A NUMERICAL SOLUTION OF THE NAVIER-STOKES AND DIFFUSION EQUATIONS FOR TWO EQUALLY SIZED SPHERES.

by

TONG-MIN SOO, B.Sc., M.Sc., D.I.C.

May, 1976.

A thesis submitted for the degree
of Doctor of Philosophy of the
University of London.

Department of Chemical Engineering
and Chemical Technology,
Imperial College of Science and
Technology,
London, S.W.7.

ABSTRACT

A theoretical study has been made of steady-state forced convective mass transfer from a system of two equally sized spheres with an isothermal, incompressible, Newtonian fluid flowing parallel to their line of centres. The stream function and vorticity distributions around the two spheres were obtained from numerical solutions of the Navier-Stokes equations and the concentration distributions from numerical solutions of the diffusion equation. Bi-spherical coordinates were used in the study because of the ease with which they can be used to describe the geometry of the flow region. The finite-difference forms of the equations were solved using an explicit extrapolated Gauss-Seidel method. Two computer programmes were developed: one for obtaining solutions of the Navier-Stokes equations and the other for obtaining solutions of the diffusion equation. Solutions were obtained for various Reynolds and Peclet numbers and for a range of sphere spacings.

Five different sphere spacings corresponding to two equally sized spheres nearly touching one another and being one, three, five, and ten diameters apart were considered in this study. For each sphere spacing, numerical solutions of the Navier-Stokes equations were obtained for a series of Reynolds numbers ranging from 0.001 to 500; also, numerical solutions of the diffusion equation were obtained for a series of Peclet numbers ranging from 0.001 to 500 using the previously obtained stream function distributions for Reynolds numbers of 0.001, 1, 10, and 100. The resultant distributions of vorticity, stream function, and concentration around the spheres were used to calculated surface

pressures, angles of flow separation, drag coefficients, and local and overall Sherwood numbers.

It was observed that the vorticity and stream function distributions were dependent on the sphere spacing and on the Reynolds number, and that the calculated rates of mass transfer from the spheres were dependent on three parameters: the sphere spacing, the Reynolds number, and the Peclet number. The distance between the spheres was found to be an important factor in determining both the fluid dynamics and the mass transfer rates. For each of the five sphere spacings considered in this study, particle-to-particle interaction was observed to exist between the spheres and to increase in extent as the sphere spacing was decreased. It was also observed that for each sphere spacing at Reynolds and Peclet numbers less than 1.0 the total drag coefficients and the overall Sherwood numbers were approximately the same for both of the spheres; while at higher Reynolds and Peclet numbers they were found to be larger for the upstream sphere than for the downstream sphere. For the larger sphere spacings the results approached those for a single isolated sphere. The results for the upstream sphere were closer to those for a single isolated sphere than were those for the downstream sphere.

ACKNOWLEDGEMENTS

I would like to express my sincere thanks and gratitude to Dr. A.R.H. Cornish for his supervision and assistance during the course of this study.

My sincere thanks and gratitude also extend to my parents for their understandings and financial assistance, and to the British Council for its Overseas Student Fee Award.

TONG-MIN SOO.

LIST OF CONTENTS

LIST OF FIGURES.

LIST OF TABLES.

LIST OF SYMBOLS

Symbol	Meaning
a	Characteristic dimension in bi-spherical coordinates defined by Figure(A-1).
a^*	a/R.
A	Cross-sectional area of spheres.
C	Concentration.
C_o	Concentration in free stream.
C_s	Concentration at surfaces of spheres.
C^*	Dimensionless concentration, $(C-C_o)/(C_s-C_o)$.
C_o^*	Dimensionless concentration in free stream.
C_s^*	Dimensionless concentration at surfaces of spheres.
C_{DF}	Frictional drag coefficient.
C_{DFA}	Frictional drag coefficient for sphere A.
C_{DFB}	Frictional drag coefficient for sphere B.
C_{DP}	Pressure drag coefficient.
C_{DPA}	Pressure drag coefficient for sphere A.
C_{DPB}	Pressure drag coefficient for sphere B.
C_{DT}	Total drag coefficient.
C_{DTA}	Total drag coefficient for sphere A.
C_{DTB}	Total drag coefficient for sphere B.
d	Characteristic dimension defined by Figure(A-1), L/2.
D_C	Diffusivity.
D_F	Frictional drag.
D_P	Pressure drag.
D_T	Total drag.
e_{ij}	Rate of strain tensor for a Newtonian fluid.

Symbol	Meaning
f	Vorticity function, defined by equation(3-3-6).
g	Vorticity function, defined by equation(3-3-5).
h	Mesh spacing in the Z-direction.
h_D	Overall mass transfer coefficient.
$h_D(\theta)$	Local mass transfer coefficient.
h_1, h_2, h_3	Scale factors in the x_1, x_2, x_3 directions.
h_Z, h_θ, h_ϕ	Scale factors in the Z, θ, ϕ directions.
k	Mesh spacing in the angle η.
k_j	Mesh spacings in the θ-direction.
K	Dimensionless pressure coefficient, $P/\frac{1}{2}\rho U^2$.
K_{AO}	Dimensionless pressure coefficient at the front stagnation point of sphere A.
$K_{A\theta}$	Dimensionless pressure coefficient at the angle θ for sphere A.
K_{BO}	Dimensionless pressure coefficient at the rear stagnation point of sphere B.
$K_{B\theta}$	Dimensionless pressure coefficient at the angle θ for sphere B.
L	Centre-to-centre distance between spheres A and B.
m	Total number of grid lines in the θ-direction.
n	Total number of grid lines in the Z-direction.
P	Pressure.
Pe	Peclet number, $2RU/D_C$.
P_S	Pressure at sphere surfaces.
P_c	Pressure in free stream.
P_n	Legendre polynomial.
r	Outer boundary radius.

Symbol	Meaning
R	Sphere radius.
R_o	Dimensionless outer boundary radius, r/d.
Re	Reynolds number, $2RU/\nu$.
S	Surface area of spheres.
Sc	Schmidt number, $\mu/\rho D_C = \nu/D_C$.
Sh_O	Overall Sherwood number, $2Rh_D/D_C$.
Sh_{AO}	Overall Sherwood number for sphere A.
Sh_{BO}	Overall Sherwood number for sphere B.
$Sh_{AL}(\theta)$, $Sh_{AL}(\eta)$	Local Sherwood number for sphere A.
$Sh_{BL}(\theta)$, $Sh_{BL}(\eta)$	Local Sherwood number for sphere B.
U	Free stream velocity.
V	Volume of spheres.
$\hat{V}$	Fluid velocity vector.
V_1, V_2, V_3	Fluid velocity components in the x_1, x_2, x_3 directions.
V_Z	Fluid velocity component in the Z-direction.
V_Z^*	Dimensionless velocity, V_Z/U.
V_θ	Fluid velocity component in the θ-direction.
V_θ^*	Dimensionless velocity, V_θ/U.
$\hat{W}$	Vorticity vector.
W_1, W_2, W_3	Vorticity vector components in the x_1, x_2, x_3 directions.
x_1, x_2, x_3	Orthogonal curvilinear coordinates.
y_1, y_2, y_3	Rectangular Cartesian coordinates.
Z	Bi-spherical coordinate.
Zs	Sphere spacing parameter.

Greek symbol	Meaning
α	Surface of sphere, $\|Zs\|$.
β	Angle defined by equation(B-4-7).
ε	Convergence criterion.
ε_{ψ^*}	Convergence criterion for the stream function.
ε_{C^*}	Convergence criterion for concentration.
ε_g	Convergence criterion for vorticity.
ζ	Vorticity.
ζ^*	Dimensionless vorticity, $R\zeta/U$.
ζ_s	Surface vorticity.
η	Angle measured from the front stagnation point of sphere A and from the rear stagnation point of sphere B.
η_{AS}	Angle of flow separation from the rear surface of sphere A.
η_{BSF}, η_{BSR}	Angles of flow separation from the front and rear surfaces of sphere B, respectively.
θ	Bi-spherical coordinate.
μ	Fluid viscosity.
ν	Fluid kinematic viscosity, μ/ρ.
ρ	Fluid density.
τ_{ij}	Symmetric stress tensor for a Newtonian fluid.
ϕ	Bi-spherical coordinate.
ψ	Stream function.
ψ^*	Dimensionless stream function, ψ/UR^2.
ω	Relaxation factor.
ω_{ψ^*}	Relaxation factor for stream function.
ω_{C^*}	Relaxation factor for concentration.
ω_g	Relaxation factor for vorticity.

The transport processes of heat, mass, and momentum from particles to fluids are important in Chemical Engineering processes. Because of the complexity of multiparticle systems in theoretical studies, a single solid sphere, liquid drop, or gas bubble is nearly always studied in order to understand transfer mechanisms.The spherical particle is the most common unit for these studies, and the results are valuable in the absence of results for multiparticle systems.

A major disadvantage of studies of single particle systems is that the particle-to-particle interactions that occur in real situations cannot be fully understood. In view of this problem, a two-particle system was thought to be a suitable starting point for multiparticle studies, and the present project was initiated to investigate steady, incompressible, isothermal, Newtonian flow around, and mass transfer rates from a system of two equally sized, stationary solid spheres placed one behind the others with their line of centres parallel to the direction of flow. Many research workers have claimed that the study of a single particle system is the first step towards gaining an understanding of the behaviour of multiparticle systems, accordingly, the present study can be claimed to be the second step in this long journey.

The transport of momentum and mass may be described by three equations: the Navier-Stokes equations, the equation of continuity, and the diffusion equation. Owing to their non-linearity, analytical solutions of the Navier-Stokes equations are very difficult to obtain. The only exact solutions available for flow around two spheres are those for Stokes flow, ie, the limiting case when the Reynolds numbers are very much less than

unity. These solutions were obtained by Stimson and Jeffery(1926). For flows at intermediate Reynolds numbers, these equations can only be solved numerically.

In this thesis, the system of equations is expressed in the two-dimensional bi-spherical coordinate system and is solved using a finite-difference method. The Navier-Stokes equations and the equation of continuity are expressed in terms of vorticity and stream function, and the resultant equations: the vorticity transport and stream function equations, which are coupled, are solved simultaneously with the appropriate boundary conditions. Using the calculated stream function distribution, the diffusion equation is then solved in order to obtain the concentration distribution.

The distance between the two spheres is an important factor in determining the influences and interactions of one sphere on the other. In the present study, five sphere spacings are considered: the two spheres nearly touching and being one, three, five, and ten diameters apart. For these sphere spacings, numerical solutions of the Navier-Stokes equations and the equation of continuity are obtained for a range of Reynolds numbers from 0.001 to as high as 500. while the diffusion equation is solved for a series of Peclet numbers from 0.001 to 500 at some selected Reynolds numbers. From the distributions of vorticity. stream function. and concentration, the drag coefficients, the surface pressure distributions, the angles of flow separation, and the local and overall Sherwood numbers for the spheres are calculated.

This study of a system of two equally sized spheres with a fluid flowing parallel to their line of centres shows the existence of particle-to-particle interaction between the spheres,

and shows that the extent of the interaction decreases as the sphere spacing increases. The distributions of vorticity, stream function, and concentration, as well as the distributions of surface pressure and local Sherwood number around the two spheres are affected by the closeness of the spheres; however, the distributions become closer to those around a single isolated sphere when the distance between the spheres becomes larger. At low Peclet numbers of 0.001 to 0.1, overall Sherwood numbers of less than 2.0 are obtained for all Reynolds numbers when the sphere spacings are small. At higher Peclet numbers, the overall rates of mass transfer from the upstream sphere are always larger than those from the downstream sphere, and the difference between the rates becomes larger when the Reynolds number is increased and when the distance between the spheres is decreased.

Two computer programmes have been developed for solving the Navier-Stokes and diffusion equations. The programmes are arranged in such a way that they can be used to solve the equations for various sphere spacings. It is hoped that this study will lead to further understanding of the complex transfer processes in multiparticle systems. The results obtained have applications in many Chemical Engineering unit operations, such as spray drying, extraction, fluidization, and combustion. The results are also useful in meteorological studies, ion exchange, and gas chromatography.

CHAPTER 2. LITERATURE SURVEY

2-1. Brief review of single sphere theoretical fluid dynamics.

The theory of viscous flow was first developed by Navier(1822) and Stokes(1845). The fourth order partial differential equations which describe the viscous flow field of a Newtonian fluid were then formulated. Because of their non-linearity, exact analytical solutions of these equations are difficult to obtain. Stokes(1851) opened a new era in theoretical viscous fluid dynamics by solving analytically the Navier-Stokes equations without the inertial term for a steady creeping flow around a solid sphere. The development of boundary layer theory by Prandtl(1904) for high Reynolds number viscous flow in which the Navier-Stokes equations can be reduced to third order partial differential equations was another great leap forward in this field.

However, for intermediate Reynolds number flows, owing to the presence of the inertial term, the only way to study the fluid dynamics is by numerical solution. Thom(1928) began the study of computational fluid dynamics by solving the Navier-Stokes equations for flow around a cylinder for a Reynolds number of 10. For the case of flow around a sphere, the first numerical solution was obtained by Kawaguti(1950) for a Reynolds number of 20 using Thom's method. Jenson(1959) obtained numerical solutions for Reynolds numbers of 5, 10, 20, and 40 using relaxation methods. He used spherical polar coordinates with an exponential transformation of the radius coordinate. With the advent of modern computers, the development of theoretical fluid dynamics has been very rapid and Hamielec, Hoffman, and Ross(1967) used Jenson's finite-difference equations to solve the

Navier-Stokes equations for viscous flow around a sphere for a series of Reynolds numbers ranging from 0.1 to 200 by the method of sucessive optimal displacement by points with relaxation. Al-Taha(1969) also used Jenson's method to obtain numerical solutions for a sphere and for oblated spheroids for Reynolds numbers between 0.001 and 500. He also investigated the effect of the location of the outer boundary on the viscous flow field and solved the energy equation for a sphere and oblated spheroids for Peclet numbers in the range of 0.001 to 2000.

2-2. Review of low Reynolds number fluid dynamics for two-sphere systems.

Nearly three quarter of a century after Stokes(1851) first solved the Navier-Stokes equations for creeping flow around a sphere, Stimson and Jeffery(1926) used bi-spherical coordinates to obtain an exact solution of the same equations for axisymmetric creeping flow around two spheres with their line of centres parallel to the direction of flow. A new chapter in theoretical fluid dynamics for multiparticle system thus opened. Their method of using bi-spherical coordinates was unique in the sense that their solutions satisfied the boundary conditions on the two spheres simultaneously and converged for all sphere spacings.

Before this exact solution was obtained, an approximate method called "the method of reflection" had been inaugurated by Smoluchowski(1911). The method of reflection was widely used for solving multiparticle problems at low Reynolds numbers. In this method, a systematic scheme of sucessive iteration was adopted for solving the Navier-Stokes equations for creeping flow to any degree of approximation by considering the boundary conditions associated with one particle at a time. The

transformation of the reflected fields from coordinates at the centre of one sphere to those at the centre of the other was accomplished in an approximate way by means of Taylor series expansions about the points corresponding to the two coordinate system origins. The results obtained using this method agreed with the exact solutions of Stimson and Jeffery for the axisymmetric two-sphere case.

Faxan and Dahl(1925) extended Smoluchowski's technique in order to study flow around two spheres along with their line of centres parallel to the direction of flow. They used a conformal transformation involving "inversion in a sphere" to transform the reflected field from coordinates at the centre of one sphere to those at the centre of the other. Their results agreed with the exact solutions of Stimson and Jeffery when sphere spacings of the two equally sized spheres were large.

Owing to the presence of inertial forces even at Reynolds numbers less than unity, Oseen(1926) presented a new treatment for the case of two spheres in which he simply used Smoluchowski's development for two spheres in creeping motion, but substituded Oseen velocity fields for Stokes fields to approximate particle interaction. For the case of two equally sized spheres following each other, he found that the force exerted by the fluid on the leading sphere was greater than that on the following sphere. For the case of two equally sized spheres falling side by side, he found that the force on each sphere was the same.

A technique involving spherical harmonics was used by Wakiya(1957) to solve two-sphere problems. The harmonics for the second sphere were developed directly with respect to the origin

of the first sphere in order to obtain a set of relationships among some characteristic constants by using the boundary conditions on the first sphere. In the same way, another set of relationships was obtained using the boundary conditions on the second sphere. By eliminating one set of these characteristic constants from the two sets of relations, a simultaneous system of equations of infinite order with respect to the other set of characteristic constants was obtained. Wakiya solved this infinite series of equations numerically by the method of sucessive approximation. His results agreed with those of Faxen and Dahl(1925) for two spheres following each other.

Kynch(1959) derived expressions for the velocity fields around two spheres moving slowly under external forces through a viscous fluid. His method was similar to that of Wakiya. He developed solutions for the second sphere with respect to the origin of the first. Instead of using spherical harmonic functions, however, the solution was developed in terms of derivatives of the basic solution. A series of equations with unknown constants was obtained and was solved by sucessive approximations for two spheres moving along and moving perpendicular to, their line of centres. Kynch noted that a general solution for any two-sphere flow problem could be obtained by combining these two solutions.

In a study of the theoretical collision efficiency of small spheres falling under the influence of gravity, Hocking(1958, 1959) noted that the two-sphere flow problem could be solved by superimposing the flows for two spheres falling along, and perpendicular to, their line of centres. He employed a method similar that of Kynch for finding numerical solutions for these

two basic problems.

A general disadvantage of these approximate methods, which are based on the method of reflection , is that the convergence of the solutions is poor when the spheres are close together or are touching. On the other hand, exact solutions in terms of bi-spherical coordinates converge for all sphere spacings.

By making use of bi-spherical coordinates, Jeffery(1915) first obtained exact solutions for the case of two spheres rotating about their line of centres. The historic work of Stimson and Jeffery(1926) then followed. They solved Stokes's equation for two spheres translating with equal velocities along their line of centres. An extension of Stimson and Jeffery's work to obtain solutions for two spheres moving with different velocities along their line of centres was carried out by Brenner(1961). These are the exact solutions for axisymmetric flow.

For the case of asymmetrical flow, exact solutions could only be obtained after Dean and O'Neill(1963) and O'Neill(1964) developed the "sphere and plane" theory for deriving exact solutions for asymmetrical flows caused by the motion of a solid sphere in a viscous fluid bounded by a plane wall.

Exact solutions for the flow field generated by two spheres moving either with equal translational velocities or with equal and opposite angular velocities perpendicular to their line of centres were obtained by O'Neill(1964), and independently by Goldman, Cox, and Brenner(1966), and by Wakiya(1967) using a modified form of the sphere and plane theory. As point out by Berker(1963), Brenner(1964), and others, the linearity of the governing differential equations and boundary conditions permits

one to decompose the general problem, in which the line of centres between the spheres is arbitrarily oriented relative to their direction of motion through the fluid, into a number of simpler sub-problems involving various types of translational and rotational motions, both parallel and perpendicular to the line of centres. O'Neill(1970) obtained another exact solution for slow viscous flow of two spheres in an infinite fluid caused by either the rotation of two equally sized spheres with uniform angular velocities about diameters perpendicular to their line of centres, or by the translation of the spheres with equal and opposite velocities along directions perpendicular to their line of centres.

2-3. Review of low Reynolds number experimental studies for two-sphere systems.

The motion of two spheres in viscous fluid at low Reynolds numbers can be resolved into the two problems of spheres falling along and perpendicular to their line of centres. It is convenient to consider these cases separately. Experimental data for both cases are available from the works of Eveson, Hall, and Wart(1959) and Bart(1959), and additional data for two spheres following each other from those of Happel and Pfeffer(1960), Isaakyan and Gasparyan(1966), and Steinberger, Pruppacher, and Neiburger(1968). In all cases, spheres were dropped in a vessel, usually cylindrical, and not in aninfinite medium as most of the theoretical works assumed.

A brief survey for the case of two spheres falling along their line of centres now follows.

The experimental data of Bart(1959) for Reynolds numbers

less than 0.05 showed good agreement with the exact theoretical results obtained by Stimson and Jeffery(1926) for two spheres nearly touching and for spheres separated by distance up to twenty diameters apart. The data of Eveson et al (1959) were also in good agreement with the solutions obtained by Stimson and Jeffery.

Happel and Pfeffer(1960) carried out experiments for two two equally sized spheres falling along their line of centres in the low Reynolds number range of 0.008 to 0.73. Their data agreed very well with the solutions obtained by Stimson and Jeffery over the Reynolds number range of 0.008 to 0.25. A definite attraction between the two spheres was observed in the Reynolds number range of 0.25 to 0.7. Happel and Pfeffer claimed that inertial forces acted to slow down the leading sphere without affecting the second sphere. Hence, their results confirmed qualitatively the prediction of Oseen(1926) that even at low Reynolds numbers of less than unity, inertial forces are important.

Isaakyan and Gasparyan(1966) carried out experiments over a Reynolds number range of 0.037 to 0.50. They observed that two equally sized spheres falling through a vertical column tended to approach each other. For the case of a large distance between the spheres, the upper sphere retarded the lower one compared with the velocity of free fall, while the upper sphere always fell with a velocity greater than that of free fall. They thus concluded that their results confirmed the Oseen solution qualitatively.

Steinberger et al(1968) studied the motion of two equally

sized spheres falling along their line of centres for Reynolds numbers ranging between 0.060 to 0.216. They observed that both spheres accelerated as they fell and that the upper sphere fell faster and accelerated more than the lower sphere. The drag coefficients for the upper sphere were also significantly smaller than those for the lower sphere.

From the above brief survey, it is obvious that most of the experimental studies of two-sphere systems were made by allowing the spheres to fall in a viscous fluid at low Reynolds numbers. However, owing to the presence of inertial forces at low Reynolds numbers, the distance between the spheres cannot be kept constant. The fluid dynamics and particle-to-particle interaction between the spheres are thus not fully understood.

2-4. Review of theoretical studies of forced convective heat and mass transfer.

The velocity fields obtained from the Navier-Stokes equations can be used to obtain solutions of the energy or diffusion equations thus enabling forced convective heat or mass transfer rates to be calculated. This survey is started with a brief study of transfer rates from a single sphere because they have been widely studied.

Langmuir(1918) showed that the value of the Nusselt number for thermal conduction from a single sphere into an infinite stagnant fluid medium was 2.0. In an experimental study of the rates of mass transfer from oblate spheroids, Cornish(1961) derived a general expression for the rates of mass transfer from oblate spheroids by molecular diffusion. His expression can be reduced to that of a single sphere as a limiting case.

By using the Stokes velocity field for low Reynolds number flow, exact solutions of the energy and diffusion equations have been obtained for both small and large Peclet numbers. In the case of small Peclet numbers, the contributions made by convection are small in comparison with those made by thermal conduction or molecular diffusion. Exact solutions of the energy equation had been obtained by Kronig and Bruijsten(1951), Yuge(1956), and Acrivos and Taylor(1962) for the rates of heat transfer from a single sphere using a perturbation method. Friedlander(1957), who employed the solution of the linearized Navier-Stokes equations due to Tomotika and Aoi(1950), solved the diffusion equation for a single sphere at both small and large Peclet numbers. On the other hand, for the case of large Peclet numbers, the effect of molecular diffusion and thermal conduction is very

small and can be neglected everywhere except within a thin boundary layer near the fluid-solid interface where the temperature or concentration variation occurs. With this boundary layer approximation, Friedlander(1957) solved the energy equation and Levich(1962) solved the diffusion equation for a single sphere at very high Peclet numbers.

For intermediate Reynolds number flows, the velocity field for flow around a single sphere is impossible to obtain analytically, hence, it is not possible to obtain an analytical solution of the diffusion and energy equations. With the help of the boundary layer approximation, Baird and Hamielec(1962) managed to predict analytically the forced convective heat and mass transfer rates from solid and fluid spheres for Reynolds numbers up to 100. The only way of solving the diffusion and energy equations is to use a numerical method with the velocity field obtained from the numerical solution of the Navier-Stokes equations.

For high Reynolds number flows, the diffusion and energy equations can be expressed in terms of boundary layer equations. As in the case of the hydrodynamic boundary layer equation, there are two kinds of solutions: exact and approximate. A method of obtaining exact solutions was developed by Frossling (1940) for flow around axisymmetric bodies of revolution. Green (1968) derived the boundary layer equations in orthogonal curvilinear coordinates and obtained exact solutions for spheres, discs, and oblate spheroids. Approximate solutions of the thermal boundary layer equation have been developed by Aksel'rud(1953), Grafton(1963) for spheres, and by Rojey(1967) for oblate spheroids.

For the case of intermediate Peclet numbers for low and intermediate Reynolds number flows, relatively few exact solutions of the energy or diffusion equation have been obtained. Al-Taha (1969) solved the energy equation numerically for spheres and oblate spheroids for a wide range of Peclet numbers from 0.001 to 2000.0. The velocity fields were obtained from the numerical solutions of the Navier-Stokes equations for a Reynolds number range from 0.001 to 500.o. This was a great advance in the study of forced convective heat and mass transfer. With the advent of modern computers, numerical solutions have become important and powerful tools for studying heat and mass transfer processes from particles of different shapes.

For multiparticle systems, Pfeffer(1964), and Pfeffer and Happel(1964)observed that the transfer rate from a single sphere decreased with an increase in the voidage. In multiparticle systems, such as fluidized beds, values of the Nusselt number less than two have been measured. Cornish(1965) presented an argument that the minimum possible rate of heat and mass transfer from a sphere may be much less than the value of two applicable to a single sphere in an infinite stagnant medium. He noted that for the case of two equally sized spheres, with their centres 100 radii apart, the Nusselt number is approximately one percent less than the limiting value of two. When the centres of the spheres are only 4 radii apart, the Nusselt number is approximately 1.6. For the limiting case when two spheres touch, Cornish predicted that the Nusselt number will be 1.386.

Solution of the diffusion equation for two-sphere systems requires the expression of the equation in bi-spherical coordinates. Solutions are difficult to obtain even though the

diffusion equation is linear. Aminzadeh(1970), Aminzadeh, Al-Taha, Cornish, Kolansky, and Pfeffer(1974), used the velocity field of Stimson and Jeffery(1926) and Al-Taha's method of solution in order to obtain numerical solutions of the diffusion equation for a range of Peclet numbers from 0.001 to 100 for two spheres of equal size. They found that at low Peclet numbers the overall Sherwood numbers for the spheres were less than two when the sphere spacings were small. They also found that for each sphere spacing at high Peclet numbers, the overall Sherwood numbers were larger for the upstream sphere than for the downstream sphere.

From this survey, it can be seen that most of the works done so far for two-sphere systems were for creeping flow. For intermediate Reynolds number flows both the inertial and convective effects are important and solutions of the Navier-Stokes equations and solutions of the energy and diffusion equations are non-existent. In order to fill this gap, the present project of forced convective mass transfer from a system of two equally sized spheres to an incompressible Newtonian fluid flowing in steady flow parallel to their line of centres was undertaken. The Navier-Stokes and diffusion equations were expressed in bi-spherical coordinates and the solutions for the equations in finite-difference form were obtained numerically using an iterative method.

CHAPTER 3. THEORETICAL ANALYSIS

3-1. The basic equations governing steady viscous fluid flow and mass transfer for two-sphere systems.

The basic equations which describe steady-state forced convective mass transfer from a system of two equally sized solid spheres to a viscous fluid flowing parallel to their line of centres are the equation of continuity, the equation of motion, and the diffusion equation. For an isothermal, incompressible, Newtonian fluid with properties continuous both in space and time, and with a small mass flux so that the density of the fluid does not change much, the three basic equations become:

The equation of continuity:

$$\nabla\cdot\hat{V} = 0 \qquad (3\text{-}1\text{-}1)$$

The Navier-Stokes equations:

$$(\hat{V}\cdot\nabla)\hat{V} = -\frac{1}{\rho}\nabla P + \nu\nabla^2\hat{V} \qquad (3\text{-}1\text{-}2)$$

Equation(3-1-2) can also be expressed in the following form:

$$\tfrac{1}{2}\nabla(\hat{V}\cdot\hat{V}) - \hat{V}\times(\nabla\times\hat{V}) = -\frac{1}{\rho}\nabla P + \nu\{\nabla(\nabla\cdot\hat{V}) - \nabla\times(\nabla\times\hat{V})\} \qquad (3\text{-}1\text{-}3)$$

The diffusion equation:

$$(\hat{V}\cdot\nabla)C = D_C\nabla^2 C \qquad (3\text{-}1\text{-}4)$$

In the above equations, $\hat{V}$ is the fluid velocity vector, C is the concentration of the transferrable material in the fluid, and ν, ρ, and D_C are the kinematic viscosity, density, and diffusivity, respectively. The term P in equations(3-1-2) and (3-1-3) is the modified fluid pressure which is measured relative to the undisturbed hydrostatic pressure which would occur if the fluid was stagnant at the point considered.

By taking the curl of equation(3-1-3) and applying the equation of continuity, the Navier-Stokes equations are transformed into the vorticity transport equation with no pressure term:

$$\nabla x(\hat{V}x\hat{W}) = \nu\nabla x(\nabla x\hat{W}) \qquad (3\text{-}1\text{-}5)$$

where the vorticity vector, $\hat{W}$, is defined as:

$$\hat{W} = \nabla x\hat{V} \qquad (3\text{-}1\text{-}6)$$

The vorticity transport equation can also be expressed in another form by taking the curl of equation(3-1-2):

$$(\hat{V}\cdot\nabla)\hat{W} = (\hat{W}\cdot\nabla)\hat{V} + \nu\nabla^2\hat{W} \qquad (3\text{-}1\text{-}7)$$

The flow of fluid with no swirl around two equally sized spheres parallel to their line of centres is axisymmetric. Hence, the orthogonal curvilinear coordinates(x_1, x_2, x_3) can be used to describe the flow with x_1 being taken in the flow direction around the surfaces, x_2 normal to the surfaces, and x_3 in the direction of rotation of the bodies about the axis of symmetry. For axisymmetric flow, the velocity and all other variables are independent of x_3-direction, and the velocity component in the x_3-direction is everywhere zero, i.e.,

$$\frac{\partial\hat{V}}{\partial x_3} = 0 \quad ; \quad \frac{\partial C}{\partial x_3} = 0 \quad ; \; V_3 = 0 \qquad (3\text{-}1\text{-}8)$$

From these conditions, it is clear that the present flow problem becomes a two-dimensional flow problem. The vorticity vector, which is defined by equation(3-1-6), has only one non-zero component $\hat{W}(0,0,\zeta)$ in the x_3-direction which is normal to the plane of flow. Also, the term $(\hat{W}\cdot\nabla)\hat{V}$ in equation(3-1-7) is zero. Hence, the vorticity transport equation(3-1-7) can be

simplified as follows:

$$(\hat{V}\cdot\nabla)\zeta = \nu\nabla^2\zeta \qquad (3\text{-}1\text{-}9)$$

Similarly, the vorticity transport equation in the form of equation(3-1-5) becomes:

$$\nabla x(\hat{V}x\zeta) = \nu\nabla x(\nabla x\zeta) \qquad (3\text{-}1\text{-}10)$$

There is a close analogy between the vorticity transport equation in the form of equation(3-1-9) and the diffusion equation(3-1-4). The terms on the right-hand side of equations (3-1-4) and (3-1-9) represent the diffusion of material and vorticity, respectively; while the terms on the left-hand side of these equations represent the convection of material and vorticity, respectively.

From the above considerations, the equations governing the present problem of forced convective mass transfer from a system of two spheres are equations(3-1-1), (3-1-4), and (3-1-10). These equations are expressed in vector form, so that an appropriate coordinate system has to be chosen before they can be solved.

3-2. System of equations in bi-spherical coordinates.

The system of equations: the equation of continuity(3-1-1), the vorticity transport equation(3-1-10), and the diffusion equation(3-1-4), is rewritten here:

$$\nabla\cdot\hat{V} = 0 \tag{3-2-1}$$

$$\nabla\times(\hat{V}\times\zeta) = \nu\nabla\times(\nabla\times\zeta) \tag{3-2-2}$$

$$(\hat{V}\cdot\nabla)C = D_C\nabla^2 C \tag{3-2-3}$$

With the help of the orthogonal curvilinear coordinate system(x_1, x_2, x_3) and their corresponding scale factors(h_1, h_2, h_3), the system of equations(3-2-1) to (3-2-3) becomes:

The equation of continuity:

$$\frac{1}{h_1h_2h_3}\{\frac{\partial}{\partial x_1}(h_2h_3V_1) + \frac{\partial}{\partial x_2}(h_1h_3V_2)\} = 0 \tag{3-2-4}$$

The vorticity transport equation:

$$\frac{V_1}{h_1}\frac{\partial}{\partial x_1}(\frac{\zeta}{h_3}) + \frac{V_2}{h_2}\frac{\partial}{\partial x_2}(\frac{\zeta}{h_3}) = \frac{\nu}{h_3^2}E^2(h_3\zeta) \tag{3-2-5}$$

where,

$$E^2 = \frac{h_3}{h_1h_2}\{\frac{\partial}{\partial x_1}(\frac{h_2}{h_1h_3}\frac{\partial}{\partial x_1}) + \frac{\partial}{\partial x_2}(\frac{h_1}{h_2h_3}\frac{\partial}{\partial x_2})\} \tag{3-2-6}$$

The diffusion equation:

$$\frac{V_1}{h_1}\frac{\partial C}{\partial x_1} + \frac{V_2}{h_2}\frac{\partial C}{\partial x_2} = \frac{D_C}{h_1h_2h_3}\{\frac{\partial}{\partial x_1}(\frac{h_2h_3}{h_1}\frac{\partial C}{\partial x_1}) + \frac{\partial}{\partial x_2}(\frac{h_1h_3}{h_2}\frac{\partial C}{\partial x_2})\} \tag{3-2-7}$$

The non-zero component of the vorticity vector, ζ, which is also called the vorticity, is derived from equation (3-1-6) as:

$$\zeta = \frac{1}{h_1 h_2}\{\frac{\partial}{\partial x_1}(h_2 V_2) - \frac{\partial}{\partial x_2}(h_1 V_1)\} \qquad (3\text{-}2\text{-}8)$$

In order to reduce the number of the variables of the system of equations by one, the stream function, ψ, is introduced to replace the velocity components V_1 and V_2. The stream function is defined by the following two expressions:

$$V_1 = \frac{-1}{h_2 h_3}\frac{\partial \psi}{\partial x_2} \qquad (3\text{-}2\text{-}9a)$$

$$V_2 = \frac{+1}{h_1 h_3}\frac{\partial \psi}{\partial x_1} \qquad (3\text{-}2\text{-}9b)$$

Equations (3-2-9a) and (3-2-9b) satisfy the equation of continuity (3-2-1). With this introduction of the stream function, the system of equations can thus be written in terms of variables: vorticity, stream function, and concentration.

The vorticity transport equation (3-2-4) becomes:

$$\frac{\partial \psi}{\partial x_1}\frac{\partial}{\partial x_2}(\frac{\zeta}{h_3}) - \frac{\partial \psi}{\partial x_2}\frac{\partial}{\partial x_1}(\frac{\zeta}{h_3}) = \nu(\frac{h_1 h_2}{h_3})E^2(h_3\zeta) \qquad (3\text{-}2\text{-}10)$$

Equation (3-2-8), which defines the vorticity, becomes the stream function equation:

$$E^2(\psi) = h_3\zeta \qquad (3\text{-}2\text{-}11)$$

and the diffusion equation (3-2-7) becomes:

$$D_C\{\frac{\partial}{\partial x_1}(\frac{h_2h_3}{h_1}\frac{\partial C}{\partial x_1}) + \frac{\partial}{\partial x_2}(\frac{h_1h_3}{h_2}\frac{\partial C}{\partial x_2})\} = \frac{\partial \psi}{\partial x_1}\frac{\partial C}{\partial x_2} - \frac{\partial \psi}{\partial x_2}\frac{\partial C}{\partial x_1} \qquad (3\text{-}2\text{-}12)$$

The bi-spherical coordinate system(Z, θ, ϕ) is an orthogonal curvilinear coordinate system. Because of the ease with which bi-spherical coordinates can be used to describe the locations of the two spheres and the boundary conditions of the system of equations, they are used in this study. A detailed description of the bi-spherical coordinate system has been given by Happel and Brenner(1965). A description is also given in Appendix A.

Hence, the three general orthogonal curvilinear coordinates become: $x_1 = Z$, $x_2 = \theta$, and $x_3 = \phi$, and the three corresponding scale factors become:

$$h_1 = h_Z = \frac{a}{\mathrm{Cosh}Z - \mathrm{Cos}\theta}$$

$$h_2 = h_\theta = \frac{a}{\mathrm{Cosh}Z - \mathrm{Cos}\theta} \qquad (3\text{-}2\text{-}13)$$

$$h_3 = h_\phi = \frac{a\mathrm{Sin}\theta}{\mathrm{Cosh}Z - \mathrm{Cos}\theta}$$

where a is the characteristic dimension in bi-spherical coordinates which is defined by Figure(A-1). With the substitution of these coordinates and scale factors, the governing system of equations in bi-spherical coordinates is finally formulated as follows:

The two velocity components, equations(3-2-9a) and (3-2-9b) become:

$$V_Z = - \left(\frac{\text{Cosh}Z - \text{Cos}\theta}{a}\right)\left(\frac{\text{Cosh}Z - \text{Cos}\theta}{a\text{Sin}\theta}\right)\frac{\partial\psi}{\partial\theta} \qquad (3\text{-}2\text{-}14)$$

$$V_\theta = + \left(\frac{\text{Cosh}Z - \text{Cos}\theta}{a}\right)\left(\frac{\text{Cosh}Z - \text{Cos}\theta}{a\text{Sin}\theta}\right)\frac{\partial\psi}{\partial Z} \qquad (3\text{-}2\text{-}15)$$

The stream function equation(3-2-11) becomes:

$$E^2(\psi) = \left(\frac{a\text{Sin}\theta}{\text{Cosh}Z - \text{Cos}\theta}\cdot\zeta\right) \qquad (3\text{-}2\text{-}16)$$

The vorticity transport equation(3-2-10) becomes:

$$E^2\left(\frac{a\text{Sin}\theta}{\text{Cosh}Z - \text{Cos}\theta}\cdot\zeta\right) = \frac{\text{Sin}\theta}{\nu}\left(\frac{\text{Cosh}Z - \text{Cos}\theta}{a}\right)\left\{\frac{\partial\psi}{\partial Z}\frac{\partial}{\partial\theta}\left(\frac{\text{Cosh}Z - \text{Cos}\theta}{a\text{Sin}\theta}\cdot\zeta\right)\right.$$

$$\left. - \frac{\partial\psi}{\partial\theta}\frac{\partial}{\partial Z}\left(\frac{\text{Cosh}Z - \text{Cos}\theta}{a\text{Sin}\theta}\cdot\zeta\right)\right\} \qquad (3\text{-}2\text{-}17)$$

where:

$$E^2 = \left(\frac{\text{Cosh}Z - \text{Cos}\theta}{a}\right)^2\left\{\frac{\partial^2}{\partial Z^2} + \left(\frac{\text{Sinh}Z}{\text{Cosh}Z - \text{Cos}\theta}\right)\frac{\partial}{\partial Z} + \frac{\partial^2}{\partial\theta^2}\right.$$

$$\left. - \frac{\text{Cosh}Z\cdot\text{Cos}\theta - 1}{\text{Sin}\theta(\text{Cosh}Z - \text{Cos}\theta)}\frac{\partial}{\partial\theta}\right\} \qquad (3\text{-}2\text{-}18)$$

The diffusion equation(3-2-12) becomes:

$$\frac{\partial^2 C}{\partial Z^2} - \left(\frac{\text{Sinh}Z}{\text{Cosh}Z - \text{Cos}\theta}\right)\frac{\partial C}{\partial Z} + \frac{\partial^2 C}{\partial\theta^2} + \frac{\text{Cosh}Z\cdot\text{Cos}\theta - 1}{\text{Sin}\theta(\text{Cosh}Z - \text{Cos}\theta)}\frac{\partial C}{\partial\theta}$$

$$= \frac{1}{D_C}\left(\frac{a\text{Sin}\theta}{\text{Cosh}Z - \text{Cos}\theta}\right)\left\{\frac{\partial\psi}{\partial Z}\cdot\frac{\partial C}{\partial\theta} - \frac{\partial\psi}{\partial\theta}\cdot\frac{\partial C}{\partial Z}\right\} \qquad (3\text{-}2\text{-}19)$$

Hence, equations(3-2-16), (3-2-17), and (3-2-19), are the model for forced convective mass transfer from a system of two spheres.

3-3. System of equations in dimensionless form.

Numerical solutions of equations(3-2-16), (3-2-17), and (3-2-19), can be obtained more conveniently if the equations are expressed in dimensionless form. In view of this, the following dimensionless quantities and groups are introduced into the present system of equations with the help of the characteristic dimension R, which is the radius of the spheres, and the undisturbed fluid velocity U:

$$a^* = \frac{a}{R} \quad , \quad \psi^* = \frac{\psi}{UR^2} \quad , \quad \zeta^* = \frac{R\zeta}{U} \quad , \quad Re = \frac{2RU}{\nu} \quad ,$$

$$C^* = \frac{C - C_o}{C_s - C_o} \quad , \quad Sc = \frac{\nu}{D_C} \quad , \quad Sh_O = \frac{2Rh_D}{D_C} \quad , \quad Pe = RexSc \qquad (3\text{-}3\text{-}1)$$

where the groups Re, Sc, Sh_O, and Pe, are the Reynolds, Schmidt, overall Sherwood, and Peclet numbers, respectively; while h_D is the overall mass transfer coefficient. The term C_s is the concentration of the transferring substance adjacent to the solid surface and C_o is the concentration in the main stream outside the outer boundary.

With these dimensionless quantities and groups, the system of equations(3-2-16), (3-2-17), and (3-2-19), can be expressed in dimensionless form.

The stream function equation becomes:

$$E^{*2}(\psi^*) = \left(\frac{a^* Sin\theta}{CoshZ - Cos\theta} \cdot \zeta^*\right) \qquad (3\text{-}3\text{-}2)$$

and the vorticity transport equation becomes:

$$E^{*2}\left(\frac{a^{*}\mathrm{Sin}\theta}{\mathrm{Cosh}Z - \mathrm{Cos}\theta}\zeta^{*}\right) = \tfrac{1}{2}\mathrm{Re}\left(\frac{a^{*}\mathrm{Sin}\theta}{\mathrm{Cosh}Z - \mathrm{Cos}\theta}\right)\left[\frac{\partial\psi^{*}}{\partial Z}\cdot\frac{\partial}{\partial\theta}\left(\frac{\mathrm{Cosh}Z - \mathrm{Cos}\theta}{a^{*}\mathrm{Sin}\theta}\zeta^{*}\right)\right.$$

$$\left. - \frac{\partial\psi^{*}}{\partial\theta}\cdot\frac{\partial}{\partial Z}\left(\frac{\mathrm{Cosh}Z - \mathrm{Cos}\theta}{a^{*}\mathrm{Sin}\theta}\zeta^{*}\right)\right] \qquad (3\text{-}3\text{-}3)$$

where,

$$E^{*2} = \left(\frac{\mathrm{Cosh}Z - \mathrm{Cos}\theta}{a^{*}}\right)^{2}\left[\frac{\partial^{2}}{\partial Z^{2}} + \left(\frac{\mathrm{Sinh}Z}{\mathrm{Cosh}Z - \mathrm{Cos}\theta}\right)\frac{\partial}{\partial Z} + \frac{\partial^{2}}{\partial\theta^{2}}\right.$$

$$\left. - \left\{\frac{\mathrm{Cosh}Z\cdot\mathrm{Cos}\theta - 1}{\mathrm{Sin}\theta(\mathrm{Cosh}Z - \mathrm{Cos}\theta)}\right\}\frac{\partial}{\partial\theta}\right] \qquad (3\text{-}3\text{-}4)$$

By defining two vorticity functions, g and f, in the following way:

$$g = \left(\frac{a^{*}\mathrm{Sin}\theta}{\mathrm{Cosh}Z - \mathrm{Cos}\theta}\zeta^{*}\right) \qquad (3\text{-}3\text{-}5)$$

$$f = \zeta^{*} \Big/ \left(\frac{a^{*}\mathrm{Sin}\theta}{\mathrm{Cosh}Z - \mathrm{Cos}\theta}\right) = \left(\frac{\mathrm{Cosh}Z - \mathrm{Cos}\theta}{a^{*}\mathrm{Sin}\theta}\zeta^{*}\right) \qquad (3\text{-}3\text{-}6)$$

equations (3-3-2) and (3-3-3) can be further simplified as follows:

$$E^{*2}(\psi^{*}) = g \qquad (3\text{-}3\text{-}7)$$

$$E^{*2}(g) = \tfrac{1}{2}\mathrm{Re}\left(\frac{a^{*}\mathrm{Sin}\theta}{\mathrm{Cosh}Z - \mathrm{Cos}\theta}\right)\left[\frac{\partial\psi^{*}}{\partial Z}\cdot\frac{\partial f}{\partial\theta} - \frac{\partial\psi^{*}}{\partial\theta}\cdot\frac{\partial f}{\partial Z}\right] \qquad (3\text{-}3\text{-}8)$$

Similarly, with the help of dimensionless quantities, the diffusion equation (3-2-19) becomes:

$$\frac{\partial^{2}C^{*}}{\partial Z^{2}} - \left(\frac{\mathrm{Sinh}Z}{\mathrm{Cosh}Z - \mathrm{Cos}\theta}\right)\frac{\partial C^{*}}{\partial Z} + \frac{\partial^{2}C^{*}}{\partial\theta^{2}} + \left\{\frac{\mathrm{Cosh}Z\cdot\mathrm{Cos}\theta - 1}{\mathrm{Sin}\theta(\mathrm{Cosh}Z - \mathrm{Cos}\theta)}\right\}\frac{\partial C^{*}}{\partial\theta}$$

$$= \tfrac{1}{2}\mathrm{Re}x\mathrm{Sc}\left(\frac{\mathrm{Cosh}Z - \mathrm{Cos}\theta}{a^{*}\mathrm{Sin}\theta}\right)\left[\frac{\partial\psi^{*}}{\partial Z}\frac{\partial C^{*}}{\partial\theta} - \frac{\partial\psi^{*}}{\partial\theta}\frac{\partial C^{*}}{\partial Z}\right] \qquad (3\text{-}3\text{-}9)$$

This system of dimensionless equations, equations(3-3-7) to (3-3-9), consists of elliptic type second order partial differential equations. Equation(3-3-8) is non-linear in ζ^*, while equations(3-3-7) and (3-3-9) are linear in ψ^* and C^*, respectively. The appropriate boundary conditions of the system of equations(3-3-7) to (3-3-9) are specified in the next section. With these boundary conditions, the coupled stream function and vorticity transport equations can be solved simultaneously for the stream function and vorticity distributions in the flow region for a series of Reynolds numbers. Using the calculated stream function distribution for any specified Reynolds number, the diffusion equation(3-3-9) can then be solved for the concentration distributions in the same flow region for a series of Peclet numbers.

3-4. Boundary conditions.

In order to solve the system of equations(3-3-7) to (3-3-9) for the stream function, vorticity, and concentration distributions in the flow region at any sphere spacing, the boundary conditions for these variables must be prescribed. For a system of two equally sized spheres with fluid flowing parallel to their line of centres, the boundary conditions are defined and given in the following sections

(1). The boundary conditions on the solid surfaces(Z=-Zs and Z=+Zs).

The locations of the two spheres are controlled by the sphere spacing parameter, Zs. For the surface of the upstream sphere, the Z-coordinate has a value of -Zs, while for the surface of the downstream sphere, it has a value of +Zs. Since the locations of the spheres are not dependent on the θ-coordinate, then, once the sphere spacing parameter Zs is specified, the positions of the surfaces of the spheres and the distance between the spheres are fixed in the space . In general, the distance between the spheres is always measured in terms of unit of R, which is the radius of the spheres.

The application of the non-slip conditions on the solid surfaces of the two spheres gives:

$$V_Z^* = V_\theta^* = 0 \quad , \quad \psi^* = 0 \quad , \quad \frac{\partial \psi^*}{\partial \theta} = \frac{\partial^2 \psi^*}{\partial \theta^2} = 0 \quad , \quad \frac{\partial \psi^*}{\partial Z} = 0 \qquad (3\text{-}4\text{-}1)$$

The vorticities at the surfaces can be obtained from the stream function equation(3-3-7) and the boundary condition(3-4-1). They have the following forms:

$$\zeta^*\Big|_{Z=-Zs} = \left(\frac{\mathrm{Cosh}(-Zs) - \mathrm{Cos}\theta}{a^* \mathrm{Sin}\theta}\right)\left(\frac{\mathrm{Cosh}(-Zs) - \mathrm{Cos}\theta}{a^*}\right) 2\frac{\partial^2\psi^*}{\partial Z^2}\Big|_{Z=-Zs} \qquad (3\text{-}4\text{-}2a)$$

and,

$$\zeta^*\Big|_{Z=+Zs} = \left(\frac{\mathrm{Cosh}(+Zs) - \mathrm{Cos}\theta}{a^* \mathrm{Sin}\theta}\right)\left(\frac{\mathrm{Cosh}(+Zs) - \mathrm{Cos}\theta}{a^*}\right) 2\frac{\partial^2\psi^*}{\partial Z^2}\Big|_{Z=+Zs} \qquad (3\text{-}4\text{-}2b)$$

The concentrations at the solid surfaces of the two spheres, C_s^*, are always maintained at a constant value, such that:

$$C_s^* = 1.0 \qquad (3\text{-}4\text{-}3)$$

(2). The boundary conditions along the axes of symmetry(θ=0 and $\theta=\pi$).

For two spheres described by the bi-spherical coordinates, the axis of symmetry(θ=0) composes two lines: one normal to the front stagnation point of the upstream sphere and the other normal to the rear stagnation point of the downstream sphere. On the other hand, the axis of symmetry($\theta=\pi$) is a straight line joining the rear stagnation point of the upstream sphere and the front stagnation point of the downstream sphere.

For the Navier-Stokes equations, the boundary conditions along these axes of symmetry are the conditions of axisymmetry which are defined as follows:

$$\psi^* = 0 \quad , \quad \frac{\partial\psi^*}{\partial Z} = \frac{\partial^2\psi^*}{\partial Z^2} = 0 \quad , \quad \frac{\partial\psi^*}{\partial\theta} = 0 \qquad (3\text{-}4\text{-}4)$$

The boundary conditions for the vorticity are obtained from the stream function equations(3-3-7) and the boundary condition(3-4-4). It is necessary to use L'Hospital's rule to obtain the following:

$$\zeta^* = 0 \quad , \quad g = 0 \quad , \quad f = 0 \tag{3-4-5}$$

For the diffusion equation, the boundary conditions along the axes of symmetry, $\theta=0$ and $\theta=\pi$, are:

$$\frac{\partial C^*}{\partial \theta} = 0 \tag{3-4-6}$$

(3). The boundary conditions along the outer boundary(Z_o, θ_o).

The outer boundary of the flow region is taken to be a large sphere which has a radius of r and a centre at the origin of the bi-spherical coordinate system. The outer boundary surrounds the two spheres completely. When values of r and Zs are specified, the coordinates along the outer boundary(Z_o, θ_o) can be obtained from equation(A-2-8) as shown in Appendix A. Along and outside this outer boundary, the flow is assumed to be uniform and parallel, so that the vorticity is zero. Also, the concentration along and outside the outer boundary is taken to be C_o. Hence, the outer boundary conditions for the system of equations can be summarized as follows:

$$\psi^* = \tfrac{1}{2}\left(\frac{a^* \mathrm{Sin}\theta_o}{\mathrm{Cosh}Z_o - \mathrm{Cos}\theta_o}\right)^2 \tag{3-4-7}$$

$$\zeta^* = 0 \quad , \quad g = 0 \quad , \quad f = 0 \tag{3-4-8}$$

$$C_o^* = 0 \tag{3-4-9}$$

With these boundary conditions, equations(3-4-1) to (3-4-9), and the system of equations(3-3-7) to (3-3-9), the problem of forced convective mass transfer from a system of two equally sized spheres with fluid flowing parallel to their line of centres is fully described. The numerical techniques employed for the solutions are presented in the next chapter.

CHAPTER 4. NUMERICAL TECHNIQUES

4-1. Introduction.

The system of equations, equations(3-3-7), (3-3-8), and (3-3-9), is rewritten here as follows:

The stream function equation:

$$\frac{\partial^2\psi^*}{\partial Z^2} + \left(\frac{\text{SinhZ}}{\text{CoshZ} - \text{Cos}\theta}\right)\frac{\partial\psi^*}{\partial Z} + \frac{\partial^2\psi^*}{\partial\theta^2} - \frac{\text{CoshZ}\cdot\text{Cos}\theta - 1}{\text{Sin}\theta(\text{CoshZ} - \text{Cos}\theta)}\cdot\frac{\partial\psi^*}{\partial\theta}$$

$$= \left(\frac{a^*}{\text{CoshZ} - \text{Cos}\theta}\right)^2 g \qquad (4\text{-}1\text{-}1)$$

The vorticity transport equation:

$$\frac{\partial^2 g}{\partial Z^2} + \left(\frac{\text{SinhZ}}{\text{CoshZ} - \text{Cos}\theta}\right)\frac{\partial g}{\partial Z} + \frac{\partial^2 g}{\partial\theta^2} - \frac{\text{CoshZ}\cdot\text{Cos}\theta - 1}{\text{Sin}\theta(\text{CoshZ} - \text{Cos}\theta)}\cdot\frac{\partial g}{\partial\theta}$$

$$= \tfrac{1}{2}\text{Re}\left(\frac{a^*\text{Sin}\theta}{\text{CoshZ} - \text{Cos}\theta}\right)\left(\frac{a^*}{\text{CoshZ} - \text{Cos}\theta}\right)^2\left[\frac{\partial\psi^*}{\partial Z}\cdot\frac{\partial f}{\partial\theta} - \frac{\partial\psi^*}{\partial\theta}\cdot\frac{\partial f}{\partial Z}\right]$$

$$(4\text{-}1\text{-}2)$$

The diffusion equation:

$$\frac{\partial^2 C^*}{\partial Z^2} - \left(\frac{\text{SinhZ}}{\text{CoshZ} - \text{Cos}\theta}\right)\frac{\partial C^*}{\partial Z} + \frac{\partial^2 C^*}{\partial\theta^2} + \frac{\text{CoshZ}\cdot\text{Cos}\theta - 1}{\text{Sin}\theta(\text{CoshZ} - \text{Cos}\theta)}\cdot\frac{\partial C^*}{\partial\theta}$$

$$= \tfrac{1}{2}\text{RexSc}\left(\frac{\text{CoshZ} - \text{Cos}\theta}{a^*\text{Sin}\theta}\right)\left[\frac{\partial\psi^*}{\partial Z}\cdot\frac{\partial C^*}{\partial\theta} - \frac{\partial\psi^*}{\partial\theta}\cdot\frac{\partial C^*}{\partial Z}\right] \qquad (4\text{-}1\text{-}3)$$

The geometrical configuration of the present system of two equally sized spheres with fluid flowing parallel to their line of centres is illustrated in Figure(4-1-1). The upstream sphere is designated as sphere A while the downstream sphere as

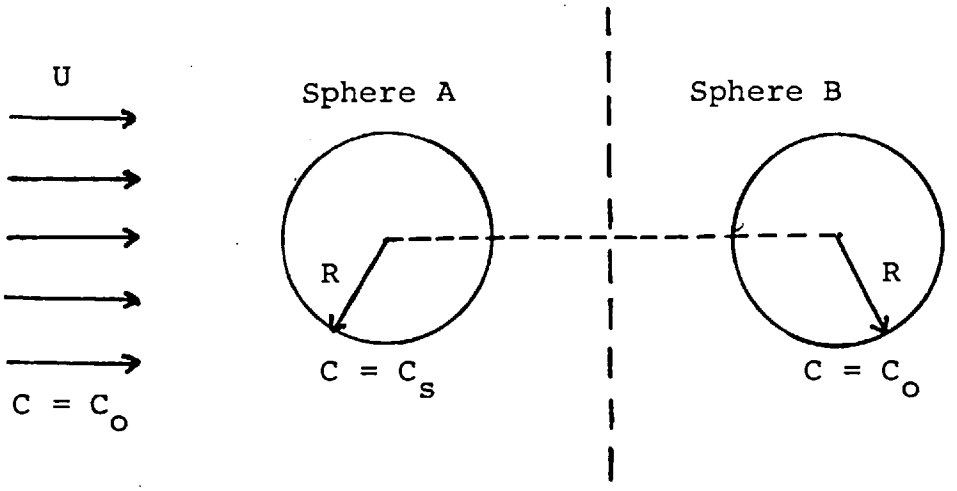

Figure(4-1-1) Flow configuration.

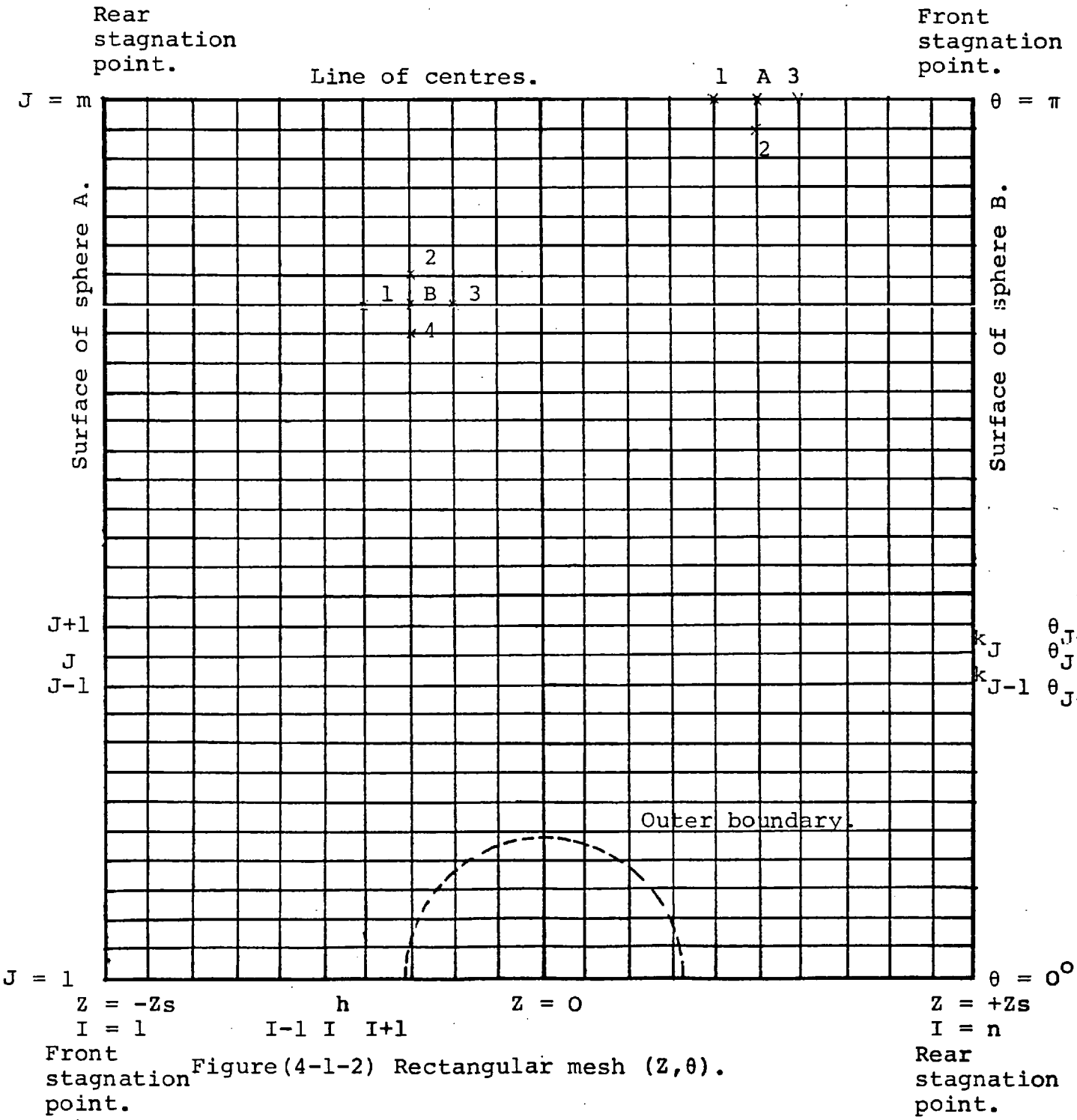

Figure(4-1-2) Rectangular mesh (Z,θ).

sphere B. The flow region is a region bounded by the solid surfaces of the two spheres and the outer boundary sphere which has a radius of r and a centre at the origin of the bi-spherical coordinate system.

By specifying the sphere spacing parameter, Zs, the locations of the two spheres are determined with $Z = -Zs$ for the surface of sphere A and with $Z = +Zs$ for the surface of sphere B. The centre- to-centre distance between the spheres, L, which equals to 2d, is $2Ra^{*} \cdot CoshZs$ or $2a \cdot CoshZs$.

In the case of a single sphere described by polar coordinates(r, θ) in a meridian plane, the angle η measured the normals to the front stagnation point and to a point on the surface, has the same value as that of the θ-coordinate which passes through the point on the surface. On the other hand, in the case of two equally sized spheres described by bi-polar coordinates(Z, θ) in a meridian plane, the angle η measured between the normals to the front stagnation point and to a point on the surface of sphere A, or between the normals to the rear stagnation point and to another point on the surface of sphere B, is not the same as that of the θ-coordinate, except at the front and rear stagnation points and unless the two spheres are an infinite distance apart.

In two-sphere fluid dynamic and mass transfer problems, many important quantities, such as surface vorticity distributions, angles of flow separation, surface pressure distributions, and local mass transfer rates, are easy to interpret using the angle η. Hence, it is desirable to develop a new scheme of distributing the grid lines for the θ-direction

using equal increments in the values of η instead of the conventional scheme of distributing the grid lines using equal increments in the values of θ. With the adoption of this new scheme, the results obtained can then be interpreted in the same way as those for a single sphere. The method of obtaining values of θ corresponding to a constant increment in the values of η is stated in section(A-3)(Appendix A). For the five sphere spacings considered in this study: Zs = 0.20. 1.32, 2.07, 2,48, and 3.09, the values of θ corresponding to a constant increment of 6^{o} in the values of η are shown in Table(A-1). It is obvious that for each sphere spacing, the values of θ and η are not the same, i.e., an equal increment in the values of θ does not result in the same increment in the values of η and vice versus. For small sphere spacings, especially the smallest sphere spacing Zs = 0.20, the differences between the values of θ and η are large; while for large sphere spacings they are generally small.

In Figures(4-1-3) to (4-1-12), the distributions of the grid lines for both the Z- and θ-directions around two equally sized spheres are shown for all the five sphere spacings considered in this study. In these figures, the grid lines for the Z-direction are distributed according to a constant increment of $|Zs/10|$ in values of Z varying from Z = -Zs to Z = +Zs, while the grid lines for the θ-direction are distributed with a constant increment of 6^{o} in the values of θ and with a constant increment of 6^{o} in the values of η. From these figures, it can be seen that the grid lines for the θ-direction are more evenly distributed in the flow region using the new scheme, especially for the two smallest sphere spacings Zs = 0.20 and Zs = 1.32. Therefore, in addition to the advantage of interpreting

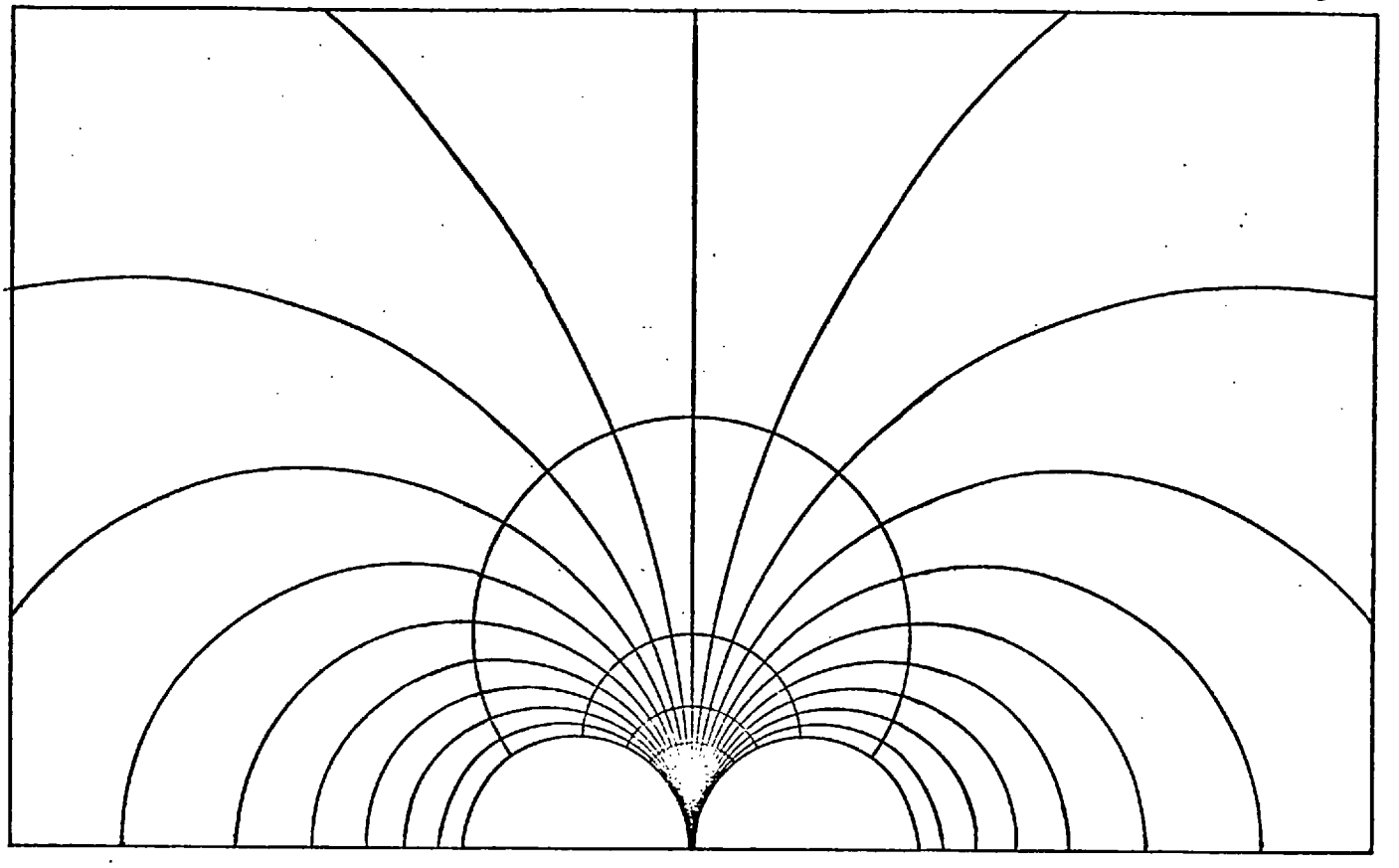

Figure(4-1-3) Distribution of grid lines for Z- and θ-directions around two spheres with Zs=0.20 ($\Delta Z=|Zs/10|, \Delta\theta=6^{o}$).

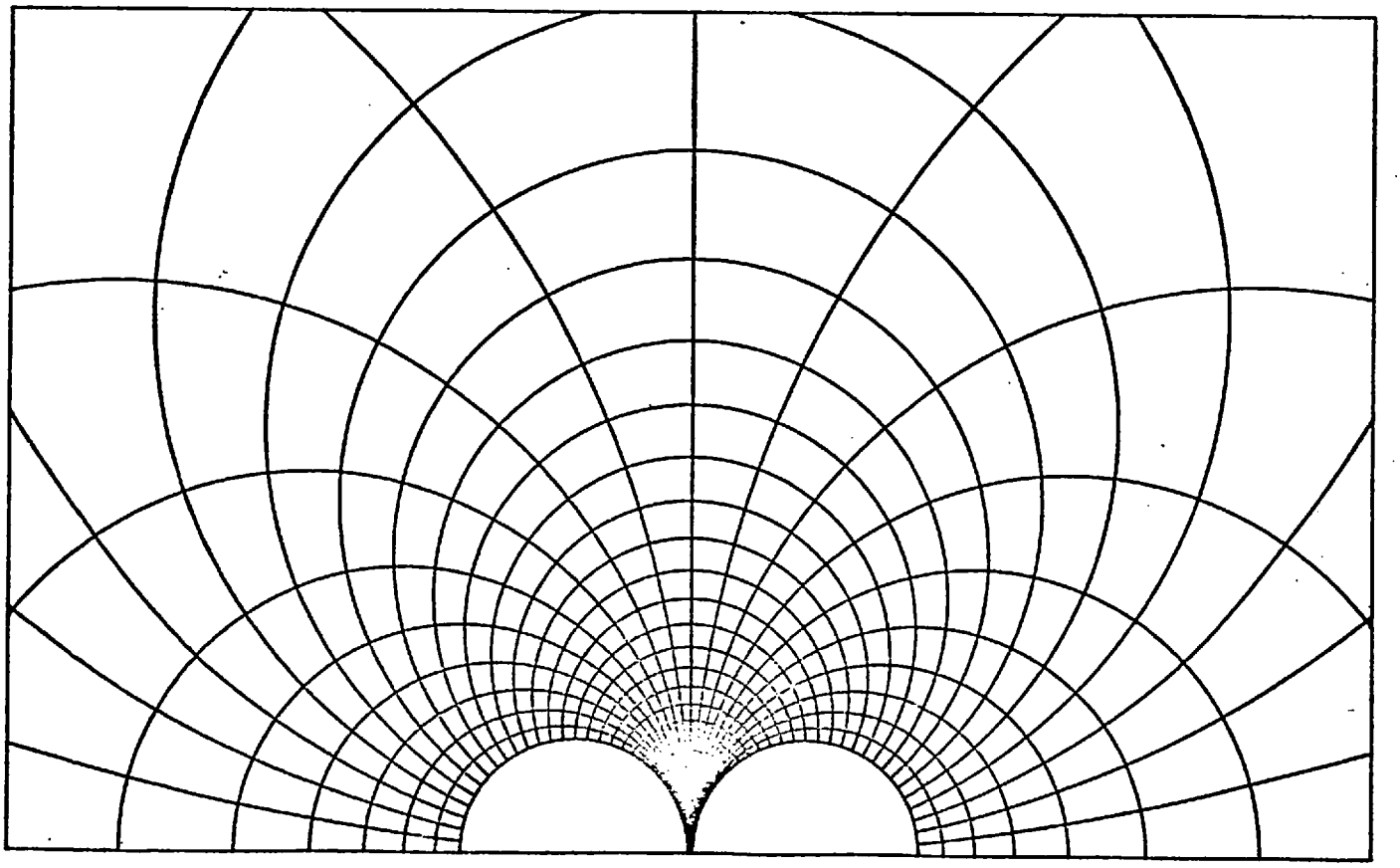

Figure(4-1-4) Distribution of grid lines for Z- and θ-directions around two spheres with Zs=0.20 ($\Delta Z=|Zs/10|, \Delta\eta=6^{o}$).

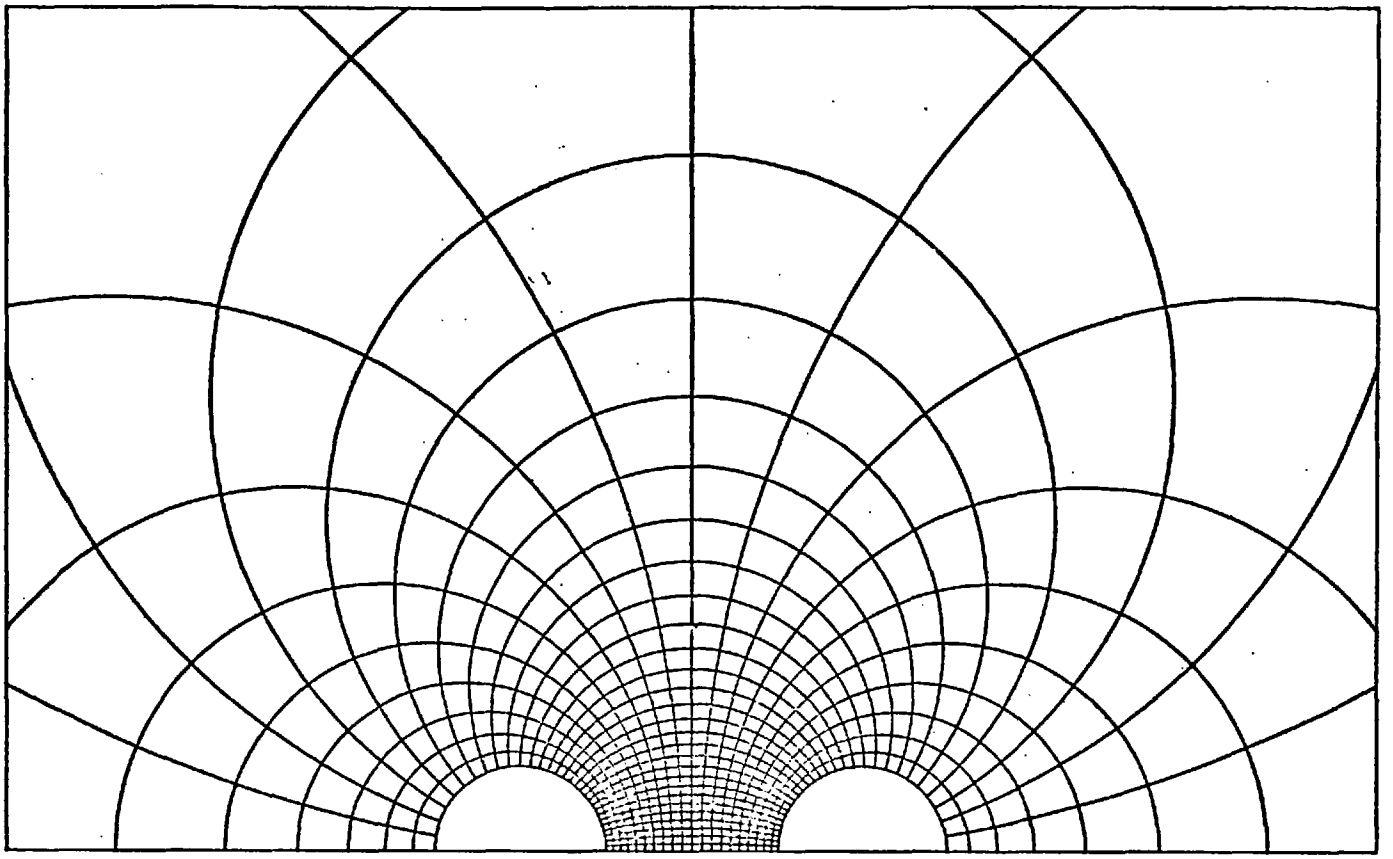

Figure(4-1-5) Distribution of grid lines for Z- and θ-directions around two spheres with Zs=1.32 ($\Delta Z=|Zs/10|, \Delta\theta=6^{\circ}$).

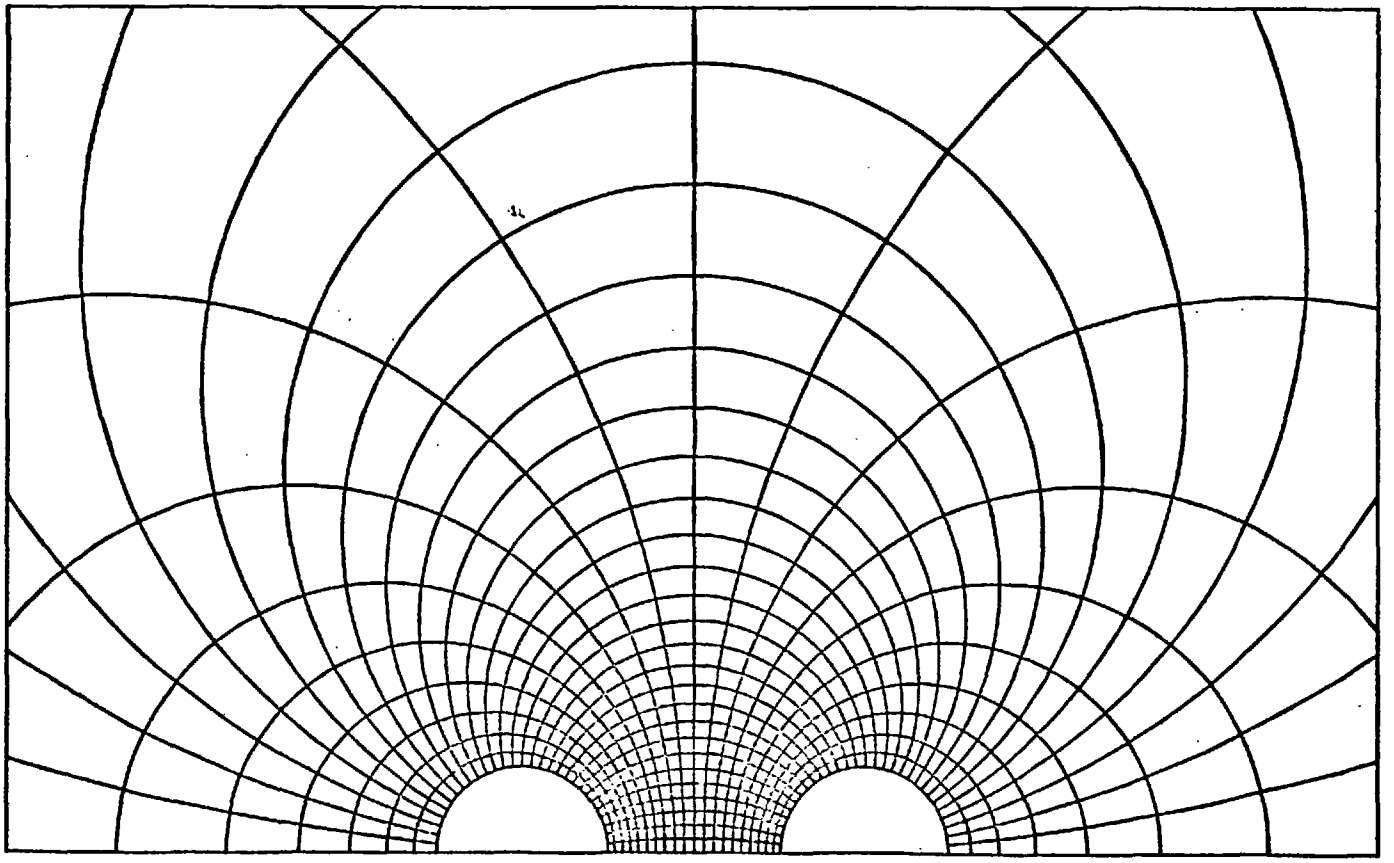

Figure(4-1-6) Distribution of grid lines for Z- and θ-directions around two spheres with Zs=1.32 ($\Delta Z=|Zs/10|, \Delta\eta=6^{\circ}$).

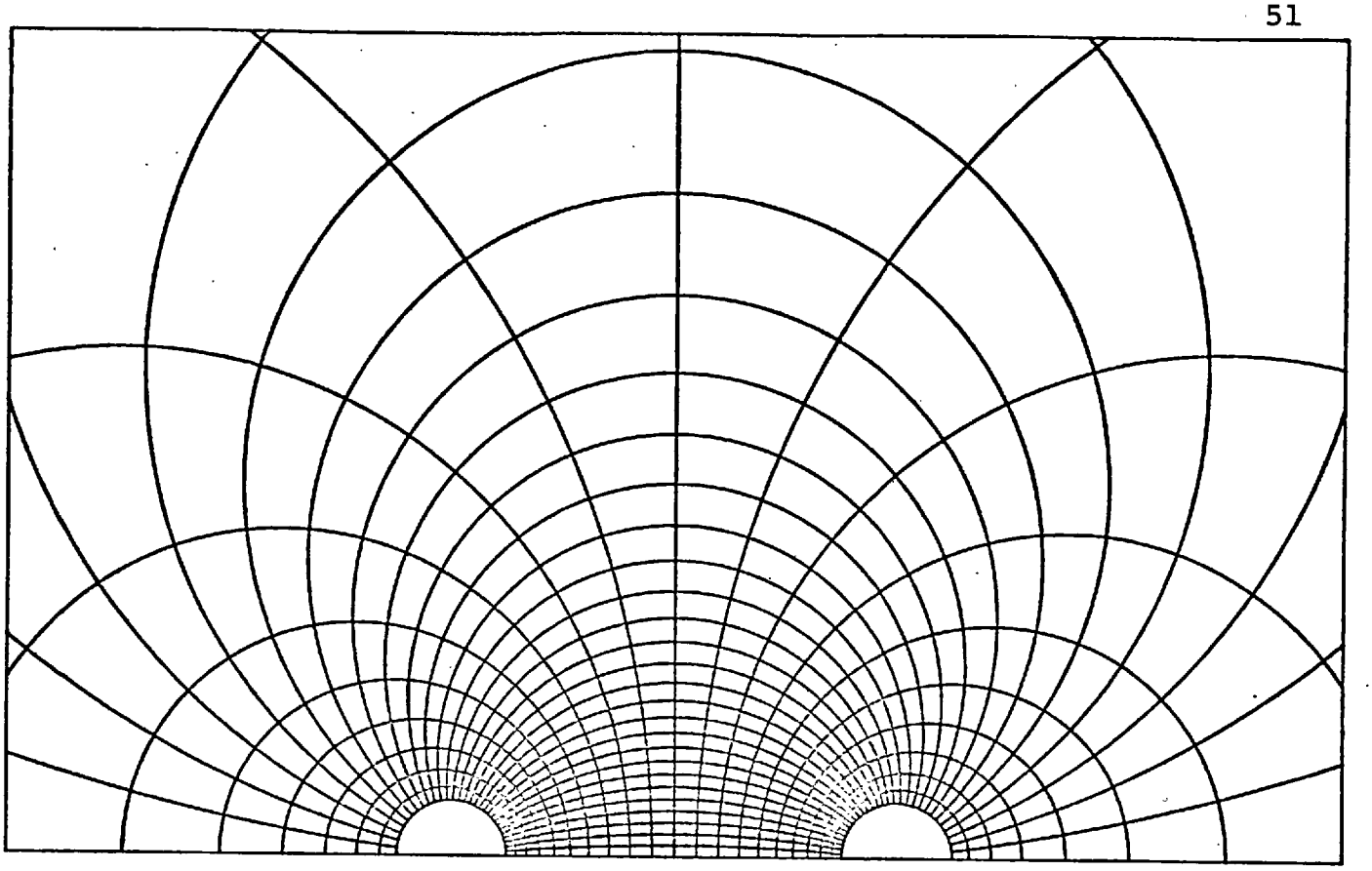

Figure(4-1-7) Distribution of grid lines for Z- and θ-directions around two spheres with Zs=2.07 ($\Delta Z=|Zs/10|, \Delta\theta=6^{o}$).

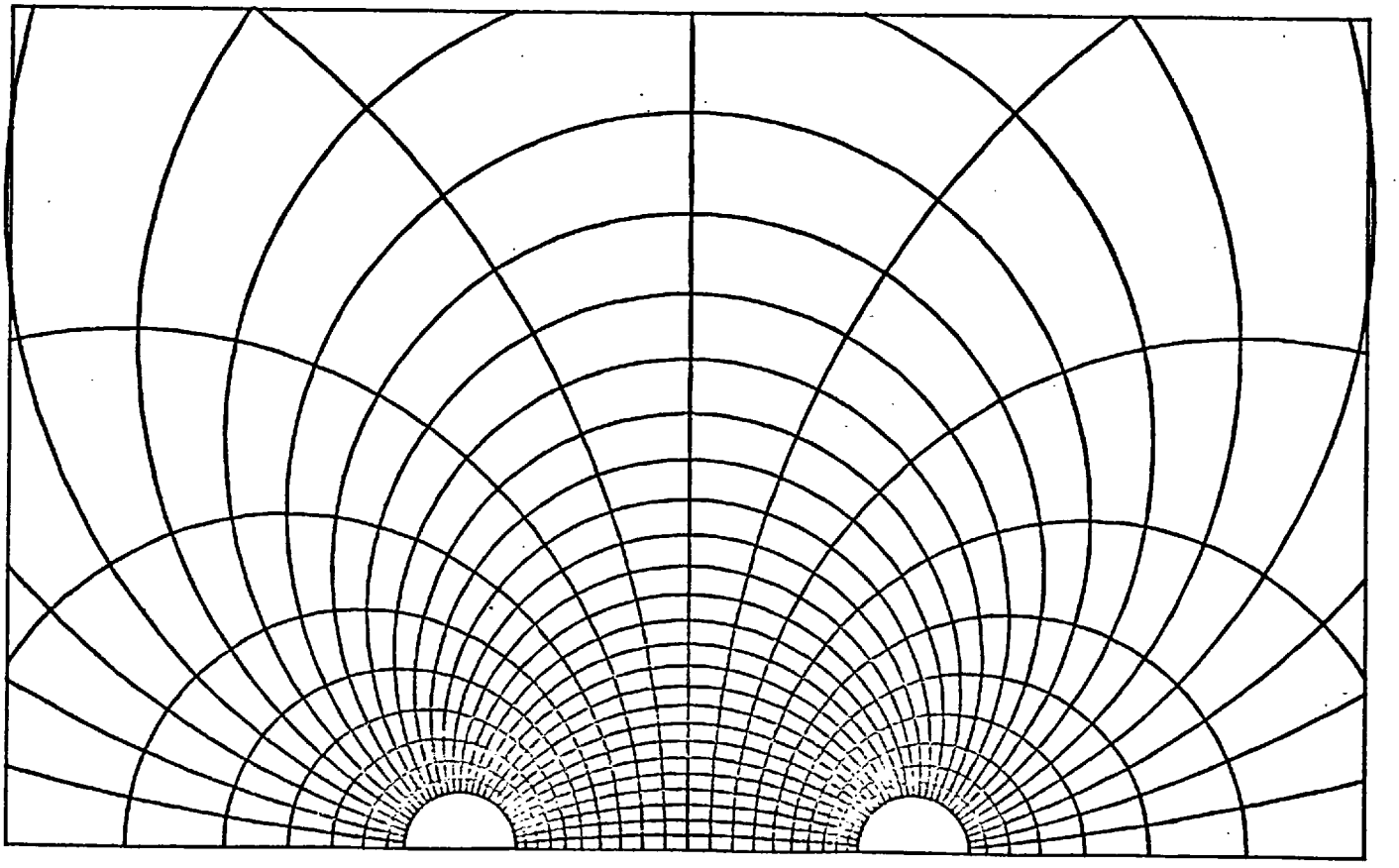

Figure(4-1-8) Distribution of grid lines for Z- and θ-directions around two spheres with Zs=2.07 ($\Delta Z=|Zs/10|, \Delta\eta=6^{o}$).

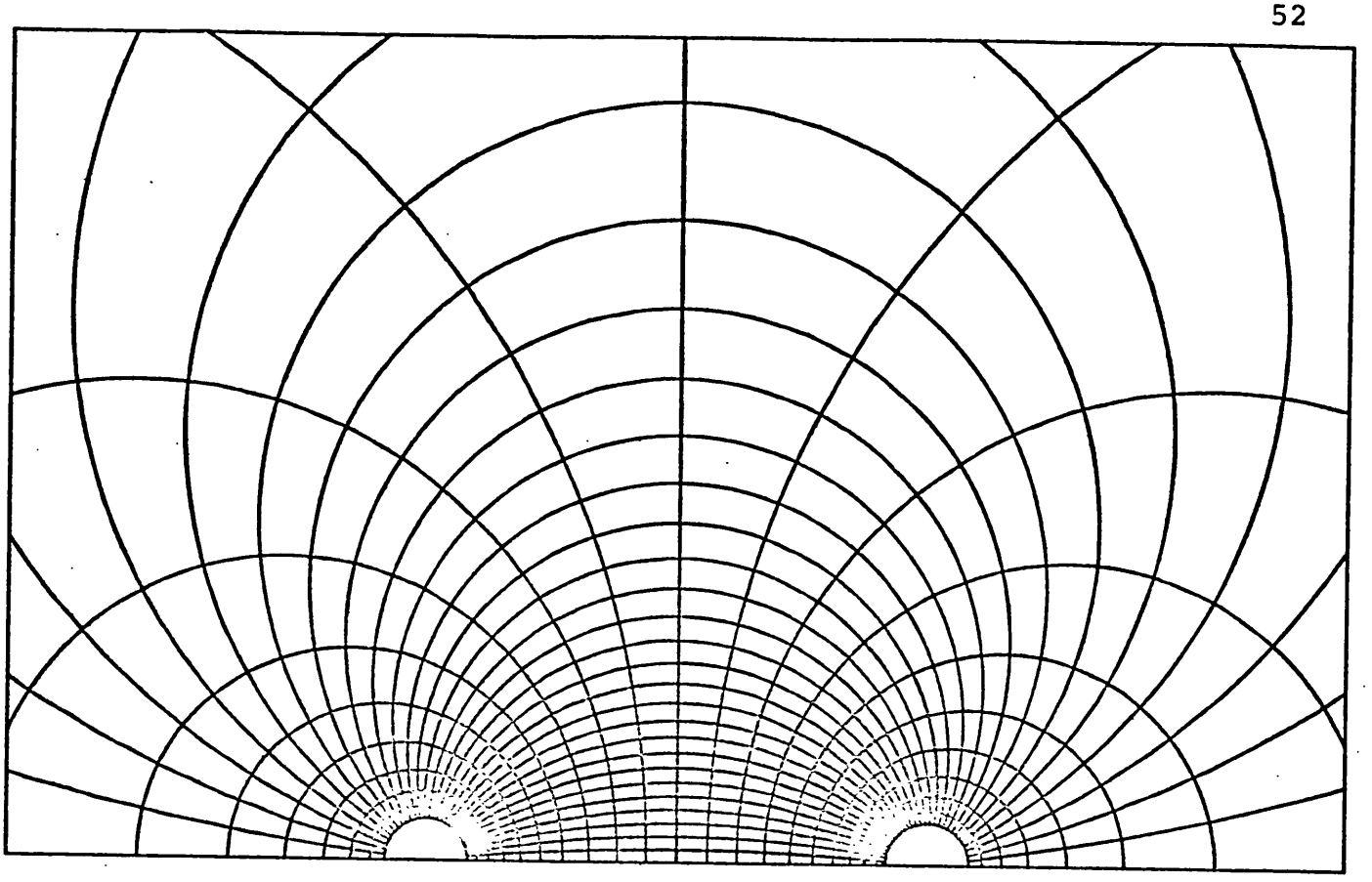

Figure(4-1-9) Distribution of grid lines for Z- and θ-directions around two spheres with Zs=2.48 ($\Delta Z=|Zs/10|, \Delta\theta=6^{o}$).

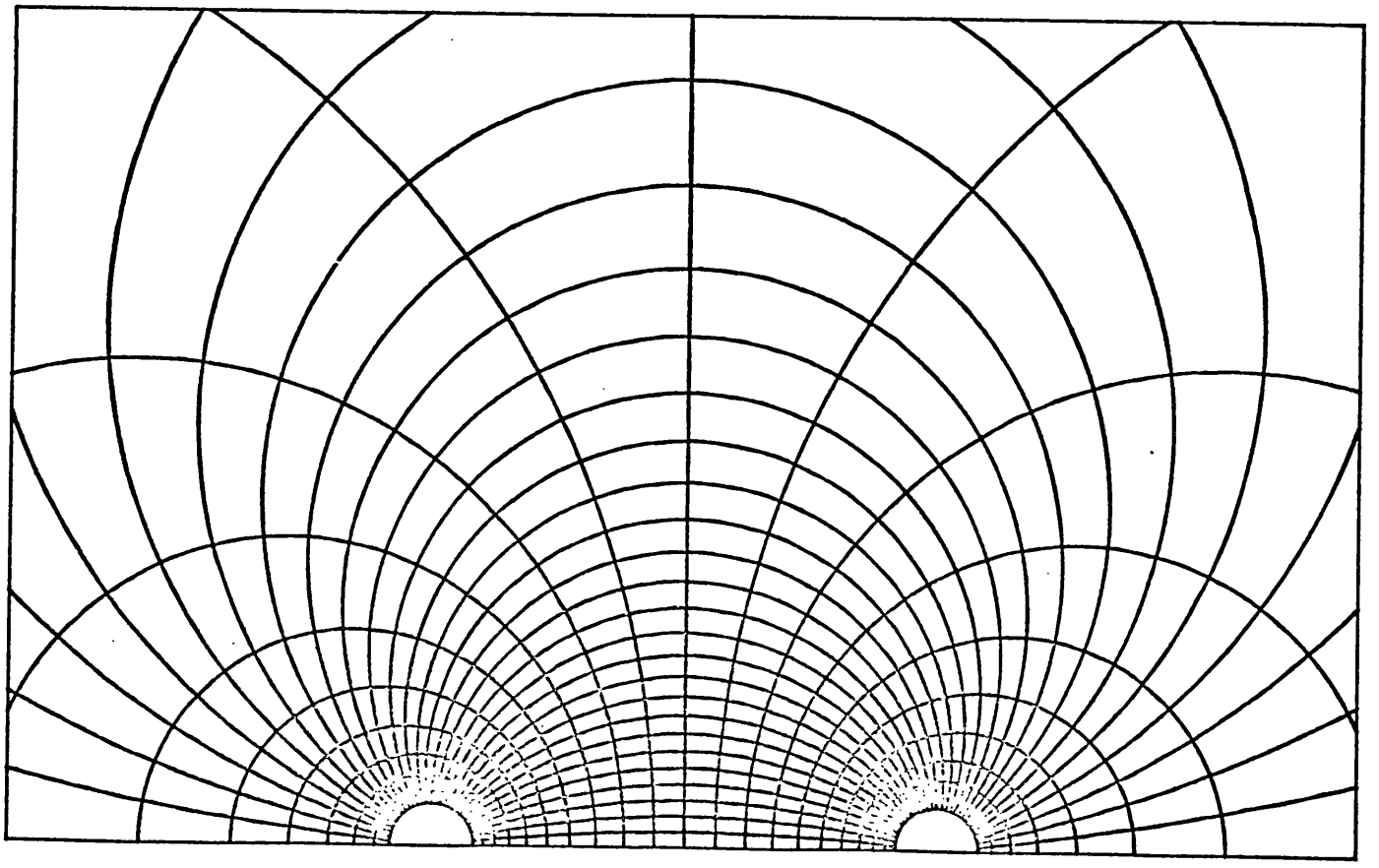

Figure(4-1-10) Distribution of grid lines for Z- and θ-directions around two spheres with Zs=2.48 ($\Delta Z=|Zs/10|, \Delta\eta=6^{o}$).

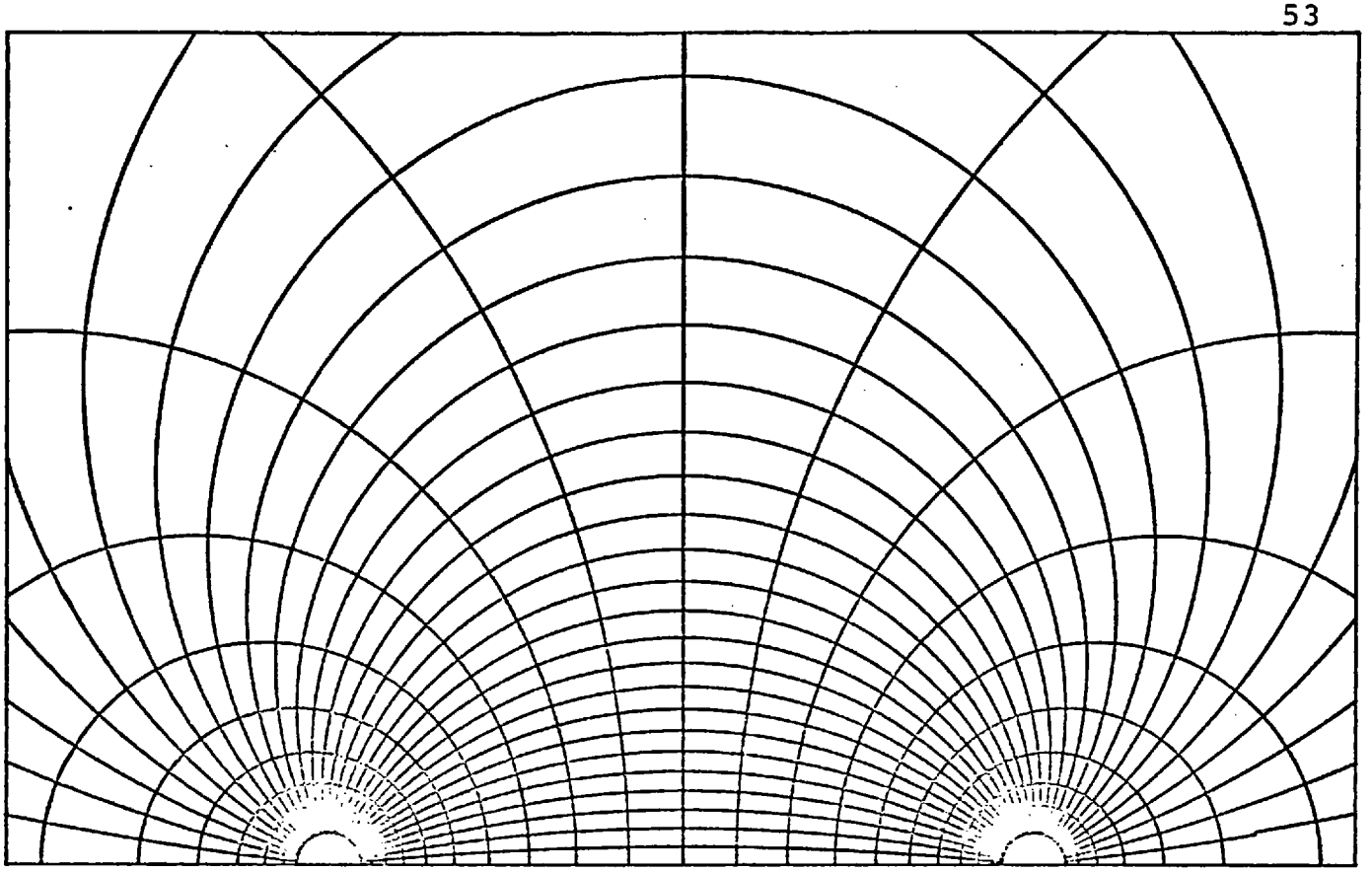

Figure(4-1-11) Distribution of grid lines for Z- and θ-directions around two spheres with Zs=3.09 ($\Delta Z=|Zs/10|, \Delta\theta=6^{o}$).

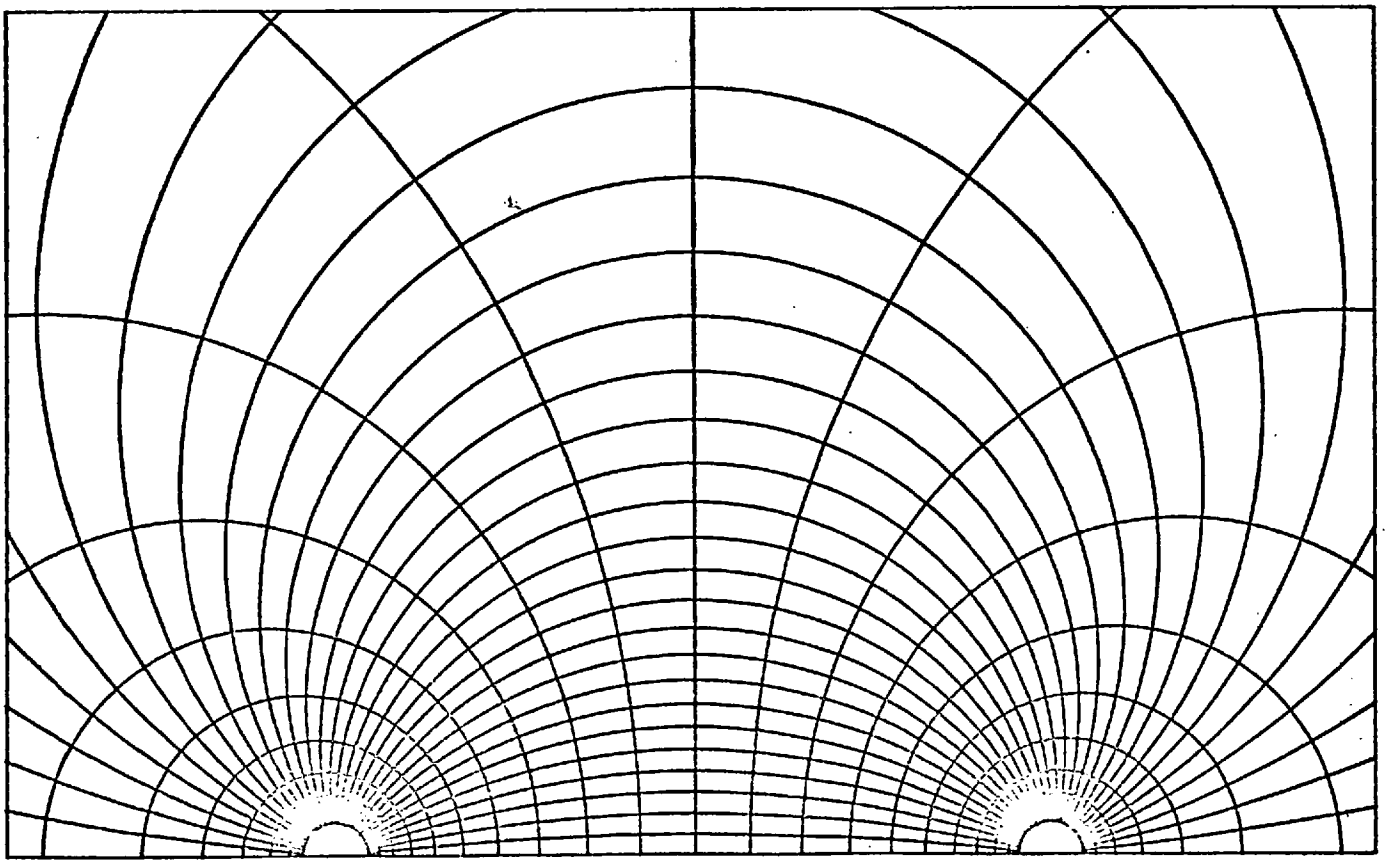

Figure(4-1-12) Distribution of grid lines for Z- and θ-directions around two spheres with Zs=3.09 ($\Delta Z=|Zs/10|, \Delta\eta=6^{o}$).

the numerical results for the two spheres in the same way as those for a single sphere, the adoption of the new scheme in the present study has the advantage of distributing the grid lines for the θ-direction more evenly in the flow region. Unfortunately, this scheme also introduces unequal increments in the values of θ which complicates the finite-difference approximations of the system of equations(4-1-1) to (4-1-3).

In Figure(4-1-2), the transformed flow region for the present two-sphere problem is shown to be bounded by four straight lines: $Z = -Zs$, $Z = +Zs$, $\theta = 0$, and $\theta = \pi$,as well as by the broken line representing the outer boundary. The rectangular mesh of the flow region corresponds to the scheme of distributing the grid lines for the Z-direction according to a constant increment in the values of $\bar{Z}$ and of distributing the grid lines for the θ-direction according to a constant increment in the values of η. For each sphere spacing, a mesh spacing of 6^{o} measured in terms of the angle η is used for the θ-direction. Because of the unequal distribution of grid lines for the Z-direction around the spheres and because of the large distances between any two neighbouring grid lines in the region upstream of sphere A, two different mesh spacings corresponding to increments of $|Zs/10|$ and $|Zs/20|$ in Z are used. Hence, for each sphere spacing, the number of mesh points in the flow region is 21x31 when an increment in Z of $|Zs/10|$ is used and 41x31 when an increment in Z of $|Zs/20|$ is used. For each sphere spacing, the system of equations is solved for the stream function, vorticity, and concentration distributions using these two different distributions of grid lines in the flow region.

The grid lines for the Z-direction are indicated by the

index i, which varies from 1 at the surface of sphere A to n at the surface of sphere B. On the other hand, the grid lines for the θ-direction are indicated by the index j, which varies from 1 at θ = 0(and η = 0) to m at θ = π(and η = π). These indicies are shown in Figure(4-1-2).

4-2. System of equations in finite-difference form.

To obtain numerical solutions of the system of equations (4-1-1) to (4-1-3), it is necessary to replace the second order partial differential equations by their finite-difference approximations. For each sphere spacing, the mesh spacing in the flow region for the Z-direction has a constant value, h, while the mesh spacings for the θ-direction are a series of unequal increments, k_1, k_2, ···, k_{j-1}, k_j, ···, k_{m-1}, which are calculated from the values of the θ-coordinate in Table(A-1) by the relations: $k_{j-1} = \theta_j - \theta_{j-1}$, $k_j = \theta_{j+1} - \theta_j$, where j = 2, 3, ··· , m-1.

A five-point star computational molecule, as shown in Figure(4-2-1), is adopted for the numerical solutions. By using

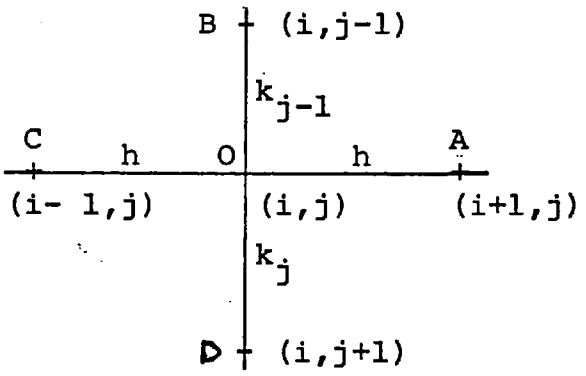

Figure(4-2-1) Five-point star computational molecule

Taylor's series expansions correct to second order derivatives, the values of any function at the four neighbouring points, (i+1,j; i-1,j; i,j+1; i,j-1), can be expressed in terms of its value at the central node, (i,j), as follows:

$$X_{i+1,j} = X_{i,j} + h\cdot\frac{\partial X_{i,j}}{\partial Z} + \frac{h^2}{2}\cdot\frac{\partial^2 X_{i,j}}{\partial Z^2} + \cdots \qquad (4\text{-}2\text{-}1)$$

$$X_{i-1,j} = X_{i,j} - h\cdot\frac{\partial X_{i,j}}{\partial Z} + \frac{h^2}{2}\cdot\frac{\partial^2 X_{i,j}}{\partial Z^2} - \cdots \qquad (4\text{-}2\text{-}2)$$

$$X_{i,j+1} = X_{i,j} + k_j \cdot \frac{\partial X_{i,j}}{\partial \theta} + \frac{k_j^2}{2} \cdot \frac{\partial^2 X_{i,j}}{\partial \theta^2} + \cdots \qquad (4\text{-}2\text{-}3)$$

$$X_{i,j-1} = X_{i,j} - k_{j-1} \cdot \frac{\partial X_{i,j}}{\partial \theta} + \frac{k_{j-1}^2}{2} \cdot \frac{\partial^2 X_{i,j}}{\partial \theta^2} - \cdots \qquad (4\text{-}2\text{-}4)$$

With appropriate manupulations and eliminations, the first and second order partial derivatives with respect to both Z and θ at the central node point (i.j), can be approximated in terms of the values at the points (i+1,j; i-1,j: i,j+1; i,j-1) of the computational molecule as shown in Figure(4-2-1).

$$\frac{\partial X_{i,j}}{\partial Z} = \frac{X_{i+1,j} - X_{i-1,j}}{2h} \qquad (4\text{-}2\text{-}5)$$

$$\frac{\partial^2 X_{i,j}}{\partial Z^2} = \frac{X_{i+1,j} - 2X_{i,j} + X_{i-1,j}}{h^2} \qquad (4\text{-}2\text{-}6)$$

$$\frac{\partial X_{i,j}}{\partial \theta} = \frac{(1-A)X_{i,j+1} - (1+B)X_{i,j-1} - \{(1-A)-(1+B)\}X_{i,j}}{(k_j + k_{j-1})} \qquad (4\text{-}2\text{-}7)$$

$$\frac{\partial^2 X_{i,j}}{\partial \theta^2} = \frac{(1-C)X_{i,j+1} - 2X_{i,j} + (1+C)X_{i,j-1}}{(k_j \cdot k_{j-1})} \qquad (4\text{-}2\text{-}8)$$

where,

$$A = \frac{k_j - k_{j-1}}{k_j}, \quad B = \frac{k_j - k_{j-1}}{k_{j-1}}, \quad C = \frac{k_j - k_{j-1}}{k_j + k_{j-1}} \qquad (4\text{-}2\text{-}9)$$

If the increments in the θ-direction are constant, i.e., $k_j = k_{j-1} = k$, then A = 0, B = 0, and C = 0, and equations(4-2-7) and (4-2-8) reduce to:

$$\frac{\partial X_{i,j}}{\partial \theta} = \frac{X_{i,j+1} - X_{i,j-1}}{k} \qquad (4\text{-}2\text{-}10)$$

$$\frac{\partial^2 X_{i,j}}{\partial \theta^2} = \frac{X_{i,j+1} - 2X_{i,j} + X_{i,j-1}}{k^2} \qquad (4\text{-}2\text{-}11)$$

Equations(4-2-10) and (4-2-11) are then similar to equations(4-2-5) and (4-2-6).

By substitution of equations(4-2-5) to (4-2-8) into equations(4-1-1) to (4-1-3), the finite-difference approximations of the Navier-Stokes and diffusion equations are formulated as follows:

The stream function equation in finite-difference form:

$$\left[\frac{1}{h^2} + \frac{1}{2h}\left(\frac{\mathrm{Sinh}Z_i}{\mathrm{Cosh}Z_i - \mathrm{Cos}\theta_j}\right)\right]\psi^*_{i+1,j} + \left[\frac{1}{h^2} - \frac{1}{2h}\left(\frac{\mathrm{Sinh}Z_i}{\mathrm{Cosh}Z_i - \mathrm{Cos}\theta_j}\right)\right]\psi^*_{i-1,j}$$

$$+ \left[\frac{(1-C)}{k_j k_{j-1}} - \frac{(1-A)}{k_j + k_{j-1}} \cdot \frac{\mathrm{Cosh}Z_i \cdot \mathrm{Cos}\theta_j - 1}{\mathrm{Sin}\theta_j(\mathrm{Cosh}Z_i - \mathrm{Cos}\theta_j)}\right]\psi^*_{i,j+1}$$

$$+ \left[\frac{(1+C)}{k_j k_{j-1}} + \frac{(1+B)}{k_j + k_{j-1}} \cdot \frac{\mathrm{Cosh}Z_i \cdot \mathrm{Cos}\theta_j - 1}{\mathrm{Sin}\theta_j(\mathrm{Cosh}Z_i - \mathrm{Cos}\theta_j)}\right]\psi^*_{i,j-1}$$

$$- \left[\frac{2}{h^2} + \frac{2}{k_j k_{j-1}} - \frac{(1-A)-(1+B)}{k_j + k_{j-1}} \cdot \frac{\mathrm{Cosh}Z_i \cdot \mathrm{Cos}\theta_j - 1}{\mathrm{Sin}\theta_j(\mathrm{Cosh}Z_i - \mathrm{Cos}\theta_j)}\right]\psi^*_{i,j}$$

$$= \left(\frac{a^*}{\mathrm{Cosh}Z_i - \mathrm{Cos}\theta_j}\right)^2 g_{i,j} \qquad (4\text{-}2\text{-}12)$$

Equation(4-2-12) can also be written in the following way:

$$\psi^*_{i,j} = B_1(i,j)\psi^*_{i+1,j} + B_2(i,j)\psi^*_{i-1,j} + B_3(i,j)\psi^*_{i,j+1}$$
$$+ B_4(i,j)\psi^*_{i,j-1} + D'_{i,j} \qquad (4\text{-}2\text{-}13)$$

where,

$$B_1(i,j) = \left[\frac{1}{h^2} + \frac{1}{2h}\left(\frac{\mathrm{Sinh}Z_i}{\mathrm{Cosh}Z_i - \mathrm{Cos}\theta_j}\right)\right] / BB(i,j)$$

$$B_2(i,j) = \left[\frac{1}{h^2} - \frac{1}{2h}\left(\frac{\mathrm{Sinh}Z_i}{\mathrm{Cosh}Z_i - \mathrm{Cos}\theta_j}\right)\right] / BB(i,j)$$

$$B_3(i,j) = \left[\frac{(1-C)}{k_j k_{j-1}} - \frac{(1-A)}{k_j + k_{j-1}} \cdot \frac{\mathrm{Cosh}Z_i \cdot \mathrm{Cos}\theta_j - 1}{\mathrm{Sin}\theta_j (\mathrm{Cosh}Z_i - \mathrm{Cos}\theta_j)}\right] / BB(i,j)$$

$$B_4(i,j) = \left[\frac{(1+C)}{k_j k_{j-1}} + \frac{(1+B)}{k_j + k_{j-1}} \cdot \frac{\mathrm{Cosh}Z_i \cdot \mathrm{Cos}\theta_j - 1}{\mathrm{Sin}\theta_j (\mathrm{Cosh}Z_i - \mathrm{Cos}\theta_j)}\right] / BB(i,j)$$

$$D'_{i,j} = -\left(\frac{a^*}{\mathrm{Cosh}Z_i - \mathrm{Cos}\theta_j}\right)^2 g_{i,j} / BB(i,j)$$

$$BB(i,j) = \left[\frac{2}{h^2} + \frac{2}{k_j k_{j-1}} - \frac{(1-A)-(1+B)}{k_j + k_{j-1}} \cdot \frac{\mathrm{Cosh}Z_i \cdot \mathrm{Cos}\theta_j - 1}{\mathrm{Sin}\theta_j (\mathrm{cosh}Z_i - \mathrm{Cos}\theta_j)}\right]$$

The vorticity transport equation in finite-difference form:

$$\left[\frac{1}{h^2} + \frac{1}{2h}\left(\frac{\mathrm{Sinh}Z_i}{\mathrm{Cosh}Z_i - \mathrm{Cos}\theta_j}\right)\right] g_{i+1,j} + \left[\frac{1}{h^2} - \frac{1}{2h}\left(\frac{\mathrm{Sinh}Z_i}{\mathrm{Cosh}Z_i - \mathrm{Cos}\theta_j}\right)\right] g_{i-1,j}$$

$$+ \left[\frac{(1-C)}{k_j k_{j-1}} - \frac{(1-A)}{k_j + k_{j-1}} \cdot \frac{\mathrm{Cosh}Z_i \cdot \mathrm{Cos}\theta_j - 1}{\mathrm{Sin}\theta_j (\mathrm{Cosh}Z_i - \mathrm{Cos}\theta_j)}\right] g_{i,j+1}$$

$$+ \left[\frac{(1+C)}{k_j k_{j-1}} + \frac{(1+B)}{k_j + k_{j-1}} \cdot \frac{\mathrm{Cosh}Z_i \cdot \mathrm{Cos}\theta_j - 1}{\mathrm{Sin}\theta_j (\mathrm{Cosh}Z_i - \mathrm{Cos}\theta_j)}\right] g_{i,j-1}$$

$$- \left[\frac{2}{h^2} + \frac{2}{k_j k_{j-1}} - \frac{(1-A)-(1+B)}{k_j + k_{j-1}} \cdot \frac{\mathrm{Cosh}Z_i \cdot \mathrm{Cos}\theta_j - 1}{\mathrm{Sin}\theta_j (\mathrm{Cosh}Z_i - \mathrm{Cos}\theta_j)}\right] g_{i,j}$$

$$= \frac{Re \cdot \mathrm{Sin}\theta_j}{4h(k_j + k_{j-1})}\left(\frac{a^*}{\mathrm{Cosh}Z_i - \mathrm{Cos}\theta_j}\right)^3 \left[(\psi^*_{i+1,j} - \psi^*_{i-1,j})\{f_{i,j+1}(1-A)\right.$$

$$- f_{i,j-1}(1+B) - f_{i,j}[(1-A)-(1+B)]\} - \{\psi^*_{i,j+1}(1-A)-\psi^*_{i,j-1}(1+B)$$

$$- \psi^*_{i,j}[(1-A)-(1+B)]\}(f_{i+1,j}-f_{i-1,j})\Big] \qquad (4\text{-}2\text{-}14)$$

Equation(4-2-14) can also be arranged in the following way:

$$g_{i,j} = B_1(i,j)g_{i+1,j} + B_2(i,j)g_{i-1,j} + B_3(i,j)g_{i,j+1}$$

$$+ B_4(i,j)g_{i,j-1} + D''_{i,j} \qquad (4\text{-}2\text{-}15)$$

where $B_1(i,j)$, $B_2(i,j)$, $B_3(i,j)$, and $B_4(i,j)$, are exactly the same as in equation(4-2-13). The non-linear term, $D''_{i,j}$, is different from that in equation(4-2-13) and is as follows:

$$D''_{i,j} = \frac{-Re\cdot Sin\theta_j}{4h(k_j+k_{j-1})}\left(\frac{a^*}{Cosh Z_i - Cos\theta_j}\right)^3\Big[(\psi^*_{i+1,j}-\psi^*_{i-1,j})\{$$

$$f_{i,j+1}(1-A)-f_{i,j-1}(1+B)-f_{i,j}[(1-A)(1+B)]\} - \{$$

$$\psi^*_{i,j+1}(1-A)-\psi^*_{i,j}(1+B)-\psi^*_{i,j}[(1-A)-(1+B)]\}(f_{i+1,j}-$$

$$f_{i-1,j})\Big] \;/\; BB(i,j)$$

The diffusion equation in finite-difference form:

$$\left[\frac{1}{h^2} - \frac{1}{2h}\left(\frac{Sinh Z_i}{Cosh Z_i - Cos\theta_j}\right) + \frac{Pe}{4h(k_j+k_{j-1})}\left(\frac{Cosh Z_i - Cos\theta_j}{a^* Sin\theta_j}\right)\{\psi^*_{i,j+1}(1-A)\right.$$

$$\left.-\psi^*_{i,j-1}(1+B)-\psi^*_{i,j}[(1-A)-(1+B)]\}\right] C^*_{i+1,j}$$

$$+\left[\frac{1}{h^2}+\frac{1}{2h}\left(\frac{\mathrm{Sinh}Z_i}{\mathrm{Cosh}Z_i-\mathrm{Cos}\theta_j}\right)-\frac{Pe}{4h(k_j+k_{j-1})}\left(\frac{\mathrm{Cosh}Z_i-\mathrm{Cos}\theta_j}{a^*\mathrm{Sin}\theta_j}\right)\{\psi^*_{i,j+1}(1-A)\right.$$

$$\left.-\psi^*_{i,j-1}(1+B)-\psi^*_{i,j}[(1-A)-(1+B)]\}\right]C^*_{i-1,j}$$

$$+\left[\frac{(1-C)}{k_jk_{j-1}}+\frac{(1-A)}{k_j+k_{j-1}}\cdot\frac{\mathrm{Cosh}Z_i\cdot\mathrm{Cos}\theta_j-1}{\mathrm{Sin}\theta_j(\mathrm{Cosh}Z_i-\mathrm{Cos}\theta_j)}\right.$$

$$\left.-\frac{Pe(1-A)}{4h(k_j+k_{j-1})}\left(\frac{\mathrm{Cosh}Z_i-\mathrm{Cos}\theta_j}{a^*\mathrm{Sin}\theta_j}\right)(\psi^*_{i+1,j}-\psi^*_{i-1,j})\right]C^*_{i,j+1}$$

$$+\left[\frac{(1+C)}{k_jk_{j-1}}+\frac{(1+B)}{k_j+k_{j-1}}\cdot\frac{\mathrm{Cosh}Z_i\cdot\mathrm{Cos}\theta_j-1}{\mathrm{Sin}\theta_j(\mathrm{Cosh}Z_i-\mathrm{Cos}\theta_j)}\right.$$

$$\left.+\frac{Pe(1+B)}{4h(k_j+k_{j-1})}\left(\frac{\mathrm{Cosh}Z_i-\mathrm{Cos}\theta_j}{a^*\mathrm{Sin}\theta_j}\right)(\psi^*_{i+1,j}-\psi^*_{i-1,j})\right]C^*_{i,j-1}$$

$$=\left[\frac{2}{h^2}+\frac{2}{k_jk_{j-1}}+\frac{(1-A)-(1+B)}{k_j+k_{j-1}}\cdot\frac{\mathrm{Cosh}Z_i\cdot\mathrm{Cos}\theta_j-1}{\mathrm{Sin}\theta_j(\mathrm{Cosh}Z_i-\mathrm{Cos}\theta_j)}\right.$$

$$\left.-\frac{Pe[(1-A)-(1+B)]}{4h(k_j+k_{j-1})}\left(\frac{\mathrm{Cosh}Z_i-\mathrm{Cos}\theta_j}{a^*\mathrm{Sin}\theta_j}\right)(\psi^*_{i+1,j}-\psi^*_{i-1,j})\right]C^*_{i,j}$$

(4-2-16)

Equation(4-2-16) can also be arranged in a different form by separating those terms on the left-hand side of the equation which contain the stream function, and grouping them into a separate term as follows:

$$\left[\frac{1}{h^2}-\frac{1}{2h}\left(\frac{\mathrm{Sinh}Z_i}{\mathrm{Cosh}Z_i-\mathrm{Cos}\theta_j}\right)\right]C^*_{i+1,j}+\left[\frac{1}{h^2}+\frac{1}{2h}\left(\frac{\mathrm{Sinh}Z_i}{\mathrm{Cosh}Z_i-\mathrm{Cos}\theta_j}\right)\right]C^*_{i-1,j}$$

$$+\left[\frac{(1-C)}{k_jk_{j-1}}+\frac{(1-A)}{k_j+k_{j-1}}\cdot\frac{\mathrm{Cosh}Z_i\cdot\mathrm{Cos}\theta_j-1}{\mathrm{Sin}\theta_j(\mathrm{Cosh}Z_i-\mathrm{Cos}\theta_j)}\right]C^*_{i,j+1}$$

$$+\left[\frac{(1+C)}{k_j k_{j-1}} - \frac{(1+B)}{k_j+k_{j-1}}\cdot\frac{\mathrm{Cosh}Z_i\cdot\mathrm{Cos}\theta_j-1}{\mathrm{Sin}\theta_j(\mathrm{Cosh}Z_i-\mathrm{Cos}\theta_j)}\right] C^*_{i,j-1}$$

$$+\frac{Pe}{4h(k_j+k_{j-1})}\left(\frac{\mathrm{Cosh}Z_i-\mathrm{Cos}\theta_j}{a^*\mathrm{Sin}\theta_j}\right)\left[\{\psi^*_{i,j+1}(1-A)-\psi^*_{i,j-1}(1+B)-\psi^*_{i,j}[(1-A)\right.$$

$$-(1+B)]\}(C^*_{i+1,j}-C^*_{i-1,j}) - (\psi^*_{i+1,j}-\psi^*_{i-1,j})\{(1-A)C^*_{i,j+1}-$$

$$\left.(1+B)C^*_{i,j-1}\}\right]$$

$$=\left[\frac{2}{h^2}+\frac{2}{k_j k_{j-1}}+\frac{(1-A)-(1+B)}{k_j+k_{j-1}}\cdot\frac{\mathrm{Cosh}Z_i\cdot\mathrm{Cos}\theta_j-1}{\mathrm{Sin}\theta_j(\mathrm{Cosh}Z_i-\mathrm{Cos}\theta_j)}\right.$$

$$\left.-\frac{Pe[(1-A)-(1+B)]}{4h(k_j+k_{j-1})}\left(\frac{\mathrm{Cosh}Z_i-\mathrm{Cos}\theta_j}{a^*\mathrm{Sin}\theta_j}\right)(\psi^*_{i+1,j}-\psi^*_{i-1,j})\right] C^*_{i,j} \qquad (4\text{-}2\text{-}17)$$

Equation(4-2-17) can further be arranged into the following form:

$$C^*_{i,j} = A_1(i,j)C^*_{i+1,j} + A_2(i,j)C^*_{i-1,j} + A_3(i,j)C^*_{i,j+1}$$

$$+ A_4(i,j)C^*_{i,j-1} + D'''_{i,j} \qquad (4\text{-}2\text{-}18)$$

where,

$$A_1(i,j) = \left[\frac{1}{h^2} - \frac{1}{2h}\left(\frac{\mathrm{Sinh}Z_i}{\mathrm{Cosh}Z_i-\mathrm{Cos}\theta_j}\right)\right] / AA(i,j)$$

$$A_2(i,j) = \left[\frac{1}{h^2} + \frac{1}{2h}\left(\frac{\mathrm{Sinh}Z_i}{\mathrm{Cosh}Z_i-\mathrm{Cos}\theta_j}\right)\right] / AA(i,j)$$

$$A_3(i,j) = \left[\frac{(1-C)}{k_j k_{j-1}} + \frac{(1-A)}{k_j+k_{j-1}}\cdot\frac{\mathrm{Cosh}Z_i\cdot\mathrm{Cos}\theta_j-1}{\mathrm{Sin}\theta_j(\mathrm{Cosh}Z_i-\mathrm{Cos}\theta_j)}\right] / AA(i,j)$$

$$A_4(i,j) = \left[\frac{(1+C)}{k_j k_{j-1}} - \frac{(1+B)}{k_j+k_{j-1}} \cdot \frac{\mathrm{Cosh}Z_i \cdot \mathrm{Cos}\theta_j - 1}{\mathrm{Sin}\theta_j (\mathrm{Cosh}Z_i - \mathrm{Cos}\theta_j)}\right] / AA(i,j)$$

$$AA(i,j) = \left[\frac{2}{h^2} + \frac{2}{k_j k_{j-1}} + \frac{(1-A)-(1+B)}{k_j+k_{j-1}} \cdot \frac{\mathrm{Cosh}Z_i \cdot \mathrm{Cos}\theta_j - 1}{\mathrm{Sin}\theta_j (\mathrm{Cosh}Z_i - \mathrm{Cos}\theta_j)}\right.$$

$$\left. - \frac{Pe\left[(1-A)-(1+B)\right]}{4h(k_j+k_{j-1})} \left(\frac{\mathrm{Cosh}Z_i - \mathrm{Cos}\theta_j}{a^* \mathrm{Sin}\theta_j}\right) (\psi^*_{i+1,j} - \psi^*_{i-1,j})\right]$$

$$D'''_{i,j} = \frac{Pe}{4h(k_j+k_{j-1})} \left(\frac{\mathrm{Cosh}Z_i - \mathrm{Cos}\theta_j}{a^* \mathrm{Sin}\theta_j}\right) \left[\psi^*_{i,j+1}(1-A) - \psi^*_{i,j-1}(1+B)\right.$$

$$- \psi^*_{i,j}\left[(1-A)-(1+B)\right](C^*_{i+1,j} - C^*_{i-1,j})$$

$$\left. - (\psi^*_{i+1,j} - \psi^*_{i-1,j})\{(1-A)C^*_{i,j+1} - (1+B)C^*_{i,j-1}\}\right] / AA(i,j)$$

Hence, equations (4-2-13), (4-2-15), and (4-2-18), are the system of equations in the required finite-difference form. The values of the dependent variables: stream function, ψ^*, vorticity function, g, and concentration, C^*, at any node point are related to their values at four neighbouring mesh points. By using these finite-difference equations at every internal mesh point in the flow region, a set of simultaneous algebraic equations is obtained, which can be solved by an iterative method using the boundary conditions which must also be expressed in finite-difference form.

4-3. Boundary conditions in finite-difference form.

For the present system of two equally sized spheres with fluid flowing parallel to their line of centres, there are two types of boundary conditions: the boundary conditions which do not change throughout the process of computation, and the boundary conditions which need special treatment or which may not remain the same during computation. The finite-difference approximations of the boundary conditions are as follows:

The constant boundary conditions:

(1). At the surface of sphere A($Z = -Zs$, $i = 1$).

$$\psi^*_{1,j} = 0 \quad , \quad C^*_{1,j} = 1 \tag{4-3-1}$$

(2). At the surface of sphere B($Z = +Zs$, $i = n$).

$$\psi^*_{n,j} = 0 \quad , \quad C^*_{n,j} = 1 \tag{4-3-2}$$

(3). Along the axis of symmetry $\theta = 0$($j = 1$).

$$\psi^*_{i,1} = 0 \quad , \quad \zeta^*_{i,1} = 0 \quad , \quad g_{i,1} = 0 \tag{4-3-3}$$

(4). Along the axis of symmetry $\theta = \pi$ ($j = m$).

$$\psi^*_{i,m} = 0 \quad , \quad \zeta^*_{i,m} = 0 \quad , \quad g_{i,m} = 0 \tag{4-3-4}$$

(5). Along the outer boundary (Z_o, θ_o).

$$\psi^*_{i,j} = \tfrac{1}{2}\left(\frac{a^* \mathrm{Sin}\theta_o}{\mathrm{Cosh}Z_o - \mathrm{Cos}\theta_o}\right)^2 \tag{4-3-5}$$

$$\zeta^*_{i,j} = 0 \quad , \quad g_{i,j} = 0 \quad , \quad f_{i,j} = 0 \quad , \quad C^*_{i,j} = 0 \tag{4-3-6}$$

For each sphere spacing Zs, the above boundary conditions remain the same throughout the numerical solution of the Navier-Stokes and diffusion equations, and have to be specified before the start of the solution procedure.

The specially treated boundary conditions.

(1). Vorticities and vorticity functions g and f at the surfaces of the spheres(i = 1 and i = n).

The surface vorticities expressed by equations(3-4-2a) and (3-4-2b) become:

$$\zeta^*_{1,j} = \left(\frac{\mathrm{Cosh}Z_1-\mathrm{Cos}\theta_j}{a^*\mathrm{Sin}\theta_j}\right)\left(\frac{\mathrm{Cosh}Z_1-\mathrm{Cos}\theta_j}{a^*}\right)^2 \frac{\partial^2\psi^*_{1,j}}{\partial Z^2} \qquad (4\text{-}3\text{-}7)$$

$$\zeta^*_{n,j} = \left(\frac{\mathrm{Cosh}Z_n-\mathrm{Cos}\theta_j}{a^*\mathrm{Sin}\theta_j}\right)\left(\frac{\mathrm{Cosh}Z_n-\mathrm{Cos}\theta_j}{a^*}\right)^2 \frac{\partial^2\psi^*_{n,j}}{\partial Z^2} \qquad (4\text{-}3\text{-}8)$$

and require evaluations of the second order stream function derivatives with respect to Z at the solid surfaces of the spheres. By using a Taylor's series expansion for the stream function in the vicinity of the surfaces, two cubic polynomials can be obtained for the second order derivatives as follows:

$$\frac{\partial^2\psi^*_{1,j}}{\partial Z^2} = \frac{8\psi^*_{2,j} - \psi^*_{3,j}}{2h^2} \qquad (4\text{-}3\text{-}9)$$

$$\frac{\partial^2\psi^*_{n,j}}{\partial Z^2} = \frac{8\psi^*_{n-1,j} - \psi^*_{n-2,j}}{2h^2} \qquad (4\text{-}3\text{-}10)$$

Hence, the vorticities at the solid surface of sphere A(Z = -Zs, i = 1) are as follows:

$$\zeta^*_{1,j} = \frac{1}{2h^2}\left(\frac{\mathrm{Cosh}Z_1-\mathrm{Cos}\theta_j}{a^*\mathrm{Sin}\theta_j}\right)\left(\frac{\mathrm{Cosh}Z_1-\mathrm{Cos}\theta_j}{a^*}\right)^2(8\psi^*_{2,j}-\psi^*_{3,j}) \tag{4-3-11}$$

$$g_{1,j} = \left(\frac{a^*\mathrm{Sin}\theta_j}{\mathrm{Cosh}Z_1-\mathrm{Cos}\theta_j}\right)\cdot\zeta^*_{1,j} \tag{4-3-12}$$

$$f_{1,j} = \zeta^*_{1,j} \Big/ \left(\frac{a^*\mathrm{Sin}\theta_j}{\mathrm{Cosh}Z_1-\mathrm{Cos}\theta_j}\right) \tag{4-3-13}$$

and the vorticities at the surface of sphere B ($Z = +Zs$, $i = n$) are as follows:

$$\zeta^*_{n,j} = \frac{1}{2h^2}\left(\frac{\mathrm{Cosh}Z_n-\mathrm{Cos}\theta_j}{a^*\mathrm{Sin}\theta_j}\right)\left(\frac{\mathrm{Cosh}Z_n-\mathrm{Cos}\theta_j}{a^*}\right)(8\psi^*_{n-1,j}-\psi^*_{n-2,j}) \tag{4-3-14}$$

$$g_{n,j} = \left(\frac{a^*\mathrm{Sin}\theta_j}{\mathrm{Cosh}Z_n-\mathrm{Cos}\theta_j}\right)\cdot\zeta^*_{n,j} \tag{4-3-15}$$

$$f_{n,j} = \zeta^*_{n,j} \Big/ \left(\frac{a^*\mathrm{Sin}\theta_j}{\mathrm{Cosh}Z_n-\mathrm{Cos}\theta_j}\right) \tag{4-3-16}$$

(2). Vorticity function f along the axes of symmetry, $\theta = 0$ and $\theta = \pi$ ($j = 1$ and $j = m$).

Since both ζ^* and $\mathrm{Sin}\theta$ are zero along the axes of symmetry $\theta = 0$ and $\theta = \pi$, the vorticity function $f_{i,1}$ and $f_{i,m}$ are undetermined. Hence, a special treatment is made for the functions by means of L'Hospital's rule.

For $\theta = 0$: $\mathrm{Sin}\theta = 0$, $\mathrm{Cos}\theta = 1$, and $\zeta^*_{i,1} = 0$, equation(3-3-6) becomes:

$$f_{i,1} = \lim_{\theta\to 0}\left|\zeta^*_{i,1} \Big/ \left(\frac{a^*\mathrm{Sin}\theta_1}{\mathrm{Cosh}Z_i-\mathrm{Cos}\theta_1}\right)\right| = \left(\frac{\partial\zeta^*_{i,1}}{\partial\theta}\right)\Big/\left(\frac{a^*}{\mathrm{Cosh}Z_i-1}\right)$$

$$= \left(\frac{\zeta^*_{i,2}}{k_1}\right) \Big/ \left(\frac{a^*}{\mathrm{Cosh}Z_i - 1}\right) \qquad (4\text{-}3\text{-}17)$$

For $\theta = \pi$: $\mathrm{Sin}\theta = 0$, $\mathrm{Cos}\theta = -1$, and $\zeta^*_{i,m} = 0$, equation (3-3-6) becomes:

$$f_{i,m} = \lim_{\theta \to \pi} \left| \zeta^*_{i,m} \Big/ \left(\frac{a^* \mathrm{Sin}\theta_m}{\mathrm{Cosh}Z_i - \mathrm{Cos}\theta_m}\right) \right| = -\left(\frac{\partial \zeta^*_{i,m}}{\partial \theta}\right) \Big/ \left(\frac{a^*}{\mathrm{Cosh}Z_i + 1}\right)$$

$$= \left(\frac{\zeta^*_{i,m-1}}{k_{m-1}}\right) \Big/ \left(\frac{a^*}{\mathrm{Cosh}Z_i + 1}\right) \qquad (4\text{-}3\text{-}18)$$

(3). The diffusion equation along the axis of symmetry $\theta = 0$ ($j = 1$).

The fourth term on the left-hand side and the term on the right-hand side of the diffusion equation (4-1-3) require special treatment because $\frac{\partial}{\partial \theta}(C^*_{i,1}) = 0$, $\frac{\partial}{\partial \theta}(\psi^*_{i,1}) = 0$, and $\mathrm{Sin}\theta = 0$. With the application of L'Hospital's rule, a limiting process is used as follows:

$$\lim_{\theta \to 0} \left| \frac{\mathrm{Cosh}Z_i \cdot \mathrm{Cos}\theta_1 - 1}{\mathrm{Sin}\theta_1 (\mathrm{Cosh}Z_i - \mathrm{Cos}\theta_1)} \cdot \frac{\partial C^*_{i,1}}{\partial \theta} \right| = + \frac{\partial^2 C^*_{i,1}}{\partial \theta^2} \qquad (4\text{-}3\text{-}19)$$

$$\lim_{\theta \to 0} \left| \frac{1}{\mathrm{Sin}\theta_1} \left(- \frac{\partial \psi^*_{i,1}}{\partial \theta} \cdot \frac{\partial C^*_{i,1}}{\partial Z} + \frac{\partial \psi^*_{i,1}}{\partial Z} \cdot \frac{\partial C^*_{i,1}}{\partial \theta} \right) \right|$$

$$= - \frac{\partial^2 \psi^*_{i,1}}{\partial \theta^2} \cdot \frac{\partial C^*_{i,1}}{\partial Z} \qquad (4\text{-}3\text{-}20)$$

By substitution these two expressions into equation (4-1-3), the diffusion equation along the axis of symmetry $\theta = 0$ becomes:

$$\frac{\partial^2 C^*_{i,1}}{\partial Z^2} - \left(\frac{\text{Sinh}Z_i}{\text{Cosh}Z_i - 1}\right)\frac{\partial C^*_{i,1}}{\partial Z} + 2\left(\frac{\partial^2 C^*_{i,1}}{\partial \theta^2}\right)$$

$$= -\tfrac{1}{2}\text{Re}\left(\frac{\text{Cosh}Z_i - 1}{a^*}\right)\cdot\frac{\partial^2 \psi^*_{i,1}}{\partial \theta^2}\cdot\frac{\partial C^*_{i,1}}{\partial Z} \qquad (4\text{-}3\text{-}21)$$

By the use of a Taylor's series expression, equation(4-2-3), the second order partial derivative with respect to θ, can be obtained along the axis of symmetry $\theta = 0$ as follows:

$$\frac{\partial^2 C^*_{i,1}}{\partial \theta^2} = \frac{2(C^*_{i,2} - C^*_{i,1})}{k_1^2} \qquad (4\text{-}3\text{-}22)$$

$$\frac{\partial^2 \psi^*_{i,1}}{\partial \theta^2} = \frac{2\psi^*_{i,2}}{k_1^2} \qquad (4\text{-}3\text{-}23)$$

From these two equations, the finite-difference approximation of equation(4-3-21) is formulated as follows:

$$\left[\frac{1}{h^2} - \frac{1}{2h}\left(\frac{\text{Sinh}Z_i}{\text{Cosh}Z_i - 1}\right) + \frac{Pe}{2hk_1^2}\left(\frac{\text{Cosh}Z_i - 1}{a^*}\right)\cdot\psi^*_{i,2}\right] C^*_{i+1,1}$$

$$+ \left[\frac{1}{h^2} + \frac{1}{2h}\left(\frac{\text{Sinh}Z_i}{\text{Cosh}Z_i - 1}\right) - \frac{Pe}{2hk_1^2}\left(\frac{\text{Cosh}Z_i - 1}{a^*}\right)\cdot\psi^*_{i,2}\right] C^*_{i-1,1}$$

$$+ \left[\frac{4}{k_1^2}\right] C^*_{i,2} - \left[\frac{2}{h^2} + \frac{4}{k_1^2}\right] C^*_{i,1} = 0 \qquad (4\text{-}3\text{-}24)$$

Equation(4-3-24) can be arranged into the following form:

$$\left[\frac{1}{h^2} - \frac{1}{2h}\left(\frac{\text{Sinh}Z_i}{\text{Cosh}Z_i - 1}\right)\right] C^*_{i+1,1} + \left[\frac{1}{h^2} + \frac{1}{2h}\left(\frac{\text{Sinh}Z_i}{\text{Cosh}Z_i - 1}\right)\right] C^*_{i-1,1}$$

$$+ \left[\frac{4}{k_1^2}\right] C^*_{i,2} + \frac{Pe\,\psi^*_{i,2}}{2hk_1^2}\left(\frac{\text{Cosh}Z_i - 1}{a^*}\right)(C^*_{i+1,1} - C^*_{i-1,1})$$

$$= \left[\frac{2}{h^2} + \frac{4}{k_1^2}\right] C^*_{i,1} \qquad (4\text{-}3\text{-}25)$$

Equation can further be arranged into the following form:

$$C^*_{i,1} = D_1(i)C^*_{i+1,1} + D_2(i)C^*_{i-1,1} + D_3C^*_{i,2} + DA' \qquad (4\text{-}3\text{-}26)$$

where,

$$D_1(i) = \left[\frac{1}{h^2} - \frac{1}{2h}\left(\frac{\mathrm{Sinh}Z_i}{\mathrm{Cosh}Z_i - 1}\right)\right] / DD$$

$$D_2(i) = \left[\frac{1}{h^2} + \frac{1}{2h}\left(\frac{\mathrm{Sinh}Z_i}{\mathrm{Cosh}Z_i - 1}\right)\right] / DD$$

$$D_3 = \left[\frac{4}{k_1^2}\right] / DD$$

$$DA' = \left[\frac{Pe\psi^*_{i,2}}{2hk_1^2}\left(\frac{\mathrm{Cosh}Z_i - 1}{a^*}\right)(C^*_{i+1,1} - C^*_{i-1,1})\right] / DD$$

$$DD = \left[\frac{2}{h^2} + \frac{4}{k_1^2}\right]$$

(4). The diffusion equation along the axis of symmetry $\theta = \pi$($j = m$).

As $\frac{\partial}{\partial\theta}(C^*_{i,m}) = 0$, $\frac{\partial}{\partial\theta}(\psi^*_{i,m}) = 0$, and $\mathrm{Sin}\theta = 0$, the diffusion equation(4-1-3) also requires the same special treatment as the previous case:

$$\lim_{\theta\to\pi}\left|\frac{\mathrm{Cosh}Z_i \cdot \mathrm{Cos}\theta_m - 1}{\mathrm{Sin}\theta_m(\mathrm{Cosh}Z_i - \mathrm{Cos}\theta_m)} \cdot \frac{\partial C^*_{i,m}}{\partial\theta}\right| = + \frac{\partial^2 C^*_{i,m}}{\partial\theta^2} \qquad (4\text{-}3\text{-}27)$$

$$\lim_{\theta\to\pi}\left|\frac{1}{\mathrm{Sin}\theta_m}\left(-\frac{\partial\psi^*_{i,m}}{\partial\theta}\cdot\frac{\partial C^*_{i,m}}{\partial Z} + \frac{\partial\psi^*_{i,m}}{\partial Z}\cdot\frac{\partial C^*_{i,m}}{\partial\theta}\right)\right|$$

$$= + \frac{\partial^2 \psi^*_{i,m}}{\partial \theta^2} \cdot \frac{\partial C^*_{i,m}}{\partial Z} \qquad (4\text{-}3\text{-}8)$$

By substitution of these two limiting expressions into equation(4-1-3), the diffusion equation along $\theta = \pi$ becomes:

$$\frac{\partial^2 C^*_{i,m}}{\partial Z^2} - \left(\frac{\text{Sinh}Z_i}{\text{Cosh}Z_i + 1}\right) \cdot \frac{\partial C^*_{i,m}}{\partial Z} + 2\left(\frac{\partial^2 C^*_{i,m}}{\partial \theta^2}\right)$$

$$= + \tfrac{1}{2}\text{Pe}\left(\frac{\text{Cosh}Z_i + 1}{a^*}\right) \cdot \frac{\partial^2 \psi^*_{i,m}}{\partial \theta^2} \cdot \frac{\partial C^*_{i,m}}{\partial Z} \qquad (4\text{-}3\text{-}29)$$

By Taylor's series expansion equation(4-2-4), the second order partial derivatives with respect to θ in equation(4-3-29) are:

$$\frac{\partial^2 C^*_{i,m}}{\partial \theta^2} = \frac{2(C^*_{i,m-1} - C^*_{i,m})}{k^2_{m-1}} \qquad (4\text{-}3\text{-}30)$$

$$\frac{\partial^2 \psi^*_{i,m}}{\partial \theta^2} = \frac{2\psi^*_{i,m-1}}{k^2_{m-1}} \qquad (4\text{-}3\text{-}31)$$

Hence, the finite-difference approximation of the diffusion equation along $\theta = \pi$, equation(4-3-29), becomes:

$$\left[\frac{1}{h^2} - \frac{1}{2h}\left(\frac{\text{Sinh}Z_i}{\text{Cosh}Z_i + 1}\right) - \frac{\text{Pe}}{2hk^2_{m-1}}\left(\frac{\text{Cosh}Z_i + 1}{a^*}\right) \cdot \psi^*_{i,m-1}\right] C^*_{i+1,m}$$

$$+ \left[\frac{1}{h^2} + \frac{1}{2h}\left(\frac{\text{Sinh}Z_i}{\text{Cosh}Z_i + 1}\right) + \frac{\text{Pe}}{2hk^2_{m-1}}\left(\frac{\text{Cosh}Z_i + 1}{a^*}\right) \cdot \psi^*_{i,m-1}\right] C^*_{i-1,m}$$

$$+ \left[\frac{4}{k^2_{m-1}}\right] C^*_{i,m-1} - \left[\frac{2}{h^2} + \frac{4}{k^2_{m-1}}\right] C^*_{i,m} = 0 \qquad (4\text{-}3\text{-}32)$$

Similarly, equation(4-3-32) can be arranged into the following form:

$$C^*_{i,m} = E_1(i)C^*_{i+1,m} + E_2(i)C^*_{i-1,m} + E_3C^*_{i,m-1} + EA' \qquad (4\text{-}3\text{-}33)$$

where,

$$E_1(i) = \left[\frac{1}{h^2} - \frac{1}{2h}\left(\frac{\mathrm{Sinh}Z_i}{\mathrm{Cosh}Z_i+1}\right)\right] / EE$$

$$E_2(i) = \left[\frac{1}{h^2} + \frac{1}{2h}\left(\frac{\mathrm{Sinh}Z_i}{\mathrm{Cosh}Z_i+1}\right)\right] / EE$$

$$E_3 = \left[\frac{1}{k_{m-1}}\right] / EE$$

$$EA = \left[\frac{-Pe\psi^*_{i,m-1}}{2hk^2_{m-1}}\left(\frac{\mathrm{Cosh}Z_i+1}{a^*}\right)(C^*_{i+1,m} - C^*_{i-1,m})\right] / EE$$

$$EE = \left[\frac{2}{h^2} + \frac{4}{k^2_{m-1}}\right]$$

Hence, equations(4-3-26) and (4-3-33) are the diffusion equations applied to the axes of symmetry: $\theta = 0$ and $\theta = \pi$. The concentration at each node point on the axes of symmetry is related to three neighbouring point values as shown in Figure(4-1-2).

During the computational process of the system of finite-difference equations(4-2-13), (4-2-15), and (4-2-18), the constant and specially treated boundary conditions are computed or specified at the beginning of each iteration until they are

prescribed everywhere on the boundaries. The system of finite-difference equations is then solved for each mesh point in the flow region. At the end of each iteration, the specially treated boundary conditions are recalculated using the newly obtained values. This process of solving the system of equations and recalculating the specially treated boundary conditions continues until the desired accuracy of the solutions has been achieved.

4-4. Iterative method with relaxation.

The system of equations, equations(4-2-13), (4-2-15), and (4-2-18) , can be written for each internal mesh point in the following general form:

$$X_{i,j} = f(X_{i+1,j}, X_{i-1,j}, X_{i,j+1}, X_{i,j-1}, D_{i,j}) \quad (4-4-1)$$

where $X_{i,j}$ stands for $\psi^*_{i,j}$, $g_{i,j}$, and $C^*_{i,j}$; while $D_{i,j}$ stands for the non-linear and convective terms of the equations. Equation(4-4-1) can be solved by successive iteration with relaxation.

In the Gauss-Seidel method, equation(4-4-1) at the n^{th} iteration is arranged as follows:

$$X^n_{i,j} = f(X^{n-1}_{i+1,j}, X^n_{i-1,j}, X^{n-1}_{i,j+1}, X^n_{i,j-1}, D^n_{i,j}) \quad (4-4-2)$$

By introduction of the coefficients from the finite-difference equations which may be denoted by $B_1(i,j)$, $B_2(i,j)$, $B_3(i,j)$, and $B_4(i,j)$, equation(4-4-2) becomes:

$$X^n_{i,j} = B_1(i,j)X^{n-1}_{i+1,j} + B_2(i,j)X^n_{i-1,j} + B_3(i,j)X^{n-1}_{i,j+1} + B_4(i,j)X^n_{i,j-1} + D^n_{i,j} \quad (4-4-3)$$

Equation(4-4-3) can be arranged in the following form by the addition and substaction of a term $X^{n-1}_{i,j}$ from the right-hand side of equation(4-4-3):

$$X^n_{i,j} = X^{n-1}_{i,j} + \left[\{B_1(i,j)X^{n-1}_{i+1,j} + B_2(i,j)X^{n}_{i-1,j} + B_3(i,j)X^{n-1}_{i,j+1} + B_4(i,j)X^{n}_{i,j-1} + D^n_{i,j}\} - X^{n-1}_{i,j}\right]$$

$$= X^{n-1}_{i,j} + (X^{*n}_{i,j} - X^{n-1}_{i,j})$$

$$= X^{n-1}_{i,j} + R^n_{i,j} \qquad (4\text{-}4\text{-}4)$$

where $X^{*n}_{i,j}$ denotes the value of $X^n_{i,j}$ calculated using equation(4-4-3), and $R^n_{i,j}$ is the amount by which the value of $X^n_{i,j}$ changes for one iteration. At complete convergence, $R^n_{i,j}$ is equal to zero.

In order to accelerate the rate of convergence, a relaxation factor, ω, which has a value that lies between 0.0 and 2.0, is introduced into equation(4-4-4) as follows:

$$X^n_{i,j} = X^{n-1}_{i,j} + \omega R^n_{i,j} = X^{n-1}_{i,j} + \omega(X^{*n}_{i,j} - X^{n-1}_{i,j}) \qquad (4\text{-}4\text{-}5)$$

This is the Gauss-Seidel iterative method with relaxation. This method is a powerful tool for solving both linear and non-linear partial differential equations expressed in finite-difference form.

Ihsan(not published) has developed a new scheme for solving a set of non-linear finite-difference equations by controlling the non-linear terms. His scheme starts with the following equation:

$$X^n_{i,j} = B_1(i,j)X^{n-1}_{i+1,j} + B_2(i,j)X^{n-1}_{i-1,j} + B_3(i,j)X^{n-1}_{i,j+1}$$

$$+ B_4(i,j)X^{n-1}_{i,j-1} + D^{n-1}_{i,j} \qquad (4\text{-}4\text{-}6)$$

By adding a term $mX^{n-1}_{i,j}$ to both sides, equation(4-4-6) becomes:

$$X^{n}_{i,j} + mX^{n-1}_{i,j} = B_1(i,j)X^{n-1}_{i+1,j} + B_2(i,j)X^{n-1}_{i-1,j} + B_3(i,j)X^{n-1}_{i,j+1}$$

$$+ B_4(i,j)X^{n-1}_{i,j-1} + (m'+w)D'^{n-1}_{i,j} \qquad (4\text{-}4\text{-}7)$$

where $mX^{n-1}_{i,j} = m'D'^{n-1}_{i,j}$ and $wD'^{n-1}_{i,j} = D^{n-1}_{i,j}$. This results in a modification to the "initial guess" before the next iteration. With the assumption that the difference between $X^{n-1}_{i,j}$ and $X^{n}_{i,j}$ is small, equation(4-4-7) can be written as follows:

$$X^{n}_{i,j} = B_1(i,j)\cdot\frac{X^{n-1}_{i+1,j}}{1+m} + B_2(i,j)\cdot\frac{X^{n-1}_{i-1,j}}{1+m} + B_3(i,j)\cdot\frac{X^{n-1}_{i,j+1}}{1+m}$$

$$+ B_4(i,j)\cdot\frac{X^{n-1}_{i,j-1}}{1+m} + \frac{(m'+w)D'^{n-1}_{i,j}}{1+m} \qquad (4\text{-}4\text{-}8)$$

When complete convergence of equation(4-4-8) has been achieved, $X^{n}_{i,j} = X^{n-1}_{i,j}$, and equations(4-4-8) and (4-4-7) become identical. Therefore, with suitable selection of the three parameters: m, m', and w, the non-linear term of equation(4-4-8) can be made to be positive in order to ensure the stability of the numerical solutions.

With these concepts in mind, a similar scheme is developed for the present system of equations. The scheme started with equation(4-4-3) and with the assumption that the difference between $X^{n-1}_{i,j}$ and $X^{n}_{i,j}$ is small, the following equation is formulated:

$$X^n_{i,j} = B_1(i,j)\,\frac{X^{n-1}_{i+1,j}}{1+m} + B_2(i,j)\,\frac{X^{n}_{i-1,j}}{1+m} + B_3(i,j)\,\frac{X^{n-1}_{i,j+1}}{1+m}$$
$$+ B_4(i,j)\,\frac{X^{n-1}_{i,j-1}}{1+m} + \frac{mX^{n-1}_{i,j} + D^n_{i,j}}{1+m} \qquad (4\text{-}4\text{-}9)$$

Equation(4-4-9) has only one extra parameter, m. When m = 0, equation(4-4-9) reduces to the Gauss-Seidel equation(4-4-3). Hence, with a suitable choice of the parameter of m at each node point, the non-linear term of equation(4-4-9) can be conditioned to be positive. The best solutions are obtained when the non-linear term is controlled to be positive, constant, and small. This scheme also ensures stability of the numerical solutions. To accelerate the rate of convergence, the value of $X^n_{i,j}$ obtained from equation(4-4-9) is then substituded into $X^{*n}_{i,j}$ of equation(4-4-5) for further relaxation.

In this computation process, the convergence criterion, ε, of each variable has to be specified before iteration process is started. In the solution of the Navier-Stokes equations, because of large differences in the values of the stream function and vorticity over the whole flow region, two different types of point-convergence tests: relative and absolute, were used:

$$\text{When } X^n_{i,j} > 1.0: \qquad \left|\frac{X^n_{i,j} - X^{n-1}_{i,j}}{X^n_{i,j}}\right| \leqslant \varepsilon \qquad (4\text{-}4\text{-}11)$$

$$\text{When } X^n_{i,j} \leqslant 1.0: \qquad \left|X^n_{i,j} - X^{n-1}_{i,j}\right| \leqslant \varepsilon \qquad (4\text{-}4\text{-}12)$$

On the other hand, in the solution of the diffusion equation, the absolute point-convergence test was used because the

concentration in the flow region varies from C^* = 1.0 to 0.0:

$$|X^n_{i,j} - X^{n-1}_{i,j}| \leq \varepsilon \qquad (4\text{-}4\text{-}13)$$

The convergence criteria for the stream function, vorticity function g, and concentration are designated as ε_{ψ^*}, ε_g, ε_{C^*}, respectively.

4-5. Calculation of surface pressures, drag coefficients, and local and overall Sherwood numbers.

For each sphere spacing Zs, the solutions of the system of equations(4-2-13), (4-2-15), and (4-2-18), produce the stream function, vorticity, and concentration distributions in the flow region at different Reynolds and Peclet numbers. From these distributions, some important quantities of the two-sphere fluid dynamic and mass transfer problems are calculated. The derivations of the appropriate relationships for the calculation of these quantities are given in Appendices B and C.

The following quantities can be obtained from the vorticity distributions:

(1). The pressures at the surfaces of the spheres are expressed in terms of the dimensionless pressure coefficient, K, which is defined as $(P_s - P_o)/\frac{1}{2}\rho U^2$, where P_s and P_o are the pressures at the sphere surfaces and in the undisturbed main stream, respectively. The dimensionless pressure coefficients at the front stagnation point of sphere A, K_{AO}, and at the rear atagnation point of sphere B, K_{BO}, are calculated from the following two expressions:

$$K_{AO} = 1.0 + \frac{8}{Re} \int_{Z=-Zs}^{Z=0} \left(\frac{\partial \zeta^*}{\partial \theta}\right)\Bigg|_{-Zs} dZ \qquad (4\text{-}5\text{-}1)$$

$$K_{BO} = 1.0 + \frac{8}{Re} \int_{Z=+Zs}^{Z=0} \left(\frac{\partial \zeta}{\partial \theta}\right)\Bigg|_{+Zs} dZ \qquad (4\text{-}5\text{-}2)$$

(2). The surface pressure distributions along the solid surfaces of the two spheres are calculated as follows: for sphere A, the calculation starts from the front stagnation point and then

proceeds along the surface towards the rear stagnation point; while for sphere B, the calculation starts from the rear stagnation point and then proceeds along the surface towards the front stagnation point.

For spheres A and B, the expressions are as follows:

$$K_{A\theta} = K_{AO} + \frac{4}{Re}\int_{O}^{\theta}\left[\left.\frac{\partial\zeta^*}{\partial Z}\right|_{-Zs} - \left(\frac{Sinh(-Zs)}{Cosh(-Zs)-Cos\theta}\right)\zeta^*_{1,j}\right]d\theta \qquad (4\text{-}5\text{-}3)$$

$$K_{B\theta} = K_{BO} + \frac{4}{Re}\int_{O}^{\theta}\left[\left.\frac{\partial\zeta^*}{\partial Z}\right|_{+Zs} - \left(\frac{-Sinh(+Zs)}{Cosh(+Zs)-Cos\theta}\right)\zeta^*_{n,j}\right]d\theta \qquad (4\text{-}5\text{-}4)$$

where $K_{A\theta}$ and $K_{B\theta}$ are the dimensionless surface pressure coefficients for spheres A and B, respectively.

(3) The total drag coefficient of each sphere consists of two components: the frictional drag coefficient and the pressure(or form) drag coefficient. For sphere A, the frictional drag coefficient, C_{DFA}, the pressure drag coefficient, C_{DPA}, and the total drag coefficient, C_{DTA}, are calculated from the following three equations, respectively:

$$C_{DFA} = \frac{8}{Re}\int_{O}^{\pi}\zeta^*_{1,j}\cdot Sin\eta\left(\frac{a^*}{Cosh(-Zs)-Cos\theta}\right)\left(\frac{a^*Sin\theta}{Cosh(-Zs)-Cos\theta}\right)d\theta \qquad (4\text{-}5\text{-}5)$$

$$C_{DPA} = +2\int_{O}^{\pi}K_{A\theta}Cos\eta\left(\frac{a^*}{Cosh(-Zs)-Cos\theta}\right)\left(\frac{a^*Sin\theta}{Cosh(-Zs)-Cos\theta}\right)d\theta \qquad (4\text{-}5\text{-}6)$$

$$C_{DTA} = C_{DFA} + C_{DPA} \qquad (4\text{-}5\text{-}7)$$

Similarly, for sphere B, the frictional drag coefficient, C_{DFB},

the pressure drag coefficient, C_{DPB}, and the total drag coefficient, C_{DTB}, are calculated using the following three equations:

$$C_{DFB} = \frac{8}{Re} \int_0^{\pi} \zeta^*_{n,j} \cdot Sin\eta \left(\frac{a^*}{Cosh(+Zs)-Cos\theta}\right)\left(\frac{a^* Sin\theta}{Cosh(+Zs)-Cos\theta}\right) d\theta \qquad (4\text{-}5\text{-}8)$$

$$C_{DPB} = -2 \int_0^{\pi} K_{B\theta} Cos\eta \left(\frac{a^*}{Cosh(+Zs)-Cos\theta}\right)\left(\frac{a^* Sin\theta}{Cosh(+Zs)-Cos\theta}\right) d\theta \qquad (4\text{-}5\text{-}9)$$

$$C_{DTB} = C_{DFB} + C_{DPB} \qquad (4\text{-}5\text{-}10)$$

From the concentration distributions in the flow region adjacent to the surfaces of the spheres the local and overall rates of mass transfer from the spheres expressed in terms of the local and overall Sherwood numbers, can be obtained as follows:

(4). The local Sherwood numbers for spheres A and B, $Sh_{AL}(\theta)$ and $Sh_{BL}(\theta)$, are given by the following two expressions:

$$Sh_{AL}(\theta) = -2.0\left(\frac{Cosh(-Zs)-Cos\theta}{a^*}\right) \left.\frac{\partial C^*}{\partial Z}\right|_{Z=-Zs} \qquad (4\text{-}5\text{-}11)$$

$$Sh_{BL}(\theta) = -2.0\left(\frac{Cosh(+Zs)-Cos\theta}{a^*}\right) \left.\frac{\partial C^*}{\partial Z}\right|_{Z=+Zs} \qquad (4\text{-}5\text{-}12)$$

(5). For each specified sphere spacing, Reynolds number, and Peclet number, the overall Sherwood numbers for spheres A and B, Sh_{AO} and Sh_{BO}, are obtained using the following two expressions:

$$Sh_{AO} = -\left[\frac{\{Cosh(-Zs)-1\}\{Cosh(-Zs)+1\}}{a^*}\right] \int_0^{\pi} \left(\frac{Sin\theta}{Cosh(-Zs)-Cos\theta}\right)$$

$$\cdot \left.\frac{\partial C^*}{\partial Z}\right|_{Z=-Zs} d\theta \qquad (4\text{-}5\text{-}13)$$

$$Sh_{BO} = -\left[\frac{\{Cosh(+Zs)-1\}\{Cosh(+Zs)+1\}}{a^*}\right] \int_0^{\pi} \left(\frac{Sin\theta}{Cosh(+Zs)-Cos\theta}\right)$$

$$\cdot \left.\frac{\partial C^*}{\partial Z}\right|_{Z=+Zs} d\theta \qquad (4\text{-}5\text{-}14)$$

where $a^* = |SinhZs|$.

In the calculation of some of the above quantities, the evaluation of first order derivatives of a function with respect to Z and θ are required. Because a constant mesh spacing is used in the Z direction and variable mesh spacings are used in the θ-direction, these derivatives have to be derived separately.

At any value of Z, say Z^*, the first order derivative of a function with respect to Z may be obtained from a Taylor's series expansion using a forward difference approximation correct up to third order derivatives, the derivative may be expressed as follows:

$$\left.\frac{\partial X}{\partial Z}\right|_{Z=Z^*} = \frac{-11X_1 + 18X_2 - 9X_3 + 2X_4}{6h} \qquad (4\text{-}5\text{-}15)$$

Equation(4-5-15) evaluates the derivative at a given value Z^* in terms of four successive equally spaced values of the function, X_1 to X_4. From equation(4-5-15), the first order derivative of the function $X_{i,j}$ with respect to Z at the surface of sphere A becomes:

$$\frac{\partial X_{1,j}}{\partial Z} = \frac{-11X_{1,j} + 18X_{2,j} - 9X_{3,j} + 2X_{4,j}}{6h} \qquad (4\text{-}5\text{-}16)$$

and the first order derivative of the function $X_{i,j}$ with respect to Z at the surface of sphere B becomes:

$$\frac{\partial X_{n,j}}{\partial Z} = \frac{-11X_{n,j} + 18X_{n-1,j} - 9X_{n-2,j} + 2X_{n-3,j}}{6h} \qquad (4\text{-}5\text{-}17)$$

Because of the variable mesh spacings in the θ-direciton, the derivation of the first order derivative of a function with respect to θ is complicated and tedious. With the same procedure and putting $L_1 = k_1$, $L_2 = k_1 + k_2$, $L_3 = k_1 + k_2 + k_3$, the derivative of a function $X_{i,j}$ with respect to θ at the axis of symmetry θ = O is:

$$\frac{\partial X_{i,1}}{\partial \theta} = \frac{\begin{array}{l} L_2^2L_1^2(L_2-L_1)(X_{i,4}-X_{i,1}) \\ - L_3^2L_1^2(L_3-L_1)(X_{i,3}-X_{i,1}) \\ + L_3^2L_2^2(L_3-L_2)(X_{i,2}-X_{i,1}) \end{array}}{L_3L_2L_1(L_3-L_2)(L_3-L_1)(L_2-L_1)} \qquad (4\text{-}5\text{-}18)$$

Similarly, by putting $L_1' = k_{m-1}$, $L_2' = k_{m-1} + k_{m-2}$, and $L_3' = k_{m-1} + k_{m-2} + k_{m-3}$, the first order derivative of the function $X_{i,j}$ with respect to θ at the axis of symmetry θ = π is:

$$\frac{\partial X_{i,m}}{\partial \theta} = \frac{\begin{array}{l} L_2'^2L_1'^2(L_2'-L_1')(X_{i,m-3}-X_{i,m}) \\ - L_3'^2L_1'^2(L_3'-L_1')(X_{i,m-2}-X_{i,m}) \\ + L_3'^2L_2'^2(L_3'-L_2')(X_{i,m-1}-X_{i,m}) \end{array}}{L_3'L_2'L_1'(L_3'-L_2')(L_3'-L_1')(L_2'-L_1')} \qquad (4\text{-}5\text{-}19)$$

If the mesh spacings in the θ-direction are constant, i.e.,

$k_1 = k_2 = k_3 = k$, and $k_{m-1} = k_{m-2} = k_{m-3} = k$, then equations(4-5-18) and (4-5-19) reduce to:

$$\frac{\partial X_{i,1}}{\partial \theta} = \frac{-11X_{i,1} + 18X_{i,2} - 9X_{i,3} + 2X_{i,4}}{6k} \qquad (4\text{-}5\text{-}20)$$

$$\frac{\partial X_{i,m}}{\partial \theta} = \frac{-11X_{i,m} + 18X_{i,m-1} - 9X_{i,m-2} + 2X_{i,m-3}}{6k} \qquad (4\text{-}5\text{-}21)$$

Equations(4-5-20) and (4-5-21) are similar to equations(4-5-16) and (4-5-17), respectively.

In the numerical integration process, the trapezoidal rule is used. For the integration of a function X(Z) over the limits Za and Zb with n-1 equally spaced intervals between them, the following expression is adopted:

$$\int_{Za}^{Zb} X(Z)dZ = h(\tfrac{1}{2}X_a + X_2 + \cdots + X_{n-2} + \tfrac{1}{2}X_b) \qquad (4\text{-}5\text{-}22)$$

Similarly, the integration of a function $X(\theta)$ over the limits θa and θb with m-1 un-equally spaced intervals k_j, where j = 1, $\cdots$, m-1, between the limits, the following expression is used:

$$\int_{\theta a}^{\theta b} X(\theta)d\theta = \tfrac{1}{2}\left[(X_a+X_2)k_1 + (X_2+X_3)k_2 + \cdots + (X_j+X_{j+1})k_j + \cdots + (X_{m-1}+X_b)k_{m-1}\right] \qquad (4\text{-}5\text{-}22)$$

With the aid of these numerical differentiation and integration expressions, the distributions of vorticity, stream function, and concentration in the flow region can be converted into quantitative physical information.

4-6. Computational procedures for the solution of the system of equations.

For each sphere spacing, the Navier-Stokes equations, expressed in terms of the stream function equation(4-2-13) and the vorticity transport equation(4-2-15), are solved simultaneously for the stream function and vorticity distributions in the flow region for a series of Reynolds numbers. The diffusion equation (4-2-18) is then solved separately for concentration distributions in the same flow region for a series of Peclet numbers using the calculated stream function distribution at any specified Reynolds number.

Two computer programmes: Program 1 and Program 2, which are listed and explained in Appendix F, are developed for the simulation of the viscous fluid flow around two equally sized spheres and the calculattion of the mass transfer rates from the spheres. Program 1 is solely for the solution of the Navier-Stokes equations while Program 2 is for the solution of the diffusion equation. In the computational process, two magnetic tapes are needed to store the flow information as well as the converged numerical results. Tape 1 is used for Program 1 and Tape 2 for Program 2.

Before entering the computational process, the flow region and the controlling parameters are specified for each sphere spacing, and the boundary conditions prescribed for each dependent variable. For the first solution obtained of the Navier-Stokes equations, the initial values for the stream function and vorticity are supplied from the analytical solutions obtained by Stimson and Jeffery(1926) for creeping flow around

two equally sized spheres at the appropriate sphere spacing. For the first solution obtained for the diffusion equation, an array of arbitary initial values for concentration is supplied. In subsequent runs, the initial values are always supplied from the converged results stored on magnetic tapes for the nearest lower Reynolds number or Peclet number.

For each specified Reynolds number, when the solution of the Navier-Stokes equations is obtained, the converged stream function and vorticity distributions in the flow region are printed out and at the same time stored on Tape 1. The surface pressures and the drag coefficients for the two spheres are then calculated. In order to understant the stream function and vorticity distributions around the spheres, the contours of the stream function and vorticity distributions are searched for and plotted using the computer. Similarly, for each specified Reynolds and Peclet numbers, when the solution of the diffusion equation is obtained, the converged concentration distribution in the flow region is printed out and stored on Tape 2. The local and overall rates of mass transfer from the spheres are calculated and the concentration contours around the spheres are located and plotted using the computer.

Detailed descriptions of the computational procedures for solving the Navier-Stokes and diffusion equations for any sphere spacing are given separately in the following sections.

(A). Summary of the computational procedures for solving the Navier-Stokes equations.

1. Specify the sphere spacing, Zs.
2. Specify the position of the outer boundary by assigning a value to the ratio, (r/d), where r is the radius of the outer boundary sphere and d is the distance between the centre of either sphere and the origin of the bi-spherical coordinate system.
3. Specify the mesh spacing in the Z-direction, h. The un-equal mesh spacings in the θ-direction, k_j, $j = 1, \cdots, m-1$, are obtained from equation(A-3-3) by assigning values of η with a constant increment of 6^o. The outer boundary coordinates(Z_o, θ_o) are obtained by solving equation(A-2-8). The number of internal mesh points in the flow region and the number of irregular mesh points which lie on the boundary and require special treatment are calculated. The total number of the unknown quantities in the finite-difference equations is the product of the dependent variables(stream function ψ^* and vorticity ζ^*) and the total number of mesh points in in the flow region. The total number of mesh points is the sum of the numbers of regular and irregular mesh points.
4. Calculate all the flow region information which are functions of Z and θ, such as SinhZ, CoshZ, Sinθ, Cosθ, etc. At this point, the flow region is fully described.
5. Specify the Reynolds number, Re, the convergence criteria and the relaxation factors for the stream function and vorticity, and the maximum number of iterations allowed for the computation.
6. Before entering the iteration process, the initial values

for the dependent variables have to be supplied. For the first solution obtained, the initial values are supplied from Stimson and Jeffery's analytical solutions for Stokes flow at the appropriate sphere spacing and these values together with the flow region information and calculated quantities are stored on Tape 1. In subsequent runs, the initial values for the dependent variables for the iteration process are supplied from the previously obtained values which have been stored on Tape 1. The values used are those for the nearest smaller value of Reynolds number.

7. Specify the constant boundary conditions for ψ^*, ζ^*, g and f at the solid surfaces of the spheres, the axes of symmetry $\theta = 0$ and $\theta = \pi$, and the outer boundary.
8. Calculate all the coefficients of the finite-difference equations(4-2-13) and (4-2-15), and the coefficients of the specially treated boundary conditions.

Up to this point, all the information and parameters required for the solution of the Navier-Stokes equations at a specified Reynolds number have been supplied. The iteration process for the solution is then started.

9. Calculate the specially treated surface vorticities and surface vorticity functions: $\zeta^*_{1,j}$, $\zeta^*_{n,j}$, $g_{1,j}$, $g_{n,j}$, $f_{1,j}$, and $f_{n,j}$, using the most recently obtained available results and apply the point convergence test of equations(4-4-11) and (4-4-12) as soon as the values at each mesh point on the solid surfaces are obtained. The values of the vorticity function f along the axes of symmetry $\theta = 0$ and $\theta = \pi$: $f_{i,1}$

and $f_{i,m}$, are also calculated using the newly obtained results.

10. The iteration process for the solution of the Navier-Stokes equations is then carried out for each internal mesh point. A set of values: $\psi^*_{i,j}$, $\zeta^*_{i,j}$, $g_{i,j}$, and $f_{i,j}$, are obtained for each mesh point. For the stream function $\psi^*_{i,j}$ and the vorticity $\zeta^*_{i,j}$, the point convergence test of equations(4-4-11) and (4-4-12) is then applied as soon as the values are obtained. At the end of each iteration a test is made to determine whether the solution has converged at every mesh point. If this test is satisfied the overall convergence has been obtained.

11. Repeat steps 9 and 10 until either overall convergence of the results is achieved or the maximum number of iterations specified is reached. When overall convergence has been achieved, an extra iteration is allowed for the specially treated boundary conditions to be satisfied as well. If overall convergence of the stream function and vorticity cannot be obtained within the maximum number of iterations allowed, a pair of new relaxation factors are supplied and the computational process is re-started from step 6.

12. When overall convergence has been achieved, the surface pressures and the drag coefficients for the spheres are calculated. The stream function and vorticity distributions around the two spheres are printed out in tabulated form and their contours located and plotted. Finally, the converged values of ψ^*, ζ^*, g, and f, together with the flow region information are stored on Tape 1, and are available for the solution of the Navier-Stokes equations at a higher Reynolds number. At this point, the numerical solution of the Navier-

Stokes equations for a particular case is complete.

13. A new case with a higher Reynolds number is initiated by starting the computational process at step 5.

(B). Summary of the computational procedures for solving the diffusion equation.

1. Specify the sphere spacing Zs and Reynolds number Re. The flow region information and the stream function distribution at the specified sphere spacing and Reynolds number are supplied from Tape 1.
2. Specify the Peclet number Pe(Pe = RexSc), the convergence criterion and the relaxation factor for the concentration, and the maximum number of iterations allowed for the computation.
3. Supply an array of initial values for the concentration. For the first solution to be obtained, the set of initial values is provided in an arbitrary way. In subsequent solutions, initial values are supplied from the converged results which have been obtained previously for a lower value of the Peclet number and which have been stored on Tape 2.
4. Specify the constant boundary conditions for the concentrations at the solid surfaces and the outer boundary of the flow region.
5. Calculate the coefficients of the diffusion equation(4-2-18) and the two modified diffusion equations(4-3-26) and (4-3-33) which apply to the axes of symmetry, $\theta = 0$ and $\theta = \pi$, respectively.

Up to this point, all the information and parameters

needed for the solution of the diffusion equation and the two modified diffusion equations at the specified Peclet number have been supplied. The iteration process for the solution of the diffusion equation then proceeds as follows:

6. Solve the modified diffusion equations along the axes of symmetry $\theta = 0$ and $\theta = \pi$ for $C^*_{i,1}$ and $C^*_{i,m}$. The diffusion equation(4-2-18) is then solved for $C^*_{i,j}$ at each internal mesh point. The point convergence test of equation(4-4-13) is applied as soon as the value at each mesh point is obtained. At the end of each iteration the results are tested for overall convergence.
7. Repeat the iteration process of step 6 until either overall convergence of the results has been achieved or the maximum number of iterations specified has been reached. When overall convergence has been achieved, an extra iteration is allowed for the boundary conditions along the axes of symmmetry $\theta = 0$ and $\theta = \pi$ to be satisfied. When overall convergence cannot be obtained within the maximum number of iterations allowed, a new relaxation factor is supplied and the computational process is re-started from step 3.
8. From the converged concentration distribution , the local and overall Sherwood numbers are calculated. Also, the distribution of concentration in the flow region is printed out in tabulated form and the concentration contours around the spheres are located and plotted. Finally, the flow region information, the stream function distribution, and the concentration distribution are stored on Tape 2 and are available for the solution of the diffusion equation at the next higher Peclet number. At this point, the numerical

solution of the diffusion equation for a particular Peclet number is complete.

9. A new case with a higher Peclet number is initiated by starting the computational process from step 2.

The procedures for solving the Navier-Stokes and diffusion equations are quite similar. However, it is important to note that Program 1 is designed such that for each sphere spacing the Navier-Stokes equations can be solved independently for a series of Reynolds numbers; while Program 2 , which is dependent upon Program 1 to supply the flow region information and the stream function distribution at any specified Reynolds number, is for the solution of the diffusion equation for a series of Peclet numbers.

CHAPTER 5.

DISCUSSION OF SOLUTIONS OF THE NAVIER-STOKES EQUATIONS.

5-1. Introduction.

Numerical solutions of the Navier-Stokes and diffusion equations for a system of two equally sized spheres with a fluid flowing parallel to their line of centres were obtained separately using two computer programmes: Program 1 and Program 2, respectively. The computer programmes were arranged in such a way that for each sphere spacing, the vorticity, stream function, and concentration distributions in the flow region could be generated over a wide range of Reynolds and Peclet numbers.

The distance between the centres of the spheres, which is governed by the sphere spacing parameter Zs, is an important factor in determining the extent of particle-to-particle interaction between the spheres. Five sphere spacings: Zs = 0.20, 1.32, 2.07, 2.48, and 3.09, corresponding to two equally sized spheres nearly touching, being one, three, five, and ten diameters apart, respectively, were considered in this study. The Navier-Stokes equations were solved by means of Program 1 for the vorticity and stream function distributions for a wide range of Reynolds numbers between 0.001 and 500. Similarly, the diffusion equation was solved by Program 2 for concentration distributions over a range of Peclet numbers from 0.001 to 500 for some selected Reynolds numbers. From the resultant concentration distributions the local and overall Sherwood numbers for the spheres were calculated. The mass transfer results will be discussed in the next chapter. The resultant vorticity and stream function distributions were used to

calculate fluid dynamic quantities; such as surface vorticity distributions, surface pressure distributions, drag coefficients and angles of flow separation. These results are discussed in this chapter.

The accuracy of the numerical solutions of the Navier-Stokes equations depends upon many factors; such as mesh spacings, convergence criteria, and numerical methods used to obtain the solution. An analysis of these factors is given in the following section(5-2). The distributions of vorticity and stream function around the spheres are given in sections(5-3) and (5-4), respectively; while the phenomenon of flow separation from the surfaces of the spheres and the surface vorticity distributions are discussed in sections(5-5). In sections(5-6) and (5-7), the surface pressure distributions and the drag coefficients for the spheres are presented separately.

5-2. Analysis of the factors affecting the numerical solutions.

The usefulness of large computers for theoretical studies in fluid dynamics often depends upon the accuracy with which numerical solutions can be obtained. In the present two-sphere problem, the accuracy of the numerical results depended upon many factors, such as the coordinate system used, the distribution of grid lines in the flow region, the choice of convergence criteria, and the methods of solution. An understanding of these factors and the influences and limitations which they imposed upon the accuracy of the numerical results is necessary.

Because of the ease with which it is possible to describe the locations of the two spheres and the associated boundary conditions, the bi-spherical coordinate system was used in the present study. However, two bi-spherical coordinates: the bi-polar coordinates Z and θ, appeared in the coefficients of the terms in the Navier-Stokes equations, equations(4-2-13) and (4-2-15), so that a large amount of computer memory storage was needed for the solutions in terms of the vorticity and stream function. Also, the replacement of the partial differential equations by their finite-difference approximations introduced a truncation error. Furthermore, during the numerical iteration process, an error called the round-off error was introduced. The dilemma of dealing with these two errors was that by reducing the size of the mesh spacings for the Z- and θ-directions in the flow region, the truncation error of the solution decreased while the round-off error of the solution generally increased. This was because of an increase in the total number of algebraic equations resulted in an increase in the number of iterations required to obtain a solution. Hence, the distribution

of grid lines in the flow region had to be chosen with these factors borne in mind.

Two distributions of the grid lines for the Z- and θ-directions in the flow region for each sphere spacing were used for the solution of the Navier-Stokes equations. In these two distributions, the grid lines for the Z-direction were distributed according to two mesh spacings of $|Zs/10|$ and $|Zs/20|$, while those for the θ-direction were distributed accroding to a constant increment of 6^{o} in the angle η. Hence, in the first case the number of mesh points was 21x31 while in the second case it was 41x31. The outer boundary of the flow region, which had its centre at the mid-point of the line of centres of the spheres, was chosen to have a radius of 7.0 times the distance between the centres of the spheres for the smallest sphere spacing Zs = 0.20, and a radius of 3.5 times the distance between the centres of the spheres for the four large sphere spacings considered. With these two distributions of grid lines in the flow region for each sphere spacing, numerical solutions of the Navier-Stokes equations were obtained using a CDC6400 computer with 65k storage locations.

The main reason for using two different distributions of grid lines in the flow region for each sphere spacing, i.e., using two different mesh spacings for the Z-coordinate, arose because of the inherent characteristic of the bi-spherical coordinate system of providing unequal distances between any two neighbouring grid lines in the Z-direction around the spheres as shown in Figures(4-1-3) to (4-1-12). A new term called the "grid-line spacing", which measures the distance between any two neighbouring grid lines along any grid line in another

direction, is introduced here to describe the uneven distributions of the grid lines for both the Z- and θ-directions. The distance between any two neighbouring grid lines in the Z-direction is called the Z-grid-line spacing, while that in the θ-direction is called the θ-grid-line spacing. It is important to note that the grid-line spacing is different from the mesh spacing which is solely used for indicating the increment in the two bi-polar coordinates: Z and θ, as well as the angle η in this study. The Z-grid-line spacings decrease around each sphere when the θ-coordinate changes from the value of $\theta = 0$ to $\theta = \pi$; hence, they are the largest along the normals to the front stagnation point of sphere A and to the rear stagnation point of sphere B; while they are smallest along the normals to the rear stagnation point of sphere A and to the front stagnation point of sphere B. These unequal Z-grid-line spacings around the spheres, especially near the upstream surface of sphere A, created some difficulties in the calculation of quantities, such as the surface pressures and the local Sherwood numbers, which were related to the vorticity and concentration distributions. This was particularly the case near the upstream surface of sphere A, because at high Reynolds and Peclet numbers the thickness of the fluid dynamic and diffusional boundary layers in that region were small in comparison with the large Z-grid-line spacings. This defect could have been overcome by a continuous reduction of the mesh spacing in Z. However, as this was done the number of mesh points in the flow region increased enormously although most of the mesh points remained concentrated in the region between the spheres where they contributed little to the improvement of the results over the upstream surface of sphere A. Also, because of

limitations imposed by the availability of computer memory storage, the flexibility of altering the mesh spacing in Z in order to improve the numerical solutions at the upstream surface of sphere A was greatly restricted. However, the use of two mesh spacings in Z allowed the sensitivity of the numerical solutions to variations of the mesh spacing in Z to be investigated

The Z-grid-line spacings, in addition to varying with position around the sphere, also increase as the distance from the surfaces of the spheres increases. Similarly, the θ-grid-line spacings are not equal along any Z-coordinate except for those adjusted to a constant increment in η which are equal along the solid surfaces of the spheres where Z = -Zs and Z = +Zs. The θ-grid-line spacings become larger when the Z-coordinate around sphere A changes from Z = -Zs to Z = O and the Z-coordinate around sphere B changes from Z = +Zs to Z = O. Hence, both the Z-grid-line and the θ-grid-line spacings are large in the region far away from the surfaces and are relatively small near the surfaces and in the region between the spheres. Accordingly, the truncation errors derived from the central finite-difference approximation of the Navier-Stokes equations were of different magnitudes throughout the flow region. The truncation errors of the solutions at the mesh points near the outer boundary of the flow region were large, and became even larger as the distances between the outer boundary and the spheres and between the centres of the spheres were increased. These large truncation errors may have been a source of numerical instability.

Because of its rapid rate of convergence and simplicity of use, the extrapolated Gauss-Seidel method was used in the present work to obtain solutions of the Navier-

Stokes equations. Over-relaxation of the solutions was found to be satisfactory for low Reynolds numbers. However, numerical solutions at high Reynolds numbers were difficult to obtain, and it is necessary to adopt a scheme of under-relaxation in order to obtain solution for a wide range of Reynolds numbers with satisfactory rates of convergence and stability. The relaxation factors, which were supplied by trial-and-error, decreased with increasing Reynolds number.

In the computational process, the convergence criteria for the stream function and vorticity were specified with consideration of two factors: the desired degree of accuracy of the numerical solutions and the computing time required. The accuracy of the solution was improved when stringent convergence criteria were specified, but a large number of iterations, and thus a large computing time, was required to achieve convergence of the solutions at every mesh point in the flow region. On the other hand, convergence of the solutions at each mesh point could have been obtain more rapidly by using less stringent convergence criteria, but at the expense of the accuracy of the solutions. Based on these considerations, the convergence criteria for the stream function and the vorticity function g were specified to be 10^{-3}. When the convergence criterion for the stream function was changed from 10^{-3} to 10^{-4} the number of iterations required to obtain a converged solution for a specified low Reynolds number was more than doubled while the results were improved only slightly. Hence, the flexibility of of altering the convergence criteria in order to improve the accuracy of the numerical solutions of the Navier-Stokes equations was restricted. In addition, because the values of

the stream function and vorticity function varied from very large to very small values, a relative point convergence test for the solutions always produced a small number of points at which the solutions did not converge no matter how many iterations were performed. The points in question were the points at which the values were small. In order to overcome this problem, a less stringent absolute convergence criterion was applied at points at which the values were less than unity. In this scheme, a relative point convergence test was applied when a point value was greater than unity, while an absolute point convergence test was used whenever a point value was equal to or less than unity. By this means, convergence of the solutions at all mesh points in the flow region was obtained rapidly. Unfortunately, the use of the absolute point convergence test in this way resulted in a decrease in the accuracy of the solutions.

5-3. Vorticity distributins around two spheres.

The numerical solutions of the Navier-Stokes equations were expressed in terms of the stream function and vorticity distributions over the whole flow region. For each sphere spacing, the tabulated results of the stream function and vorticity distributions at each Reynolds number were interpolated and the streamlines and vorticity contours plotted around the spheres. Using these plots, the fluid dynamics as well as the variation of the flow patterns with Reynolds number and sphere spacing were studied qualitatively. The vorticity distributions around the spheres are discussed in this section and the stream function distributions in the next section(5-4).

The vorticity distributions around two equally sized spheres at five sphere spacings: Zs = 0.20, 1.32, 2.07, 2.48, and 3.09, obtained using a mesh spacing of $|Zs/10|$ in Z and a mesh spacing of 6^{o} in η, are shown in Figures(5-3-1) to (5-3-19) for a wide range of Reynolds numbers. In each figure, five vorticity contours with values of ζ^{*} of 0, 0.1, 0.5, 1.0, and 2.0, are plotted around the spheres. It is important to note that the axes of symmetry are coincident with the zero vorticity contour.

For the largest sphere spacing considered in this study: Zs = 3.09, L/R = 22.022, the vorticity distributions around the spheres are shown in Figures(5-3-1) to (5-3-3) for some selected Reynolds numbers ranging from 0.001 to 150. At low Reynolds numbers of 0.001 to 0.1, the vorticity contours change very little and are symmetrical about a plane through the mid-point of the line of centres normal to the direction of flow. This shows that the effect of convection upon the diffusion of

vorticity from the spheres is almost negligible at these low Reynolds numbers. However, when the Reynolds numbers reaches unity, the vorticities around both spheres begin to be convected more rapidly towards the rear than they diffuse forwards from the surfaces of the spheres. As the Reynolds number is further increased, the vorticity contours upstream of each sphere are confined to an increasingly narrower region and at high Reynolds numbers a fluid dynamic boundary layer is developed over the upstream surface of each sphere. At the same time the vorticity contours downstream of each sphere extend rapidly rearwards. These results indicate that when the Reynolds number is greater than unity, the effect of convection upon the diffusion of vorticity from the spheres is significant and increases with increasing Reynolds number. Also, the larger extension of the vorticity contours rearwards from sphere A than from sphere B indicates that the effect of convection upon the diffusion of vorticity from sphere A is larger than upon that from sphere B. As a result, the difference between the vorticity distributions around the two spheres increases with increasing Reynolds number, and the onset of flow separation from the rear surface of each sphere occurs at a different Reynolds number. For sphere A, a flow separation is observed at a Reynolds number of 20, while for sphere B it is not observed until the Reynolds number is 50. A detailed discussion of flow separation is given in section(5-5). It is important to note that as the outer boundary of the flow region is thirty-three diameters upstream from the front stagnation point of sphere A and is the same distance downstream from the rear stagnation point of sphere B, the effect of the location of the outer boundary upon the vorticity

distributions near the surfaces of the spheres is likely to be small.

The vorticity distributions around the two spheres have common features in that the most intensive vorticities are always generated at the upstream surfaces of each sphere and that these vorticities are subsequently convected rearwards and persist at large distances downstream from the surfaces of the spheres. However, the continuous process of convection of vorticity downstream from the surface of sphere A eventually results in an interaction of the vorticities from sphere A with the vorticities diffused upstream from the surface of sphere B. This interaction is illustrated at a Reynolds number of 30 in Figure(5-3-2) by the vorticity contour $\zeta^* = 0.1$. Instead of separate contours existing around each sphere, the contour generated around sphere A extends downstream and meets that diffusing upstream from sphere B so that the two contours become combined together in the region between the spheres. For the present axisymmetrical flow, the vorticity, which is defined as the differential circulation per unit area enclosed in the fluid, is also the angular velocity of the fluid around a direction normal to the plane of flow, so that when vorticity diffusing and convecting downstream from sphere A interacts with vorticity diffusing upstream from sphere B the vorticity contours change their positions in the region where the vorticities interact. Furthermore, the distributions of vorticity around the spheres, especially in the region between the spheres, are quite different from those around a single isolated sphere at the same Reynolds number. This indicates the existence of particle-to-particle interaction between the spheres.

For the sphere spacings: Zs = 2.48, L/R = 12.025; and Zs = 2.07, L/R = 8.0510, the vorticity distributions around the spheres are shown in Figures(5-3-4) to (5-3-7) for some Reynolds numbers ranging from 0.001 to 200, and in Figures(5-3-8) to (5-3-10) for some selected Reynolds numbers ranging from 0.001 to 180, respectively. For each sphere spacing, the variation of the distributions of vorticity around the spheres with Reynolds number is similar to that for the largest sphere spacing Zs = 3.09. However, because of the smaller distance between the spheres, the interaction between the vorticity diffusing and convecting downstream from the surface of sphere A and the vorticity diffusing upstream from the surface of sphere B becomes apparent at a lower Reynolds number than that for the largest sphere spacing. This can be seen from Figures(5-3-6) and (5-3-9) which show that as the spheres become closer together the two separate contours with a vorticity of 0.1 merge into a combined contour at progressively lower Reynolds numbers, also the distributions of vorticity around the spheres become increasingly unlike those around a single isolated sphere. Based on these observations, it is clear that the extent of particle-to-particle interaction between the spheres increases when the spacing between the spheres decreases.

On decreasing the sphere spacing further to Zs = 1.32, L/R = 4.0106, the vorticity distributions around the spheres, given in Figures(5-3-11) to (5-3-14) for some selected Reynolds numbers ranging from 0.001 to 300, become more complicated, particularly in the region between the spheres. The contours $\zeta^* = 0.1$ become a combined contour joining the two spheres at

a Reynolds number as low as 0.001. This is because the distance between the spheres is so small that the vorticities diffusing downstream from the rear surface of sphere A and upstream from the front surface of sphere B interact in the small region between the spheres even at very low Reynolds number. Despite this, the vorticity distributions around the spheres remain almost unchanged as the Reynolds number is increased from 0.001 to 0.1. Also, the vorticity distributions remain symmetrical about a plane pass through the mid-point of the line of centres and normal to the direction of flow. Thus, at low Reynolds numbers the effect of forced convection upon the diffusion of vorticity from the surfaces of the spheres is negligible.

For Reynolds numbers greater than unity, the vorticity around each sphere is convected more rapidly rearwards than it diffuses forwards from the surface of the sphere. This pattern of behaviour is similar to that for larger sphere spacings. Similarly, the vorticity contours in the region upstream of sphere A are confined to an increasingly smaller region and at high Reynolds numbers a fluid dynamic boundary layer is formed for sphere A. On the other hand, because of the very small distance between the spheres and the strong interaction of vorticities in the region between the spheres, a fluid dynamic boundary layer does not become fully developed at the upstream surface of sphere B even at high Reynolds numbers. Another feature of the vorticity distributions for this sphere spacing is that when the Reynolds number is greater than 30, there are two zero vorticity contours in the region between the spheres: one originating from the rear surface of sphere A and the other from the front surface of sphere B. In addition, when the

Reynolds number reaches 100, a third zero vorticity contour originating from the rear surface of sphere B appears.Points of flow separation are characterized by the intersection of a solid surface with a zero vorticity contour. The appearance of flow separation from the front surface of sphere B may be a result of the closeness of the spheres in that more and more vorticity is convected downstream from sphere A to the vicinity of the front surface of sphere B. Eventually, a backward flow is induced near the upstream surface of sphere B resulting in the establishment of a standing eddy or vortex in the region between the spheres.

For the smallest sphere spacing considered in this study: Zs = 0.20, L/R = 2.0402, the vorticity distributions around the two nearly touching spheres for Reynolds numbers ranging from 0.001 to 500 are shown in Figures(5-3-15) to (5-3-19). The pattern of the variation of the vorticity distribution with Reynolds number is similar to that for the sphere spacing Zs = 1.32. However, there are some observable differences between the distributions of vorticity for these two smallest sphere spacings. The two zero vorticity contours in the region between the spheres, which appear at a Reynolds number of 50 for sphere spacing Zs = 1.32, become one combined contour joining the two spheres at Reynolds numbers as low as 0.001 for the smallest sphere spacing Zs = 0.20. This indicates that flow separation from the front surface of sphere B occurs at about the same Reynolds number as that at which flow separation appears at the rear of sphere A. Also, for this closest sphere spacing, the merging of two separate vorticity contours with the same magnitude of vorticity into a combined contour joining

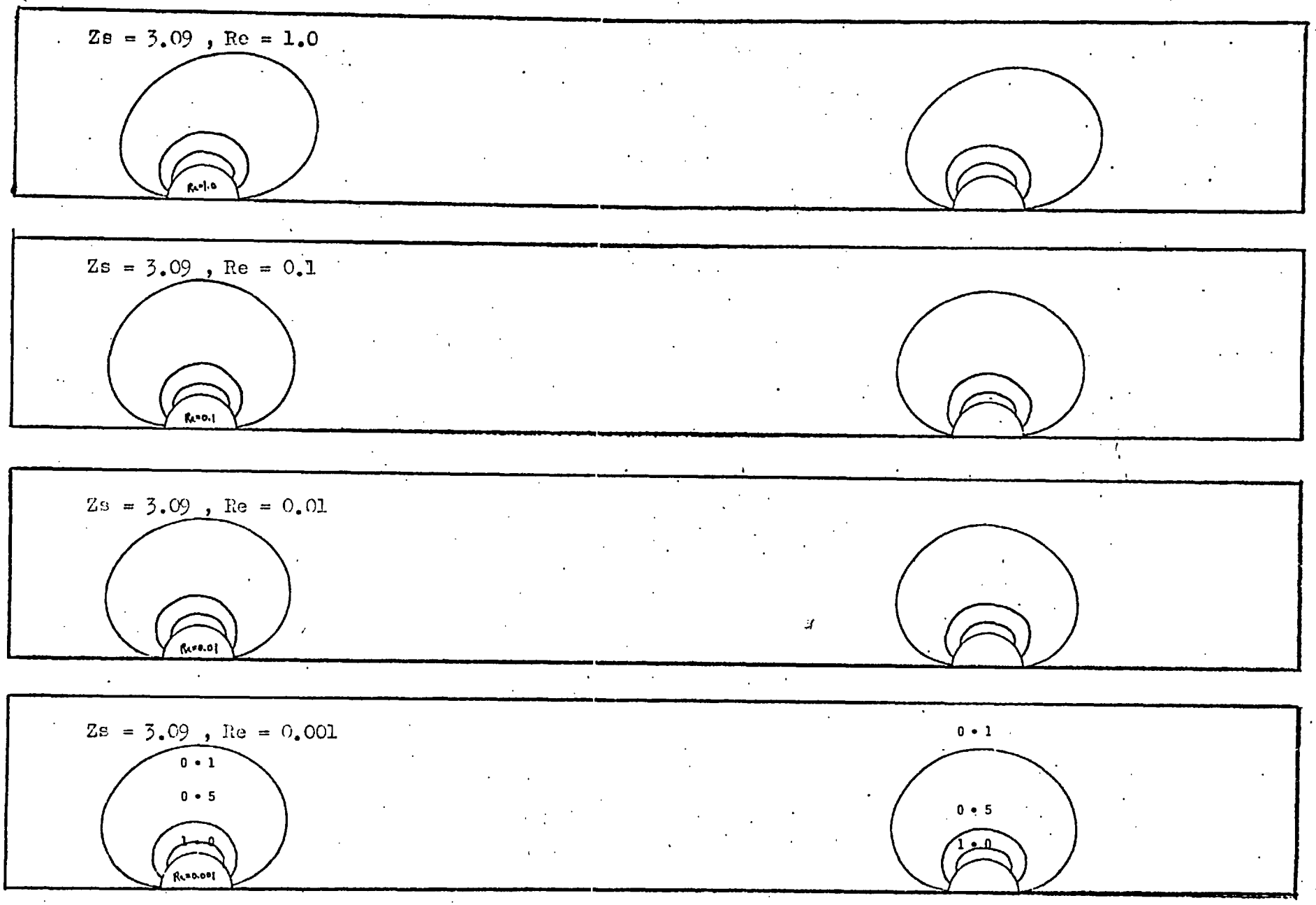

Figure(5-3-1). Vorticity distributions around two spheres with Zs = 3.09.

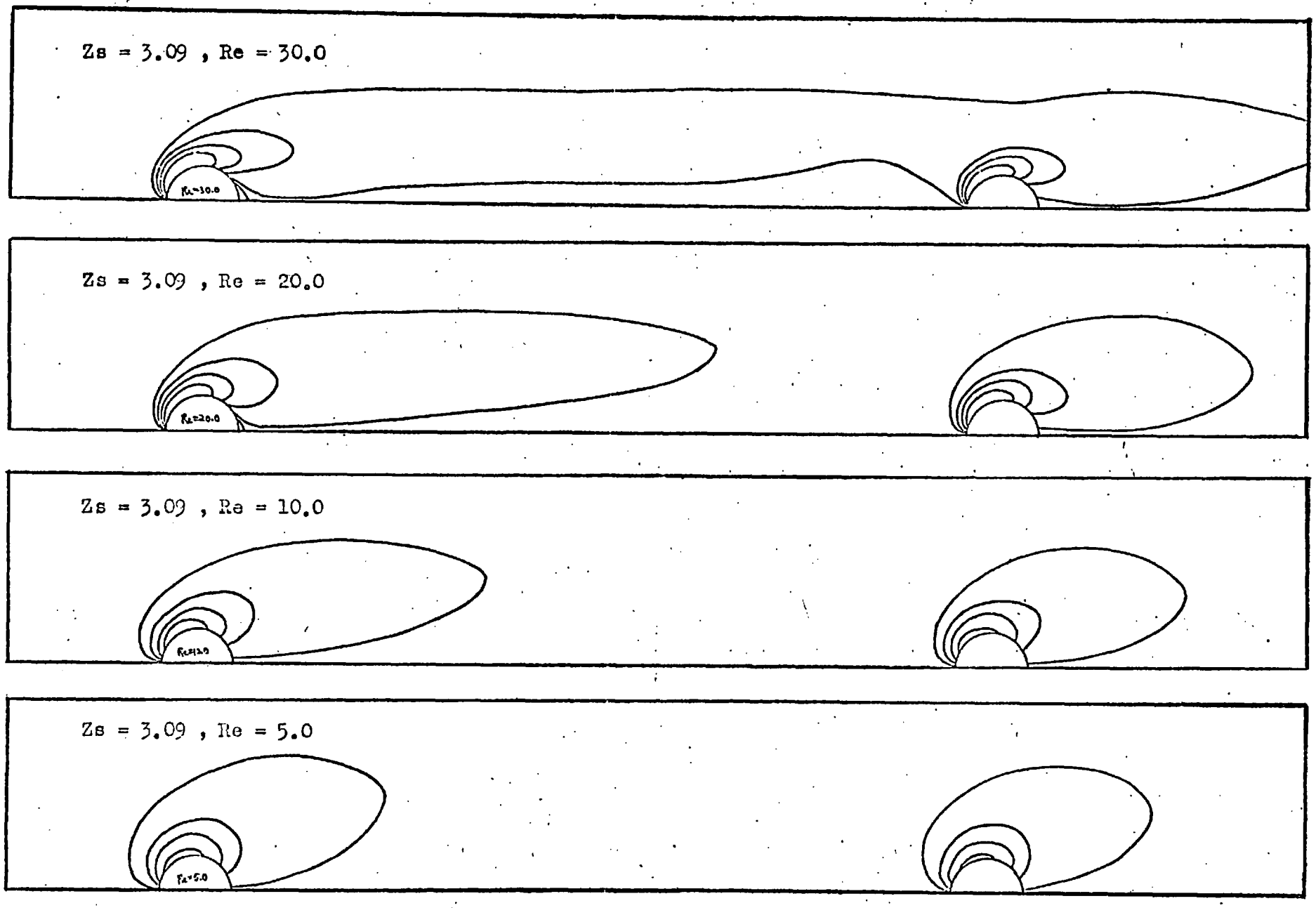

Figure(5-3-2). Vorticity distributions around two spheres with Zs = 3.09.

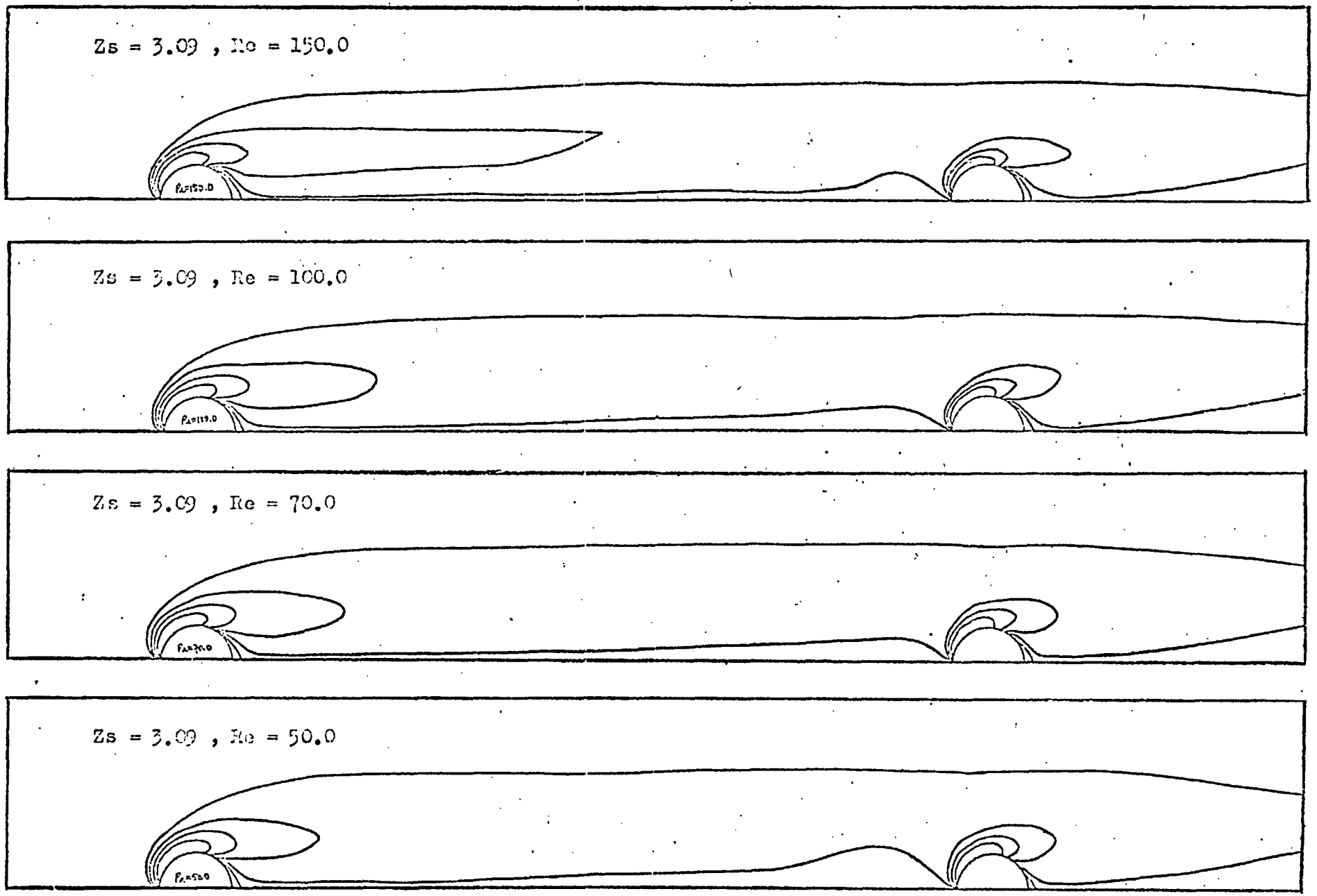

Figure(5-3-3). Vorticity distributions around two spheres with Zs = 3.09.

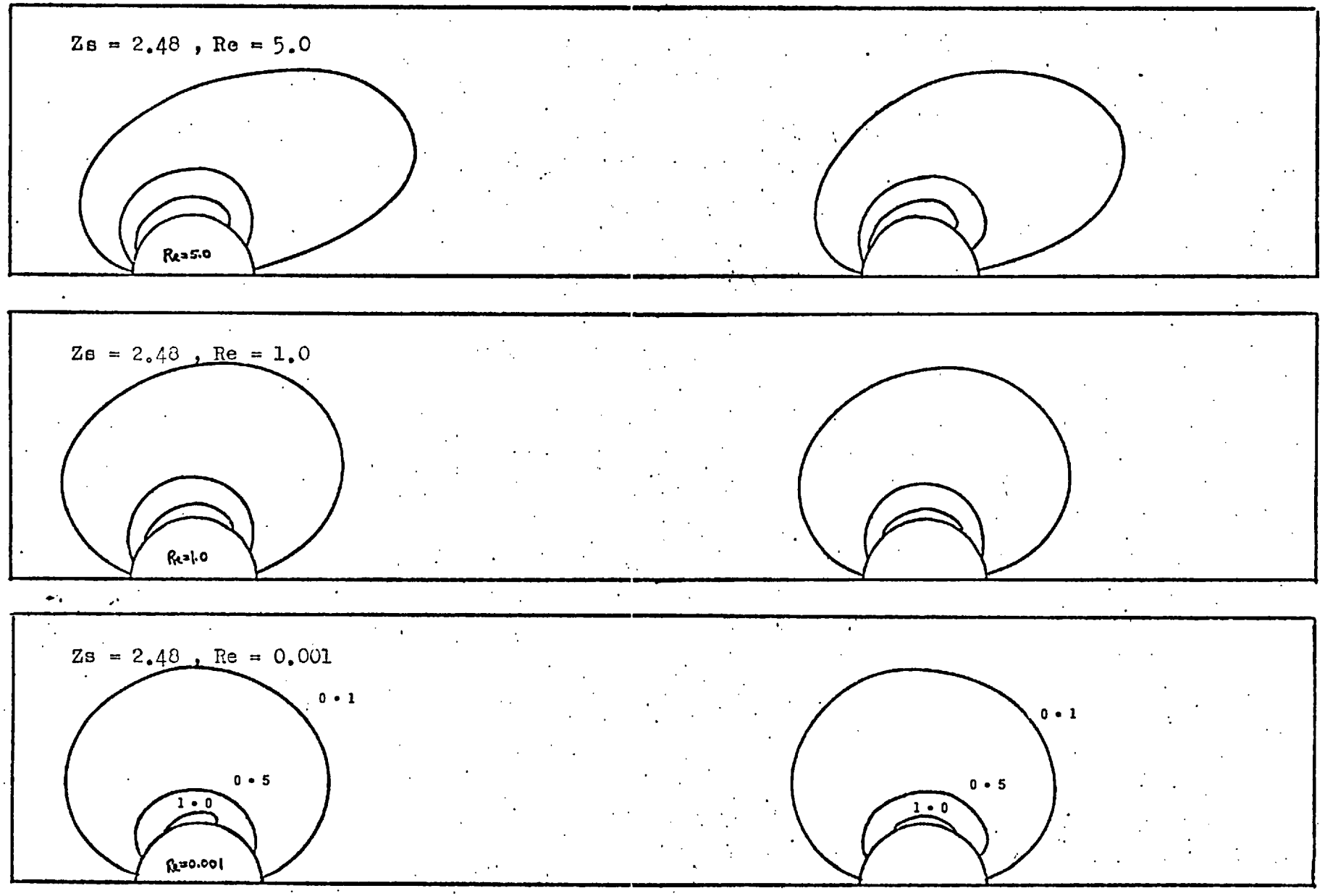

Figure(5-3-4). Vorticity distributions around two spheres with Zs = 2.48.

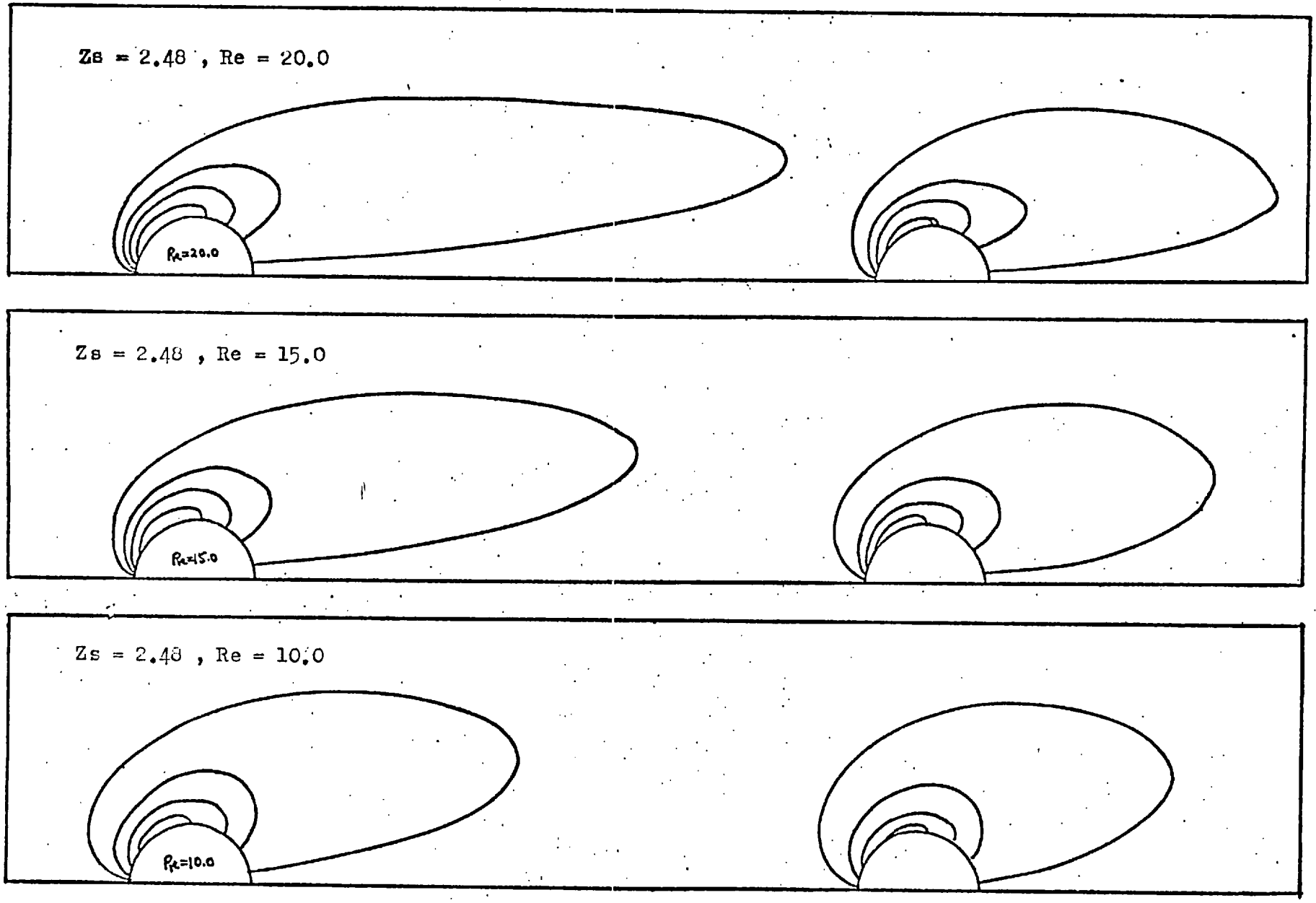

Figure(5-3-5). Vorticity distributions around two spheres with Zs = 2.48.

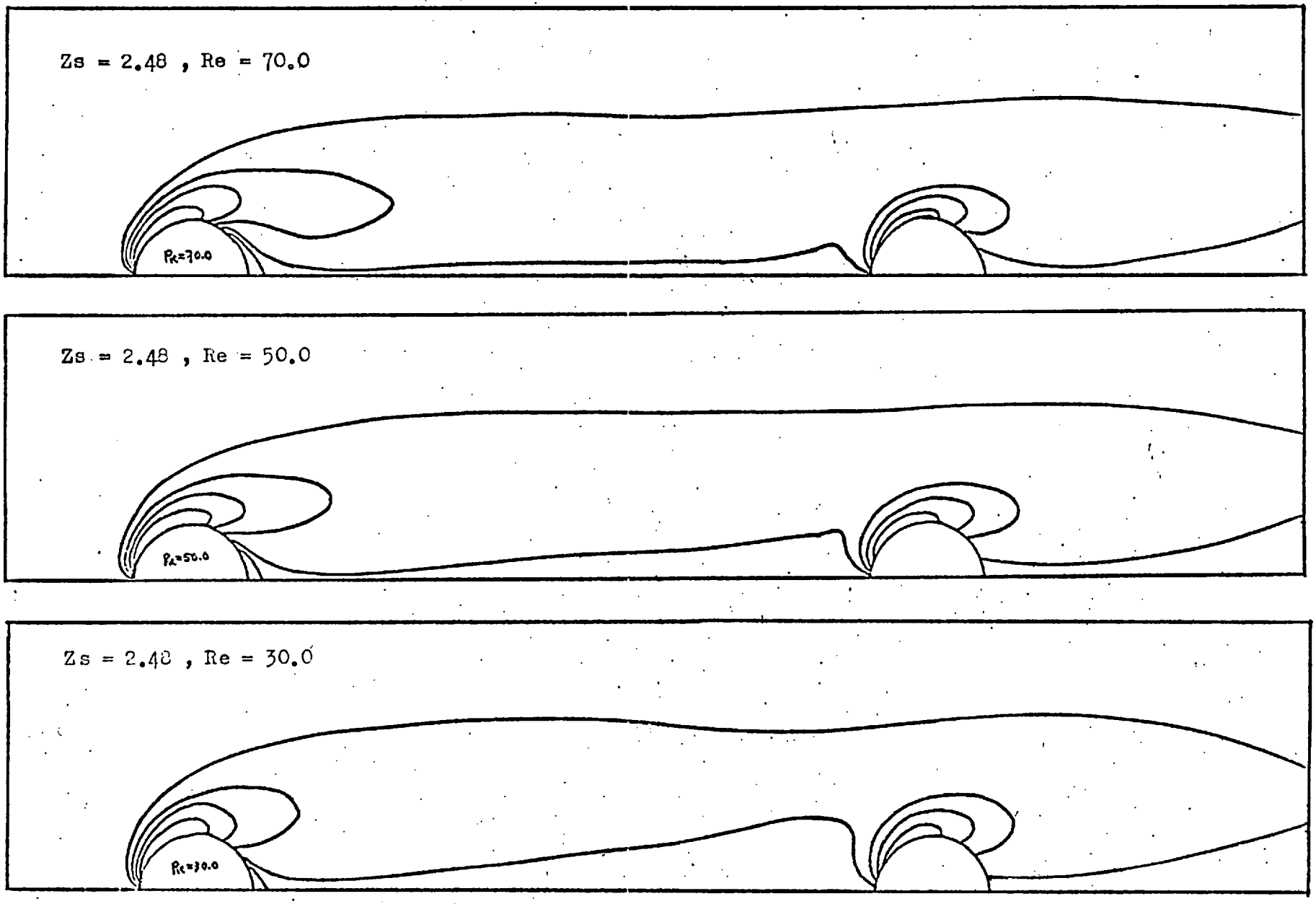

Figure(5-3-6). Vorticity distributions around two spheres with Zs = 2.48.

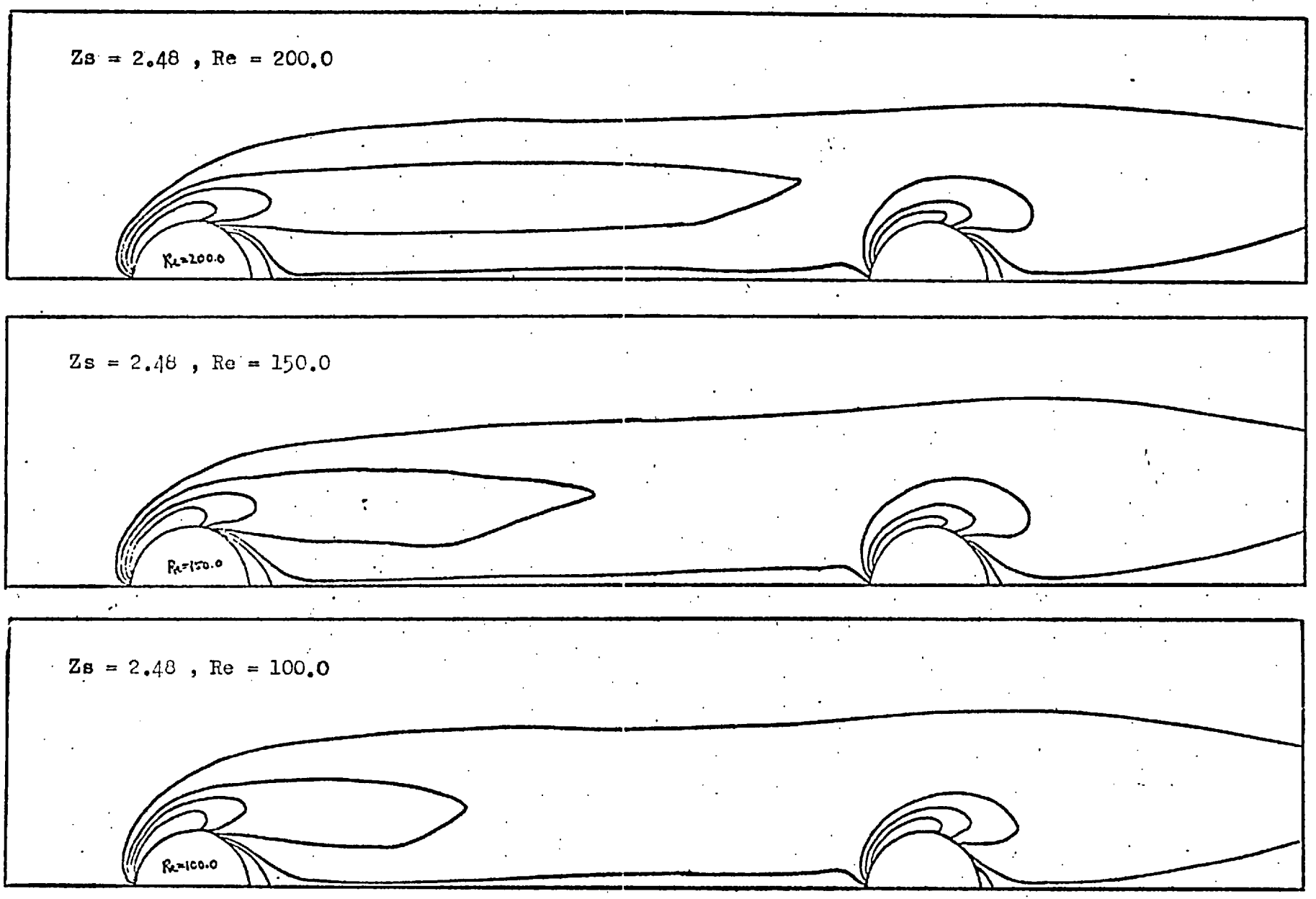

Figure(5-3-7). Vorticity distributions around two spheres with Zs = 2.48.

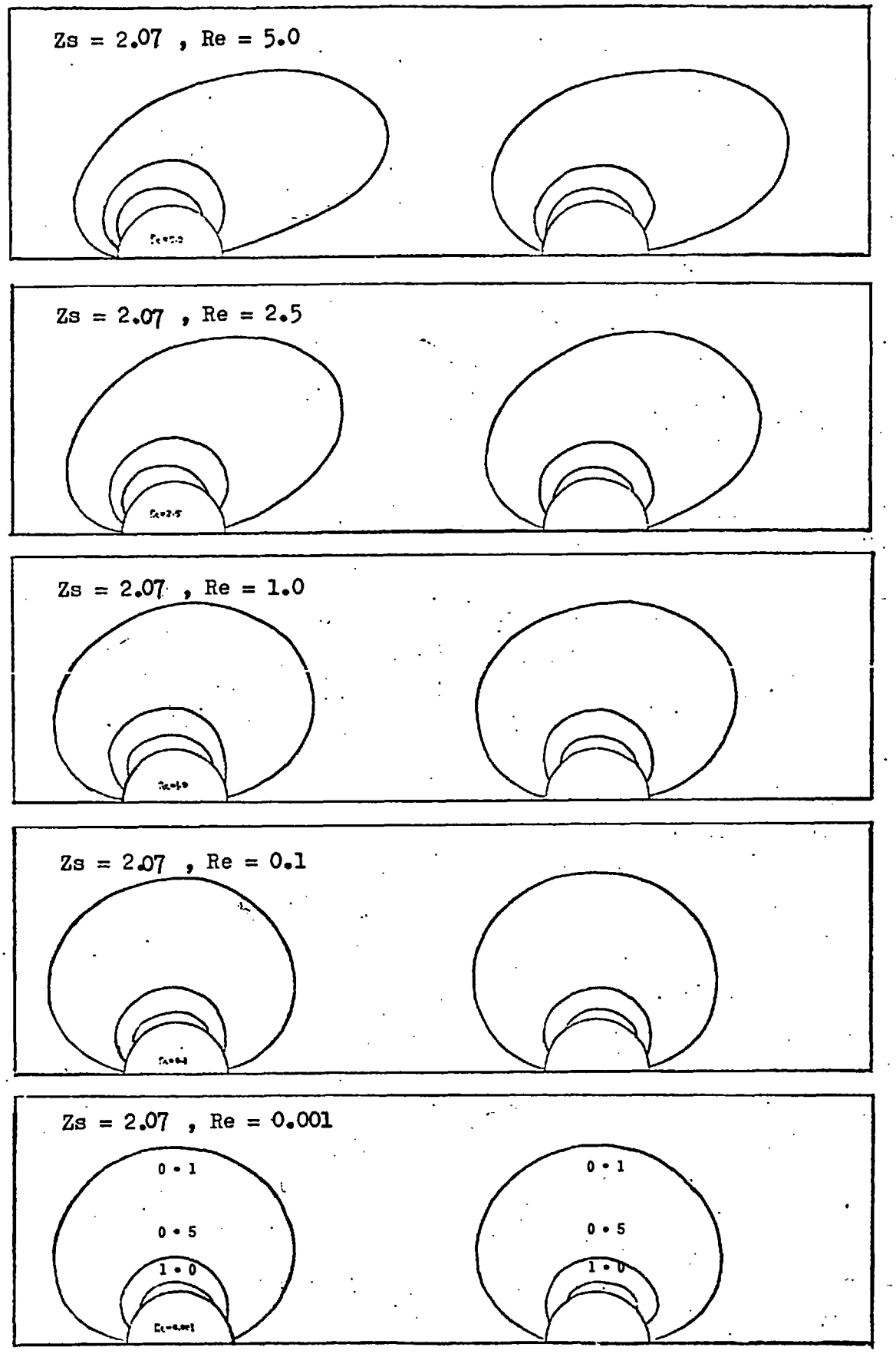

Figure(5-3-8). Vorticity distributions around two spheres with Zs = 2.07.

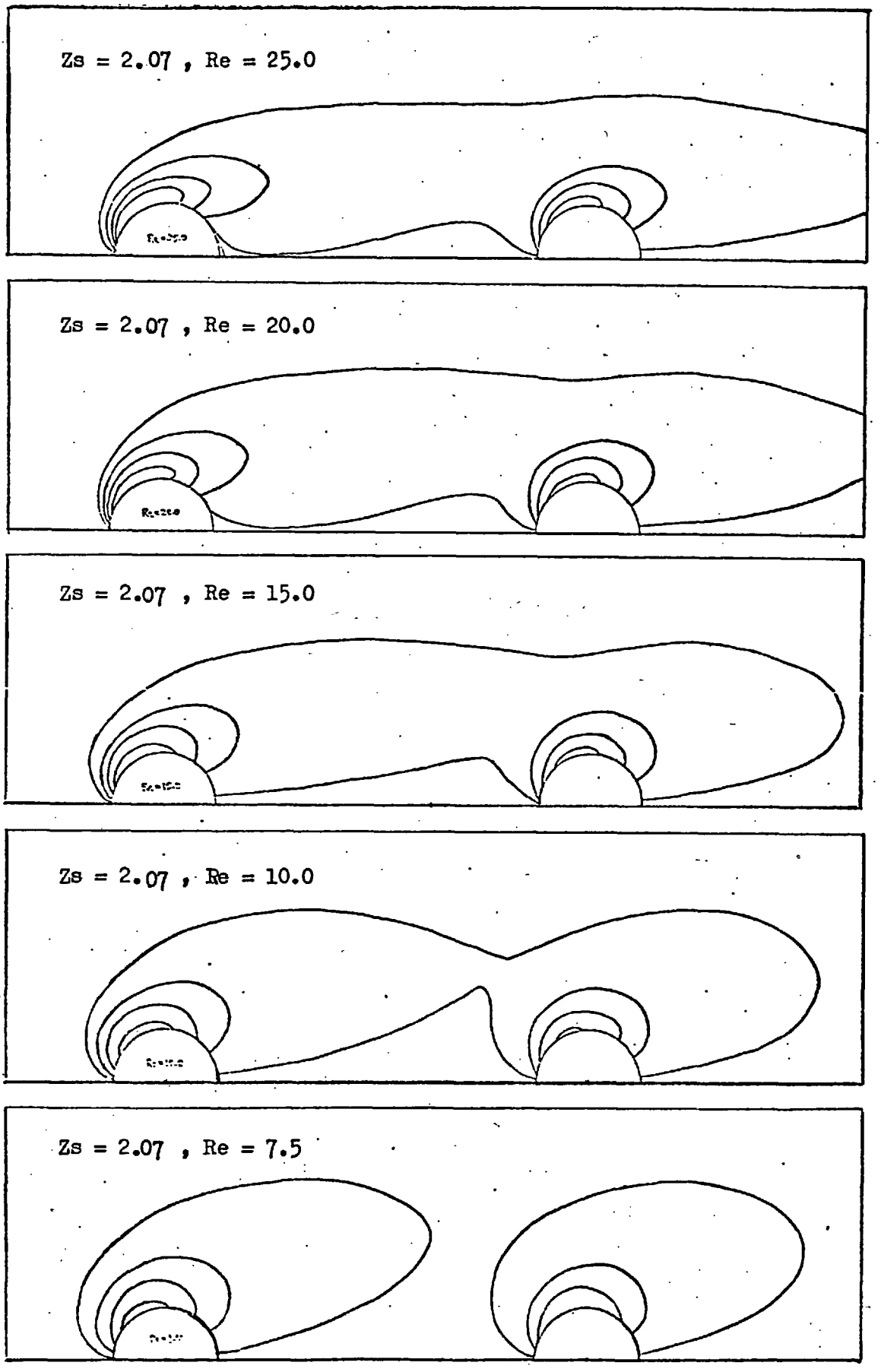

Figure (5-3-9). Vorticity distributions around two spheres with Zs = 2.07.

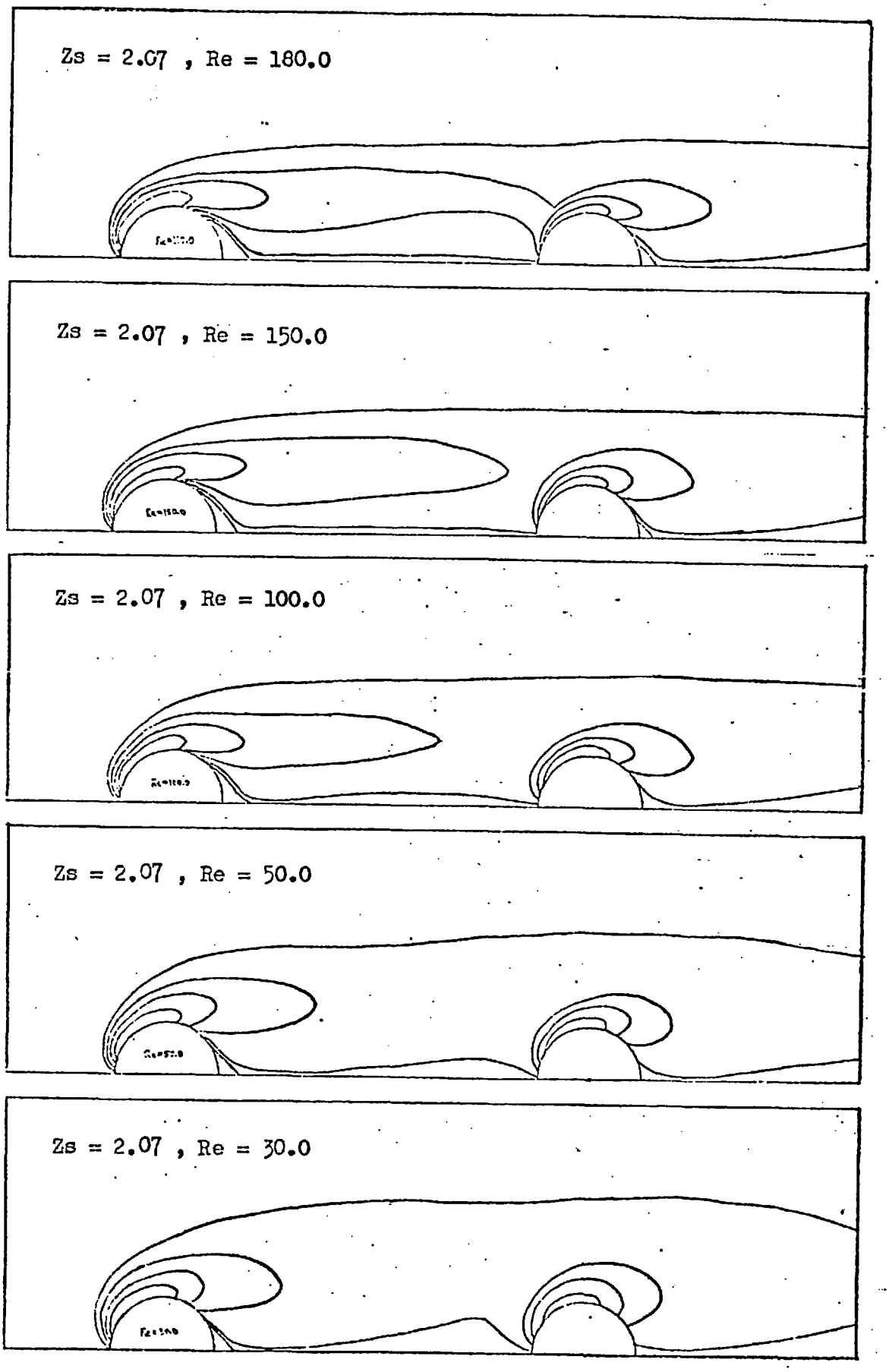

Figure(5-3-10). Vorticity distributions around two spheres with Zs = 2.07.

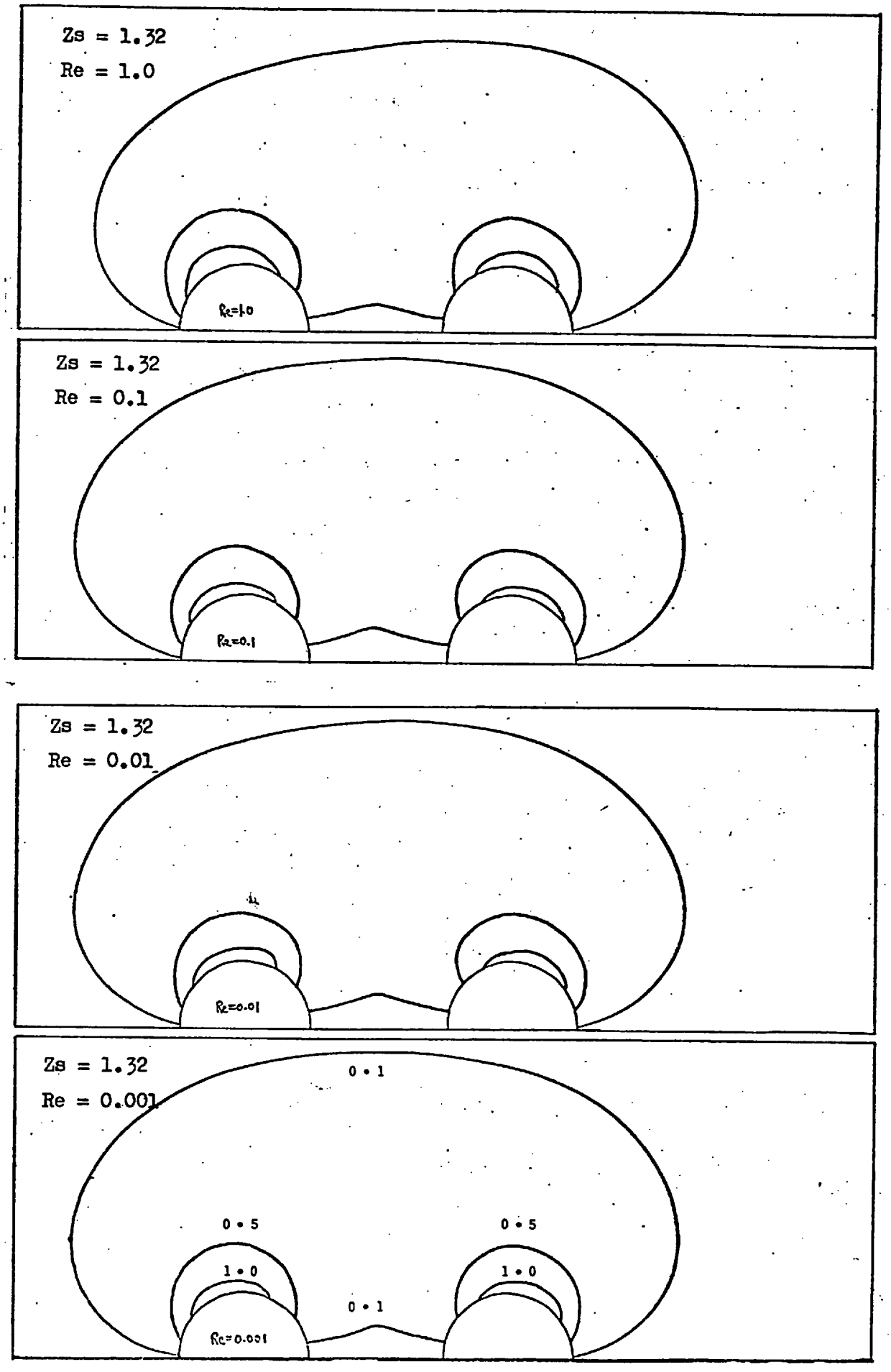

Figure(5-3-11). Vorticity distributions around two spheres with Zs = 1.32.

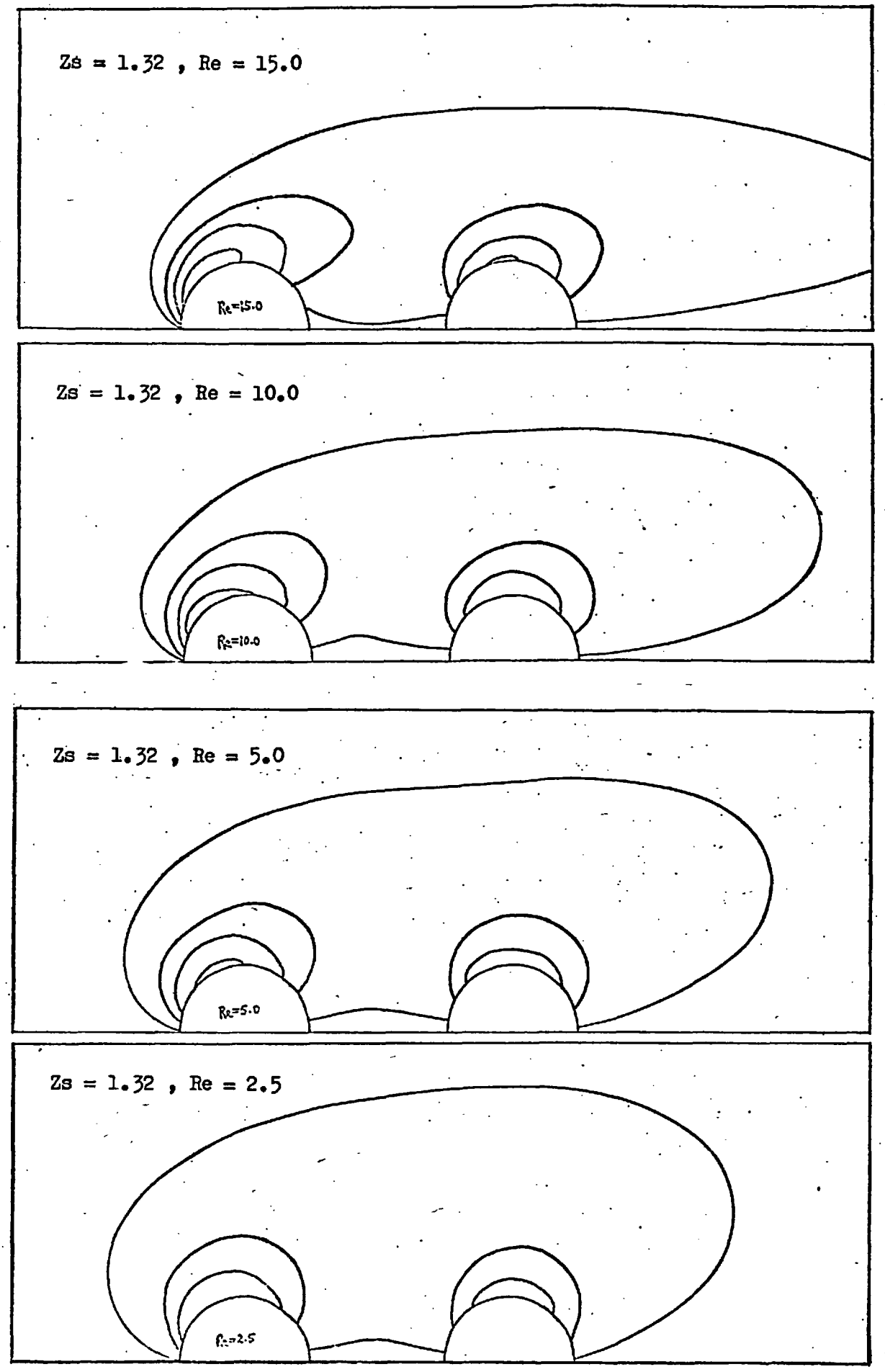

Figure(5-3-12). Vorticity distributions around two spheres with Zs = 1.32.

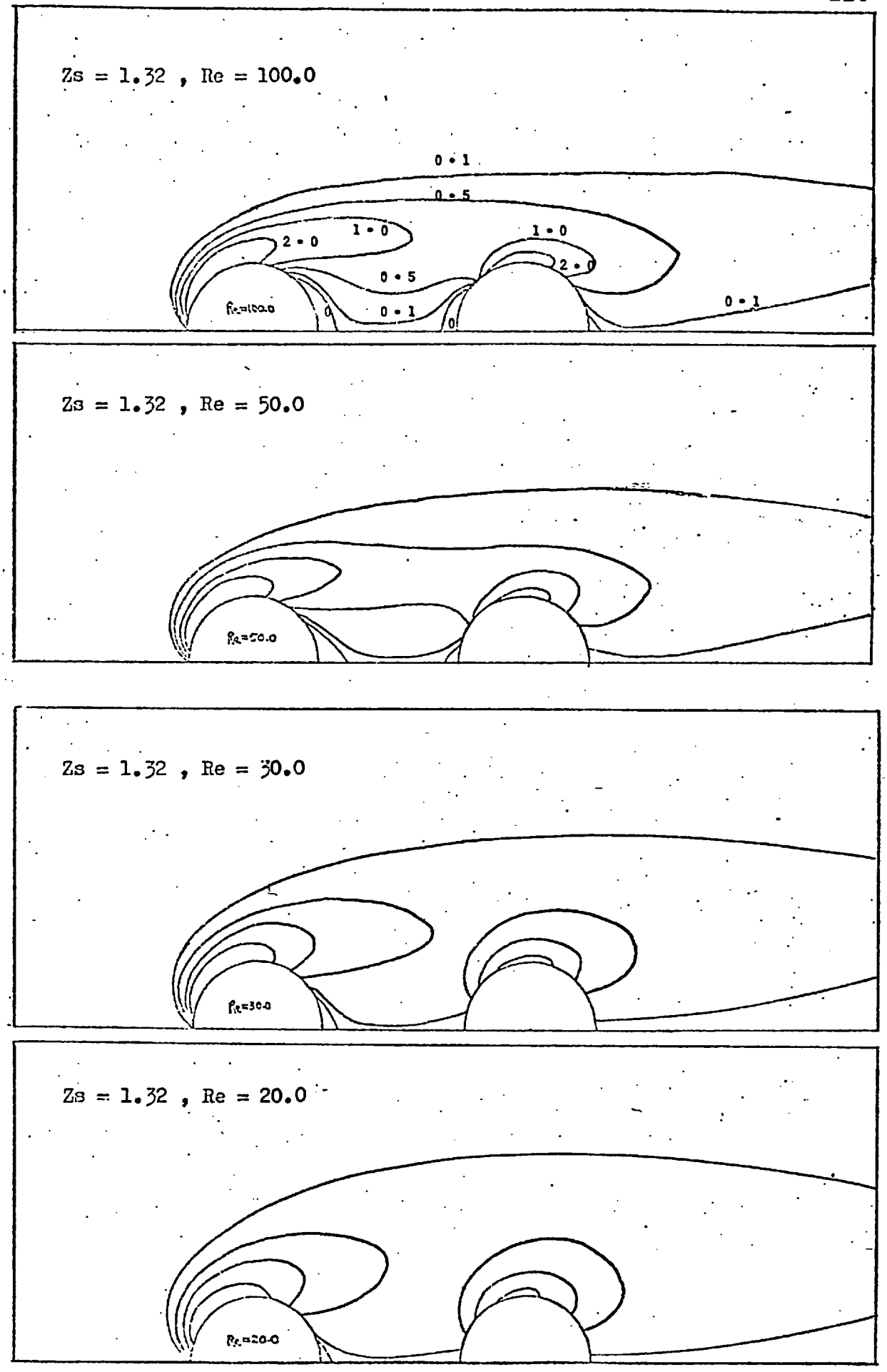

Figure(5-3-13). Vorticity distributions around two spheres with Zs = 1.32.

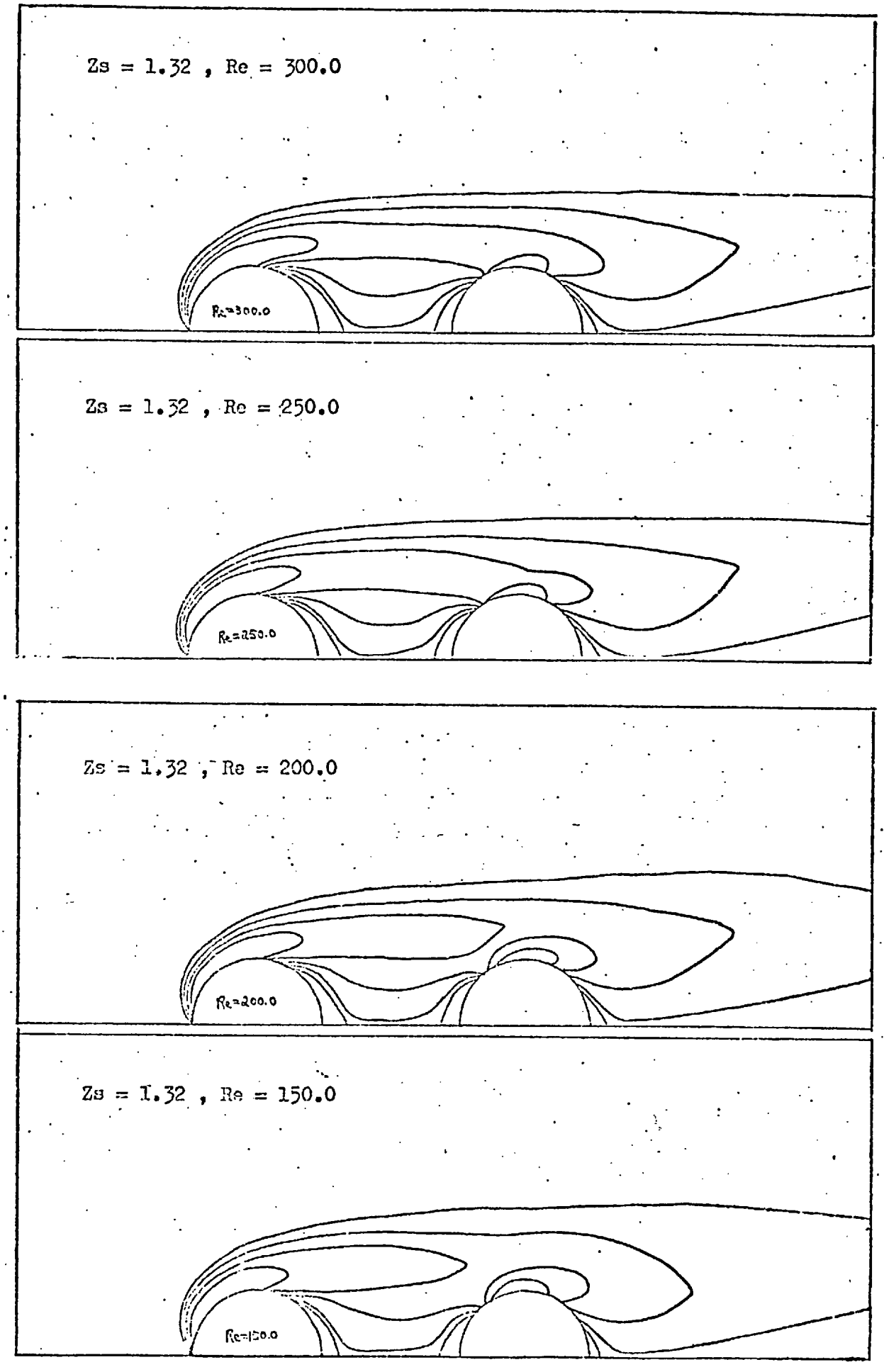

Figure(5-3-14). Vorticity distributions around two spheres with Zs = 1.32.

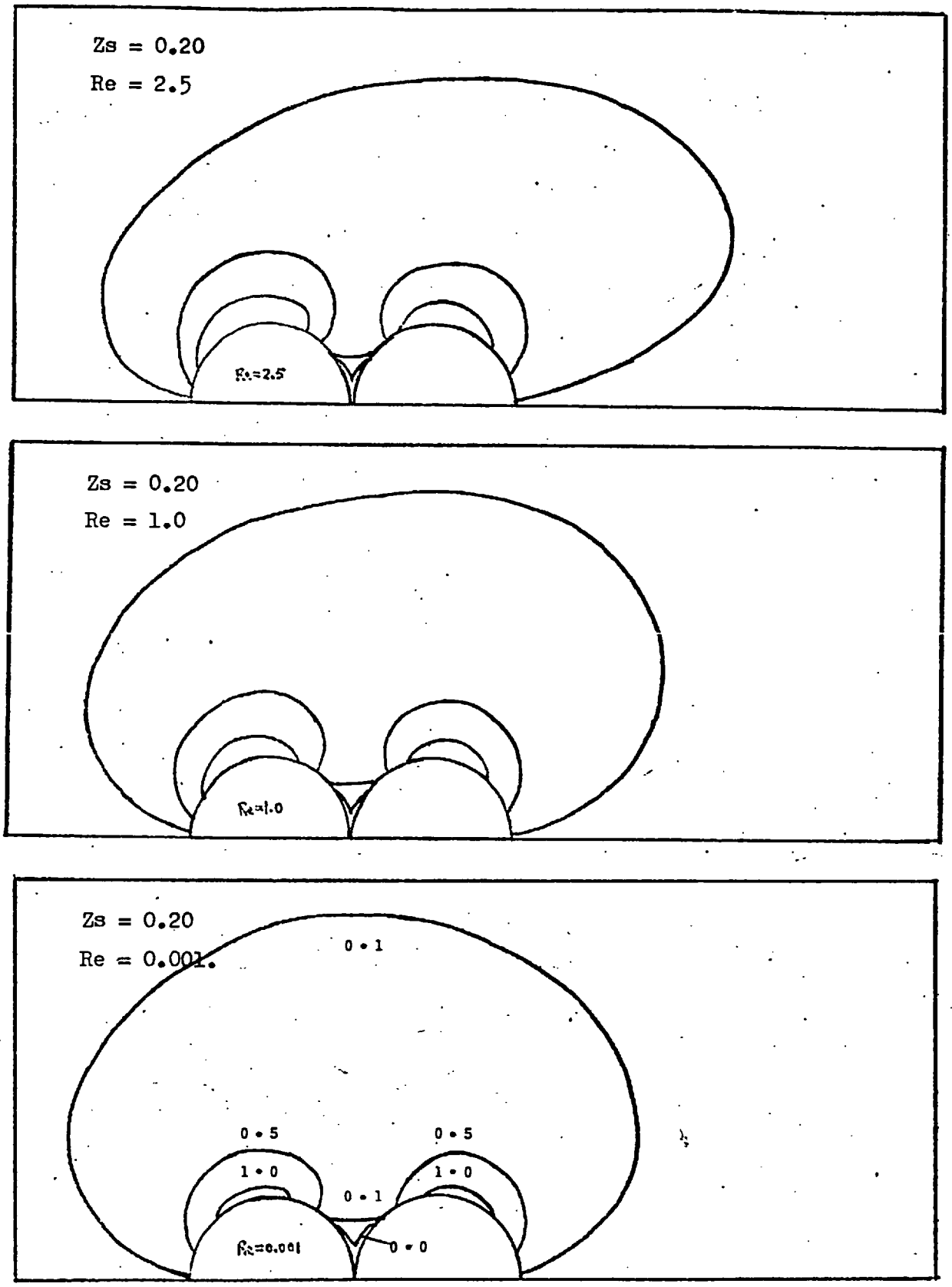

Figure(5-3-15). Vorticity distributions around two spheres with Zs = 0.20.

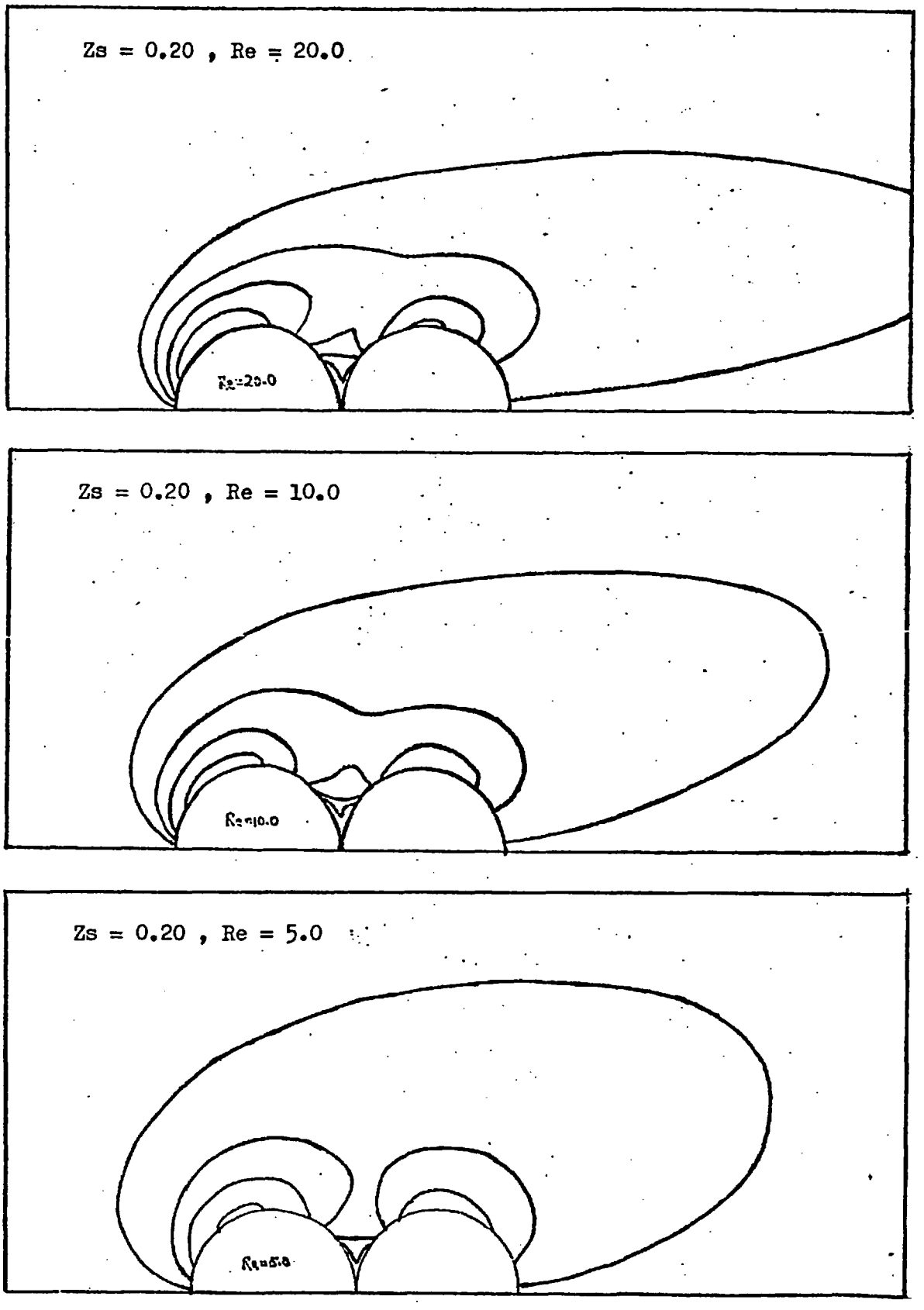

Figure(5-3-16). Vorticity distributions around two spheres with Zs = 0.20.

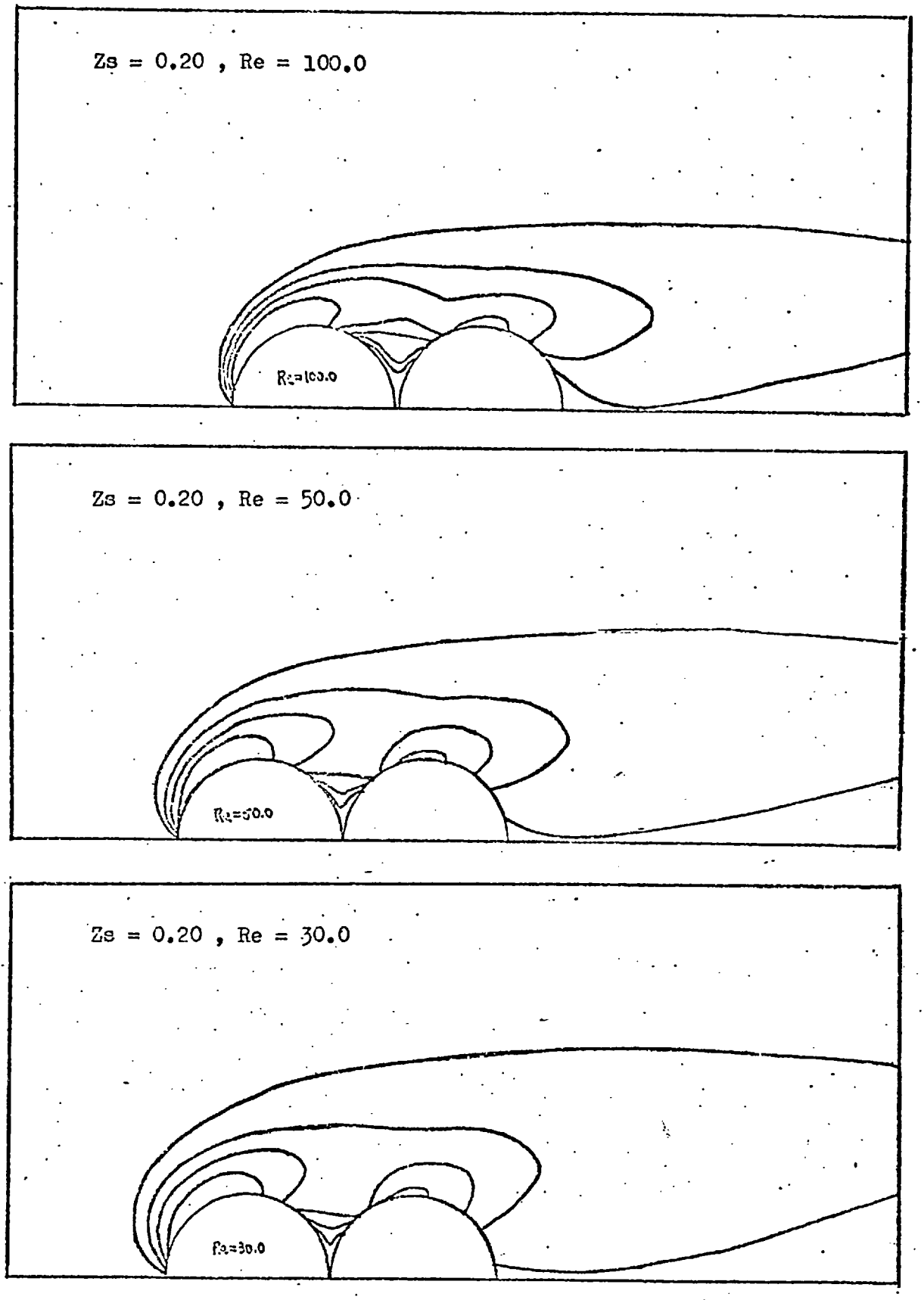

Figure(5-3-17). Vorticity distributions around two spheres with Zs = 0.20.

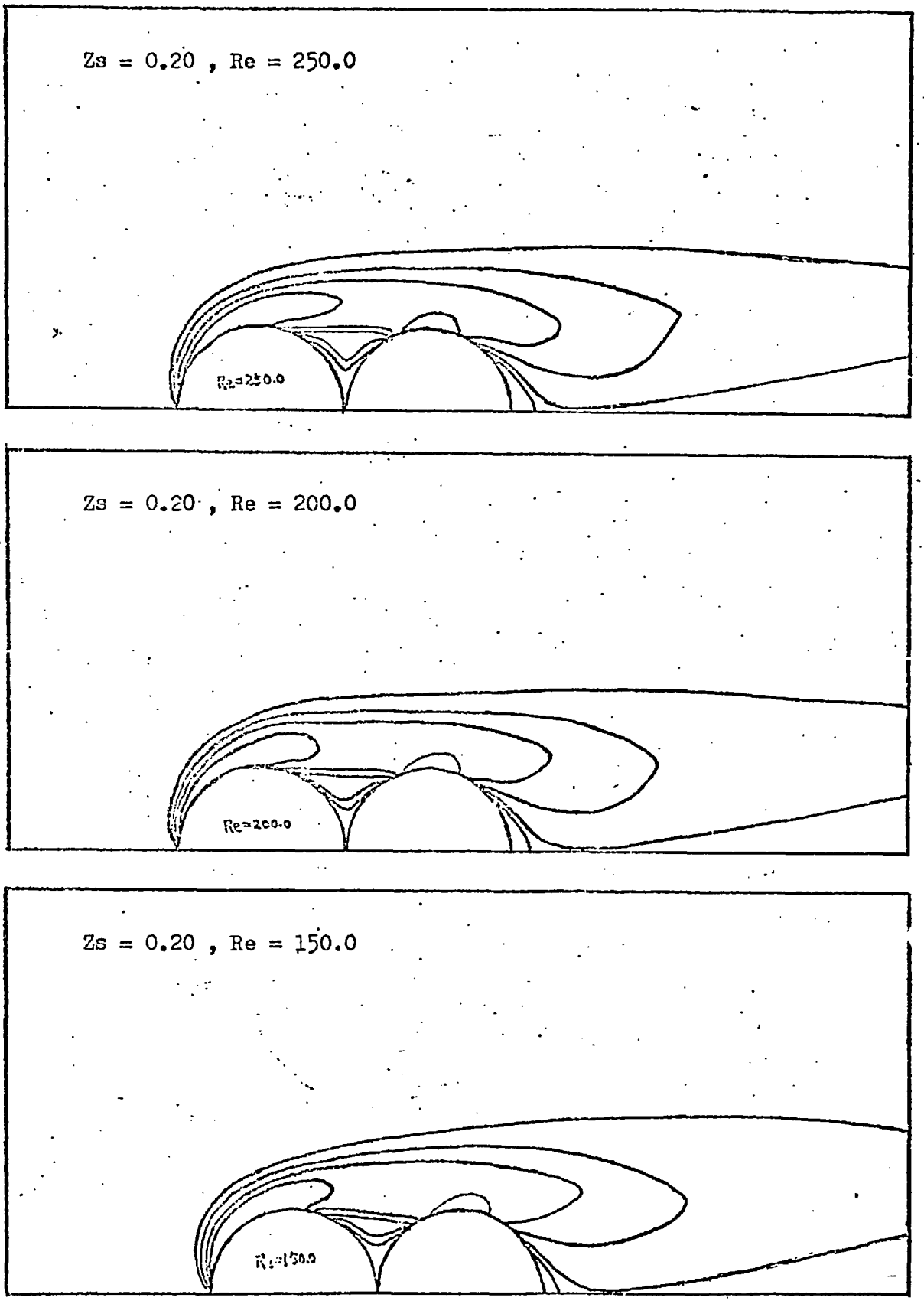

Figure(5-3-18). Vorticity distributions around two spheres with Zs = 0.20.

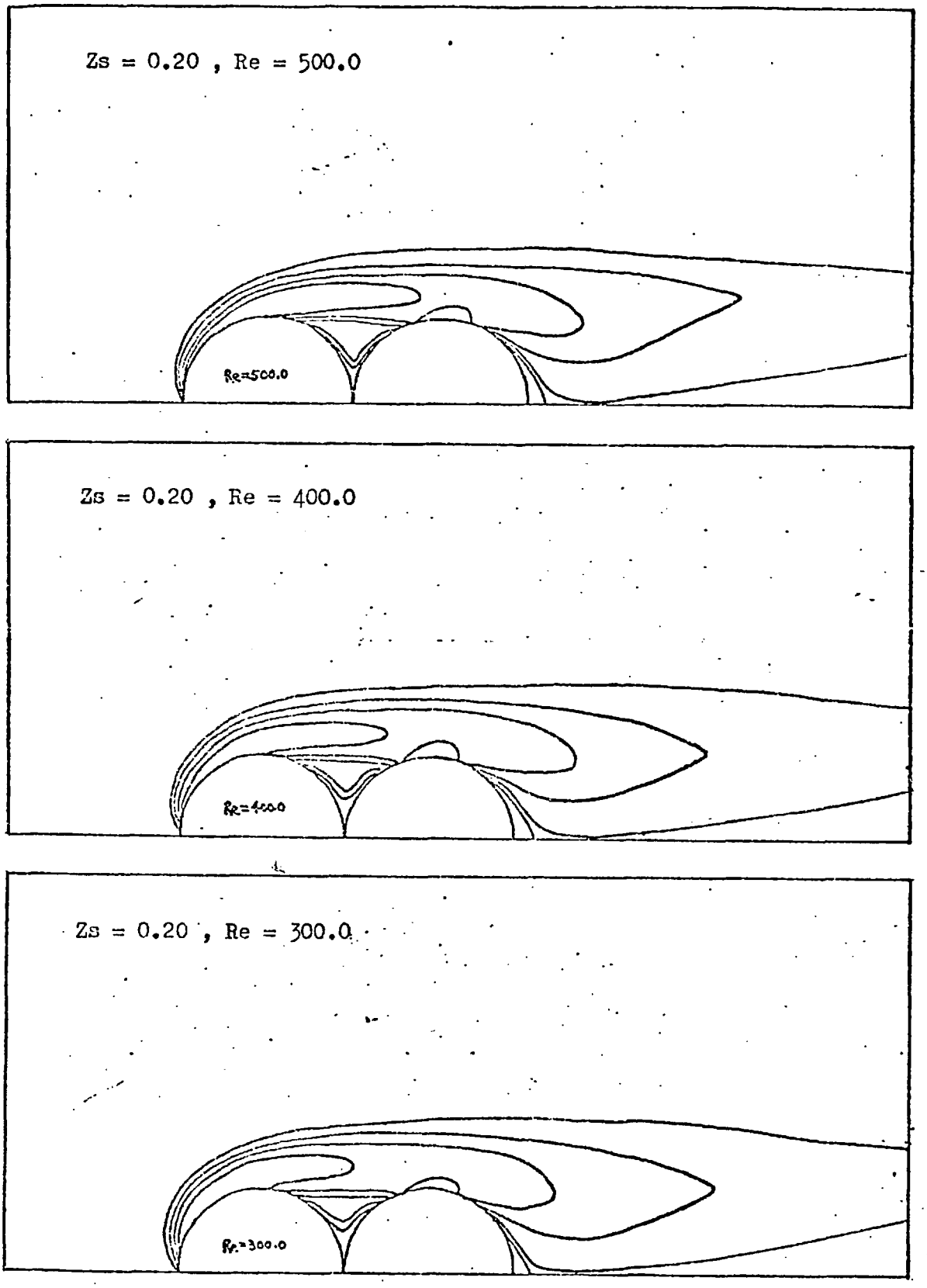

Figure(5-3-19). Vorticity distributions around two spheres with Zs = 0.20.

the spheres occurs at very low Reynolds numbers in comparison with the larger sphere spacings. For instance, for this smallest sphere spacing the formation of combined contours with large vorticities of 0.50 and 1.0 takes place at Reynolds numbers of 10 and 100, respectively; while for the sphere spacing Zs = 1.32 these combined contours are formed at Reynolds numbers of 50 and 250, respectively. As a result of this strong interaction of vorticity in the region between the spheres, the distributions of vorticity around the two nearly touching spheres become very complicated and quite different from those around a single isolated sphere. This indicates the existence of very strong particle-to-particle interaction between the spheres.

From the above discussion, it is clear that the distributions of vorticity around a system of two equally sized spheres with fluid flowing parallel to their line of centres are dependent on the Reynolds number and the sphere spacing. A brief summary of the behaviour can be summarized as follows. For each sphere spacing, the vorticity distributions at low Reynolds numbers of 0.001 to 0.1 are symmetrical about a plane through the mid-point of the line of centres normal to the direction of flow, and the diffusion of vorticity from the spheres is predominant. At higher Reynolds numbers, the vorticity is convected more rapidly rearwards than it diffuses forwards. Hence, the effect of convection upon the transport of vorticity becomes significant and increases in importance with increasing Reynolds number, however, it is always stronger for sphere A than for sphere B. As a result, at high Reynolds numbers a fluid dynamic boundary layer is developed at the upstream surface of each sphere, however, the development of

a boundary layer at the upstream surface of sphere B becomes less obvious as the sphere spacing is decreased.

Another feature of the distributions of vorticity is the interaction of the vorticities diffusing and convecting downstream from sphere A and those diffusing upstream from sphere B in the region between the spheres. The interaction of vorticity becomes apparent at a lower Reynolds number when the distance between the spheres is decreased. As a result, for each sphere spacing considered in this study the distributions of vorticity around the two spheres are always at least slightly different from those around a single isolated sphere; the difference becomes larger when the sphere spacing decreases. This indicates the existence of a particle-to-particle interaction between the spheres and the extent of interparticle interaction increases with decreasing sphere spacing.

5-4. Stream function distributions around two spheres.

The distributions of the stream function around two spheres at five different sphere spacings: Zs = 0.20, 1.32, 2.07, 2.48, and 3.09, are shown in Figures(5-4-1) to (5-4-13) for a wide range of Reynolds numbers. In each figure, five streamlines with values of ψ^* of 0, 0.1, 1.0, 2.0, and 4.0, are plotted around the spheres. It is important to note that the axis of symmetry $\theta = 0$ in the region upstream of sphere A, the surface of sphere A, the axis of symmetry $\theta = \pi$ in the region between the spheres, the surface of sphere B, and the axis of symmetry $\theta = 0$ in the region downstream of sphere B, are all coincident with the streamline with zero stream function. In these plots, a qualitative picture of the flow pattern around the spheres is presented.

For the three largest sphere spacings: Zs = 3.09, 2.48, and 2.07, the distributions of the stream function around the spheres for some selected Reynolds numbers are shown in Figures(5-4-1) to (5-4-2), Figures(5-4-3) to (5-4-5), and Figures(5-4-6) to (5-4-7), respectively. In the following discussion, it is useful and convenient to divide the region between the spheres into two regions: an inner region and an outer region. The region bounded by the rear surface of sphere A, the front surface of sphere B, and the surface of a cylinder obtained by the rotation of a straight line which is parallel to the line of centres between the spheres and is one sphere radius from it, is referred to as the inner region between the spheres; while all the other part of the region downstream of sphere A and upstream of sphere B is referred to as the outer region between the spheres. For each of the three largest sphere spacings, the

streamlines are approximately parallel to the axis of symmetry $\theta = 0$. The presence of sphere A forces the streamlines to change their direction as the fluid flows around it.In the region downstream of sphere A but upstream of sphere B, the streamline $\psi^* = 0.1$ moves into the inner region between the spheres and close to the line of centres, whereas the streamlines with larger values of stream function stay in the outer region between the spheres and are almost parallel to one another. Similarly, the streamlines change their direction once again when the fluid flows around sphere B and eventually become approximately parallel to the axis of symmetry $\theta = 0$ in the region well downstream of the sphere. It is obvious from the figures that the distributions of the stream function around the spheres at low Reynolds numbers in the range of 0.001 to 1.0 do not change much as the Reynolds number is increased and that the distributions are almost symmetrical about a plane through the mid-point of the line of centres of the spheres and normal to the direction of flow.

For Reynolds numbers greater than 1.0, the distributions of the stream function around the spheres become asymmetrical about a plane through the mid-point of the line of centres normal to the direction of flow. Upstream of each sphere the streamlines generally move closer to the surface of each sphere as well as closer to the axes of symmetry. With the exception of the streamline $\psi^* = 0.1$, the streamlines downstream of each sphere also tend to move slightly closer to the axes of symmetry. However, when flow separation from the rear surface of each sphere occurs, the streamlines generally move away from the axes of symmetry. It is important to note that the onset of flow

separation from the rear surface of sphere A always appears at a lower Reynolds number than from the rear surface of sphere B. The regions enclosed within the separated streamlines with zero stream function, which are termed the wake region, increases in extent with increasing Reynolds number. For each of the three sphere spacings, the wake region downstream of sphere A is always larger than the wake region downstream of sphere B.

For the sphere spacing Zs = 1.32, the distributions of the stream function are shown in Figures(5-4-8) to (5-4-10) for a wide range of Reynolds numbers from 0.001 to 300. The main difference between the flow patterns around the spheres at this sphere spacing and those at larger sphere spacings is that for all Reynolds numbers, the streamline $\psi^* = 0.1$ does not move into the inner region between the spheres and does not come close to the upstream surface of sphere B. When the Reynolds number reaches 100, the streamline $\psi^* = 0.1$ becomes almost parallel to the streamlines with larger values of the stream function and remains outside of the inner region between the spheres; hence, almost the entire inner region between the spheres is contained within the volume bounded by the streamline with zero stream function(wake region). Flow separation from the rear surface of sphere A first appears at a Reynolds number of 20 and as the Reynolds number increases the separated region extends downstream of the sphere towards the upstream surface of sphere B. At a Reynolds number of 70 the streamline with zero stream function reaches the upstream surface of sphere B and a backward flow is induced in the inner region between the spheres. This development continues until at a Reynolds number

of 100 most of the inner region between the spheres becomes a wake region. In addition, at a Reynolds number of 100 another wake region appears in the region downstream of sphere B, however, it is always small compared with that in the inner region between the spheres.

For the smallest sphere spacing considered in this study: Zs = 0.20, the stream function distributions around the two nearly touching spheres are shown in Figures(5-4-11) to (5-4-13) for Reynolds numbers ranging from 0.001 to 500. With the exception of the streamline with zero stream function, which separates from the rear surface of sphere A and reaches the front surface of sphere B at a Reynolds number as low as 0.001, the distributions of the streamlines around the spheres and their variation with Reynolds number are similar to those obtained for the sphere spacing Zs = 1.32. Hence, a wake region always exists in the tiny region between the spheres, and when the Reynolds number reaches 100 it nearly occupies the whole region. On the other hand, the separation of the streamline with zero stream function from the rear surface of sphere B does not appear for a Reynolds number less than 200. As the streamline $\psi^* = 0.1$ and the streamlines with larger values of the stream function always lie outside of the inner region between the spheres and are approximately parallel to each other, it is obvious that the two nearly touching spheres behave like a single combined object when the fluid flows around them.

From the above discussion, it is clear that the stream function distributions around a system of two equally sized

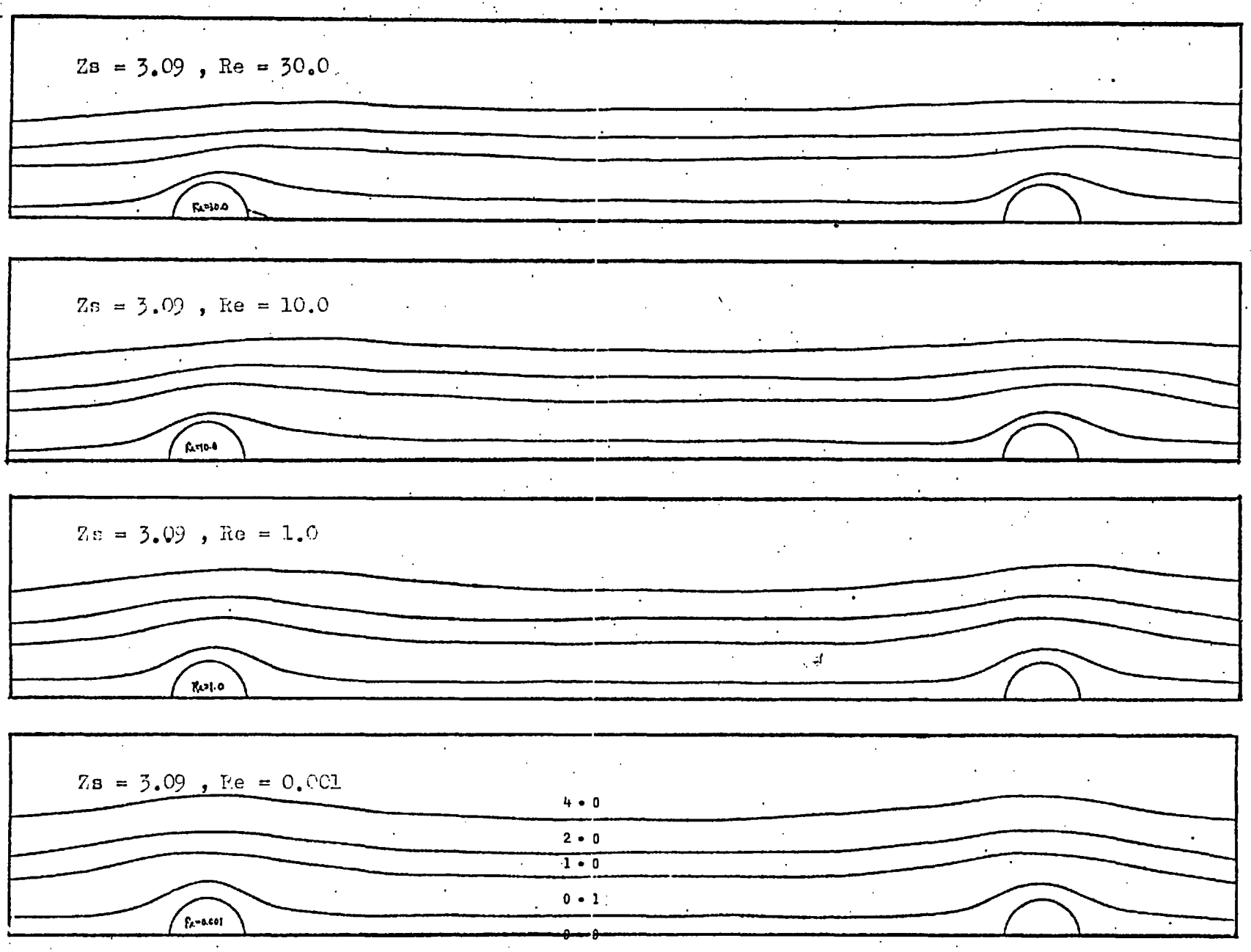

Figure(5-4-1). Stream function distributions around two spheres with Zs = 3.09.

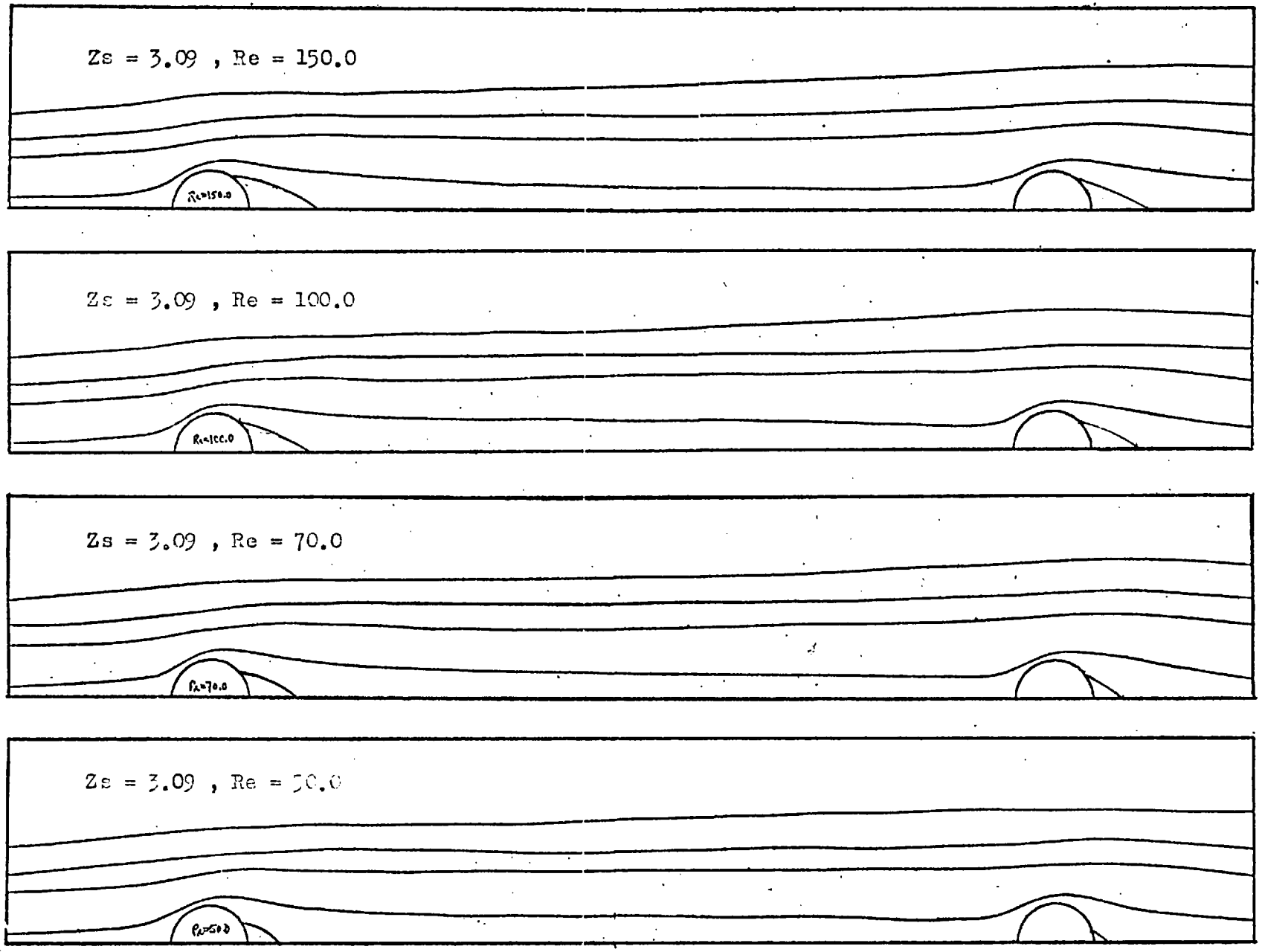

Figure(5-4-2). Stream function distributions around two spheres with Zs = 3.09.

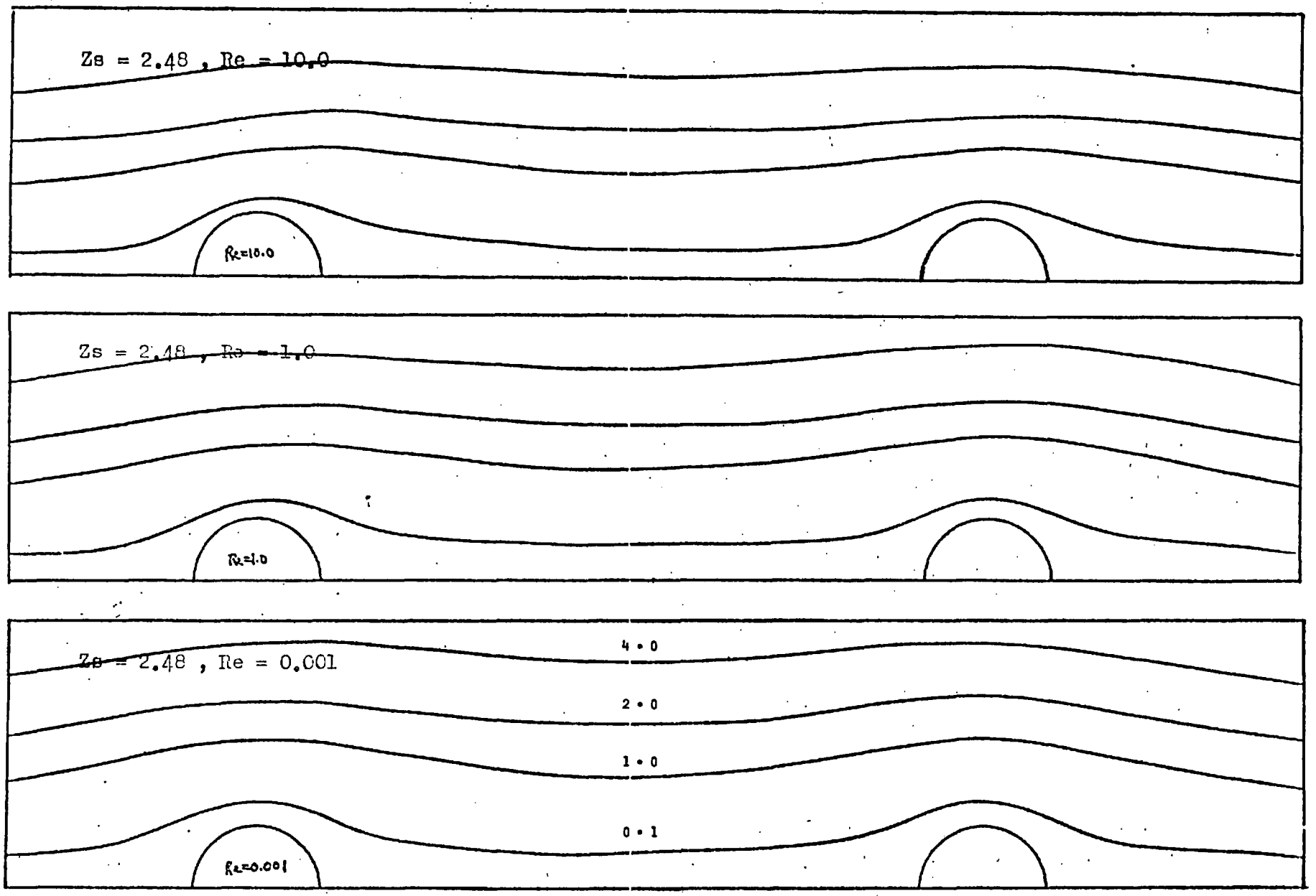

Figure(5-4-3). Stream function distributions around two spheres with Zs = 2.48.

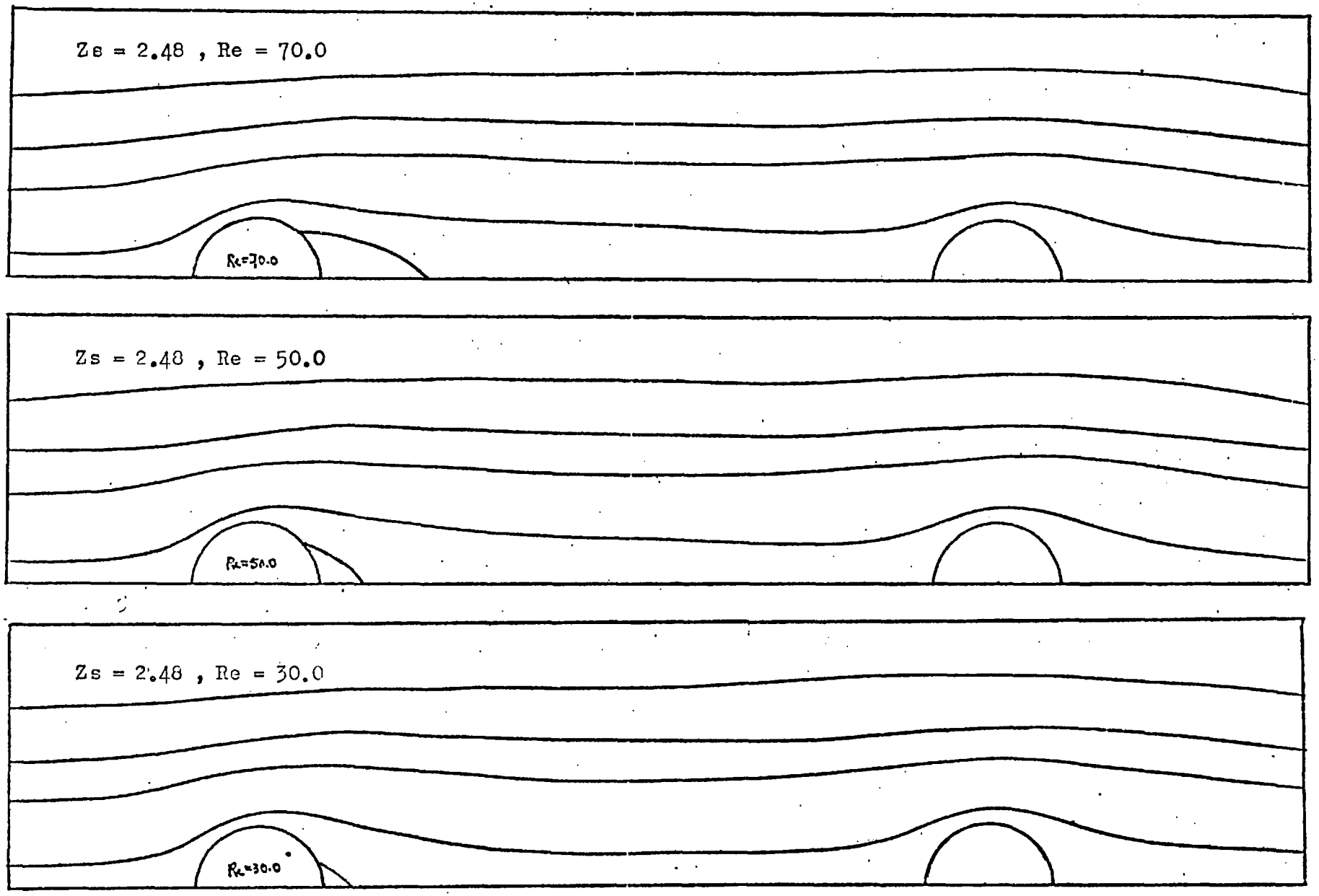

Figure(5-4-4). Stream function distributions around two spheres with Zs = 2.48.

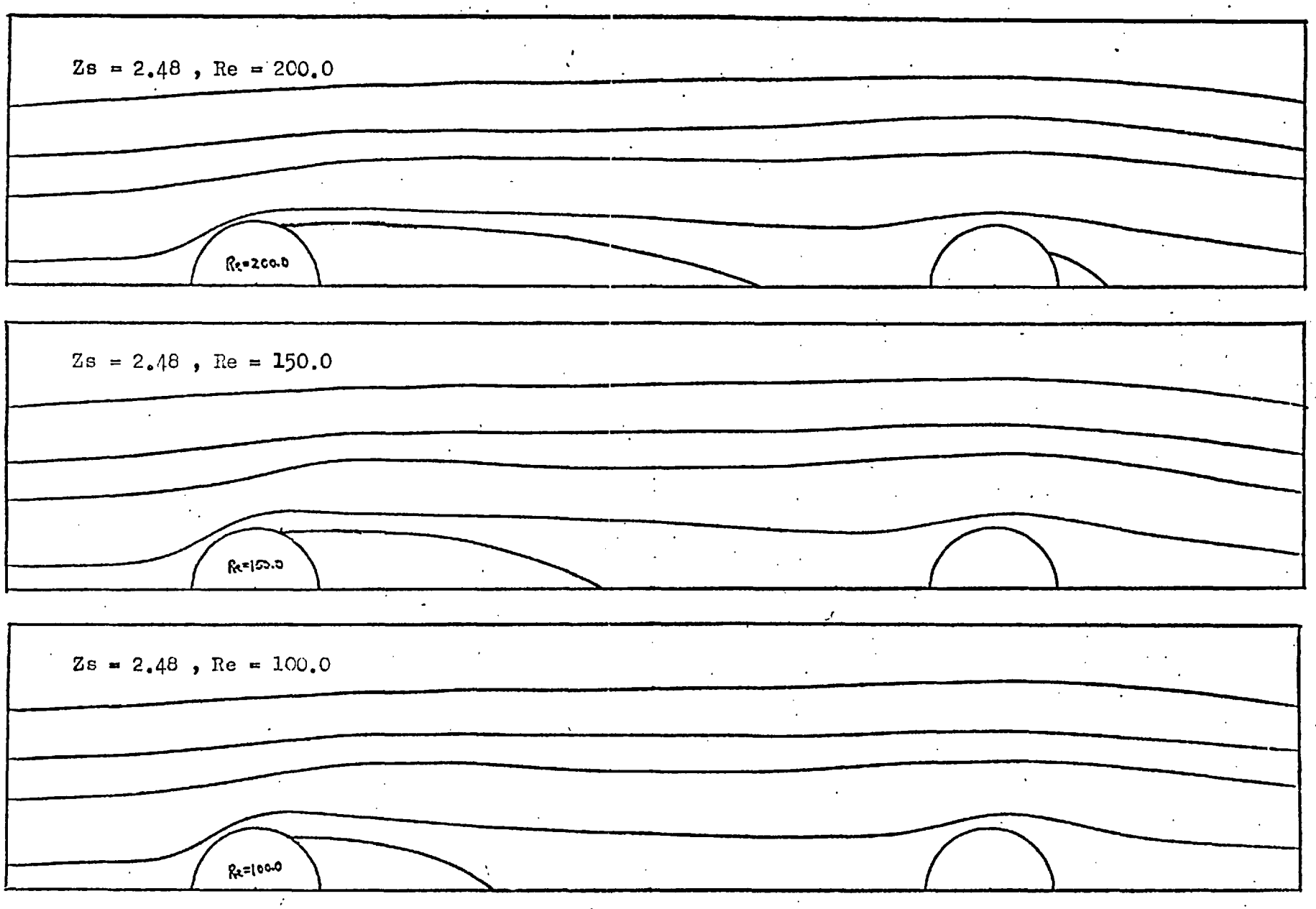

Figure(5-4-5). Stream function distributions around two spheres with Zs = 2.48.

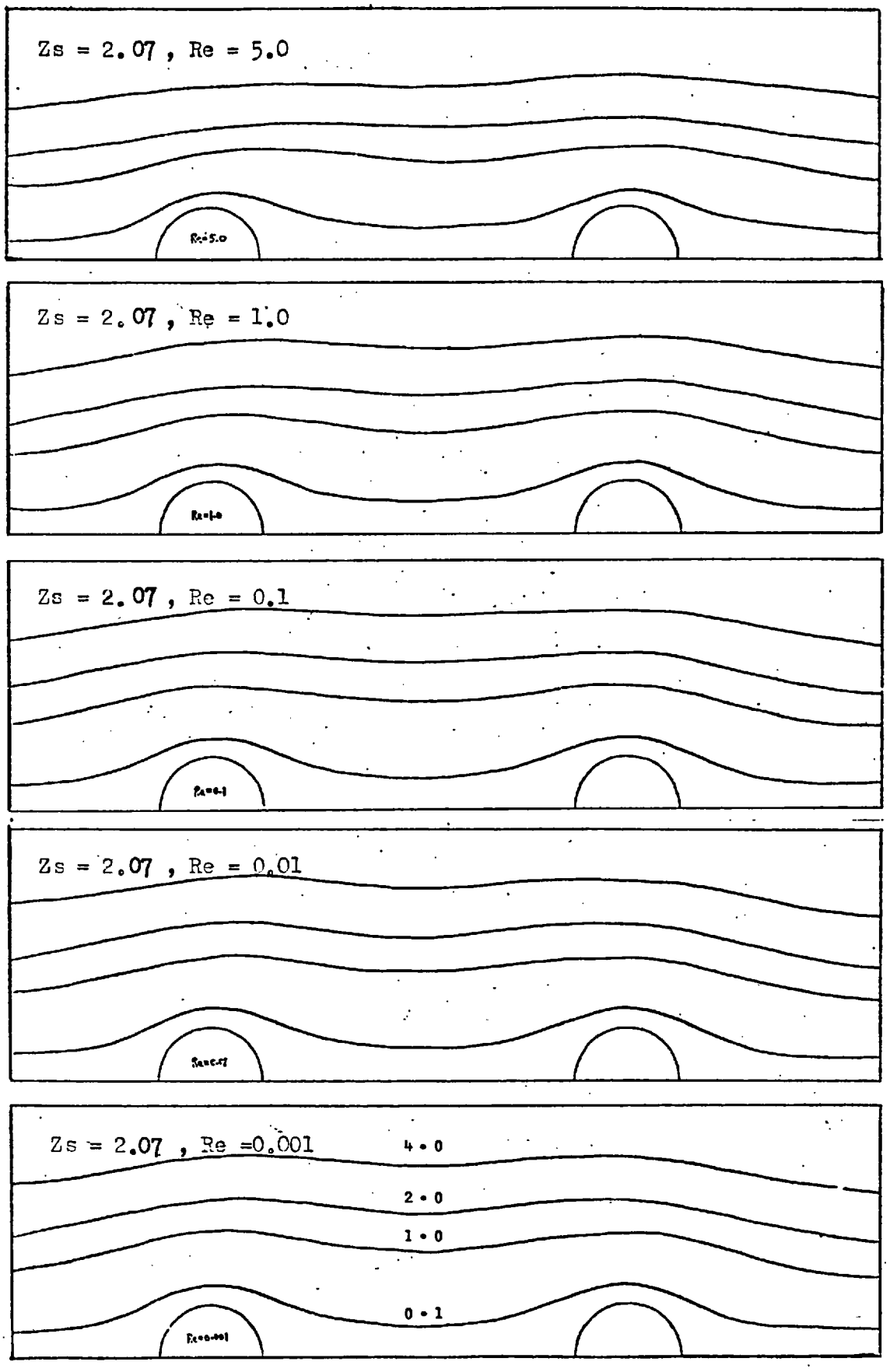

Figure(5-4-6). Stream function distributions around two spheres with Zs = 2.07.

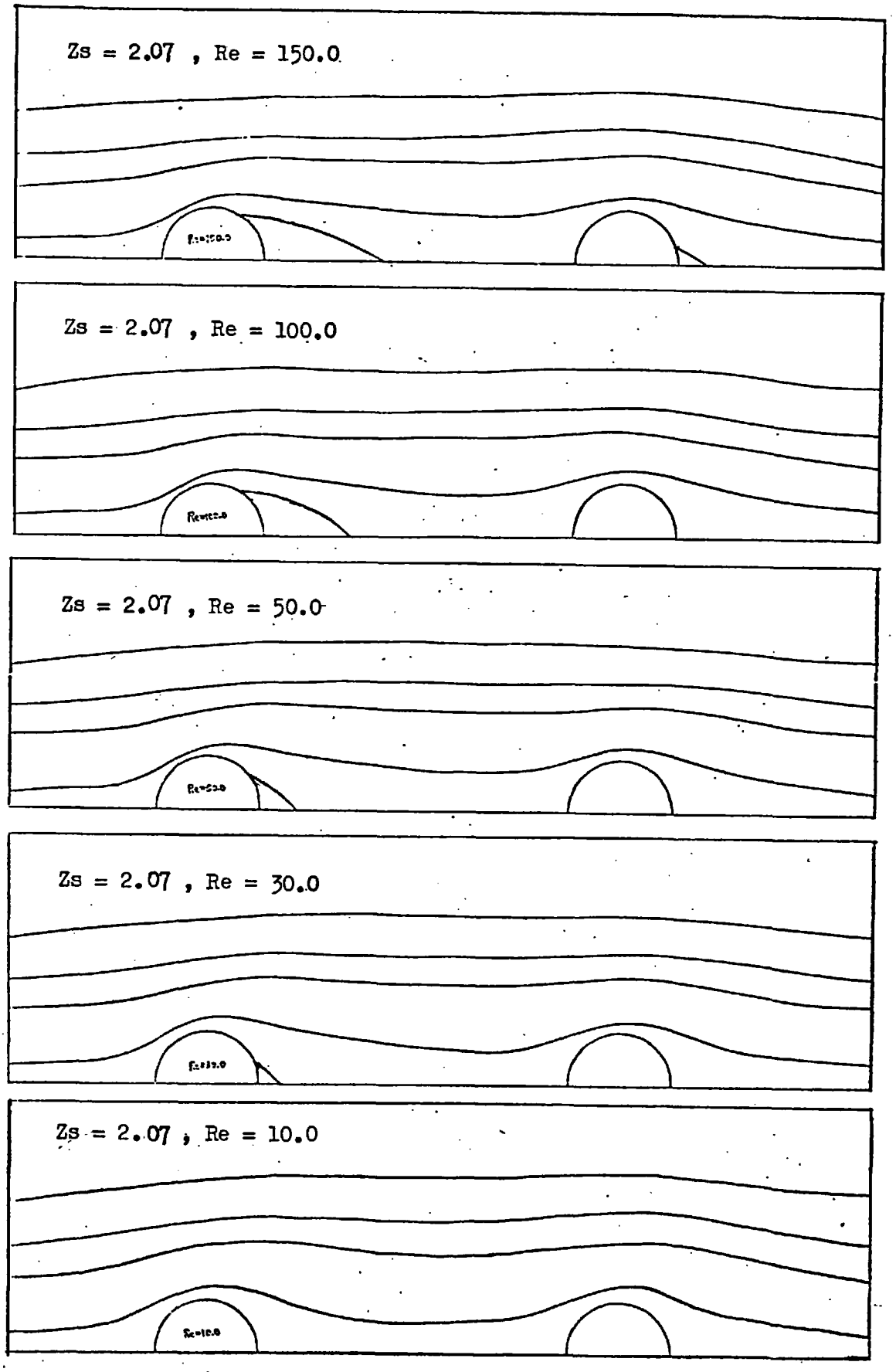

Figure(5-4-7). Stream function distributions around two spheres with Zs = 2.07.

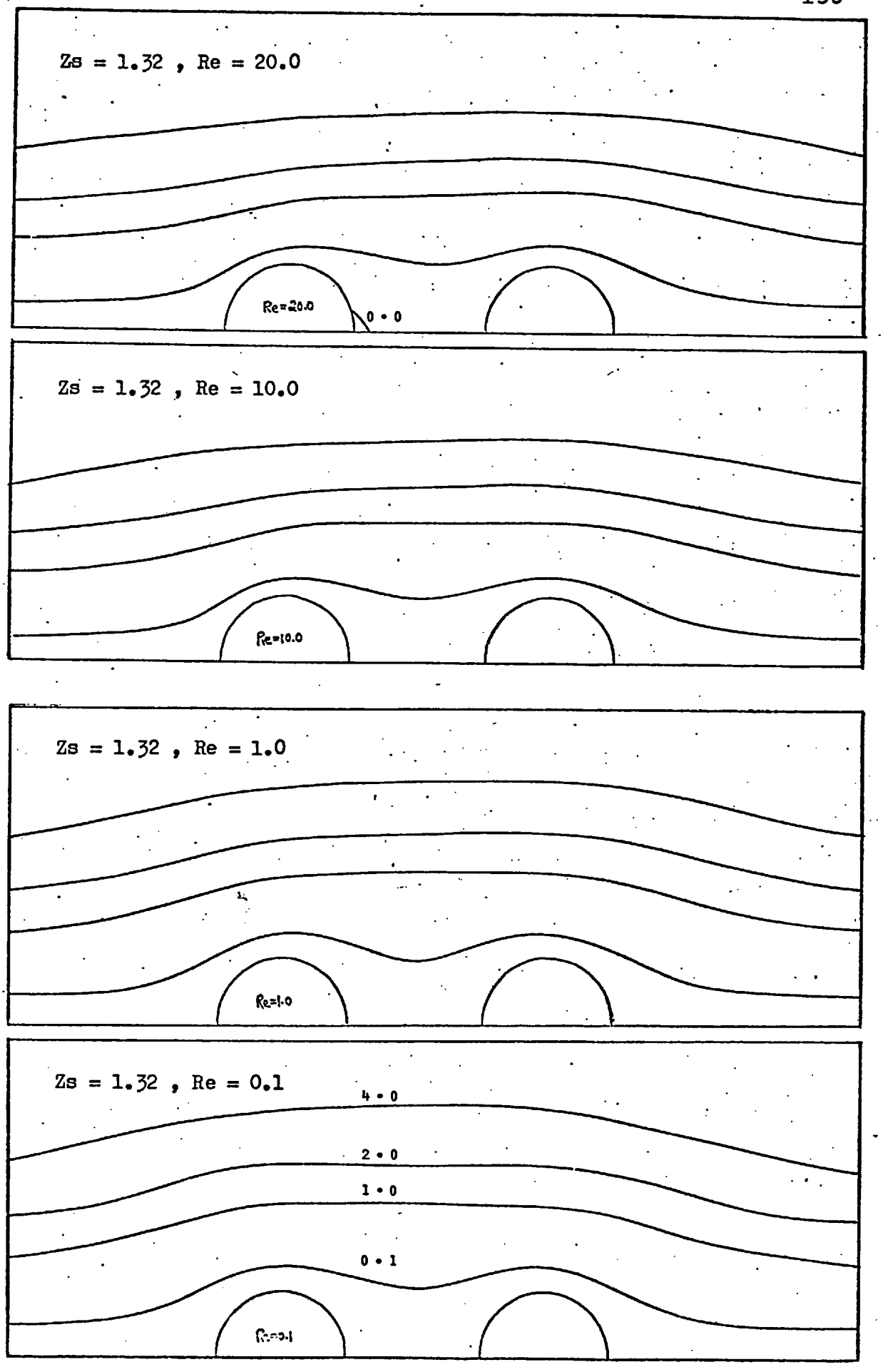

Figure(5-4-8). Stream function distributions around two spheres with Zs = 1.32.

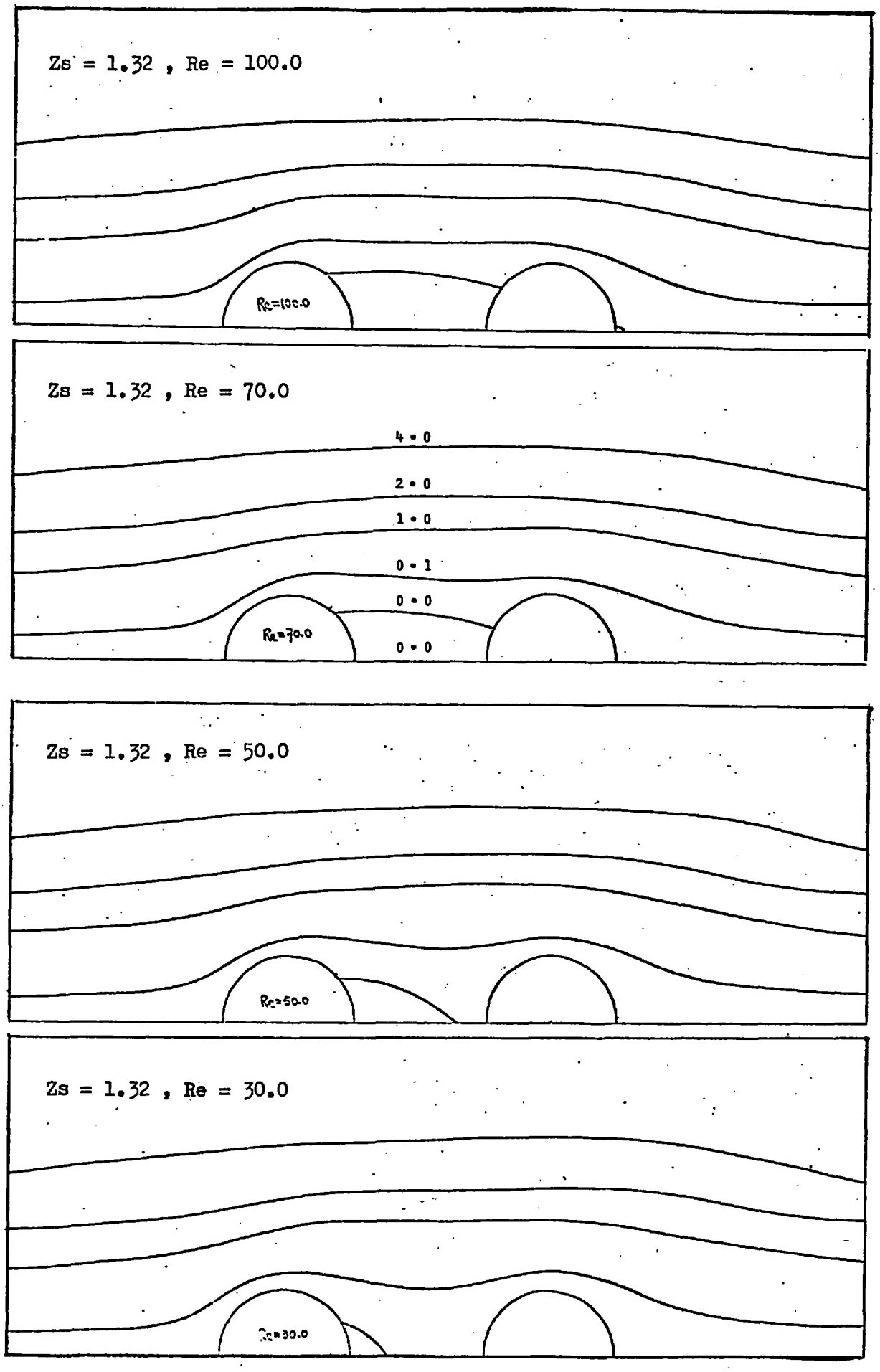

Figure(5-4-9). Stream function distributions around two spheres with Zs = 1.32.

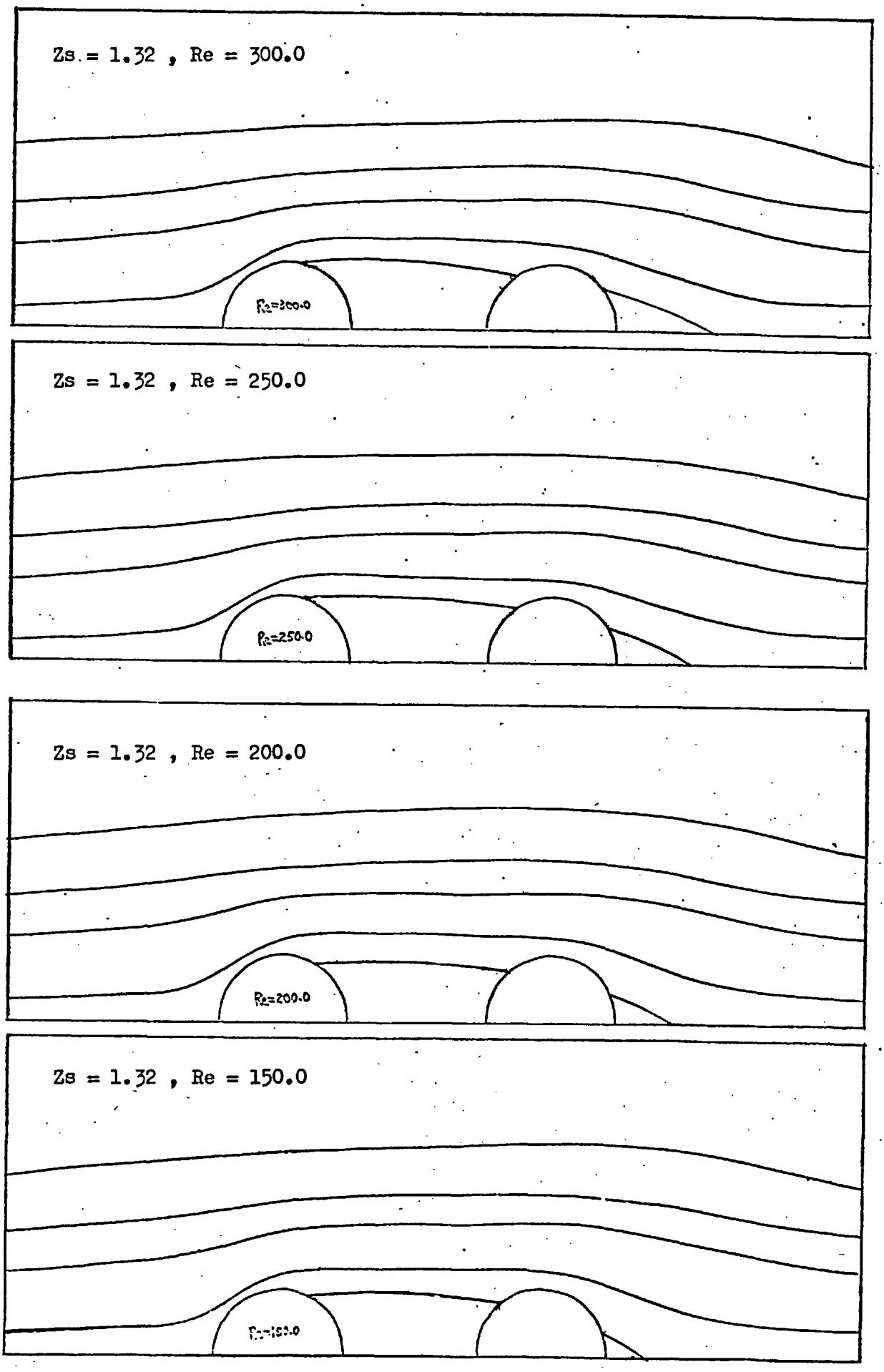

Figure(5-4-10). Stream function distributions around two spheres with Zs = 1.32.

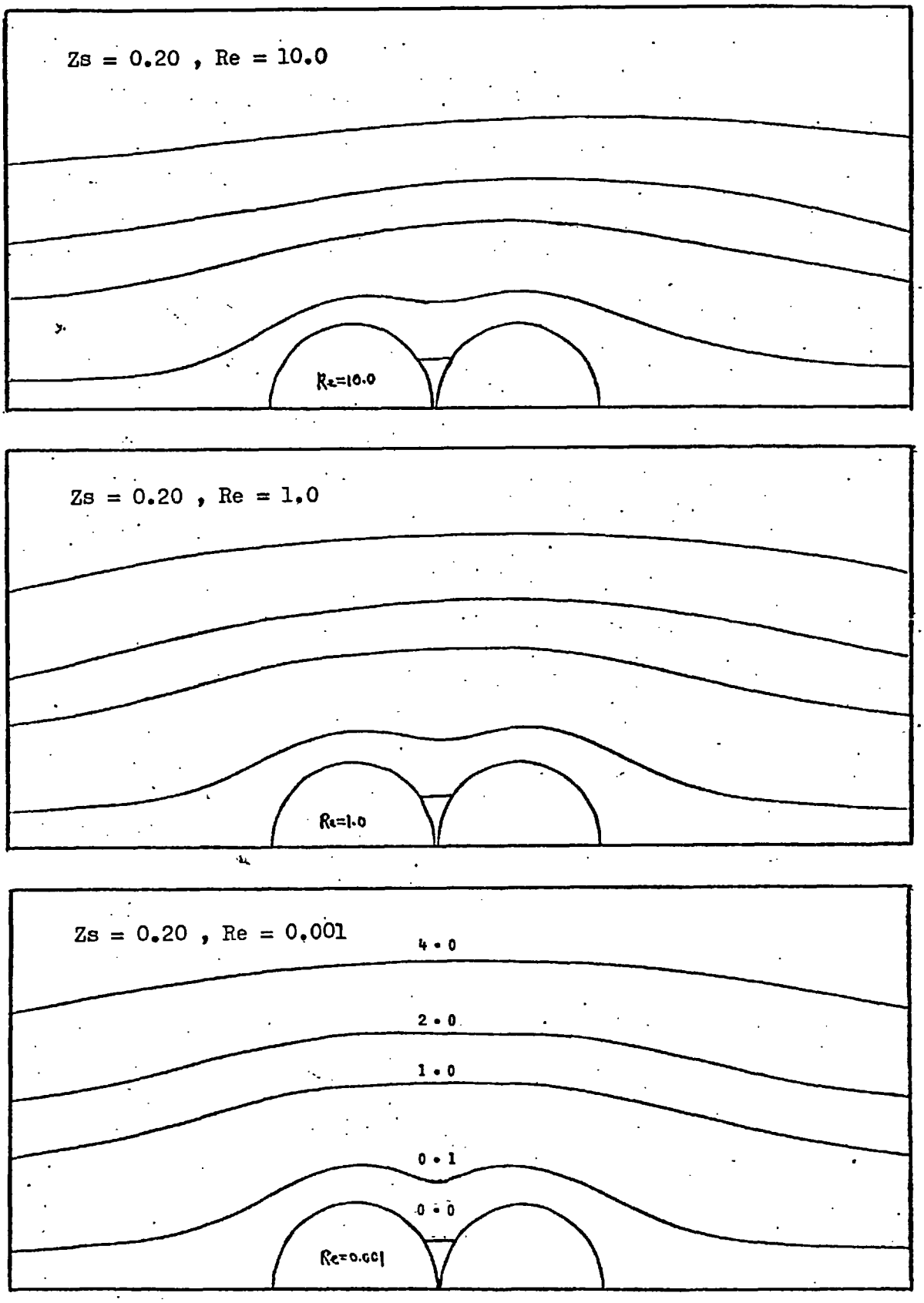

Figure(5-4-11). Stream function distributions around two spheres with Zs = 0.20.

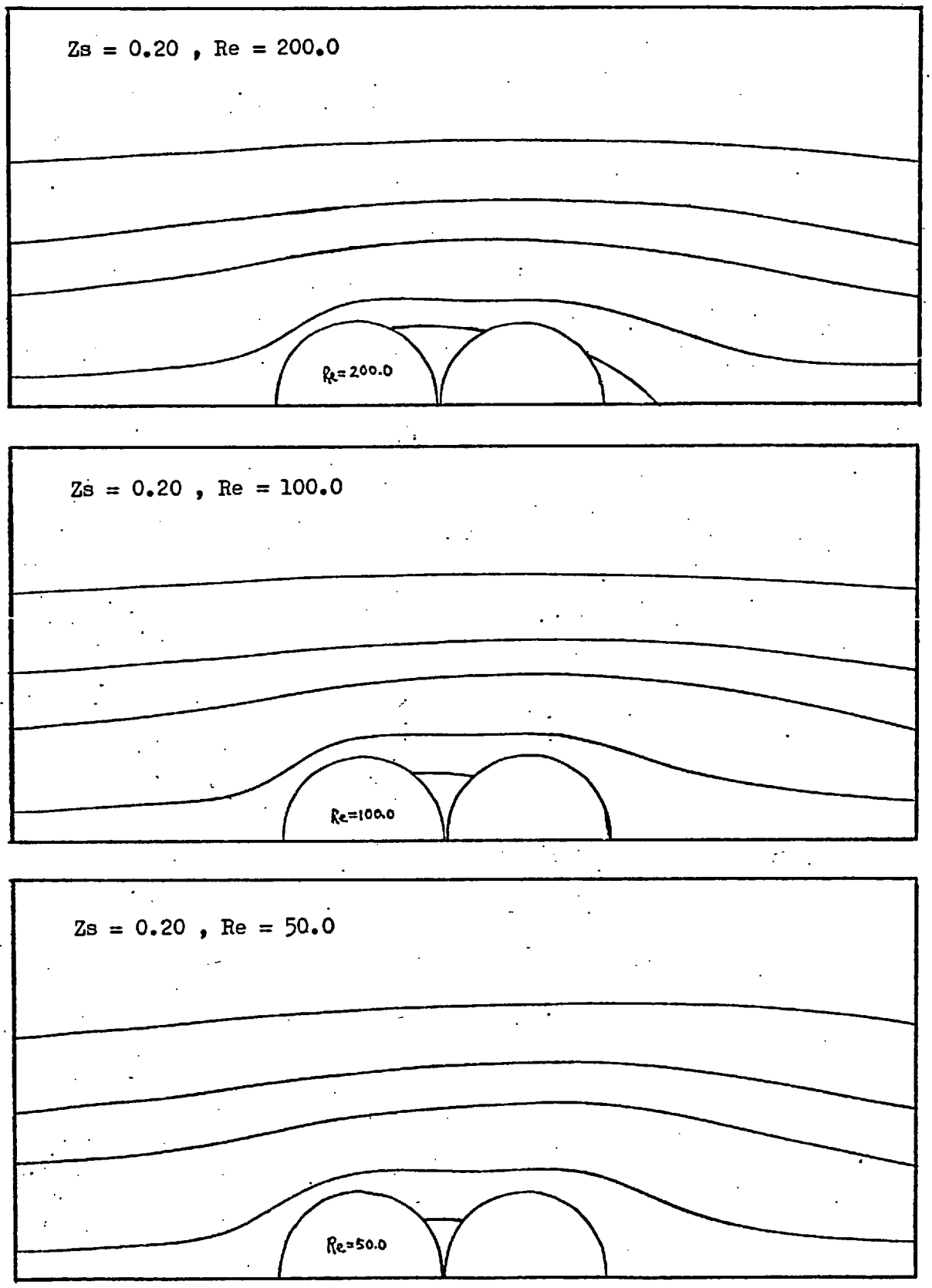

Figure(5-4-12). Stream function distributions around two spheres with Zs = 0.20.

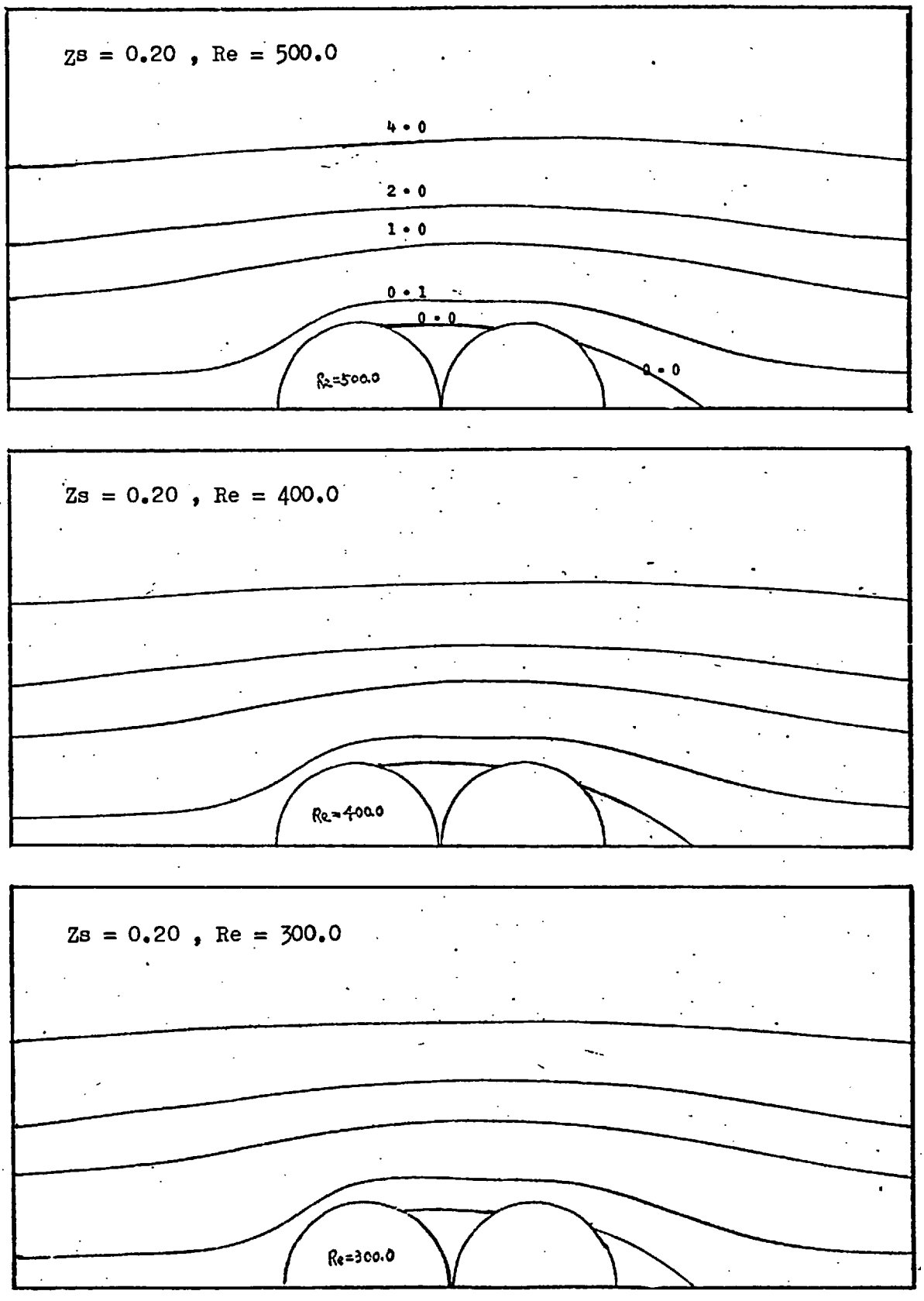

Figure(5-4-13). Stream function distributions around two spheres with Zs = 0.20.

spheres are dependent on Reynolds number and on sphere spacing. A brief summary of the behaviour is given as follows. At low Reynolds numbers of 0.001 to 1.0, the distributions of the stream function around the spheres for each sphere spacing are almost symmetrical while at higher Reynolds numbers the distributions of the stream function around the spheres are asymmetrical about a plane through the mid-point of the line of centres normal to the direction of flow. The separation of the streamline with zero stream function from the rear surface of sphere A always appears at a lower Reynolds number than for sphere B. As a result, the wake region downstream of sphere A is always larger than that downstream of sphere B. For the two smallest sphere spacings, because of the small distance between the spheres, at high Reynolds numbers almost the entire inner region between the spheres becomes a wake region.

The variation of sphere spacing has a significant effect upon the distributions of the stream function especially on those in the inner region between the spheres. As the sphere spacing decreases, the most obvious change is shown by the streamline $\psi^* = 0.1$ which moves away from the line of centres of the spheres, and becomes completely outside of the inner region between the spheres for the two smallest sphere spacings Zs = 1.32 and 0.20. Meanwhile, the deflection of the streamline $\psi^* = 0.1$ downstream of sphere A becomes larger while that downstream of sphere B becomes smaller; consequently, the separation of the streamline with zero stream function from the rear surface of sphere A first appears at increasingy lower Reynolds numbers while separation from the rear surface of sphere B first appears at increasingly higher Reynolds numbers.

This may be because as the two spheres come closer to each other, they behave more and more like a combined and elongated object when a fluid flows around them. On the other hand, the distributions of the streamlines with large values of the stream function change only slightly with variation in sphere spacing, and the streamlines remain approximately parallel to each other outside of the inner region between the spheres. Moreover, for each sphere spacing the distributions of the stream function around the spheres are always at least slightly different from those around a single isolated sphere with the same Reynolds number, and the difference becomes larger as the sphere spacing decreases. This indicates the existence of particle-to-particle interaction between the spheres for all the five sphere spacings considered in this study, and the extent of interparticle interaction increases with decreasing sphere spacing. The conclusion that there is interaction between the spheres is exactly the same as that drawn from the distributions of vorticity around the spheres as discussed in the previous section (5-3).

5-5. Surface vorticity distributions and flow separation.

The phenomenon of flow separation occurs when the Reynolds number is sufficiently high. Accoring to non-slip condition, the surface vorticity is zero at the point where the flow separates from the surface of a sphere or bluff body. Hence, the angle of flow separation can be determined either by numerical interpolation of the surface vorticities which change from positive to negative values or by plotting the surface vorticities against the angle η, and determining the point at which the curve cuts the η-axis corresponding to zero surface vorticity. However, the results obtained graphically were less accurate than those obtained by interpolation. Hence, interpolation was used to determine the angles of flow separation for the two spheres and the results are shown in Tables(5-5-1) to (5-5-5) for the five sphere spacings considered in this study. For each sphere spacing, there are two sets of results corresponding to the two solutions obtained from the Navier-Stokes equations using two different distributions of grid lines. In the tables, the angles of flow separation are recorded in terms of the angle η. For sphere A, the angles of flow separation are denoted by η_{AS}; while for sphere B, they are denoted by η_{BSF} and η_{BSR} for flow separation from the front and rear surfaces of sphere B, respectively. It is important to note that for sphere A, the angle η is measured from the normal to the front stagnation point while for sphere B, it is measured from the normal to the rear stagnation point.

Because of a close relationship between the angles of flow separation and the surface vorticity distributions, the surface vorticities for each sphere spacing are plotted for

the two spheres against the angle η for some selected Reynolds numbers. The surface vorticity distributions for the five sphere spacings obtained using a smaller mesh spacing of $|Zs/20|$ in Z are shown in Figures(5-5-1) to (5-5-5); while those obtained using a larger mesh spacing of $|Zs/10|$ in Z are shown in Figures(5-5-6) to (5-5-10).

For the largest sphere spacing: Zs = 3.09, the surface vorticity distributions and their variation with Reynolds number, as shown in Figures(5-5-1) and (5-5-6), are similar to those for a single isolated sphere. For Reynolds numbers greater than 30 for sphere A and for Reynolds numbers greater than 50 for sphere B, the surface vorticities near the rear stagnation points of the spheres become negative. This indicates the existence of a backward flow as well as the occurence of flow separation from the rear surfaces of the spheres. As the Reynolds number increases, the vorticities at the front surface of each sphere become larger and the point at which the surface vorticity is the most intensive move closer to the front stagnation point; on the other hand, the vorticities at the rear surface of each sphere become smaller and the point of minimum surface vorticity moves away from the rear stagnation point. Another important feature of the distributions is that as the Reynolds number increases, the vorticities at the front surface of sphere A increase faster than those for sphere B; while the vorticities at the rear surface of sphere A decrease more rapidly than those for sphere B. Consequently, at Reynolds numbers greater than 10, the vorticities at the front surface of sphere A are larger than those at the front surface of sphere B and the region where the surface vorticities have negative

values is larger for sphere A than for sphre B.

For the sphere spacings Zs = 2.48 and 2.07, the surface vorticity distributions for the two spheres and their variation with Reynolds number are similar to those for the largest sphere spacing. The main observable difference is that the surface vorticities close to the front stagnation point of sphere B begin to decrease instead of increasing when the Reynolds number is greater than 100 for the sphere spacing Zs = 2.48, and when the Reynolds number is greater than 50 for the smaller sphere spacing Zs = 2.07. This is a consequence of the closeness of the spheres in that flow separation from the rear surface of sphere A cause the vorticities at the front surface of sphere B to decrease. This eventually results in the development of a very small backward flow at the upstream surface of sphere B when the Reynolds number reaches 150. As the sphere spacing decreases, particle-to-particle interaction becomes more intense and the decrease in the front surface vorticities of sphere B first occurs at lower Reynolds numbers, meanwhile, the most intensive vorticity at the surface of sphere B move further downstream from the front stagnation point.

When the sphere spacing is reduced to Zs = 1.32, the surface vorticity distributions and their variation with Reynolds number, shown in Figures(5-5-4) and (5-5-9), are similar to those for the sphere spacing Zs = 2.07. However; because of the smaller distance between the spheres and the increase in particle-to-particle interaction, the surface vorticities at the front of sphere B begin to decrease at a Reynolds number of 30 and become negative when the Reynolds number reaches 100, and a reverse flow is developed at the

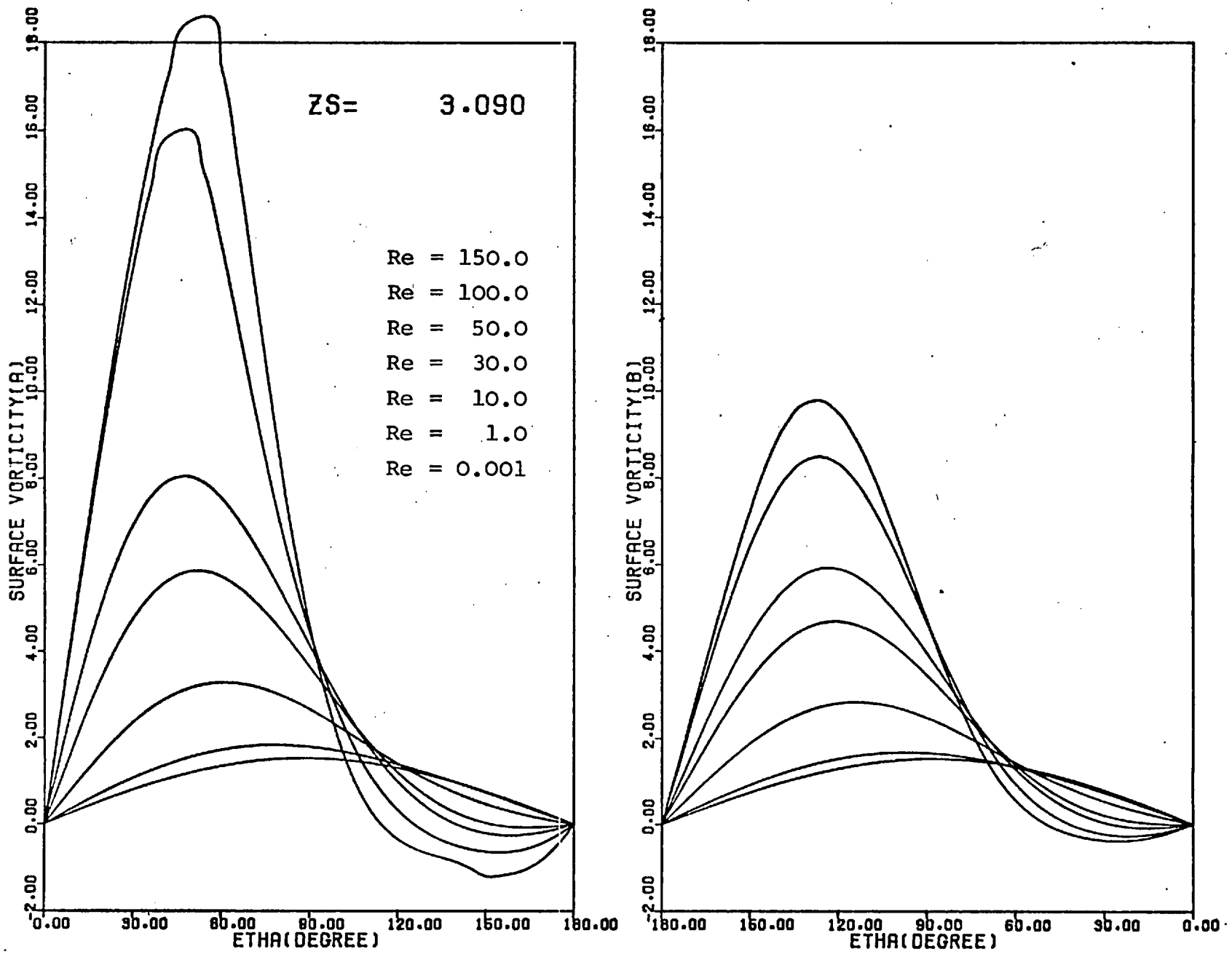

Figure(5-5-1). Surface vorticity distributions for two spheres with Zs = 3.09.

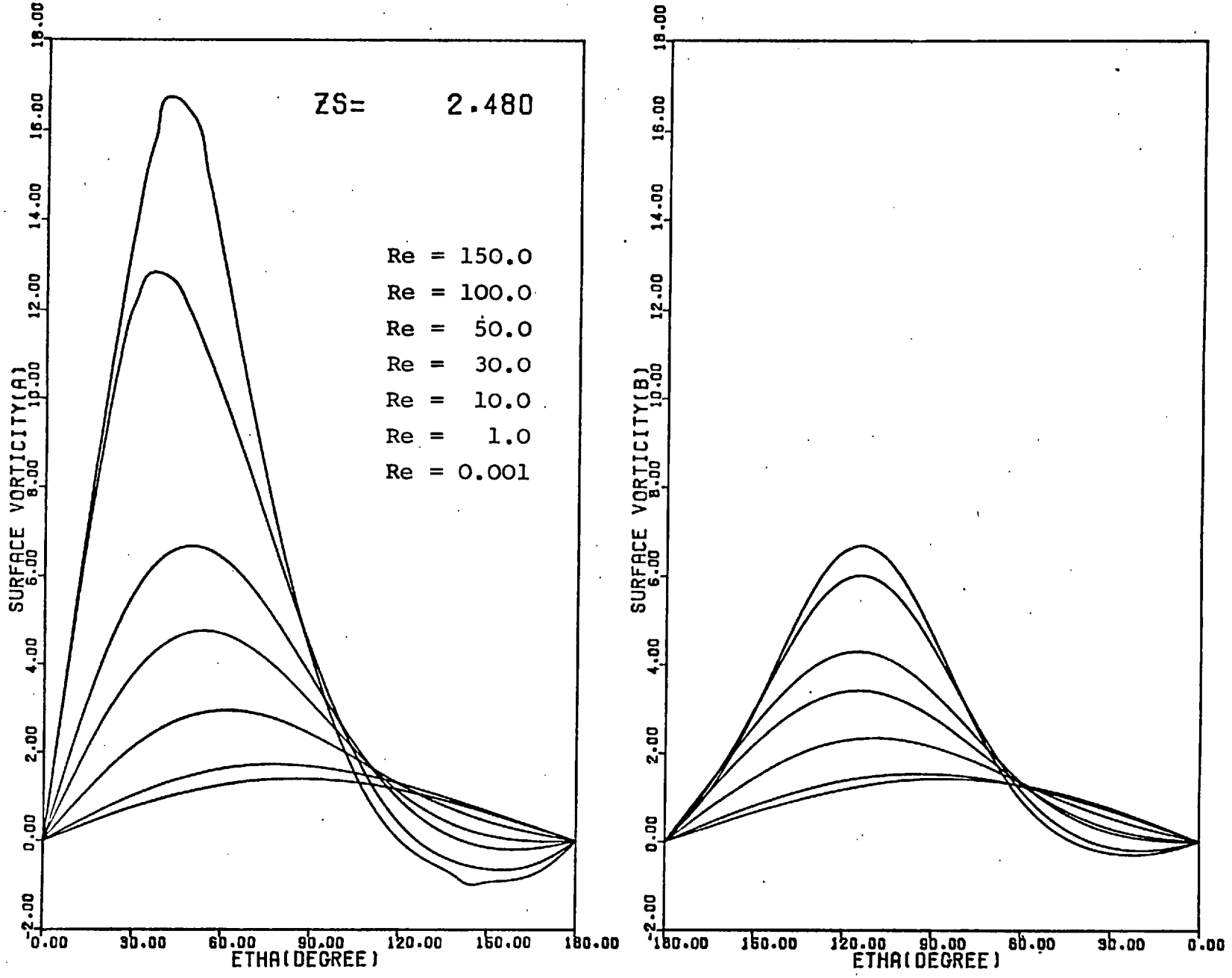

Figure(5-5-2). Surface vorticity distributions for two spheres with Zs = 2.48.

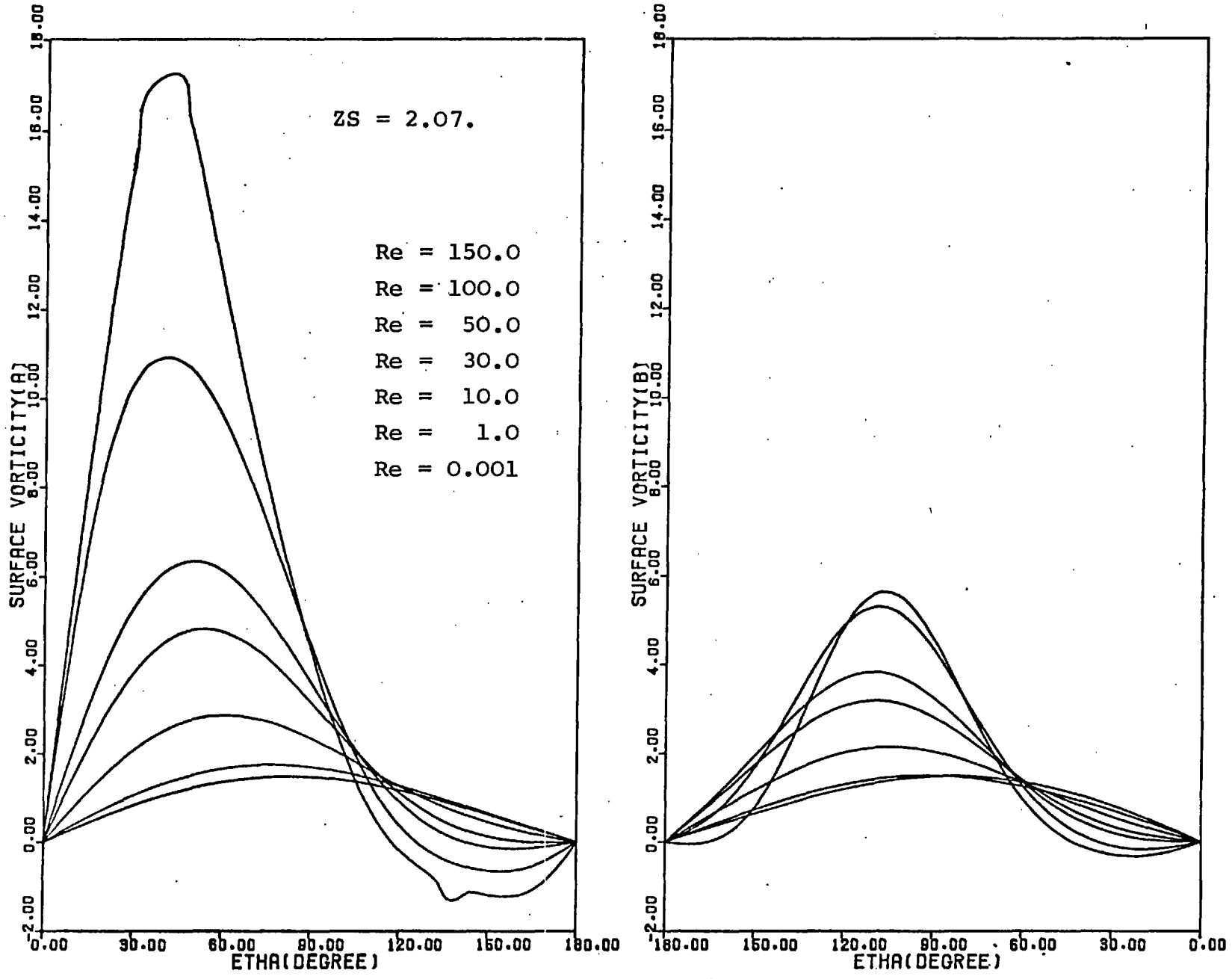

Figure(5-5-3). Surface vorticity distributions for two spheres with Zs = 2.07.

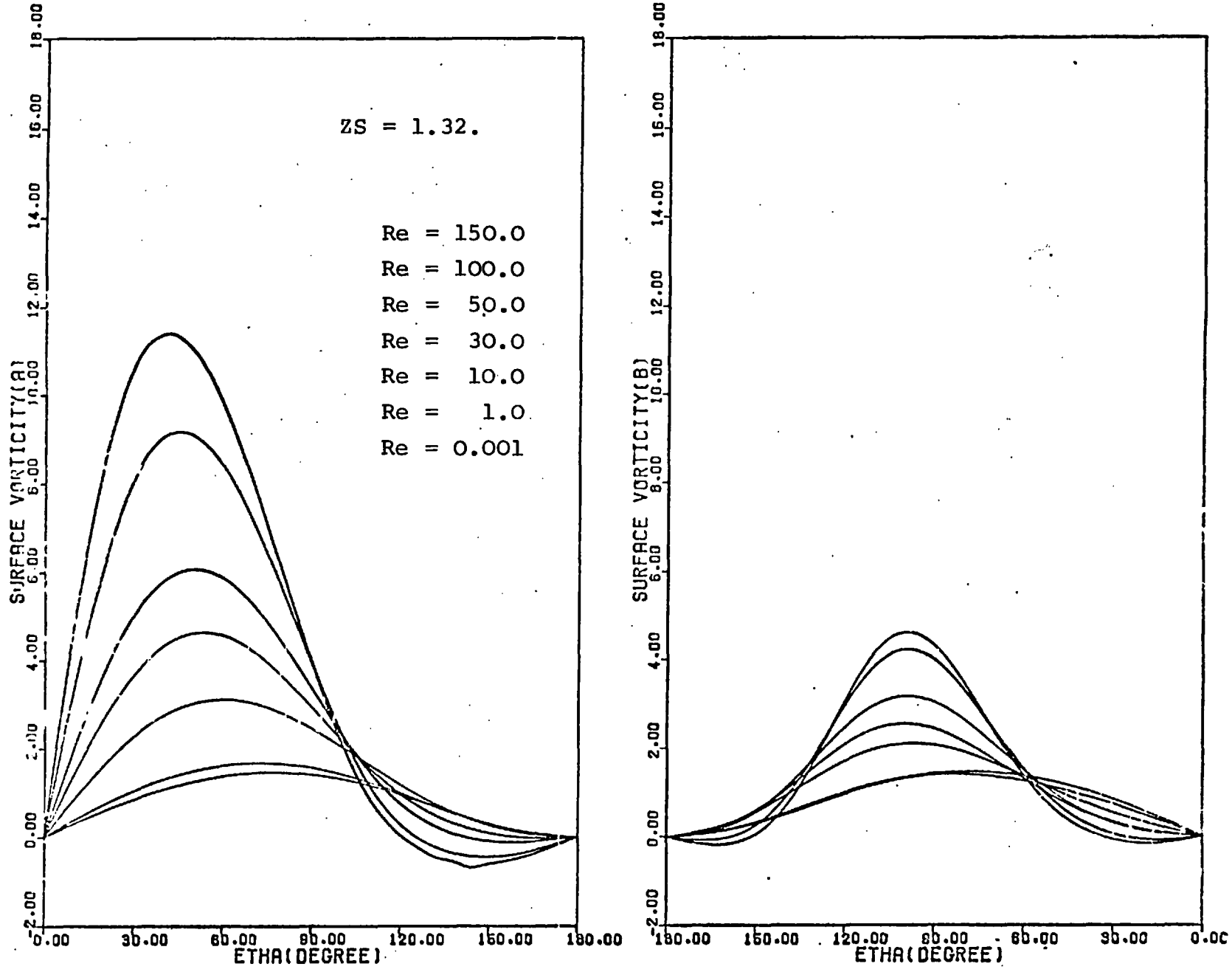

Figure(5-5-4). Surface vorticity distributions for two spheres with Zs = 1.32.

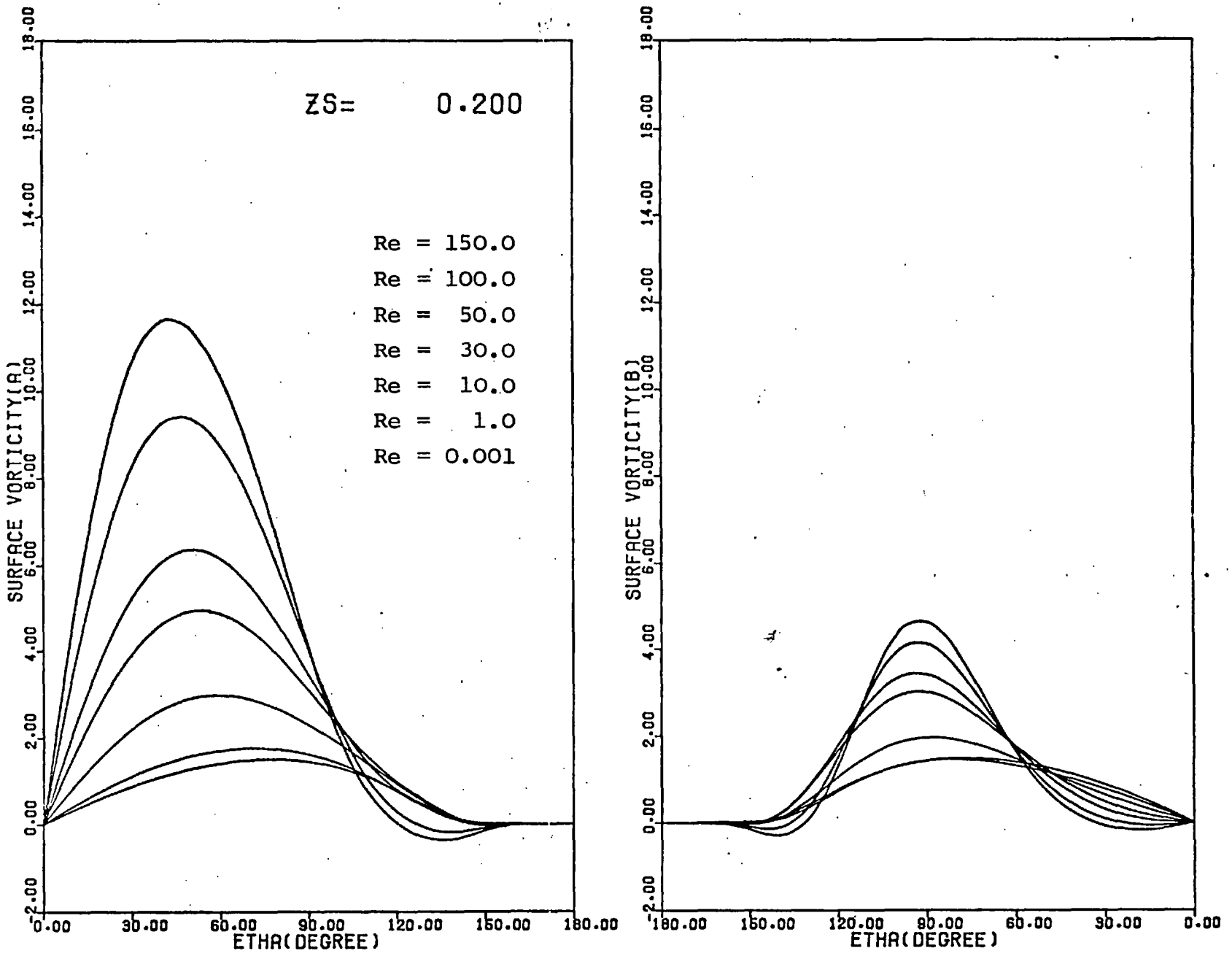

Figure(5-5-5). Surface vorticity distributions for two spheres with Zs = 0.20.

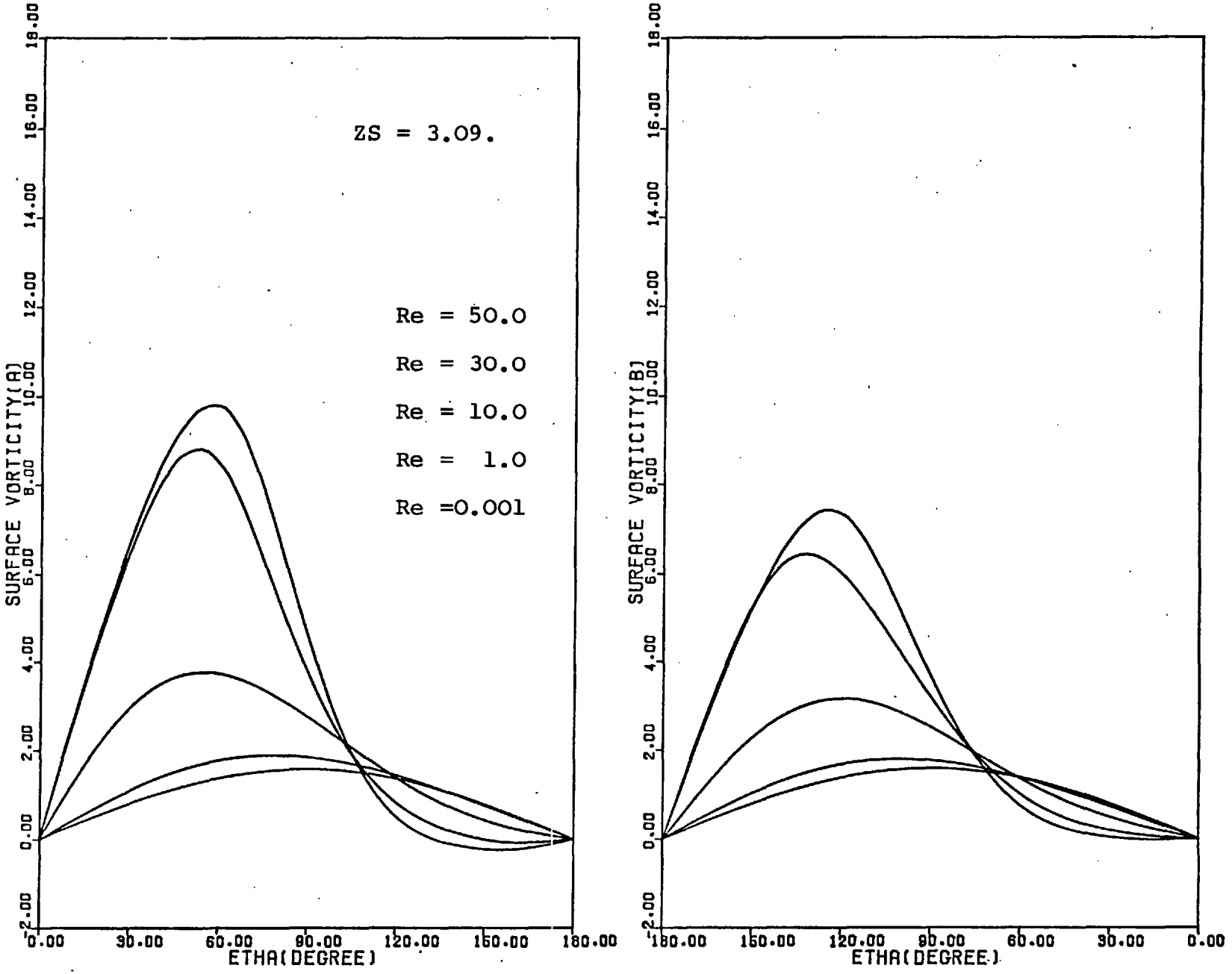

Figure(5-5-6). Surface vorticity distributions for two spheres with Zs = 3.09.

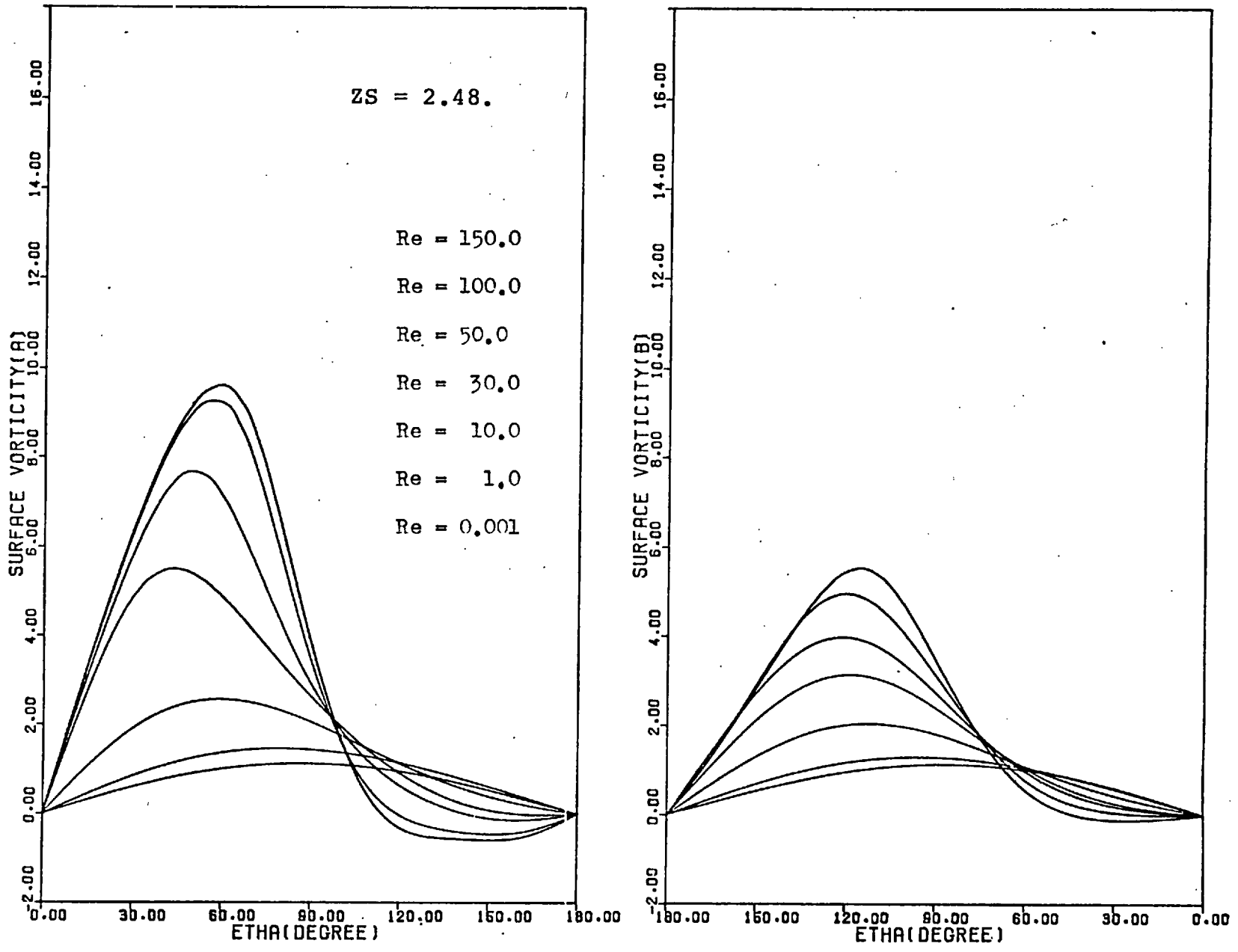

Figure(5-5-7). Surface vorticity distributions for two spheres with Zs = 2.48.

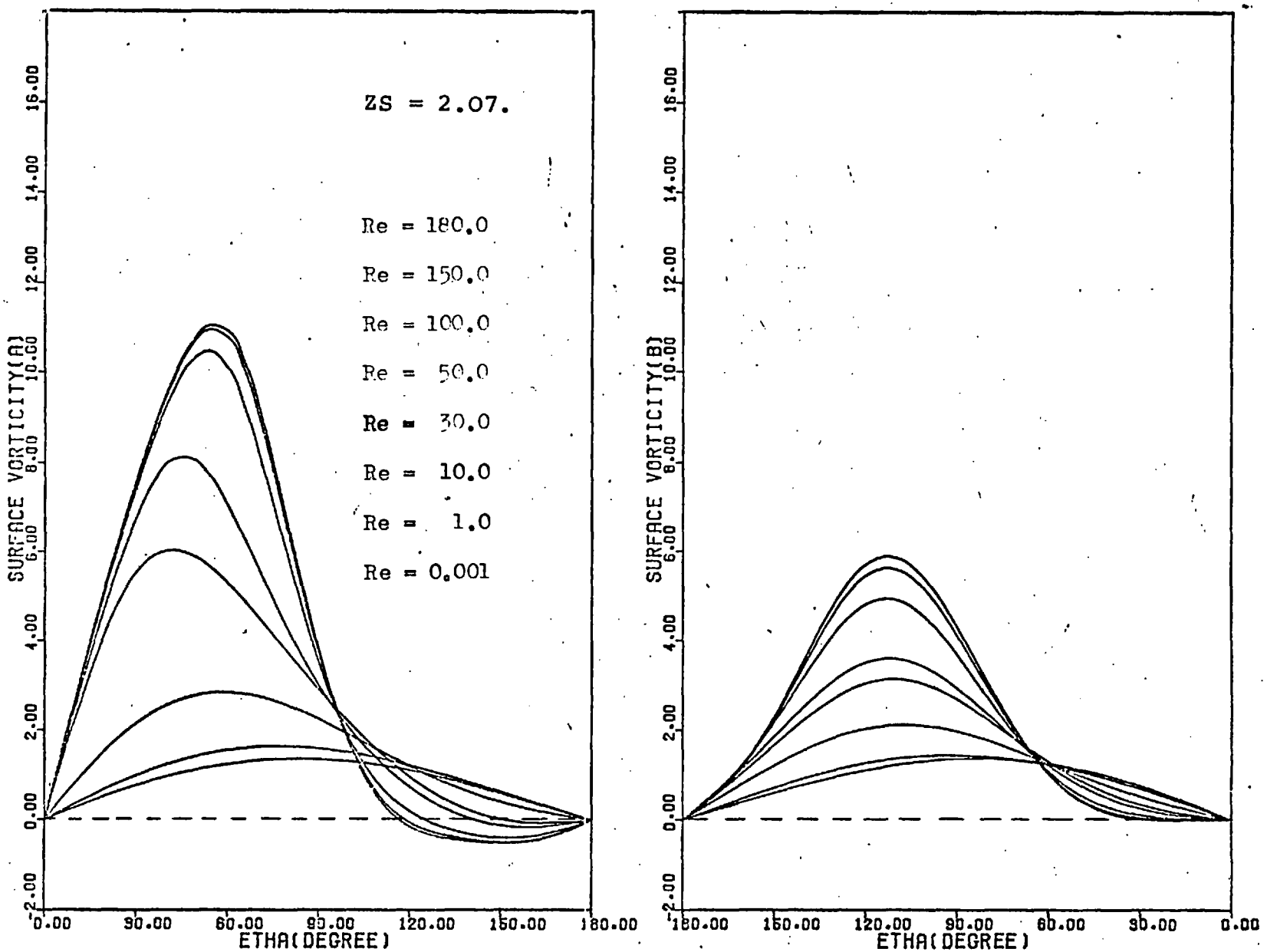

Figure(5-5-8). Surface vorticity distributions for two spheres with Zs = 2.07.

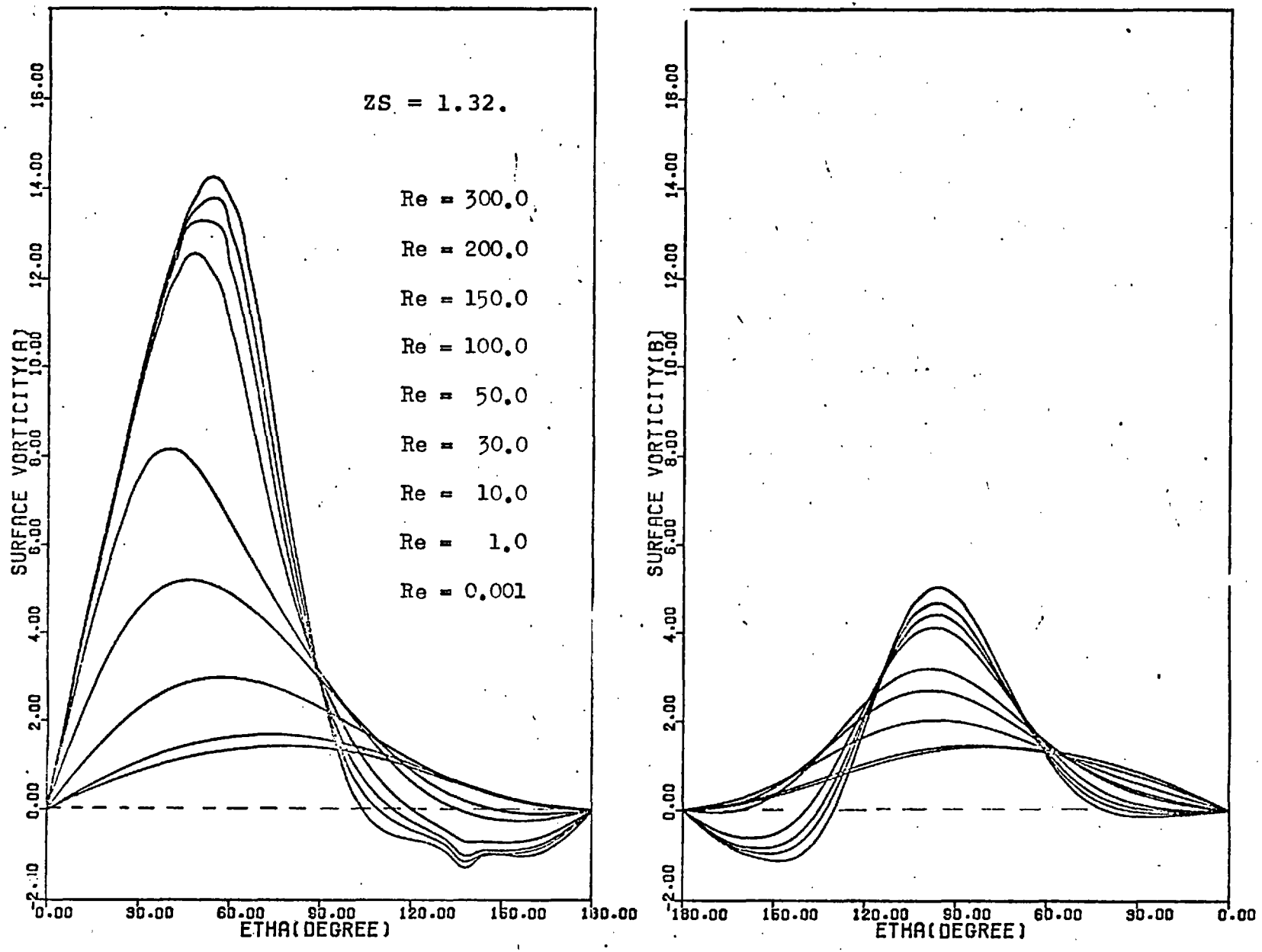

Figure(5-5-9). Surface vorticity distributions for two spheres with Zs = 1.32.

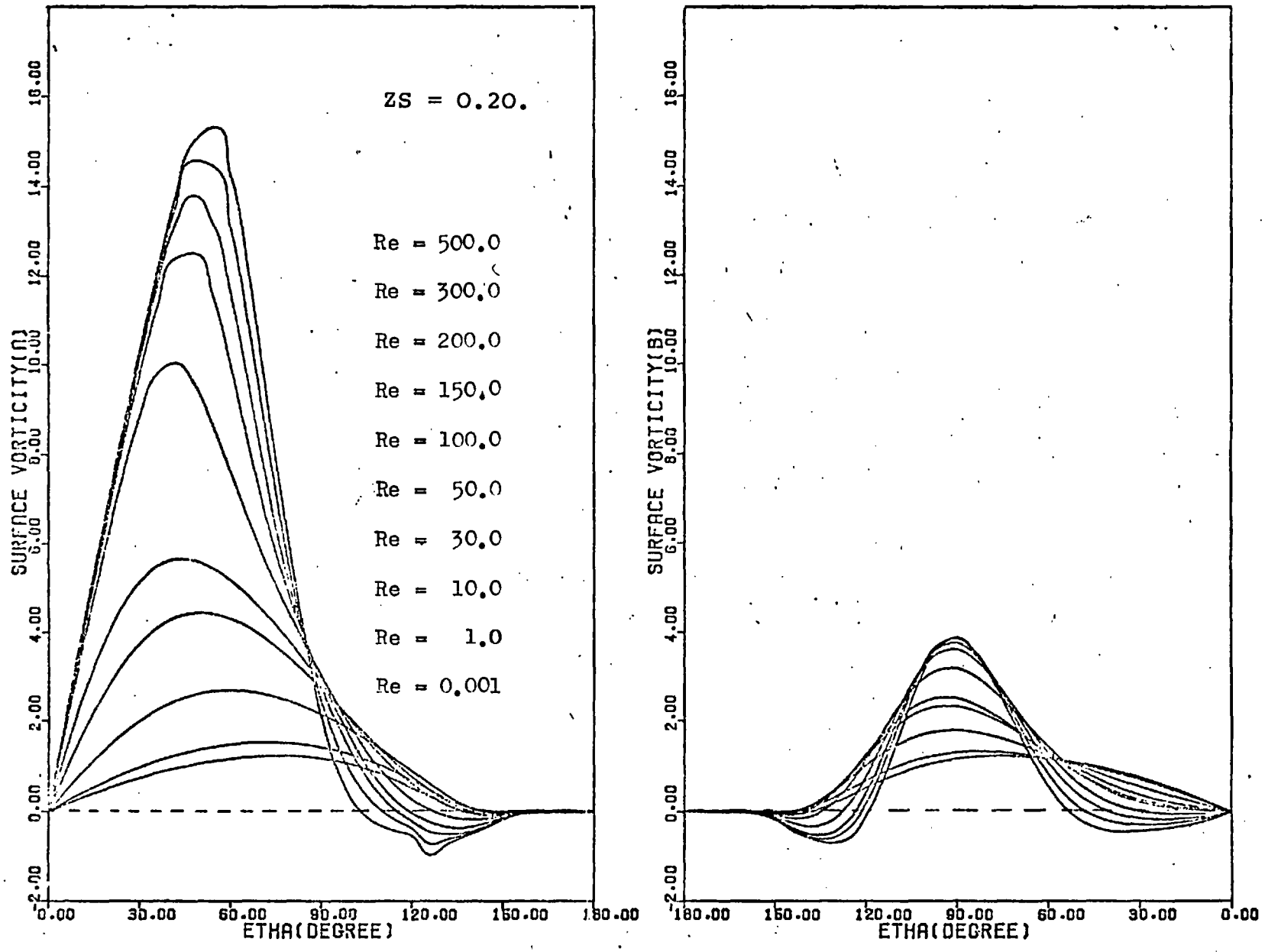

Figure(5-5-10). Surface vorticity distributions for two spheres with Zs = 0.20.

upstream surface of sphere B. Hence, in addition to the flow separation from the back of each sphere, there is flow separation from the front of sphere B.

For the smallest sphere spacing: Zs = 0.20, the surface vorticity distributions for the two nearly touching spheres have some distinctive differences from those for the sphere spacing Zs = 1.32. The most interesting feature of the distributions is the existence of a small region between $\eta = 156^{o}$ and $\eta = 180^{o}$ on each sphere where the surface vorticities are nearly zero. These regions, which are near the rear stagnation point of sphere A and the front stagnation point of sphere B may be due to the existence of stagnant fluid in the tiny inner region between the spheres. For this smallest sphere spacing, the surface vorticity distributions from $\eta = 0^{o}$ to $\eta = 156^{o}$ are similar to those from $\eta = 0^{o}$ to $\eta = 180^{o}$ for the sphere spacing Zs = 1.32. Also, the variation of the surface vorticity distributions with Reynolds number is similar. For this smallest sphere spacing, in addition to flow separation from the back of each sphere, there is also flow separation from the front surface of sphere B.

From this discussion, it is clear that when the spheres are not far apart, the surface vorticity distributions for the two spheres and their variation with Reynolds number are not similar to those around a single isolated sphere, except for the surface vorticities at the front of sphere A and at the back of sphere B. As the sphere spacing is decreased, then at any specified high Reynolds number the vorticities at the front surface of sphere B become smaller and the point at which the

surface vorticity is most intense move further downstream from the front stagnation point. A backward flow is induced at the front surface of sphere B for the two smallest sphere spacings, Zs = 0.20 and 1.32.

It is important to note that at high Reynolds numbers, the vorticities over part of the front surface of sphere A for each sphere spacing and the vorticities at the front surface of sphere B for the largest sphere spacing Zs = 3.09, become independent of Reynolds number. This is mainly a result of the inherent characteristic of the bi-spherical coordinate system of providing unequal distances between any two neighbouring grid lines in the Z-direction around the spheres, as has been described in section(5-2), combined with the existence of a fluid dynamic boundary layer at the upstream surface of each sphere. For each sphere, the boundary layer becomes thinner as the Reynolds number increases; and it becomes so thin at high Reynolds numbers that the boundary layer over part of the upstream surface is contained within the Z-grid-line spacing immediately next to the surface of the sphere. As a result, the surface vorticities which were calculated using equations(4-3-7) and (4-3-8) become independent of Reynolds number. As the Reynolds number is further increased, the vorticities become independent of Reynolds number over a larger part of the upstream surface of each sphere because a larger section of the increasingly thinner boundary layer becomes contained within the first Z-grid-line spacing. Another consequence of this development is that as the Reynolds number is increased, the most intensive surface vorticity moves further downstream from the front stagnation point instead of moving closer to it.

Because the Z-grid-line spacings upstream of sphere B are always much smaller than those upstream of sphere A, the region where the surface vorticities become independent of Reynolds number is much smaller for sphere B than for sphere A. On the other hand, as the sphere spacing increases the vorticities become independent of Reynolds number over a larger part of the front surface of sphere A. This is because for a constant number of mesh points, the grid-line spacing for the Z-direction becomes coarser as the sphere spacing is increased. However, for each sphere spacing, when a smaller mesh spacing in Z was used, the anomalies were greatly reduced and did not occur until higher Reynolds numbers were attained(see Figures(5-5-1) to (5-5-5)).

The separation of flow from the surfaces of the two spheres is closely associated with the existence of regions where the surface vorticities have negative values. It is thus clear from the surface vorticity distributions that for each sphere spacing and at sufficiently high Reynolds number, there is always flow separation from the back of each sphere, and for the two smallest sphere spacings Zs = 0.20 and 1.32 there is also flow separation from the front of sphere B. As the regions where the surface vorticities are negative increase in extent with increasing Reynolds number, the angles of flow separation measured from the rear stagnation point of each sphere together with the angles of flow separation measured from the front stagnation point of sphere B also become larger with increasing Reynolds number as shown in Tables(5-5-1) to (5-5-5). It is important to note that for each specified sphere spacing and

Reynolds number, the angle of flow separation measured from the rear stagnation point of sphere A is larger than that measured from the rear stagnation point of sphere B. Also, for the two smallest sphere spacing the angle of flow separation measured from the rear stagnation point of sphere A is always larger than that measured from the front stagnation point of sphere B. Moreover, the pattern of the variation of angles of flow separation with Reynolds number remains nearly the same when the mesh spacing in Z changes from |Zs/10| to |Zs/20|.

The size of sphere spacing has a noticeable effect upon the angles of flow separation. As the sphere spacing decreases, the angle of flow separation measured from the rear stagnation point of sphere A becomes larger while that measured from the rear stagnation point of sphere B becomes smaller. This is because when the two spheres approch each other they behave more and more like a combined and elongated object as discussed in the previous section. For small sphere spacings, the angles of flow separation from the back of sphere A are larger while those from the back of sphere B are smaller than the angles of flow separation from the back of a single isolated sphere obtained by Al-Taha(1969). However, as the sphere spacing increases, the angles of flow separation from the back of each sphere become closer to those of a single isolated sphere. The angles of flow separation measured from the front stagnation point of sphere B become smaller with increasing sphere spacing. and eventually there is no flow separation from the front of sphere B.

5-6. Surface pressure distributions.

The pressures along the surfaces of the two spheres are expressed in terms of the dimensionless pressure coefficients which are defined by equation(B-3-8). The dimensionless surface pressure distributions for sphere A were calculated using equation(4-5-1) and (4-5-3); while those for sphere B were calculated using equations(4-5-2) and (4-5-4). Detailed derivations of the equations are given in Appendix B. For each sphere spacing, the resultant surface pressures are plotted against the angle η for seven selected Reynolds numbers of 1, 2.5, 5, 10, 25, 50, and 100. For the five sphere spacings considered in this study, the surface pressure distributions obtained for the two spheres using a mesh spacing of $|Zs/20|$ in Z are shown in Figures(5-6-1) to (5-6-5); while those obtained using a larger mesh spacing of $|Zs/10|$ in Z are shown in Figures(5-6-6) to (5-6-10).

For the three largest sphere spacings: Zs = 3.09, 2.48, and 2.07, the pressure distributions at the surfaces of the spheres are generally similar to those at the surface of a single isolated sphere. For Reynolds numbers up to 5.0, the pressures at the surface of each sphere decrease continuously from maximum values at the front stagnation point to minimum values at the rear stagnation point. This pattern becomes different for higher Reynolds numbers as the region of minimum surface pressure moves away from the rear stagnation point. As a result, the surface pressures for each sphere decrease from maximum values at the front stagnation point to minimum values and then increase slowly until the rear stagnation point is

reached. From the figures it can be seen that as the Reynolds number increases, the dimensionless pressure coefficients at the front surface of each sphere become smaller while those at the rear surface of each sphere become larger.

For the two smallest sphere spacings considered in this study : Zs = 1.32 and 0.20, the pressure distributions at the front surface of sphere A and at the rear surface of sphere B are generally similar to those for the three largest sphere spacings, however, the pressures at the rear surface of sphere A and at the front surface of sphere B are affected by the closeness of the spheres. For the sphere spacing Zs = 1.32, the surface pressures for sphere A always decrease from maximum values at the front stagnation point to minimum values and then increase slowly until the rear stagnation point is reached. For sphere B, the surface pressures increase slowly from the front stagnation point to maximum values at the front surface of the sphere and then decrease continuously to minimum values at the rear stagnation point. Hence, the surface pressure distributions show that for this sphere spacing and at low Reynolds numbers, the minimum surface pressures of sphere A are not at the rear stagnation point of the sphere and the maximum surface pressures of sphere B are not at the front stagnation point of the sphere. For the smallest sphere spacing Zs = 0.20, the surface pressure distributions for the spheres are similar to those for the sphere spacing Zs = 1.32 except near to the rear stagnation point of sphere A and near to the front stagnation point of sphere B where the surface pressures become independent of position. The regions of constant surface pressure may be a result of the existence of stagnant fluid in

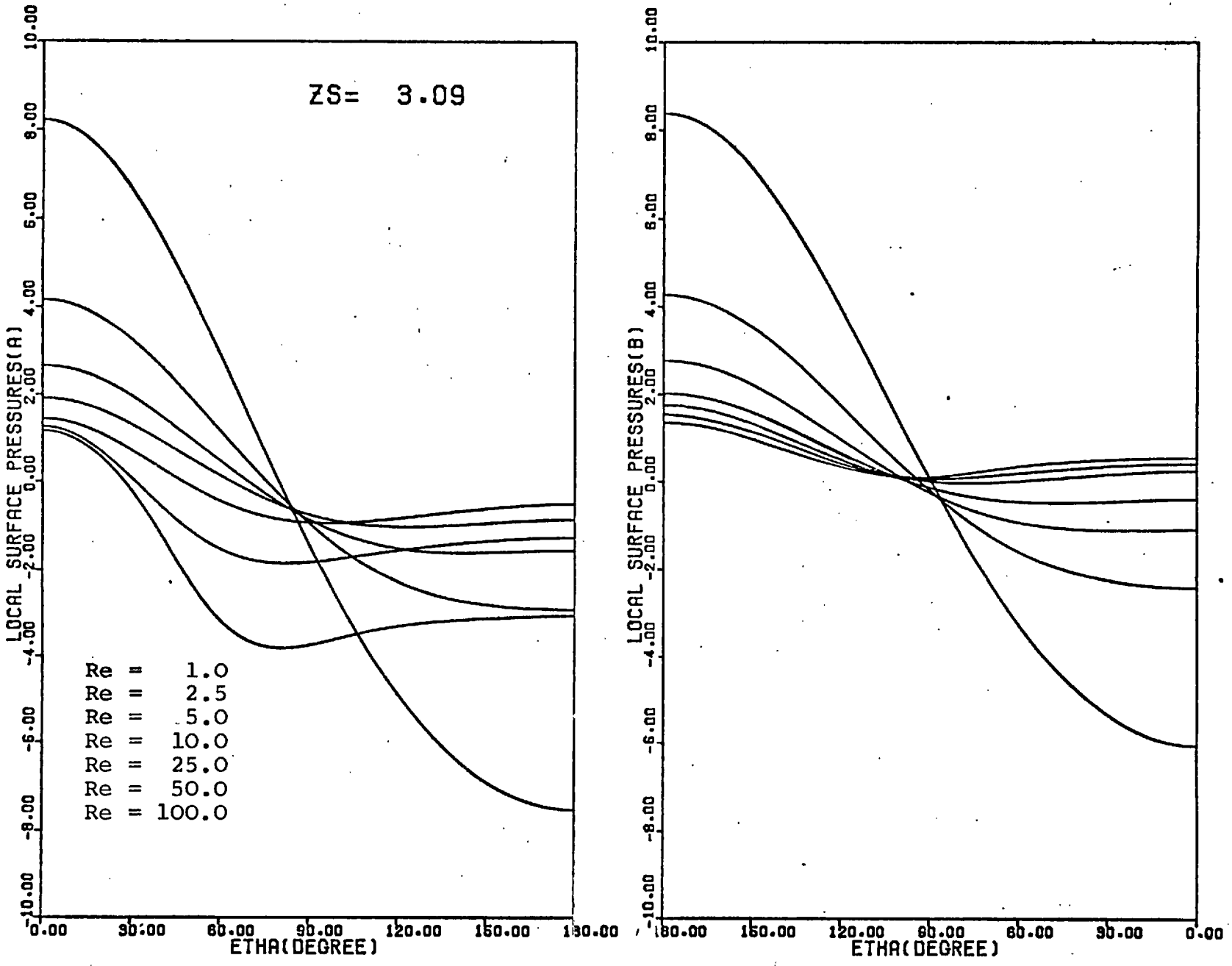

Figure(5-6-1). Surface pressure distributions for two spheres with Zs = 3.09.

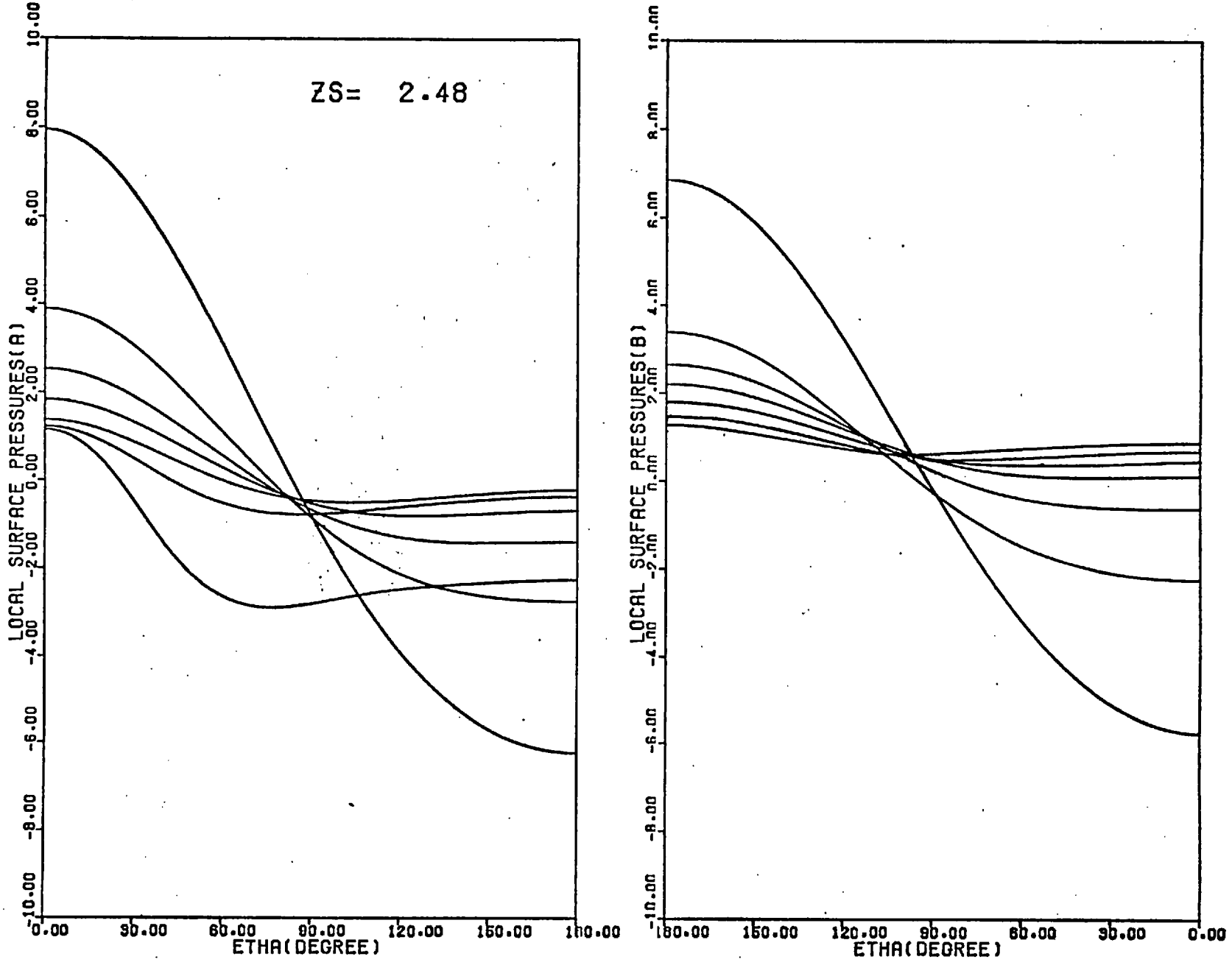

Figure(5-6-2). Surface pressure distributions for two spheres with Zs = 2.48.

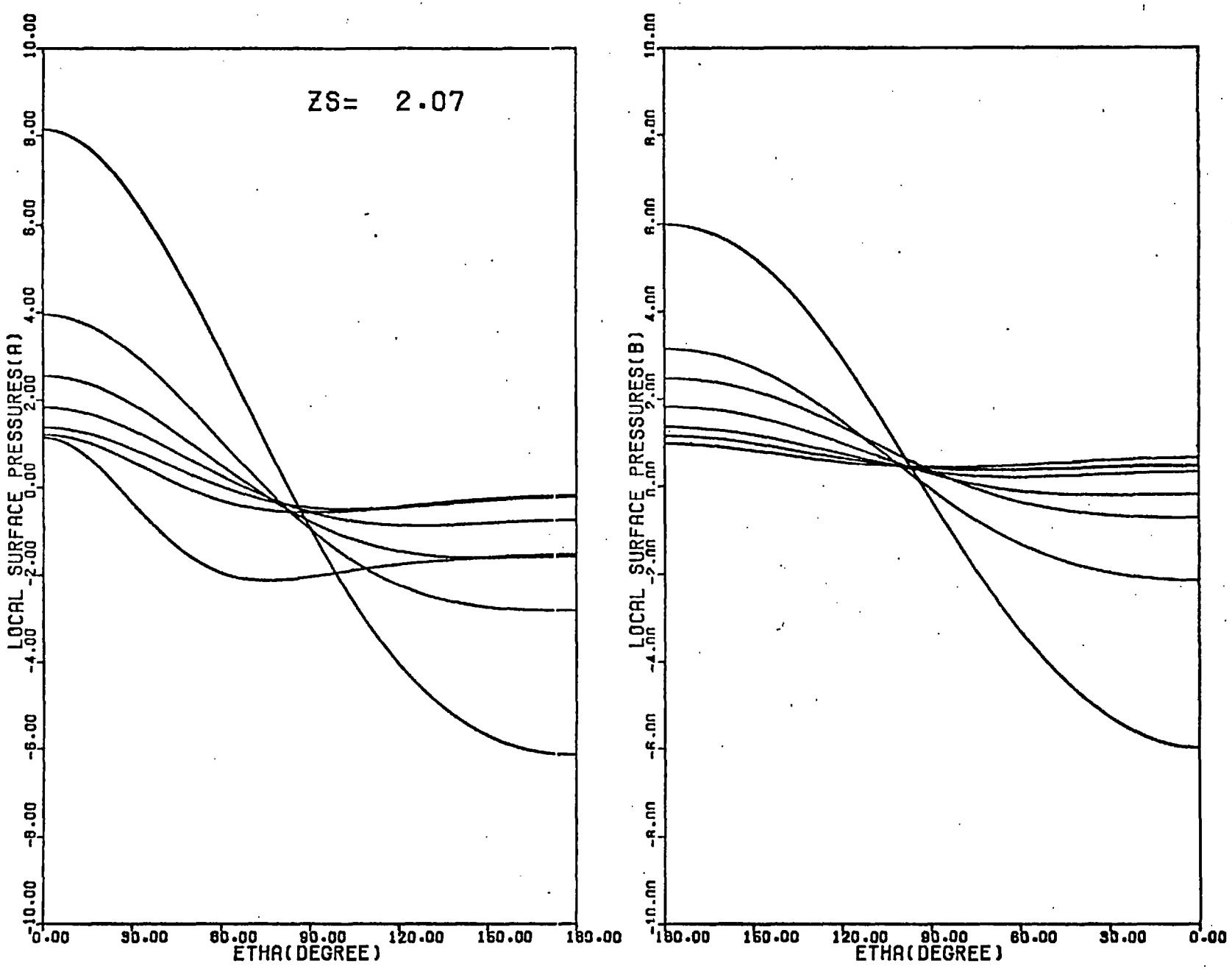

Figure(5-6-3). Surface pressure distributions for two spheres with Zs = 2.07.

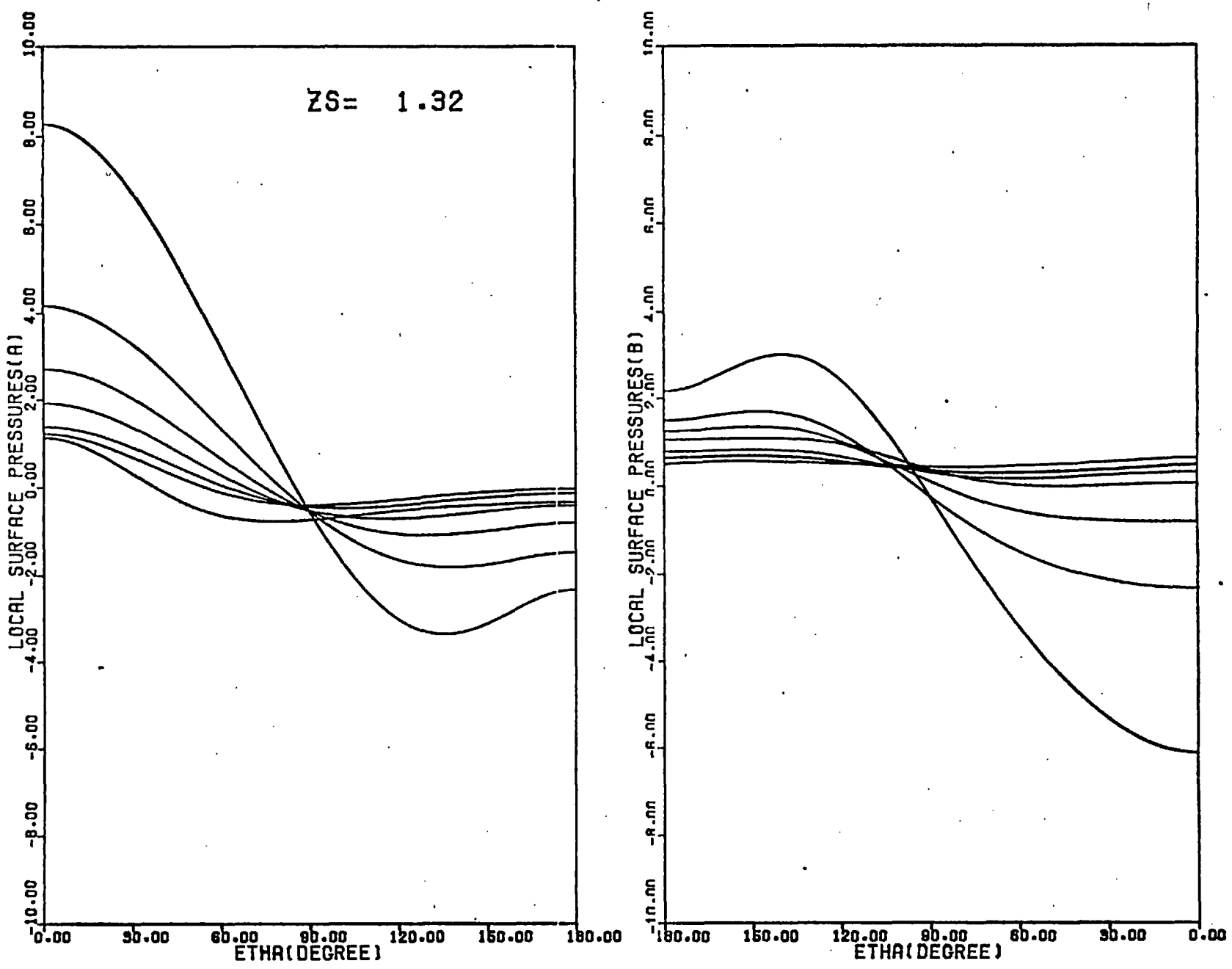

Figure(5-6-4). Surface pressure distributions for two spheres with Zs = 1.32.

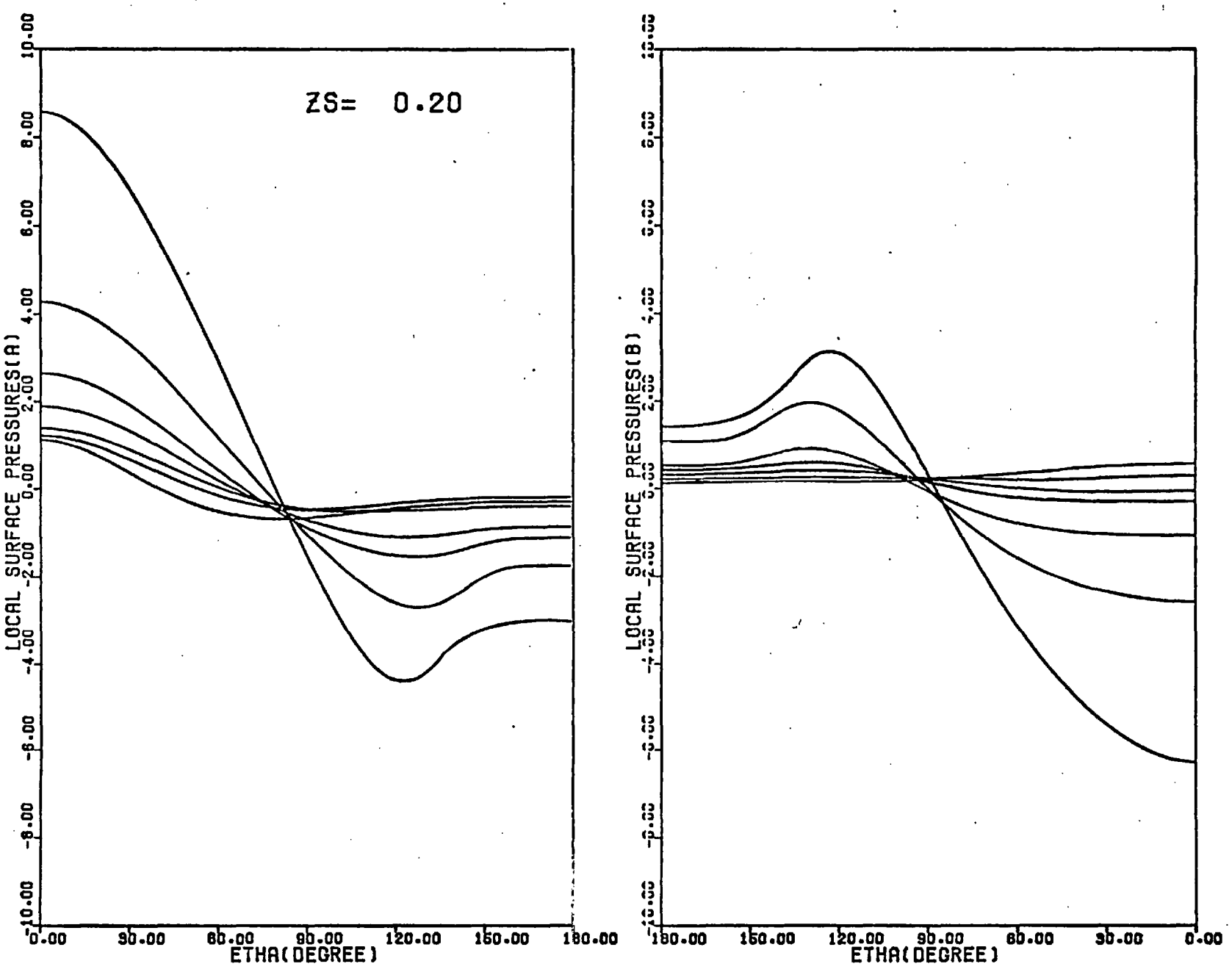

Figure(5-6-5). Surface pressure distributions for two spheres with Zs = 0.20.

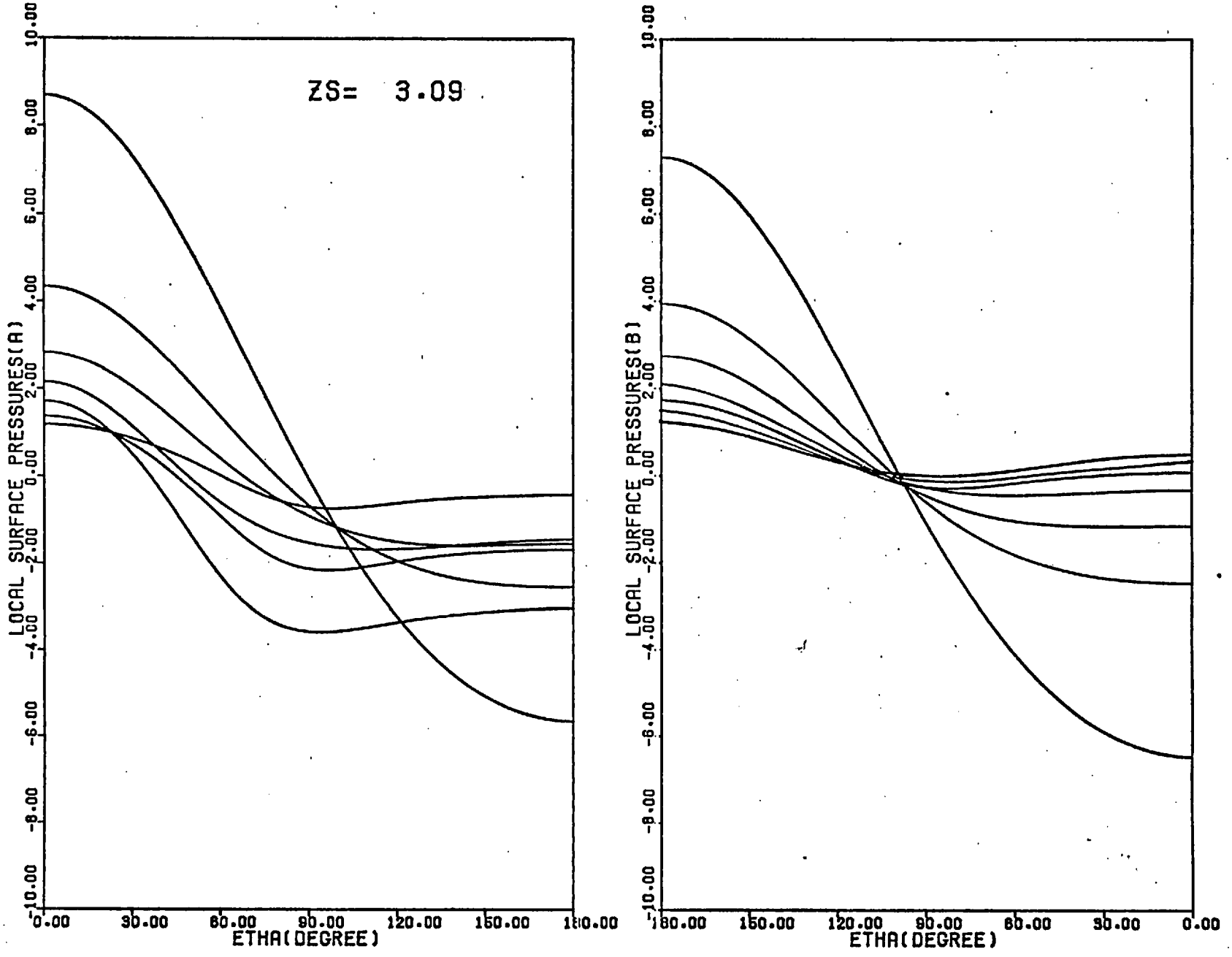

Figure(5-6-6). Surface pressure distributions for two spheres with Zs = 3.09.

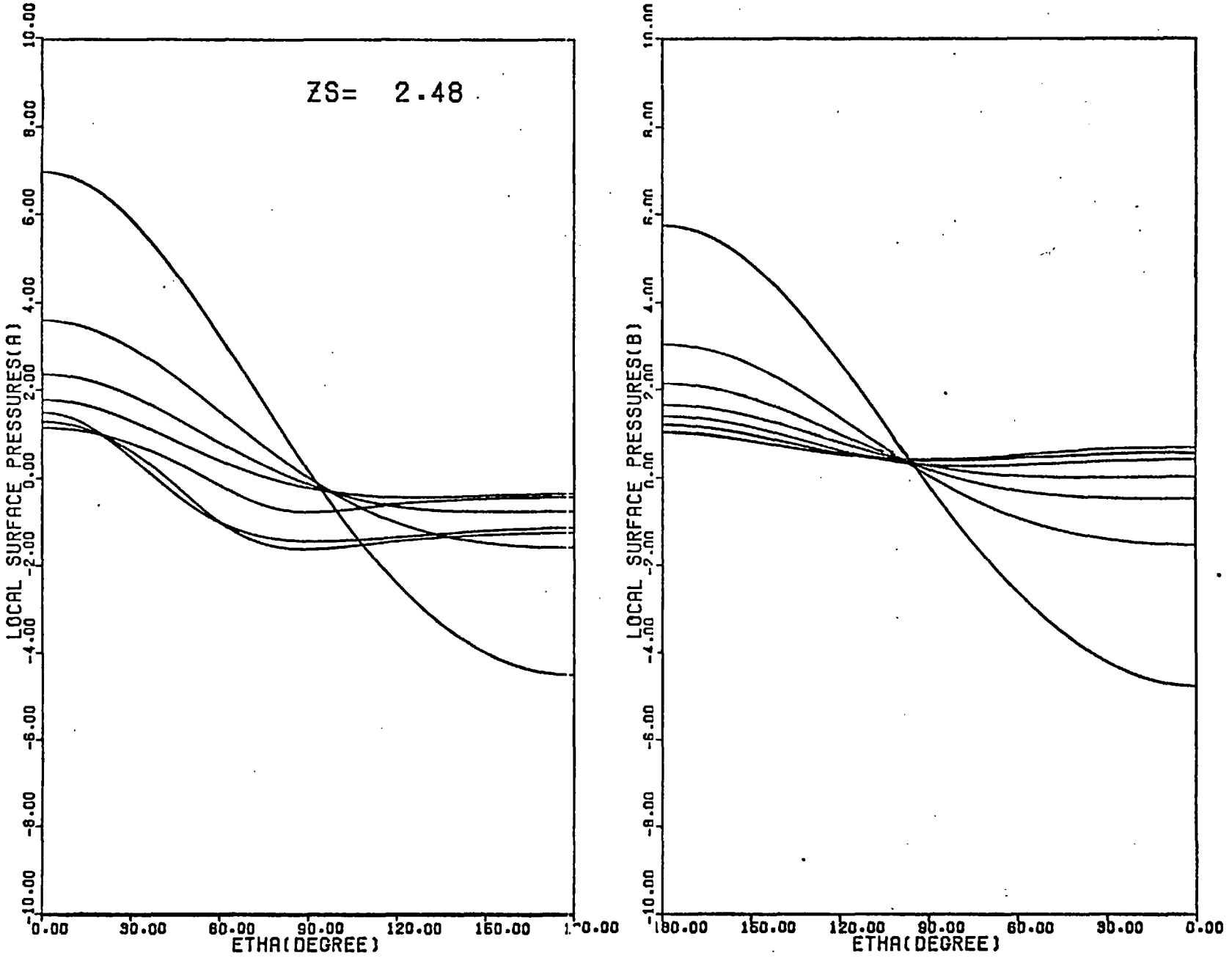

Figure(5-6-7). Surface pressure distributions for two spheres with Zs = 2.48.

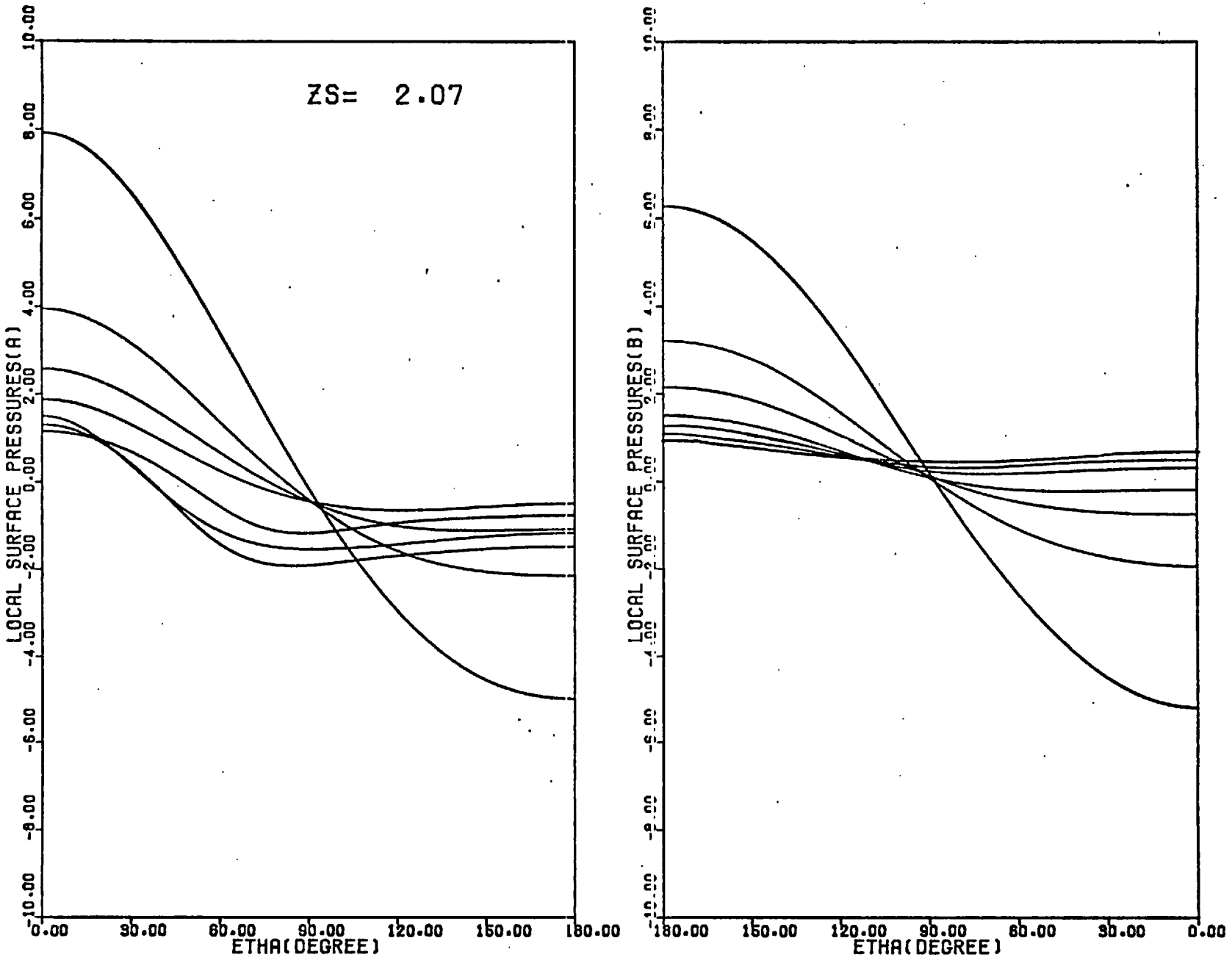

Figure(5-6-8). Surface pressure distributions for two spheres with Zs = 2.07.

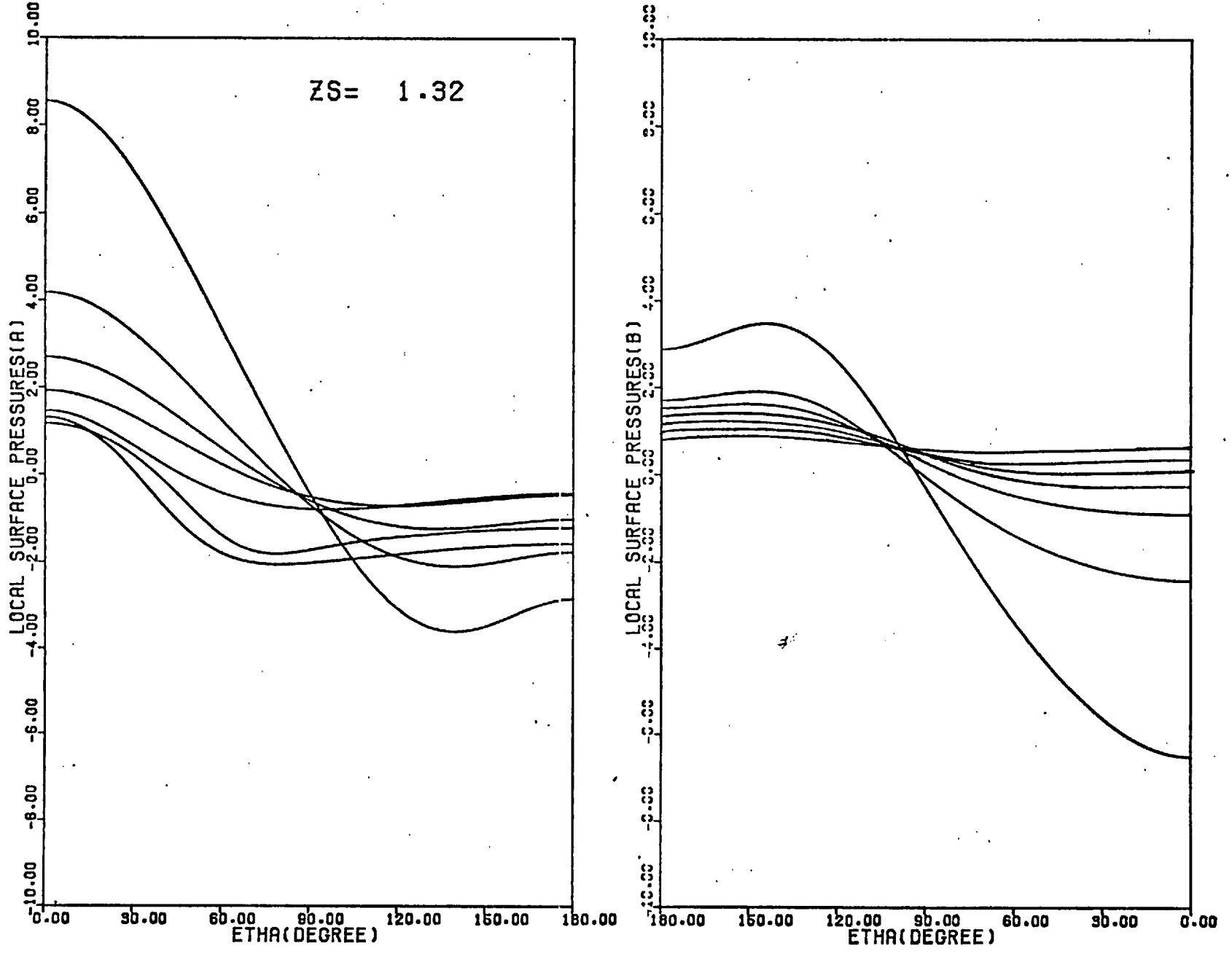

Figure(5-6-9). Surface pressure distributions for two spheres with Zs = 1.32.

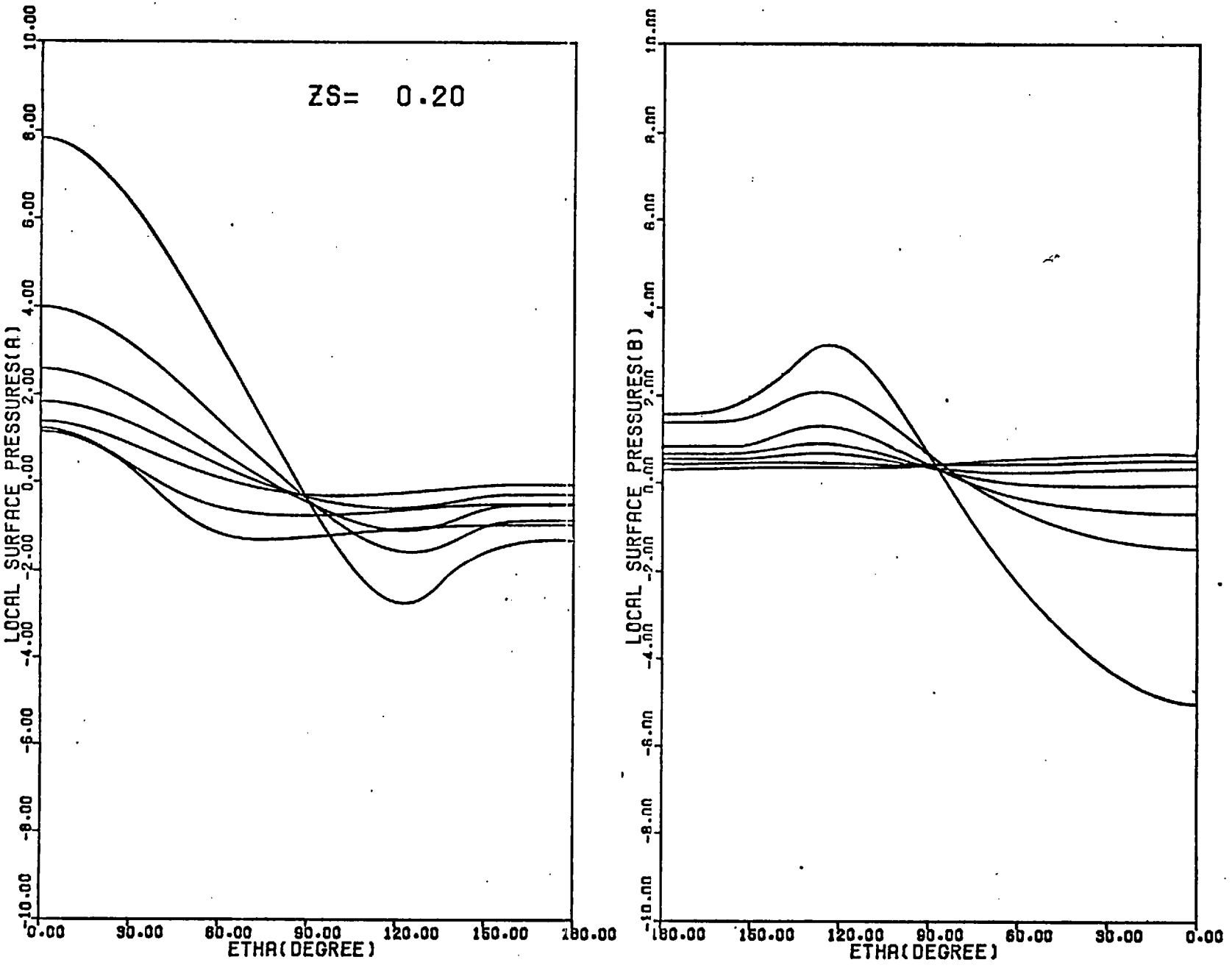

Figure(5-6-10). Surface pressure distributions for two spheres with Zs = 0.20.

the inner region between the spheres. The variation of surface pressures with Reynolds number for these two smallest sphere spacings is similar to those for the larger sphere spacings in that as the Reynolds number increases the dimensionless pressure coefficients at the front surface of each sphere become smaller while those at the rear surface of each sphere become larger.

From the above discussion, it is clear that the closeness of the spheres affects the pressure distributions at the rear surface of sphere A and at the front surface of sphere B. As the sphere spacing decreases, the dimensionless pressure coefficients at the rear surface of sphere A become larger while those at the front surface of sphere B become smaller so that the surface pressure distributions for the two spheres become further away from those for a single isolated sphere. On the other hand, the pressure distributions at the front surface of sphere A and at the rear surface of sphere B do not change much when the sphere spacing decreases from $Z_s = 3.09$ to $Z_s = 0.20$.

It is important to note that in comparison with the behaviour at smaller Reynolds numbers, the surface pressures over sphere A decrease very rapidly from the front stagnation and affect the pressure distributions at the rear surface of the sphere. The absolute values of the negative dimensionless pressure coefficients at the rear surface of sphere A are larger at Reynolds numbers of 50 and 100 than at a Reynolds number of 25. This dependence of the downstream surface pressure coefficients on the Reynolds number appear to be abnormal.

This may be a result of the combined effect of the large Z-grid-line spacings adjacent to the upstream surface of sphere A and the existence of a thin fluid dynamic boundary layer. The boundary layer becomes sufficiently thin at high Reynolds numbers of 50 and 100 that the boundary layer over part of the upstream surface of sphere A is contained within the large Z-grid-line spacing immediately next to the surface of sphere A. As a result, the dimensionless pressure coefficients at the upstream surface of sphere A obtained from the vorticity distributions in that region are too small. This fact thus contributes to the anomalous pressure distributions calculated for the downstream surface of sphere A because the surface pressures calculated for the downstream surface of sphere A are dependent on the accuracy of the surface pressures calculated for the upstream surface of the sphere. Fortunately, this anomaly becomes less acute when either the sphere spacing or the mesh spacing in Z is made smaller.

5-7. Drag coefficients.

When a viscous fluid flow around a solid sphere , a drag force is produced in the direction of flow which tends to resist the motion of the sphere in the fluid. The total drag, D_T, on the submerged sphere is the sum of the frictional drag, D_F, which is a result of the shear stresses acting on the sphere and is thus dependent upon the extent and character of the boundary layer; and the pressure drag, D_p, which arises from the pressure variation over the surface and is thus dependent upon the shape of the immersed object and on flow separation. The frictional drag on the sphere is obtained by integration of all the shear forces on the sphere which are tangential to the surface, while the pressure drag is obtained from the integration of the pressures on the sphere. The drag forces exerted on the sphere are expressed in terms of drag coefficients which are obtained from the division of the drag forces by $\frac{1}{2}\rho U^2 A$, where A is the cross-sectional area of the sphere. Hence, the total drag coefficient, C_{DT}, is the sum of the frictional drag coefficient,C_{DF}, and the pressure drag coefficient, C_{DP}.

Similarly, for a Newtonian fluid flowing around a system of two equally sized spheres parallel to their line of centres, the resistance to the motion of the spheres or the drag forces exerted upon the spheres are also expressed in terms of drag coefficients. For sphere A, the frictional drag coefficient, C_{DFA}, the pressure drag coefficient, C_{DPA}, and the total drag coefficient, C_{DTA}, were calculated using equations(4-5-5) to (4-5-7), respectively; while for sphere B, the frictional drag

coefficient, C_{DFB}, the pressure drag coefficient, C_{DPB}, and the total drag coefficient, C_{DTB}, were calculated using equations(4-5-8) to (4-5-10), respectively . Detailed descriptions of the derivations of these equations are given in Appendix B.

For each sphere spacing, there are two sets of results corresponding to the two solutions obtained from the Navier-Stokes equations using two different mesh spacings in Z. For the five sphere spacings: Zs = 3.09, 2.48, 2.07, 1.32, and 0.20, the total drag coefficients, the frictional drag coefficients, and the pressure drag coefficients of the two spheres are plotted against Reynolds number as shown in Figures(5-7-1) to (5-7-10), and the numerical results are given in Tables(5-7-1) to (5-7-10)(Appendix E). The results obtained using a mesh spacing of |Zs/20| in Z are shown in Figures(5-7-1) to (5-7-5) and in Tables(5-7-1) to (5-7-5); while those obtained using a larger mesh spacing of |Zs/10| in Z are shown in Figures(5-7-6) to (5-7-10) and in Tables(5-7-6) to (5-7-10).

For each sphere spacing, except those at high Reynolds numbers, the frictional drag coefficients, the pressure drag coefficients, and the total drag coefficients of the two spheres decrease nearly linearly with increasing Reynolds number on logarithmic plots, and the frictional drag coefficients are always larger than the pressure drag coefficients. It is important to note that flow separation from the surfaces of the spheres results in the pressure drag coefficients being larger than the frictional drag coefficients. Hence, at high Reynolds numbers the pressure drag coefficients are larger

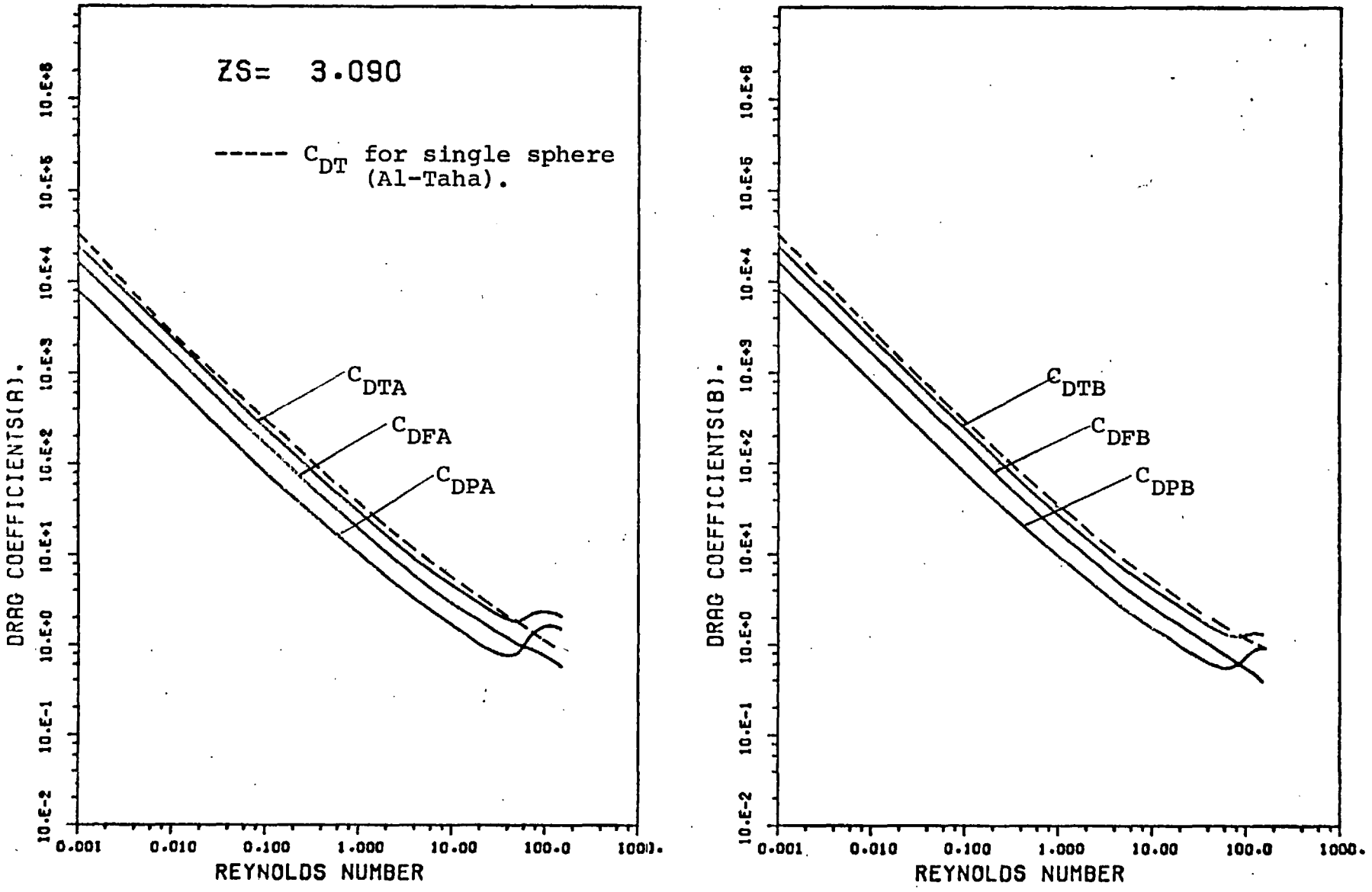

Figure(5-7-1). Drag coefficients for two spheres with Zs = 3.09.

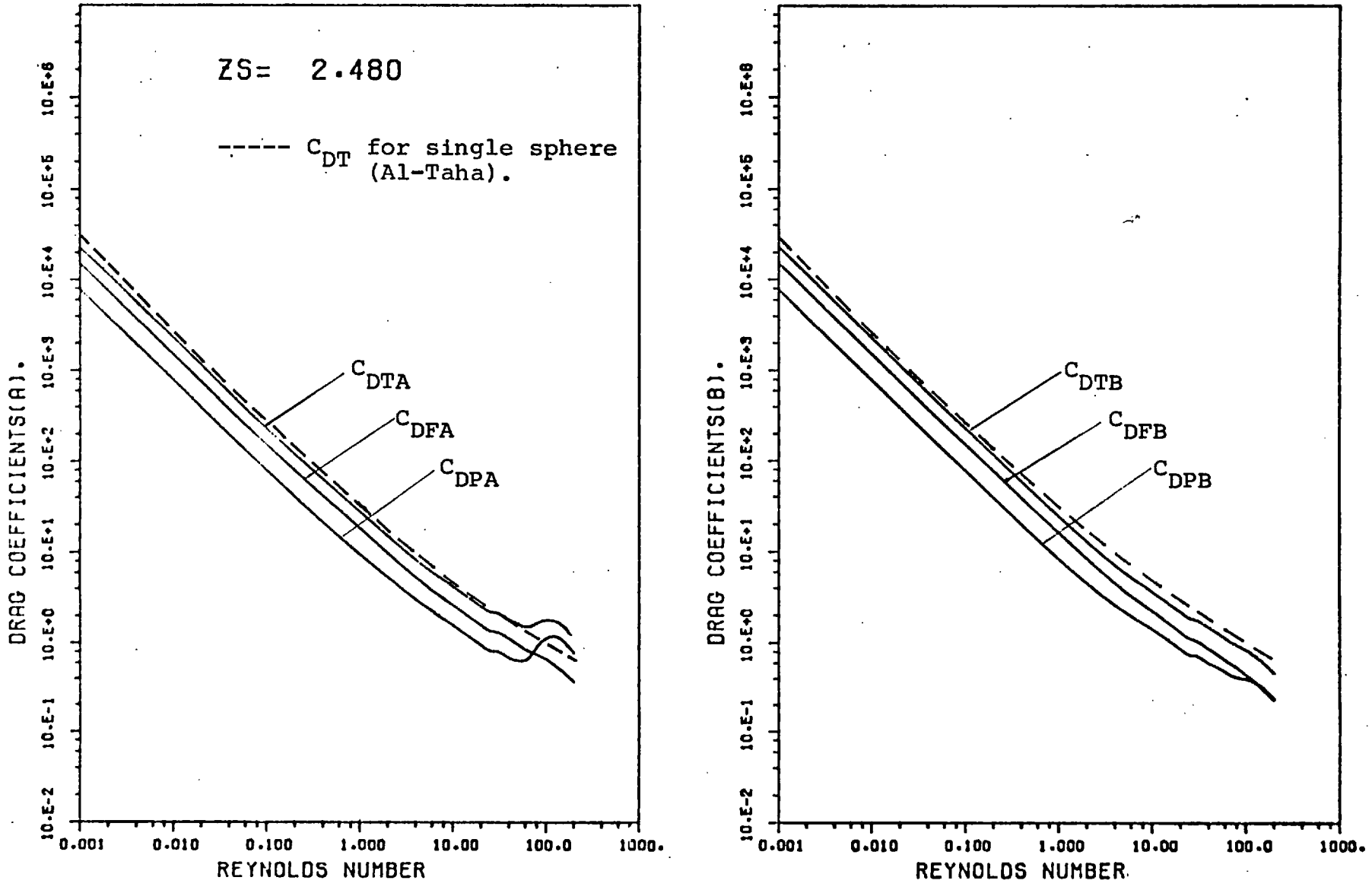

Figure(5-7-2). Drag coefficients for two spheres with Zs = 2.48.

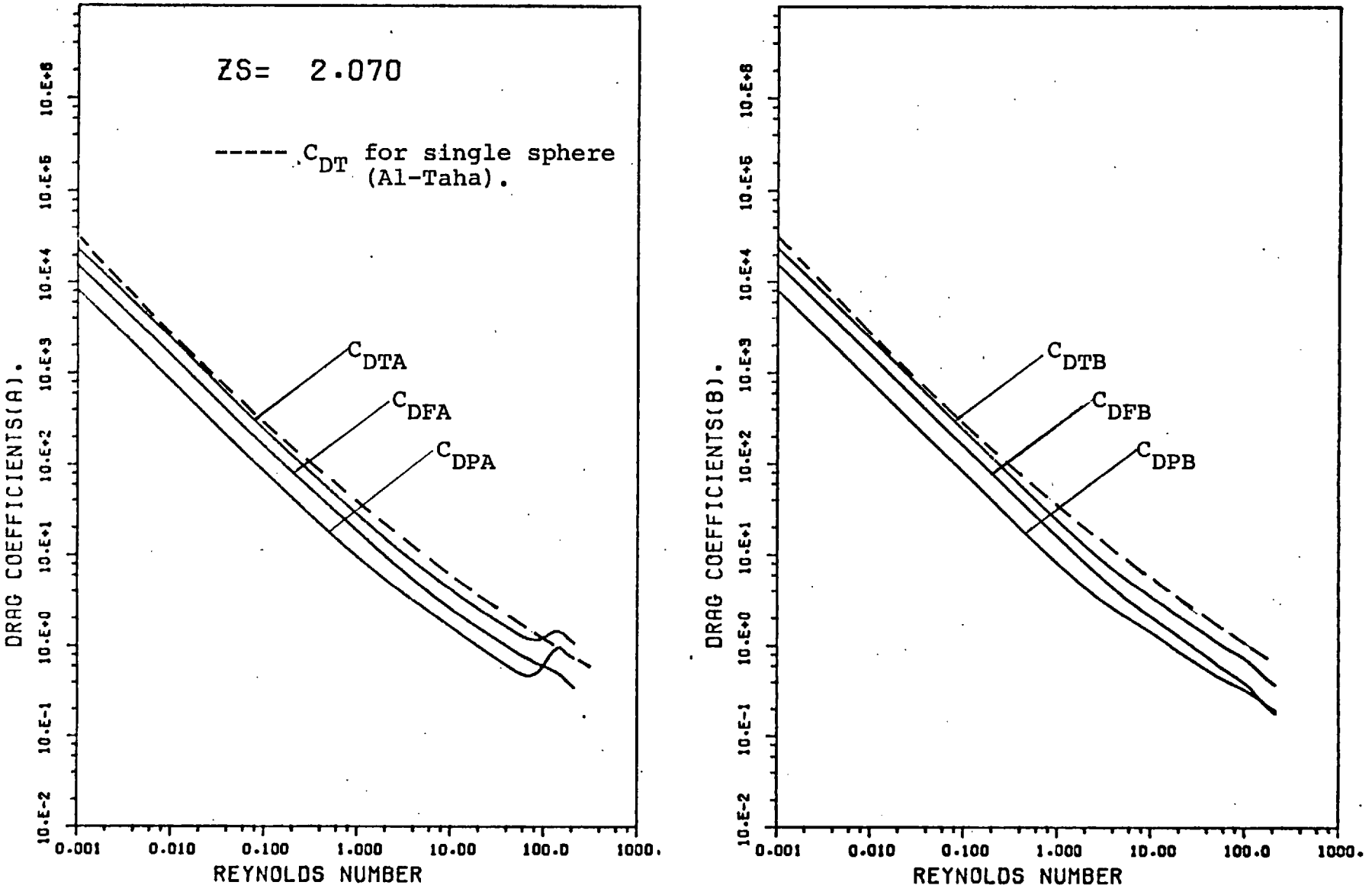

Figure(5-7-3). Drag coefficients for two spheres with Zs = 2.07.

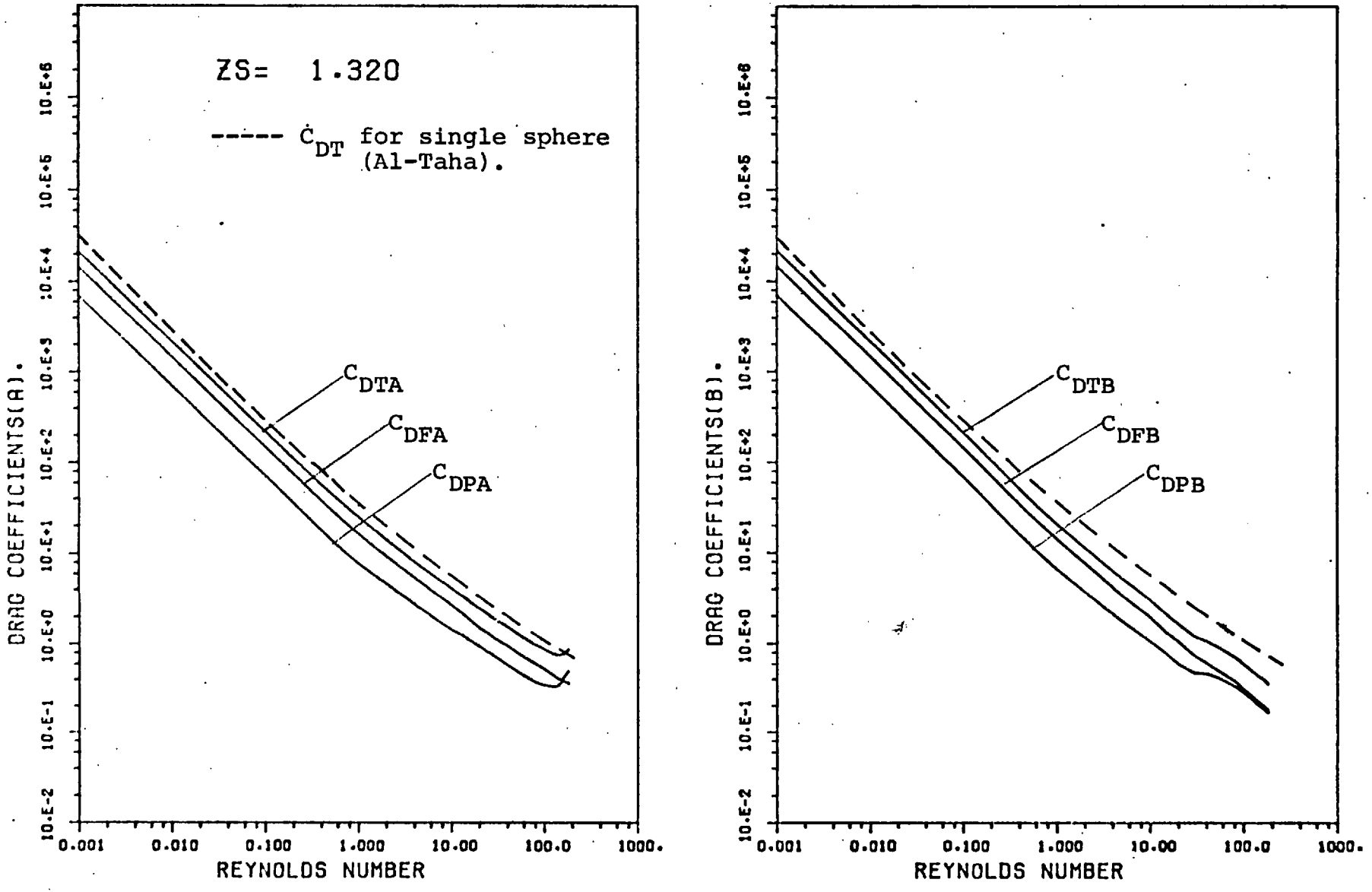

Figure(5-7-4). Drag coefficients for two spheres with Zs = 1.32.

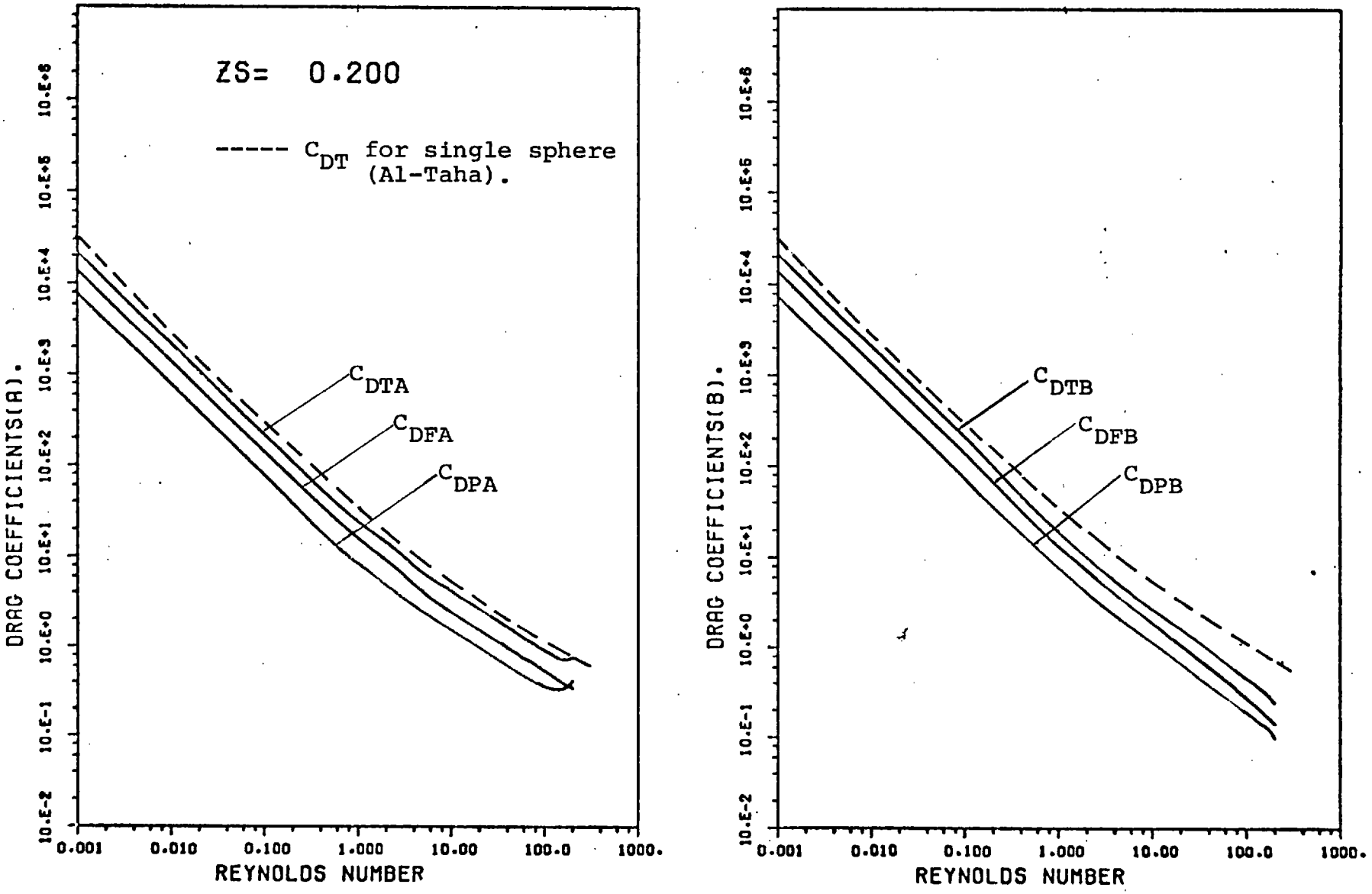

Figure(5-7-5). Drag coefficients for two spheres with Zs = 0.20.

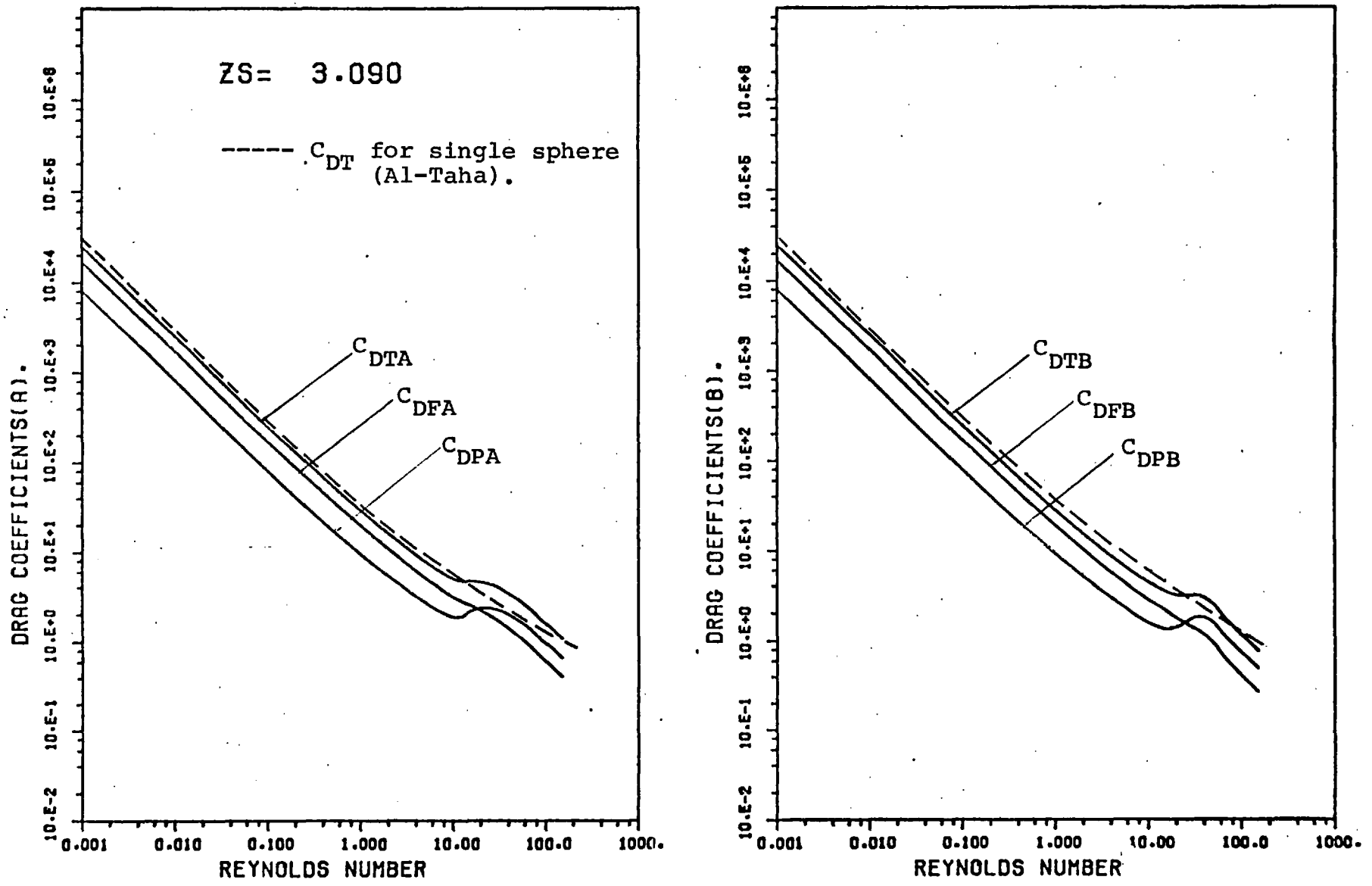

Figure(5-7-6). Drag coefficients for two spheres with Zs = 3.09.

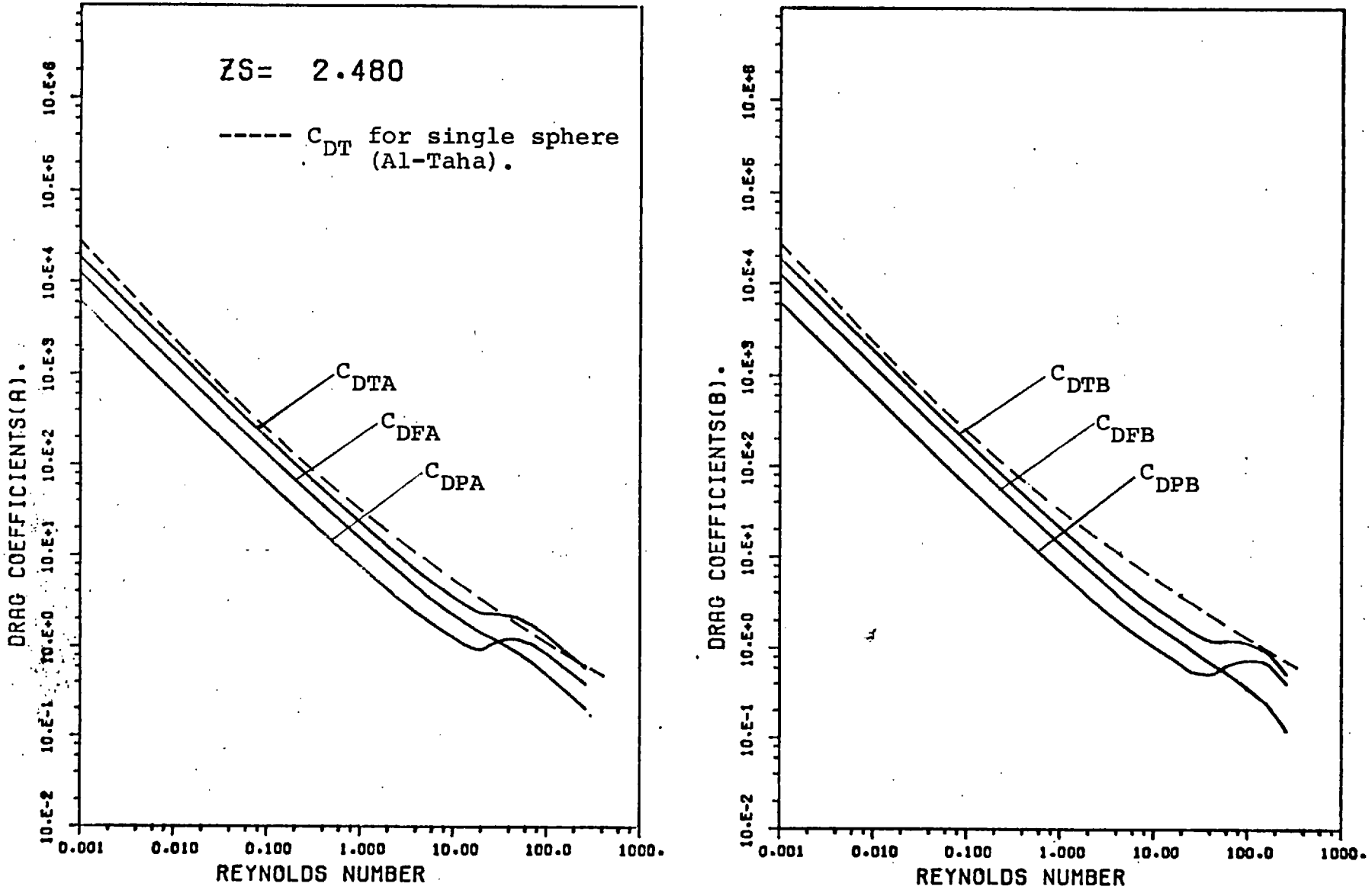

Figure(5-7-7). Drag coefficients for two spheres with Zs = 2.48.

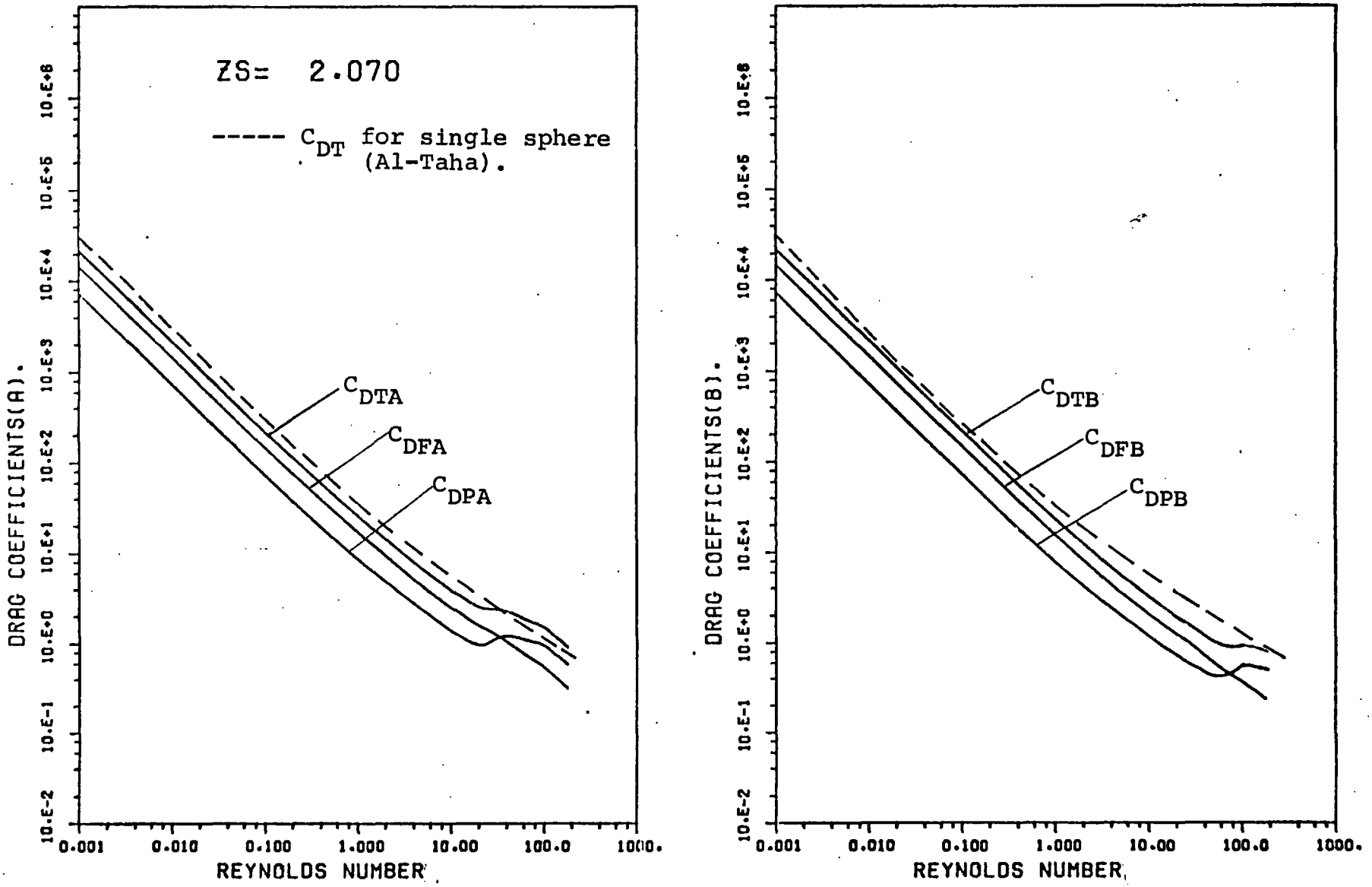

Figure(5-7-8). Drag coefficients for two spheres with Zs = 2.07.

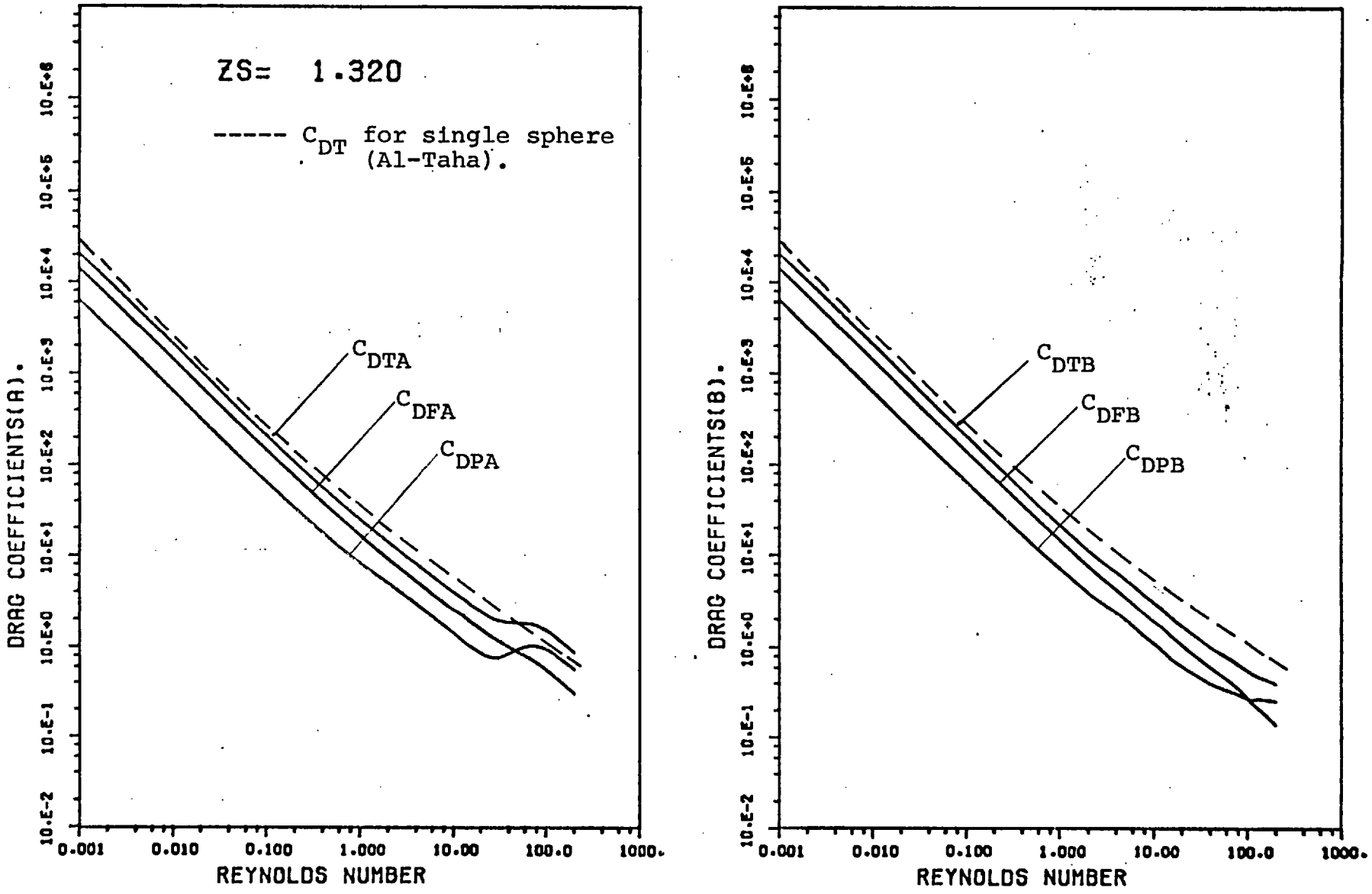

Figure(5-7-9). Drag coefficients for two spheres with Zs = 1.32.

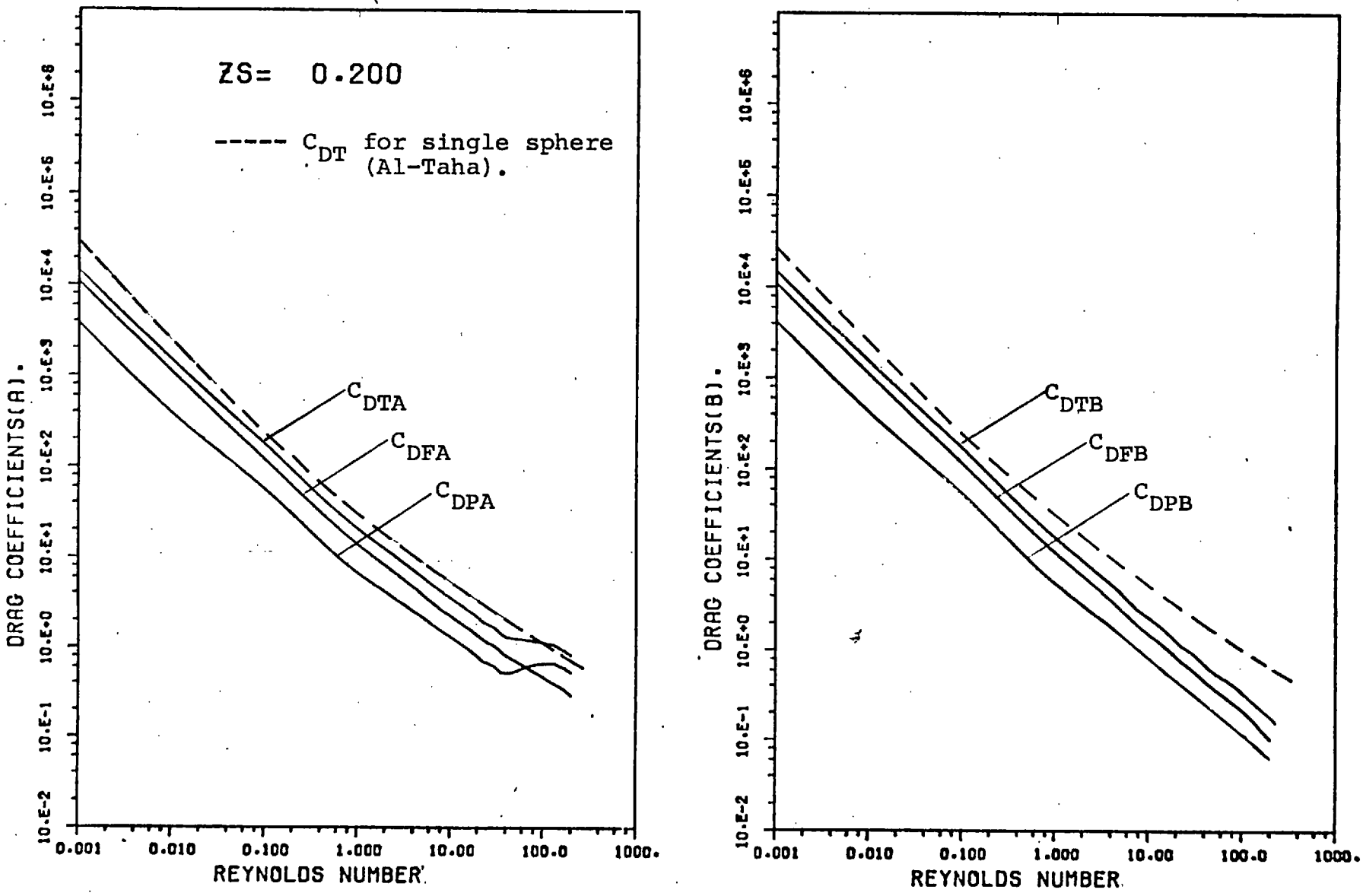

Figure(5-7-10). Drag coefficients for two spheres with Zs = 0.20.

than the frictional drag coefficients except for sphere B for the smallest sphere spacing Zs = 0.20 where the pressure drag coefficients are always smaller than the frictional drag coefficients. The range of Reynolds numbers over which the drag coefficients decrease nearly linearly with the Reynolds number is smaller for sphere A than for sphere B. This may be because for each sphere spacing, the flow separation from the back of sphere A is always larger than that from the back of sphere B. It is important to note that for each sphere spacing, the pattern of the variation of the drag coefficients with Reynolds number remains similar when the mesh spacing in Z changes from |Zs/20| to |Zs/10|.

Except at high Reynolds numbers, the total drag coefficients of sphere A for each sphere spacing are smaller than those of a single isolated sphere obtained by Al-Taha(1969). Also, except at high Reynolds numbers for the largest sphere spacing Zs = 3.09 the total drag coefficients of sphere B are always smaller than those of a single isolated sphere obtained by Al-Taha(1969). It is clear from Figures(5-7-1) to (5-7-10) that for each sphere spacing, the agreement of the present results with those of a single isolated sphere obtained by Al-Taha(1969) is better for sphere A than for sphere B; on the other hand, the agreements of the present results of the two spheres with those of a single isolated sphere are better for large sphere spacings than for small sphere spacings.

CHAPTER 6.

DISCUSSION OF SOLUTIONS OF THE DIFFUSION EQUATION.

6-1. Introduction.

In the present two-sphere forced convective mass transfer problem, numerical solutions of the diffussion equation were obtained separately after the corresponding numerical solutions of the Navier-Stokes equations had been obtained. For each sphere spacing, the solution of the diffusion equation over a flow region required the stream function distribution in the flow region at a specified Reynolds number. The computer programme, Program 2, used for the solution of the diffusion equation was arranged is such a way that for each sphere spacing and Reynolds number the concentration distributions in the flow region could be generated for a wide range of Peclet numbers.

The distance between the spheres, which is governed by the sphere spacing parameter Zs, is an important factor in the study of the particle-to-particle interaction between the spheres in the two-sphere mass transfer problem. Five sphere spacings: Zs = 0.20, 1.32, 2.07, 2.48, and 3.09, corresponding to two equally sized spheres nearly touching, being one, three, five, and ten diameters apart, respectively, were considered in this study. For each sphere spacing, four Reynolds numbers of 0.001, 1.0, 10.0, and 100.0, were selected in order to study the fluid dynamic effect upon the rates of mass transfer from the spheres. For each sphere spacing and Reynolds number, the diffusion equation was then solved for concentration distributions for a wide range of Peclet numbers from 0.001 to as high as 500. From the resultant concentrations, the

concentration contours around the spheres were interpolated and plotted by the computer line-printer, and the local and overall rates of mass transfer from the spheres were also calculated.

The study of the present two-sphere mass transfer problem is divided into four sections. The factors affecting the accuracy of the numerical solutions of the diffusion equation are analyzed in section(6-2). The qualitative study of the concentration profiles around the spheres is given in section(6-3), while the quantitative studies of the local and overall rates of mass transfer from the spheres are presented in sections(6-4) and (6-5), respectively. In the last three sections, the variations of the concentration distributions around the spheres, the local and overall rates of mass transfer from the spheres, with three parameters: sphere spacing, Reynolds number, and Peclet number, are considered in detail. Because of the similarity between the forms of the diffusion equation and the vorticity transport equation, the methods of solution and the arrangements of the computer programmes for solving the diffusion equation were generally similar to those for solving the Navier-Stokes equations, and the resultant distributions of concentration and vorticity around the spheres were also similar in character.

6-2. Analysis of the factors affecting the numerical solutions.

The factors affecting the accuracy of the numerical solutions of the diffusion equation, such as the coordinate system used, the distributions of grid lines in the flow region, the methods of solution, and the choice of convergence criterion, etc, were similar to the factors affecting the accuracy of the numerical solutions of the Navier-Stokes equations. An understanding of these factors and the influences and limitations which they imposed upon the accuracy of the numerical results of the diffusion equation is necessary.

Bi-spherical coordinates were used in the present study because of the ease with which they can be used to describe the locations of the two spheres and the associated boundary conditions of the Navier-Stokes and diffusion equations. It is important to note that the flow region and the distributions of grid lines in the flow region for which the solutions of the diffusion equation were obtained were exactly the same as those with which the solutions of the Navier-Stokes equations were obtained. For each sphere spacing, two distributions of grid lines in the flow region were used. In these two distributions, the grid lines for the Z-direction were distributed according to two different mesh spacings of $|Zs/10|$ and $|Zs/20|$ in Z, while those for the θ-direction were distributed according to a constant increment of 6^{o} in the angle η; hence, the numbers of mesh points in each flow region were 21x31 and 41x31, respectively. The outer boundary of the flow region, which has its centre at the mid-point of the line of centres of the spheres, was chosen to have a radius of 7.0 times the distance between the centres of the spheres for the

smallest sphere spacing Zs = 0.20, and a radius of 3.5 times the distance between the centres of the spheres for the four larger sphere spacings considered.

The reason for using two different distributions of grid lines in the flow region at each sphere spacing, arose because as has been described in section(5-2), of the inherent characteristic of the bi-spherical coordinate system of providing unequal distance between any two neighbouring grid lines in the Z-direction around the spheres. The large Z-grid-line spacings around the upstream surface of sphere A created some difficulties in the calculation of the correct local Sherwood numbers in that region and subsequently affected the accuracy of the overall Sherwood numbers obtained for sphere A at high Peclet numbers. This was because at high Peclet numbers the thickness of the diffusional boundary layer in the region upstream of sphere A was very small compared with the large Z-grid-line spacings. The limitations imposed by the availability of computer memory storages upon the solutions of the Navier-Stokes equations, restricted the flexibility of altering the mesh spacing in Z in order to improve the numerical solutions of the diffusion equation at the upstream surface of sphere A.

Because of its rapid rate of convergence and simplicity of use, the extrapolated Gauss-Seidel method was used to obtain solutions of the diffusion equation. Although over-relaxation of the solutions was found to give a faster rate of convergence, at high Peclet numbers numerical solutions of the diffusion equation were difficult to obtain and it was necessary to adopt a scheme of under-relaxation. The relaxation factor, which was

supplied by trial-and-error, was decreased with increasing Peclet number. The convergence criterion for the dimensionless concentration was specified to be 10^{-4}, and an absolute point-convergence test was used. With this method, convergence of the solutions at all mesh points in the flow region was obtained.

In order to understand the influence of the convergence criterion for the dimensionless concentration on the numerical solutions of the diffusion equation, solutions were obtained for the limiting case of zero Peclet number for two different magnitudes of the convergence criterion: 10^{-4} and 10^{-6}. Similarly, in order to understand the influence of the distribution of grid lines in the flow region on the numerical solutions of the diffusion equation, for each specified sphere spacing solutions were obtained for the limiting case of zero Peclet number for three different distributions of mesh points: 21x31, 41x31, and 41x61. In each case, the stream function was set to zero throughout the flow region. The overall Sherwood numbers obtained from these solutions are presented in Table(6-2-1) for each of the five sphere spacings considered in this work. It can be seen from the table that, as predicted by Cornish(1965), all the values of the overall Sherwood numbers are less than the limiting value of 2.0 obtained from a single isolated sphere with molecular diffusion alone to an infinite medium. For each sphere spacing and value of the convergence criterion for the dimensionless concentration, the overall Sherwood numbers increase slightly when the distribution of mesh points changes from 21x31 to 41x31; however, they become smaller when the distribution of mesh points is further changed from 41x31 to 41x61. It is interesting to note that the

Table(6-2-1). The effects of the variations of convergence criterion and distribution of grid lines upon the overall Sherwood numbers of the spheres at zero Peclet number.

Zs.	ε_C*	The distributions of mesh points.						R_o=r/d
		21x31		41x31		41x61		
		Sh_{AO}	Sh_{BO}	Sh_{AO}	Sh_{BO}	Sh_{AO}	Sh_{BO}	
0.20	10^{-4}	1.59584	1.59109	1.60807	1.59280	1.58067	1.57592	14.0
	10^{-6}	1.57808	1.57804	1.58704	1.58690	1.56881	1.56875	14.0
1.32	10^{-4}	1.84224	1.83902	1.85567	1.85092	1.82892	1.82216	7.0
	10^{-6}	1.82715	1.82711	1.83198	1.83194	1.81441	1.81434	7.0
2.07	10^{-4}	1.92461	1.92211	1.93429	1.92979	1.91659	1.91097	7.0
	10^{-6}	1.90781	1.90778	1.90950	1.90945	1.89999	1.89993	7.0
2.48	10^{-4}	1.95779	1.95535	1.96021	1.95565	1.95160	1.94622	7.0
	10^{-6}	1.93828	1.93826	1.93281	1.93277	1.93310	1.93304	7.0
3.09	10^{-4}	1.98106	1.97857	1.99244	1.98781	1.98232	1.97698	7.0
	10^{-6}	1.95427	1.95424	1.95967	1.95962	1.95915	1.95909	7.0

Table(6-2-2). Comparison of numerical overall Sherwood numbers for the limiting case of zero Peclet number with theoretical values.

Zs.	Theoretical values (Cornish).	Numerical results (Aminzadeh et al).		Present results $\Delta Z=\lvert Zs/20\rvert, \Delta\eta=3^o$		ε_C*
		Sh_{AO}	Sh_{BO}	Sh_{AO}	Sh_{BO}	
0.20	1.3920	1.39239	1.39231	1.44563	1.44555	10^{-6}
1.00	1.5232	1.54658	1.54653	1.56287	1.56280	10^{-6}
2.10	1.7852	1.80739	1.80693	1.80723	1.80662	10^{-5}
3.00	1.9056	1.92645	1.92597	1.91962	1.91907	10^{-5}

limiting overall Sherwood numbers for the spheres obtained using the distributions of mesh points of 21x31 and 41x61 are close to each other even though the mesh spacings for the Z- and θ-directions have been each reduced by half. On the other hand, for each sphere spacing and distribution of mesh points, the limiting overall Sherwood numbers for the spheres decrease by less than 2% when the convergence criterion for the dimensionless concentration decrease from 10^{-4} to 10^{-6}, and the small improvement in the results was obtained at a great expense in computing time. Hence, it can be concluded that the use of a value of 10^{-4} for the convergence criterion for the dimensionless concentration and the use of the distributions of mesh points of 21x31 and 41x31 in the present work were appropriate.

Aminzadeh, Al-Taha, Cornish, Kolansky, and Pfeffer(1974) computed the overall Sherwood numbers for the limiting case of zero Peclet number for four sphere spacings of Zs = 0.20, 1.00, 2.10, and 3.00, by using a large value for the outer boundary, r/d = 40, and by setting the velocity components V_Z^* and V_θ^* equal to zero. In order to compare the effect on the solutions of the diffusion equation of distributing the grid lines for the θ-direction according to a constant increment in the angle η, with the effect of distributing the grid lines for the θ-direction according to a constant increment in the values of θ as used by Aminzadeh et al, overall Sherwood numbers were calculated for the limiting case of zero Peclet number for the four sphere spacings with the same outer boundary specification, convergence criterion, and number of mesh points in the flow region as used by Aminzadeh et al, but with the distribution

of grid lines for the θ-direction set with a constant increment in the angle η and by setting the stream function equal to zero. The two results together with the theoretical values predicted by Cornish(1965) are listed in Table(6-2-2). It is clear from the table that for the two largest sphere spacings, the present results are in very good agreement with the theoretical values predicted by Cornish and with the numerical results obtained by Aminzadeh et al. However, for the two smallest sphere spacings, especially the smallest sphere spacing Zs = 0.20, the present results are noticeably larger than the theoretical values predicted by Cornish and the numerical results obtained by Aminzadeh et al. The difference in the two sets of numerical results may be because the present scheme provides a more even distribution of grid lines for the θ-direction in the flow region than the scheme used by Aminzadeh et al, particularly when the sphere spacing is very small, as shown in Figures(4-1-3) to (4-1-12).

6-3. Concentration distributions.

The numerical solutions of the diffusion equation were expressed in terms of the concentration distributions over the whole flow region. For each sphere spacing, the tabulated results of the concentration distributions at each specified Reynolds number and Peclet number were interpolated and the concentration contours plotted around the spheres. From these plots, the variation of the concentration profiles with Peclet number, Reynolds number, and sphere spacing, can be studied.

The concentration profiles around two equally sized spheres at five different sphere spacings: Zs = 0.20, 1.32, 2.07, 2.48, and 3.09, are shown in Figures(6-3-1) to (6-3-29) for some of the four selected Reynolds numbers of 0.001, 1.0, 10.0, and 100.0, each for a wide range of Peclet numbers. In each figure, six concentration contours with values of C^* of 1.0, 0.80, 0.50, 0.25, 0.10, and 0.05, are plotted around the spheres. It is important to note that the surfaces of the two spheres are coincident with the contours $C^* = 1.0$.

For the smallest sphere spacing considered in this study: Zs = 0.20, L/R = 2.0402, the distributions of concentration around the two nearly touching spheres are shown in Figures(6-3-1) to (6-3-6) for three selected Reynolds numbers of 0.001, 1.0, and 100.0, each for a series of Peclet numbers. The most interesting feature of the distributions is that for all the Reynolds and Peclet numbers shown, all of the contours, except those with $C^* = 1.0$, envelop the two spheres and the inner region between them. This indicates that the two nearly touching spheres behave like a single combined object and that the fluid

in the inner region between the spheres contains a high concentration of the material transferred. As a consequence, the rates of mass transfer from the spheres to the fluid in the inner region between the spheres are greatly depressed.

For each Reynolds number, the concentration profiles around the spheres at low Peclet numbers of 0.001 to 0.1 remain almost unchanged and are symmetrical about a plane placed normal to the direction of flow and passing through the mid-point of the line of centres. This is because the transfer of material from the solid surfaces to the flowing fluid is mainly by means of molecular diffusion and thus the material diffuses uniformly in all directions. However, for Peclet numbers greater than 0.1, the concentration contours upstream of sphere A move closer to the front surface of that sphere, those in the region between the spheres move nearer to the line of centres, while those downstream of sphere B extend further away from the rear surface of that sphere and eventually develop into a tail at high Peclet numbers. This is because the material around the spheres is convected more rapidly rearwards than it diffuses forwards from the surfaces of the spheres. Hence, at high Peclet numbers the concentration profiles upstream of sphere A are confined in an increasingly narrower region and a diffusional boundary layer is developed at the upstream surface of the sphere. On the other hand, because of the closeness of the two spheres and the existence of a pool of highly concentrated fluid in the inner region between the spheres, the concentration profiles upstream of sphere B do not change much with increasing Peclet number and a diffusional boundary layer is not developed at the upstream surface of sphere B even at high Peclet numbers.

It is clear that for Peclet numbers greater than 0.1, the effect of convection on the rates of mass transfer from the spheres is significant, and increases in importance with increasing Peclet number. However, the effect of convection on the rates of mass transfer is always stronger for sphere A than for sphere B.

At low Peclet numbers of 0.001 to 0.1, variations in the flow field around the two spheres have very little effect upon the concentration profiles which remain almost unchanged when the Reynolds number changes from 0.001 to 100.0. On the other hand, at high Peclet numbers the concentration profiles are influenced by variations in the flow region, in particular, the contours with small values of concentration move closer to the front surface of sphere A and the line of centres between the spheres when the Reynolds number becomes larger. This suggests that at high Peclet numbers, the strong effect of convection upon the rates of mass transfer from the spheres is further strengthened at higher Reynolds number.

For the enlarged sphere spacing: Zs = 1.32, L/R = 4.0106, the concentration profiles for three selected Reynolds numbers of 0.001, 1.0, and 100.0, each for a series of Peclet numbers, are shown in Figures(6-3-7) to (6-3-12). Because of the larger distance between the spheres and the consequent lower concentration of the fluid in the inner region between the spheres, the concentration profiles for this sphere spacing have some obvious difference from those for the smallest sphere spacing. The contour $C^* = 0.80$, which envelops the two nearly touching spheres and the inner region between them at the previous sphere spacing, becomes two separate contours

each forming a closed path around a sphere, and the contour $C^* = 0.50$ becomes the first contour to envelop the two spheres which are at one diameter apart, and the inner region between them. On the other hand, the variations of the concentration profiles with Peclet and Reynolds numbers for this sphere spacing are similar to those for the smallest sphere spacing, except for the contour $C^* = 0.80$ in the inner region between the spheres and upstream of sphere B. When the Peclet number is increased, for Reynolds numbers of 0.001 and 1.0 the contour $C^* = 0.80$ move closer to the front surface of the sphere and for a Reynolds number of 100 the contour moves further away from the front surface of sphere B. This may be because at a high Reynolds number of 100 the flow separates from both the rear surface of sphere A and from the front surface of sphere B so that nearly the whole inner region between the spheres becomes a wake region with a consequent increase in the concentration of the fluid in the inner region between the spheres, especially upstream of sphere B.

For the sphere spacing: Zs = 2.07, L/R = 8.0510, the concentration profiles for three selected Reynolds numbers of 1.0, 10.0, and 100.0, each over a wide range of Peclet numbers, are shown in Figures(6-3-13) to (6-3-18). From the figures, it is clear that for all Reynolds and Peclet numbers, the contours $C^* = 0.80$ and $C^* = 0.50$ form closed paths around each of the two spheres, while the contour $C^* = 0.25$ is the first contour to envelop the two spheres and the inner region between them. For each Reynolds number, the concentration profiles at low Peclet numbers of 0.001 to 0.1 remain almost unchanged and are symmetrical about a plane through the mid-point of the line of

centres normal to the direction of flow showing that the transfer of material from the spheres is dominated by molecular diffusion. However, for higher Peclet numbers the material around the spheres is convected more rapidly rearwards than it diffuses forwards from the surfaces of the spheres. Hence, the effect of convection upon the rates of mass transfer from the spheres becomes significant and increases in importance with increasing Peclet number. Because of the larger distance between the spheres, the concentration profiles in the inner region between the spheres vary rapidly with increasing Peclet number and the contour forming closed paths around sphere A move further downstream while the contours forming closed paths around sphere B move closer to the front surface of sphere B. As a result, at high Peclet numbers a diffusional boundary layer is observed to have developed at the upstream surface of each sphere, however, its development at the upstream surface of sphere B is less well established than that at the upstream surface of sphere A. It is important to note that the numerical solution for a Reynolds number of 100.0 shows that flow separation occurs from the rear surface of sphere A and that at high Peclet numbers a pool of highly concentrated fluid is formed near the point of flow separation and over the downstream surface of sphere A where the rates of mass transfer will be greatly depressed.

When the Reynolds number changes from 1.0 to 100.0, the concentration profiles at low Peclet numbers of 0.001 to 0.1 remain almost the same. However, at higher Peclet numbers the concentration profiles change with Reynolds number, in particular, as the Reynolds number is increased the contours with small values of concentration move closer to the front surface of

each sphere as well as closer to the line of centres between the spheres. This indicates that at high Peclet numbers, the already strong effect of convection upon the rates of mass transfer from the spheres is further strengthened by an increase in the Reynolds number. However, for high Peclet numbers and all Reynolds numbers the effect of convection upon the rates of mass transfer is always stronger for sphere A than for sphere B.

The concentration profiles for four selected Reynolds numbers of 0.001, 1.0, 10.0, and 100.0, each for a series of Peclet numbers are shown in Figures(6-3-19) to (6-3-25) for the increased sphere spacing: Zs = 2.48, L/R = 12.0250. It is clear from the figures that the variations of the concentration profiles with both the Peclet number and the Reynolds number are similar to those for the sphere spacing Zs = 2.07. Similarly, at this sphere spacing, the contours C^* = 0.80 and C^* = 0.50 form closed paths around each sphere, while the contour C^* = 0.25 is the first contour to envelop the two spheres and the inner region between them; however, when the Peclet number reaches unity, the contour C^* = 0.25 becomes two separate contours and the contour C^* = 0.10 becomes the first contour to envelop the two spheres and the inner region between them. This may indicate that for each sphere spacing, the concentration of the lowest concentration contour which envelops both spheres is primarily dependent on Peclet number. On the other hand, because of the larger distance between the spheres, the development of a diffusional boundary layer at the upstream surface of sphere B becomes more clearly established for this sphere spacing than for the sphere spacing Zs = 2.07.

For the largest sphere spacing considered in this study: Zs = 3.09, L/R = 22.022, the concentration profiles are shown in Figures(6-3-26) to (6-3-29) for two selected Reynolds numbers of 1.0 and 100.o, each for a series of Peclet numbers. From these figures, it can be seen that the variations of the concentration profiles with Peclet number and Reynolds number are similar to those for the sphere spacing Zs = 2.48. On the other hand, because of the very large distance between the spheres, all contours except those with C^* = 0.10 and C^* = 0.05 form closed paths around each of the spheres. The most interesting feature of the concentration profiles is that when the Peclet number reaches unity, the contour C^* = 0.10 which envelops the spheres and the inner region between them at Peclet numbers less than 1.0 becomes two separate contours and the contours C^* = 0.05 becomes the sole contour to envelop the two spheres. Furthermore, as the Peclet number is further increased, the contour C^* = 0.10 which forms a closed path around sphere A extends rapidly downstream and eventually recombines with the contour C^* = 0.10 which forms a closed path around sphere B. The combined contour envelops once again the spheres and the inner region between them. This phenomenon occurs at Peclet numbers of 100 and 50 for the Reynolds numbers of 1.0 and 100.o, respectively. Because of the very large distance between the spheres, a diffusional boundary layer is always developed at the upstream surface of each sphere when the Peclet number is high; however, its development at the upstream surface of sphere A is always more advanced than that at the upstream surface of sphere B. It is clear that for this largest sphere spacing, the concentration profiles around the spheres are generally very similar to those around a single isolated sphere.

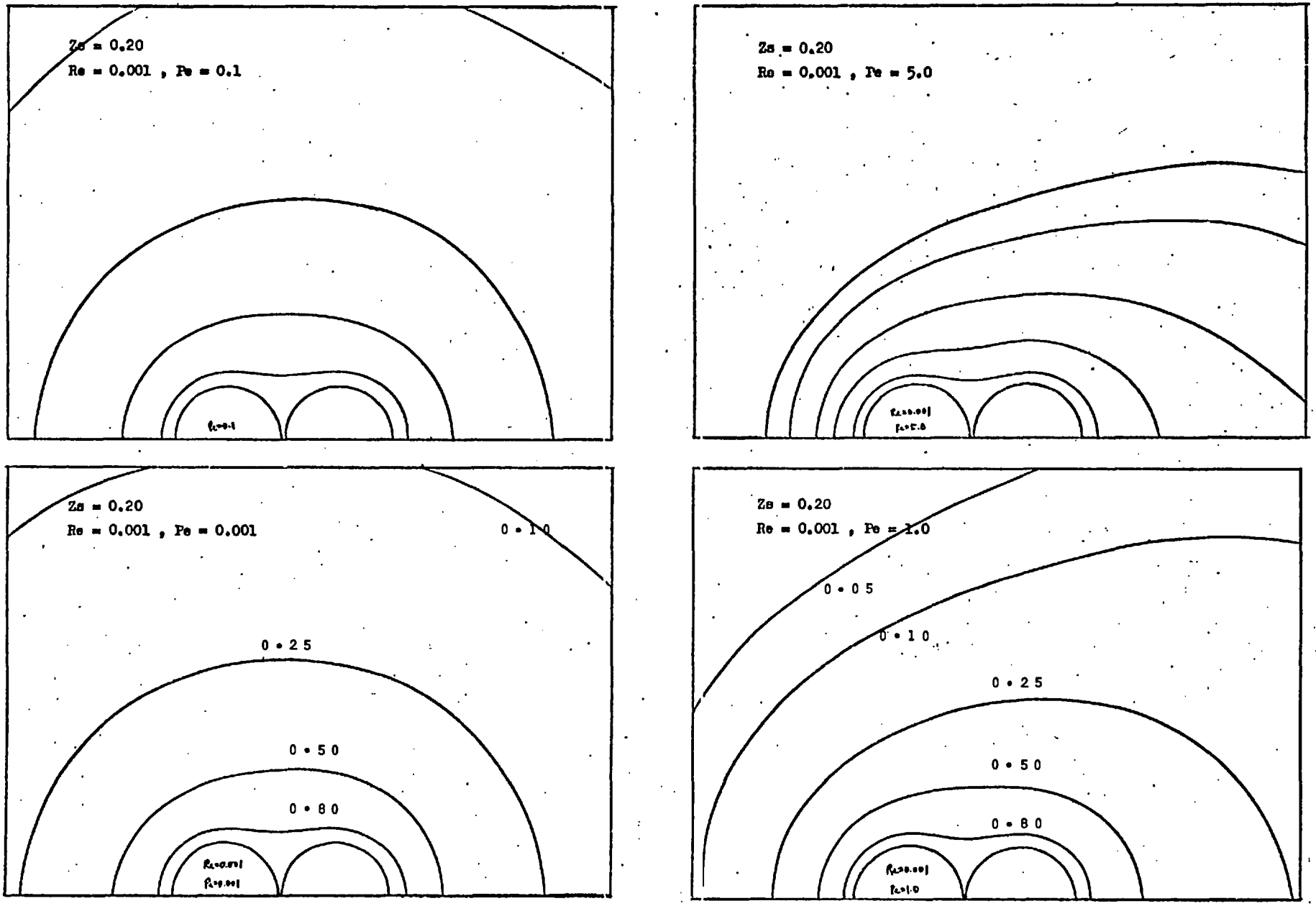

Figure(6-3-1). Concentration profiles around two spheres with Zs = 0.20.

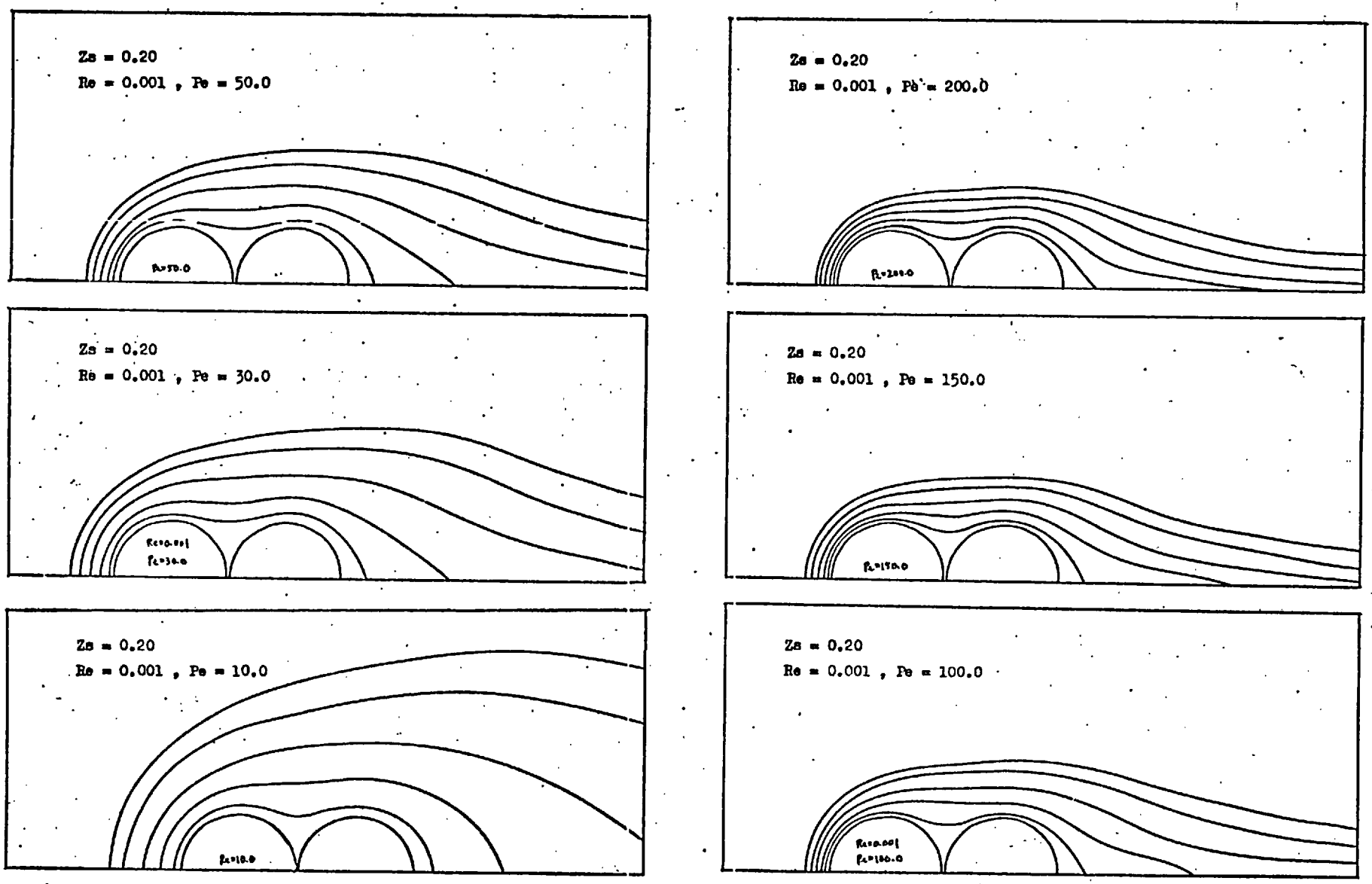

Figure(6-3-2). Concentration profiles around two spheres with Zs = 0.20.

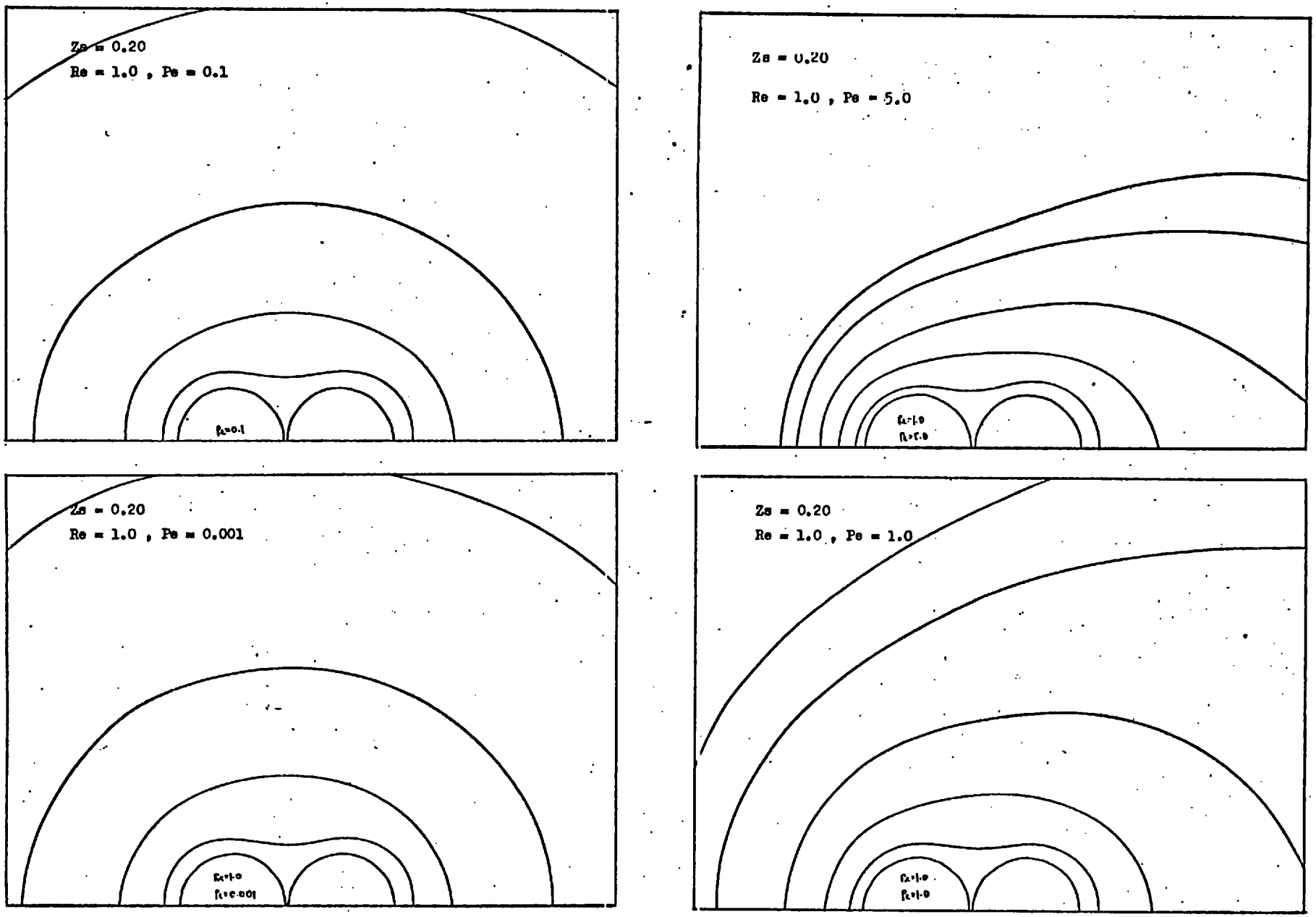

Figure(6-3-3). Concentration profiles around two spheres with Zs = 0.20.

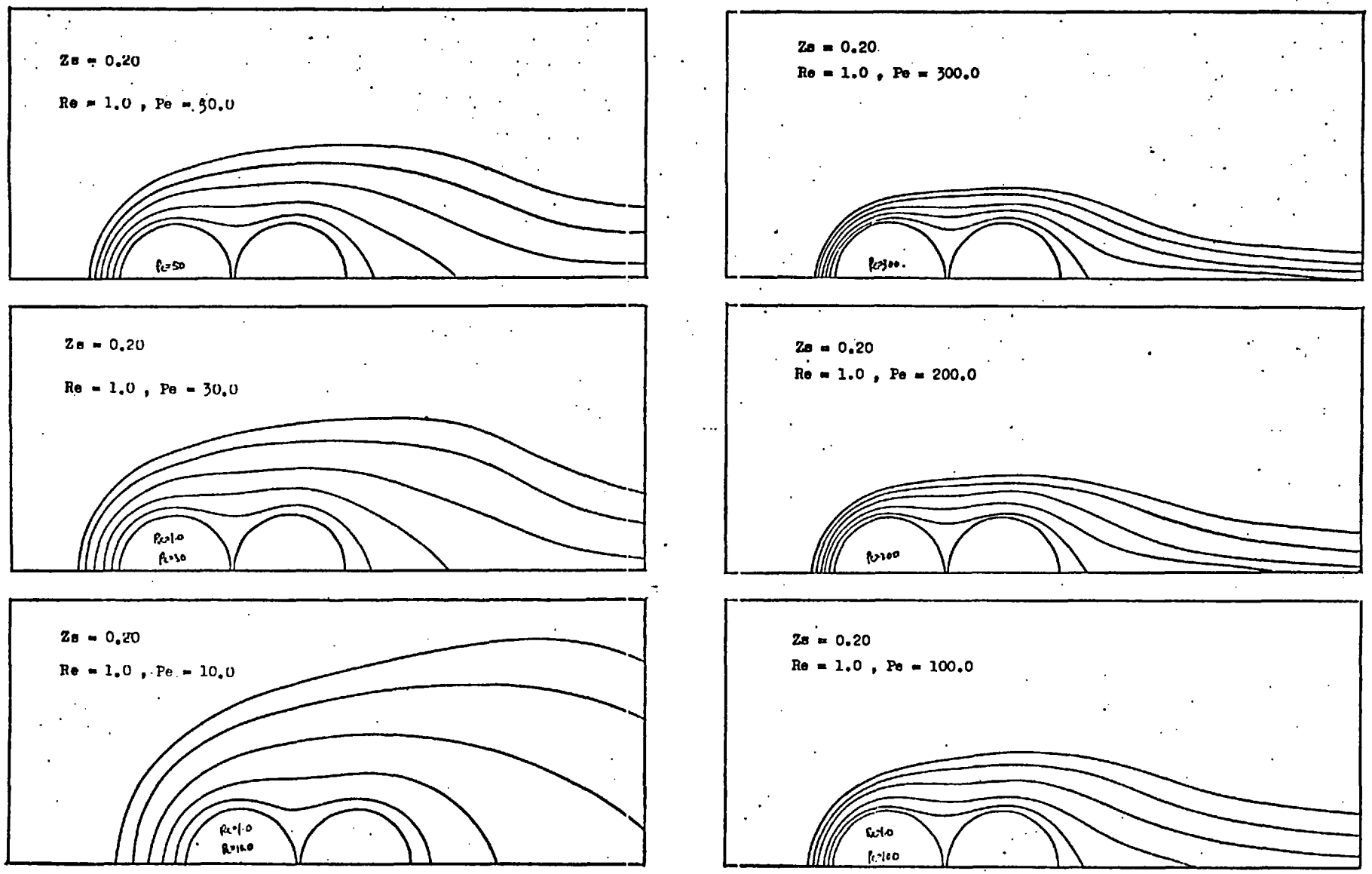

Figure(6-3-4). Concentration profiles around two spheres with Zs = 0.20.

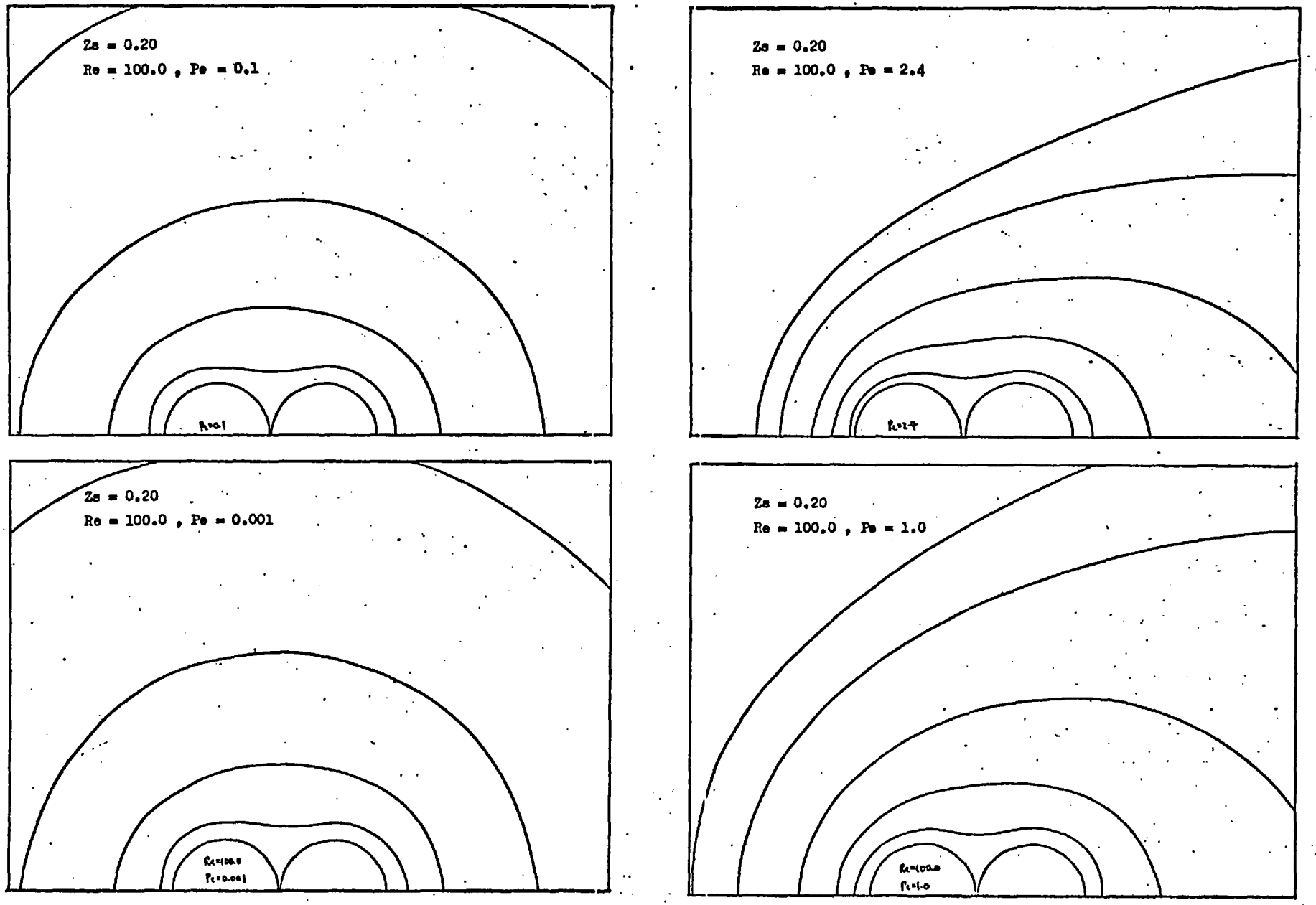

Figure(6-3-5). Concentration profiles around two spheres with Zs = 0.20.

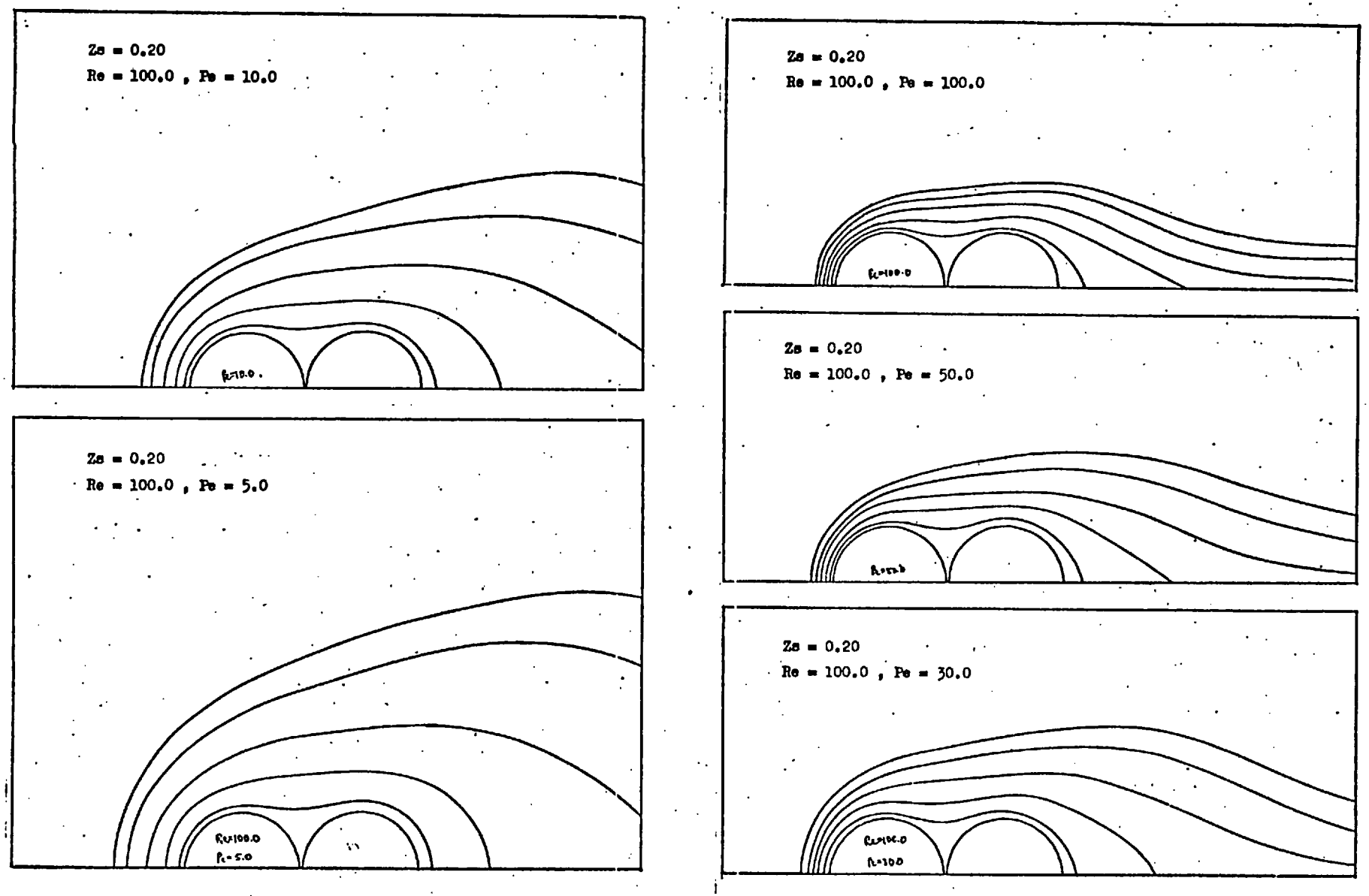

Figure(6-3-6). Concentration profiles around two spheres with Zs = 0.20.

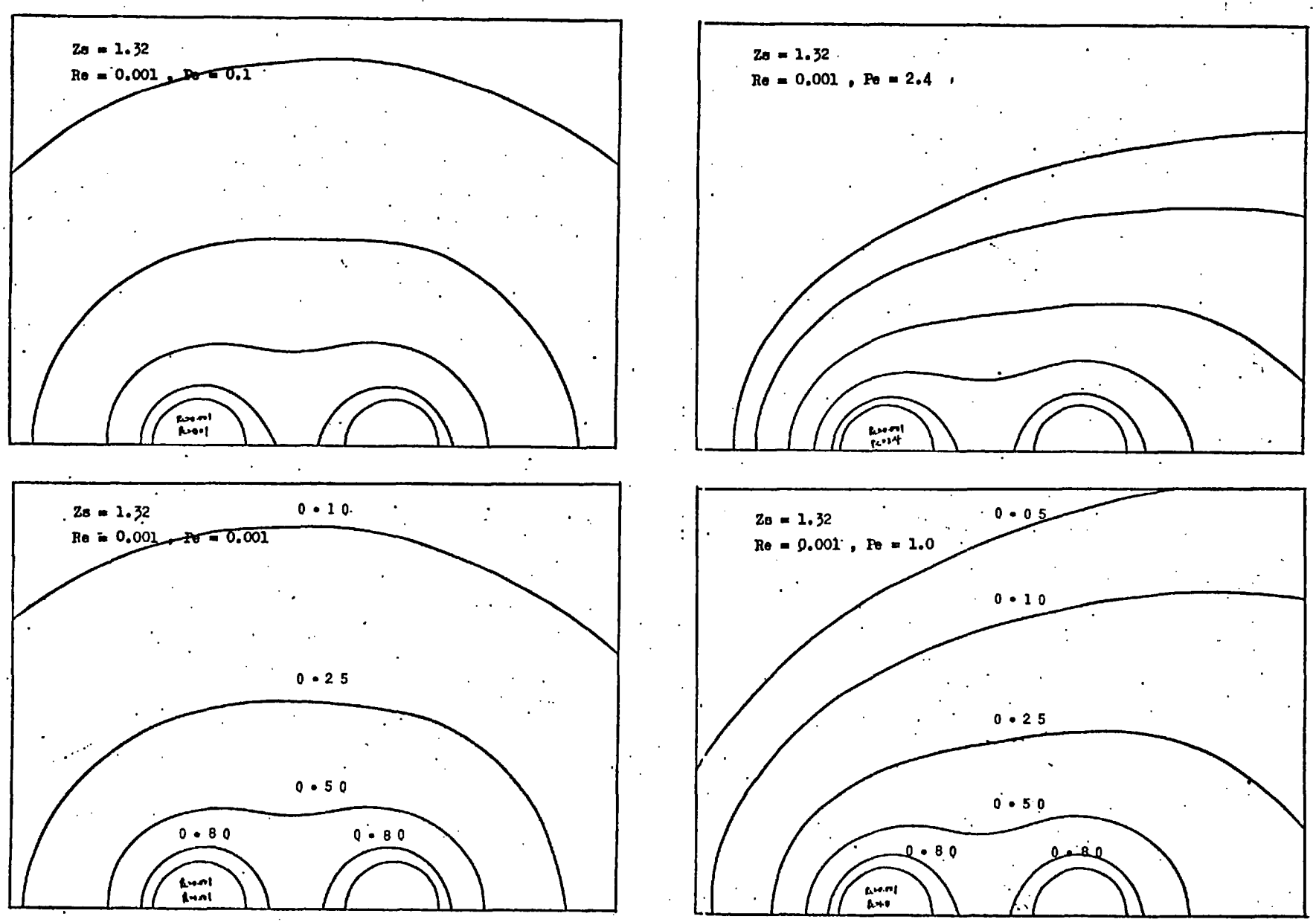

Figure(6-3-7). Concentration profiles around two spheres with Zs = 1.32.

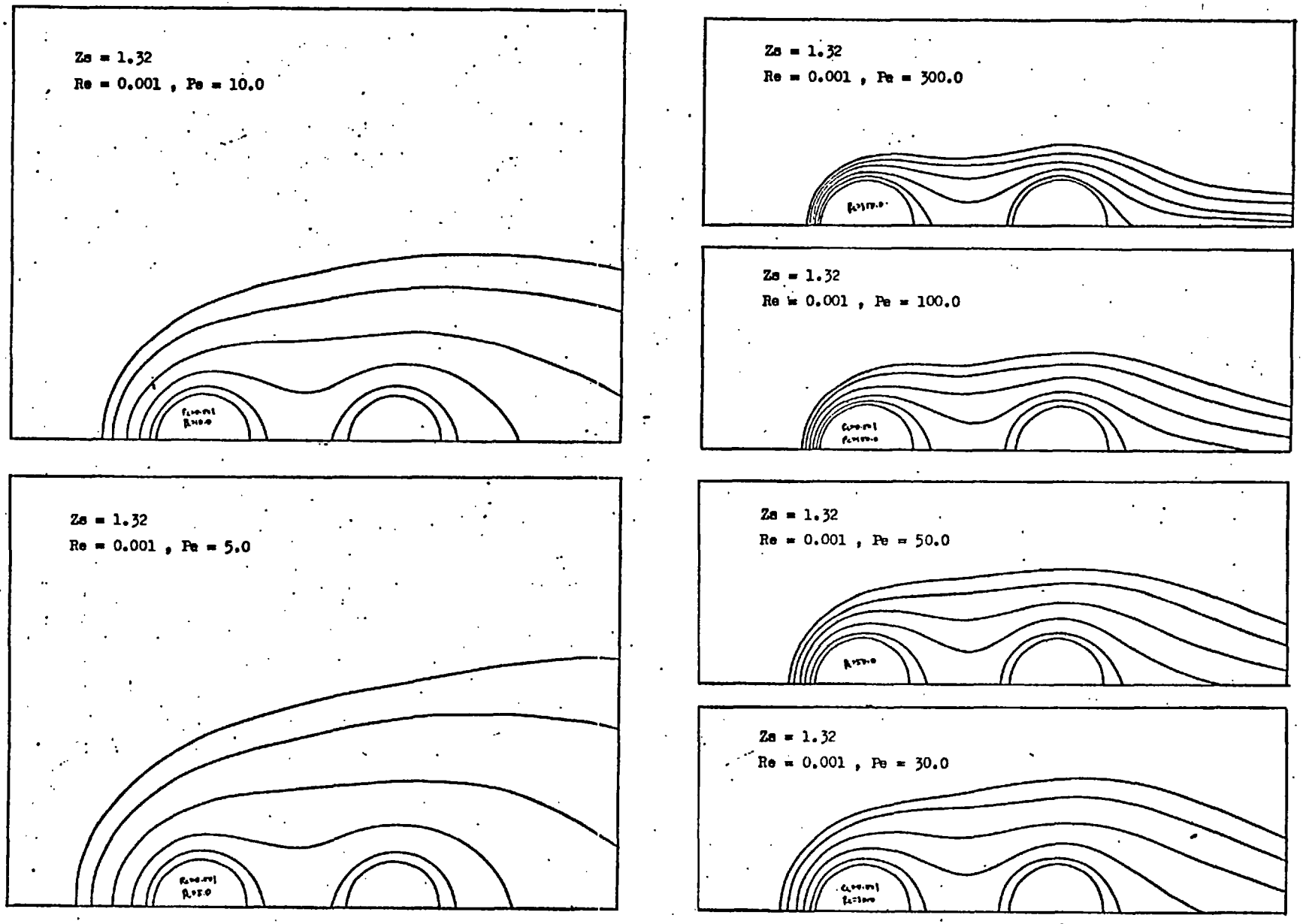

Figure(6-3-8). Concentration profiles around two spheres with Zs = 1.32.

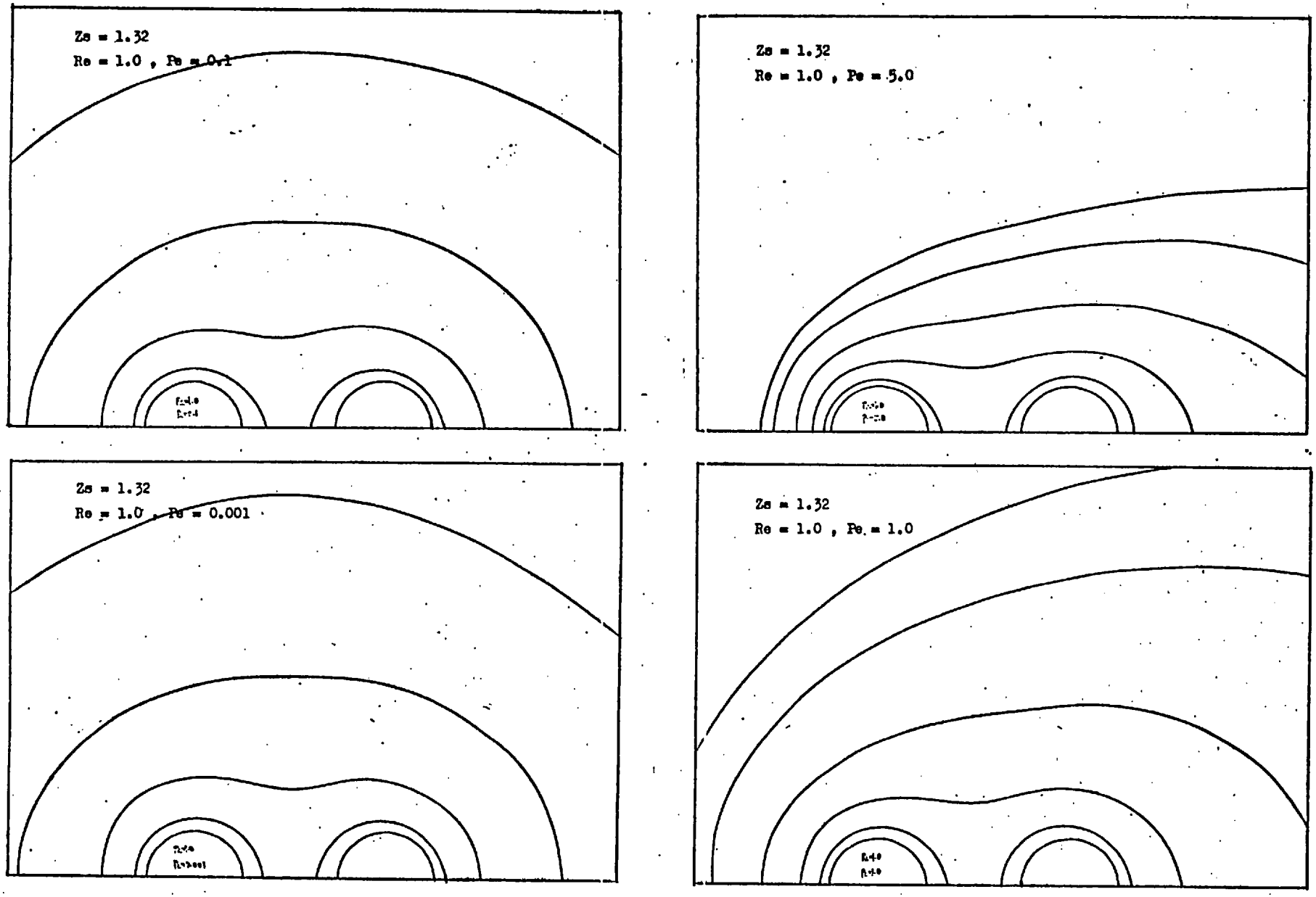

Figure(6-3-9). Concentration profiles around two spheres with Zs = 1.32.

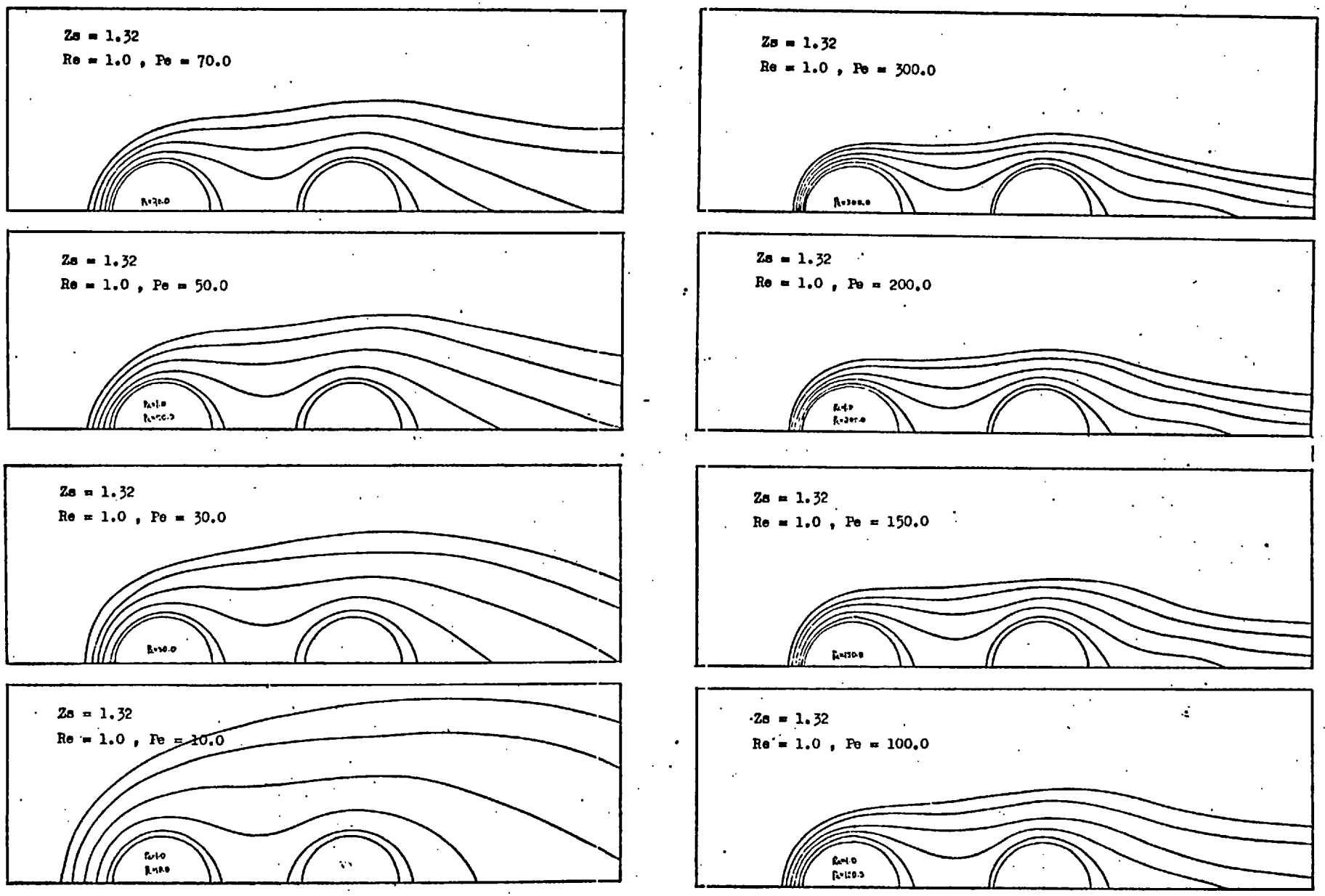

Figure(6-3-10). Concentration profiles around two spheres with Zs = 1.32.

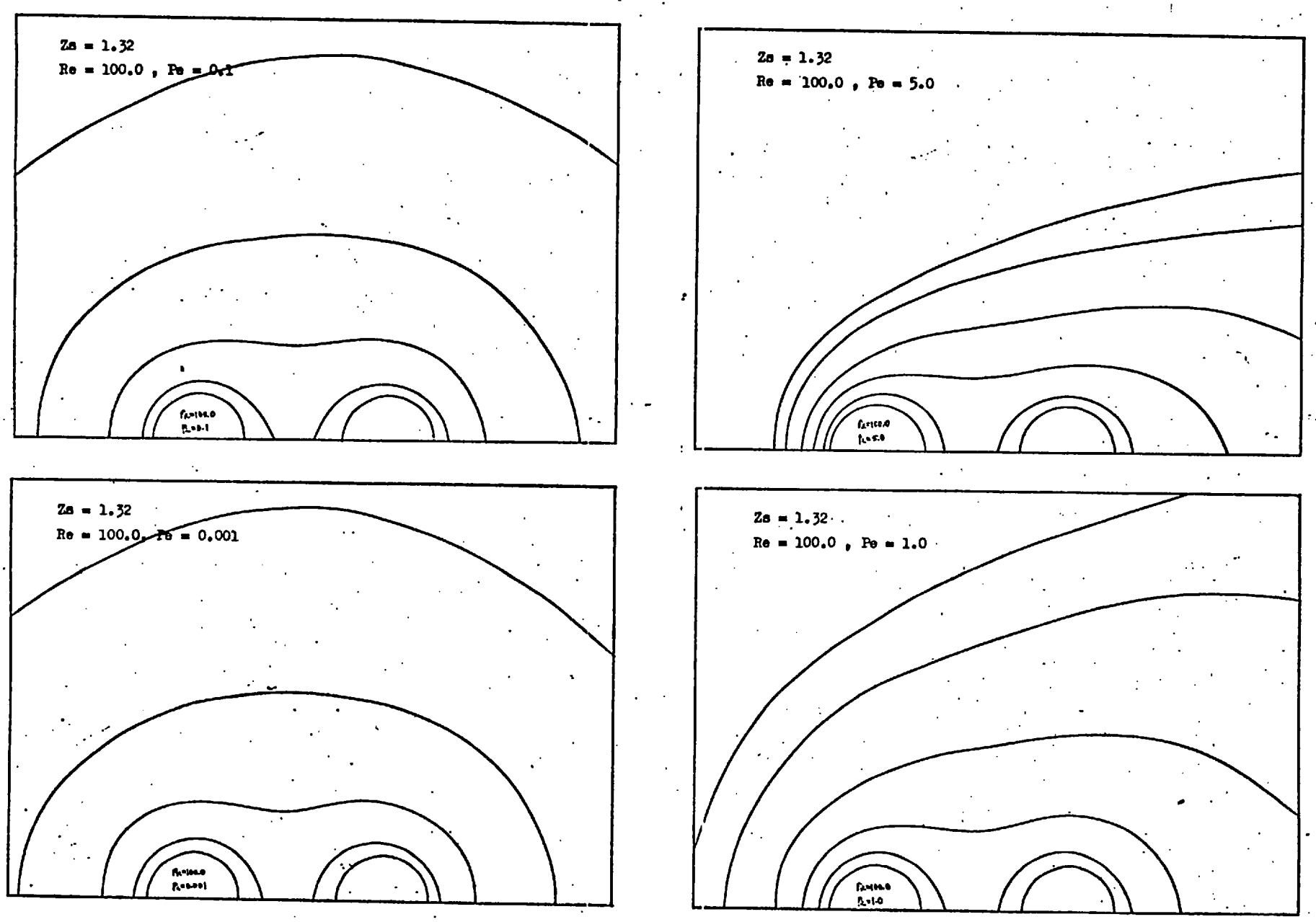

Figure(6-3-11). Concentration profiles around two spheres with Zs = 1.32.

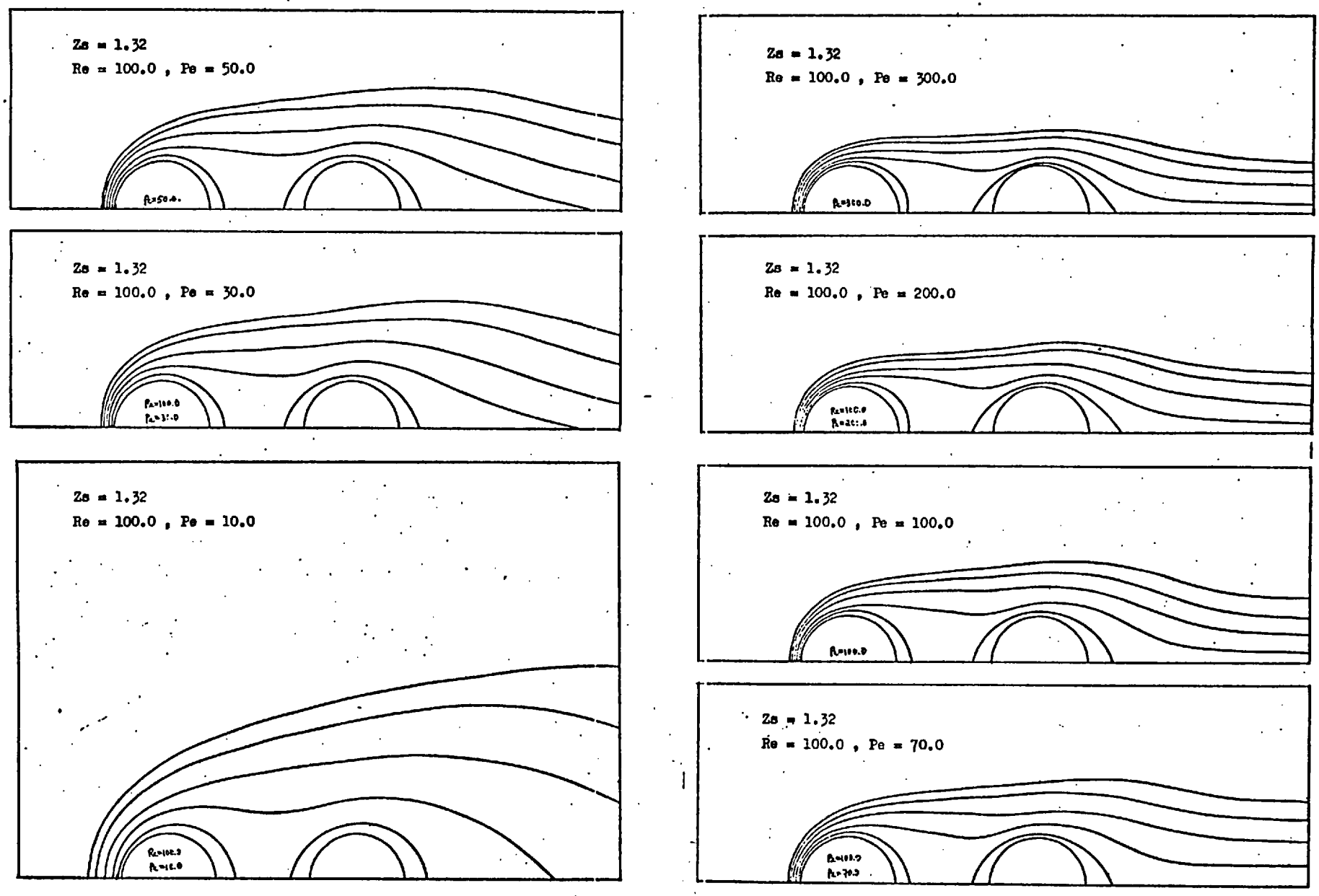

Figure(6-3-12). Concentration profiles around two spheres with Zs = 1.32.

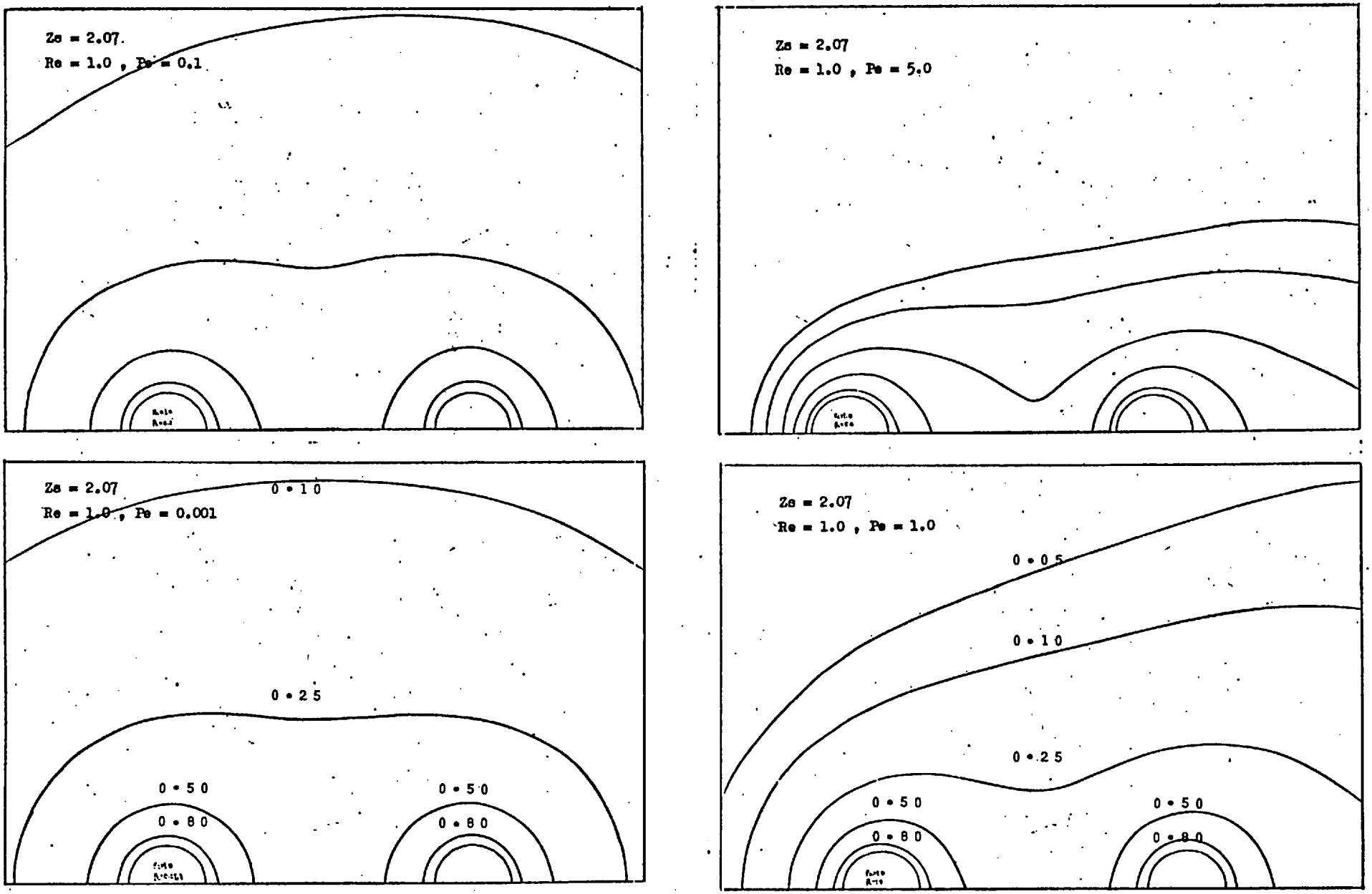

Figure(6-3-13). Concentration profiles around two spheres with Zs = 2.07.

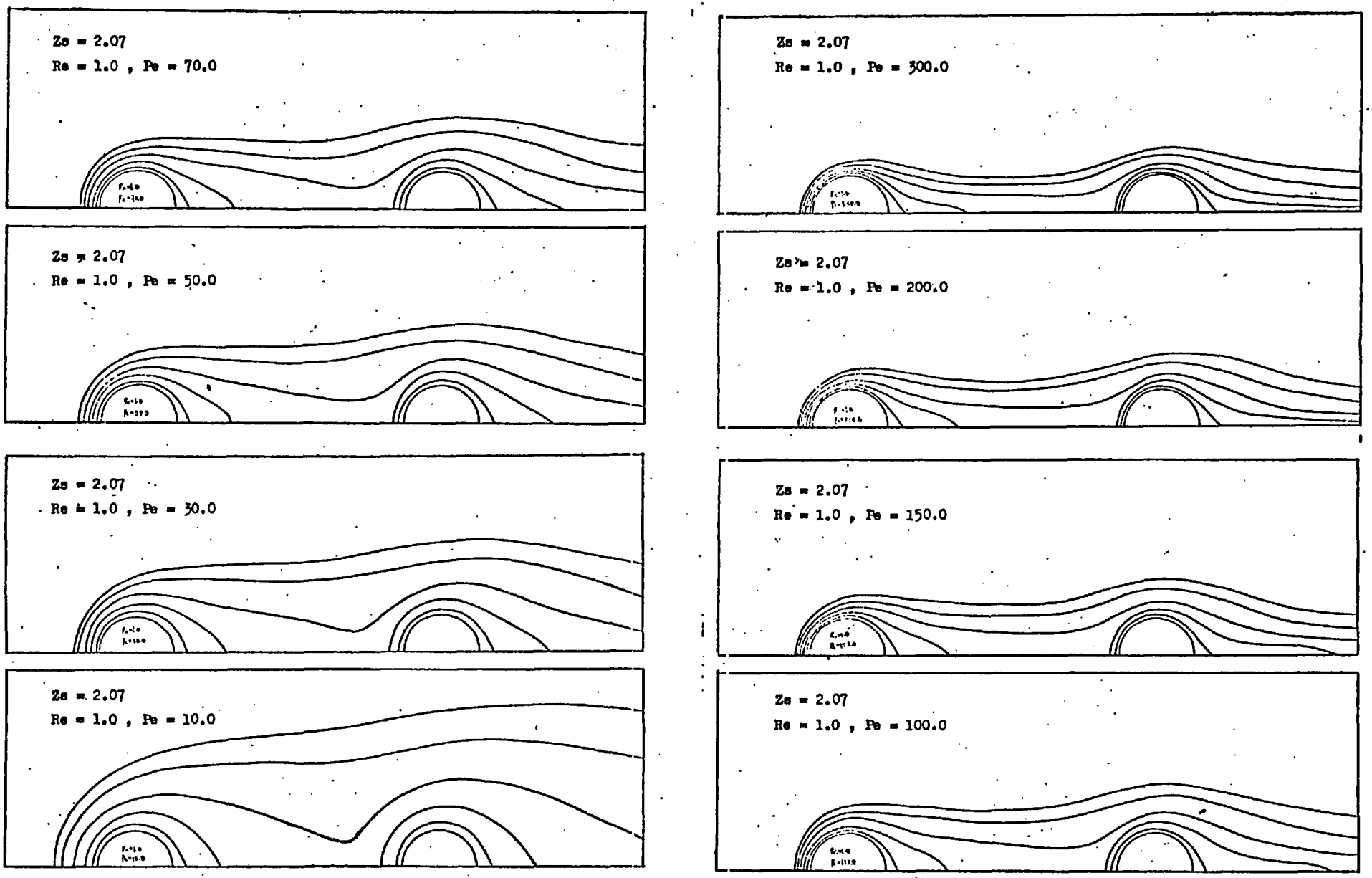

Figure(6-3-14). Concentration profiles around two spheres with Zs = 2.07.

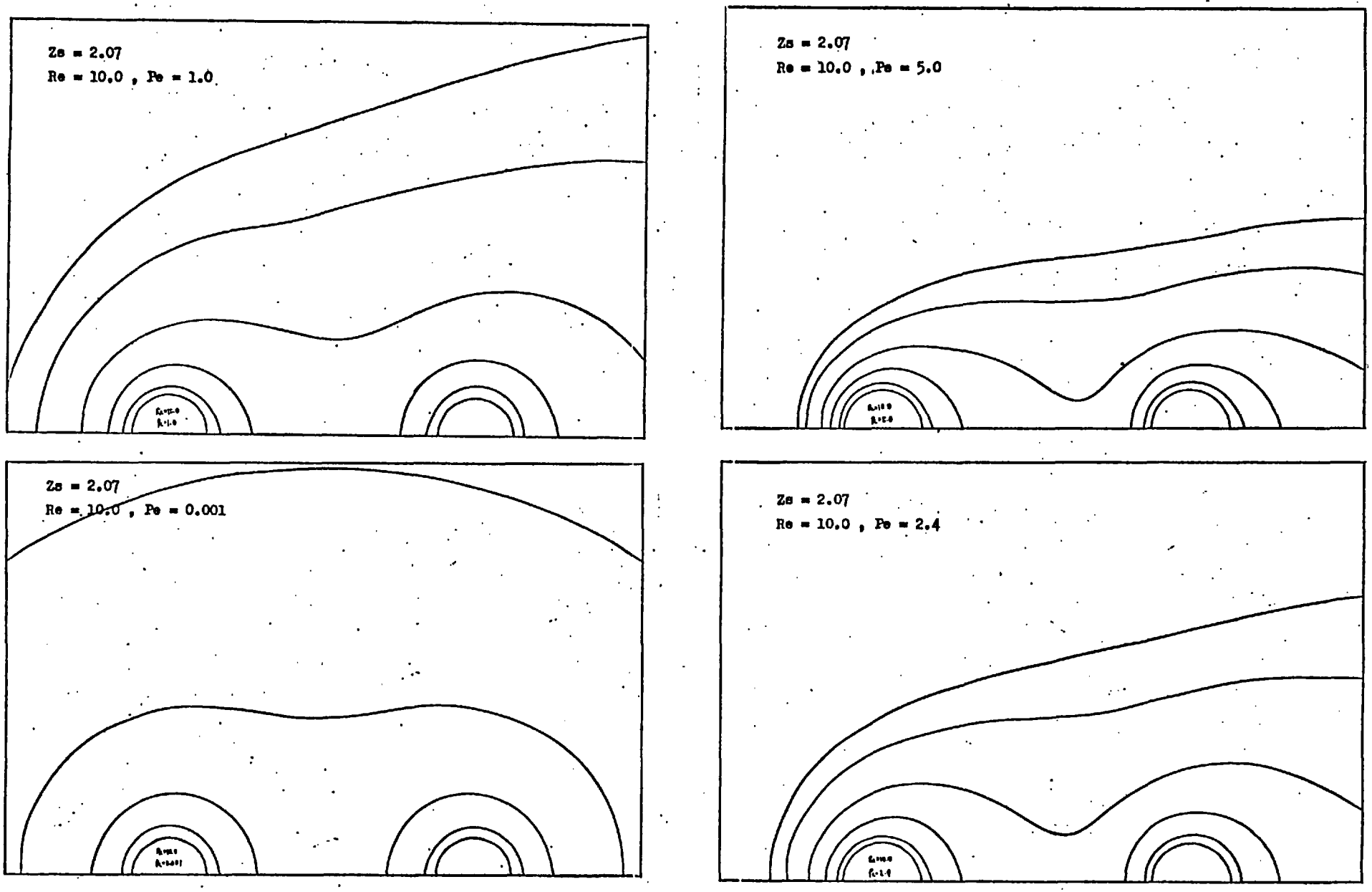

Figure(6-3-15). Concentration profiles around two spheres with Zs = 2.07.

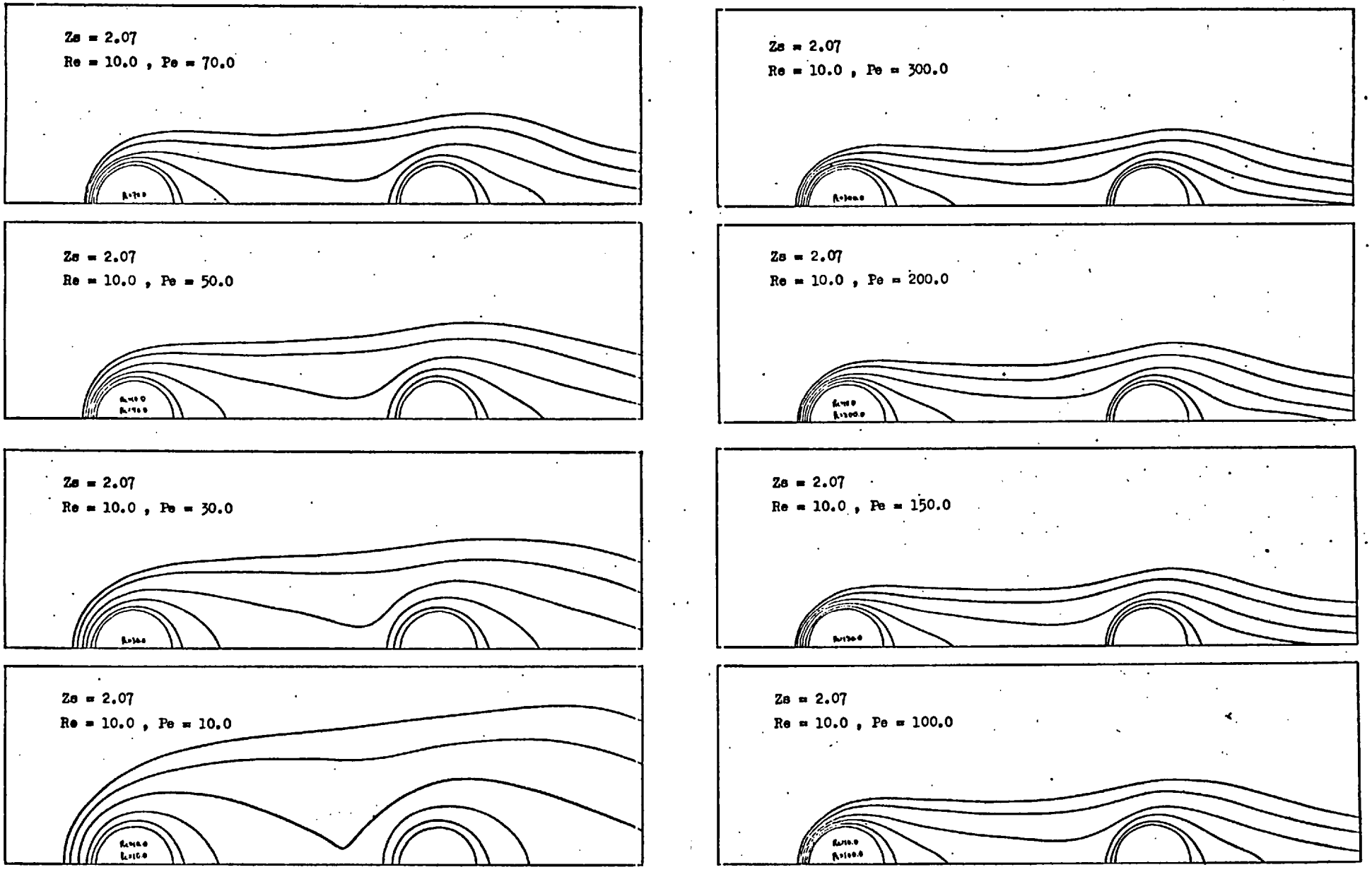

Figure(6-3-16). Concentration profiles around two spheres with Zs = 2.07.

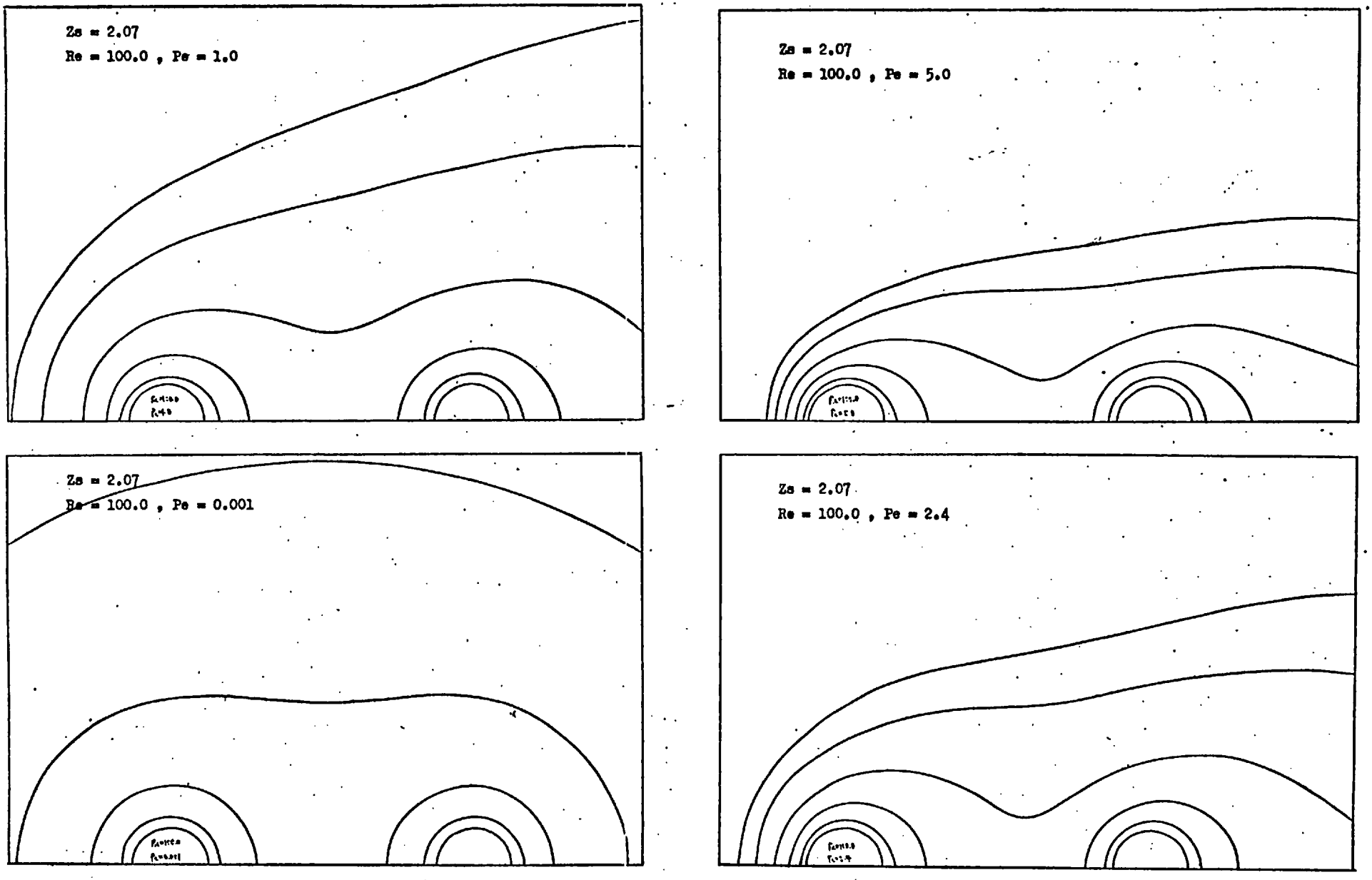

Figure(6-3-17). Concentration profiles around two spheres with Zs = 2.07.

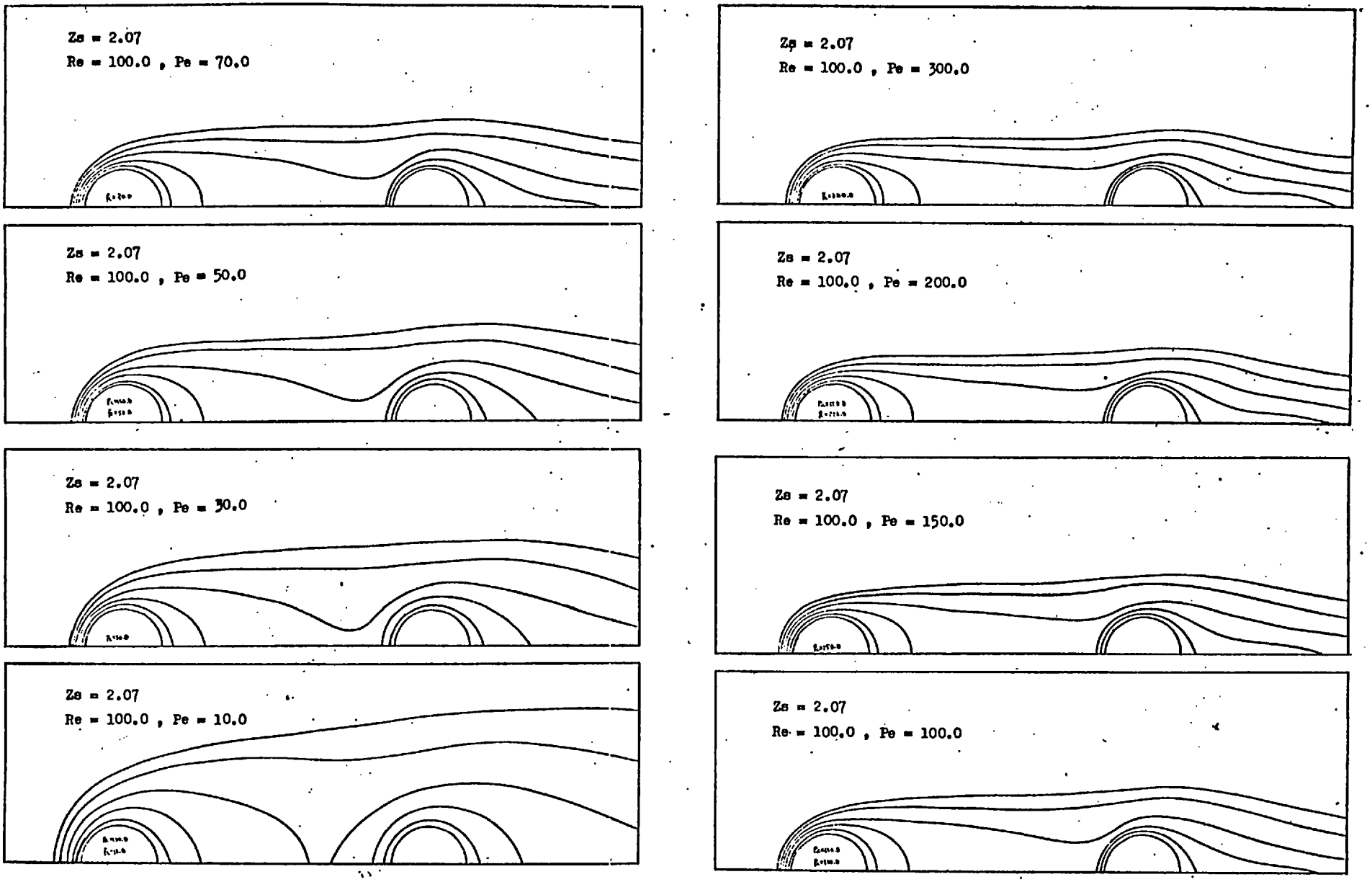

Figure(6-3-18). Concentration profiles around two spheres with Zs = 2.07.

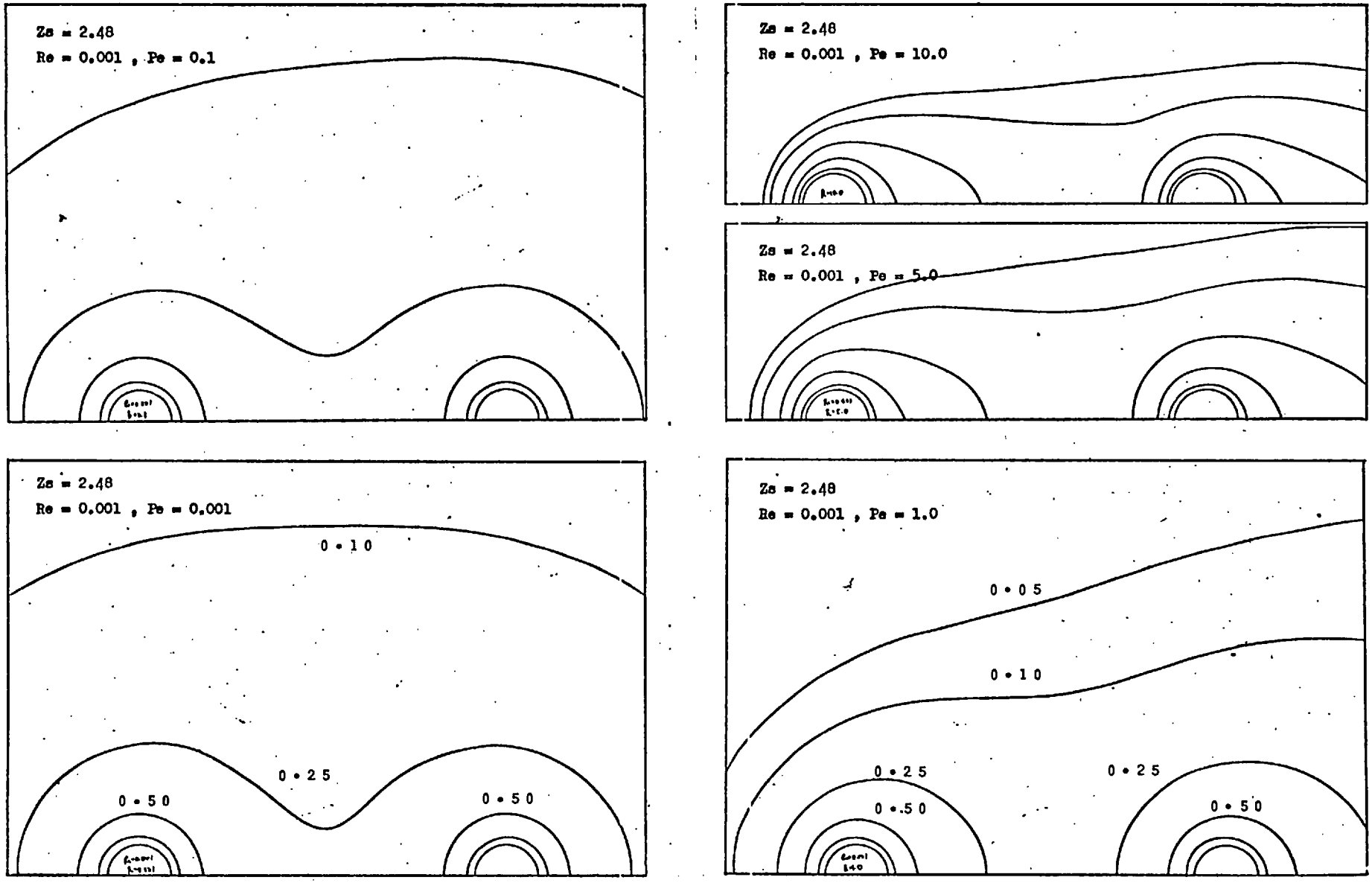

Figure(6-3-19). Concentration profiles around two spheres with Zs = 2.48.

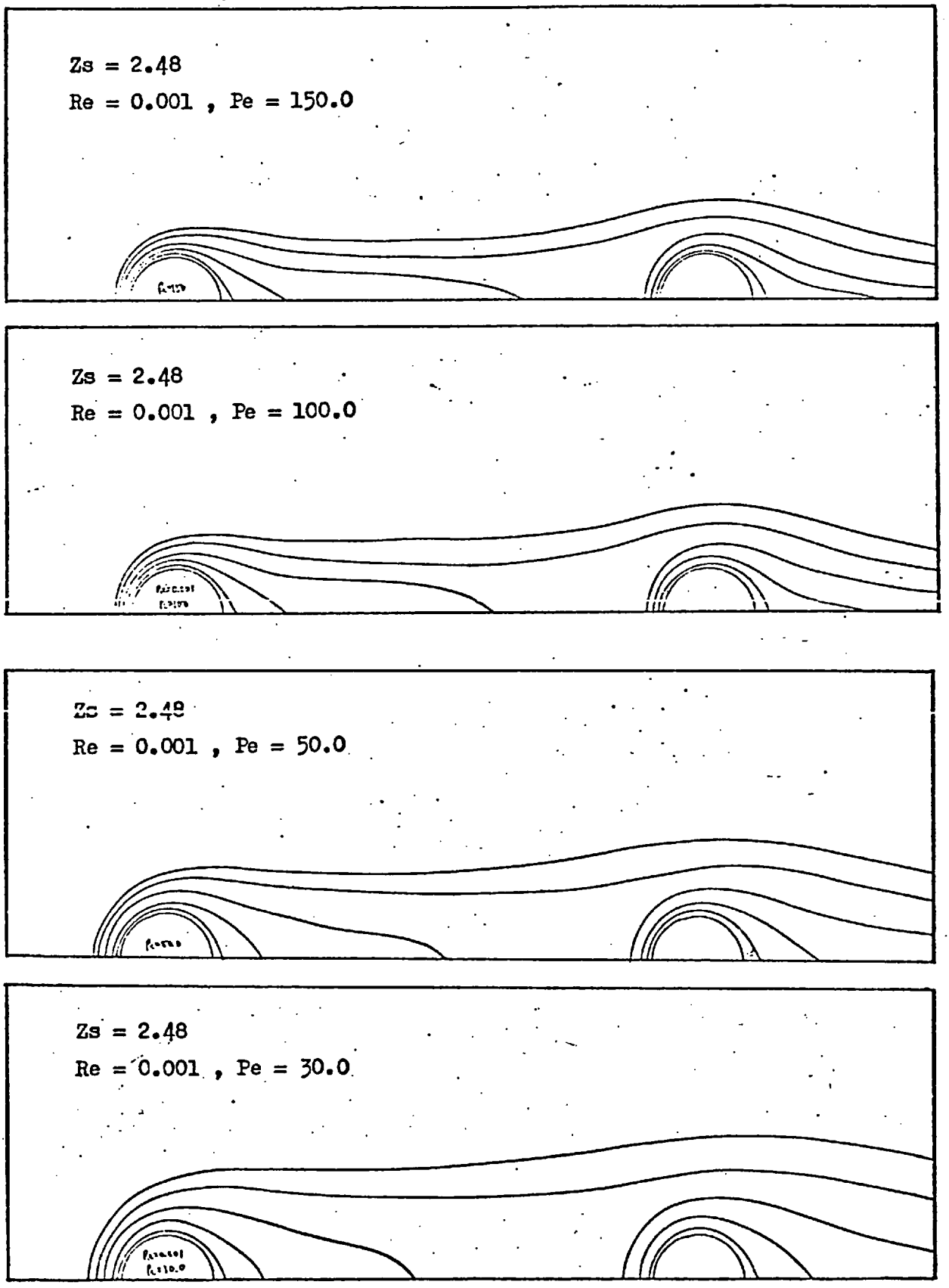

Figure(6-3-20). Concentration profiles around two spheres with Zs = 2.48.

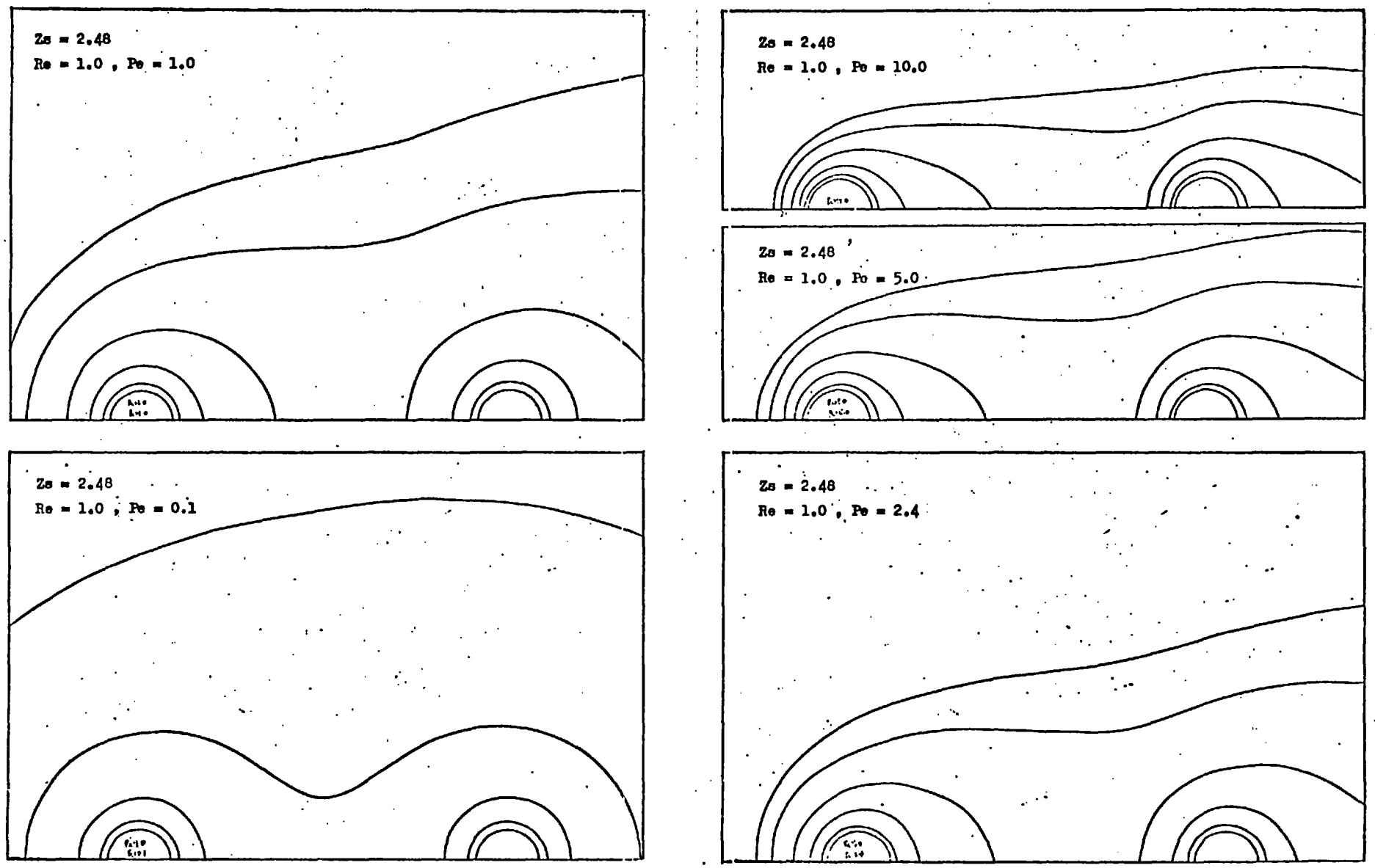

Figure(6-3-21). Concentration profiles around two spheres with Zs = 2.48.

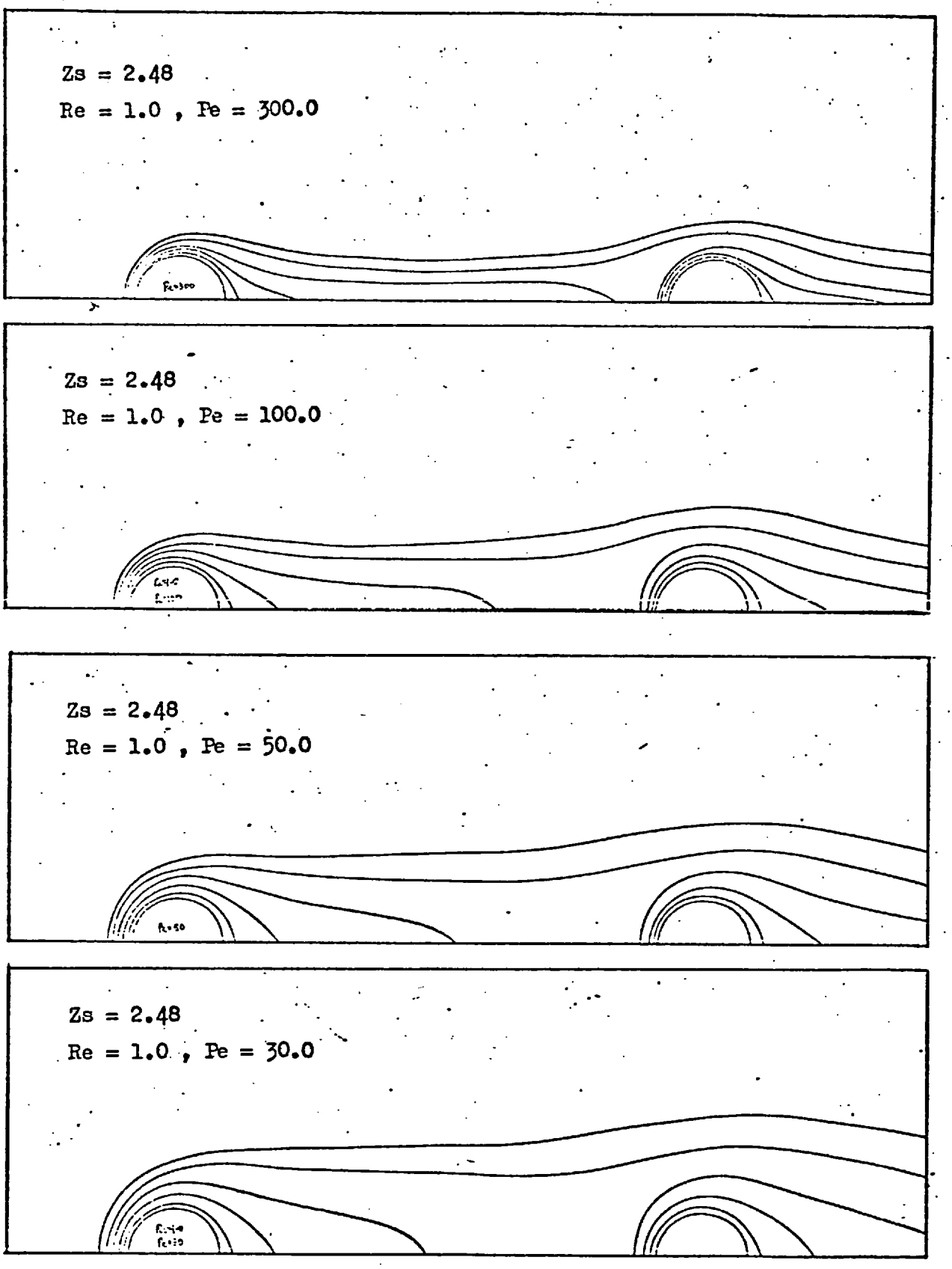

Figure(6-3-22). Concentration profiles around two spheres with Zs = 2.48.

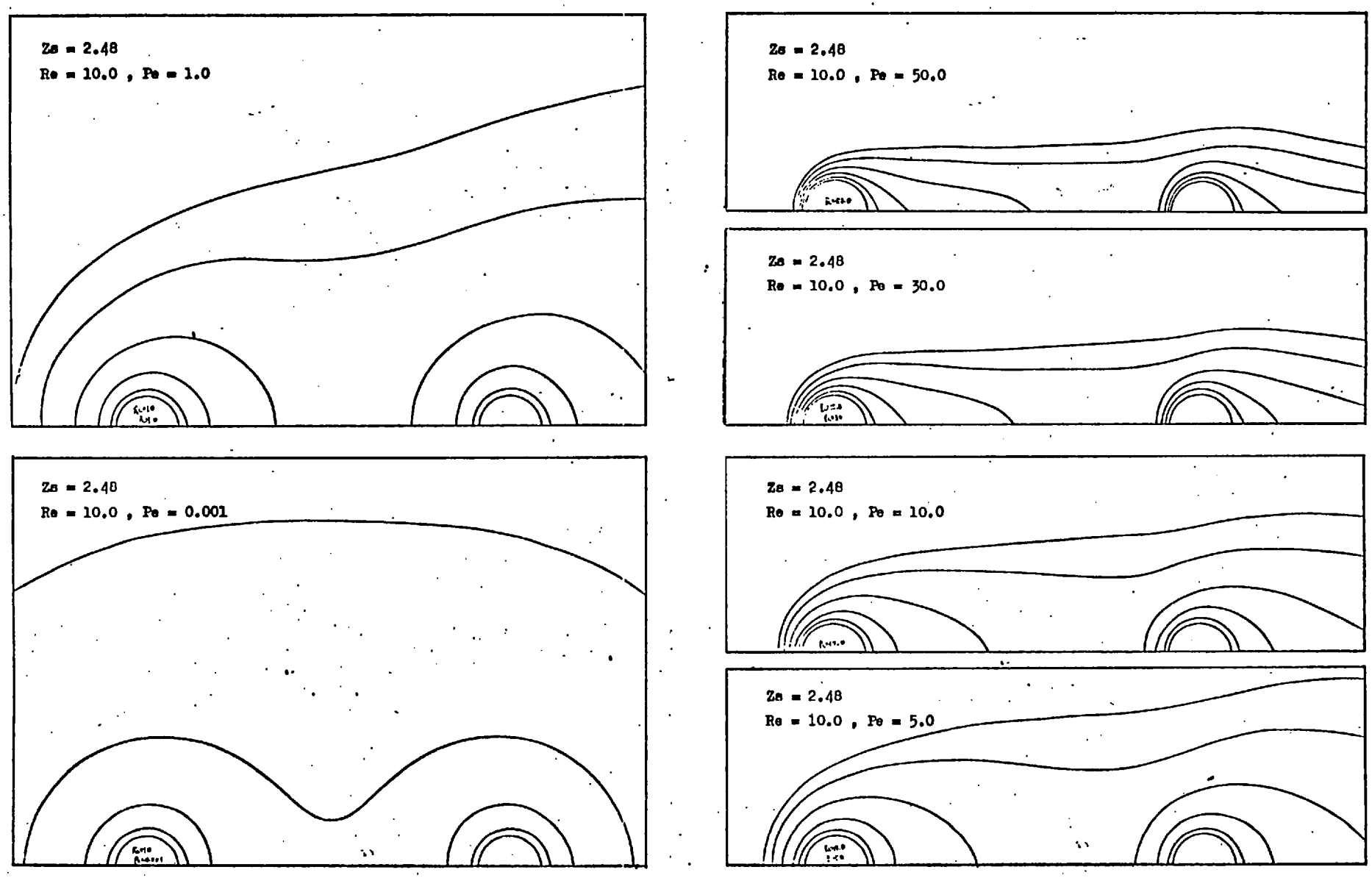

Figure(6-3-23). Concentration profiles around two spheres with Zs = 2.48.

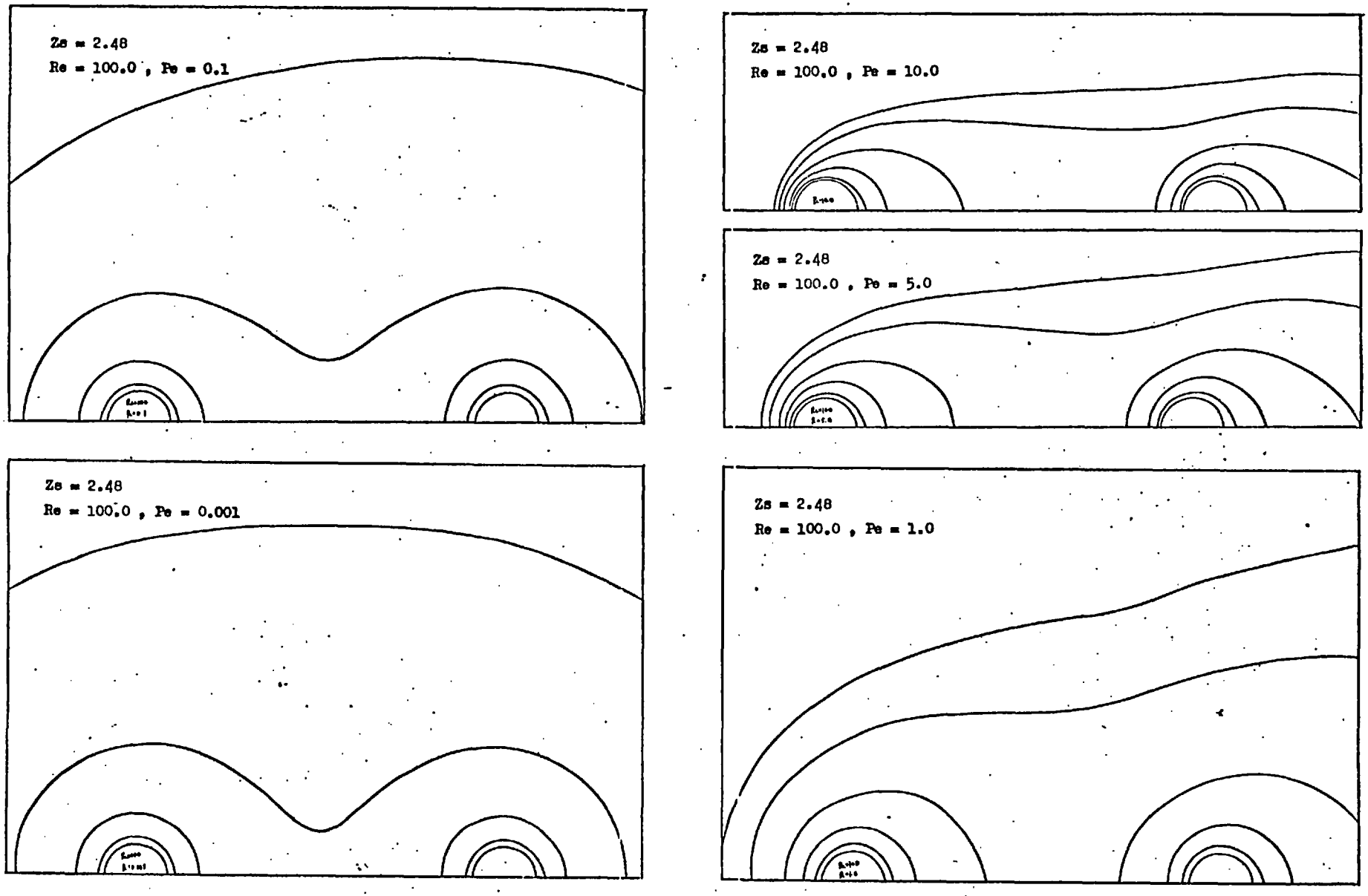

Figure(6-3-24). Concentration profiles around two spheres with Zs = 2.48.

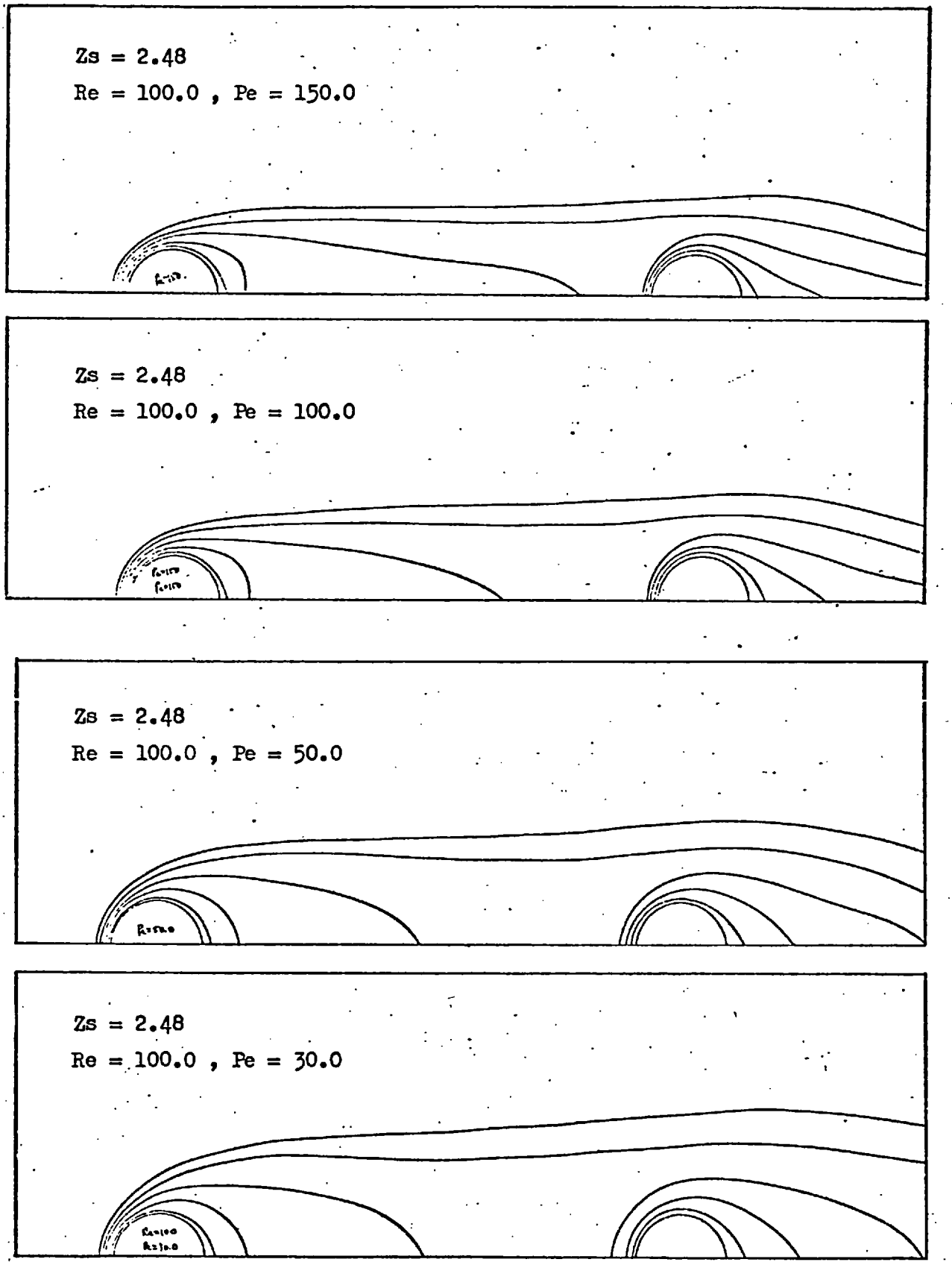

Figure (6-3-25). Concentration profiles around two spheres with Zs = 2.48.

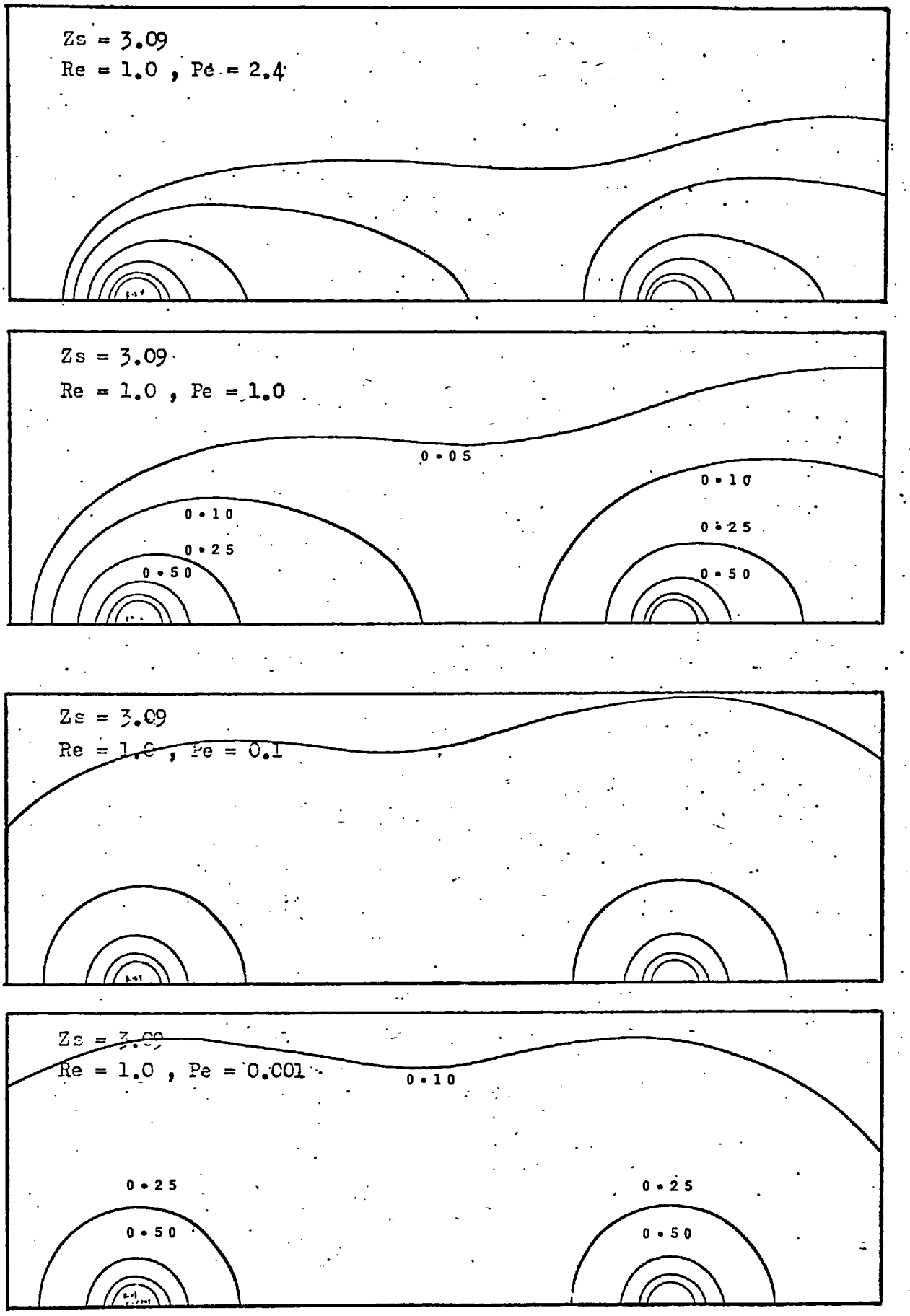

Figure(6-3-26). Concentration profiles around two spheres with Zs = 3.09.

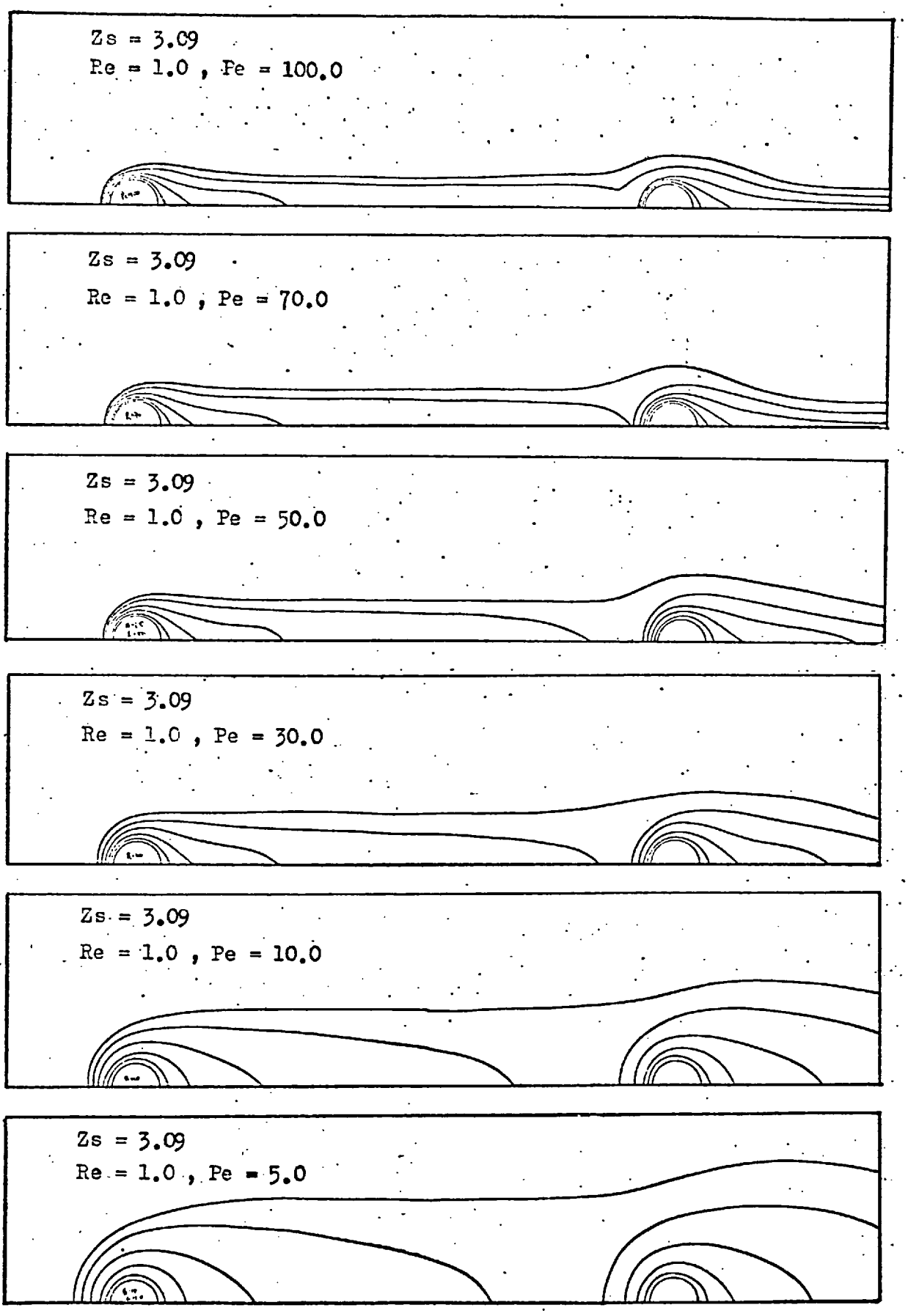

Figure(6-3-27). Concentration profiles around two spheres with Zs = 3.09.

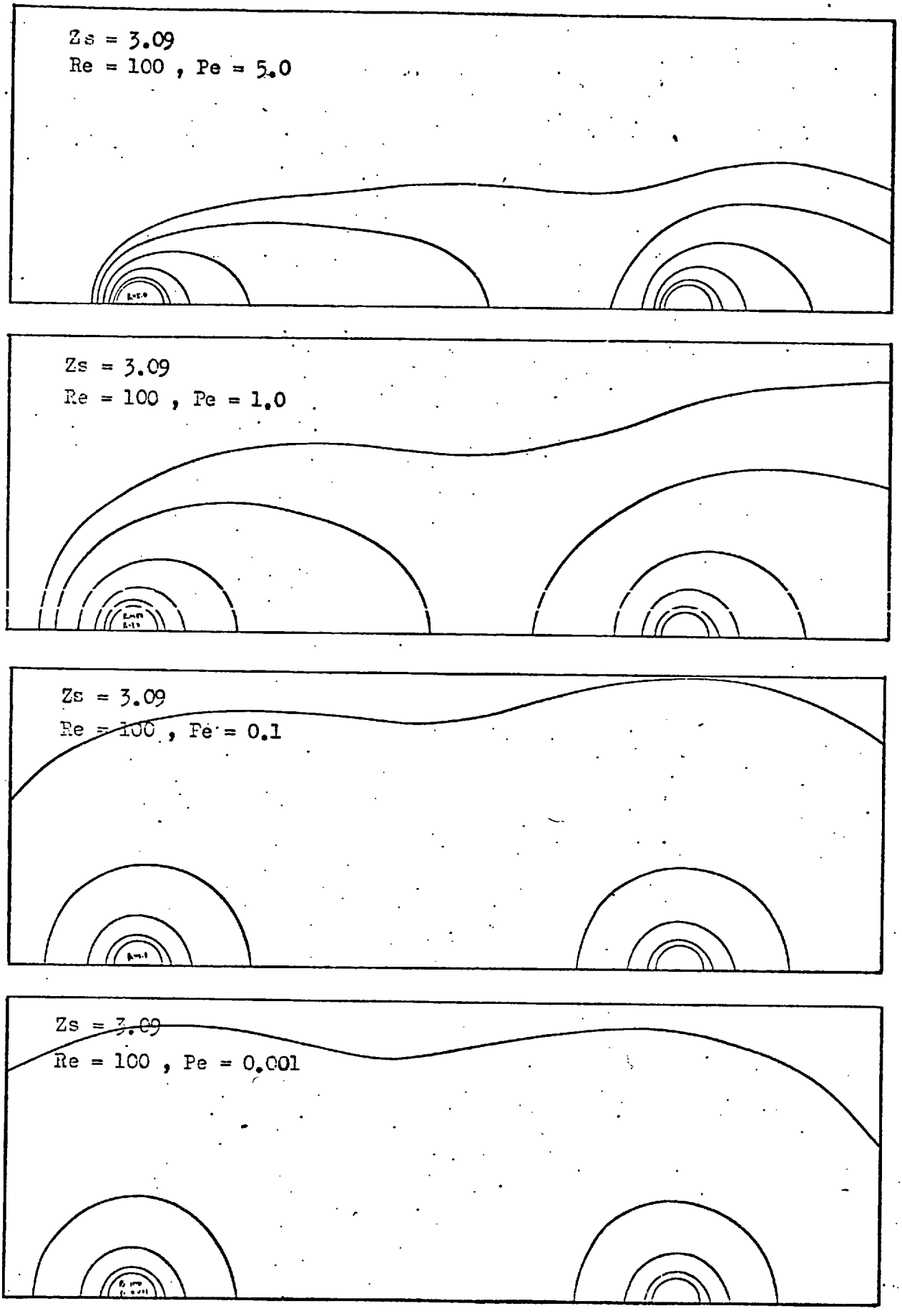

Figure(6-3-28). Concentration profiles around two spheres with Zs = 3.09.

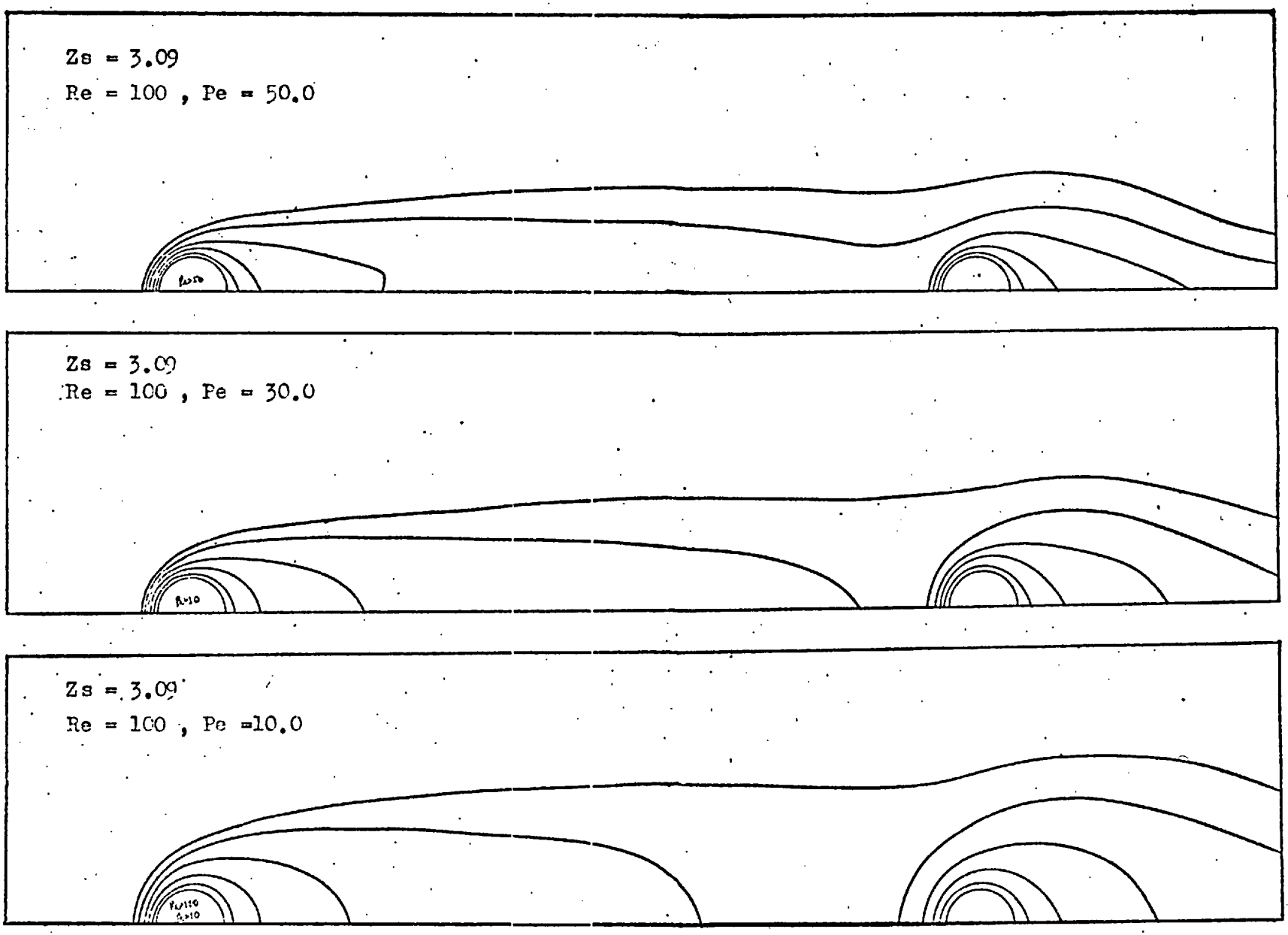

Figure(6-3-29). Concentration profiles around two spheres with Zs = 3.09.

From the above discussion, it is clear that the concentration distributions around two equally sized spheres with a fluid flowing parallel to their line of centres is dependent on the Peclet number, the Reynolds number, and the spacing between the spheres. A brief summary of this dependence is as follows.

For each sphere spacing and Reynolds number, the concentration profiles at low Peclet numbers of 0.001 to 0.1 remain almost unchanged and are symmetrical about a plane through the mid-point of the line of centres normal to the direction of flow. This is because molecular diffusion is the dominant mode of transfer and the material diffuses uniformly in all directions. At higher Peclet numbers, the material is convected more rapidly rearwards than it diffuses forwards from the surface of each sphere. Hence, the effect of convection upon the rates of mass transfer from the spheres becomes significant and increases in importance with increasing Peclet number. The convective effect is, however, always stronger for sphere A than for sphere B. As a result, at high Peclet numbers a diffusional boundary layer is always developed at the upstream surface of sphere A whereas when the sphere spacing is small, a diffusional boundary layer is not developed at the upstream surface of sphere B. However, as the sphere spacing increases, a diffusional boundary layer does become established at the upstream surface of sphere B.

For each sphere spacing, the concentration profiles at low Peclet numbers of 0.001 to 0.1 remain almost the same when the Reynolds number changes from 0.001 to 100.0. On the other hand, at higher Peclet numbers the concentration profiles are

influenced by the fluid dynamics, in particular, as the Reynolds number increases the contours with small values of concentration move closer to the front surface of sphere A and closer to the line of centres, also for large sphere spacings move closer to the front surface of sphere B. This indicates that at high Peclet numbers, the already strong effect of convection upon the rates of mass transfer from the spheres is further strengthened by an increase in the Reynolds number.

The distance between the spheres is an important factor affecting the concentration profiles around the spheres especially in the region between the spheres. As the sphere spacing increases, the number of contours in the figures which form closed paths around each sphere increase so that the concentration of the lowest concentration contour which envelops the two spheres and the inner region between them decreases. For the smallest sphere spacing Zs = 0.20, all contours shown in the figures envelop the two nearly touching spheres and the inner region between them, while for the largest sphere spacing Zs = 3.09, nearly all contours form closed paths around each sphere except for the contours C^* = 0.10 and C^* = 0.05 which envelop the two spheres and the large inner region between them. It is clear that as the sphere spacing increases, the concentration profiles in the inner region between the spheres change significantly and the concentration profiles around the two spheres become closer to those around a single isolated sphere. It is important to note that for each of the five sphere spacings considered in this study, the concentration profiles around the two equally sized spheres are always slightly different from those around a single isolated sphere, and the difference

becomes smaller when the two spheres are further apart. This indicates the existence of particle-to-particle interaction between the spheres. As the sphere spacing increases, the extent of inter-particle interaction upon the rates of mass transfer from the spheres decreases.

6-4. Local Sherwood numbers.

In this two-sphere mass transfer problem, quantitative insight into the rates of mass transfer from the two spheres to the flowing fluid around them was obtained from studies of the local and overall rates of mass transfer from the spheres in relation to sphere spacing, Reynolds number, and Peclet number. The results of the studies of the local and overall rates of mass transfer from the spheres are given in this and the next sections, respectively. The local rates of mass transfer from spheres A and B were expressed in terms of the local Sherwood numbers, $Sh_{AL}(\eta)$ and $Sh_{BL}(\eta)$, which were obtained from the concentration profiles using equations(4-5-11) and (4-5-12), respectively.

For each of the five sphere spacings considered in this study: Zs = 0.20, 1.32, 2.07, 2.48, and 3.09, and each of the four selected Reynolds numbers of 0.001, 1.0, 10.0, and 100.0, the plots of the local Sherwood numbers against the angle η obtained using a mesh spacing of |Zs/20| in Z are shown in Figures(6-4-1) to (6-4-10); while those obtained using a larger mesh spacing of |Zs/10| in Z are shown in Figures(6-4-11) to (6-4-20). The Sherwood number curves in Figures(6-4-1) to (6-4-10) are plotted for seven selected Peclet numbers of 0.001, 1.0, 10.0, 30.0, 50.0, 100.0, and 200.0; while those in Figures(6-4-11) to (6-4-20) are plotted for six selected Peclet numbers of 0.001, 1.0, 10.0, 30.0, 50.0, and 100.0. It should be noted that for sphere A, the angle η is 0^{o} at the front stagnation point and is 180^{o} at the rear stagnation point; while for sphere B, the angle η is 180^{o} at the front stagnation point and is 0^{o} at the rear stagnation point. From these plots, the

the local rates of mass transfer from the two spheres and their variations with the three parameters: sphere spacing, Reynolds number, and Peclet number, can be investigated. At the end of this section, the influence of the mesh spacing in Z upon the results, especially at the front surface of sphere A, will also be discussed.

For the smallest sphere spacing considered in this study: Zs = 0.20, L/R = 2.0402, the most important feature of the local Sherwood number curves for the two nearly touching spheres as shown in Figures(6-4-1) to (6-4-2) and in Figures(6-4-11) to (6-4-12), is the existence of two regions where the local Sherwood numbers are approximately zero for all Reynolds and Peclet numbers: one near the rear stagnation point of sphere A and the other near the front stagnation point of sphere B. The very small values of the local Sherwood numbers in these regions arise because of the closeness of the two spheres so that the highly concentrated stagnant fluid in the tiny inner region between the spheres reduces the driving force for mass transfer to nearly zero.

For each Reynolds number and Peclet number, the local Sherwood numbers for sphere A always decrease from their maximum value at the front stagnation point to almost zero in the region near the rear stagnation point. As the Peclet number increases, the local Sherwood numbers at the front surface of sphere A increase rapidly because of the decrease in the thickness of the diffusional boundary layer; while those at the rear surface of sphere A increase only slightly or remain unchanged. On the other hand, at low Peclet numbers of 0.001 to 1.0 the local Sherwood numbers for sphere B increase

continuously from the region at which their values are very low to the rear stagnation point; while at higher Peclet numbers they rise to a maximum value at around $\eta = 90^{o}$ and then fall off until the rear stagnation point is reached. Except in the regions close to the front and rear stagnation points the local Sherwood numbers for sphere B increase with increasing Peclet number. It is thus clear that for this smallest sphere spacing, the difference between the rates of mass transfer from the front surfaces of the spheres is very large and that it becomes even larger when the Peclet number is increased.

At low Peclet numbers of 0.001 to 1.0, the local Sherwood number curves remain nearly the same when the Reynolds number is increased from 0.001 to 100.0; however, at higher Peclet numbers the local Sherwood number curves change with Reynolds number, in particular, the local Sherwood numbers at the front surface of sphere A increase rapidly with increasing Reynolds number. As a result, at higher Reynolds numbers the difference between the rates of mass transfer from the front surfaces of the spheres becomes even larger. The very rapid increase in the local Sherwood numbers near the front stagnation point of sphere A when the Reynolds number increases from 10.0 to 100.0, may be a result of the development of increasingly thinner fluid dynamic and diffudional boundary layers. For sphere B, this phenomenon does not appear because of the very small distance between the spheres so that neither a fluid dynamic nor a diffusional boundary layer is formed even at high Reynolds and Peclet numbers.

For the sphere spacing: Zs = 1.32, L/R = 4.0106, the curves of Figures(6-4-3) to (6-4-4) and Figures(6-4-13) to

(6-4-14) show that the local Sherwood numbers near the rear stagnation point of sphere A and those near the front stagnation point of sphere B are no longer close to zero. This is because the larger distance between the spheres results in a lower concentration of the diffusing material in the fluid in the inner region between the spheres and thus a larger rate of mass transfer from the surfaces adjacent to the inner region between the spheres. All the curves, except those for a Reynolds number of 100 at high Peclet numbers show that the local Sherwood numbers for sphere A decrease continuously from their maximum values at the front stagnation point to their minimum values at the rear stagnation point. For a Reynolds number of 100 and for high Peclet numbers, the local Sherwood numbers for sphere A decrease to a minimum at the back of the sphere at an angle which is approximately coincident with the point of flow separation, and then increase slowly until the rear stagnation point is reached. On the other hand, at low Peclet numbers of 0.001 to 1.0 the local Sherwood numbers for sphere B increase steadily from the front stagnation point to the rear stagnation point; while at higher Peclet numbers they first increase to a maximum and then fall off until the rear stagnation point is reached. This indicates that when the two spheres are one diameter apart, the depression of the rates of mass transfer from the front surface of sphere B by the concentrated fluid in the inner region between the spheres is still very marked even though it is smaller than that for the smallest sphere spacing. It is important to note that for each Reynolds number, the rates of mass transfer from the front surfaces of the two spheres increase with increasing Peclet number although the increase is much faster for sphere A than for sphere B.

In a similar way to that for the smallest sphere spacing, the local Sherwood number curves for Peclet numbers of 0.001 to 1.0 remain almost unchanged when the Reynolds number is increased from 0.001 to 100.0. On the other hand, at higher Peclet numbers the local Sherwood numbers at the front surfaces of the spheres generally become larger when the Reynolds number is increased, however, there is an exception for the local Sherwood numbers near the front stagnation point of sphere B which at high Peclet numbers of 100 and 200 become smaller when the Reynolds number is increased from 10.0 to 100.0. The reason for this exception is that at a Reynolds number of 100.0, there is flow separation from the back of sphere A as well as from the front of sphere B. This flow separation results in nearly the whole of the inner region between the spheres becoming a wake region with a consequent increase in the concentration of the diffusing material in the fluid near the upstream surface of sphere B thus depressing the rates of mass transfer from that region.

For the sphere spacing: Zs = 2.07, L/R = 8.0510, the local Sherwood number curves for the two spheres are shown in Figures(6-4-5) to (6-4-6) and in Figures(6-4-15) and (6-4-16). For each Reynolds number, the distributions of the local Sherwood number around sphere A and their variation with Peclet number for this sphere spacing are similar to those for the last sphere spacing that was discussed. However, because of the larger distance between the spheres and thus the lower concentration of the diffusing material in the inner region between the spheres, the rates of mass transfer from the front surface of sphere B although depressed are greater than those in the previous case. The depression in the rates of mass

transfer from the front surface of sphere B is particularly obvious at a Reynolds number of 100.0 because at this Reynolds number the flow separations from the rear surface of sphere A and the highly concentrated fluid in the inner region between the spheres is convected close to the front stagnation point of sphere B thus reducing the driving force for mass transfer from that region. On the whole, the local Sherwood numbers at the front surfaces of the two spheres increase with increasing Peclet number. Except at very high Peclet numbers the local Sherwood numbers for sphere B generally decrease continuously from the front to rear stagnation points. At very high Peclet numbers the local Sherwood numbers for sphere B first increase to a maximum and then decrease continuously until the rear stagnation point is reached.

At low Peclet numbers of 0.001 to 1.0, the local Sherwood numbers for the spheres remain nearly the same when the Reynolds number changes from 0.001 to 100.0. On the other hand, at higher Peclet numbers the local Sherwood numbers for the spheres change with Reynolds number, in particular, the local Sherwood numbers at the front surfaces of the spheres increase rapidly as the Reynolds number is increased. The most important feature of the distributions of the local Sherwood number around the spheres at this sphere spacing is that the rates of mass transfer from the front surfaces of the spheres increase with both Peclet and Reynolds numbers although the increase is always faster for sphere A than for sphere B.

For the sphere spacing: Zs = 2.48, L/R = 12.0250, the local Sherwood number curves of Figures(6-4-7) to (6-4-8) and Figures(6-4-17) to (6-4-18) show a similar variation with both

Peclet and Reynolds numbers as those for the sphere spacing Zs = 2.07. However, because of the larger distance between the spheres and thus the lower concentration of the diffusing material in the inner region between the spheres, the rates of mass transfer from the front surface of sphere B are larger than in the previous case although still depressed at high Peclet and Reynolds numbers. Except at a Reynolds number of 100.0 and at high Peclet numbers, the local Sherwood numbers for both spheres always decrease from the front to rear stagnation points. At a Reynolds number of 100.0 and high Peclet numbers, the local Sherwood numbers for sphere A decrease to a minimum value at the back of the sphere at an angle which is approximately coincident with that of flow separation and then increase slowly until the rear stagnation point is reached; while those for sphere B increase to a maximum value at the front of the sphere and then fall off until the rear stagnation point is reached.

For the largest sphere spacing considered in this study: Zs = 3.09, L/R = 22.022, the local Sherwood number curves of Figures(6-4-9) to (6-4-10) and of Figures(6-4-19) to (6-4-20) show that the variations of the local Sherwood numbers for the two spheres with Peclet number and Reynolds number are similar to those for the previous sphere spacing Zs = 2,48. For both spheres, the rates of mass transfer from the front surfaces increase with both Peclet and Reynolds numbers. Because of the very large distance between the spheres, the depression of the rates of mass transfer from the front surface of sphere B by the concentrated fluid in the inner region between the spheres is quite small, and the distributions of the local Sherwood

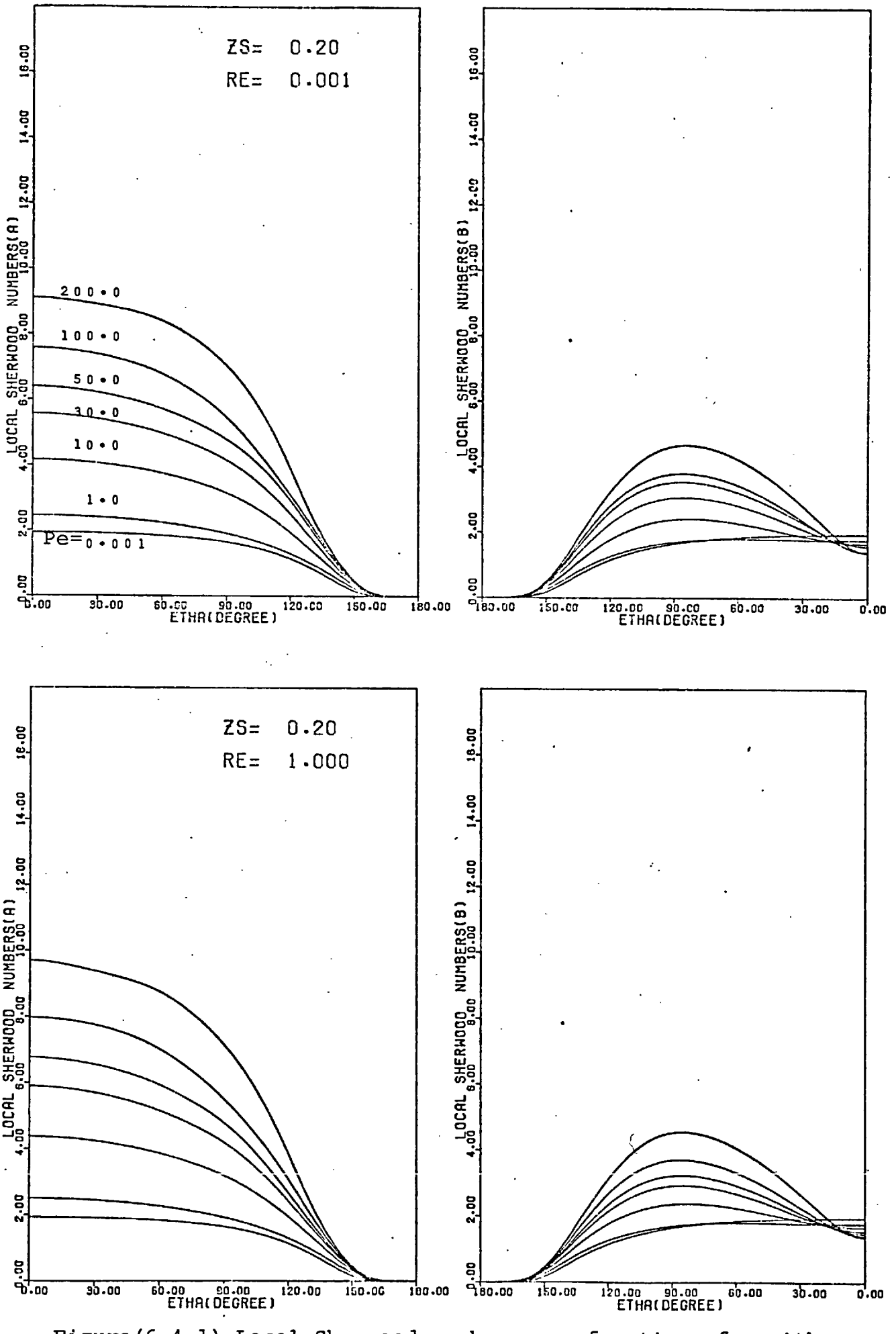

Figure(6-4-1) Local Sherwood number as a function of η with Peclet number as a parameter.

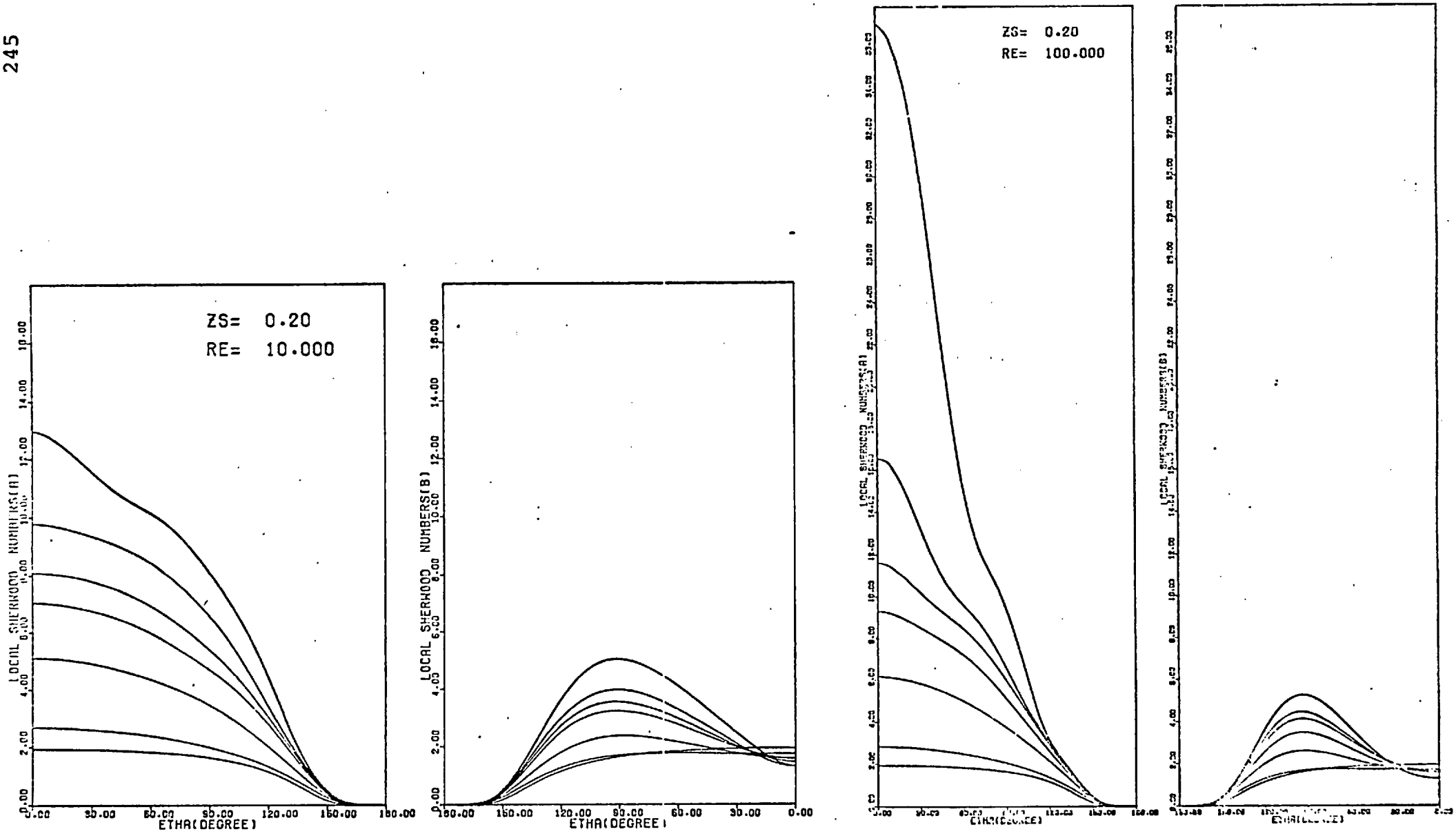

Figure(6-4-2) Local Sherwood number as a function of η with Peclet number as a parameter.

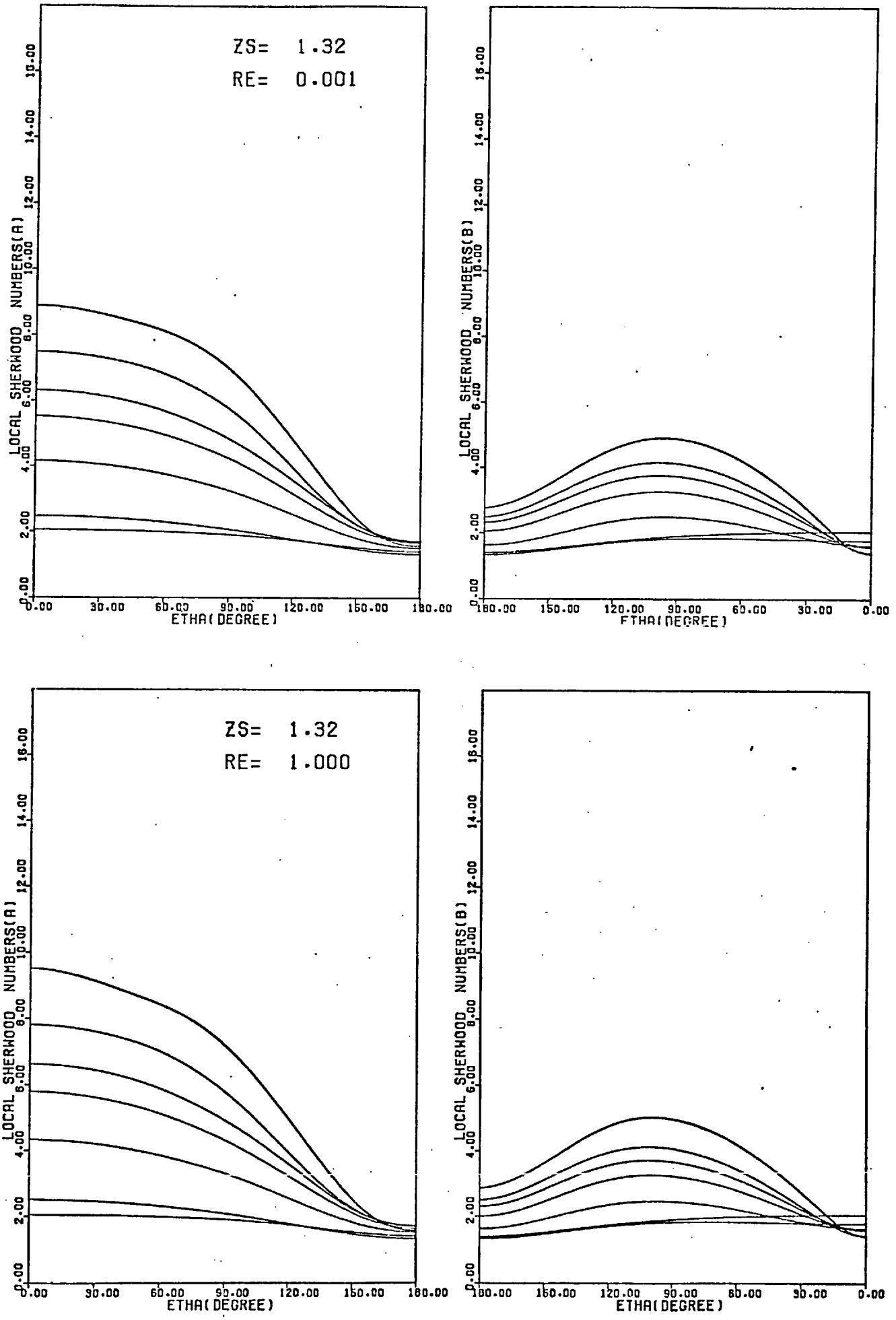

Figure(6-4-3) Local Sherwood number as a function of η with Peclet number as a parameter.

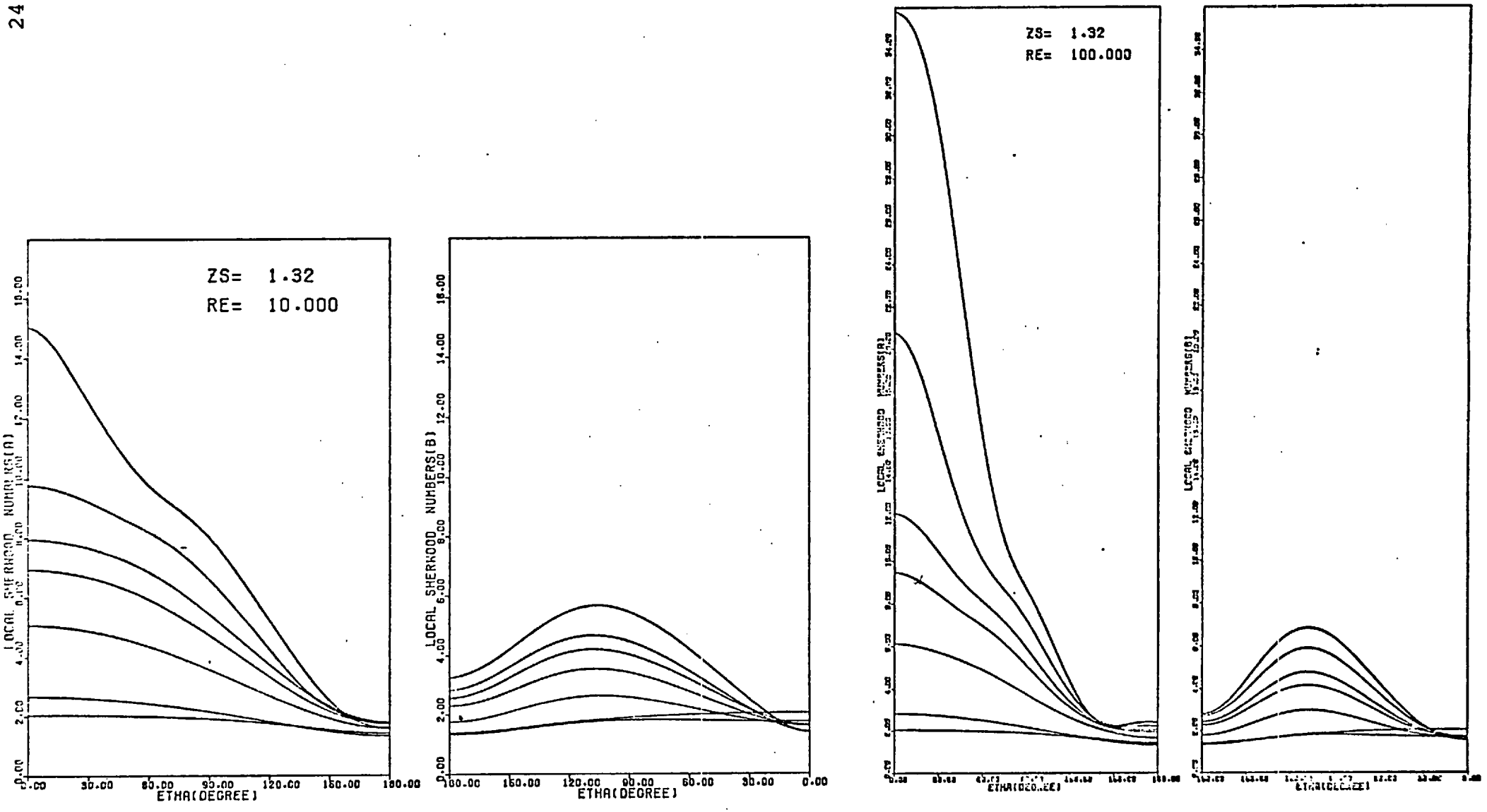

Figure(6-4-4) Local Sherwood number as a function of η with Peclet number as a parameter.

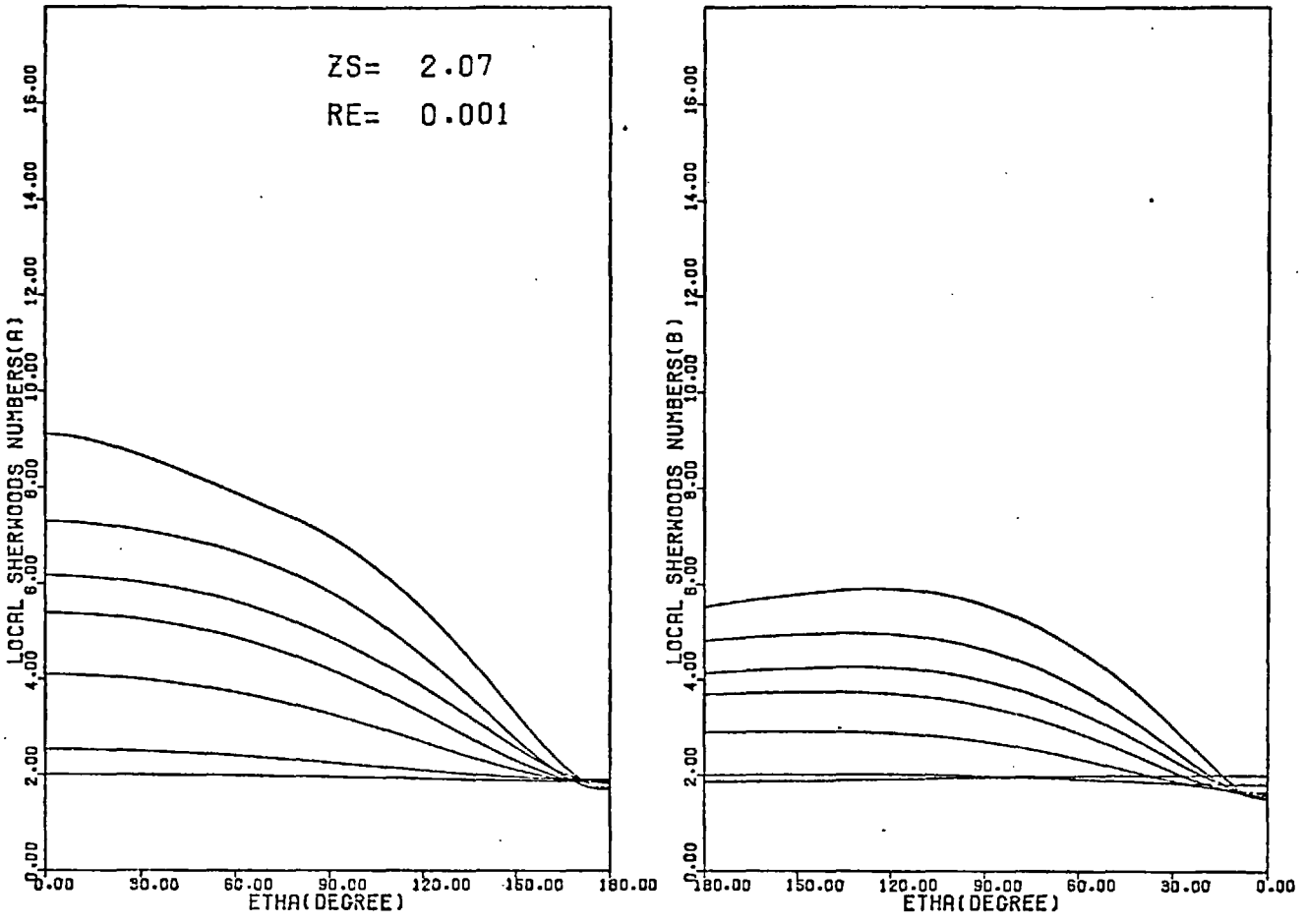

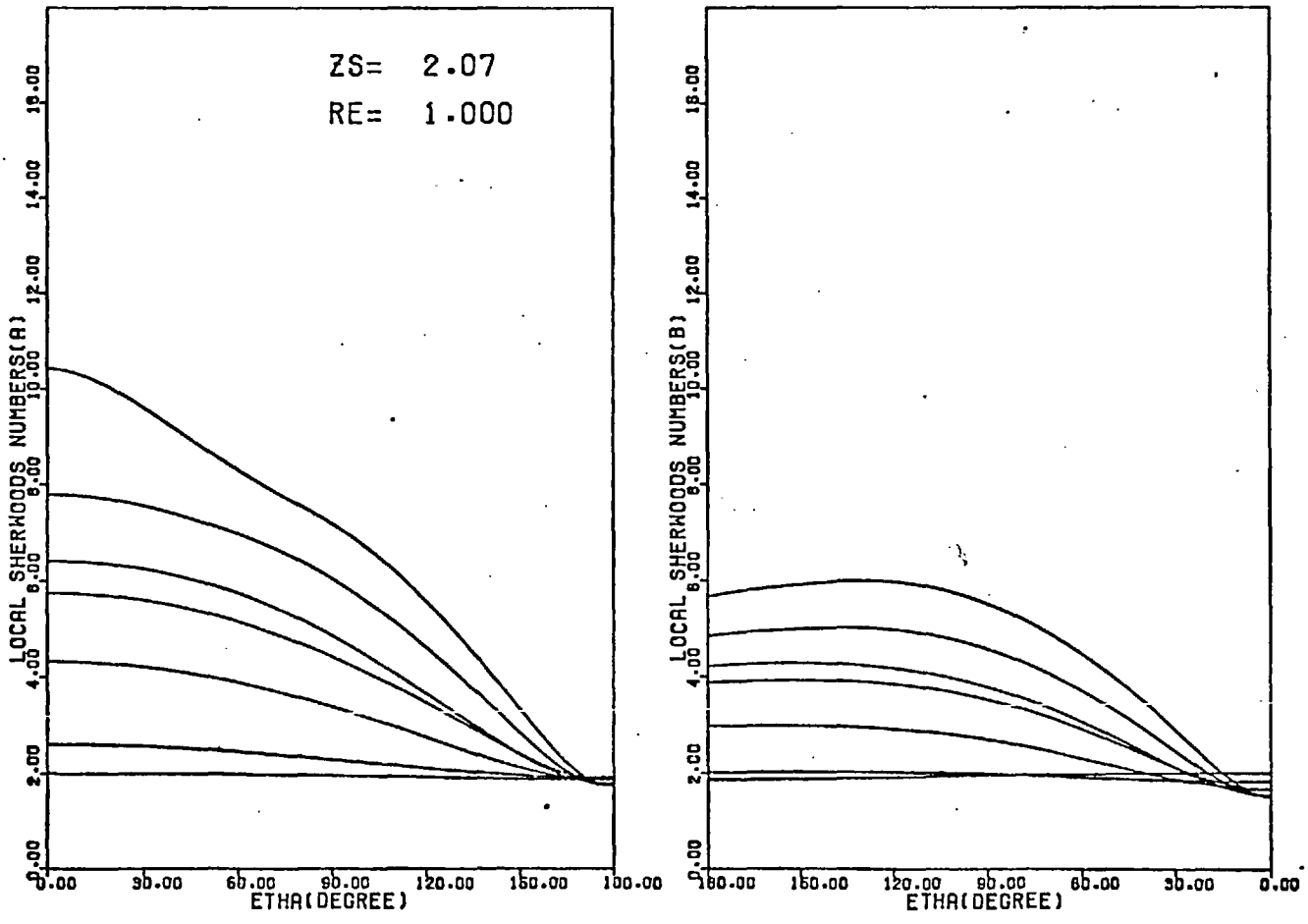

Figure(6-4-5) Local Sherwood number as a function of η with Peclet number as a parameter.

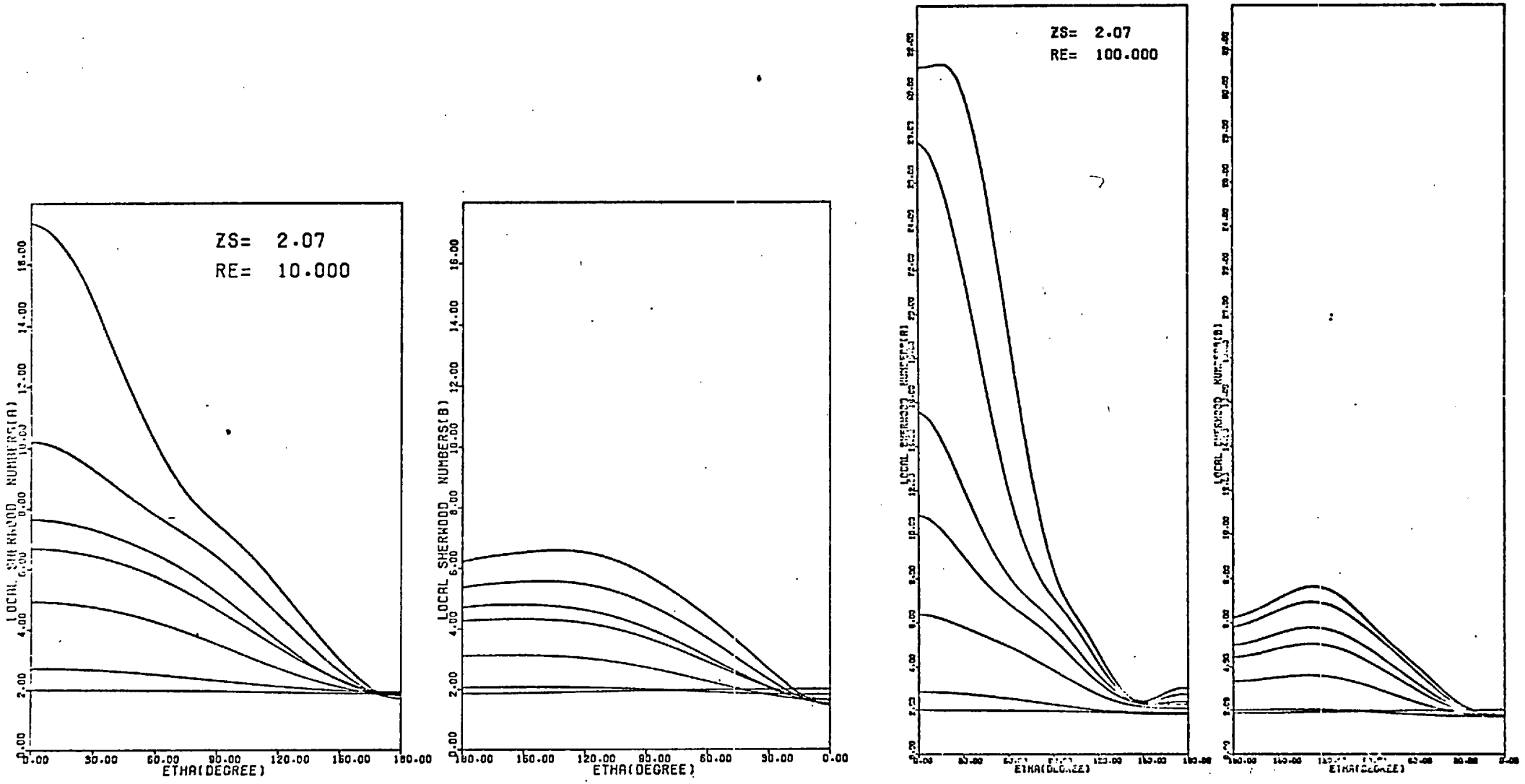

Figure(6-4-6) Local Sherwood number as a function of η with Peclet number as a parameter.

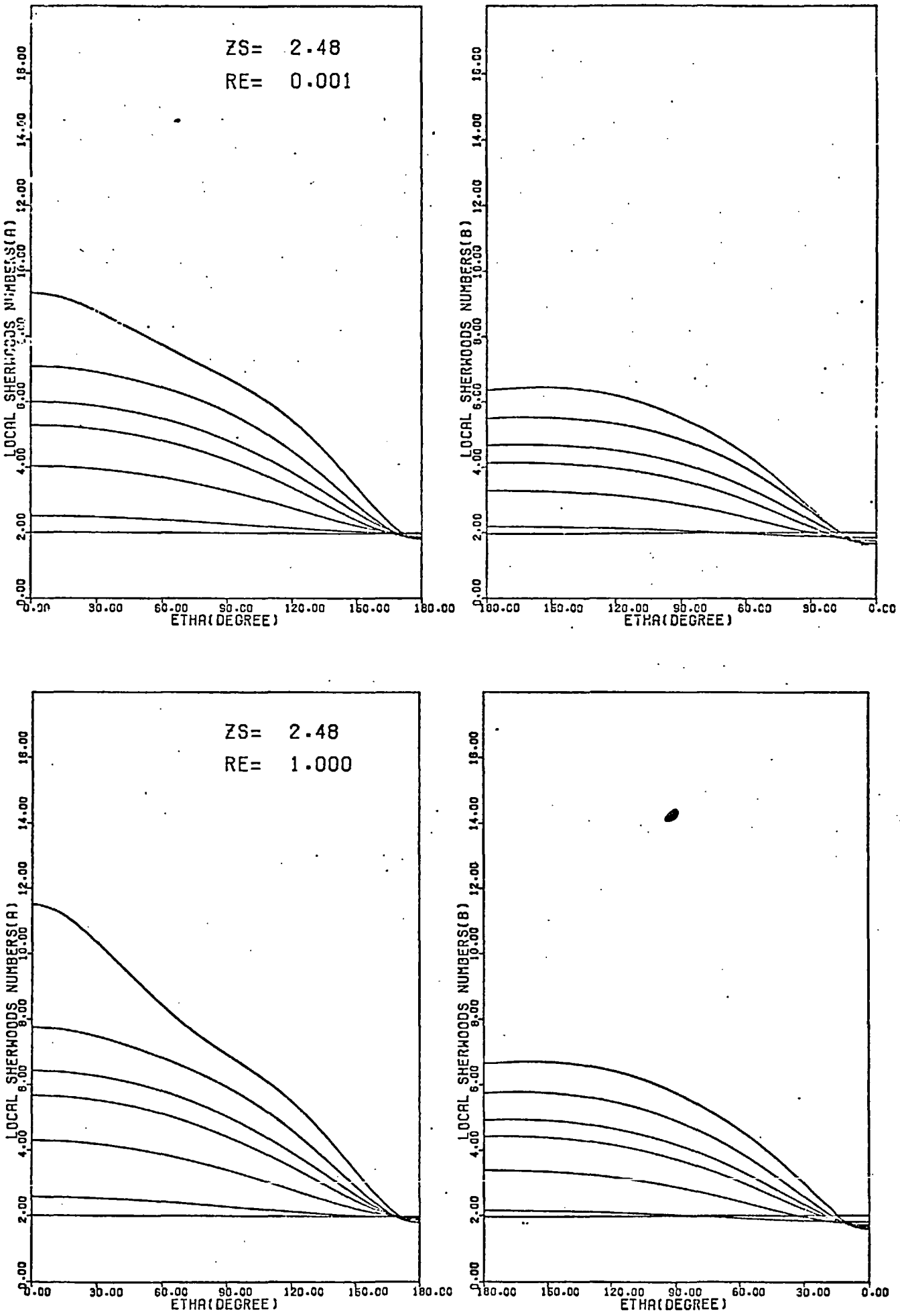

Figure(6-4-7) Local Sherwood number as a function of η with Peclet number as a parameter.

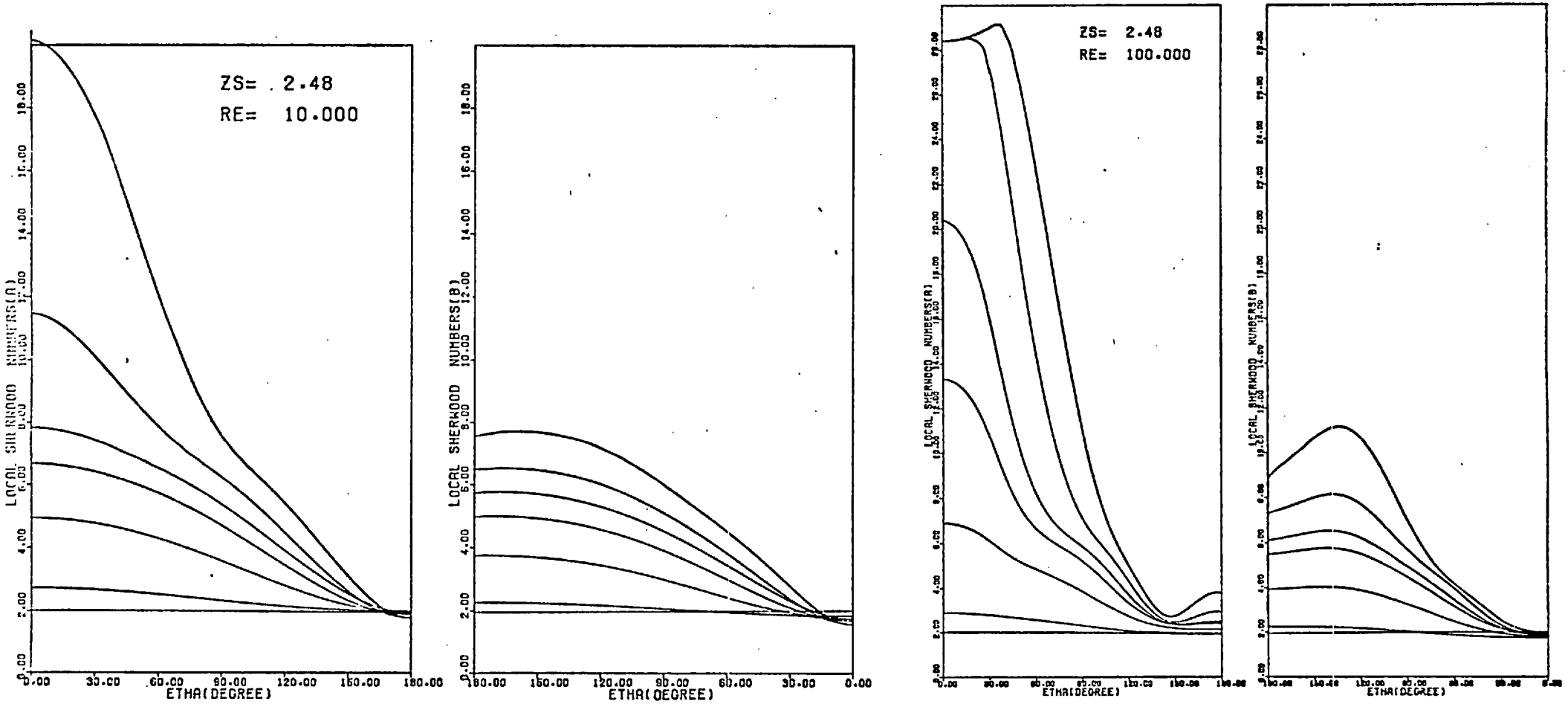

Figure(6-4-8) Local Sherwood number as a function of η with Peclet number as a parameter.

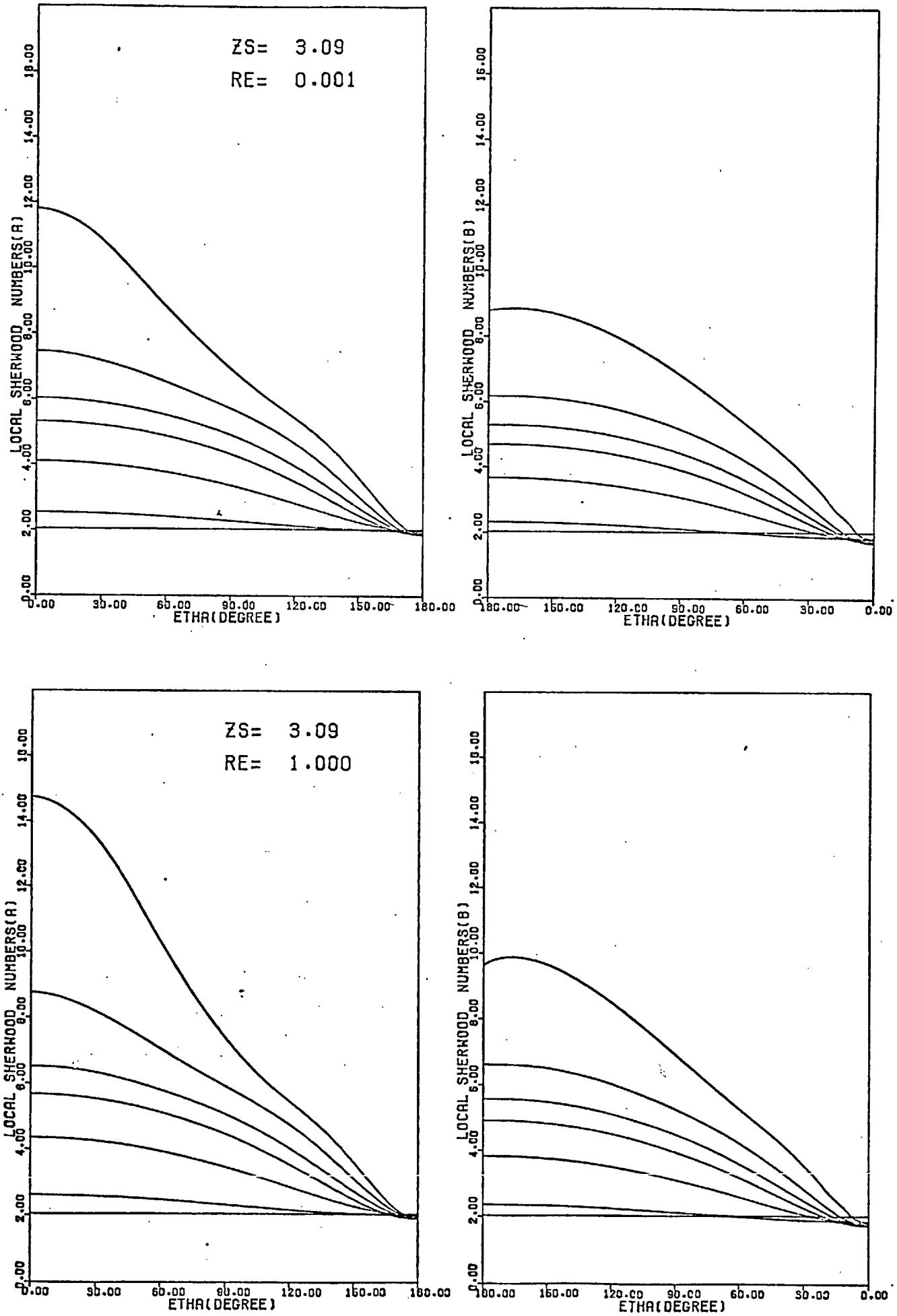

Figure(6-4-9) Local Sherwood number as a function of η with Peclet number as a parameter.

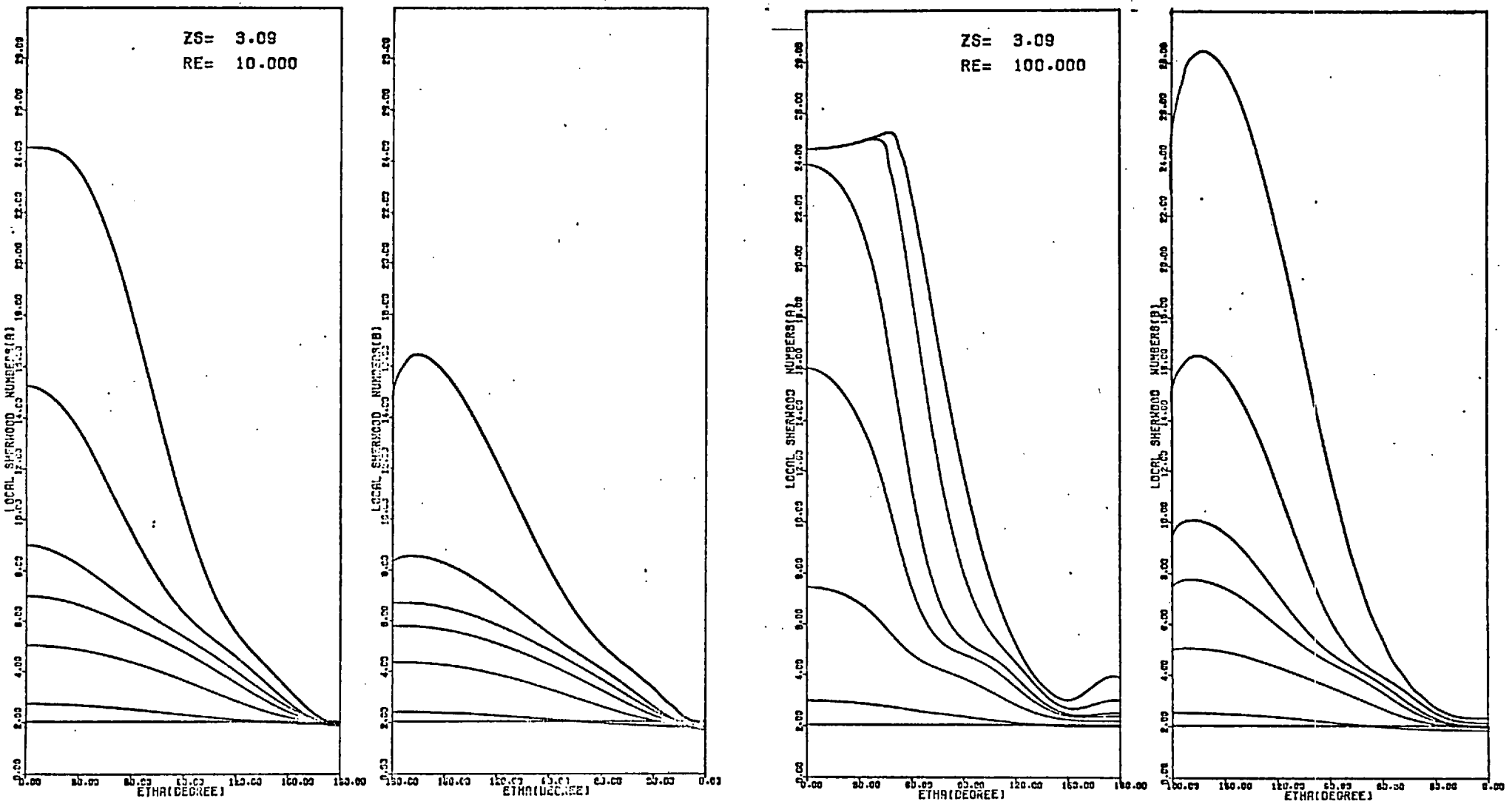

Figure(6-4-10) Local Sherwood number as a function of η with Peclet number as a parameter.

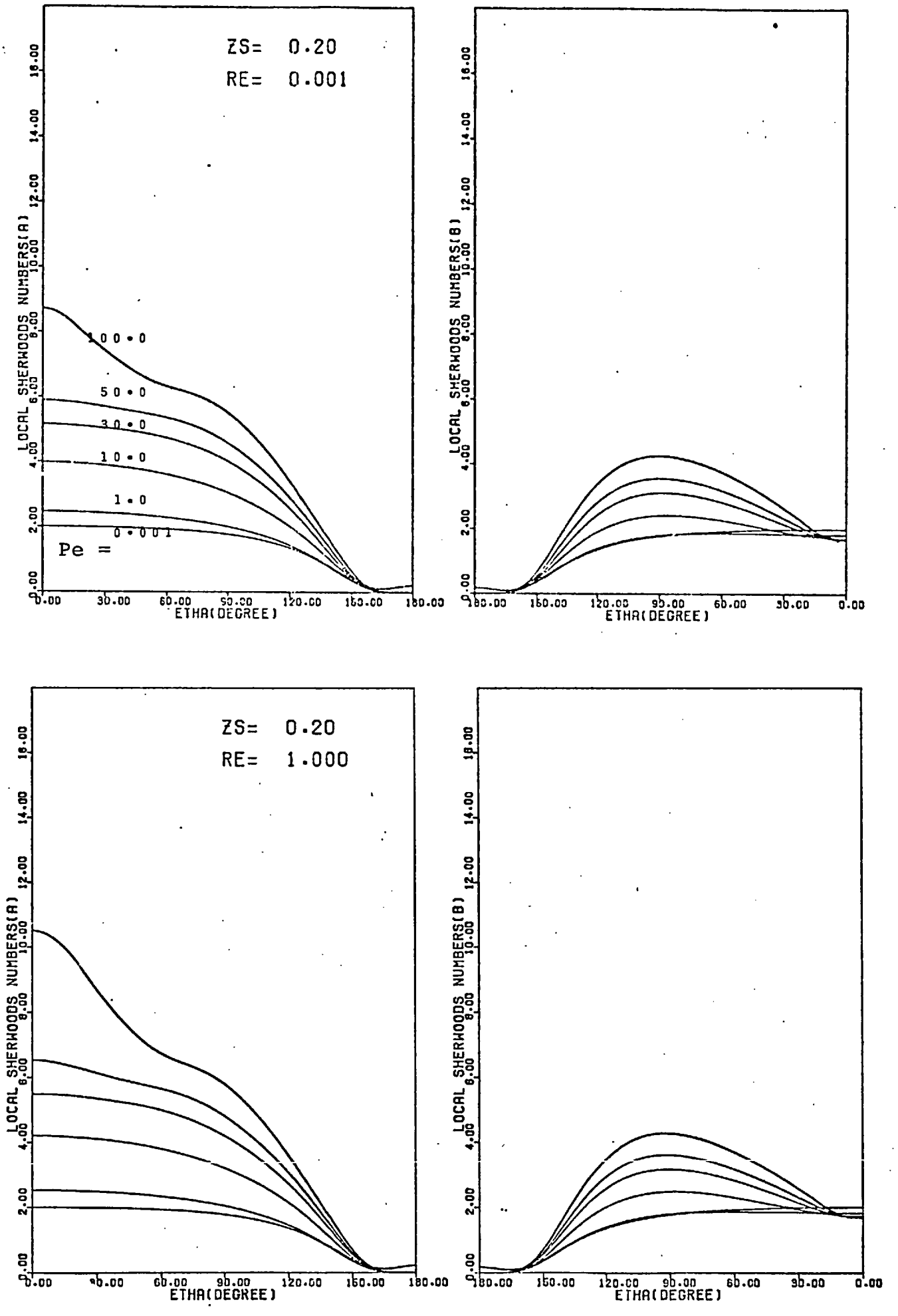

Figure(6-4-11) Local Sherwood numbers as a function of η with Peclet number as a parameter.

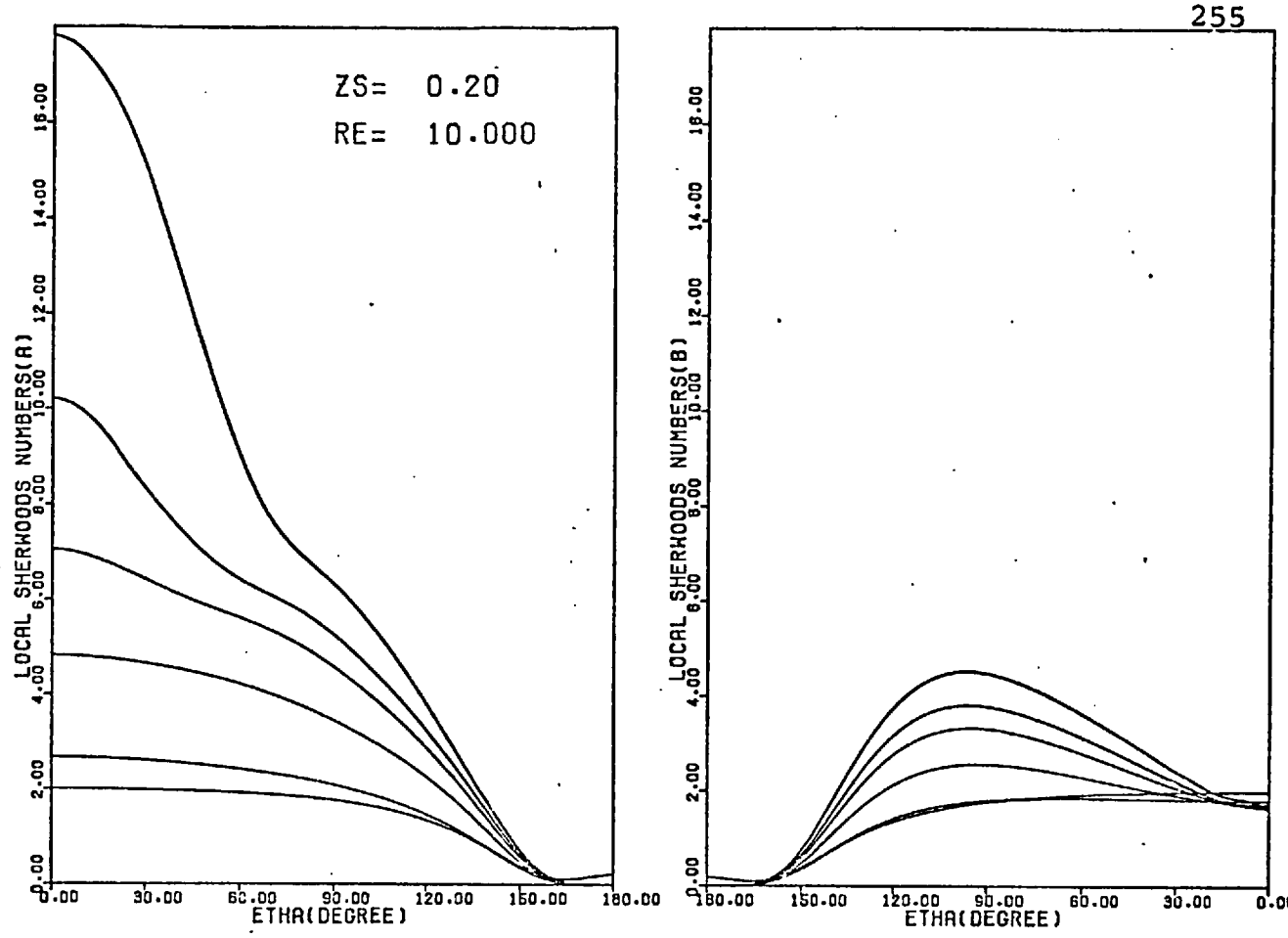

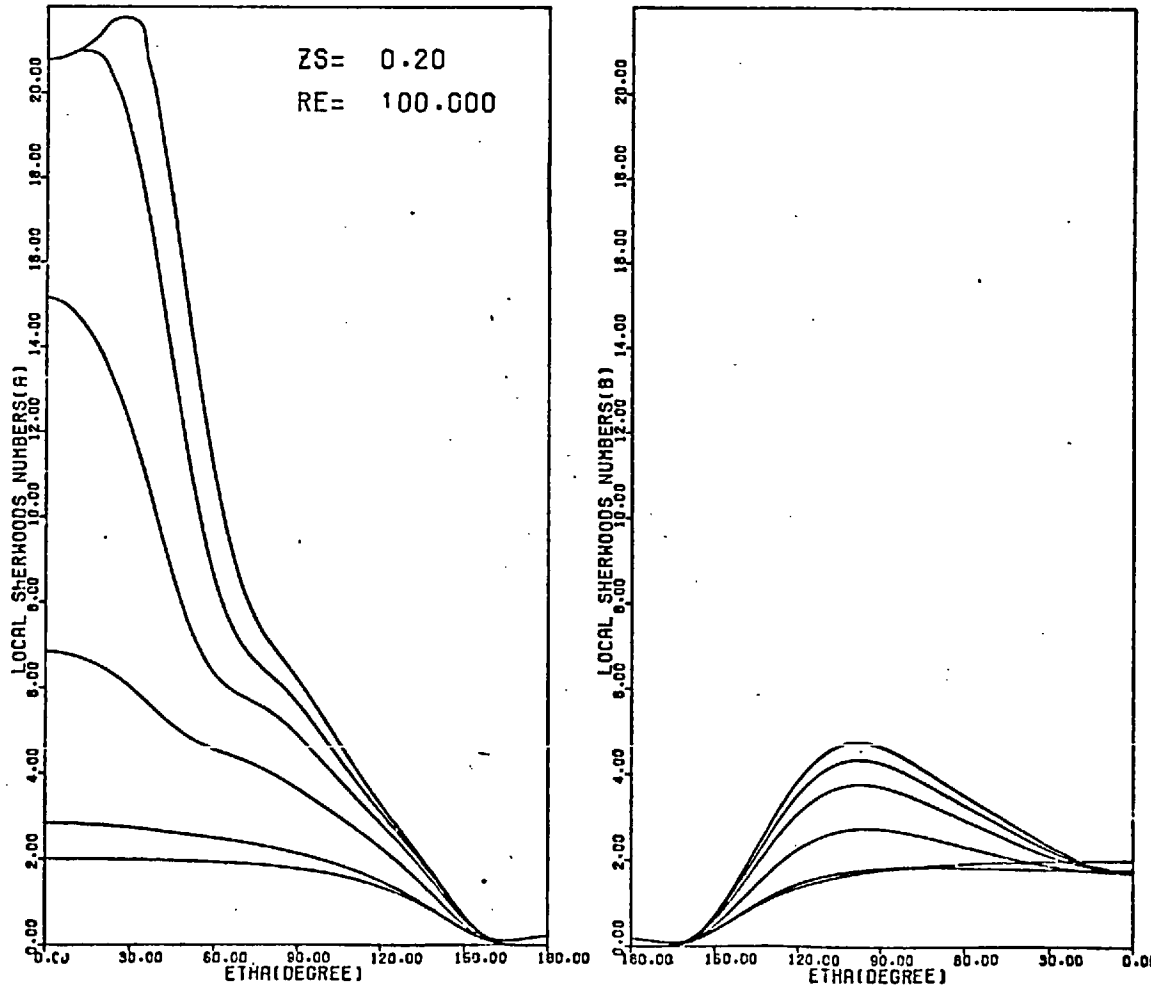

Figure(6-4-12) Local Sherwood number as a function of η with Peclet number as a parameter.

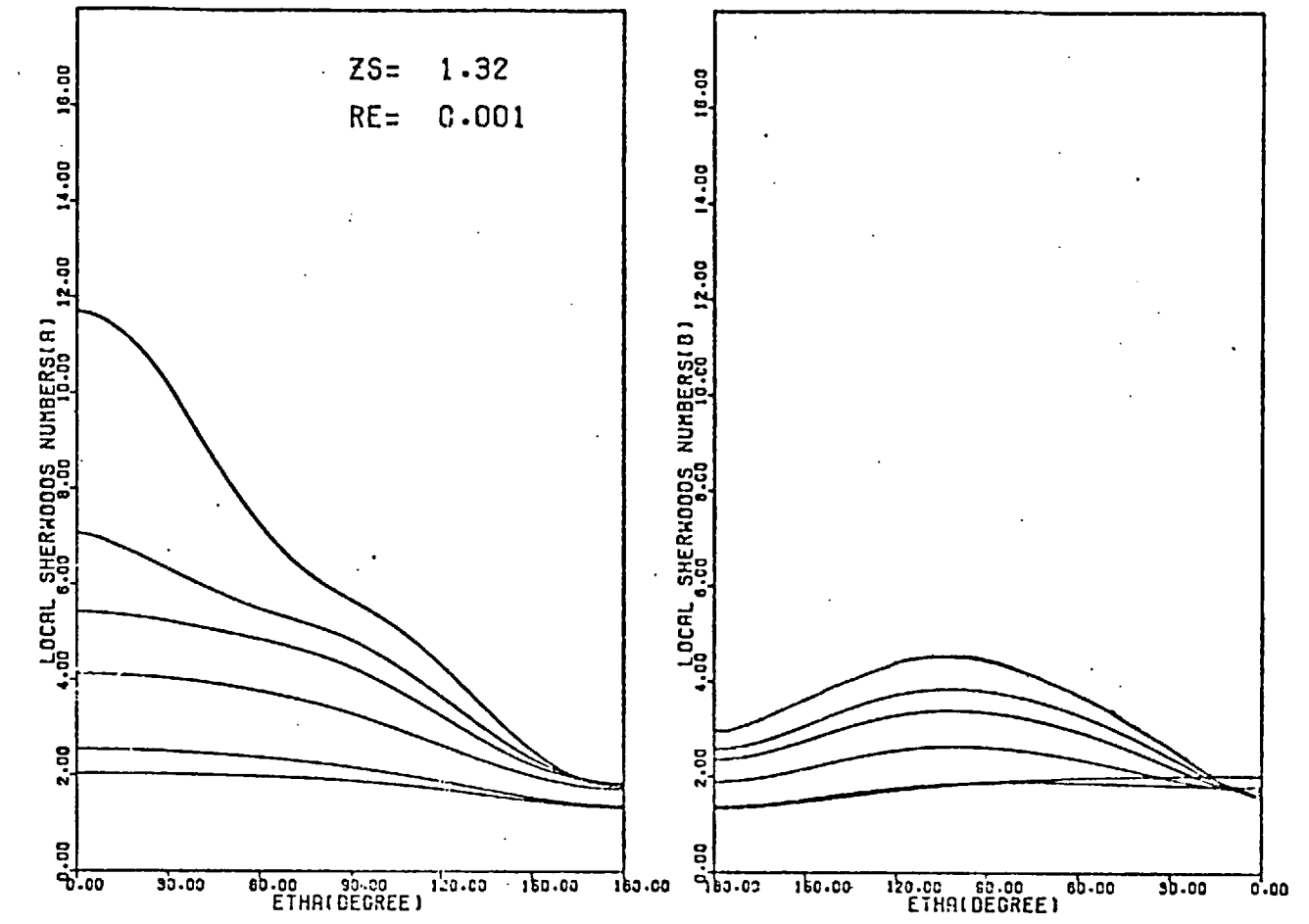

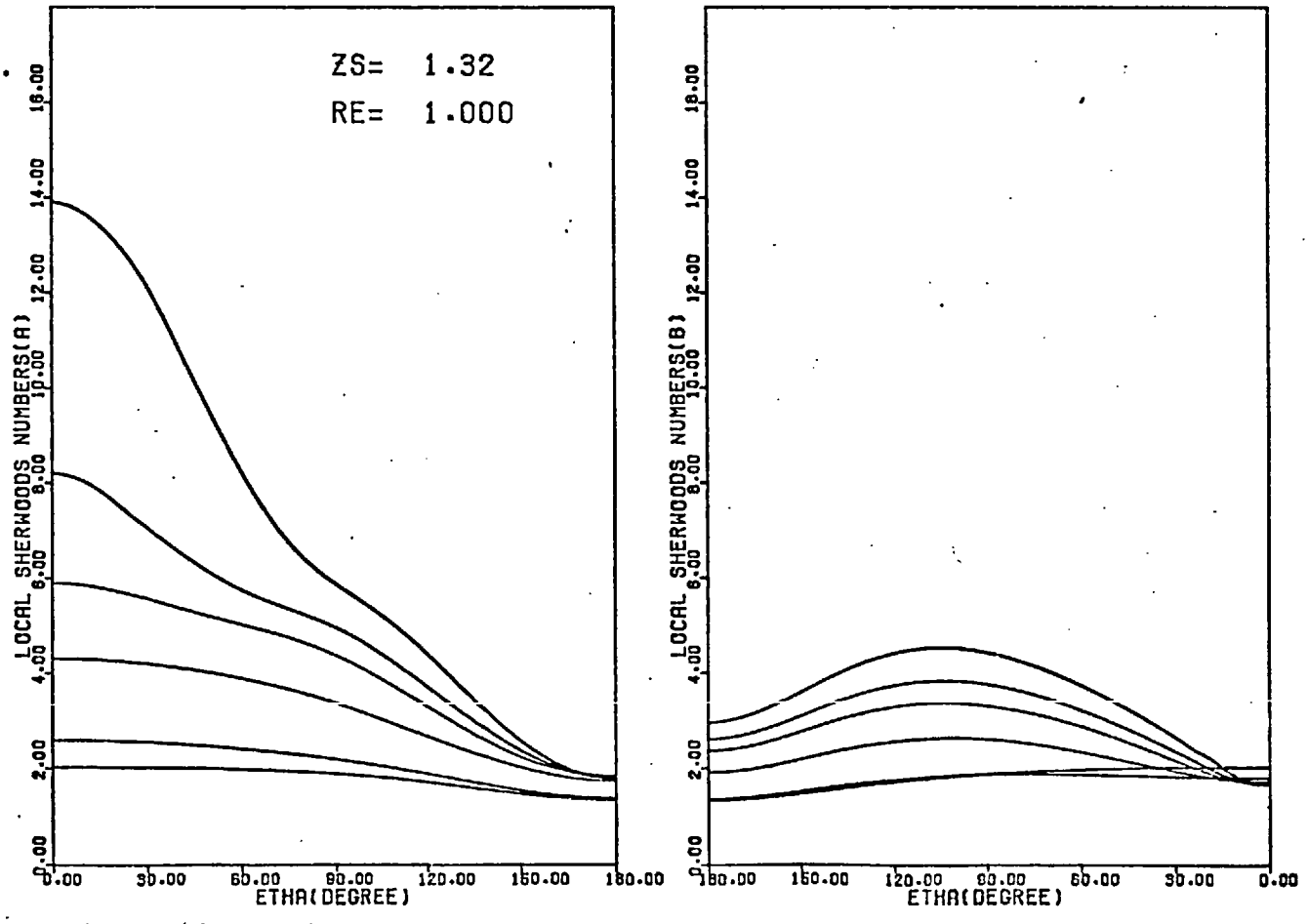

Figure(6-4-13) Local Sherwood number as a function of η with Peclet number as a parameter.

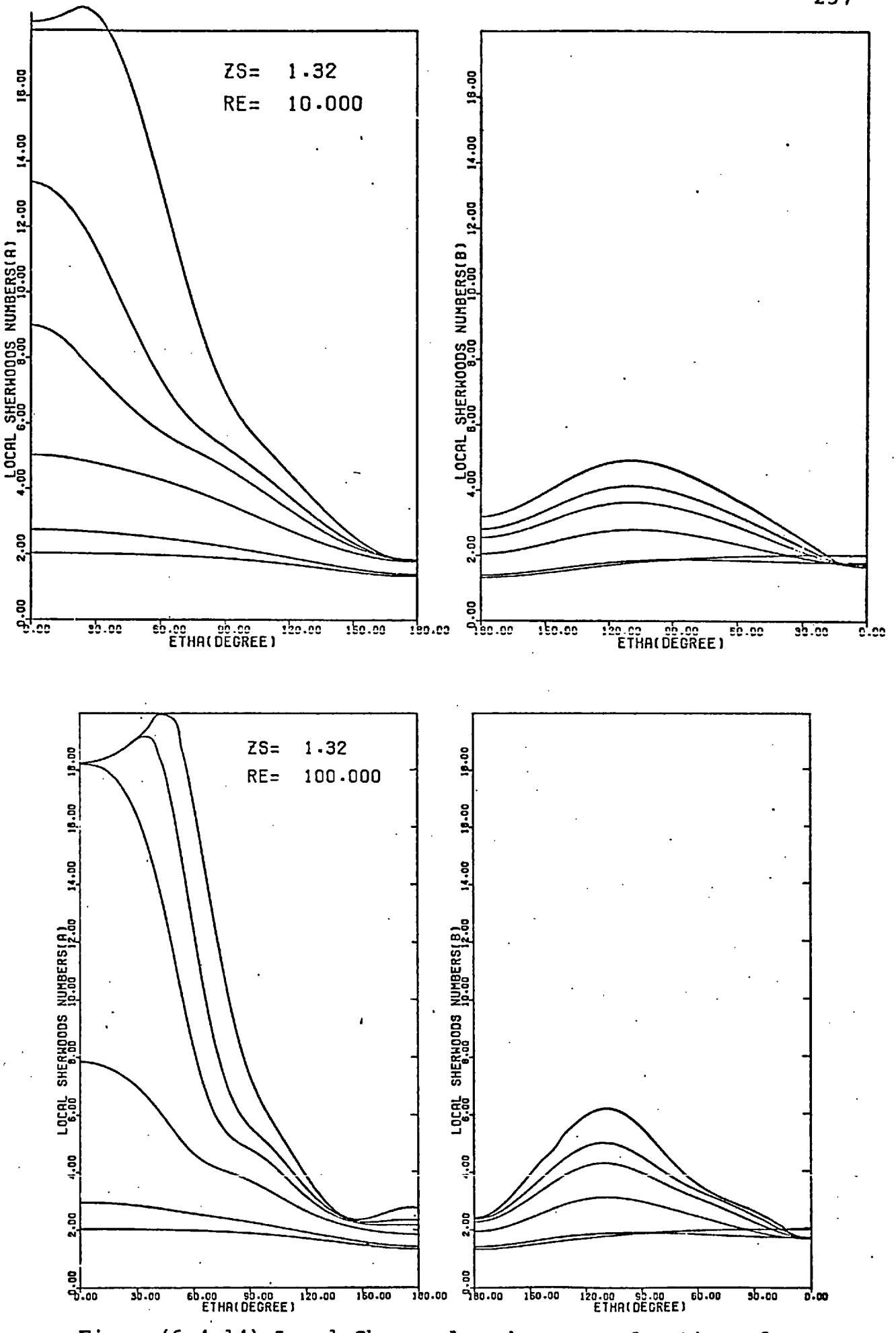

Figure(6-4-14) Local Sherwood number as a function of η with Peclet number as a parameter.

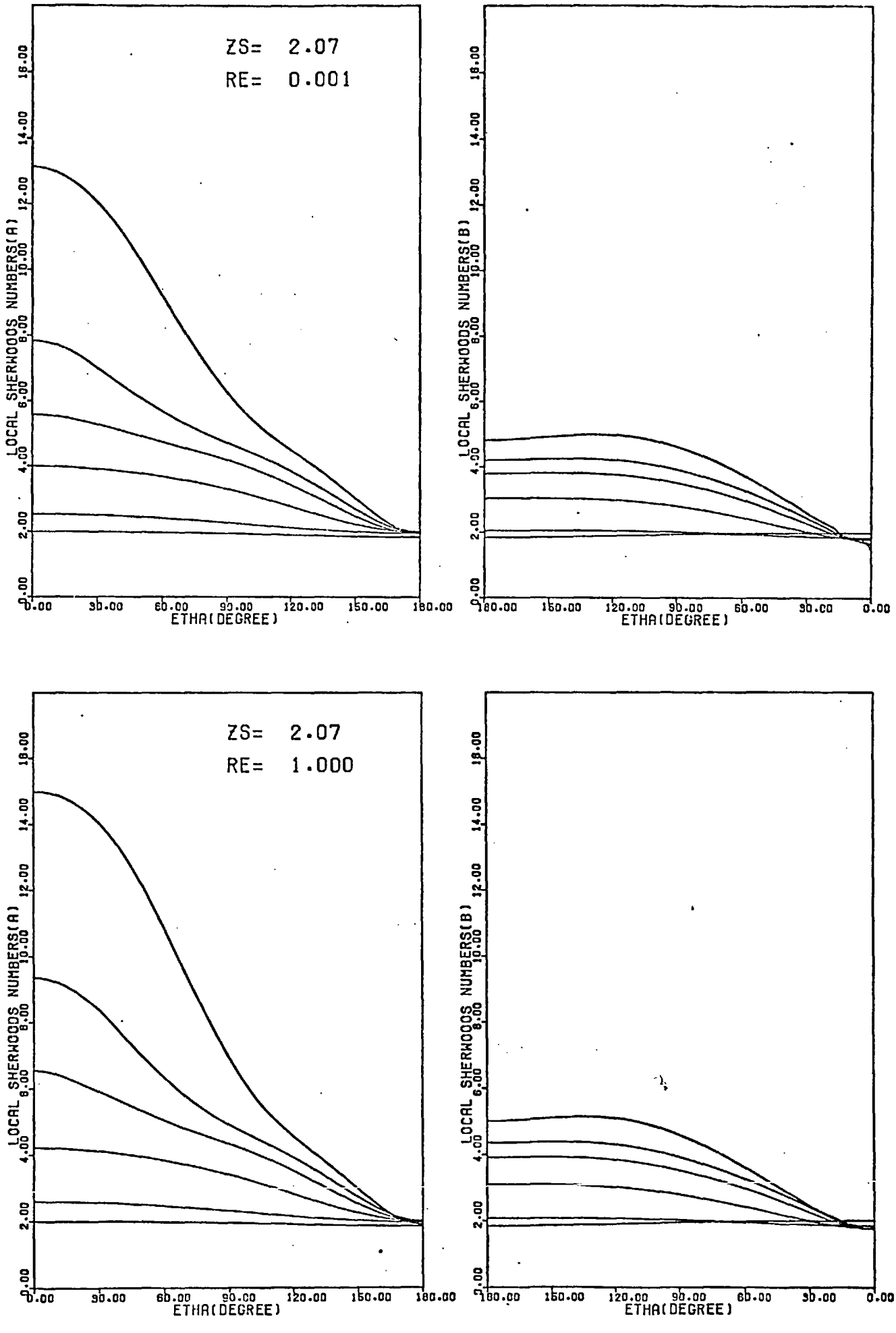

Figure(6-4-15) Local Sherwood number as a function of η with Peclet number as a parameter.

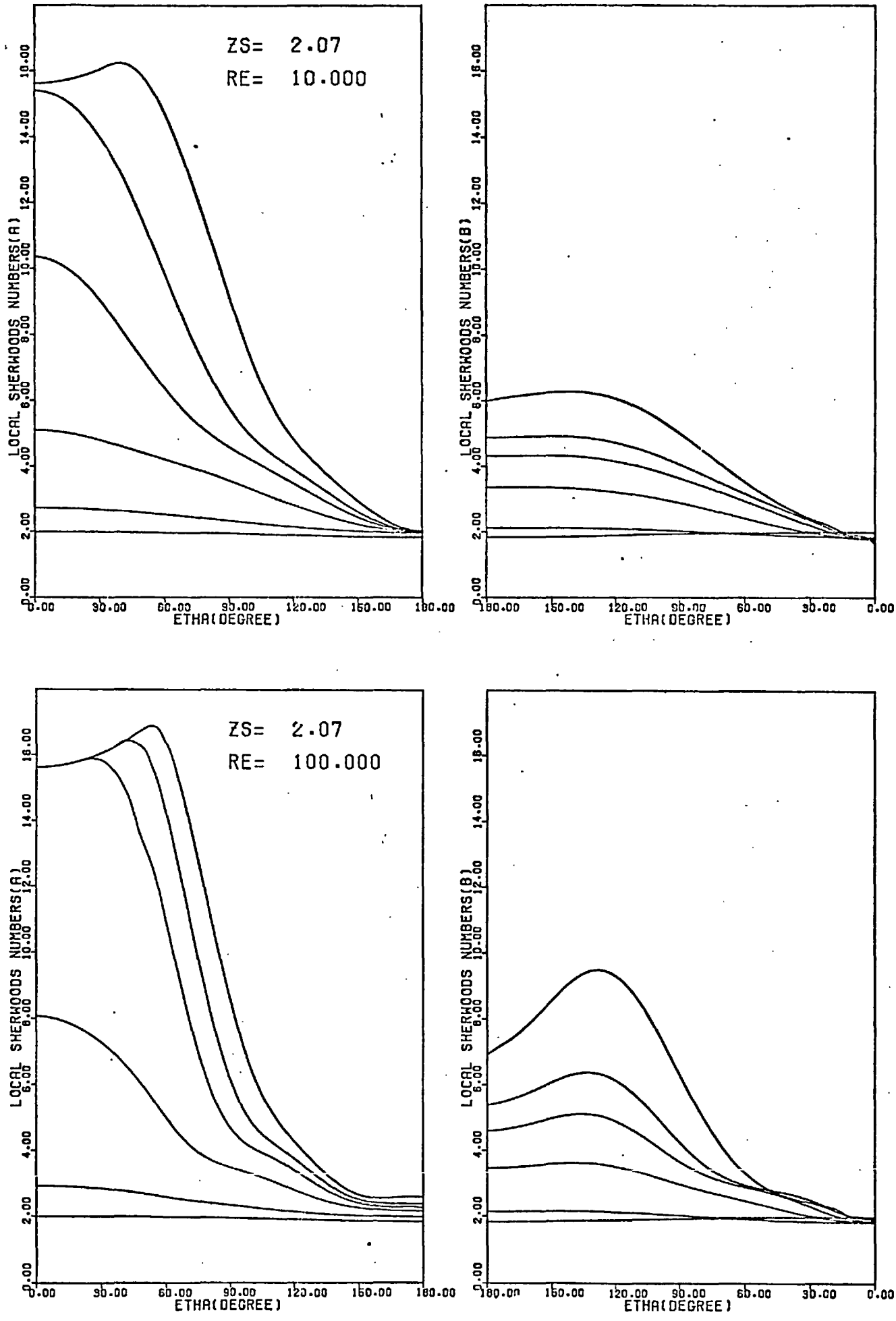

Figure(6-4-16) Local Sherwood number as a function of η with Peclet number as a parameter.

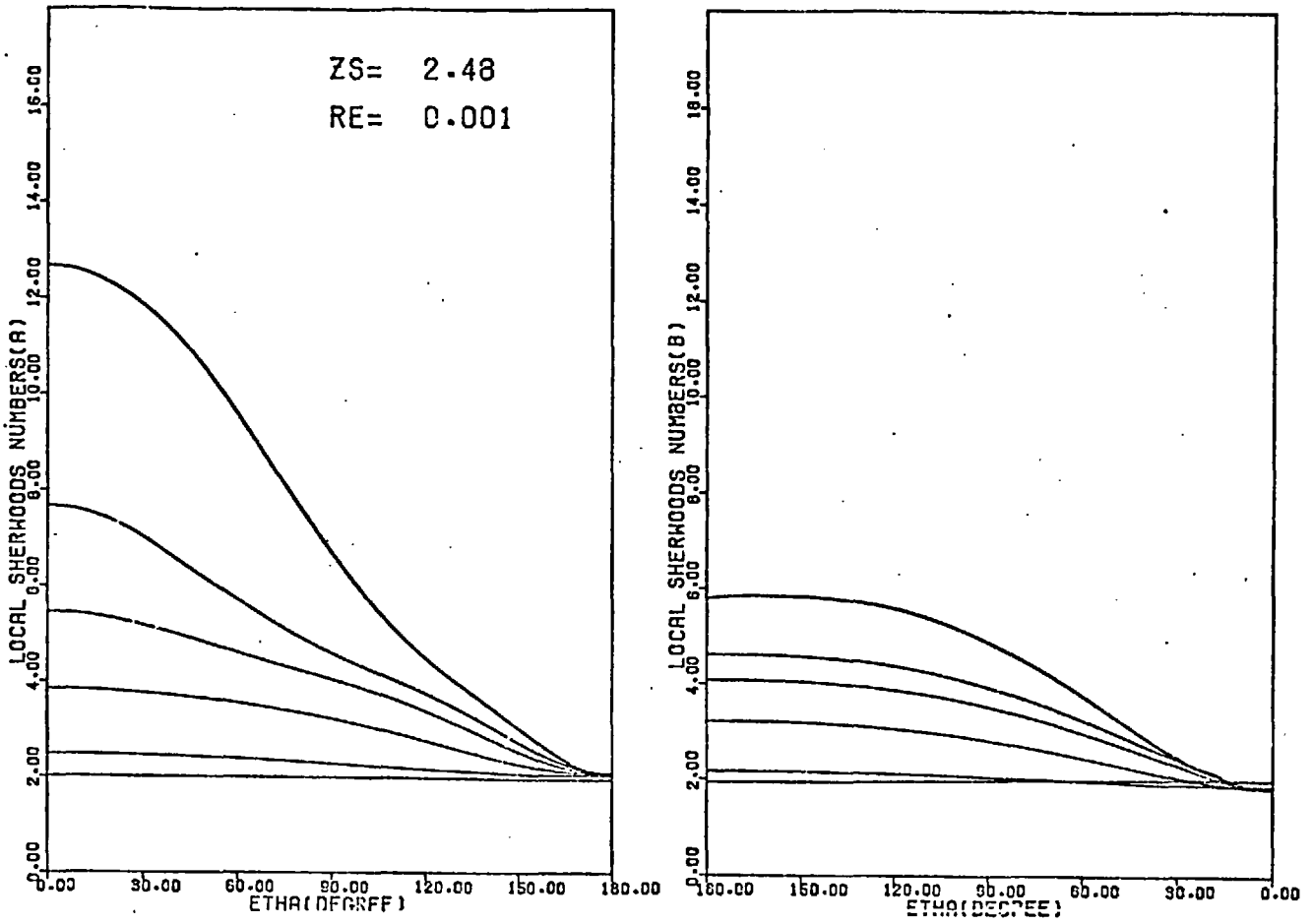

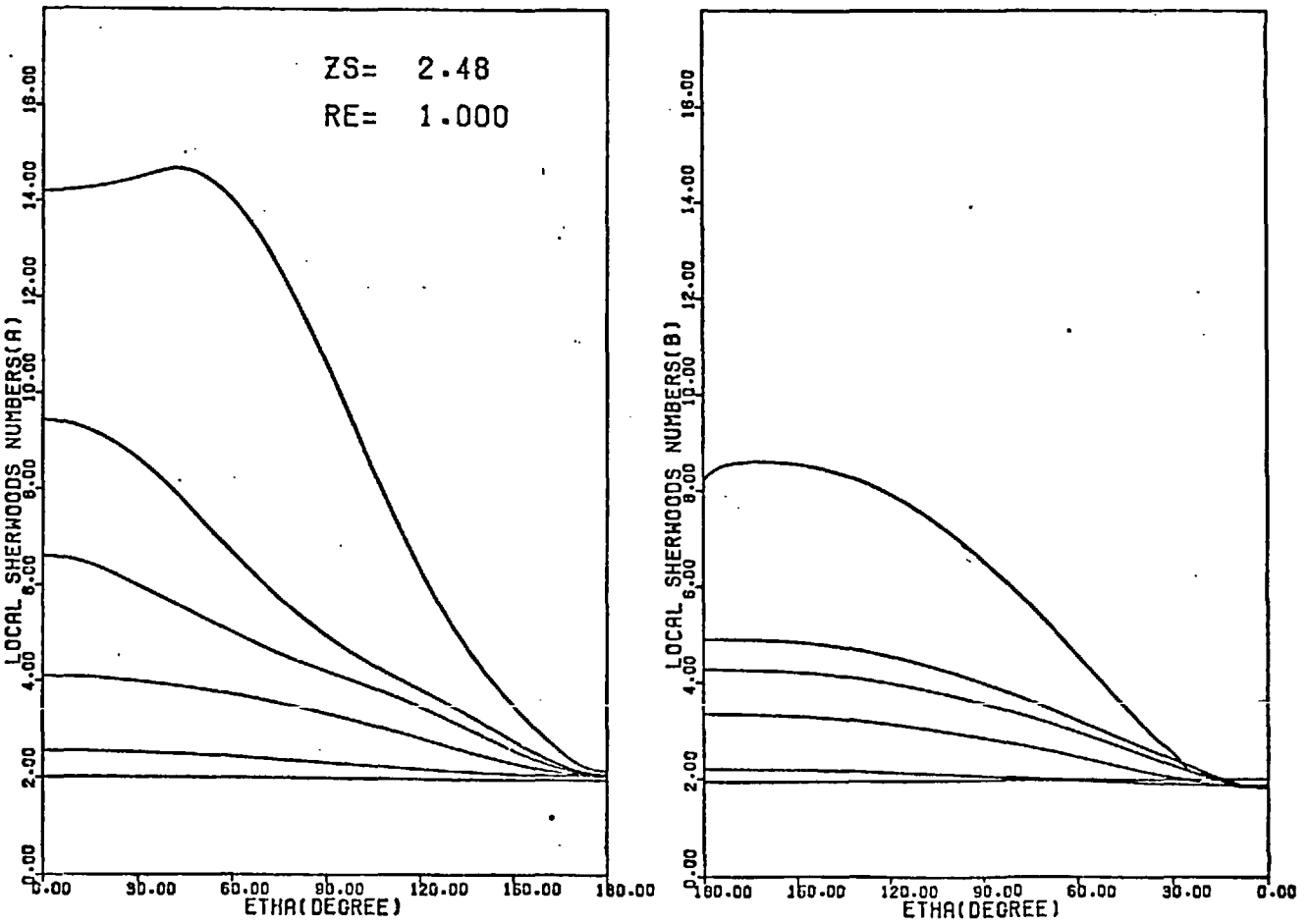

Figure(6-4-17) Local Sherwood number as a function of η with Peclet number as a parameter.

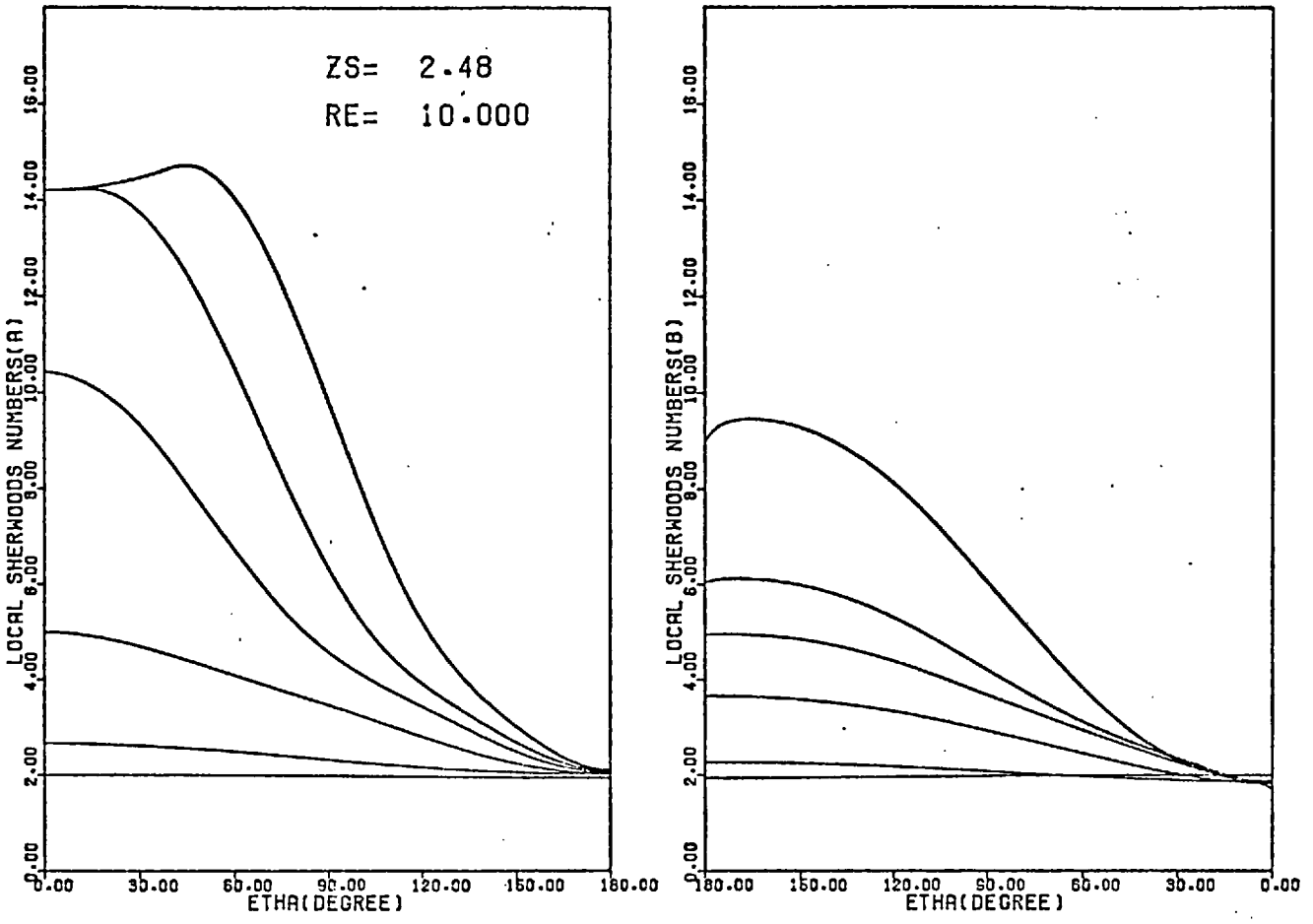

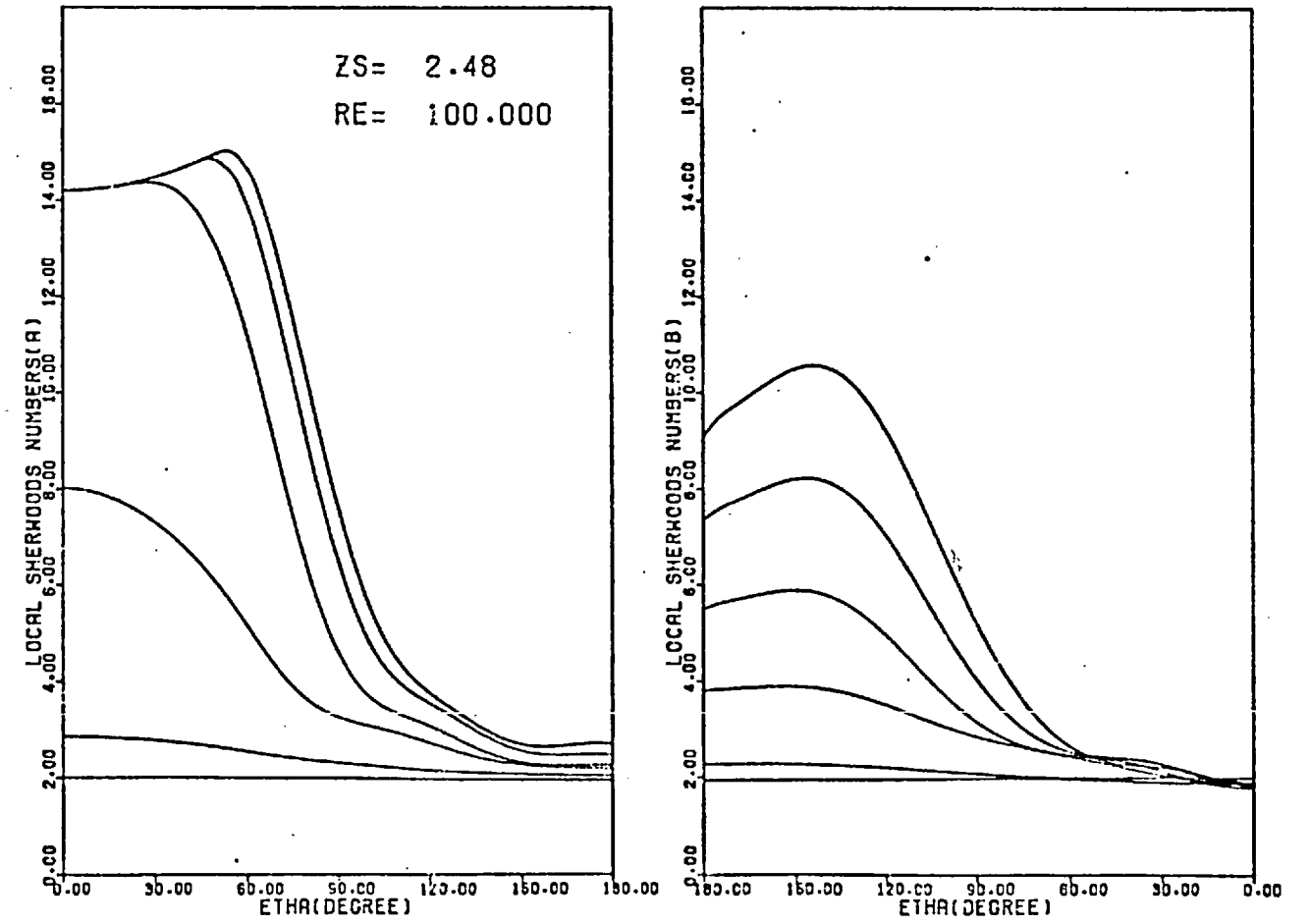

Figure(6-4-18) Local Sherwood number as a function of η with Peclet number as a parameter.

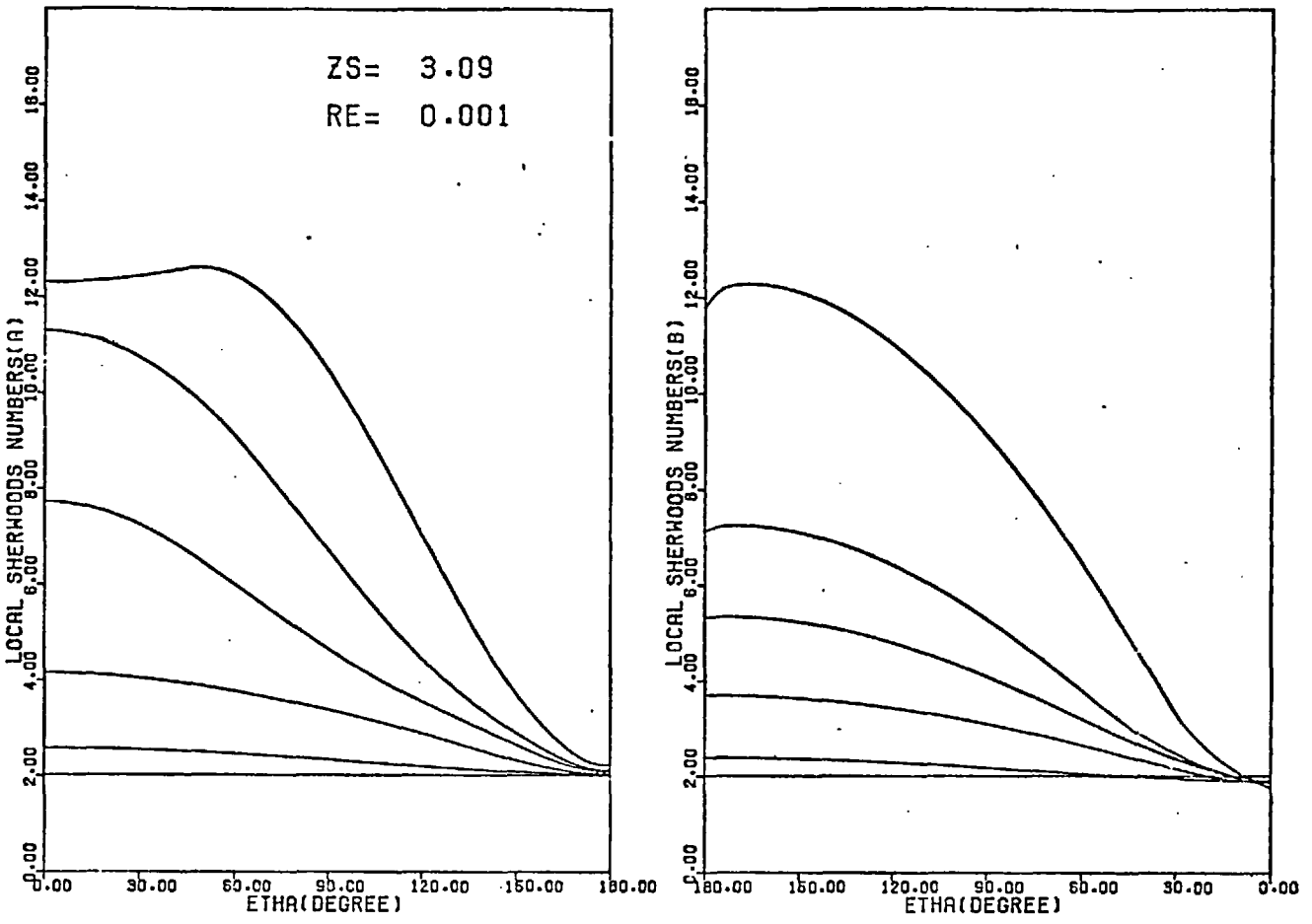

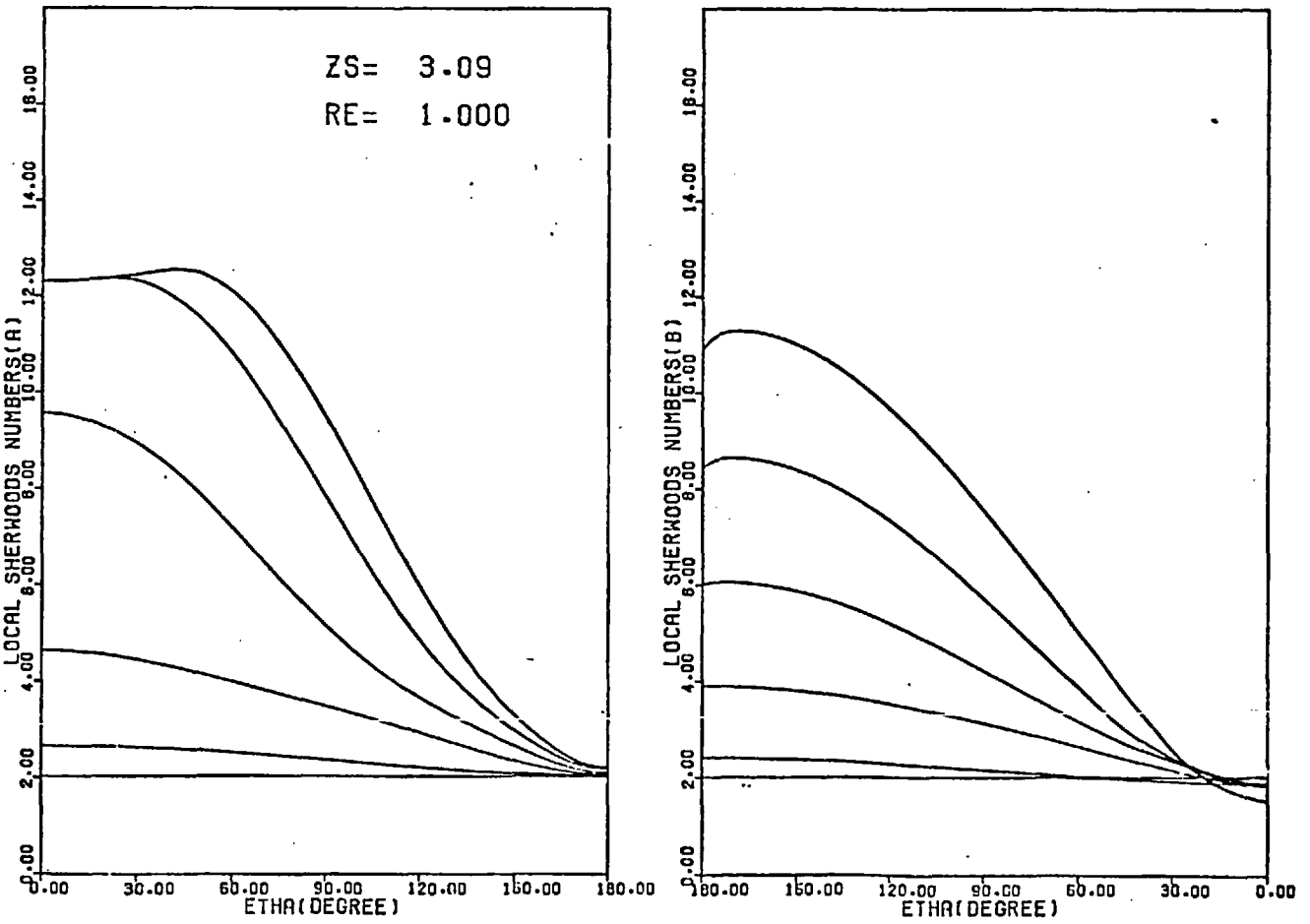

Figure(6-4-19) Local Sherwood number as a function of η with Peclet number as a parameter.

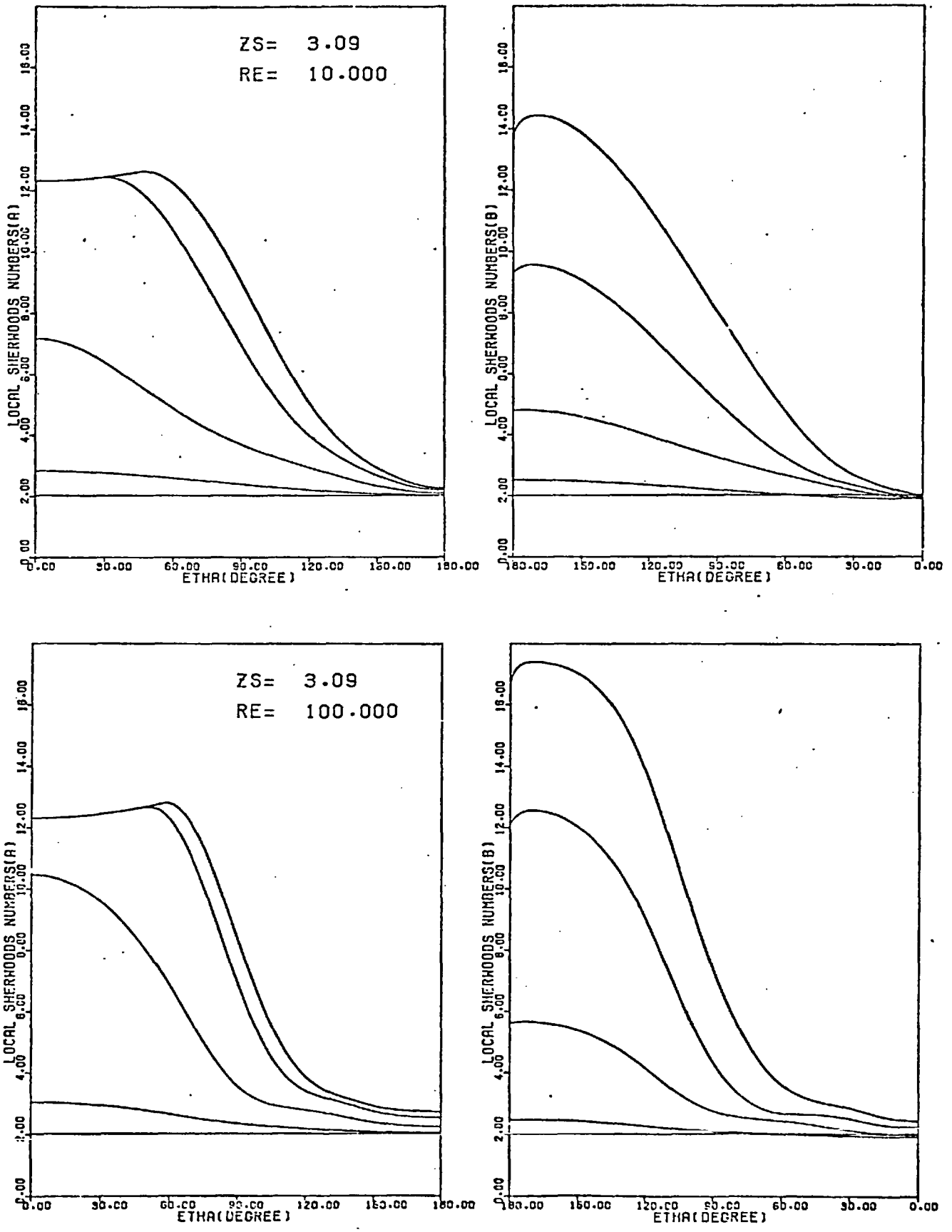

Figure(6-4-20) Local Sherwood number as a function of η with Peclet number as a parameter.

number around the two spheres are generally similar to each other and are also similar to those around a single isolated sphere.

Before summarizing the results for the five sphere spacings, there are two important features regarding the values of the local Sherwood numbers near the front stagnation point of sphere A which must be considered. The first feature is the rapidity of the increase in the local Sherwood numbers near the front stagnation point with increasing Peclet number. The second feature is that for the large sphere spacings the rapid increase in the local Sherwood numbers with increasing Peclet number suddenly ceases and the local Sherwood numbers become independent of Peclet number over a region near the front stagnation point of sphere A. The maximum values of the local Sherwood numbers appear to be dependent upon Peclet and Reynolds numbers and upon sphere spacing. The anomalous behaviour is mainly a result of the combined effect of the inherent characteristic of the bi-spherical coordinate system of providing large Z-grid-line spacings upstream of sphere A and the existence of a thin diffusional boundary layer at the upstream surface of sphere A at high Peclet numbers. It is clear that as the Peclet number increases, the thickness of the diffusional boundary layer decreases. Hence, when the Peclet number is sufficiently high, the diffusional boundary layer over part of the front surface of sphere A falls within the three Z-grid-line spacings closest to the front surface of sphere A and, as a result, the concentration gradients at the surface calculated using equation(4-5-16), which is based on a four-point forward difference approximation, become abnormally

large. Similarly, when the Peclet number is further increased, the diffusional boundary layer over the front surface of sphere A becomes so thin that over part of the surface of sphere A it falls within the Z-grid-line spacing closest to the front surface of sphere A with the result that the local Sherwood numbers near the front stagnation point of sphere A calculated using equations(4-5-11) and (4-5-16) become independent of Peclet number. It is important to note that the size of the region over which the local Sherwood numbers become independent of Peclet number increases with Peclet number, Reynolds number, and sphere spacing. Also, as the sphere spacing is increased the local Sherwood numbers near the front stagnation point of sphere A first become independent of Peclet number at lower values of the Peclet and Reynolds numbers. The dependence on sphere spacing arises because, for a constant number of mesh points used in each flow region the Z-grid-line spacings become coarser as the sphere spacing increases so that the diffusional boundary layer over part of the upstream surface of sphere A becomes contained within the first Z-grid-line spacing at lower Peclet and Reynolds numbers. It should be noted that for each sphere spacing when the mesh spacing in Z was reduced from $|Zs/10|$ to $|Zs/20|$ the anomalous behaviour associated with the combined effect of the large Z-grid-line spacings and the thin diffusional boundary layer over part of the upstream surface of sphere A was greatly reduced and did not occur until higher Reynolds and Peclet numbers had been attained. For sphere B these problems did not occur even for large sphere spacings and at high Reynolds and Peclet numbers. This is because the Z-grid-line spacings upstream of sphere B were generally very small compared with those upstream of sphere A.

From the above discussion, it is clear that the local rates of mass transfer from a system of two equally sized spheres with fluid flowing parallel to their line of centres, are dependent on the Peclet number, Reynolds number, and sphere spacing. A brief summary of this behaviour is made as follows.

Except from the front surface of sphere B for the smallest sphere spacing, the rates of mass transfer from the front surfaces of the two spheres for each specified sphere spacing and Reynolds number increase with increasing Peclet number. The increase is always larger for sphere A than for sphere B. At low Peclet numbers of 0.001 to 1.0 the local rates of mass transfer remain nearly the same at each sphere spacing as the Reynolds number is increased from 0.001 to 100.0. At higher Peclet numbers the local rates of mass transfer increase with Reynolds number, particularly from the front surfaces of the spheres, and the increases are larger for sphere A than for sphere B. As a result, for each sphere spacing the difference between the rates of mass transfer from the front surfaces of the spheres is very large at high Reynolds and Peclet numbers. In contrast, for each sphere spacing the rates of mass transfer from the rear surfaces of the two spheres either remain nearly the same or change only slightly with Reynolds and Peclet numbers. Also, for each sphere spacing the distributions of the local Sherwood numbers around the two spheres do not change much when the mesh spacing in Z is changed from $|Zs/10|$ to $|Zs/20|$ except over that part of the front surface of sphere A which at high Peclet and Reynolds numbers are affected by the relative thinness of the diffusional boundary layer in comparison with the relative coarseness of the Z-grid-line spacings.

The distance between the spheres is an important factor which affects the distributions of the local Sherwood number around the spheres especially at the front surface of sphere B. Except for the anomalous results at high Peclet and Reynolds numbers, the local Sherwood numbers at the front surface of sphere A do not change much as the sphere spacing is increased although at the rear surface of sphere A they do increase, particularly when the sphere spacing is increased from Zs = 0.20 to Zs = 1.32. On the other hand, the rates of mass transfer from the front surface of sphere B increase while those from the rear surface of sphere B remain nearly the same when the sphere spacing is increased. The increase in the rates of mass transfer from the front surface of sphere B with increasing sphere spacing is mainly because the larger distance between the spheres results in a lower concentration of the diffusing material in the fluid in the inner region between the spheres and thus in increased rates of mass transfer from the front surface of sphere B. As a consequence, when the distance between the spheres increases the difference between the rates of mass transfer from the front surfaces of the two spheres becomes smaller and the distributions of the local Sherwood number around the two spheres become closer to each other as well as closer to those around a single isolated sphere.

6-5. Overall Sherwood numbers.

The overall rates of mass transfer from a system of two equally sized spheres were expressed in terms of the overall Sherwood numbers Sh_{AO} and Sh_{BO} for spheres A and B, respectively. For each specified sphere spacing, Reynolds number, and Peclet number, the overall Sherwood numbers for the two spheres were obtained from the integration of the local Sherwood numbers over the entire surfaces of the spheres using equations(4-5-13) and (4-5-14) for spheres A and B, respectively.

For each of the five sphere spacings considered in this study: Zs = 0.20, 1.32, 2.07, 2.48, and 3.09, and for each of the four selected Reynolds numbers of 0.001, 1.0, 10.0, and 100.0, there are two sets of results corresponding to the mesh spacings of |Zs/20| and |Zs/10| in Z used in the solution of the diffusion equation. The overall Sherwood numbers obtained using the smaller mesh spacing of |Zs/20| in Z are tabulated in Tables(6-5-1) to (6-5-5); while those obtained using the larger mesh spacing of |Zs/10| in Z are tabulated in Tables(6-5-6) to (6-5-10). Plots of the overall Sherwood numbers against Peclet number are shown in Figures(6-5-1) to (6-5-16). For each specified sphere spacing and Reynolds number, the overall Sherwood numbers for the two spheres are plotted against Peclet number as shown in Figures(6-5-1) to (6-5-9). From these plots, the difference between the overall Sherwood numbers for the two spheres at each specified sphere spacing and Reynolds number can immediately be seen over a wide range of Peclet numbers. Also, in Figures(6-5-10) to (6-5-16) the overall Sherwood numbers for the two spheres at each specified sphere spacing are plotted against Peclet number separately

with the four selected Reynolds numbers as parameter. From these plots, the influence of Reynolds number upon the overall Sherwood numbers for each of the two spheres can easily be studied.

From Figures(6-5-1) to (6-5-9), it is clear that for each sphere spacing and Reynolds number, the overall Sherwood numbers of the two spheres are approximately equal and constant at low Peclet numbers of 0.001 to 0.1 in which range the transfer of material is mainly by means of molecular diffusion. At higher Peclet numbers, the overall Sherwood numbers for the two spheres increase steadily with increasing Peclet number, and the increase is larger for sphere A than for sphere B. These indicate the increasing importance of convection upon the transfer of material from the spheres and the effect of convection is greater for sphere A than for sphere B. Hence, as the Peclet number is increased the difference between the overall rates of mass transfer from the two spheres becomes larger. This is because sphere A is upstream of sphere B and encounters fresher fluid than sphere B; also, the diffusional boundary layer at the upstream surface of sphere A may be more highly developed than that at the upstream of sphere B. For these reasons there is a larger driving force for mass transfer from the front surface of sphere A than from the front surface of sphere B. It should be noted that the front surfaces of the spheres contribute most to the overall rates of mass transfer from the spheres. For each sphere spacing, except at high Reynolds and Peclet numbers the overall Sherwood numbers for the spheres generally do not change much when the mesh spacing in Z changes from $|Zs/10|$ to $|Zs/20|$. At high Reynolds and

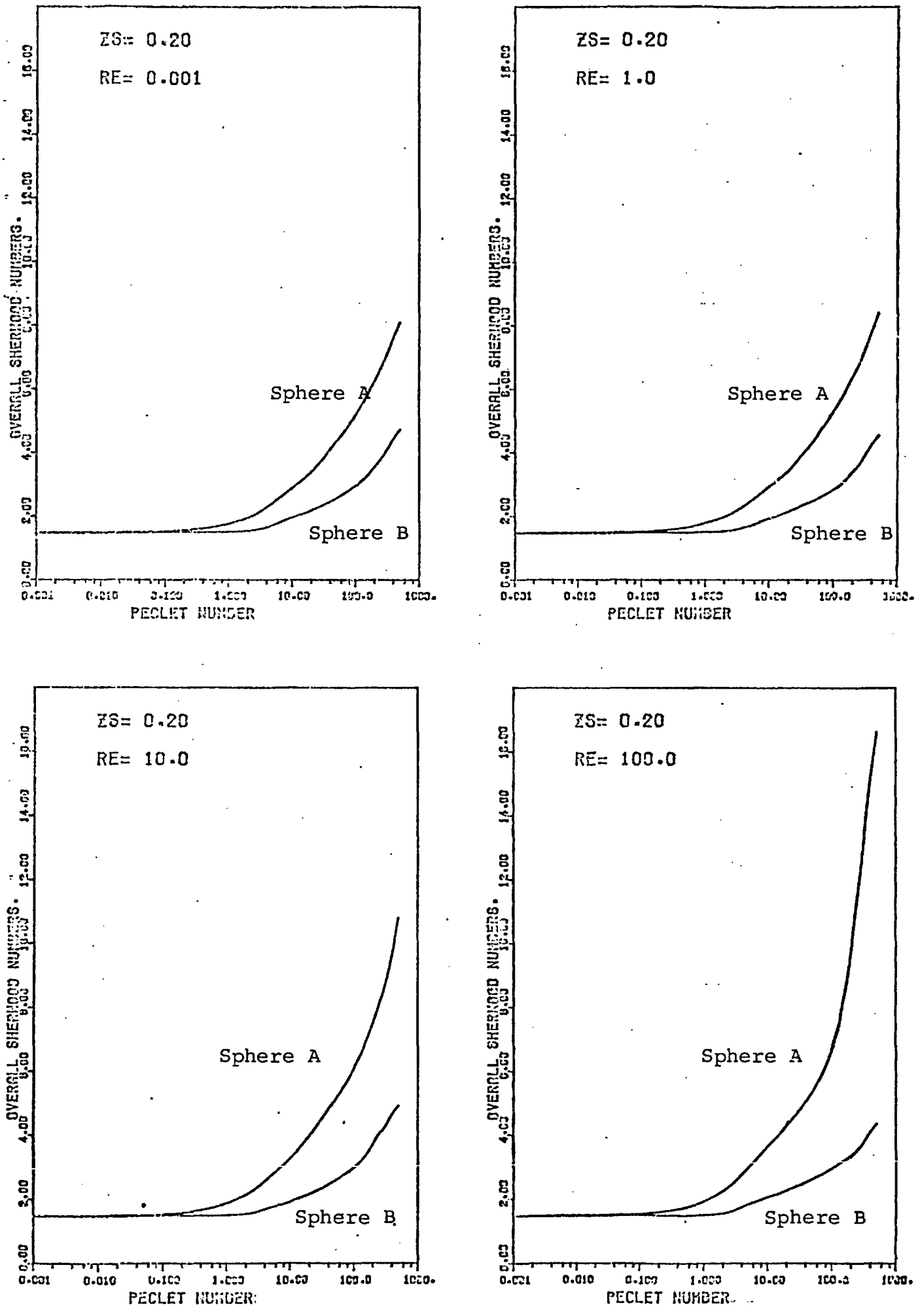

Figure(6-5-1). Overall Sherwood number as a function of Peclet number.

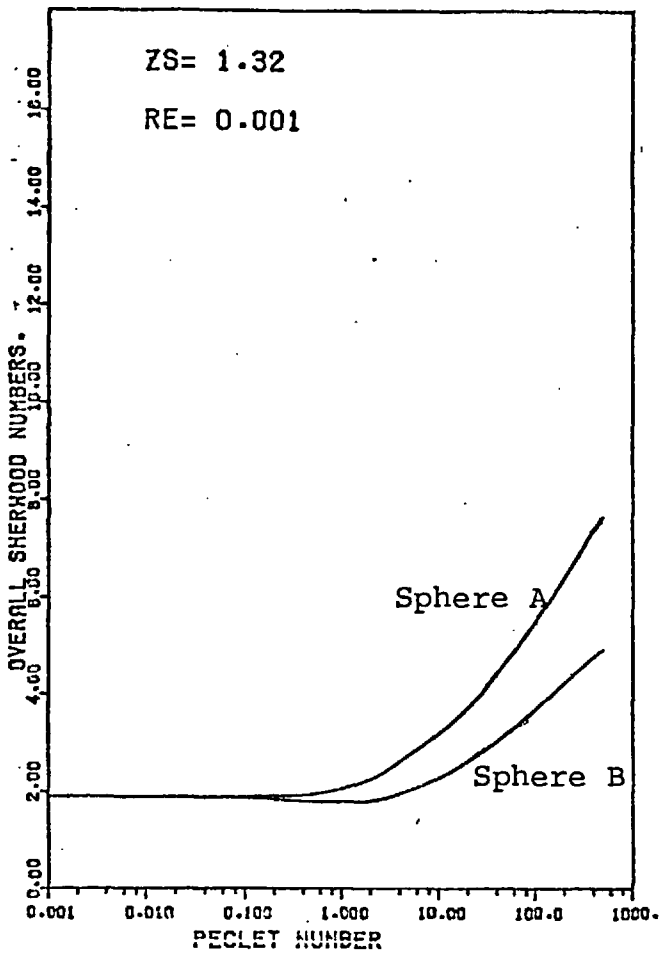

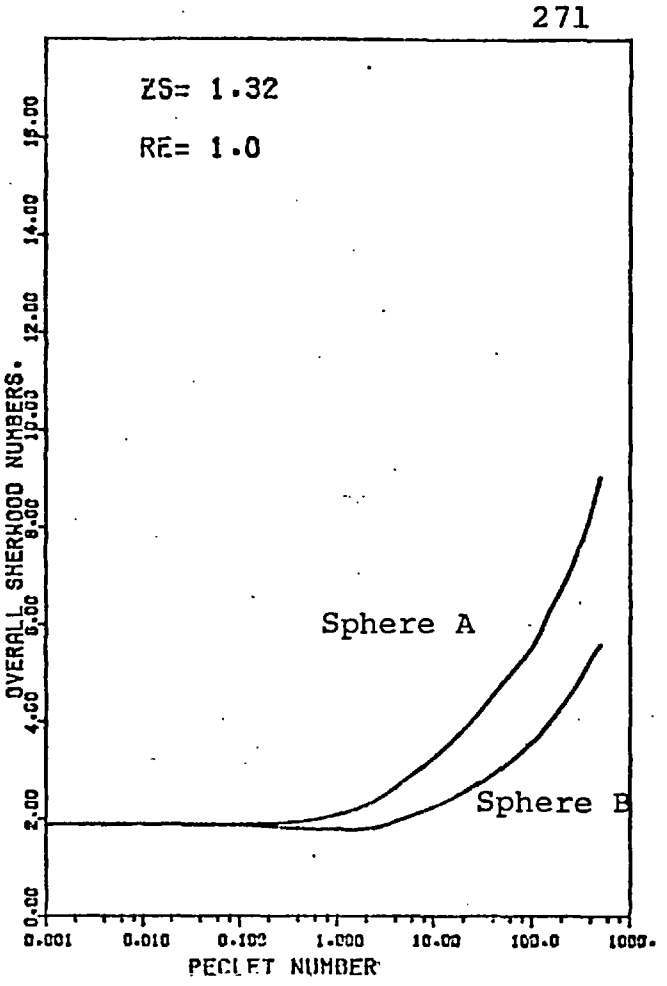

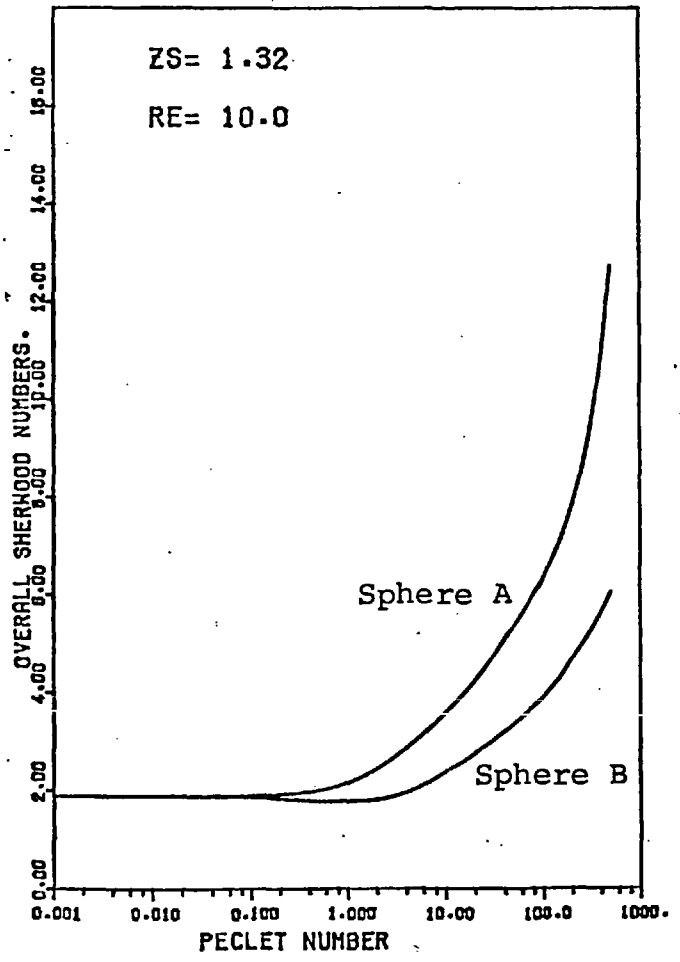

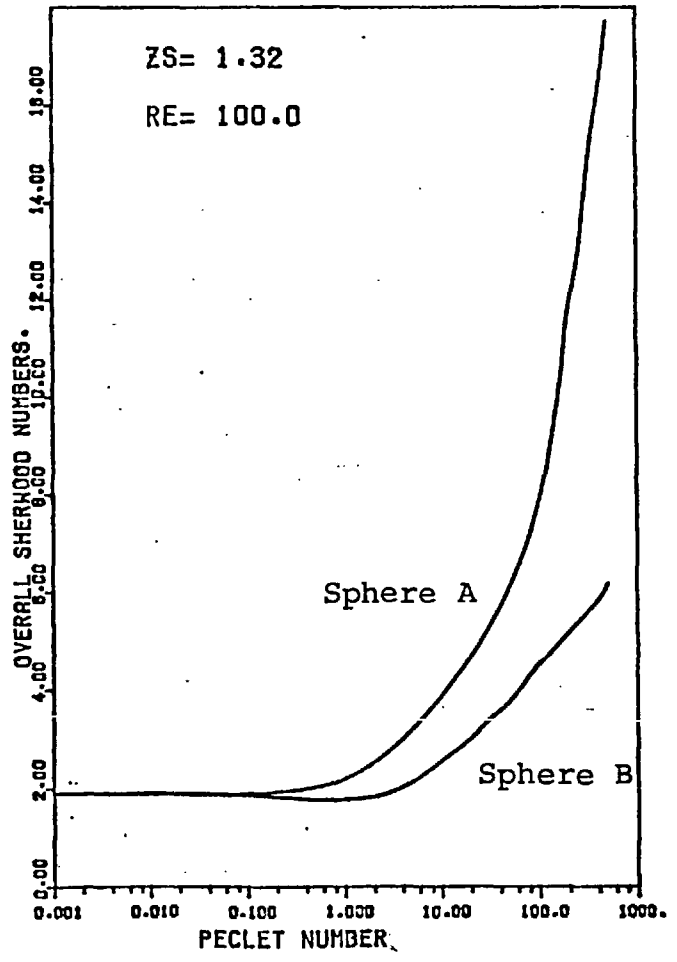

Figure(6-5-2) Overall Sherwood number as a function of Peclet number.

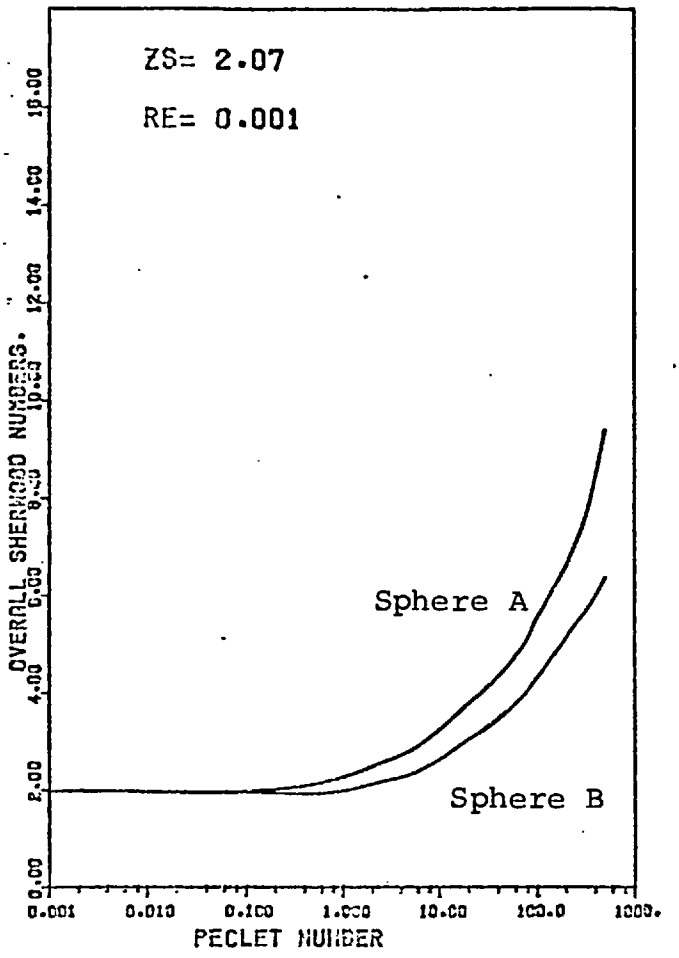

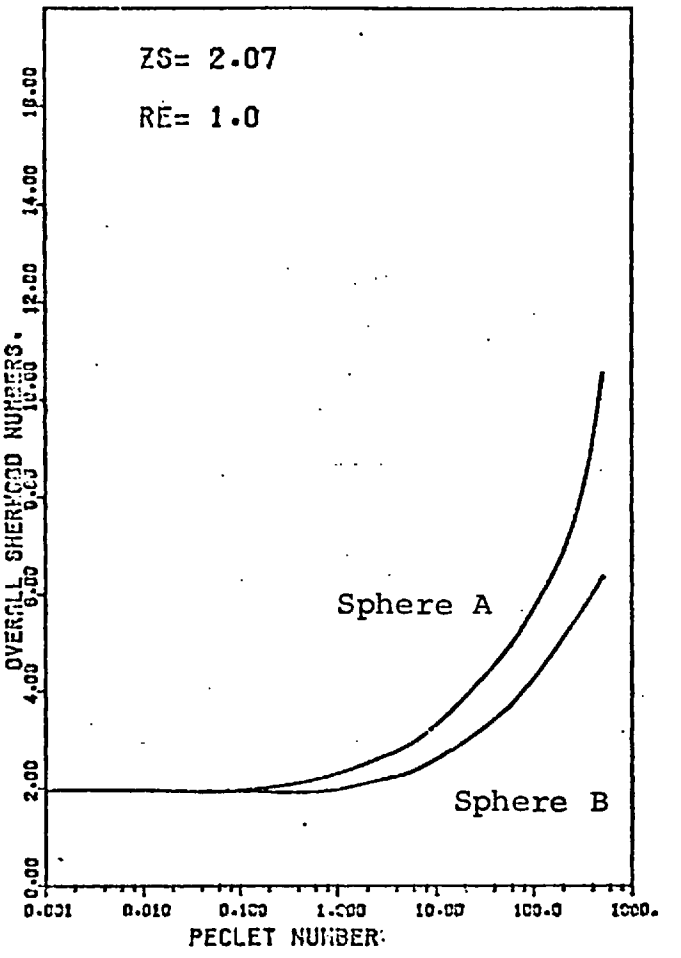

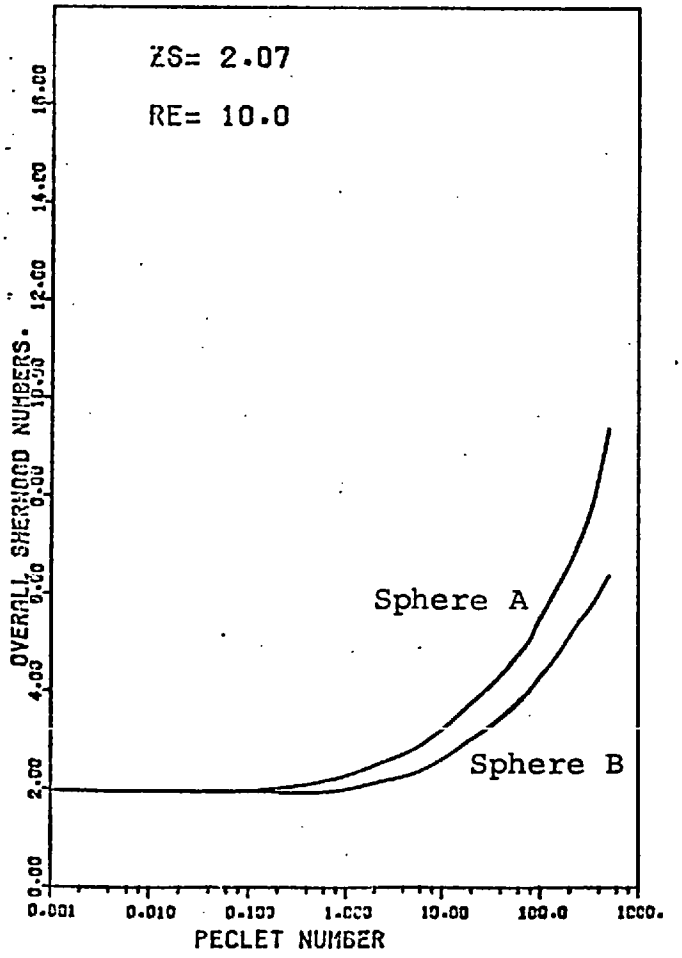

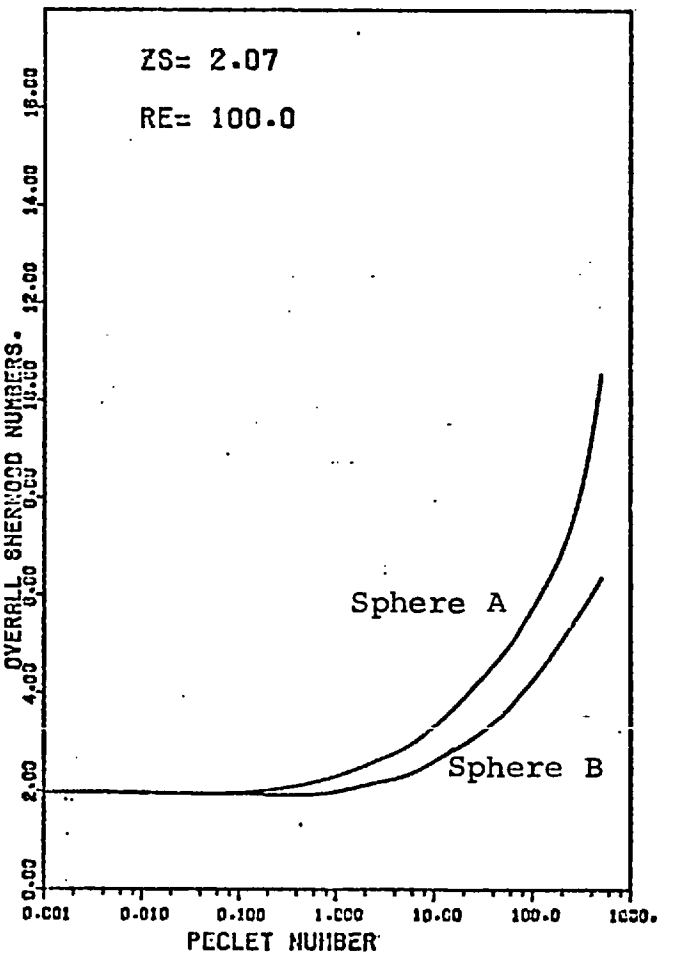

Figure(6-5-3). Overall Sherwood number as a function of Peclet number.

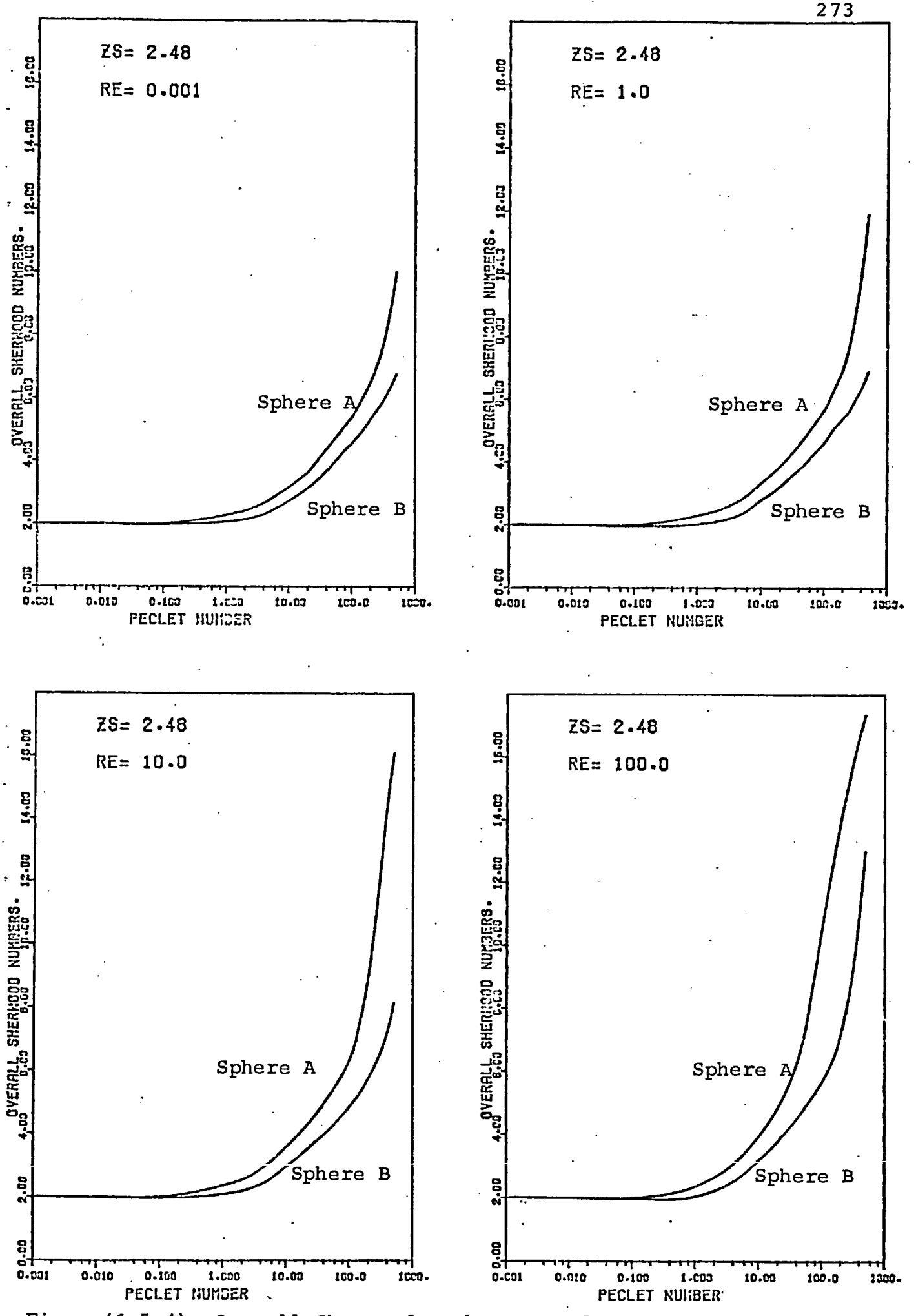

Figure(6-5-4). Overall Sherwood number as a function of Peclet number.

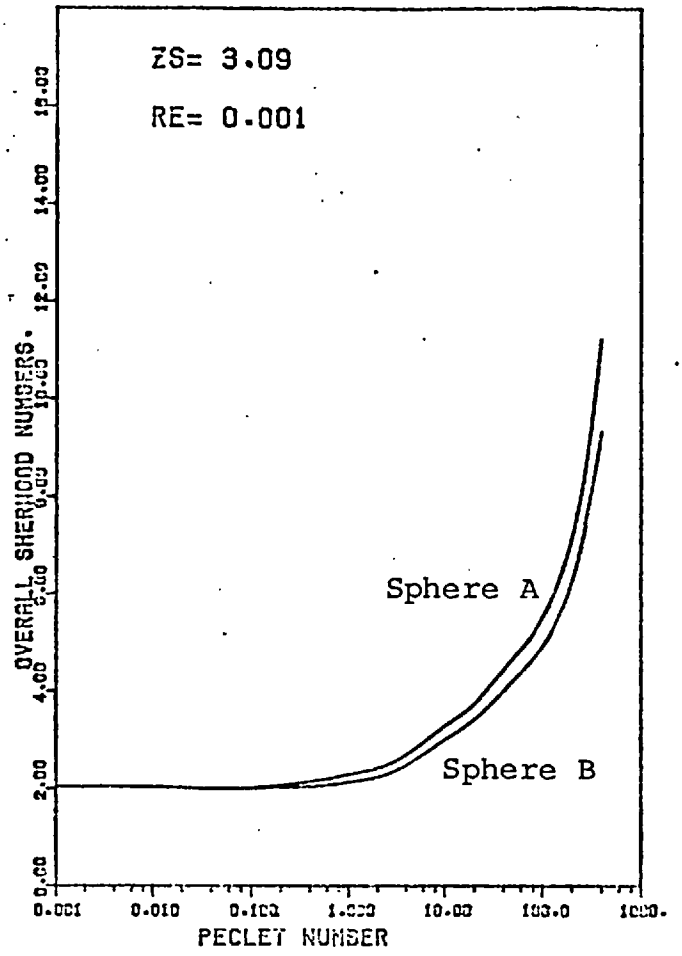

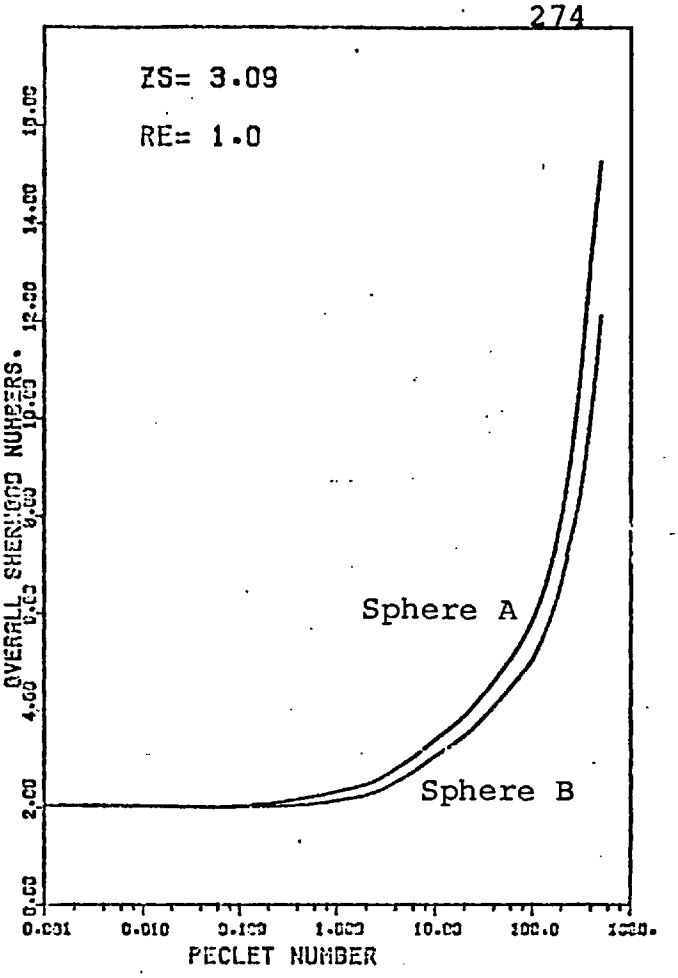

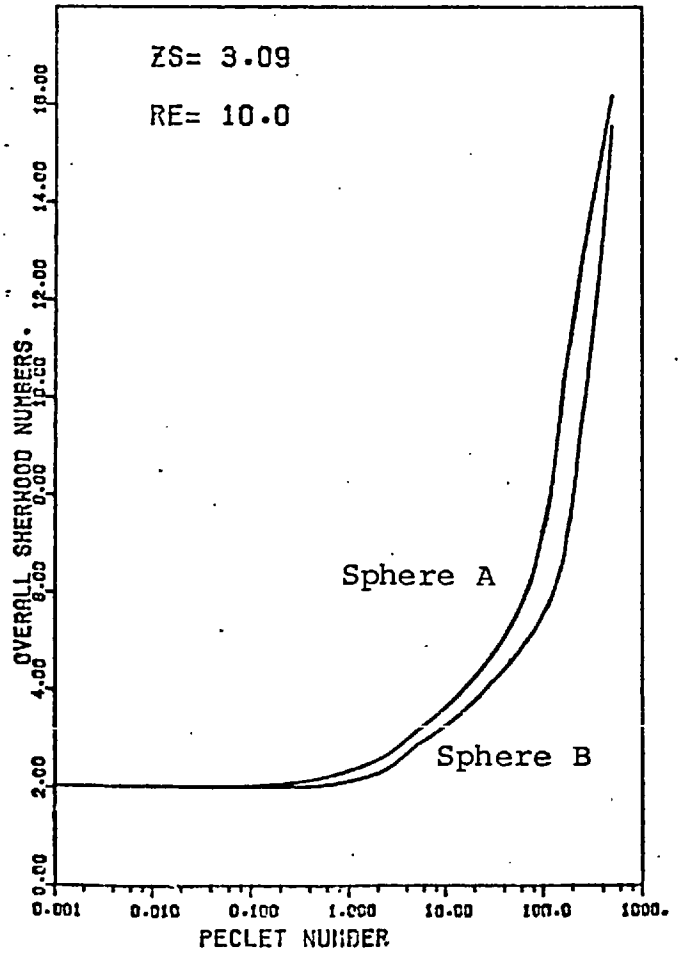

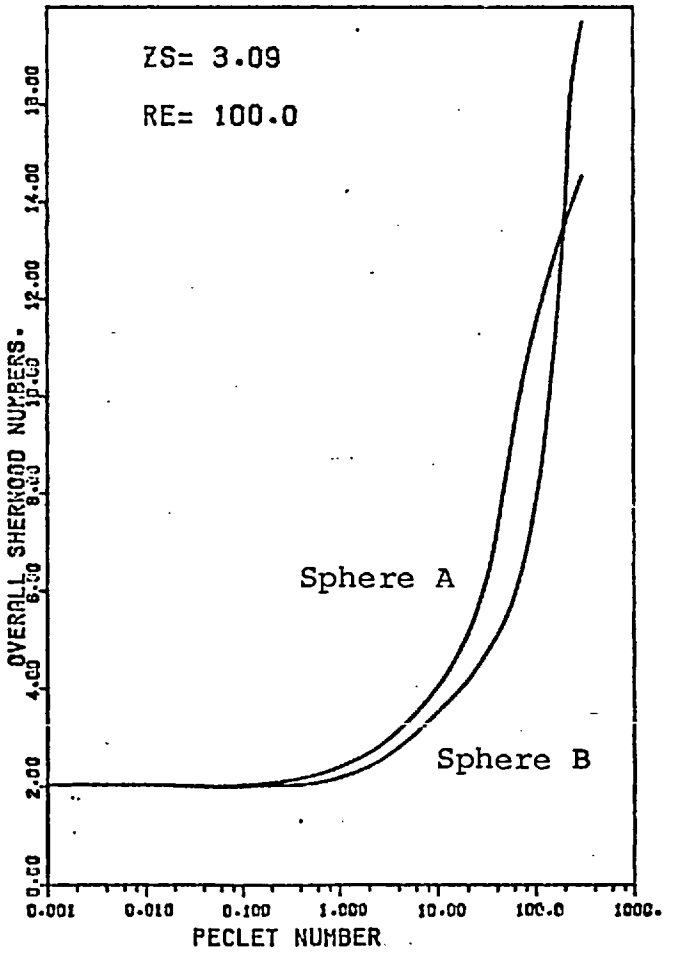

Figure(6-5-5). Overall Sherwood number as a function of Peclet number.

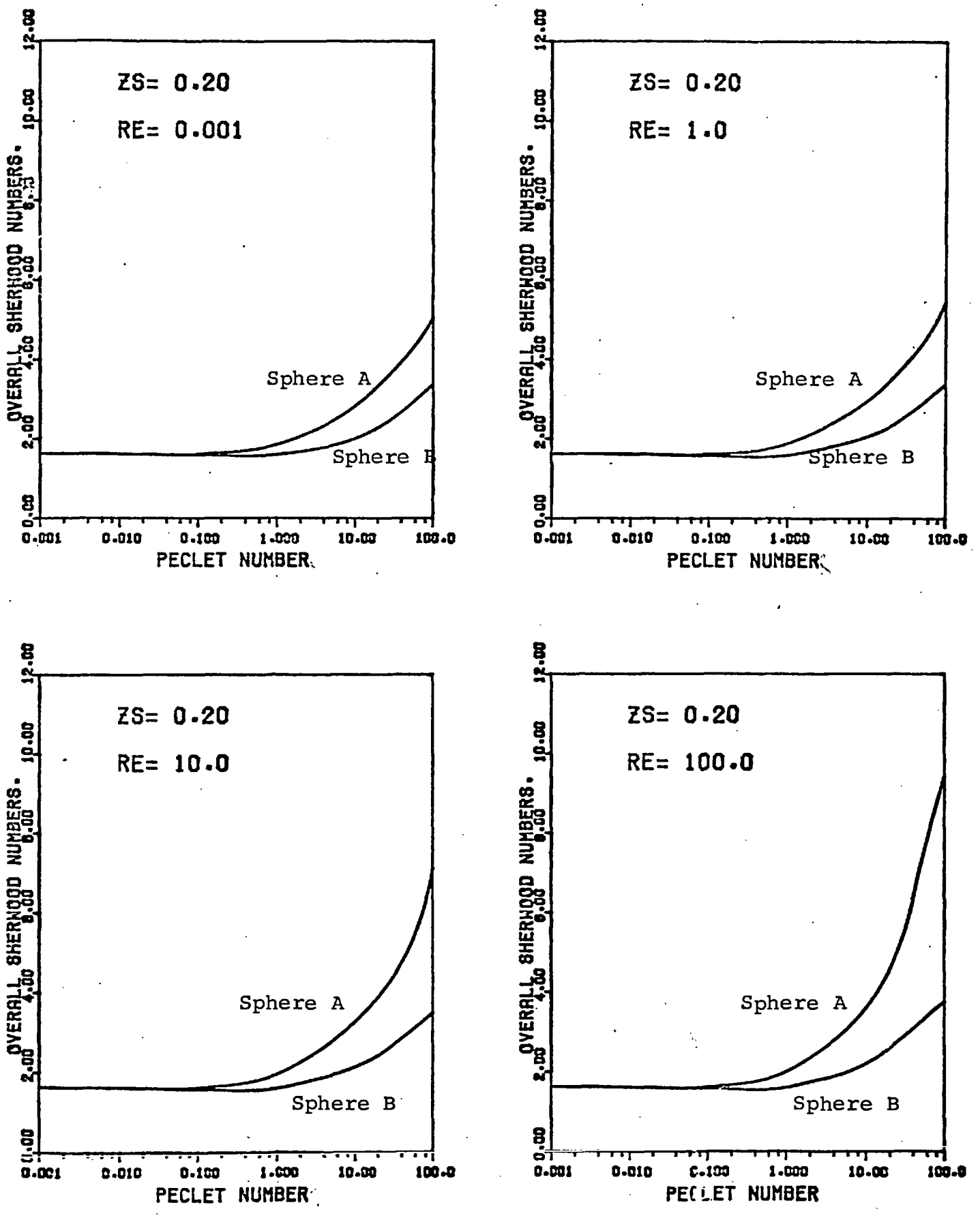

Figure(6-5-6) Overall Sherwood number as a function of Peclet number.

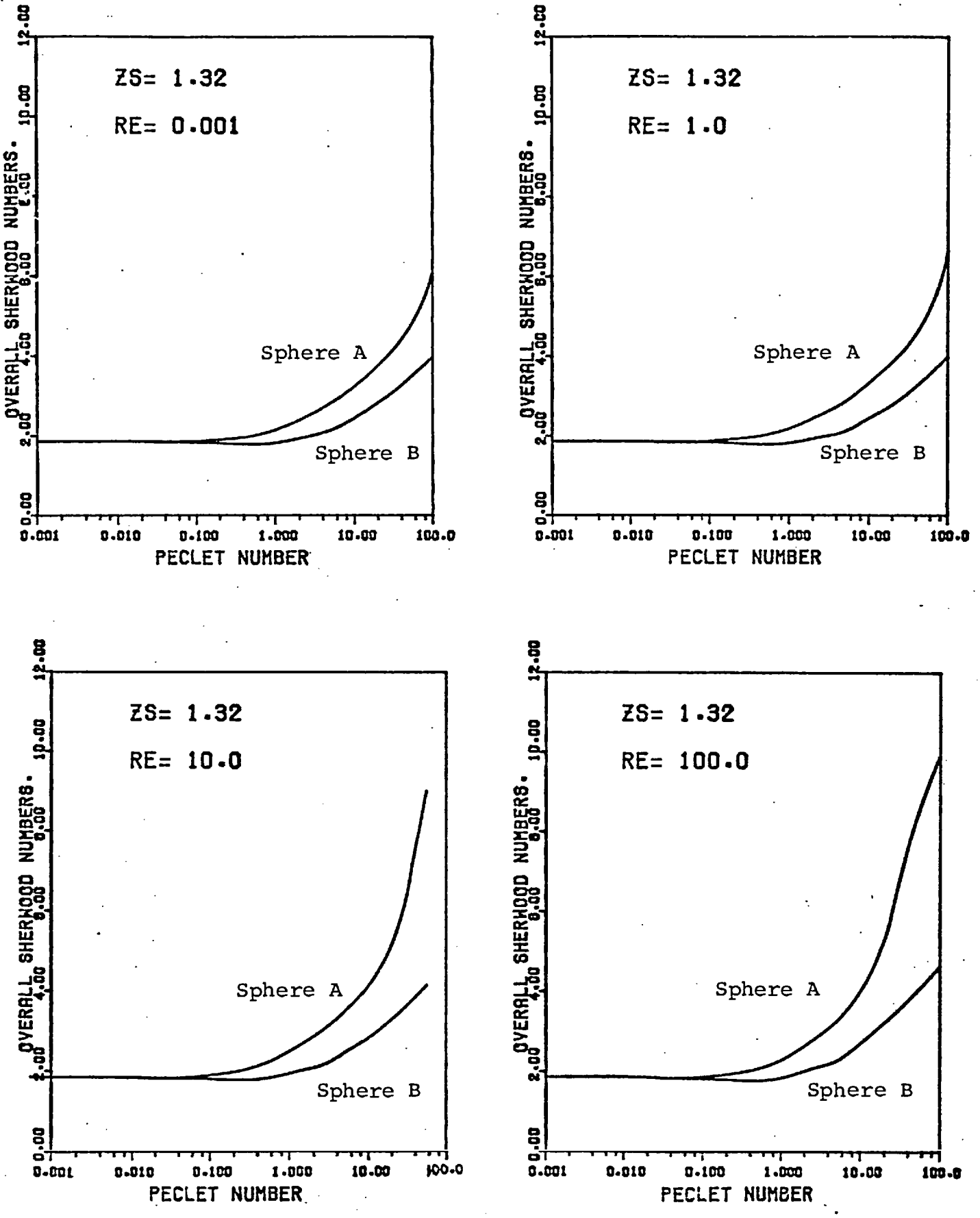

Figure(6-5-7). Overall Sherwood number as a function of Peclet number.

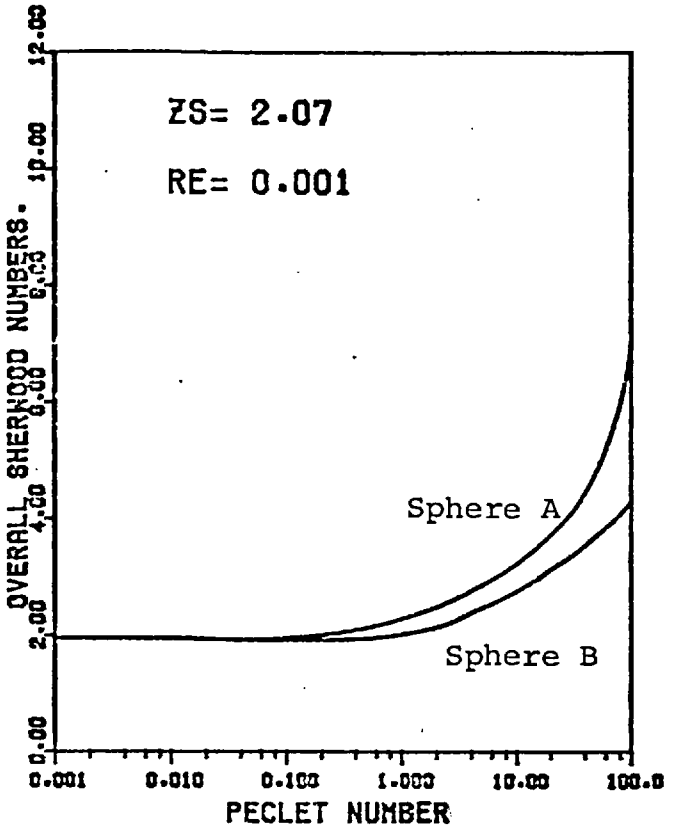

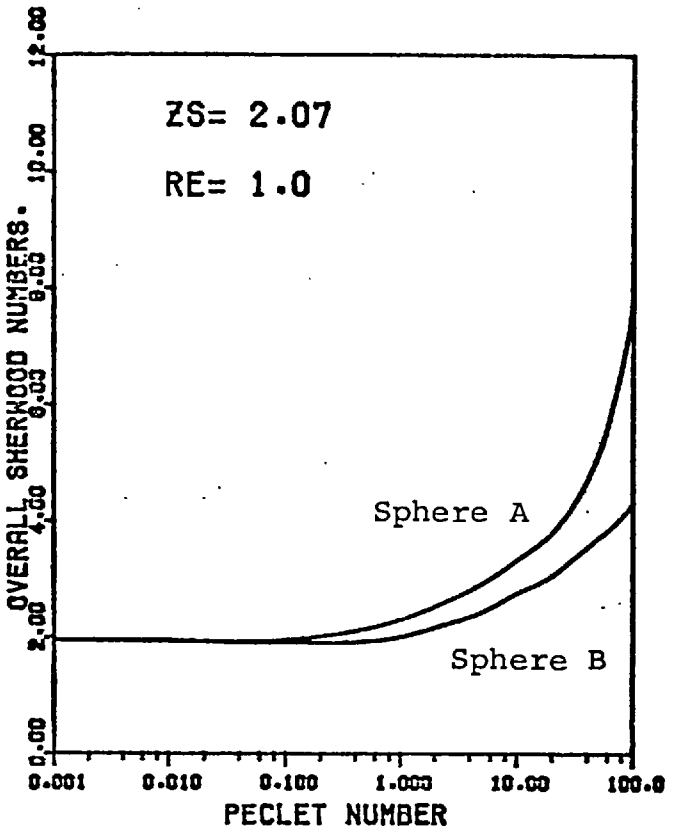

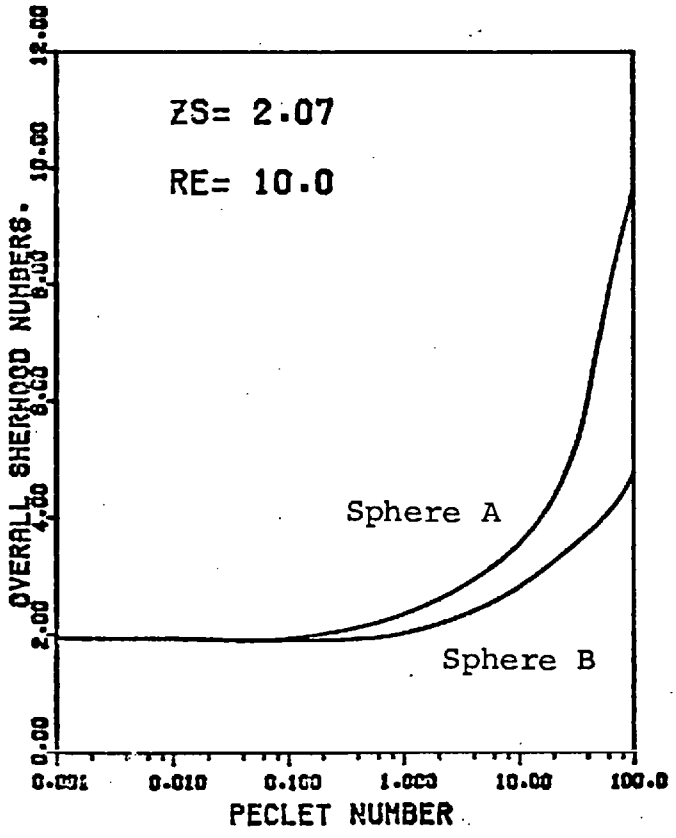

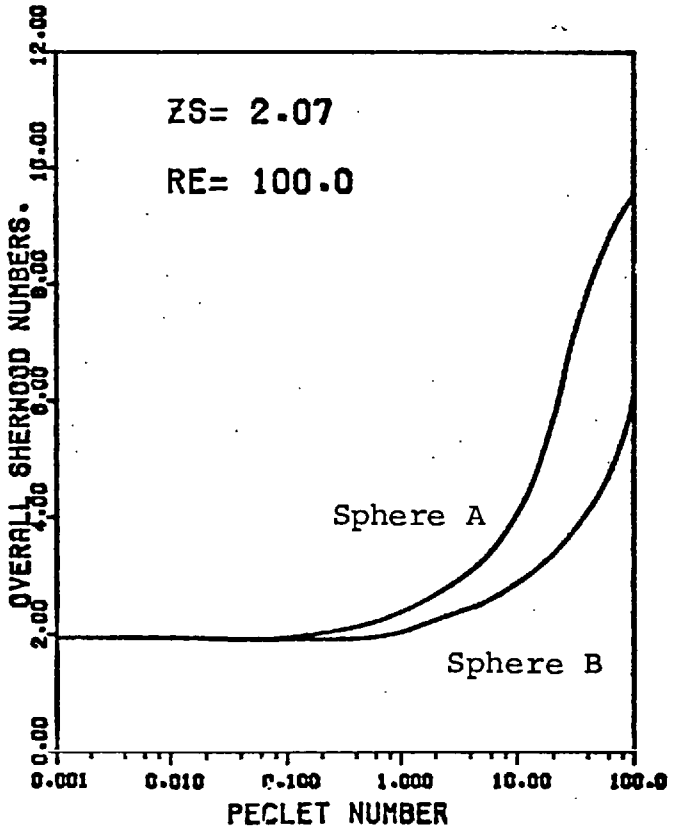

Figure(6-4-8). Overall Sherwood number as a function of Peclet number.

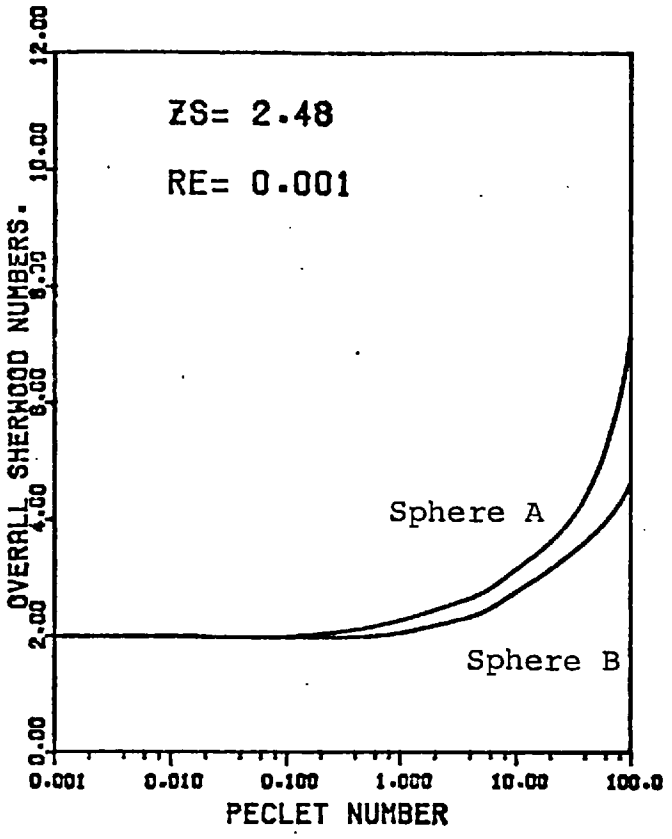

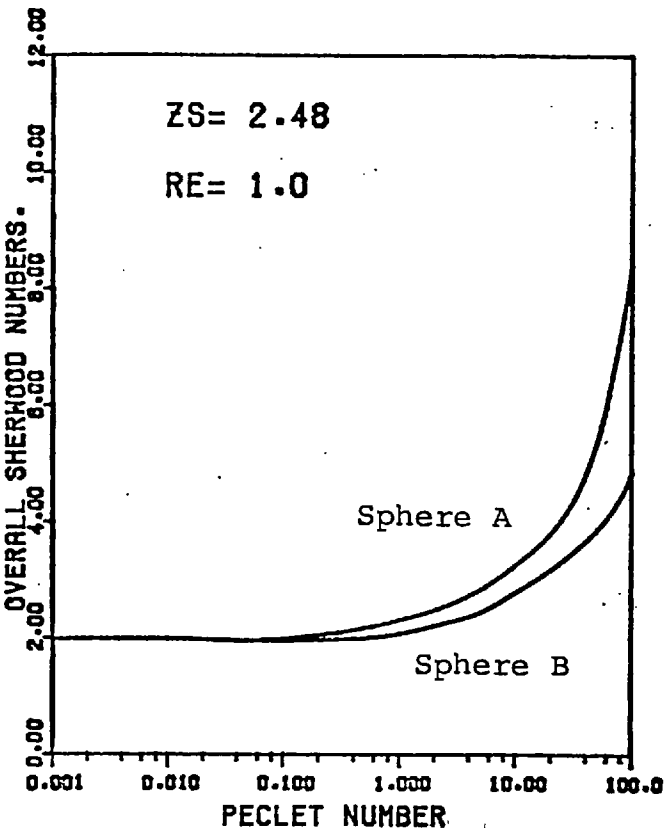

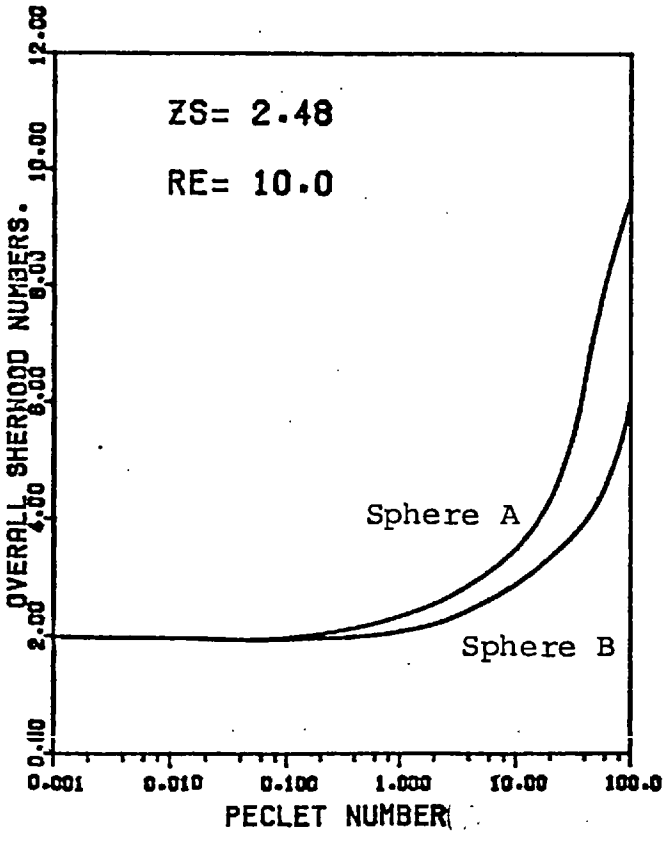

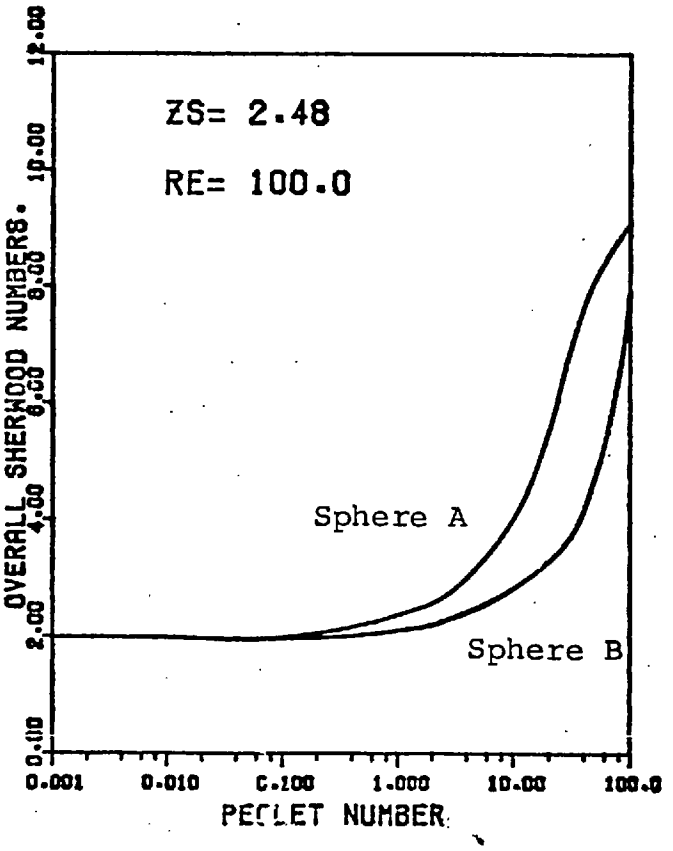

Figure(6-5-9). Overall Sherwood number as a function of Peclet number.

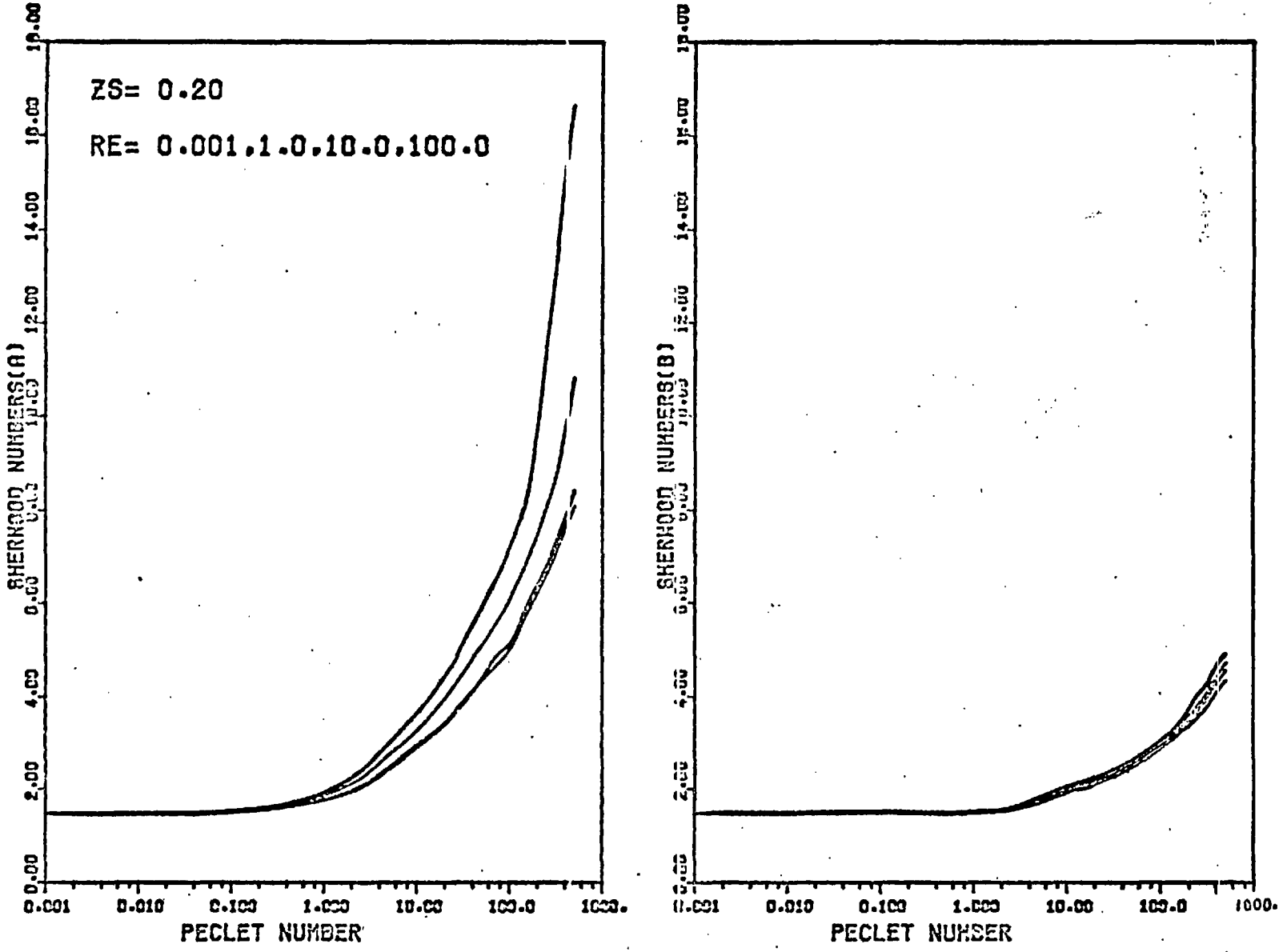

Figure(6-5-10). Overall Sherwood number as a function of Peclet number with Reynolds number as a parameter.

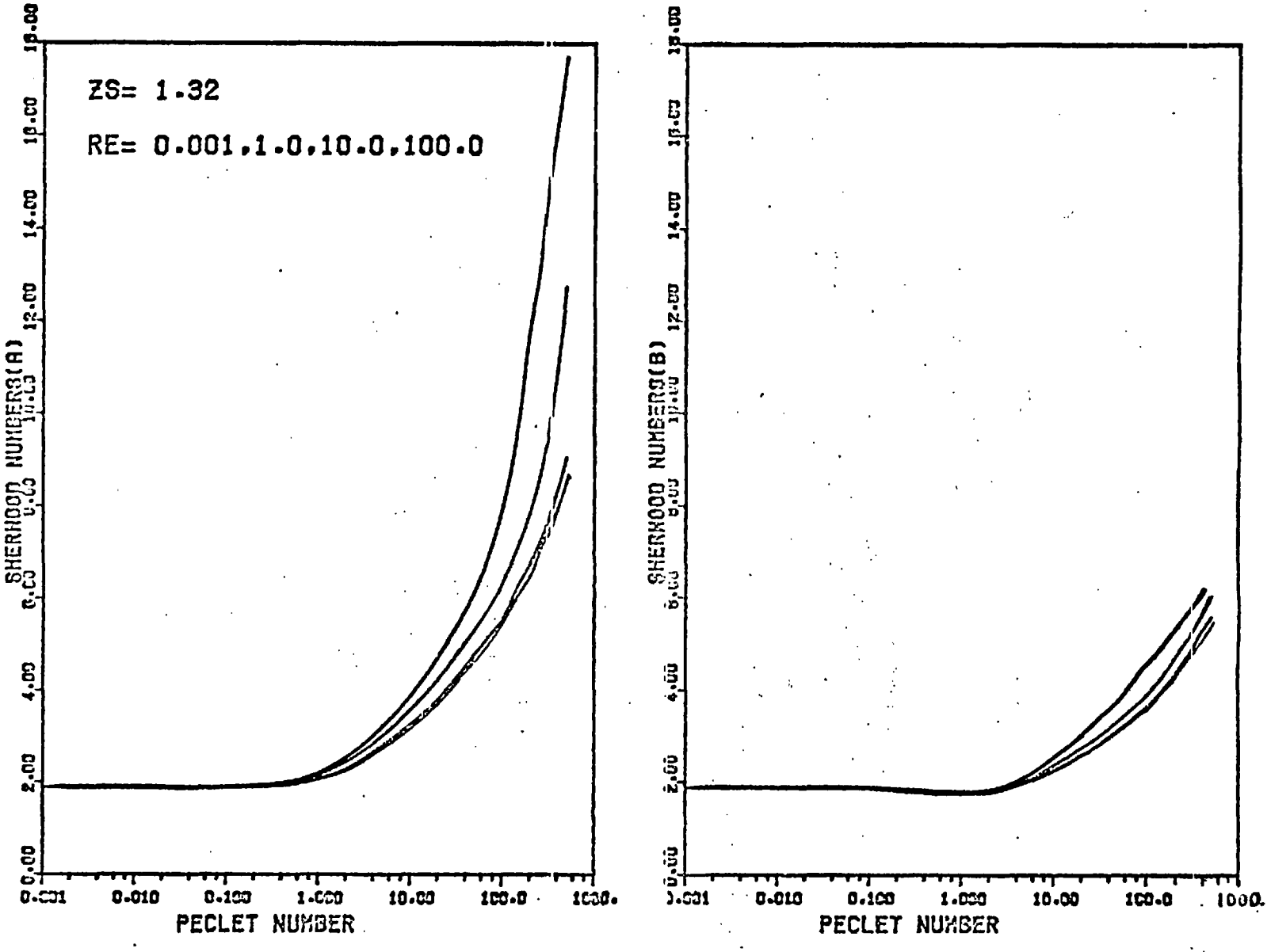

Figure(6-5-11). Overall Sherwood number as a function of Peclet number with Reynolds number as a parameter.

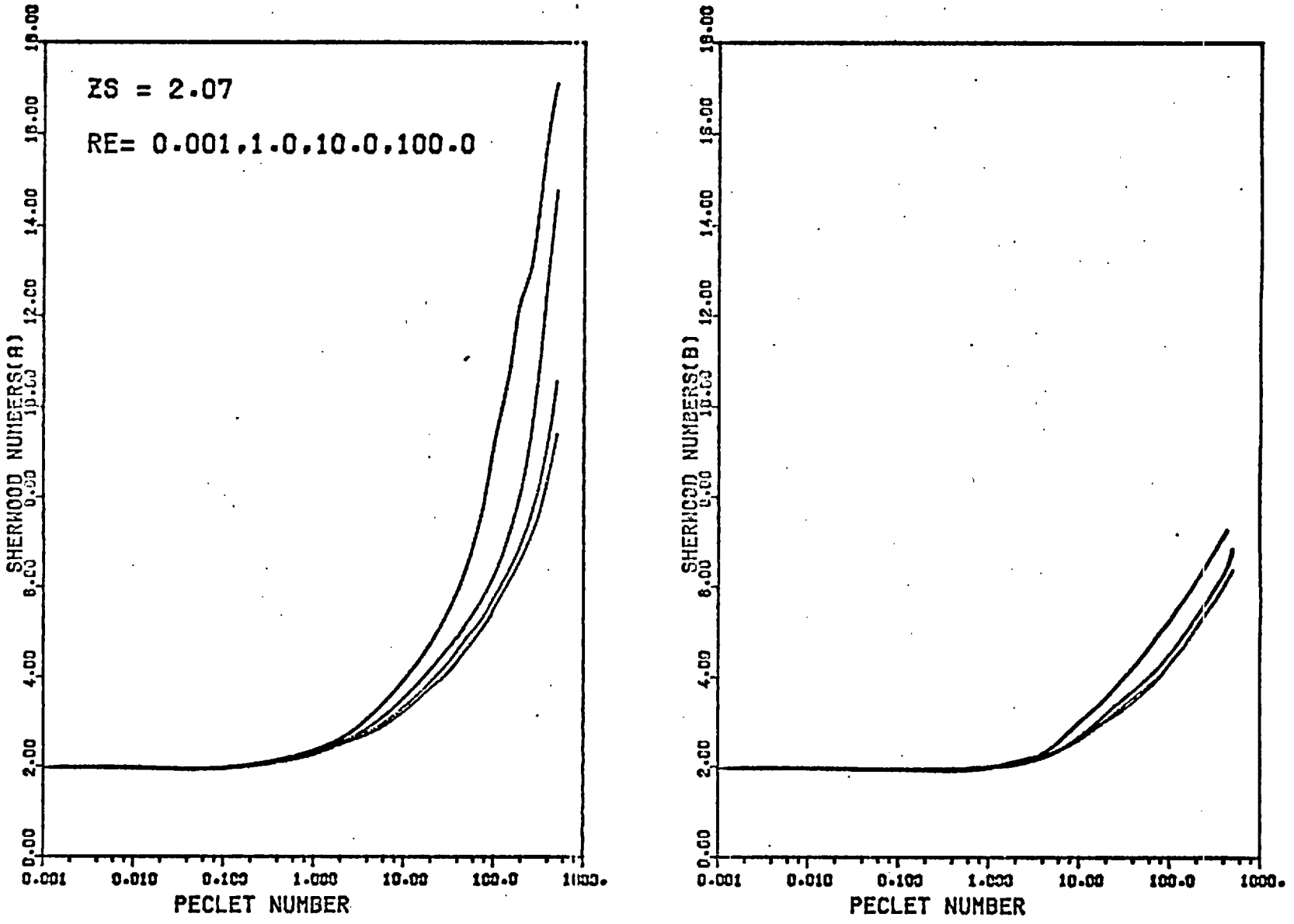

Figure(6-5-12). Overall Sherwood number as a function of Peclet number with Reynolds number as a parameter.

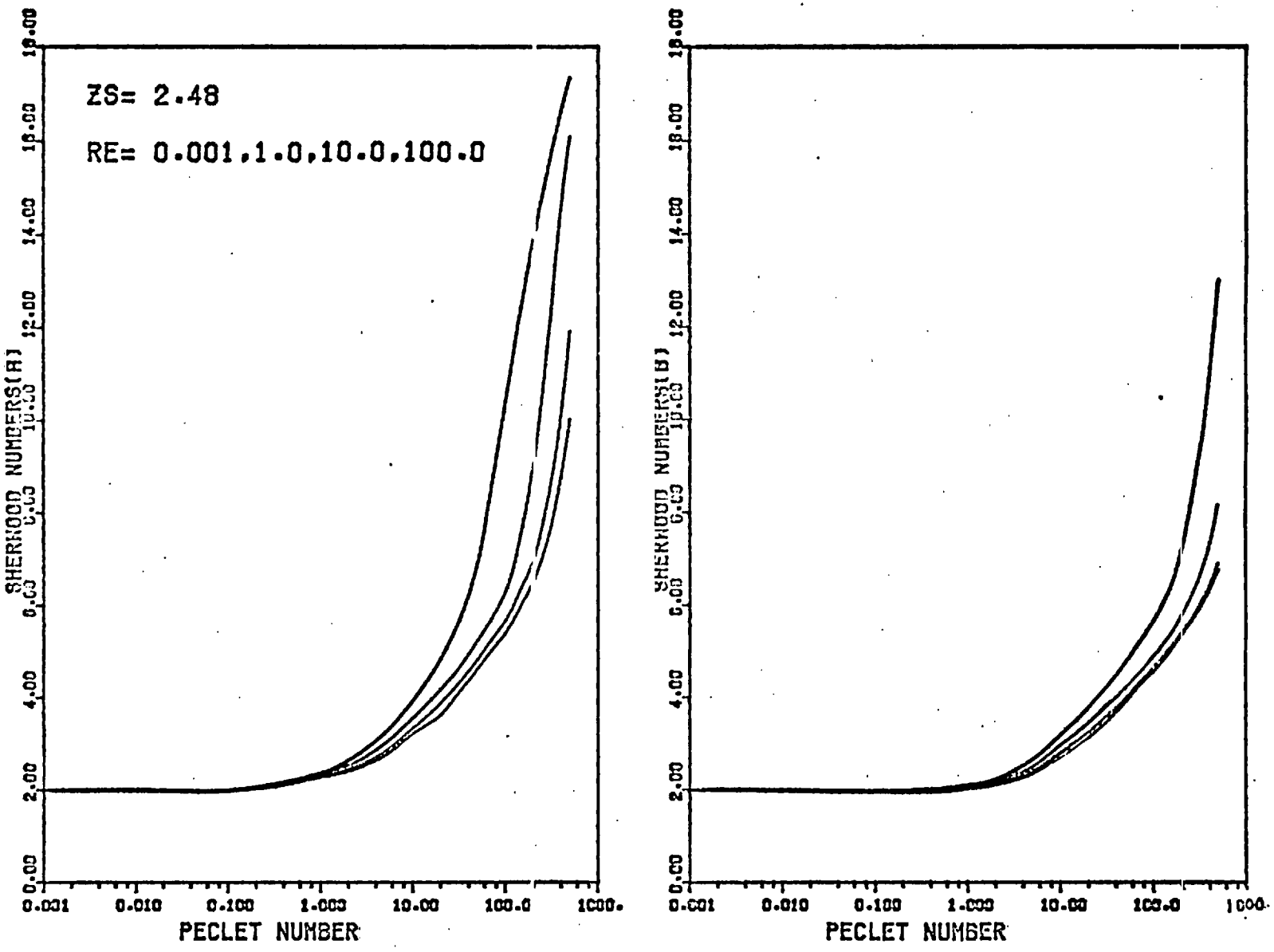

Figure(6-5-13). Overall Sherwood number as a function of Peclet number with Reynolds number as a parameter.

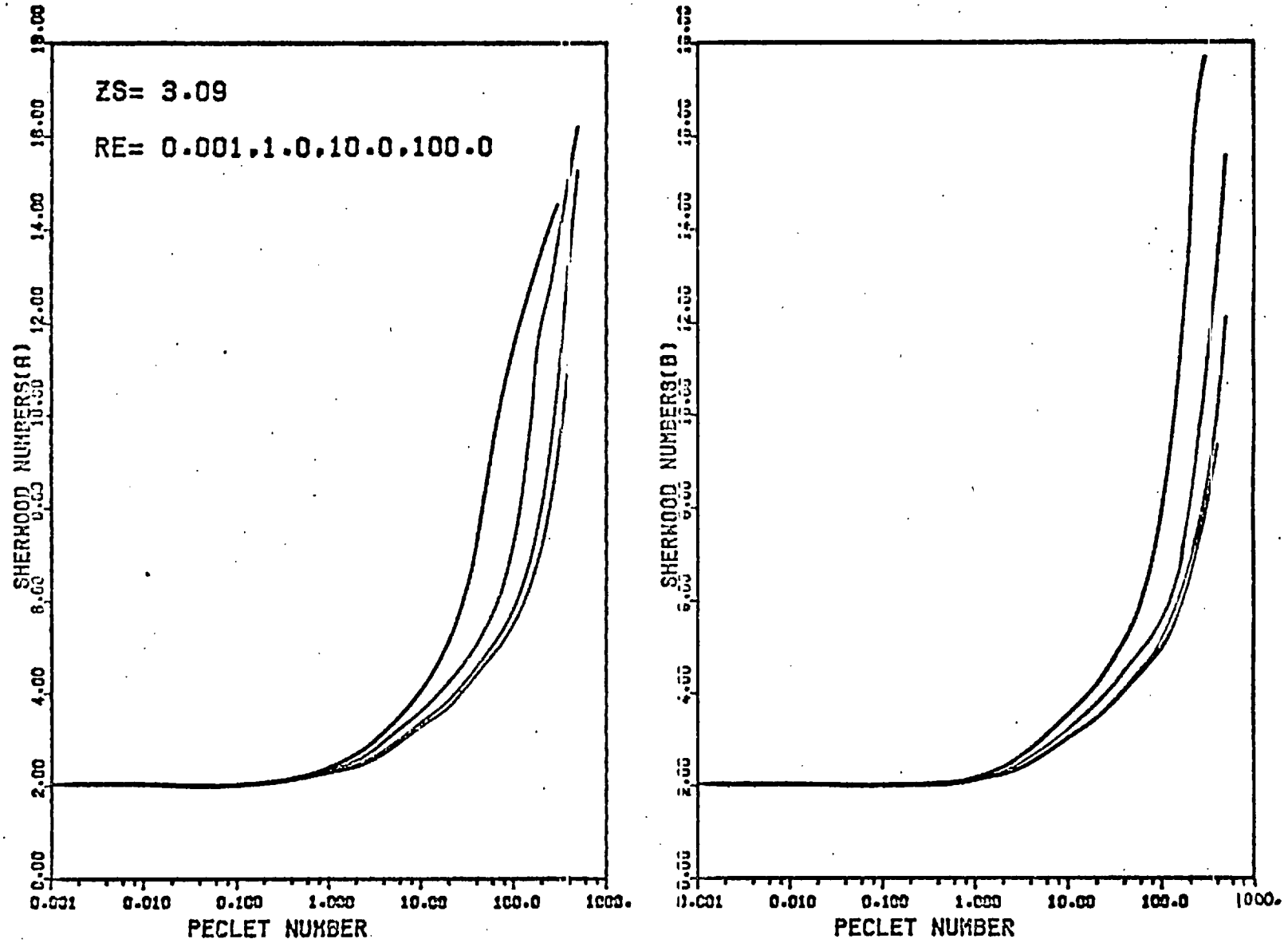

Figure(6-5-14). Overall Sherwood number as a function of Peclet number with Reynolds number as a parameter.

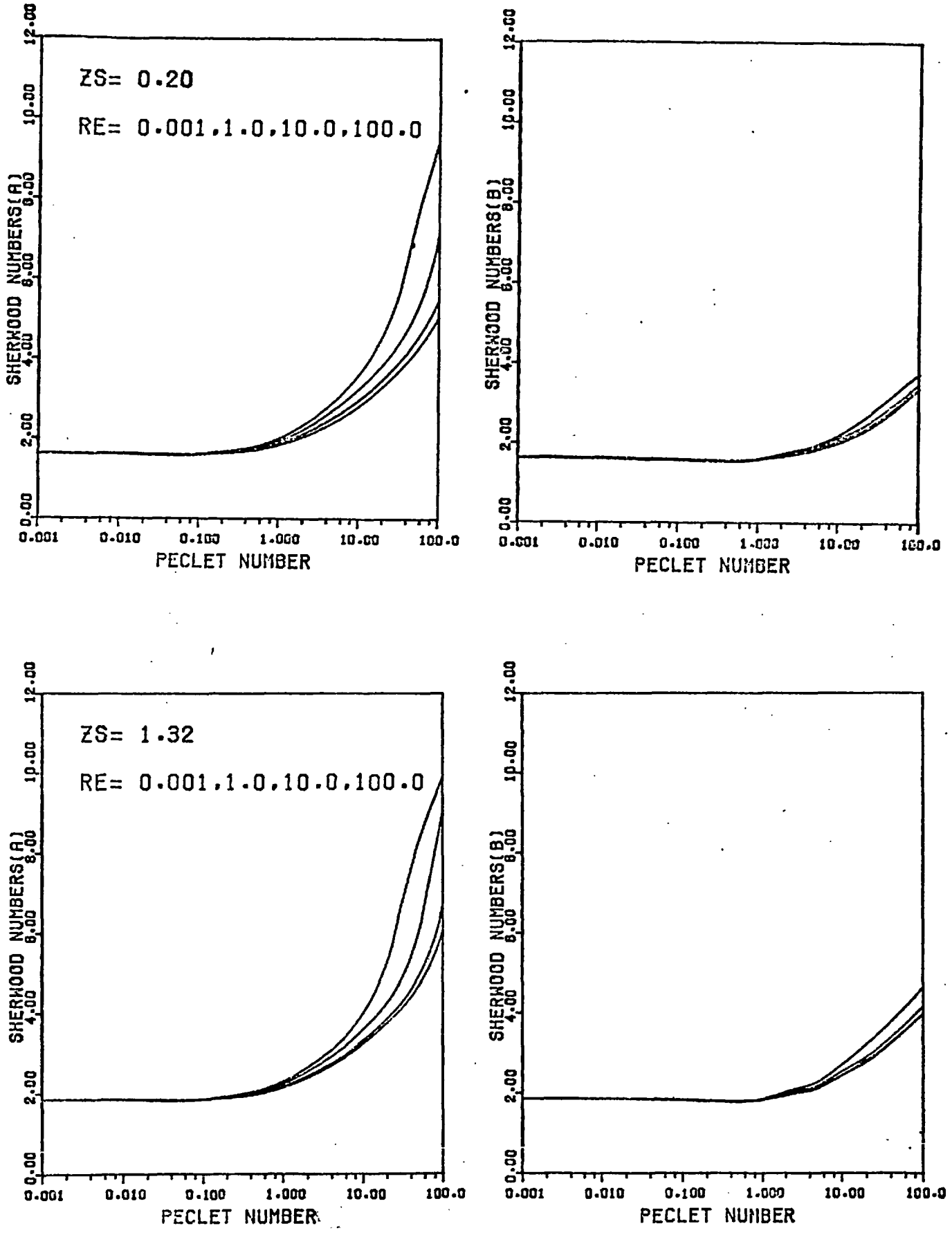

Figure(6-5-15). Overall Sherwood number as a function of Peclet number with Reynolds number as a parameter.

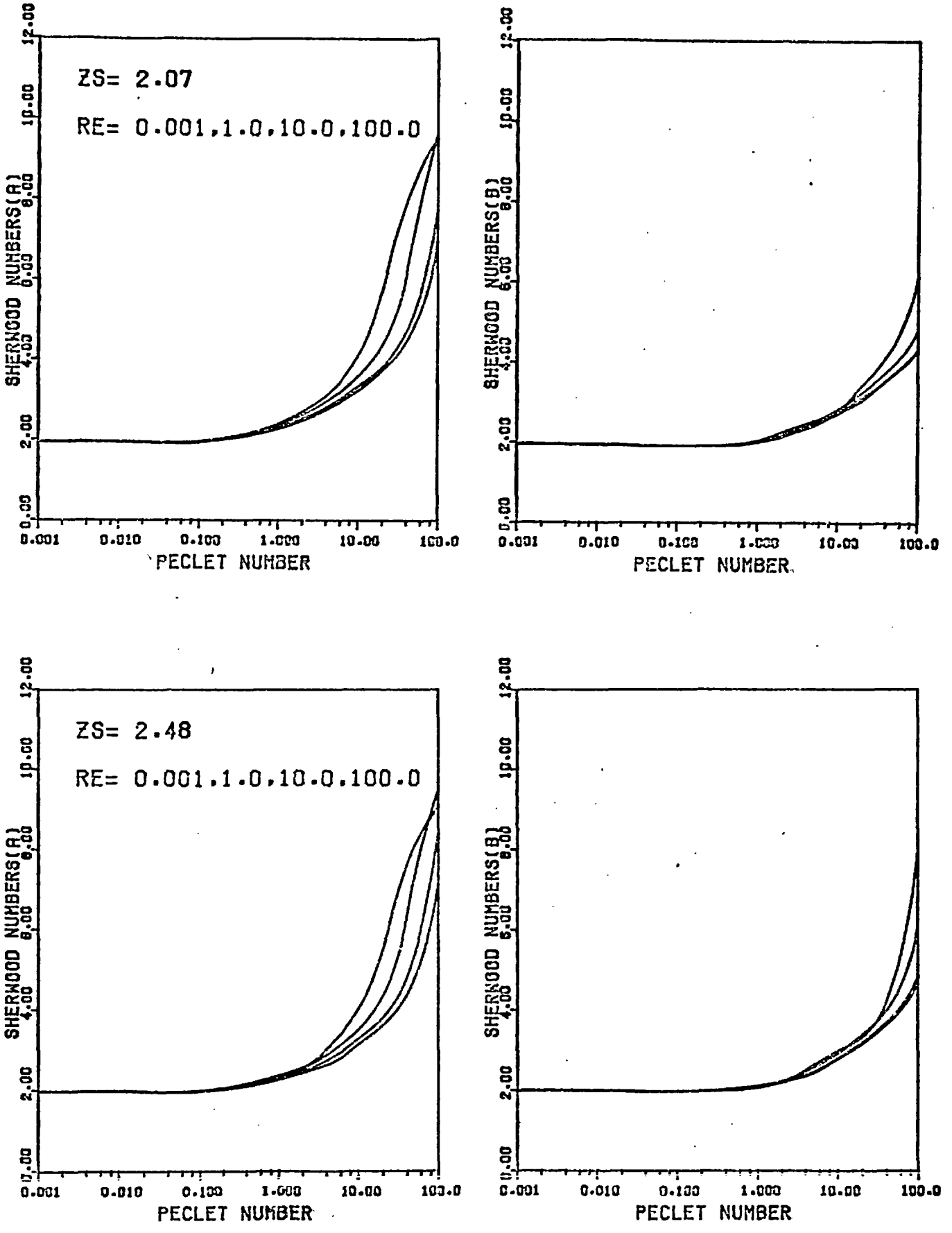

Figure(6-5-16). Overall Sherwood number as a function of Peclet number with Reynolds number as a parameter.

Peclet numbers, the overall Sherwood numbers for sphere A are influenced by the combined effect of the large Z-grid-line spacings and the thin diffusional boundary layer over part of the upstream surface of sphere A (this has been discussed in the previous section). A further consequence of this combined effect is that the overall Sherwood numbers for sphere A increase more slowly than those for sphere B with increasing Peclet number, and at high Peclet numbers the overall Sherwood numbers for sphere A eventually become smaller than those for sphere B. It is important to note that this anomalous behaviour is generally not obvious except for the two largest sphere spacings considered in this study: Zs = 2.48 and Zs = 3.09.

For each sphere spacing, the influence of Reynolds number upon the overall rates of mass transfer from the spheres can be seen directly from Figures(6-5-10) to (6-5-16). For sphere A, the overall Sherwood numbers are independent of Reynolds number over the range of Peclet numbers from 0.001 to 0.1; while for sphere B, the overall Sherwood numbers are independent of Reynolds number over the larger range of Peclet numbers from 0.001 to 1.0. The range of Peclet numbers over which the overall Sherwood numbers for sphere B are independent of Reynolds number become larger when the sphere spacing becomes smaller. On the other hand, at higher Peclet numbers the overall Sherwood numbers for the two spheres increase with increasing Reynolds number although the increase is always larger for sphere A than for sphere B. Hence, when both the Reynolds and Peclet numbers are large the difference between the overall rates of mass transfer from the two spheres is also large.

From Figures(6-5-1) to (6-5-16) and Tables(6-5-1) to (

6-5-10), it can be seen that the overall rates of mass transfer from the spheres increase with increasing sphere spacing, however, the increase is always larger for sphere B than for sphere A. The reason for this larger increase in the overall Sherwood numbers for sphere B than for sphere A is that increases in the distances between the spheres result in the lower concentration of the diffusing material in the fluid in the inner region between the spheres and thus in the larger rates of mass transfer from the front surface of sphere B. Except when the sphere spacing changes from Zs = 0.20 to Zs = 1.32, the rates of mass transfer from the rear surface of sphere A increase only slightly with increasing distance between the two spheres. As a result, when the sphere spacing is increased, the difference between the overall rates of mass transfer from the spheres becomes smaller.

It is important to note that for each sphere spacing and for all Reynolds numbers considered in this study, the overall Sherwood numbers for sphere A in the Peclet number range of 0.001 to 0.1 and the overall Sherwood numbers for sphere B in the Peclet number range of 0.001 to 1.0 are either less than or slightly larger than the limiting value of 2.0 obtained for a single isolated sphere with molecular diffusion alone to an infinite medium. These values also increase with increasing sphere spacing.

CHAPTER 7. CONCLUSIONS

The results of the present study are summarized as follows:

1. Numerical solutions of the Navier-Stokes and diffusion equations have been obtained for a system of two equally sized spheres with a steady, isothermal, incompressible, Newtonian fluid flowing parallel to their line of centres.

2. The bi-spherical coordinate system was used in the present study because of the ease with which it may be used to describe the locations of the two spheres and the boundary conditions of the system of governing equations. Unfortunately, it also introduced unequal distributions of grid lines in both the Z- and θ-directions in the flow region.

In order to remove the unequal increments along the surfaces of the two spheres which arose from using the conventional scheme of distributing the grid lines for the θ-direction according to a constant increment in the value of θ, a new scheme of distributing the grid lines according to a constant increment in the angle η was adopted. This new scheme had the advantages of distributing the grid lines for the θ-direction more evenly in the flow region, particularly when the sphere spacings were small, and of allowing many important quantities for the two-sphere fluid dynamic and mass transfer problems to be studied and interpreted in the same way as those for a single isolated sphere.

3. An explicit extrapolated Gauss-Seidel method with under-relaxation was used to obtain solutions of the finite-

difference forms of the Navier-Stokes and diffusion equations. Suitable values of the relaxation factors were supplied by trial-and-error in order to ensure that at each mesh point the solution converged with the desired accuracy. Computational times were reduced by using results obtained for immediately lower Reynolds and Peclet numbers as initial values for the iterative solutions of the Navier-Stokes and diffusion equations, respectively.

4. In this study, five different sphere spacings: Zs = 0.20, 1.32, 2.07, 2.48, and 3.09, corresponding to two equally sized spheres having a centre-to-centre distance of 2.0402, 4.0106, 8.0510, 12.025, and 22.022 radii, respectively, were considered. The Navier-Stokes equations were solved for the stream function and vorticity distributions in the flow region for a series of Reynolds numbers ranging from 0.001 to 500; while the diffusion equation was solved separately for the concentration distributions in the same flow region for four selected Reynolds numbers of 0.001, 1.0, 10.0, and 100.0, each for a series of Peclet numbers from 0.001 to 500. The resultant distributions of vorticity and stream function were used to calculate the surface pressures, angles of flow separation, and drag coefficients for the spheres. Similarly, the resultant distributions of concentration were used to calculate the local and overall Sherwood numbers.

5. The vorticity distributions obtained for flow around two equally sized spheres were found to be dependent on the Reynolds number and on the sphere spacing. For each sphere spacing, the vorticity distributions at Reynolds numbers less than unity were symmetrical and those at higher Reynolds numbers

were unsymmetrical about a plane through the mid-point of the line of centres normal to the direction of flow. At high Reynolds numbers, a fluid dynamic boundary layer was observed to have developed at the upstream surfaces of the spheres, however, its development at the upstream surface of the downstream sphere, sphere B, became less pronounced when the distance between the spheres was decreased.

It was also observed that for each of the five sphere spacings considered, the distributions of vorticity around the two spheres were always at least slightly different from those around a single isolated sphere and that the difference became larger as the distance between the spheres decreased. This showed the effect of particle-to-particle interaction between the spheres upon the flow around the spheres. The extent of the interparticle interaction increased with decreasing sphere spacing.

6. The stream function distributions around the two spheres were also found to be dependent on the Reynolds number and on the sphere spacing. For each sphere spacing, the distributions of stream function at low Reynolds numbers of 0.001 to 0.1 were symmetrical while those at higher Reynolds numbers were unsymmetrical about a plane through the mid-point of the line of centres normal to the direction of flow. The main influence of sphere spacing upon the stream function distributions was shown particularly in the inner region between the spheres. As the sphere spacing was decreased, the streamlines with small values of the stream function moved further away from the line of centres of the spheres. For the

two smallest sphere spacings: Zs = 0.20 and 1.32, at high Reynolds numbers nearly the whole inner region between the spheres became a wake region.

7. The distributions of surface vorticity at the front surface of the upstream sphere, sphere A, and at the rear surface of the downstream sphere, sphere B, were found to be almost independent of sphere spacing whereas those at the rear surface of sphere A and at the front surface of sphere B were affected by the closeness of the spheres. In particular, as the sphere spacing was decreased the surface vorticities at the rear surface of sphere A for high Reynolds numbers became negative over a larger region while those at the front surface of sphere B for high Reynolds numbers decreased and eventually became negative for the two smallest sphere spacings considered in this study: Zs = 0.20 and 1.32. Also, for the smallest sphere spacing Zs = 0.20 the surface vorticities near the rear stagnation point of sphere A and near the front stagnation point of sphere B were found to be nearly zero for all Reynolds numbers indicating the existence of stagnant fluid in the tiny inner region between the two nearly touching spheres.

8. For each sphere spacing, at high Reynolds numbers there was flow separation from the rear surface of each sphere and that the angles of flow separation were always larger for sphere A than for sphere B. As the sphere spacing was increased, the angles of flow separation from the back of sphere A generally became smaller while those from the back of sphere B became larger until they both became close to that for a single isolated sphere. For the two smallest sphere spacings: Zs = 0.20 and 1.32, flow separation from the front surface of sphere B

was observed; and the angle of flow separation was smaller for the larger of these two sphere spacings.

9. It was observed that the distributions of surface pressure at the front surface of sphere A and at the rear surface of sphere B did not change much with sphere spacing; while those at the rear surface of sphere A and at the front surface of sphere B were affected by the closeness of the spheres. As the sphere spacing was decreased, the surface pressures at the rear surface of sphere A became larger while those at the front surface of sphere B became smaller so that as a result, the distributions of surface pressure around the two equally sized spheres became further away from those around a single isolated sphere. It was also observed that for each sphere spacing, the dimensionless surface pressures at the front surface of each sphere decreased with increasing Reynolds number.

10. It was found that for each sphere spacing, the pattern of variation of the frictional, pressure, and total drag coefficients for the spheres with increasing Reynolds number was generally similar to that for a single isolated sphere. It was also found that the total drag coefficients for each of the two spheres were less than those obtained by Al-Taha(1969) for a single isolated sphere. As the sphere spacing was increased, the total drag coefficients for each of the two spheres became closer to those for a single isolated sphere although the approach was closer for sphere A than for sphere B.

11. The concentration profiles around the two spheres were found to be dependent on three parameters: the Peclet

number, the Reynolds number, and the sphere spacing.

At low Peclet numbers of 0.001 to 0.1, the concentration profiles were symmetrical about a plane through the mid-point of the line of centres normal to the direction of flow, and remained nearly unchanged when the Reynolds number was increased. At higher Peclet numbers, the region of high concentration of the diffusing material was confined into a narrow zone upstream of each sphere. Also, the regions of high concentration became increasingly thinner as the Peclet number was increased so that at high Peclet numbers a diffusional boundary layer was observed to have developed at the upstream surface of each sphere. However, the development of a diffusional boundary layer at the upstream surface of sphere B became less pronounced when the sphere spacing was decreased. Meanwhile, at high Peclet numbers the concentration profiles around the spheres were influenced by the fluid dynamics, in particular, as the Reynolds number increased the regions of high concentration of diffusing material were confined into narrower regions upstream of the spheres.

It was also observed that for each of the five sphere spacings considered, the concentration profiles around the two spheres were always at least slightly different from those around a single isolated sphere, and the difference became larger when the distance between the spheres was decreased. This showed that the particle-to-particle interaction between the spheres affected the rates of mass transfer from the spheres and that the effect of the interparticle interaction increased with decreasing sphere spacing.

12. It was observed that the local Sherwood numbers at the rear surface of sphere A and at the front surface of sphere B were affected by the closeness of the spheres. As the sphere spacing was decreased, the higher concentration of the diffusing material in the fluid in the inner region between the spheres reduced the rates of mass transfer from the regions near the rear stagnation point of sphere A and near the front stagnation point of sphere B, and for the smallest sphere spacing $Z_s = 0.20$ the mass transfer rates were nearly zero for all Reynolds and Peclet numbers. As a result, the distributions of local Sherwood number around the two spheres became different from those around a single isolated sphere.

Except for sphere B at the smallest sphere spacing, the local Sherwood numbers at the front surfaces of the spheres increased with increasing Peclet number because of the decrease in the thickness of the diffusional boundary layer. It was observed that at low Peclet numbers of 0.001 to 0.1, the local Sherwood numbers for the spheres were almost independent of Reynolds number although at higher Peclet numbers the local Sherwood numbers at the front surfaces of the spheres increased with increasing Reynolds number. It was found that the increase in the local Sherwood numbers with increasing Reynolds and Peclet numbers was always larger for sphere A than for sphere B. In contrast, the local Sherwood numbers at the rear surfaces of the spheres either remained nearly the same or increased only slightly when the Reynolds and Peclet numbers were increased.

13. At low Peclet numbers of 0.001 to 0.1, the overall Sherwood numbers for the spheres were approximately equal and

and constant. For the three smallest sphere spacings, the overall Sherwood numbers were less than the limiting value of 2.0 obtained for a single isolated sphere by molecular diffusion alone to an infinite medium whereas for the two largest sphere spacings they were slightly greater than 2.0. At higher Peclet numbers the overall Sherwood numbers for the two spheres increased with increasing Peclet number although the increase was observed to be larger for sphere A than for sphere B.

The overall Sherwood numbers for sphere A were independent of the Reynolds number over the Peclet numbers range of 0.001 to 0.1; while those for sphere B were independent of the Reynolds number over the larger Peclet number range of 0.001 to 1.0. At higher Peclet numbers, the overall Sherwood numbers for the spheres increased with increasing Reynolds number, however, the increase was larger for sphere A than for sphere B.

It was also observed that the overall Sherwood numbers for the spheres increased with increasing sphere spacing; however, at high Peclet numbers the rate of increase was faster for sphere B than for sphere A. As a result, when the distance between the two spheres was increased the overall Sherwood numbers for the two spheres became closer to each other as well as closer to those for a single isolated sphere.

14. The use of the bi-spherical coordinate system in the present study had a disadvantage which arose mainly from the inherently unequal distances between any two neighbouring

grid lines in the Z-direction around the spheres.

At high Reynolds and Peclet numbers the thicknesses of the fluid dynamic and diffusional boundary layers at the upstream surface of sphere A were both small in comparison with the large Z-grid-line spacings close to the upstream surface of sphere A. This resulted in some anomalous behaviours of the surface vorticities, surface pressures, and local Sherwood numbers obtained for that region which subsequently affected the accuracy of the drag coefficients and the overall Sherwood numbers for sphere A. Fortunately, this effect was significantly reduced when the sphere spacing was small and when a smaller mesh spacing in the Z-direction was used in the solutions of the Navier-Stokes and diffusion equations. For sphere B, this disadvantage was either not present or very small because the Z-grid-line spacings close to the upstream surface of sphere B were generally very small in comparison with those close to the upstream surface of sphere A.

15. The computer programmes used in the present study were developed solely to predict the flow conditions around two equally sized spheres parallel to their line of centres and to predict the rates of mass transfer from them. However, there is scope for these programmes to be used in studies of two spheres of different sizes. Furthermore, with appropriate modification and combination, the computer programmes can be extended to studies of two-sphere free convective, interacting free and forced convective mass transfer problems, as well as to studies of time-dependent two-sphere fluid dynamic and mass transfer problems.

APPENDIX A. BI-SPHERICAL COORDINATE SYSTEM.

A-1. Bi-spherical coordinates(Z,θ,ϕ).

A system of two spheres is formed by the rotation of two circles about their line of centres. The relationships between the bi-spherical coordinates(Z,θ,ϕ) and the rectangular Cartesian coordinates(y_1,y_2,y_3) are as follows:

$$y_1 = \frac{a\,\mathrm{Sinh}Z}{\mathrm{Cosh}Z - \mathrm{Cos}\theta} \qquad \text{(A-1-1)}$$

$$y_2 = \frac{a\,\mathrm{Sin}\theta\,\mathrm{Sin}\phi}{\mathrm{Cosh}Z - \mathrm{Cos}\theta} \qquad \text{(A-1-2)}$$

$$y_3 = \frac{a\,\mathrm{Sinh}Z\,\mathrm{Cos}\phi}{\mathrm{Cosh}Z - \mathrm{Cos}\theta} \qquad \text{(A-1-3)}$$

with the ranges of the coordinates as follows:

$$-\infty < Z < +\infty \quad , \quad 0 \leqslant \theta \leqslant \pi \quad , \quad 0 \leqslant \phi \leqslant 2\pi \qquad \text{(A-1-4)}$$

For an orthogonal curvilinear coordinate system, the scale factors, $(h_i,\ i = 1,2,3)$, are related to the rectangular Cartesian coordinate system by the following expression:

$$h_i = \left[\sum_{k=1}^{3} \left(\frac{\partial y_k}{\partial x_i}\right)^2 \right]^{\frac{1}{2}} \qquad \text{(A-1-4)}$$

where $(y_k,\ k = 1,2,3)$ represent the rectangular Cartesian coordinates, and $(x_i,\ i = 1,2,3)$ represent the orthogonal curvilinear coordinate system.

For the bi-spherical coordinates, $x_1 = Z$, $x_2 = \theta$, $x_3 = \phi$, the following scale factors: $h_1 = h_Z$, $h_2 = h_\theta$, and $h_3 = h_\phi$, are

obtained by substituting equations(A-1-1) to (A-1-3) into equation(A-1-4):

$$h_Z = h_\theta = \frac{a}{\text{Cosh}Z - \text{Cos}\theta} \quad , \quad h_\phi = \frac{a\text{Sin}\theta}{\text{Cosh}Z - \text{Cos}\theta} \qquad \text{(A-1-5)}$$

The element of area on the surfaces of the spheres with $Z = \pm Zs$ ($Z = -Zs$ represents the upstream sphere while $Z = +Zs$ represents the downstream sphere) is:

$$dS = h_2 h_3 dx_2 dx_3$$

$$= \left(\frac{a}{\text{Cosh}(\pm Zs) - \text{Cos}\theta}\right)\left(\frac{a\text{Sin}\theta}{\text{Cosh}(\pm Zs) - \text{Cos}\theta}\right) \qquad \text{(A-1-6)}$$

and the total surface area of each of the spheres is:

$$S = \frac{4\pi a^2}{\text{Cosh}^2(\pm Zs) - 1} = 4\pi\left|\frac{a^2}{\text{Sinh}^2(\pm Zs)}\right| \qquad \text{(A-1-7)}$$

Similarly, the element of volume of each of the spheres is:

$$dV = h_1 h_2 h_3 dx_1 dx_2 dx_3$$

$$= \left(\frac{a}{\text{Cosh}(\pm Zs) - \text{Cos}\theta}\right)^2\left(\frac{a\text{Sin}\theta}{\text{Cosh}(\pm Zs) - \text{Cos}\theta}\right) dZ d\theta d\phi \qquad \text{(A-1-8)}$$

and the volume of each of the spheres is:

$$V = \frac{4}{3}\pi \cdot \left|\frac{a^3}{\text{Sinh}^3(\pm Zs)}\right| \qquad \text{(A-1-9)}$$

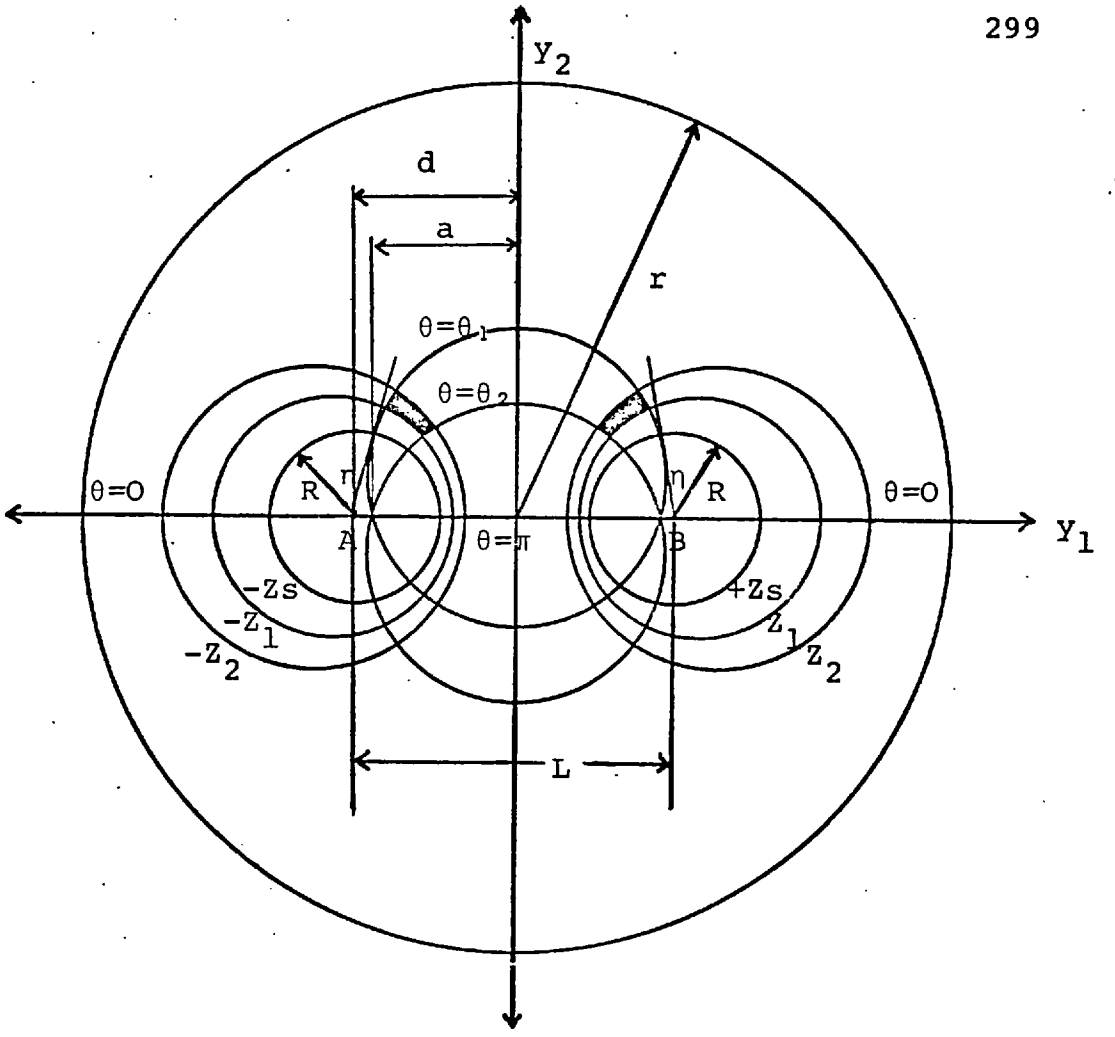

Figure(A-1) Bi-polar coordinates (Z,θ) in a meridian plane.

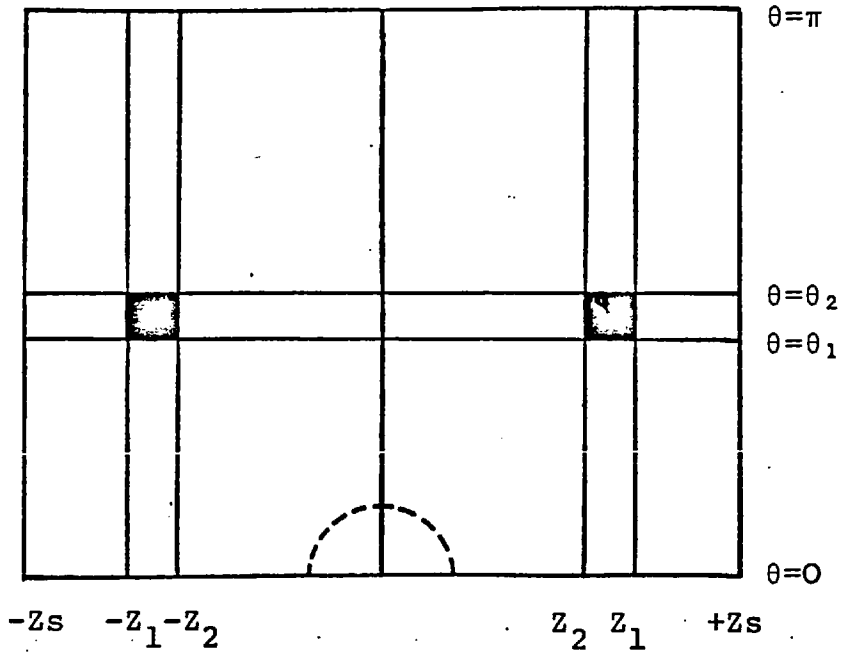

Figure(A-2) Transformed bi-polar coordinate(Z,θ) plane.

A-2. Reduction of bi-spherical coordinates to bi-polar coordinates.

The flow of a fluid around two equally sized spheres parallel to their line of centres is independent of the angle of rotation, ϕ, and is axisymmetrical. Hence, the bi-spherical coordinate system may be reduced to the bi-polar(Z,θ) coordinate system so that the bi-polar coordinates(Z,θ) in a meridian plane are the only coordinates required to describe the flow.

The relationships between the bi-polar coordinates(Z,θ) and the Cartesian coordinates(y_1,y_2) are obtained from the transformation of:

$$y_1 + iy_2 = ia\cdot\mathrm{Cot}\tfrac{1}{2}(\theta + iZ) \qquad \text{(A-2-1)}$$

with $a > 0$

which, on equating the real and imaginary parts, leads to the following relations:

$$y_1 = \frac{a\mathrm{Sinh}Z}{\mathrm{Cosh}Z - \mathrm{Cos}\theta} \qquad \text{(A-2-2)}$$

$$y_2 = \frac{a\mathrm{Sin}\theta}{\mathrm{Cosh}Z - \mathrm{Cos}\theta} \qquad \text{(A-2-3)}$$

Equations(A-2-2) and (A-2-3) describe the physical plane shown in Figure(A-1).

On eliminating θ from equations(A-2-2) and (A-2-3), the following relationship is obtained:

$$(y_1 - a\mathrm{Coth}Z)^2 + y_2^2 = a^2\mathrm{Csch}^2Z \qquad \text{(A-2-4)}$$

Equation(A-2-4) describes, for different values of Z, a family of non-intersecting, coaxial circles with their centres lying along the y_1-axis. For Z = -Zs = constant, it describes a circle lying entirely to the left of the plane $y_1 = 0$ which has its centre at the point(y_1 = aCoth(-Zs), $y_2 = 0$) and which has a radius of aCsch(-Zs); while for Z = +Zs = constant, it describes another circle lying entirely to the right of the plane $y_1 = 0$ which has its centre at the point (y_1 = aCoth(+Zs), y_2 = 0) and which has a radius of aCsch(+Zs). It is important to note that these two circles have the same radius and that their centres are the same distance from the origin of the bi-polar coordinate system. The points (-a, 0) and (+a, 0), are the centres of the two circles of zero radius ($Z = -\infty$ and $Z = +\infty$).

When Z is eliminated from equations(A-2-2) and (A-2-3), the following relation is obtained:

$$y_1^2 + (y_2 - a\text{Cot}\theta)^2 = a^2\text{Csc}^2\theta \qquad \text{(A-2-5)}$$

which describes, for different values of θ, a family of circles with their centres lying along the y_2-axis.

The conformal mapping of the bi-polar coordinates(Z,θ) into the rectangular Cartesian coordinates(y_1,y_2) is obtained through an exponential function: $F = e^{Z + i\theta} = e^{y_1 + iy_2}$, which gives: $y_1 = Z$ and $y_2 = \theta$. The transformed coordinates(Z,θ) are shown in Figure(A-2). It is clear that the two planes of Figures (A-1) and (A-2) correspond to each other. The semicircles Z = constant and the circular arcs θ = constant shown in the upper half of the physical plane of Figure(A-1) corresponding to the vertical lines Z = constant and to the horizontal lines θ =

constant, respectively, in Figure(A-2). Similarly, the two shaded areas in the two figures also correspond to each other.

For a system of two equally sized circles with Z = -Zs and Z = +Zs, surrounded by a large boundary circle of radius r which has its centre at the mid-point of the line of centres, the flow region in the upper half of the physical plane of Figure(A-1) which is bounded by $\theta = 0$, $\theta = \pi$, Z = -Zs, Z = +Zs, and the enveloping large semicircle, maps into a rectangular plane of Figure(A-2) which is bounded by the straight lines $\theta = 0$, $\theta = \pi$, Z = -Zs, Z = +Zs, and by the curve corresponding to the enveloping semicircle.

The location of the enveloping semicircle is determined as follows:

$$r^2 = y_1^2 + y_2^2 = \left(\frac{a\,\mathrm{Sinh}Z_o}{\mathrm{Cosh}Z_o - \mathrm{Cos}\theta_o}\right)^2 + \left(\frac{a\,\mathrm{Sin}\theta_o}{\mathrm{Cosh}Z_o - \mathrm{Cos}\theta_o}\right)^2$$

$$= a^2\left(\frac{\mathrm{Cosh}Z_o + \mathrm{Cos}\theta_o}{\mathrm{Cosh}Z_o - \mathrm{Cos}\theta_o}\right) \qquad \text{(A-2-6)}$$

Division of equation(A-2-6) by d^2, where $d = a|\mathrm{Coth}Zs|$ is the distance between the centre of either circles to the origin of the bi-polar coordinate system, gives:

$$\left(\frac{r}{d}\right)^2 = \left(\frac{a}{d}\right)^2\left(\frac{\mathrm{Cosh}Z_o + \mathrm{Cos}\theta_o}{\mathrm{Cosh}Z_o - \mathrm{Cos}\theta_o}\right) = \tanh^2 Zs\left(\frac{\mathrm{Cosh}Z_o + \mathrm{Cos}\theta_o}{\mathrm{Cosh}Z_o - \mathrm{Cos}\theta_o}\right) \qquad \text{(A-2-7)}$$

rearrangement of equation(A-2-7) gives:

$$\mathrm{Cosh}Z_o = \left[\frac{\{(r/d)^2/\tanh^2 Zs\} + 1}{\{(r/d)^2/\tanh^2 Zs\} - 1}\right]\mathrm{Cos}\theta_o \qquad \text{(A-2-8)}$$

Table(A-1). Values of θ corresponding to values of η incremented by a constant value of 6^{o}.

Zs =	0.20	1.32	2.07	2.48	3.09
η	θ				
0	0.0	0.0	0.0	0.0	0.0
6	0.6	3.5	4.7	5.1	5.5
12	1.2	7.0	9.3	10.2	11.0
18	1.8	10.5	14.0	15.3	16.5
24	2.4	14.0	18.7	20.4	22.0
30	3.1	17.6	23.5	25.5	27.5
36	3.7	21.3	28.3	30.7	33.0
42	4.4	25.0	33.2	36.0	38.6
48	5.1	28.9	38.1	41.3	44.2
54	5.8	32.8	43.1	46.6	49.9
60	6.6	36.9	48.3	52.0	55.6
66	7.4	41.2	53.5	57.5	61.3
72	8.3	45.6	58.8	63.1	67.1
78	9.2	50.2	64.3	68.8	73.0
84	10.3	55.0	69.9	74.6	78.8
90	11.4	60.1	75.6	80.4	84.8
96	12.6	65.4	81.5	86.4	90.8
102	14.0	71.1	87.6	92.5	96.9
108	15.6	77.0	93.8	98.7	103.0
114	17.5	83.0	100.1	104.9	109.1
120	19.6	90.1	106.7	111.3	115.4
126	22.1	97.2	113.4	117.8	121.7
132	25.2	104.8	120.3	124.5	128.0
138	29.1	112.9	127.4	131.2	134.4
144	34.1	121.3	134.6	138.0	140.8
150	40.8	130.3	141.9	144.8	147.3
156	50.2	139.6	149.4	151.8	153.8
162	64.4	149.4	156.9	158.8	160.3
168	87.0	159.4	164.6	165.8	166.9
174	124.5	169.6	172.3	172.9	173.4
180	180.0	180.0	180.0	180.0	180.0

When values of Zs and (r/d) are specified, equation(A-2-8) can be solved for Z_o for any specified value of θ_o. Pairs of values of Z_o and θ_o are the bi-polar coordinates of the outer boundary of the flow region which, when plotted, provided the dashed-line curve in Figure(A-2).

A-3. Calculation of the value of θ which correspond to values of η incremented by a constant value.

From Figure(A-1), it is clear that for each specified value of θ there are two points on the circumferences of the circles: one on each circle, with the same value of angle η measured from the axis of symmetry $\theta = 0^o$. For sphere A, η is the angle between the normal to the front stagnation point and the normal to a point on the circumference; while for sphere B, it is the angle between the normal to the rear stagnation point and the normal to a point on the circumference. Except at the front and rear stagnation points of the circles, the value of θ is always different from that of η.

In order to study and understand the results of the two-sphere fluid dynamic and mass transfer problems in the same way as those for a single isolated sphere, it is desirable to adopt a scheme of distributing the grid lines for the θ-direction with a constant increment in the values of η instead of retaining a constant increment in the value of θ. From the relationship between η and θ as shown in Figure(A-1), the following expressions are obtained using equations(A-2-2) and (A-2-3):

For circle A (Z = -Zs).

$$y_{1A} = \frac{a\mathrm{Sinh}(-Zs)}{\mathrm{Cosh}(-Zs) - \mathrm{Cos}\theta} \qquad \text{(A-3-1)}$$

$$y_{2A} = \frac{a\mathrm{Sin}\theta}{\mathrm{Cosh}(-Zs) - \mathrm{Cos}\theta} \qquad \text{(A-3-2)}$$

$$\tan\eta = \frac{y_{1A}}{y_{2A} + |\mathrm{Cosh}(-Zs)|} \qquad \text{(A-3-3)}$$

For circle B (Z = +Zs).

$$y_{1B} = \frac{a\mathrm{Sinh}(+Zs)}{\mathrm{Cosh}(+Zs) - \mathrm{Cos}\theta} \qquad \text{(A-3-4)}$$

$$y_{2B} = \frac{a\mathrm{Sin}\theta}{\mathrm{Cosh}(+Zs) - \mathrm{Cos}\theta} \qquad \text{(A-3-5)}$$

$$\tan\eta = \frac{y_{1B}}{y_{2B} - |\mathrm{Cosh}(+Zs)|} \qquad \text{(A-3-6)}$$

When values of the sphere spacing Zs and the constant increment in η, are specified, then, because of symmetry values of θ can be obtained from either equations(A-3-1) to (A-3-3) or from equations(A-3-4) to (A-3-6).

Values of θ for five sphere spacings: Zs = 0.20, 1.32, 2.07, 2.48, and 3.09, and for a constant increment in the angle η of 6^{o} are shown in Table(A-1). It is clear that the values of θ and η are not the same, and that the difference between them are very large when the sphere spacing is small. This scheme of distributing the grid lines for the θ-direction according to a constant increment in η also has the advantage of distributing the grid lines more evenly in the flow region than that using a constant increment in θ.

APPENDIX B. SURFACE PRESSURE DISTRIBUTIONS AND DRAG COEFFICIENTS.

B-1. Physical components of the stress tensor for an incompressible Newtonian fluid.

For an incompressible Newtonian fluid, the symmetrical Newtonian stress tensor is as follows:

$$\tau_{ij} = -p \cdot \delta_{ij} + \mu \cdot e_{ij} \qquad \text{(B-1-1)}$$

where p is the static-fluid pressure, δ_{ij} is the Kronecker delta ($\delta_{ij} = 1$ for $i = j$, and $\delta_{ij} = 0$ for $i \neq j$), and e_{ij} is the symmetrical rate of strain tensor.

The nine components of the stress tensor expressed in bi-spherical coordinates (Z, θ, ϕ) are as follows:

$$\tau_{ZZ} = -p + 2\mu\left(\frac{\text{Cosh}Z-\text{Cos}\theta}{a}\right)\left[\frac{\partial V_Z}{\partial Z} - \left(\frac{\text{Sin}\theta}{\text{Cosh}Z-\text{Cos}\theta}\right)V_\theta\right] \qquad \text{(B-1-2)}$$

$$\tau_{\theta\theta} = -p + 2\mu\left(\frac{\text{Cosh}Z-\text{Cos}\theta}{a}\right)\left[\frac{\partial V_\theta}{\partial \theta} - \left(\frac{\text{Sinh}Z}{\text{Cosh}Z-\text{Cos}\theta}\right)V_Z\right] \qquad \text{(B-1-3)}$$

$$\tau_{\phi\phi} = -p + 2\mu\left(\frac{\text{Cosh}Z-\text{Cos}\theta}{a}\right)\left[\frac{1}{\text{Sin}\theta}\frac{\partial V_\phi}{\partial \phi} - \left(\frac{\text{Sinh}Z}{\text{Cosh}Z-\text{Cos}\theta}\right)V_Z + \left(\frac{\text{Cosh}Z\cdot\text{Cos}\theta-1}{\text{Sin}\theta\,(\text{Cosh}Z-\text{Cos}\theta)}\right)V_\theta\right] \qquad \text{(B-1-4)}$$

$$\tau_{Z\theta} = \tau_{\theta Z} = \mu\left(\frac{\text{Cosh}Z-\text{Cos}\theta}{a}\right)\left[\frac{\partial V_Z}{\partial Z} + \left(\frac{\text{Sin}\theta}{\text{Cosh}Z-\text{Cos}\theta}\right)V_Z + \frac{\partial V_\theta}{\partial Z} + \left(\frac{\text{Sinh}Z}{\text{Cosh}Z-\text{Cos}\theta}\right)V_\theta\right] \qquad \text{(B-1-5)}$$

$$\tau_{Z\phi} = \tau_{\phi Z} = \mu\left(\frac{\text{Cosh}Z-\text{Cos}\theta}{a}\right)\left[\frac{1}{\text{Sin}\theta}\cdot\frac{\partial V_Z}{\partial \phi} + \frac{\partial V_\phi}{\partial Z} + \left(\frac{\text{Sinh}Z}{\text{Cosh}Z-\text{Cos}\theta}\right)V_\phi\right] \qquad \text{(B-1-6)}$$

$$\tau_{\theta\phi} = \tau_{\phi\theta} = \mu\left(\frac{\text{Cosh}Z-\text{Cos}\theta}{a}\right)\left[\frac{1}{\text{Sin}\theta}\frac{\partial V_\theta}{\partial \phi} + \frac{\partial V_\phi}{\partial \theta} - \left\{\frac{\text{Cosh}Z\ \text{Cos}\theta-1}{\text{Sin}\theta(\text{Cosh}\,Z-\text{Cos}\theta)}\right\}V_\theta\right] \qquad \text{(B-1-7)}$$

B-2. The Navier-Stokes and diffusion equations in bi-spherical coordinates.

For steady incompressible Newtonian flows, the continuity, Navier-Stokes and diffusion equations are given as follows:

$$\nabla\cdot\hat{V} = 0 \qquad \text{(B-2-1)}$$

$$\hat{V}\cdot\nabla C = D_C\nabla^2 C \qquad \text{(B-2-2)}$$

$$\tfrac{1}{2}\nabla(\hat{V}\cdot\hat{V}) - \hat{V}\times(\nabla\times\hat{V}) = -\frac{1}{\rho}\nabla P + \nu\left[\nabla(\nabla\cdot\hat{V}) - \nabla\times(\nabla\times\hat{V})\right] \qquad \text{(B-2-3)}$$

When expressed in terms of bi-spherical coordinates these equations become as follows:

1. The continuity equation in bi-spherical coordinates:

$$\left(\frac{\text{Cosh}Z-\text{Cos}\theta}{a}\right)\left[\left\{\frac{\partial V_Z}{\partial Z} - 2\left(\frac{\text{Sinh}Z}{\text{Cosh}Z-\text{Cos}\theta}\right)V_Z\right\} + \left\{\frac{\partial V_\theta}{\partial \theta}\right.\right. \qquad \text{(B-2-4)}$$

$$\left.\left. + \left(\frac{\text{Cosh}Z\cdot\text{Cos}\theta-1}{\text{Sin}\theta(\text{Cosh}Z-\text{Cos}\theta)} - \frac{\text{Sin}\theta}{\text{Cosh}Z-\text{Cos}\theta}\right)V_\theta\right\} + \frac{1}{\text{Sin}\theta}\cdot\frac{\partial V_\phi}{\partial \phi}\right] = 0$$

2. The diffusion equation in bi-spherical coordinates:

$$\left(\frac{\mathrm{Cosh}Z-\mathrm{Cos}\theta}{a}\right)\left[V_Z\cdot\frac{\partial C}{\partial Z}+V_\theta\cdot\frac{\partial C}{\partial\theta}+\frac{V_\phi}{\mathrm{Sin}\theta}\frac{\partial C}{\partial\phi}\right]=D_C\,\nabla^2C \qquad \text{(B-2-5)}$$

where:

$$\nabla^2=\left(\frac{\mathrm{Cosh}Z-\mathrm{Cos}\theta}{a}\right)^2\left[\frac{\partial^2}{\partial Z^2}+\left(\frac{-\mathrm{Sinh}Z}{\mathrm{Cosh}Z-\mathrm{Cos}\theta}\right)\frac{\partial}{\partial Z}+\frac{\partial^2}{\partial\theta^2}\right.$$

$$\left.+\frac{\mathrm{Cosh}Z\cdot\mathrm{Cos}\theta-1}{\mathrm{Sin}\theta(\mathrm{Cosh}Z-\mathrm{Cos}\theta)}\frac{\partial}{\partial\theta}+\frac{1}{\mathrm{Sin}^2\theta}\frac{\partial^2}{\partial\phi^2}\right] \qquad \text{(B-2-6)}$$

3. The Z-, θ-, and φ-components of the Navier-Stokes equations in bi-spherical coordinates are as follows:

Z-component of the Navier-Stokes equations:

$$\left(\frac{\mathrm{Cosh}Z-\mathrm{Cos}\theta}{a}\right)\left[V_Z\cdot\frac{\partial V_Z}{\partial Z}+V_\theta\frac{\partial V_Z}{\partial\theta}+\frac{V_\phi}{\mathrm{Sin}\theta}\cdot\frac{\partial V_Z}{\partial\theta}+\left(\frac{-\mathrm{Sin}\theta}{\mathrm{Cosh}Z-\mathrm{Cos}\theta}\right)V_\theta V_Z\right.$$

$$\left.-\left(\frac{-\mathrm{Sinh}Z}{\mathrm{Cosh}Z-\mathrm{Cos}\theta}\right)V_\theta^2+\left(\frac{-\mathrm{Sinh}Z}{\mathrm{Cosh}Z-\mathrm{Cos}\theta}\right)V_\phi^2\right]$$

$$=-\frac{1}{\rho}\left(\frac{\mathrm{Cosh}Z-\mathrm{Cos}\theta}{a}\right)\cdot\frac{\partial P}{\partial Z}+\nu\left(\frac{\mathrm{Cosh}Z-\mathrm{Cos}\theta}{a}\right)^2\left[\left(\frac{a}{\mathrm{Cosh}Z-\mathrm{Cos}\theta}\right)^2\cdot\nabla^2V_Z\right.$$

$$+\left\{-2\left(\frac{-\mathrm{Sinh}Z}{\mathrm{Cosh}Z-\mathrm{Cos}\theta}\right)^2+\left(\frac{-\mathrm{Sin}\theta}{\mathrm{Cosh}Z-\mathrm{Cos}\theta}\right)^2\right\}V_Z$$

$$+\left\{2\left(\frac{-\mathrm{Sinh}Z}{\mathrm{Cosh}Z-\mathrm{Cos}\theta}\right)^2+\left(\frac{-\mathrm{Sinh}Z}{\mathrm{Cosh}Z-\mathrm{Cos}\theta}\right)\left(\frac{-\mathrm{Sin}\theta}{\mathrm{Cosh}Z-\mathrm{Cos}\theta}\right)\right\}V_\theta$$

$$\left.+2\left\{\left(\frac{-\mathrm{Sin}\theta}{\mathrm{Cosh}Z-\mathrm{Cos}\theta}\right)\cdot\frac{\partial V_\theta}{\partial Z}-\left(\frac{-\mathrm{Sinh}Z}{\mathrm{Cosh}Z-\mathrm{Cos}\theta}\right)\cdot\frac{\partial V_\theta}{\partial\theta}\right.\right.$$

$$- \frac{1}{\text{Sin}\theta}\left(\frac{-\text{Sinh}Z}{\text{Cosh}Z-\text{Cos}\theta}\right)\frac{\partial V_\phi}{\partial \phi}\Big\}\Bigg] \qquad \text{(B-2-7)}$$

θ-component of the Navier-Stokes equations:

$$\left(\frac{\text{Cosh}Z-\text{Cos}\theta}{a}\right)\Bigg[V_Z\cdot\frac{\partial V_\theta}{\partial Z} + V_\theta\cdot\frac{\partial V_\theta}{\partial \theta} + \frac{V_\phi}{\text{Sin}\theta}\frac{\partial V_\theta}{\partial \phi} - \left(\frac{-\text{Sin}\theta}{\text{Cosh}Z-\text{Cos}\theta}\right)V_Z^2$$

$$+ \left(\frac{-\text{Sinh}Z}{\text{Cosh}Z-\text{Cos}\theta}\right)V_Z V_\theta + \frac{\text{Cosh}Z\cdot\text{Cos}\theta-1}{\text{Sin}\theta(\text{Cosh}Z-\text{Cos}\theta)}V_\phi^2\Bigg]$$

$$= -\frac{1}{\rho}\left(\frac{\text{Cosh}Z-\text{Cos}\theta}{a}\right)\cdot\frac{\partial P}{\partial \theta} + \nu\left(\frac{\text{Cosh}Z-\text{Cos}\theta}{a}\right)^2\Bigg[\left(\frac{a}{\text{Cosh}Z-\text{Cos}\theta}\right)^2\nabla^2 V_\theta$$

$$+ 2\Big\{-\left(\frac{-\text{Sin}\theta}{\text{Cosh}Z-\text{Cos}\theta}\right)\cdot\frac{\partial V_Z}{\partial Z} + \left(\frac{-\text{Sinh}Z}{\text{Cosh}Z-\text{Cos}\theta}\right)\cdot\frac{\partial V_Z}{\partial \theta}$$

$$- \frac{1}{\text{Sin}\theta}\cdot\frac{\text{Cosh}Z\cdot\text{Cos}\theta-1}{\text{Sin}\theta(\text{Cosh}Z-\text{Cos}\theta)}\cdot\frac{\partial V_\phi}{\partial \phi}\Big\} - \left(\frac{-\text{Sin}\theta}{\text{Cosh}Z-\text{Cos}\theta}\right)\left(\frac{-\text{Sinh}Z}{\text{Cosh}Z-\text{Cos}\theta}\right)V_Z$$

$$- V_\theta\Big\{\left(\frac{-\text{Sinh}Z}{\text{Cosh}Z-\text{Cos}\theta}\right)^2 + \left(\frac{-\text{Sin}\theta}{\text{Cosh}Z-\text{Cos}\theta}\right)^2 + \left(\frac{\text{Cosh}Z\cdot\text{Cos}\theta-1}{\text{Sin}\theta(\text{Cosh}Z-\text{Cos}\theta)}\right)^2\Big\}\Bigg]$$

(B-2-8)

ϕ-component of the Navier-Stokes equations:

$$\left(\frac{\text{Cosh}Z-\text{Cos}\theta}{a}\right)\Bigg[V_Z\cdot\frac{\partial V_\phi}{\partial Z} + V_\theta\cdot\frac{\partial V_\phi}{\partial \theta} + \frac{V_\phi}{\text{Sin}\theta}\cdot\frac{\partial V_\phi}{\partial \phi}$$

$$+ \left(\frac{-\text{Sinh}Z}{\text{Cosh}Z-\text{Cos}\theta}\right)V_Z V_\theta + \frac{\text{Cosh}Z\cdot\text{Cos}\theta-1}{\text{Sin}\theta(\text{Cosh}Z-\text{Cos}\theta)}\cdot V_\theta V_\phi\Bigg]$$

$$= -\frac{1}{\rho}\left(\frac{\text{Cosh}Z-\text{Cos}\theta}{a}\right)\cdot\frac{\partial P}{\partial \phi} + \nu\left(\frac{\text{Cosh}Z-\text{Cos}\theta}{a}\right)^2\Bigg[\left(\frac{a}{\text{Cosh}Z-\text{Cos}\theta}\right)^2\cdot\nabla^2 V_\phi$$

$$+\frac{2}{\text{Sin}\theta}\left(\frac{-\text{Sinh}Z}{\text{Cosh}Z-\text{Cos}\theta}\right)\cdot\frac{\partial V_Z}{\partial\phi}+\frac{2}{\text{Sin}\theta}\cdot\frac{\text{Cosh}Z\cdot\text{Cos}\theta-1}{\text{Sin}\theta(\text{Cosh}Z-\text{Cos}\theta)}\cdot\frac{\partial V_\theta}{\partial\phi}$$

$$-V_\theta\left\{\left(\frac{-\text{Sinh}Z}{\text{Cosh}Z-\text{Cos}\theta}\right)^2+\left(\frac{\text{Cosh}Z\cdot\text{Cos}\theta-1}{\text{Sin}\theta(\text{Cosh}Z-\text{Cos}\theta)}\right)^2\right\}\Bigg] \qquad \text{(B-2-10)}$$

For axisymmetrical flow with no swirl, V_ϕ, its derivatives, and all derivatives with respect to ϕ are zero so that equations (B-2-4) to (B-2-10) reduce to simpler forms.

B-3. Surface pressure distributions.

The pressures at the surfaces of the two equally sized spheres can be determined from the Navier-Stokes equations when the vorticity distributions around the spheres are known. For an axisymmetrical flow without swirl, there are only two components of the Navier-Stokes equations so that the two components of velocity: V_Z and V_θ, are related to the single component of vorticity of the fluid, ζ, in the ϕ-direction. Therefore, a relationship can be obtained for the surface pressure distributions in terms of the vorticity distributions around the spheres. This relationship is derived below.

The components of the Navier-Stokes equations in the Z- and θ-directions, when expressed in terms of vorticity become as follows:

The Z-component of the Navier-Stokes equations:

$$V_Z\cdot\frac{\partial V_Z}{\partial Z}+\frac{1}{\rho}\cdot\frac{\partial P}{\partial Z}=-\nu\left(\frac{\partial\zeta}{\partial\theta}+\frac{\text{Cosh}Z\cdot\text{Cos}\theta-1}{\text{Sin}\theta(\text{Cosh}Z-\text{Cos}\theta)}\cdot\zeta\right) \qquad \text{(B-3-1)}$$

The θ-component of the Navier-Stokes equations:

$$(V_Z \cdot \frac{\partial V_\theta}{\partial Z} + V_\theta \cdot \frac{\partial V_\theta}{\partial \theta}) + (\frac{-\text{Sinh}Z}{\text{Cosh}Z-\text{Cos}\theta}) \cdot V_Z V_\theta - (\frac{-\text{Sin}\theta}{\text{Cosh}Z-\text{Cos}\theta}) \cdot V_Z^2$$

$$+ \frac{1}{\rho} \frac{\partial P}{\partial \theta} = \nu \cdot \{\frac{\partial \zeta}{\partial Z} + (\frac{-\text{Sinh}Z}{\text{Cosh}Z-\text{Cos}\theta}) \cdot \zeta\} \qquad \text{(B-3-2)}$$

where,

$$\zeta = (\frac{\text{Cosh}Z-\text{Cos}\theta}{a}) \left[\frac{\partial V_\theta}{\partial Z} + (\frac{-\text{Sin}\theta}{\text{Cosh}Z-\text{Cos}\theta}) \cdot V_\theta - \frac{\partial V_Z}{\partial \theta}\right.$$

$$\left. + (\frac{-\text{Sinh}Z}{\text{Cosh}Z-\text{Cos}\theta}) \cdot V_Z\right] \qquad \text{(B-3-3)}$$

The pressures at the front stagnation point of sphere A and at the rear stagnation point of sphere B can be obtained in the following ways:

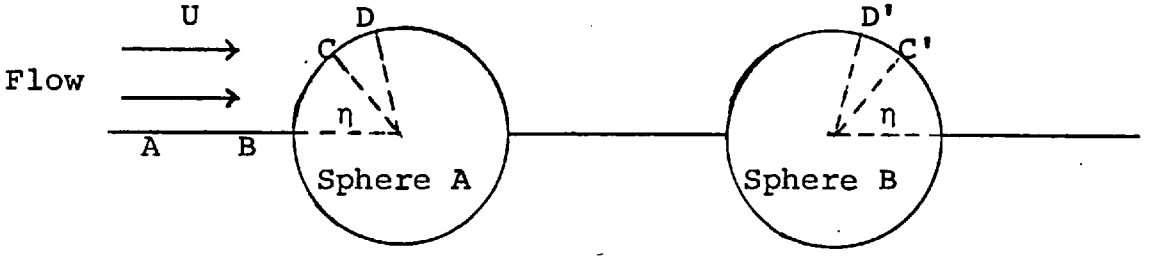

Figure B-1. Fluid flows around a system of two equally sized spheres.

Along the axis of symmetry, θ = 0: ψ, V_θ, and all their derivatives with respect to Z are zero, and the vorticity ζ defined by equation (B-3-3) becomes zero also. Because the second term on the right-hand side of equation (B-3-1) is

indeterminate, it is necessary to use the limiting rule of L'Hospital to give:

$$\lim_{\theta \to O} \frac{\text{Cosh}Z \cdot \text{Cos}\theta - 1}{\text{Sin}\theta(\text{Cosh}Z - \text{Cos}\theta)} \cdot \zeta = \frac{\frac{\partial \zeta}{\partial \theta}}{\text{Cos}\theta} = \frac{\partial \zeta}{\partial \theta} \qquad \text{(B-3-4)}$$

Hence, equation(B-3-1) becomes:

$$V_Z \cdot \frac{\partial V_Z}{\partial Z} + \frac{1}{\rho} \cdot \frac{\partial P}{\partial Z} = -2\nu \left(\frac{\partial \zeta}{\partial \theta}\right) \qquad \text{(B-3-5)}$$

Integrating equation(B-3-5) along the axis of symmetry from points A to B gives:

$$\frac{1}{\rho}(P_B - P_A) + \tfrac{1}{2}(V_Z^2)\Big|_B - \tfrac{1}{2}(V_Z^2)\Big|_A = -2\nu \int_A^B \left(\frac{\partial \zeta}{\partial \theta}\right) dZ \qquad \text{(B-3-6)}$$

The dimensionless pressure coefficient K may be defined as follows:

$$K = \frac{P_s - P_o}{\tfrac{1}{2}\rho U^2} \qquad \text{(B-3-7)}$$

where P_s is the pressure at the surfaces of the spheres and P_o is the pressure in the undisturbed fluid. The dimensionless pressure coefficients at the points A and B are denoted by K_A and K_B, respectively.

Also, introduction of the dimensionless velocity u*, where $u^* = V_Z/U$, into equation(B-3-6), gives:

$$K_B - K_A + u_B^{*2} - u_A^{*2} = \frac{-8}{Re} \int_A^B \left(\frac{\partial \zeta}{\partial \theta}\right) dZ \qquad \text{(B-3-8)}$$

If point A is well upstream of sphere A and point B is at the front stagnation point of sphere A, then:

$$u_B^* = 0,\ u_A^* = 1,\ K_A = 0,\ \text{and}\ K_B = K_{AO}$$

so that equation(B-3-8) becomes:

$$K_{AO} = 1.0 + \frac{8.0}{Re} \int_{Z=-Zs}^{Z=0} \left(\frac{\partial \zeta^*}{\partial \theta}\right) dZ \qquad \text{(B-3-9)}$$

Similarly, if point A is at the rear stagnation point of sphere B and point B is well downstream of sphere B, then:

$$u_B^* = 1,\ u_A^* = 0,\ K_A = K_{BO},\ \text{and}\ K_B = 0$$

so that equation(B-3-8) becomes:

$$K_{BO} = 1.0 + \frac{8.0}{Re} \int_{Z=+Zs}^{Z=0} \left(\frac{\partial \zeta^*}{\partial \theta}\right) dZ \qquad \text{(B-3-10)}$$

where K_{AO} and K_{BO} are the dimensionless pressure coefficients at the front stagnation point of sphere A and at the rear stagnation point of sphere B, respectively.

The surface pressure distributions for the two equally sized spheres can be obtained from equation(B-3-2), the θ-component of the Navier-Stokes equations, in the following way:

On the surfaces of the spheres, $Z = \pm Zs$: ψ, V_Z, V_θ, and all their derivatives with respect to θ are zero. Also, from the continuity equation, $\partial V_Z/\partial Z = 0$. Hence, equation(B-3-2) becomes:

$$\frac{1}{\rho}\cdot\frac{\partial P}{\partial \theta} = \nu\frac{\partial \zeta}{\partial Z} - \left(\frac{\text{Sinh}Z}{\text{Cosh}Z - \text{Cos}\,\theta}\right)\cdot\zeta_s \qquad \text{(B-3-11)}$$

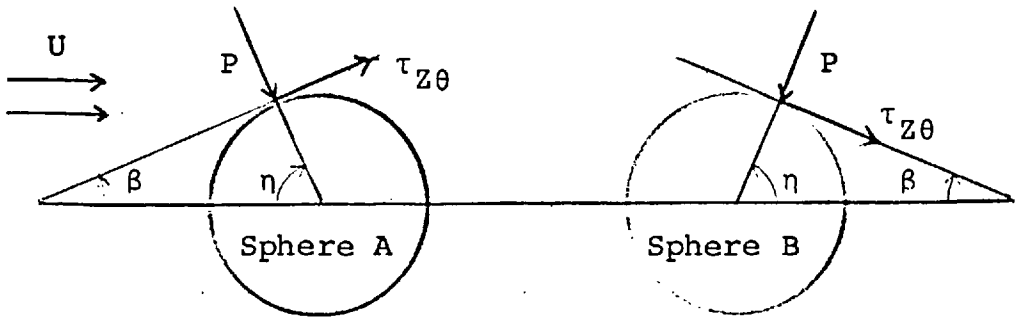

Figure(B-2) Pressures and viscous stresses on the surfaces of the spheres.

For sphere A, the integration of equation(B-3-11) around the surface from points C to D, as shown in Figure(B-2), gives:

$$\frac{1}{\rho}(P_D - P_C) = \nu \int_C^D \left[\frac{\partial \zeta^*}{\partial Z} - \left(\frac{\text{Sinh}(-Zs)}{\text{Cosh}(-Zs)-\text{Cos}\theta}\right)\cdot\zeta_s^*\right] d\theta \qquad \text{(B-3-12)}$$

In terms of dimensionless functions, equations(B-3-12) becomes:

$$K_D = K_C + \frac{4}{Re}\int_C^D \left[\frac{\partial \zeta^*}{\partial Z} - \left(\frac{\text{Sinh}(-Zs)}{\text{Cosh}(-Zs)-\text{Cos}\theta}\right)\zeta_s^*\right] d\theta \quad \text{(B-3-13)}$$

If the point C is considered to be at the front stagnation point of sphere A and the point D to be on the surface at a reference angle θ, then $K_C = K_{AO}$ and $K_D = K_{A\theta}$. Thus equation(B-3-13) can be rewritten as:

$$K_{A\theta} = K_{AO} + \frac{4}{Re}\int_O^\theta \left[\frac{\partial \zeta}{\partial Z} - \left(\frac{\text{Sinh}(-Zs)}{\text{Cosh}(-Zs)-\text{Cos}\theta}\right)\zeta_s^*\right] d\theta \quad \text{(B-3-14)}$$

where K_{AO} is given by equation(B-3-9) , while $K_{A\theta}$ is the dimensionless pressure coefficient at an angle θ on the surface of sphere A.

On the other hand, for sphere B the integration of equation(B-3-11) around the surface from points C' to D' gives:

$$\frac{1}{\rho}(P_{D'}-P_{C'}) = \nu \int_{C'}^{D'} \left[\frac{\partial \zeta}{\partial Z} - \left(\frac{-\text{Sinh}(+Zs)}{\text{Cosh}(+Zs)-\text{Cos}\theta}\right)\zeta_s\right] d\theta \quad \text{(B-3-15)}$$

In terms of dimensionless functions, equation(B-3-15) becomes:

$$K_{D'} = K_{C'} + \frac{4}{Re}\int_{C'}^{D'} \left[\frac{\partial \zeta^*}{\partial Z} - \left(\frac{-\text{Sinh}(+Zs)}{\text{Cosh}(+Zs)-\text{Cos}\theta}\right)\zeta_s^*\right] d\theta \quad \text{(B-3-16)}$$

If the point C' is considered to be at the rear stagnation point of sphere B and the point D' to be on the surface at a reference angle θ, then $K_{C'} = K_{BO}$ and $K_{D'} = K_{B\theta}$. Thus, equation(B-3-16) becomes:

$$K_{B\theta} = K_{BO} + \frac{4}{Re}\int_{O}^{\theta} \left[\frac{\partial \zeta^*}{\partial Z} + \left(\frac{\text{Sinh}(+Zs)}{\text{Cosh}(+Zs)-\text{Cos}\theta}\right)\zeta_s^*\right] d\theta \quad \text{(B-3-17)}$$

where K_{BO} is given by equation(B-3-10), while $K_{B\theta}$ is the dimensionless pressure coefficient at an angle θ on the surface of sphere B.

B-4. Drag forces and drag coefficients.

The total drag force on each of the two spheres is the sum of the pressure and viscous forces exerted by the fluid on the surface of each sphere in the direction of flow. Hence, the total drag force, D_T, can be expressed as the sum of the frictional drag force, D_F, and the pressure drag force, D_F:

$$D_T = D_F + D_P \quad \text{(B-4-1)}$$

Dividing each term of equation(B-4-1) by $\frac{1}{2}\rho U^2 A$, where A is the cross-sectional area of each sphere gives:

$$C_{DT} = C_{DF} + C_{DP} \qquad \text{(B-4-2)}$$

where C_{DT}, C_{DF}, and C_{DP}, are the total, frictional, and pressure drag coefficients, respectively.

For each sphere, the frictional drag force is evaluated from the sum of the tangential viscous stresses in the direction of flow at all points on the surface; while the pressure drag force is obtained from the summation of the pressure forces in the direction of flow at all points on the surface.

On the surfaces of the two equally sized spheres, $Z = \pm Z_s$: V_Z, V_θ, and all their derivatives with respect to θ are zero, hence, from equation (B-1-5) $\tau_{Z\theta}$, which is the only non-zero component of the Newtonian stress tensor, becomes:

$$\tau_{Z\theta} = \mu\left(\frac{\text{Cosh}Z-\cos\theta}{a}\right)\cdot\frac{\partial V_\theta}{\partial Z} = \mu\zeta_s \qquad \text{(B-4-4)}$$

Also, the average normal pressure at any point on the sphere surface is P. It is important to note that the horizontal components of the pressure and viscous forces contribute to the drag force; while the vertical components of the pressure and viscous forces contribute to the lift force which is zero in the present case of flow around a system of two equally sized spheres parallel to their line of centres.

Hence, the frictional drag force for each sphere is:

$$D_F = \iint_S \tau_{Z\theta}\cdot\text{Cos}\beta \; dS \qquad \text{(B-4-5)}$$

and the pressure drag force for each sphere is:

$$D_P = \iint_S P\cdot\text{Sin}\beta \; dS \qquad \text{(B-4-6)}$$

where β is the angle between the tangential plane and the direction of flow far from the spheres as shown in Figure(B-2), and dS is the element of surface area given by equation(A-1-6).

From Figure(B-2), it is clear that the relationship between β and η is as follows:

$$\beta = \tfrac{1}{2}\pi - \eta \qquad \text{(B-4-7)}$$

Hence,

$$\mathrm{Cos}\beta = \mathrm{Sin}\eta \qquad \text{(B-4-8)}$$

$$\mathrm{Sin}\beta = \mathrm{Cos}\eta \qquad \text{(B-4-9)}$$

where η can be obtained either from equation(A-3-3) of equation(A-3-6).

From equations(B-4-4), (B-4-5), and (B-4-8), the expressions for the frictional drag forces on spheres A and B: D_{FA} and D_{FB}, are obtained as follows:

$$D_{FA} = 2\pi\mu \int_0^{\pi} \zeta_s \mathrm{Sin}\eta \left(\frac{a}{\mathrm{Cosh}(-Zs)-\mathrm{Cos}\theta}\right)\left(\frac{a\mathrm{Sin}\theta}{\mathrm{Cosh}(-Zs)-\mathrm{Cos}\theta}\right) d\theta \qquad \text{(B-4-10)}$$

$$D_{FB} = 2\pi\mu \int_0^{\pi} \zeta_s \mathrm{Sin}\eta \left(\frac{a}{\mathrm{Cosh}(+Zs)-\mathrm{Cos}\theta}\right)\left(\frac{a\mathrm{Sin}\theta}{\mathrm{Cosh}(+Zs)-\mathrm{Cos}\theta}\right) d\theta \qquad \text{(B-4-11)}$$

Similarly, from equations(B-4-6) and (B-4-9), the expressions for the pressure drag forces on spheres A and B: D_{PA} and D_{PB}, are obtained as follows:

$$D_{PA} = 2\pi \int_0^{\pi} +P\mathrm{Cos}\eta \left(\frac{a}{\mathrm{Cosh}(-Zs)-\mathrm{Cos}\theta}\right)\left(\frac{a\mathrm{Sin}\theta}{\mathrm{Cosh}(-Zs)-\mathrm{Cos}\theta}\right) d\theta \qquad \text{(B-4-12)}$$

$$D_{PB} = 2\pi \int_0^{\pi} -P\,\mathrm{Cos}\eta \left(\frac{a}{\mathrm{Cosh}(+Zs)-\mathrm{Cos}\theta}\right)\left(\frac{a\cdot\mathrm{Sin}\theta}{\mathrm{Cosh}(+Zs)-\mathrm{Cos}\theta}\right) d\theta \qquad \text{(B-4-13)}$$

In terms of drag coefficients, the above four expressions become:

$$C_{DFA} = \frac{8}{Re} \int_0^{\pi} \zeta_s^* \mathrm{Sin}\eta \left(\frac{a^*}{\mathrm{Cosh}(-Zs)-\mathrm{Cos}\theta}\right)\left(\frac{a^*\cdot\mathrm{Sin}\theta}{\mathrm{Cosh}(-Zs)-\mathrm{Cos}\theta}\right) d\theta \qquad \text{(B-4-14)}$$

$$C_{DFB} = \frac{8}{Re} \int_0^{\pi} \zeta_s^* \mathrm{Sin}\eta \left(\frac{a^*}{\mathrm{Cosh}(+Zs)-\mathrm{Cos}\theta}\right)\left(\frac{a^*\cdot\mathrm{Sin}\theta}{\mathrm{Cosh}(+Zs)-\mathrm{Cos}\theta}\right) d\theta \qquad \text{(B-4-15)}$$

$$C_{DPA} = +2 \int_0^{\pi} K_\theta \mathrm{Cos}\eta \left(\frac{a^*}{\mathrm{Cosh}(-Zs)-\mathrm{Cos}\theta}\right)\left(\frac{a^*\cdot\mathrm{Sin}\theta}{\mathrm{Cosh}(-Zs)-\mathrm{Cos}\theta}\right) d\theta \qquad \text{(B-4-16)}$$

$$C_{DPB} = -2 \int_0^{\pi} K_\theta \mathrm{Cos}\eta \left(\frac{a^*}{\mathrm{Cosh}(+Zs)-\mathrm{Cos}\theta}\right)\left(\frac{a^*\cdot\mathrm{Sin}\theta}{\mathrm{Cosh}(+Zs)-\mathrm{Cos}\theta}\right) d\theta \qquad \text{(B-4-17)}$$

and the total drag coefficients for the spheres are:

$$C_{DTA} = C_{DFA} + C_{DPA} \qquad \text{(B-4-18)}$$

$$C_{DTB} = C_{DFB} + C_{DPB} \qquad \text{(B-4-19)}$$

where C_{DFA}, C_{DPA}, C_{DTA}, are the frictional, pressure, and total drag coefficients for sphere A; while C_{DFB}, C_{DPB}, and C_{DTB}, are the frictional, pressure, and total drag coefficients for sphere B.

APPENDIX C. LOCAL AND OVERALL SHERWOOD NUMBERS.

C-1. Local Sherwood numbers.

According to Fick's law of mass diffusion the local diffusional mass fluxes normal to the surfaces of the two spheres are:

For sphere A: $$J_A = \frac{-D_C}{h_Z}\left(\frac{\partial C}{\partial Z}\right)_{Z = -Zs} \qquad (C\text{-}1\text{-}1)$$

For sphere B: $$J_B = \frac{-D_C}{h_Z}\left(\frac{\partial C}{\partial Z}\right)_{Z = +Zs} \qquad (C\text{-}1\text{-}2)$$

where D_C is the diffusivity of the diffusing material in the fluid.

The local mass fluxes can also be expressed in terms of the local mass transfer coefficient, $h_D(\theta)$, as follows:

$$J_A = h_D(\theta)(C_s - C_o) \qquad (C\text{-}1\text{-}3)$$

$$J_B = h_D(\theta)(C_s - C_o) \qquad (C\text{-}1\text{-}4)$$

Hence, equations (C-1-1) to (C-1-4) give:

For sphere A: $$\frac{h_D(\theta)}{D_C} = -\left(\frac{\mathrm{Cosh}(-Zs) - \mathrm{Cos}\theta}{a}\right)\frac{1}{C_s - C_o}\left(\frac{\partial C}{\partial Z}\right)_{Z=-Zs} \qquad (C\text{-}1\text{-}5)$$

For sphere B: $$\frac{h_D(\theta)}{D_C} = -\left(\frac{\mathrm{Cosh}(+Zs) - \mathrm{Cos}\theta}{a}\right)\frac{1}{C_s - C_o}\left(\frac{\partial C}{\partial Z}\right)_{Z=+Zs} \qquad (C\text{-}1\text{-}6)$$

The local Sherwood numbers for the two spheres, spheres A and B, are defined as follows:

$$Sh_{AL}(\theta) = \frac{2R \cdot h_D(\theta)}{D_C} \qquad (C\text{-}1\text{-}7)$$

$$Sh_{BL}(\theta) = \frac{2R \cdot h_D(\theta)}{D_C} \qquad (C\text{-}1\text{-}8)$$

where R is the radius of the spheres.

Hence, from equations(C-1-5) and (C-1-7), the local Sherwood number for sphere A is obtained as follows:

$$Sh_{AL}(\theta) = -2.0\left(\frac{\mathrm{Cosh}(-Zs)-\mathrm{Cos}\theta}{a^*}\right)\left(\frac{\partial C^*}{\partial Z}\right)_{Z=-Zs} \qquad (C\text{-}1\text{-}9)$$

and from equations(C-1-6) and (C-1-8), the local Sherwood number for sphere B becomes:

$$Sh_{BL}(\theta) = -2.0\left(\frac{\mathrm{Cosh}(+Zs)-\mathrm{Cos}\theta}{a^*}\right)\left(\frac{\partial C^*}{\partial Z}\right)_{Z=+Zs} \qquad (C\text{-}1\text{-}10)$$

where $a^* = |\mathrm{Sinh}Zs|$. Thus, when the concentration distributions around the two spheres are known, the local Sherwood numbers for the spheres can be obtained using equations(C-1-9) and (C-1-10).

C-2. Overall Sherwood numbers.

The overall rates of mass transfer from the spheres to the fluid flowing around them, are either expressed in terms of the overall mass transfer coefficient, h_D, or the overall Sherwood number ($Sh_O = 2R \cdot h_D/D_C$).

The total mass flux from the surface of each sphere, Q_D, is evaluated by the summation of the products of mass flux and

area for all points on the surface.

For sphere A: $$Q_{DA} = \iint_S J_A \, dS \qquad (C\text{-}2\text{-}1)$$

For sphere B: $$Q_{DB} = \iint_S J_B \, dS \qquad (C\text{-}2\text{-}2)$$

where dS is an element of surface area.

On the other hand, the total mass fluxes from the spheres can also be expressed in terms of the total mass transfer coefficients, h_{DA} and h_{DB}, as follows:

For sphere A: $$Q_{DA} = h_{DA} S (C_s - C_o) \qquad (C\text{-}2\text{-}3)$$

For sphere B: $$Q_{DB} = h_{DB} S (C_s - C_o) \qquad (C\text{-}2\text{-}4)$$

where S is the total surface area of the spheres.

From equations (C-2-1), (C-2-3), and (C-1-1), and from equations (C-2-2), (C-2-4), and (C-1-2), the overall rates of mass transfer from the spheres, measured in terms of the overall Sherwood number coefficients, are obtained as follows:

For sphere A: $$\frac{h_{DA}}{D_C} = \frac{1}{S(C_s - C_o)} \iint_S \frac{1}{h_Z} \left(\frac{\partial C}{\partial Z}\right)_{Z=-Zs} dS \qquad (C\text{-}2\text{-}5)$$

For sphere B: $$\frac{h_{DB}}{D_C} = \frac{1}{S(C_s - C_o)} \iint_S \frac{1}{h_Z} \left(\frac{\partial C}{\partial Z}\right)_{Z=+Zs} dS \qquad (C\text{-}2\text{-}6)$$

where, for a system of two equally sized spheres dS and S are:

$$dS = \frac{a^2 \mathrm{Sin}\theta}{(\mathrm{Cosh}(\pm Zs) - \mathrm{Cos}\theta)^2} \, d\theta d\phi \ , \text{ and } S = \frac{4\pi a^2}{\mathrm{Cosh}^2(\pm Zs) - 1} \ .$$

By substitution of these values into equations(C-2-5) and (C-2-6), the overall Sherwood numbers for the two spheres are obtained as follows:

For sphere A:

$$Sh_{AO} = \left(\frac{\cosh^2(-Zs)-1}{a^*}\right) \int_0^{\pi} \left(\frac{-\sin\theta}{\cosh(-Zs)-\cos\theta}\right) \left(\frac{\partial C^*}{\partial Z}\right)_{Z=-Zs} d\theta \qquad \text{(C-2-7)}$$

For sphere B:

$$Sh_{BO} = \left(\frac{\cosh^2(+Zs)-1}{a^*}\right) \int_0^{\pi} \left(\frac{-\sin\theta}{\cosh(+Zs)-\cos\theta}\right) \left(\frac{\partial C^*}{\partial Z}\right)_{Z=+Zs} d\theta \qquad \text{(C-2-8)}$$

where Sh_{AO} and Sh_{BO} are the overall Sherwood numbers for spheres A and B, respectively.

APPENDIX D. STIMSON AND JEFFERY'S ANALYTICAL SOLUTIONS.

For steady-state creeping flow, the continuity and Navier-Stokes equations are as follows:

$$\nabla \cdot \hat{V} = 0 \tag{D-1}$$

$$\nabla P = \mu \nabla^2 \hat{V} \tag{D-2}$$

Equations(D-1) and (D-2) had been solved by Stimson and Jeffery(1926) in bi-polar coordinates(Z,θ) for the case of two equally sized spheres falling parallel to their line of centres in an incompressible Newtonian fluid. The solution in term of the Stokes stream function is given as follows:

$$\psi(Z,\theta) = (\mathrm{Cosh}Z - \mathrm{Cos}\theta)^{-3/2} \sum_{n=1} U_n(Z) V_n(\theta) \tag{D-3}$$

where,

$$U_n(Z) = A_n \mathrm{Cosh}(n-\tfrac{1}{2})Z + B_n \mathrm{Cos}(n+1.5)Z \tag{D-4}$$

$$A_n = -(2n+3)K\left[\frac{2(1-e^{-(2n+1)\alpha})+(2n+1)(e^{2\alpha}-1)}{2\mathrm{Sinh}(2n+1)\alpha + (2n+1)\mathrm{Sinh}2\alpha}\right] \tag{D-5}$$

$$B_n = (2n-1)K\left[\frac{2(1-e^{-(2n+1)\alpha})+(2n+1)(1-e^{-2\alpha})}{2\mathrm{Sinh}(2n+1)\alpha + (2n+1)\mathrm{Sinh}2\alpha}\right] \tag{D-6}$$

$$K = \frac{a^2 U(n+1)n}{\{2(2n-1)(2n+1)(2n+3)\}^{\frac{1}{2}}} \tag{D-7}$$

$$\alpha = |Zs|, \text{ surfaces of the spheres.} \tag{D-8}$$

$$V_n(\theta) = P_{n-1}(\text{Cos}\theta) - P_{n+1}(\text{Cos}\theta) \qquad \text{(D-8)}$$

P_n = Legendre function.

For the case of two fixed spheres with fluid flowing around them parallel to their line of centres, the solution of equations (D-1) and (D-2) is given as follows:

$$\psi(Z,\theta) = \tfrac{1}{2}U\left(\frac{a\text{Sin}\theta}{\text{Cosh}Z-\text{Cos}\theta}\right)^2 + (\text{Cosh}Z-\text{Cos}\theta)^{-3/2} \sum_{n=1} U_n(Z)V_n(\theta) \qquad \text{(D-10)}$$

where the first term on the right-hand-side of equation (D-10) is the stream function in the undisturbed bulk flow.

APPENDIX E. TABLES OF RESULTS.

Tables(5-5-1) to (5-5-5).

Tables(5-7-1) to (5-7-10).

Tables(6-5-1) to (6-5-10).

Table(5-5-1). Angles of flow separation for two spheres with Zs = 0.20.

	$\Delta Z = \lvert Zs/10 \rvert$, $\Delta\eta = 6^{o}$			$\Delta Z = \lvert Zs/20 \rvert$, $\Delta\eta = 6^{o}$		
Re	η_{AS}	η_{BSF}	η_{BSR}	η_{AS}	η_{BSF}	η_{BSR}
2.5	146.6	147.1		143.5	143.7	
5.0	143.1	143.2		144.2	144.8	
7.5	143.5	143.8				
10.0	143.7	143.9		146.2	146.7	
12.5	143.5	143.8				
15.0	143.3	143.7		146.9	147.5	
17.5	143.2	143.6				
20.0	143.0	143.5		147.3	147.9	
25.0	142.4	143.2		147.8	148.4	
30.0	140.1	141.9		148.7	149.3	
40.0	139.3	141.5		148.9	149.6	
50.0	137.5	140.7		148.4	149.4	
60.0	135.8	139.6		147.2	148.9	12.7
70.0	134.0	138.2		135.1	142.8	21.6
80.0	131.7	137.3		131.3	140.7	23.7
90.0	129.9	136.5		129.3	137.9	24.4
100.0	127.6	135.4		126.6	136.6	24.7
110.0	125.5	134.2		124.7	135.2	26.8
120.0	124.1	132.6	12.5	123.1	133.8	28.8
130.0	121.1	130.0	22.8	121.8	132.2	31.1
140.0	120.5	129.2	24.4	121.4	131.9	31.3
150.0	119.3	128.2	28.2	120.5	131.5	33.2
160.0	117.6	125.5	33.4	119.9	131.3	34.5
170.0	117.3	125.1	34.6	119.1	131.0	36.0
180.0	116.8	124.8	36.4	118.5	130.7	36.7
190.0	115.8	124.4	38.1	117.5	130.3	37.7
200.0	115.2	124.1	39.3	116.2	129.8	38.8
225.0	113.7	123.5	42.3	113.4	128.6	41.3
250.0	112.4	122.8	44.4	111.5	126.3	43.2
275.0	112.1	122.6	44.8	109.6	123.8	45.0
300.0	110.4	121.9	47.6	107.9	120.4	47.1
350.0	107.5	120.8	49.8	106.2	117.6	49.7
400.0	107.1	120.5	50.2			
450.0	104.0	119.5	52.5			
500.0	103.4	119.2	52.9			

Table(5-5-2). Angles of flow separation for two spheres with Zs = 1.32.

	$\Delta Z = \lvert Zs/10 \rvert$, $\Delta\eta = 6^o$			$\Delta Z = \lvert Zs/20 \rvert$, $\Delta\eta = 6^o$		
Re	η_{AS}	η_{BSF}	η_{BSR}	η_{AS}	η_{BSF}	η_{BSR}
15.0				170.6		
17.5	167.5					
20.0	161.3			168.3		
22.5	158.6					
25.0	154.6			166.1		
30.0	148.2			161.6		
40.0	140.7	169.6		147.8		
50.0	135.8	161.9		142.8		
60.0	131.5	155.7		137.4		
70.0	127.8	149.1		133.2	172.0	11.3
80.0	125.2	145.7		130.0	165.2	18.6
90.0	122.8	142.4		128.0	161.2	22.4
100.0	120.3	139.5	8.1	125.8	157.9	25.9
110.0	118.32	136.6	17.8	125.0	161.9	27.4
120.0	117.2	136.4	18.5	123.9	160.8	29.6
130.0	116.1	136.0	20.9	122.4	159.1	31.5
140.0	115.1	135.6	23.4	122.1	158.6	31.8
150.0	114.1	135.2	24.9	121.3	157.5	32.8
160.0	113.0	134.8	26.9	119.7	149.9	34.8
170.0	112.0	134.3	29.6	118.7	148.6	36.2
180.0	110.9	133.6	31.4	117.9	147.1	37.1
190.0	110.8	133.6	31.6			
200.0	109.8	133.1	32.9			
250.0	106.2	131.1	38.5			
300.0	104.7	130.4	40.2			

Table(5-5-3). Angles of flow separation for two spheres with Zs = 2.07.

	$\Delta Z = \lvert Zs/10 \rvert$, $\Delta\eta = 6^o$			$\Delta Z = \lvert Zs/20 \rvert$, $\Delta\eta = 6^o$		
Re	η_{AS}	η_{BSF}	η_{BSR}	η_{AS}	η_{BSF}	η_{BSR}
22.5	168.1					
25.0	159.5					
30.0	152.1			164.0		
35.0	148.2					
40.0	146.4			148.3		
45.0	143.1					
50.0	142.0			142.8		6.9
60.0	138.0			137.8		14.5
70.0	135.2			134.0		20.0
80.0	131.5			131.1		25.3
90.0	128.5			128.2		30.8
100.0	125.4			125.9		34.1
110.0	122.9		6.8	124.4		36.7
120.0	122.7		7.2	122.7		38.6
130.0	121.6		9.7	120.8		40.7
140.0	118.8		15.1	118.8	167.2	42.2
150.0	118.7		21.8	117.9	166.0	42.9
160.0	118.6		22.4			
170.0	118.0		25.0			
180.0	117.0		29.0			

Table(5-5-4). Angles of flow separation for two spheres with Zs = 2.48.

	$\Delta Z = \lvert Zs/10 \rvert$, $\Delta\eta = 6^o$		$\Delta Z = \lvert Zs/20 \rvert$, $\Delta\eta = 6^o$	
Re	η_{AS}	η_{BSR}	η_{AS}	η_{BSR}
25.0	170.6		173.8	
30.0	159.1		163.4	
40.0	149.4		149.3	
50.0	142.2		142.1	6.3
60.0	136.8		137.4	11.0
70.0	128.8		134.4	25.7
80.0	125.0	9.4	131.3	29.8
90.0	121.9	14.4	128.9	33.2
100.0	119.2	18.5	126.5	36.5
110.0	117.2		124.9	38.0
120.0	116.1		123.7	39.5
130.0	115.3		122.3	41.1
140.0	114.4		120.8	42.4
150.0	113.8			
160.0	113.4			
170.0	113.0			
180.0	112.7	16.6		
190.0	112.4	24.7		
200.0	112.2	26.5		
210.0	112.0	28.9		
220.0	111.8	30.5		
230.0	111.7	31.3		
240.0	111.6	31.8		
250.0	111.5	32.4		

Table(5-5-5). Angles of flow separation for two spheres with Zs = 3.09.

	$\Delta Z = \lvert Zs/10 \rvert$, $\Delta\eta=6^{o}$		$\Delta Z = \lvert Zs/20 \rvert$, $\Delta\eta=6^{o}$	
Re	η_{AS}	η_{BSR}	η_{AS}	η_{BSR}
20.0	173.3		171.2	
22.5	164.2			
25.0	157.9		157.9	
30.0	149.4		152.1	7.6
40.0	140.8		144.6	19.8
50.0	133.3	21.5	139.9	27.5
60.0	128.3	38.7	136.4	31.4
70.0	125.6	42.8	132.9	35.4
80.0	125.4	45.5	130.7	37.2
90.0	125.4	45.8	128.1	39.0
100.0	123.5	49.3	125.4	41.4
110.0	123.1	50.3	123.6	43.0
120.0	122.9	51.0	120.6	45.0
130.0	122.8	51.1	118.4	46.1
140.0	122.7	51.3	116.6	47.5
150.0	122.6	51.5	114.3	49.1

Table(5-7-1). Drag coefficients for two spheres with Zs = 0.20.
($\Delta Z = |Zs/20|$, $\Delta\eta = 6^{o}$)

Re	$\omega_\psi{}^*, \omega_g$	C_{DFA}	C_{DPA}	C_{DTA}	C_{DFB}	C_{DPB}	C_{DTB}
0.001	1.00,0.80	13859.359	7901.519	21760.879	13810.748	7440.773	21251.221
0.01	1.00,0.80	1385.7464	786.0597	2171.8061	1380.2568	739.7086	2119.9654
0.1	1.00,0.80	138.4757	77.3069	215.7827	137.7387	72.6073	210.3460
1.0	1.00,0.80	15.7137	8.3114	24.0252	13.2921	6.3193	19.6114
2.5	0.80,0.50	7.4858	4.4658	11.9516	5.9801	3.4302	9.4103
5.0	0.50,0.30	3.9735	2.5301	6.5036	2.9710	1.6045	4.5756
10.0	0.40,0.25	2.4185	1.7602	4.1787	1.6865	1.2684	2.9550
15.0	0.40,0.25	1.9739	1.4315	3.4054	1.3371	1.0013	2.3385
20.0	0.40,0.25	1.6220	1.0994	2.7214	1.0603	0.7683	1.8287
25.0	0.40,0.25	1.2656	0.9360	2.2017	0.8524	0.7344	1.5869
30.0	0.40,0.25	1.1804	0.8039	1.9844	0.7965	0.6627	1.4592
40.0	0.40,0.25	0.9607	0.6626	1.6233	0.6173	0.5044	1.1217
50.0	0.40,0.25	0.8354	0.5574	1.3929	0.5156	0.4175	0.9332
60.0	0.30,0.20	0.7334	0.4876	1.2210	0.4380	0.3522	0.7902
70.0	0.30,0.20	0.6856	0.4280	1.1137	0.3856	0.2629	0.6486
80.0	0.30,0.20	0.6219	0.3985	1.0205	0.3348	0.2215	0.5563
90.0	0.30,0.20	0.5735	0.3735	0.9470	0.2992	0.2032	0.5025
100.0	0.30,0.20	0.5365	0.3547	0.8912	0.2743	0.1925	0.4669
110.0	0.30,0.20	0.5049	0.3407	0.8457	0.2535	0.1798	0.4334
120.0	0.20,0.10	0.4755	0.3330	0.8085	0.2348	0.1676	0.4024
130.0	0.20,0.10	0.4513	0.3292	0.7811	0.2188	0.1579	0.3767
140.0	0.10,0.05	0.4214	0.3020	0.7234	0.2033	0.1457	0.3490
150.0	0.10,0.05	0.4039	0.3244	0.7283	0.1905	0.1418	0.3324
160.0	0.10,0.05	0.3846	0.3234	0.7080	0.1791	0.1342	0.3133
170.0	0.10,0.05	0.3703	0.3413	0.7117	0.1691	0.1279	0.2970
180.0	0.10,0.05	0.3561	0.3508	0.7070	0.1598	0.1203	0.2802
190.0	0.10,0.05	0.3455	0.3765	0.7221	0.1514	0.1117	0.2631
200.0	0.10,0.05	0.3376	0.4113	0.7489	0.1433	0.1005	0.2438
225.0	0.10,0.05	0.3176	0.4806	0.7983	0.1254	0.0748	0.2002
250.0	0.10,0.05	0.3000	0.5287	0.8287	0.1082	0.0389	0.1472

Table(5-7-2). Drag coefficients for two spheres with Zs = 1.32.
($\Delta Z = |Zs/20|$, $\Delta\eta = 6^{o}$)

Re	ω_ψ* , ω_g	C_{DFA}	C_{DPA}	C_{DTA}	C_{DFB}	C_{DPB}	C_{DTB}
0.001	1.00 0.80	14606.9990	7022.7204	21629.7195	14617.1312	7011.6375	21628.7682
0.01	1.00 0.80	1461.0836	702.1453	2163.2289	1461.9492	700.9800	2162.9293
0.1	1.00 0.80	147.8850	71.1841	219.0691	144.7703	68.5987	213.3690
1.0	1.00 0.80	16.3051	7.7674	24.0725	14.2159	6.6614	20.8774
2.5	0.80 0.50	7.7786	3.8925	11.6712	6.3433	3.1320	9.4753
5.0	0.50 0.30	4.4706	2.3076	6.7783	3.4401	1.7795	5.2196
10.0	0.50 0.30	2.6564	1.4196	4.0761	1.9628	1.0584	3.0213
15.0	0.50 0.30	1.9051	1.1265	3.0317	1.3265	0.7652	2.0917
20.0	0.30 0.20	1.4846	0.8092	2.2939	1.0555	0.5954	1.6509
25.0	0.30 0.20	1.2874	0.7955	2.0830	0.8579	0.5217	1.3796
30.0	0.30 0.20	1.1240	0.7058	1.8298	0.7316	0.4717	1.2034
40.0	0.30 0.20	0.9491	0.5805	1.5297	0.6118	0.4618	1.0736
50.0	0.30 0.20	0.8054	0.4969	1.3024	0.5227	0.4279	0.9506
60.0	0.30 0.20	0.7138	0.4384	1.1523	0.4616	0.3914	0.8530
70.0	0.30 0.20	0.6489	0.3966	1.0455	0.4146	0.3594	0.7740
80.0	0.30 0.20	0.5995	0.3695	0.9691	0.3770	0.3322	0.7092
90.0	0.20 0.15	0.5541	0.3509	0.9050	0.3481	0.3036	0.6454
100.0	0.20 0.15	0.5189	0.3440	0.8629	0.3131	0.2807	0.5938
110.0	0.10 0.10	0.4830	0.3359	0.8190	0.2865	0.2579	0.5444
120.0	0.10 0.10	0.4541	0.3402	0.7943	0.2645	0.2412	0.5058
130.0	0.10 0.10	0.4336	0.3621	0.7957	0.2462	0.2260	0.4722
140.0	0.05 0.05	0.4050	0.3357	0.7408	0.2287	0.2075	0.4363
150.0	0.05 0.05	0.3870	0.3673	0.7544	0.2144	0.1998	0.4142
160.0	0.05 0.05	0.3759	0.4144	0.7903	0.2028	0.1946	0.3974
170.0	0.05 0.05	0.3677	0.4574	0.8241	0.1981	0.1831	0.3749
180.0	0.05 0.05	0.3570	0.4905	0.8476	0.1809	0.1698	0.3507

Table(5-7-3). Drag coefficients for two spheres with Zs = 2.07.
($\Delta Z = |Zs/20|$, $\Delta\eta = 6^{o}$)

Re	ω_{ψ^*}, ω_g	C_{DFA}	C_{DPA}	C_{DTA}	C_{DFB}	C_{DPB}	C_{DTB}
0.001	1.00 0.80	15721.5803	8287.9309	24009.5113	15787.4513	8129.3211	23916.7725
0.01	1.00 0.80	1573.3286	826.8176	2400.1462	1579.1992	811.2530	2390.4523
0.1	1.00 0.80	157.6160	82.0900	239.7061	158.0019	80.6187	238.6206
1.0	1.00 0.80	18.1597	9.4672	27.6270	15.8949	8.1472	24.0422
2.5	0.70 0.40	7.8707	4.4388	12.3096	6.6271	3.6490	10.2761
5.0	0.40 0.25	4.3697	2.6789	7.0486	3.5650	2.2250	5.7901
10.0	0.40 0.25	2.5507	1.6064	4.1572	2.0986	1.4168	3.5155
15.0	0.40 0.25	1.8971	1.1977	3.0949	1.5598	1.0700	2.6298
20.0	0.40 0.25	1.5582	0.9795	2.5377	1.2601	0.8599	2.1201
25.0	0.40 0.25	1.3431	0.8378	2.1810	1.0697	0.7430	1.8127
30.0	0.40 0.25	1.1932	0.7378	1.9311	0.9381	0.6610	1.5992
40.0	0.40 0.25	0.9955	0.6110	1.6066	0.7612	0.5487	1.3100
50.0	0.30 0.20	0.8526	0.5276	1.3802	0.6364	0.4755	1.1120
60.0	0.30 0.20	0.7627	0.4826	1.2454	0.5584	0.4303	0.9887
70.0	0.30 0.20	0.7107	0.4680	1.1787	0.5075	0.3947	0.9022
80.0	0.30 0.20	0.6523	0.4707	1.1230	0.4611	0.3796	0.8408
90.0	0.30 0.20	0.6290	0.5346	1.1636	0.4272	0.3512	0.7784
100.0	0.30 0.20	0.5987	0.6213	1.2200	0.3931	0.3289	0.7221
110.0	0.25 0.15	0.5730	0.7213	1.2943	0.3627	0.3127	0.6754
120.0	0.25 0.15	0.5499	0.8092	1.3591	0.3337	0.2948	0.6286
130.0	0.25 0.15	0.5290	0.8881	1.4171	0.3042	0.2742	0.5822
140.0	0.20 0.15	0.5063	0.9454	1.4517	0.2704	0.2563	0.5268
150.0	0.15 0.10	0.4804	0.9513	1.4317	0.2529	0.2529	0.5064
160.0	0.10 0.05	0.4530	0.9165	1.3696	0.2359	0.2364	0.4723

Table(5-7-4). Drag coefficients for two spheres with Zs = 2.48.

($\Delta Z = |Zs/20|$, $\Delta\eta = 6^{o}$).

Re	ω_{ψ^*}, ω_g	C_{DFA}	C_{DPA}	C_{DTA}	C_{DFB}	C_{DPB}	C_{DTB}
0.001	1.00 0.80	15033.4306	7872.4978	22905.9285	15178.4670	7823.9431	23002.4102
0.01	1.00 0.80	1505.6325	787.0880	2292.7205	1519.3672	781.9425	2301.3098
0.1	1.00 0.80	151.3662	78.5653	229.9415	152.4424	77.9537	230.3961
1.0	1.00 0.80	18.0925	9.3736	27.4661	16.3326	8.4516	24.7842
2.5	0.70 0.40	7.8553	4.3653	12.2207	6.8946	3.7958	10.6904
5.0	0.50 0.30	4.3503	2.5397	6.8901	3.7670	2.2197	5.9868
10.0	0.50 0.30	2.6167	1.5648	4.1815	2.2534	1.4057	3.6591
15.0	0.50 0.30	1.9391	1.1711	3.1103	1.6592	1.0655	2.7247
20.0	0.40 0.25	1.5667	0.9542	2.5210	1.3245	0.8635	2.1880
25.0	0.40 0.25	1.3520	0.8231	2.1752	1.1267	0.7427	1.8694
30.0	0.40 0.25	1.3114	0.8129	2.1243	1.0543	0.7272	1.7816
40.0	0.40 0.25	1.1120	0.6826	1.7947	0.8695	0.6019	1.4714
50.0	0.40 0.25	0.9553	0.6351	1.5905	0.7481	0.5419	1.2901
60.0	0.40 0.25	0.8431	0.6384	1.4816	0.6504	0.4835	1.1339
70.0	0.30 0.20	0.7859	0.7366	1.5225	0.5835	0.4381	1.0217
80.0	0.30 0.20	0.7403	0.8950	1.6354	0.5323	0.4213	0.9536
90.0	0.30 0.20	0.6997	1.0319	1.7316	0.4853	0.4041	0.8895
100.0	0.30 0.20	0.6582	1.1114	1.7696	0.4445	0.3866	0.8312
110.0	0.20 0.15	0.6195	1.1596	1.7791	0.4112	0.3860	0.7972
120.0	0.10 0.10	0.5870	1.1963	1.7833	0.3810	0.3782	0.7593
130.0	0.10 0.10	0.5418	1.1043	1.6462	0.3517	0.3490	0.7008
140.0	0.10 0.10	0.5201	1.1429	1.6630	0.3285	0.3431	0.6716
150.0	0.05 0.05	0.4855	1.0659	1.5514	0.3065	0.3192	0.6257
160.0	0.05 0.05	0.4552	0.9977	1.4530	0.2873	0.2985	0.5858
170.0	0.05 0.05	0.4284	0.9358	1.3642	0.2703	0.2796	0.5499

Table(5-7-5). Drag coefficients for two spheres with Zs = 3.09.

($\Delta Z = |Zs/20|$, $\Delta\eta = 6^{o}$)

Re	ω_{ψ^*}, ω_g	C_{DFA}	C_{FPA}	C_{DTA}	C_{DFB}	C_{DPB}	C_{DTB}
0.001	1.00 0.80	16476.8832	8018.3040	24495.1870	16438.3902	8005.6204	24444.0106
0.01	1.00 0.80	1647.2863	801.6569	2448.9432	1643.4864	800.4306	2443.9170
0.1	1.00 0.80	164.5631	80.1122	244.6753	164.1736	79.9415	244.1152
1.0	0.80 0.50	19.2479	10.4051	29.6531	17.7909	9.6104	27.4014
2.5	0.50 0.30	8.6531	4.6409	13.2944	8.1119	4.4469	12.5588
5.0	0.50 0.30	4.7629	2.7228	7.4858	4.4169	2.5510	6.9679
10.0	0.50 0.30	2.8827	1.6901	4.5729	2.6200	1.5551	4.1751
15.0	0.50 0.30	2.2003	1.2416	3.4420	1.9813	1.2084	3.1897
20.0	0.50 0.30	1.8607	0.9977	2.8585	1.6783	0.9666	2.6450
25.0	0.50 0.30	1.5865	0.8849	2.4715	1.4198	0.8344	2.2543
30.0	0.50 0.30	1.4003	0.8072	2.2075	1.2395	0.7512	1.9908
40.0	0.50 0.30	1.1863	0.7504	1.9367	1.0194	0.6261	1.6455
50.0	0.30 0.20	1.0212	0.7890	1.8102	0.8730	0.5812	1.4542
60.0	0.20 0.15	0.9399	0.9879	1.9279	0.7727	0.5480	1.3207
70.0	0.20 0.15	0.8890	1.2521	2.1411	0.6986	0.5619	1.2627
80.0	0.10 0.10	0.8293	1.3953	2.2246	0.6366	0.5946	1.2312
90.0	0.10 0.10	0.7872	1.5235	2.3108	0.5895	0.6469	1.2364
100.0	0.10 0.10	0.7452	1.5897	2.3350	0.5505	0.7194	1.2700
110.0	0.10 0.10	0.6991	1.5860	2.2851	0.5180	0.8009	1.3190
120.0	0.10 0.10	0.6669	1.6138	2.2807	0.4861	0.8824	1.3685
130.0	0.10 0.10	0.6299	1.5851	2.2150	0.4509	0.9101	1.3611
140.0	0.10 0.10	0.5954	1.5465	2.1420	0.4204	0.9298	1.3503
150.0	0.10 0.05	0.5631	1.4944	2.0576	0.3901	0.9112	1.3013

Table(5-7-6) Drag coefficients for two spheres with Zs = 0.20.
($\Delta Z = |Zs/10|$, $\Delta\eta = 6^{o}$)

Re	ω_{ψ^*}, ω_g	C_{DFA}	C_{DPA}	C_{DTA}	C_{DFB}	C_{DPB}	C_{DTB}
0.001	1.00 0.80	10849.8113	3810.0517	14659.8631	10901.2203	4155.3803	15056.6002
0.01	1.00 0.80	1085.2755	384.8513	1470.1269	1090.9970	419.2379	1510.2350
0.1	1.00 0.80	118.2033	56.0603	174.2636	116.3036	53.9319	170.2355
1.0	1.00 0.80	13.6737	6.6439	20.3176	11.9996	5.4787	17.4783
2.5	0.80 0.50	6.7309	3.4949	10.2258	5.4089	2.6139	8.0229
5.0	0.50 0.30	3.8370	2.1539	5.9910	2.8669	1.4964	4.3633
7.5	0.50 0.30	2.7419	1.5860	4.3284	1.9384	0.9517	2.8901
10.0	0.50 0.30	2.2262	1.3111	3.5374	1.5141	0.7911	2.3053
12.5	0.50 0.30	1.8998	1.1206	3.0204	1.2682	0.6812	1.9495
15.0	0.50 0.30	1.6740	0.9867	2.6608	1.0926	0.5795	1.6722
17.5	0.40 0.25	1.4929	0.8729	2.3658	0.9505	0.4851	1.4357
20.0	0.30 0.20	1.3461	0.7821	2.1283	0.8383	0.4163	1.2547
22.5	0.20 0.15	1.2203	0.6997	1.9201	0.7482	0.3709	1.1191
25.0	0.20 0.15	1.1327	0.6666	1.7993	0.6780	0.3363	1.0143
30.0	0.20 0.15	1.0400	0.6189	1.6589	0.5990	0.3211	0.9200
35.0	0.10 0.10	0.9024	0.5304	1.4328	0.5174	0.2762	0.7936
40.0	0.10 0.10	0.8073	0.4996	1.3069	0.4554	0.2441	0.6996
50.0	0.10 0.10	0.7099	0.5382	1.2481	0.3724	0.1959	0.5684
60.0	0.10 0.10	0.6386	0.5881	1.2267	0.3228	0.1826	0.5054
80.0	0.10 0.10	0.5340	0.6412	1.1752	0.2583	0.1572	0.4156
100.0	0.10 0.10	0.4665	0.6608	1.1273	0.2151	0.1297	0.3449
150.0	0.10 0.10	0.3582	0.6233	0.9816	0.1437	0.0710	0.2147
200.0	0.06 0.06	0.2863	0.5291	0.8155	0.1010	0.0402	0.1413
250.0	0.04 0.04	0.2359	0.4453	0.6812	0.0776	0.0338	0.1115
300.0	0.02 0.02	0.1992	0.3748	0.5741	0.0627	0.0330	0.0957
350.0	0.02 0.02	0.1732	0.3255	0.4987	0.0517	0.0325	0.0842
400.0	0.01 0.01	0.1519	0.2806	0.4325	0.0446	0.0295	0.0742
450.0	0.01 0.01	0.1363	0.2518	0.3882	0.0379	0.0316	0.0695
500.0	0.01 0.01	0.1230	0.2241	0.3472	0.0337	0.0299	0.0637

Table(5-7-7). Drag coefficients for two spheres with Zs = 1.32.
($\Delta Z = |Zs/10|$, $\Delta\eta = 6^{o}$)

Re	ω_{ψ^*}, ω_g	C_{DFA}	C_{DPA}	C_{DTA}	C_{DFB}	C_{DPB}	C_{DTB}
0.001	1.00 0.80	14381.2595	6372.5549	20753.8145	14307.8766	6421.3984	20729.2750
0.01	1.00 0.80	1437.2063	637.4898	2074.6962	1430.2022	642.5788	2072.7810
0.1	1.00 0.80	143.3138	63.8835	207.1973	142.7738	64.5178	207.2916
1.0	1.00 0.80	16.6161	8.1718	24.7880	14.6344	7.2537	21.8881
2.5	0.60 0.40	7.5968	4.1079	11.7047	6.1838	3.2906	9.4744
5.0	0.50 0.30	4.3321	2.4349	6.7670	3.4468	1.9964	5.4433
7.5	0.50 0.30	3.1404	1.7635	4.9039	2.4323	1.3854	3.8178
10.0	0.50 0.30	2.5378	1.4180	3.9558	1.9137	1.1002	3.0139
12.5	0.50 0.30	2.2181	1.1674	3.3855	1.6250	0.9094	2.5344
15.0	0.50 0.30	1.9113	1.0256	2.9369	1.3696	0.7613	2.1309
17.5	0.40 0.25	1.7028	0.9314	2.6342	1.1940	0.6776	1.8716
20.0	0.40 0.25	1.5506	0.8642	2.4148	1.0683	0.6238	1.6922
22.5	0.30 0.20	1.4165	0.7982	2.2148	0.9656	0.5730	1.5386
25.0	0.30 0.20	1.3184	0.7694	2.0878	0.8872	0.5384	1.4256
30.0	0.30 0.20	1.1763	0.7556	1.9319	0.7706	0.4850	1.2557
40.0	0.20 0.15	0.9896	0.8436	1.8332	0.6131	0.4031	1.0163
50.0	0.20 0.15	0.8676	0.9322	1.7999	0.5173	0.3654	0.8828
60.0	0.20 0.15	0.7825	0.9860	1.7686	0.4522	0.3396	0.7918
80.0	0.20 0.15	0.6544	0.9965	1.6510	0.3529	0.2989	0.6519
100.0	0.20 0.15	0.5550	0.9244	1.4794	0.2810	0.2787	0.5598
120.0	0.10 0.10	0.4732	0.8212	1.2945	0.2299	0.2670	0.4969
140.0	0.06 0.06	0.4120	0.7346	1.1466	0.1992	0.2634	0.4625
150.0	0.04 0.04	0.3866	0.6944	1.0810	0.1861	0.2578	0.4439
200.0	0.02 0.02	0.2983	0.5597	0.8580	0.1408	0.2516	0.3924
250.0	0.02 0.02	0.2440	0.4713	0.7153	0.1135	0.2574	0.3710
300.0	0.01 0.01	0.2044	0.3967	0.6011	0.0954	0.2465	0.3419

Table(5-7-8). Drag coefficients for two spheres with Zs = 2.07.

($\Delta Z = |Zs/10|$, $\Delta\eta = 6^{o}$)

Re	ω_{ψ^*}, ω_g	C_{DFA}	C_{DPA}	C_{DTA}	C_{DFB}	C_{DPB}	C_{DTB}
0.001	1.00 0.80	14505.4272	7276.5202	21781.9474	14550.8926	7228.6553	21779.5469
0.01	1.00 0.80	1451.2047	727.2688	2178.2688	1455.5387	722.3004	2177.8391
0.1	1.00 0.80	145.4019	72.4000	217.8019	145.7338	71.9528	217.6866
1.0	1.00 0.80	17.0813	8.5093	25.5906	15.3290	7.7070	23.0360
2.5	0.80 0.50	7.6149	3.9842	11.5991	6.6126	3.4993	10.1120
5.0	0.50 0.30	4.2184	2.3197	6.5382	3.5737	1.9918	5.5655
7.5	0.50 0.30	3.1000	1.7155	4.8156	2.5895	1.4683	4.0579
10.0	0.40 0.25	2.4862	1.3777	3.8640	2.0443	1.1621	3.2065
12.5	0.40 0.25	2.1658	1.1910	3.3568	1.7408	0.9777	2.7185
15.0	0.40 0.25	1.8908	1.0630	2.9538	1.5012	0.8588	2.3601
17.5	0.40 0.25	1.7029	0.9928	2.6957	1.3426	0.7843	2.1269
20.0	0.40 0.25	1.5660	0.9575	2.5235	1.2199	0.7145	1.9345
22.5	0.40 0.25	1.4643	0.9576	2.4219	1.1217	0.6564	1.7782
25.0	0.40 0.25	1.3930	1.0054	2.3985	1.0411	0.6044	1.6455
30.0	0.30 0.20	1.2579	1.1231	2.3810	0.9023	0.5420	1.4443
35.0	0.20 0.15	1.1388	1.1754	2.3143	0.7941	0.5062	1.3003
40.0	0.10 0.10	1.0304	1.1614	2.1918	0.7069	0.4617	1.1686
45.0	0.10 0.10	0.9614	1.1967	2.1581	0.6465	0.4514	1.0979
50.0	0.06 0.06	0.8837	1.1412	2.0250	0.5891	0.4195	1.0086
60.0	0.06 0.06	0.7757	1.1138	1.8896	0.5111	0.4219	0.9331
80.0	0.06 0.06	0.6382	1.0394	1.6777	0.4208	0.4679	0.8887
100.0	0.06 0.06	0.5424	0.9424	1.4848	0.3644	0.5386	0.9031
120.0	0.02 0.02	0.4622	0.8207	1.2829	0.3162	0.5405	0.8568
140.0	0.02 0.02	0.4033	0.7362	1.1396	0.2857	0.5994	0.8852
150.0	0.01 0.01	0.3768	0.6883	1.0651	0.2675	0.5663	0.8338
160.0	0.01 0.01	0.3535	0.6460	0.9996	0.2514	0.5473	0.7988
170.0	0.01 0.01	0.3338	0.6121	0.9460	0.2398	0.5377	0.7776
180.0	0.01 0.01	0.3171	0.5870	0.9040	0.2317	0.5303	0.7621

Table(5-7-9). Drag coefficients for two spheres with Zs = 2.48.

($\Delta Z = |Zs/10|$, $\Delta\eta = 6^{o}$)

Re	ω_{ψ^*}, ω_g	C_{DFA}	C_{DPA}	C_{DTA}	C_{DFB}	C_{DPB}	C_{DTB}
0.001	1.00 0.80	12536.5133	6207.2107	18743.7244	12628.3063	6237.1321	18865.4383
0.01	1.00 0.80	1254.8536	621.1800	1876.0337	1263.9118	624.0446	1887.9583
0.1	1.00 0.80	130.2453	64.4085	194.6539	128.0635	61.3363	189.3999
1.0	0.90 0.75	15.2650	7.5806	22.8457	13.9335	6.9900	20.9236
2.5	0.80 0.50	6.8379	3.4009	10.2388	6.0797	3.0434	9.1231
5.0	0.50 0.30	3.7150	1.9957	5.7107	3.2336	1.7306	4.9643
10.0	0.50 0.30	2.2310	1.2486	3.4796	1.8858	1.0510	2.9369
15.0	0.50 0.30	1.6944	0.9828	2.6773	1.4190	0.8081	2.2272
20.0	0.50 0.30	1.4123	0.9177	2.3300	1.1621	0.6566	1.8188
25.0	0.50 0.30	1.2693	1.0360	2.3053	0.9861	0.5579	1.5541
30.0	0.30 0.20	1.1431	1.1251	2.2682	0.8625	0.5366	1.3992
40.0	0.30 0.20	0.9705	1.1961	2.1667	0.7001	0.5170	1.2171
50.0	0.30 0.20	0.8488	1.1831	2.0319	0.6087	0.5705	1.1793
60.0	0.30 0.20	0.7418	1.1052	1.8470	0.5414	0.6428	1.1842
80.0	0.20 0.15	0.5966	0.9650	1.5605	0.3896	0.6189	1.0086
100.0	0.20 0.15	0.4928	0.8368	1.3296	0.3422	0.7453	1.0876
120.0	0.20 0.15	0.4158	0.7199	1.1357	0.3018	0.7336	1.0354
140.0	0.10 0.10	0.3603	0.6342	0.9946	0.2743	0.7256	1.0000
150.0	0.10 0.10	0.3385	0.6000	0.9385	0.2600	0.7118	0.9718
160.0	0.10 0.10	0.3192	0.5697	0.8889	0.2445	0.6876	0.9321
180.0	0.08 0.08	0.2878	0.5226	0.8104	0.2092	0.6221	0.8313
200.0	0.06 0.06	0.2610	0.4787	0.7398	0.1802	0.5520	0.7323
220.0	0.06 0.06	0.2386	0.4253	0.6801	0.1580	0.4959	0.6539
240.0	0.04 0.04	0.2197	0.4089	0.6286	0.1405	0.4496	0.5901
250.0	0.04 0.04	0.2113	0.3945	0.6058	0.1331	0.4304	0.5635

Table(5-7-10). Drag coefficients for two spheres with Zs = 3.09.

($\Delta Z = |Zs/10|$, $\Delta\eta = 6^{o}$)

Re	ω_{ψ^*}, ω_g	C_{DFA}	C_{DPA}	C_{DTA}	C_{DFB}	C_{DPB}	C_{DTB}
0.001	1.00 0.80	16973.1418	8179.5579	25152.6997	16965.3059	8070.1682	25035.4742
0.01	1.00 0.80	1697.7022	816.9335	2514.6358	1696.6237	806.1358	2502.7623
0.1	1.00 0.80	169.9186	79.8014	249.2010	169.0169	78.5502	247.5671
1.0	1.00 0.80	19.8887	9.4823	29.3710	18.8448	9.0937	27.9386
2.5	0.80 0.50	8.9352	4.4840	13.4193	8.3280	4.1904	12.5185
5.0	0.50 0.30	5.0674	2.7138	7.7812	4.6393	2.4735	7.1128
7.5	0.40 0.25	3.7742	2.1064	5.8806	3.3858	1.8355	5.2213
10.0	0.40 0.25	3.1204	1.8721	4.9925	2.7630	1.5471	4.3102
12.5	0.40 0.25	2.7625	1.8859	4.6485	2.4161	1.4033	3.8195
15.0	0.40 0.25	2.5525	2.1261	4.6786	2.1324	1.3196	3.4521
17.5	0.40 0.25	2.3628	2.2767	4.6396	1.9148	1.3293	3.2442
20.0	0.40 0.25	2.2033	2.3499	4.5533	1.7478	1.3661	3.1140
22.5	0.30 0.25	2.0578	2.3605	4.4184	1.6181	1.4410	3.0592
25.0	0.30 0.25	1.9392	2.3545	4.2938	1.5247	1.5674	3.0922
30.0	0.30 0.25	1.7275	2.2626	3.9902	1.3705	1.7394	3.1100
40.0	0.10 0.10	1.3918	1.9818	3.3737	1.1407	1.7638	2.9045
50.0	0.08 0.08	1.1658	1.7389	2.9047	0.9233	1.5408	2.4642
60.0	0.06 0.06	1.0009	1.5316	2.5326	0.7271	1.2477	1.9749
70.0	0.04 0.04	0.8668	1.3460	2.2129	0.5965	1.0344	1.6309
80.0	0.02 0.02	0.7595	1.1804	1.9399	0.5194	0.9018	1.4213
90.0	0.01 0.01	0.6756	1.0509	1.7265	0.4606	0.8004	1.2611
100.0	0.01 0.01	0.6137	0.9752	1.5890	0.4090	0.7290	1.1381
110.0	0.01 0.01	0.5605	0.8957	1.4563	0.3710	0.6678	1.0388
120.0	0.01 0.01	0.5157	0.8281	1.3438	0.3396	0.6161	0.9557
130.0	0.005 0.005	0.4765	0.7660	1.2425	0.3134	0.5696	0.8831
140.0	0.005 0.005	0.4429	0.7129	1.1558	0.2910	0.5299	0.8209
150.0	0.005 0.005	0.4140	0.6678	1.0818	0.2715	0.4960	0.7676

Table(6-5-1). Overall Sherwood numbers for two spheres with Zs = 0.20.

($\Delta Z = |Zs/20|$, $\Delta\eta = 6^{o}$)

	Re = 0.001			Re = 1.0			Re = 10.0			Re = 100.0		
Pe	ω_{C*}	Sh_{AO}	Sh_{BO}	ω_{C*}	Sh_{AO}	Sh_{BO}	ω_{C*}	Sh_{AO}	Sh_{BO}	ω_{C*}	Sh_{AO}	Sh_{BO}
0.001	0.80	1.4725	1.4809	0.80	1.4725	1.4809	0.80	1.4725	1.4808	0.80	1.4726	1.4808
0.01	0.80	1.4748	1.4830	0.80	1.4752	1.4834	0.80	1.4753	1.4833	0.80	1.4753	1.4833
0.1	0.70	1.5090	1.5020	0.70	1.5113	1.5029	0.70	1.5185	1.5026	0.70	1.5227	1.5009
1.0	0.50	1.7606	1.5037	0.50	1.7802	1.5028	0.50	1.8627	1.4981	0.50	1.9218	1.4922
2.4	0.30	2.0295	1.5552	0.30	2.0484	1.5481	0.30	2.2212	1.5591	0.30	2.3599	1.5746
5.0	0.30	2.4071	1.7104	0.30	2.4610	1.7011	0.30	2.7269	1.7470	0.30	2.9675	1.8196
10.0	0.30	2.8706	1.9552	0.30	2.9393	1.9369	0.20	3.2493	1.9137	0.30	3.6296	2.0494
20.0	0.20	3.3857	2.1812	0.15	3.4285	2.0818	0.20	3.9613	2.2512	0.10	4.2884	2.2624
30.0	0.20	3.7812	2.4208	0.15	3.8541	2.3077	0.20	4.4418	2.5077	0.10	5.0339	2.5533
50.0	0.20	4.3533	2.7692	0.10	4.3905	2.5148	0.10	5.0782	2.7099	0.10	5.8966	2.9546
70.0	0.10	4.6503	2.8659	0.10	4.8467	2.7765	0.05	5.3780	2.7683	0.05	6.4547	3.0898
100.0	0.05	5.0021	2.9502	0.05	5.1215	2.8456	0.05	6.0813	2.9792	0.05	6.8040	3.1209
150.0	0.05	5.7444	3.2349	0.05	5.9048	3.1220	0.05	6.8480	3.3220	0.05	8.1445	3.1970
200.0	0.05	6.2402	3.5402	0.05	6.4168	3.4196	0.05	7.4799	3.6798	0.05	9.6639	3.3210
250.0	0.05	6.6224	3.7811	0.05	6.7968	3.6318	0.05	8.0656	4.0233	0.05	11.3509	3.5245
300.0	0.05	6.9749	4.0145	0.05	7.1837	3.8756	0.05	8.5544	4.1942	0.05	12.6378	3.6935
400.0	0.05	7.6060	4.4318	0.05	7.8572	4.2779	0.05	9.6930	4.6390	0.05	15.1210	4.0857
500.0	0.05	8.0799	4.7059	0.05	8.4066	4.5418	0.05	10.7916	4.8975	0.05	16.6059	4.3403

Table(6-5-2). Overall Sherwood numbers for two spheres with Zs = 1.32.

($\Delta Z = |Zs/20|, \Delta\eta = 6^{o}$).

	Re = 0.001			Re = 1.0			Re = 10.0			Re = 100.0		
Pe	ω_{C*}	Sh_{AO}	Sh_{BO}	ω_{C*}	Sh_{AO}	Sh_{BO}	ω_{C*}	Sh_{AO}	Sh_{BO}	ω_{C*}	Sh_{AO}	Sh_{BO}
0.001	0.80	1.8929	1.8879	0.80	1.8929	1.8879	0.80	1.8930	1.8878	0.80	1.8930	1.8878
0.01	0.80	1.8925	1.8875	0.80	1.8925	1.8874	0.80	1.8925	1.8874	0.80	1.8925	1.8874
0.1	0.70	1.8841	1.8721	0.70	1.8846	1.8723	0.70	1.8858	1.8690	0.70	1.8868	1.8656
1.0	0.50	2.0573	1.7860	0.50	2.0759	1.7817	0.50	2.1502	1.7688	0.50	2.1908	1.7653
2.4	0.30	2.3179	1.8134	0.30	2.3574	1.8062	0.30	2.5244	1.8237	0.30	2.6290	1.8561
5.0	0.30	2.7358	2.0178	0.30	2.7927	2.0057	0.25	3.0085	2.0255	0.25	3.1925	2.1205
10.0	0.25	3.1705	2.2747	0.25	3.2452	2.2551	0.25	3.5739	2.3725	0.25	3.8662	2.5374
20.0	0.20	3.7107	2.6114	0.20	3.8075	2.5871	0.20	4.2297	2.7363	0.20	4.6846	3.0096
30.0	0.20	4.0932	2.9028	0.20	4.2121	2.8800	0.20	4.6881	3.0543	0.10	5.2585	3.3728
50.0	0.20	4.6495	3.3116	0.20	4.7730	3.2511	0.20	5.3475	3.5491	0.10	6.1099	3.7711
70.0	0.05	4.7977	3.3664	0.10	5.1278	3.4163	0.05	5.6532	3.6237	0.10	6.8391	4.1353
100.0	0.05	5.4109	3.6278	0.05	5.5212	3.5705	0.05	6.3073	3.8866	0.05	7.8783	4.5436
150.0	0.05	6.0650	3.9990	0.05	6.2677	4.0058	0.05	7.1010	4.2863	0.05	9.7011	4.8608
200.0	0.05	6.4581	4.2399	0.05	6.7219	4.3055	0.05	7.8186	4.6659	0.04	11.8098	5.1749
250.0	0.05	6.9361	4.5988	0.05	7.1379	4.5775	0.05	8.5145	4.9503	0.04	12.9151	5.2912
300.0	0.04	7.3033	4.7985	0.05	7.5227	4.8186	0.05	9.2454	5.1933	0.04	14.4099	5.5468
400.0				0.05	8.3209	5.2872	0.05	10.8938	5.6349	0.04	16.2257	5.8329
500.0				0.05	9.0211	5.5711	0.05	12.7151	6.0293	0.04	17.6917	6.1679

Table(6-5-3). Overall Sherwood numbers for two spheres with Zs = 2.07.

($\Delta Z = |Zs/20|, \Delta\eta = 6^{o}$)

	Re = 0.001			Re = 1.0			Re = 10.0			Re = 100.0		
Pe	ω_{C*}	Sh_{AO}	Sh_{BO}	ω_{C*}	Sh_{AO}	Sh_{BO}	ω_{C*}	Sh_{AO}	Sh_{BO}	ω_{C*}	Sh_{AO}	Sh_{BO}
0.001	0.80	1.9735	1.9687	0.80	1.9735	1.9687	0.80	1.9735	1.9687	0.80	1.9735	1.9687
0.01	0.80	1.9726	1.9679	0.80	1.9726	1.9679	0.80	1.9726	1.9678	0.80	1.9724	1.9676
0.1	0.80	1.9622	1.9431	0.80	1.9630	1.9422	0.80	1.9643	1.9395	0.80	1.9653	1.9419
1.0	0.80	2.2661	1.9829	0.70	2.2973	1.9836	0.70	2.3435	2.0046	0.40	2.3093	1.9318
2.4	0.50	2.5386	2.1596	0.50	2.5899	2.1609	0.30	2.5484	2.0847	0.25	2.6997	2.0940
5.0	0.30	2.7900	2.3070	0.30	2.8701	2.3099	0.20	2.9795	2.2801	0.20	3.2435	2.4324
10.0	0.20	3.2141	2.6028	0.20	3.3185	2.6027	0.15	3.5160	2.6513	0.20	3.9243	2.9732
20.0	0.15	3.7659	3.0280	0.15	3.8983	3.0319	0.15	4.1673	3.1782	0.15	4.7530	3.5373
30.0	0.10	4.0662	3.2577	0.15	4.2848	3.3458	0.10	4.5928	3.5251	0.15	5.3660	3.9494
50.0	0.10	4.6936	3.7300	0.05	4.7722	3.5756	0.05	5.0852	3.8192	0.10	6.4097	4.4600
70.0	0.05	4.9217	3.9096	0.05	5.2128	3.9062	0.05	5.6297	4.1412	0.10	7.4407	4.8566
100.0	0.05	5.5046	4.3092	0.05	5.7338	4.2620	0.05	6.2247	4.5015	0.05	9.1387	5.2353
150.0	0.05	6.1407	4.7414	0.05	6.3732	4.7298	0.05	7.1656	4.9674	0.04	11.8959	5.6438
200.0	0.05	6.6115	5.1343	0.05	6.9224	5.1043	0.04	8.1196	5.3371	0.04	12.3629	5.6407
250.0	0.05	7.0489	5.4232	0.05	7.4653	5.3954	0.04	9.1720	5.6195	0.04	12.9520	5.6610
300.0	0.04	7.4446	5.6203	0.05	8.0167	5.6348	0.04	10.3177	5.8691	0.04	13.9373	5.7581
400.0	0.04	8.4260	6.0145	0.05	9.2206	6.0205	0.04	12.8268	6.2808	0.04	15.9366	6.2469
500.0	0.04	9.3737	6.3584	0.05	10.5342	6.3573	0.04	14.7548	6.6787	0.04	17.0903	6.8264

Table(6-5-4). Overall Sherwood numbers for two spheres with Zs = 2.48.

($\Delta Z = |Zs/20|$, $\Delta\eta = 6^{o}$).

	Re = 0.001			Re = 1.0			Re = 10.0			Re = 100.0		
Pe	ω_{C*}	Sh_{AO}	SH_{BO}	ω_{C*}	Sh_{AO}	Sh_{BO}	ω_{C*}	Sh_{AO}	Sh_{BO}	ω_{C*}	Sh_{AO}	Sh_{BO}
0.001	0.80	2.0040	2.0000	0.80	2.0044	1.9997	0.80	2.0044	1.9997	0.80	2.0044	1.9997
0.01	0.80	2.0026	1.9987	0.80	2.0028	1.9981	0.80	2.0028	1.9981	0.80	2.0028	1.9982
0.1	0.80	1.9899	1.9723	0.80	1.9909	1.9708	0.80	1.9920	1.9685	0.80	1.9930	1.9665
1.0	0.80	2.2846	2.0641	0.50	2.2902	2.0204	0.70	2.3586	2.0871	0.40	2.3516	2.0379
2.4	0.40	2.4693	2.1759	0.30	2.5010	2.1370	0.30	2.5959	2.2142	0.30	2.7335	2.2799
5.0	0.25	2.7586	2.3845	0.20	2.8289	2.3581	0.20	2.9999	2.4780	0.20	3.2436	2.6373
10.0	0.25	3.2219	2.7911	0.20	3.3376	2.7927	0.20	3.5574	2.9439	0.20	3.9404	3.1761
20.0	0.10	3.6276	3.1206	0.15	3.8839	3.2316	0.15	4.1754	3.4336	0.15	4.8251	3.7756
30.0	0.10	4.0651	3.4380	0.15	4.2698	3.5599	0.15	4.5854	3.7721	0.15	5.5513	4.2911
50.0	0.10	4.6173	3.8974	0.10	4.8211	3.9628	0.15	5.2262	4.3434	0.15	6.9328	4.7543
70.0	0.10	5.0003	4.2474	0.10	5.2269	4.2991	0.10	5.6847	4.5869	0.10	8.5036	5.1641
100.0	0.05	5.3930	4.5626	0.05	5.6525	4.6163	0.04	6.2909	4.8582	0.05	10.3937	5.6388
150.0	0.05	6.0254	4.9721	0.05	6.3951	5.1235	0.04	7.5931	5.2930	0.05	12.4773	6.3251
200.0	0.05	6.5241	5.3433	0.04	6.9604	5.3978	0.04	8.9787	5.7434	0.05	13.8443	7.1130
250.0	0.05	7.0355	5.6257	0.04	7.6865	5.6430	0.04	10.4849	6.1206	0.05	14.8149	7.9835
300.0	0.05	7.5619	5.8642	0.04	8.4416	5.9296	0.04	12.0050	6.4885	0.05	15.5513	8.9114
400.0	0.05	8.7562	6.3378	0.04	10.0915	6.3887	0.04	14.5287	7.2373	0.05	16.6113	10.8438
500.0	0.05	10.0114	6.7586	0.04	11.3989	6.8822	0.04	16.0824	8.1392	0.05	17.3391	12.9881

Table(6-5-5). Overall Sherwood numbers for two spheres with Zs = 3.09.

($\Delta Z = |Zs/20|$, $\Delta\eta = 6^{o}$)

	Re = 0.001			Re = 1.0			Re = 10.0			Re = 100.0		
Pe	ω_{C*}	Sh_{AO}	Sh_{BO}	ω_{C*}	Sh_{AO}	Sh_{BO}	ω_{C*}	Sh_{AO}	Sh_{BO}	ω_{C*}	Sh_{AO}	Sh_{BO}
0.001	0.80	2.0471	2.0431	0.80	2.0471	2.0431	0.80	2.0471	2.0431	0.80	2.0471	2.0431
0.01	0.80	2.0414	2.0375	0.80	2.0409	2.0370	0.80	2.0407	2.0367	0.80	2.0400	2.0360
0.1	0.80	2.0253	2.0110	0.80	2.0257	2.0100	0.70	2.0268	2.0133	0.60	2.0277	2.0169
1.0	0.60	2.2892	2.1283	0.60	2.3221	2.1413	0.40	2.3318	2.1251	0.50	2.3979	2.1851
2.4	0.30	2.4728	2.2825	0.30	2.5303	2.3069	0.25	2.6289	2.3547	0.30	2.7870	2.4901
5.0				0.25	2.9204	2.6317	0.25	3.1256	2.8356	0.25	3.3518	2.9597
10.0	0.25	3.2858	3.0050	0.25	3.3843	3.0477	0.20	3.6117	3.2425	0.25	4.0549	3.5265
20.0	0.10	3.7331	3.4187	0.10	3.8761	3.4693	0.15	4.2439	3.7694	0.20	5.1156	4.1575
30.0	0.10	4.1362	3.7523	0.10	4.2804	3.8046	0.15	4.6772	4.1466	0.20	6.1415	4.6768
50.0	0.10	5.0063	4.5376	0.10	4.8527	4.2999	0.10	5.4029	4.7135	0.10	8.4107	5.4622
70.0	0.05	5.0063	4.5376	0.10	5.2612	4.6438	0.10	6.0778	5.0356	0.10	10.0869	6.3358
100.0	0.05	5.5036	4.9079	0.10	5.8410	5.0413	0.05	7.2061	5.5316	0.10	11.4495	7.7738
150.0	0.05	6.3305	6.0432	0.05	6.8377	6.1462	0.05	9.5730	6.4647	0.05	12.7111	10.5650
200.0	0.05	7.1273	6.5827	0.05	7.9551	6.8191	0.05	11.9561	8.7574	0.05	13.5036	13.6448
250.0	0.05	8.0359	7.1743	0.05	9.2108	7.5457	0.04	12.7570	9.6098	0.05	14.0773	16.7084
300.0	0.05	10.1029	8.5713	0.05	10.5438	8.3296	0.04	13.6579	10.8306	0.05	14.5122	17.6828
400.0	0.05	11.2107	9.3234	0.05	13.3007	10.1380	0.04	15.0669	13.2085	0.05	15.1823	18.2884
500.0				0.05	15.2440	12.0942	0.04	16.1793	15.5447	0.05	15.6098	18.8208

Table(6-5-6). Overall Sherwood numbers for two spheres with Zs = 0.20.

($\Delta Z = |Zs/10|$, $\Delta\eta = 6^{o}$)

	Re = 0.001			Re = 1.0			Re = 10.0			Re = 100.0		
Pe	ω_{C*}	Sh_{AO}	Sh_{BO}	ω_{C*}	Sh_{AO}	Sh_{BO}	ω_{C*}	Sh_{AO}	Sh_{BO}	ω_{C*}	Sh_{AO}	Sh_{BO}
0.001	0.80	1.6307	1.6248	0.80	1.6307	1.6248	0.80	1.6307	1.6247	0.80	1.6308	1.6247
0.01	0.80	1.6262	1.6207	0.80	1.6262	1.6207	0.80	1.6257	1.6201	0.80	1.6248	1.6191
0.1	0.80	1.6122	1.5901	0.80	1.6132	1.5886	0.80	1.6156	1.5846	0.80	1.6174	1.5808
1.0	0.80	1.8538	1.6013	0.80	1.8823	1.6012	0.80	1.9475	1.6030	0.80	1.9963	1.6019
2.4	0.50	2.1283	1.7033	0.80	2.2064	1.7380	0.80	2.3371	1.7574	0.80	2.4483	1.7810
5.0	0.30	2.4395	1.8302	0.50	2.5559	1.8842	0.50	2.7598	1.9221	0.30	2.9410	1.9409
10.0	0.20	2.8257	2.0118	0.30	2.9721	2.0711	0.30	3.2578	2.1287	0.20	3.5919	2.2049
20.0				0.20	3.4914	2.3334	0.20	3.8724	2.4093	0.20	4.5524	2.6005
30.0	0.15	3.6697	2.5064	0.20	3.8631	2.5678	0.30	4.3252	2.6514	0.20	5.4298	2.8829
50.0	0.15	4.1625	2.8455	0.20	4.3961	2.8931	0.20	5.0986	2.9878	0.20	7.2101	3.2541
70.0	0.15	4.5486	3.1069	0.20	4.8469	3.1482	0.15	5.8548	3.2241	0.15	8.3243	3.5135
100.0	0.10	5.0515	3.3687	0.10	5.4549	3.3843	0.10	7.1116	3.4892	0.10	9.3751	3.7519
150.0	0.10	5.8663	3.7337	0.10	6.5348	3.7415	0.10	9.0847	3.8656	0.05	10.4714	4.0144
200.0	0.05	6.6516	3.9109	0.05	7.6224	3.9189	0.05	10.2651	4.0703	0.05	11.2103	4.1760
250.0	0.05	7.6024	4.1458	0.05	8.8272	4.1553	0.05	11.1710	4.3117	0.05	11.7565	4.3943
300.0	0.05	8.4921	4.3267	0.05	9.7655	4.3542	0.05	11.8625	4.5126	0.05	12.1642	4.5740
400.0	0.05	10.1052	4.6835				0.05	12.9111	4.8417	0.05	12.7484	4.8244
500.0							0.05	13.6631	5.1114	0.05	13.1668	5.0557

Table(6-5-7). Overall Sherwood numbers for two spheres with Zs = 1.32.

($\Delta Z = |Zs/10|$, $\Delta\eta = 6^{o}$)

	Re = 0.001			Re = 1.0			Re = 10.0			Re = 100.0		
Pe	ω_{C^*}	Sh_{AO}	Sh_{BO}	ω_{C^*}	Sh_{AO}	Sh_{BO}	ω_{C^*}	Sh_{AO}	Sh_{BO}	ω_{C^*}	Sh_{AO}	Sh_{BO}
0.001	0.80	1.8666	1.8630	0.80	1.8666	1.8630	0.80	1.8667	1.8630	0.80	1.8667	1.8629
0.01	0.80	1.8650	1.8615	0.80	1.8653	1.8618	0.80	1.8651	1.8614	0.80	1.8645	1.8608
0.1	0.80	1.8603	1.8345	0.80	1.8613	1.8340	0.80	1.8641	1.8299	0.80	1.8662	1.8262
1.0	0.80	2.1532	1.8310	0.80	2.1743	1.8273	0.80	2.2411	1.8350	0.80	2.2897	1.8496
2.4	0.50	2.4739	1.9784	0.50	2.5144	1.9732	0.50	2.6407	2.0100	0.50	2.7475	2.0746
5.0	0.25	2.8165	2.1433	0.25	2.8573	2.1130	0.25	3.0510	2.1768	0.20	3.2432	2.2694
10.0	0.25	3.2423	2.4398	0.25	3.3235	2.4362	0.25	3.5816	2.5324	0.20	3.9976	2.7044
20.0	0.20	3.7588	2.8188	0.20	3.8534	2.7727	0.20	4.2386	2.8932	0.20	5.2788	3.2175
30.0	0.20	4.1032	3.0619	0.20	4.2298	3.0320	0.20	4.8049	3.1682	0.20	6.6525	3.5273
50.0	0.20	4.6805	3.4343	0.20	4.8949	3.4086	0.20	6.0002	3.5534	0.20	8.2670	3.9737
70.0	0.15	5.2095	3.6896	0.20	5.5455	3.6878	0.20	7.4121	3.8400	0.15	9.1043	4.2786
100.0	0.10	6.0452	3.9623	0.15	6.6369	3.9787	0.15	9.0143	4.1484	0.10	9.8723	4.6313
150.0	0.10	7.6895	4.3380	0.10	8.6450	4.3178	0.10	10.5248	4.5130	0.10	10.6668	5.1855
200.0	0.05	9.0215	4.5369	0.05	9.9174	4.5225	0.05	11.4486	4.7476	0.05	11.1441	5.8276
250.0	0.05	10.2918	4.7828	0.05	10.9423	4.7762	0.05	12.1457	5.0100	0.05	11.4597	6.3714
300.0	0.05	11.1213	5.0202	0.05	11.6727	5.0074	0.05	12.6680	5.2571	0.05	11.7092	6.9368
400.0	0.05	12.3398	5.4329	0.05	12.7609	5.4141	0.05	13.4343	5.6956	0.05	12.0724	8.1375
500.0	0.05	13.1817	5.8108	0.05	13.5187	5.7532	0.05	13.9648	6.0973	0.05	12.3280	9.2361

Table(6-5-8). Overall Sherwood numbers for two spheres with Zs = 2.07.

($\Delta Z = |Zs/10|$, $\Delta\eta = 6^{o}$)

	Re = 0.001			Re = 1.0			Re = 10.0			Re = 100.0		
Pe	ω_{C*}	Sh_{AO}	Sh_{BO}	ω_{C*}	Sh_{AO}	Sh_{BO}	ω_{C*}	Sh_{AO}	Sh_{BO}	ω_{C*}	Sh_{AO}	Sh_{BO}
0.001	0.80	1.9515	1.9487	0.80	1.9513	1.9484	0.80	1.9516	1.9486	0.80	1.9516	1.9486
0.01	0.80	1.9501	1.9472	0.80	1.9496	1.9468	0.80	1.9501	1.9472	0.80	1.9497	1.9467
0.1	0.80	1.9463	1.9207	0.80	1.9477	1.9186	0.80	1.9501	1.9166	0.80	1.9512	1.9149
1.0	0.80	2.2850	2.0100	0.80	2.3176	2.0144	0.80	2.3635	2.0334	0.80	2.3907	2.0465
2.4	0.50	2.5484	2.1852	0.50	2.6027	2.1947	0.50	2.6942	2.2432	0.80	2.7857	2.3092
5.0	0.25	2.8652	2.4776	0.30	2.9212	2.4045	0.30	3.0789	2.5021	0.25	3.2594	2.5274
10.0	0.25	3.2316	2.7113	0.20	3.3313	2.7015	0.20	3.5658	2.8245	0.25	4.0723	2.9694
20.0	0.20	3.7361	3.1294	0.20	3.8741	3.1183	0.15	4.3399	3.2479	0.15	5.6786	3.4361
30.0	0.15	4.0936	3.3474	0.15	4.3161	3.3661	0.15	5.1313	3.5309	0.15	7.1168	3.7995
50.0	0.15	4.8305	3.7134	0.15	5.2409	3.7297	0.15	7.0770	3.9313	0.15	8.3991	4.4308
70.0	0.10	5.5951	3.9656	0.10	6.2877	3.9842	0.10	8.4473	4.2585	0.10	9.0431	5.0522
100.0	0.10	6.9688	4.2970	0.05	7.7983	4.2799	0.10	9.6356	4.7751	0.10	9.5210	6.1263
150.0	0.10	9.2005	4.8655	0.05	9.9201	4.8780	0.05	10.7317	5.7154	0.05	10.1441	8.1390
200.0	0.05	10.4543	5.4812	0.05	10.9737	5.6292	0.05	11.3944	6.8846	0.05	10.4520	10.2403
250.0	0.05	11.2672	6.1592	0.05	11.6835	6.4097	0.05	11.8444	8.1169	0.05	10.6669	12.2500
300.0	0.05	11.8762	6.8585	0.05	12.2014	7.2248	0.05	12.1788	9.3309	0.05	10.8291	14.0544
400.0	0.05	12.7259	8.2332	0.05	12.9269	8.7745	0.05	12.6363	11.5656			
500.0	0.05	13.2750	9.7346	0.05	13.3972	10.3911	0.05	12.9397	13.3126			

Table(6-5-9). Overall Sherwood numbers for two spheres with Zs = 2.48.

($\Delta Z = |Zs/10|$, $\Delta\eta = 6^{o}$)

	Re = 0.001			Re = 1.0			Re = 10.0			Re = 100.0		
Pe	ω_{C*}	Sh_{AO}	Sh_{BO}	ω_{C*}	Sh_{AO}	Sh_{BO}	ω_{C*}	Sh_{AO}	Sh_{BO}	ω_{C*}	Sh_{AO}	Sh_{BO}
0.001	0.80	1.9898	1.9871	0.80	1.9899	1.9871	0.80	1.9899	1.9870	0.80	1.9899	1.9870
0.01	0.80	1.9882	1.9854	0.80	1.9879	1.9852	0.80	1.9882	1.9854	0.80	1.9884	1.9856
0.1	0.80	1.9808	1.9588	0.80	1.9821	1.9572	0.80	1.9837	1.9558	0.80	1.9847	1.9550
1.0	0.80	2.2744	2.0595	0.80	2.3083	2.0696	0.80	2.3443	2.0895	0.80	2.3705	2.1011
2.4	0.80	2.4981	2.2262	0.40	2.5322	2.2195	0.40	2.6262	2.2697	0.30	2.6623	2.2442
5.0	0.25	2.7262	2.3964	0.25	2.8419	2.4425	0.24	3.0038	2.5518	0.23	3.2222	2.6193
10.0	0.25	3.1459	2.7527	0.25	3.2633	2.7950	0.20	3.4848	2.8987	0.20	4.0256	2.9607
20.0	0.20	3.6161	3.1356	0.20	3.7909	3.1843	0.20	4.3147	3.3489	0.05	5.5049	3.2764
30.0	0.20	3.9908	3.4014	0.20	4.2717	3.4573	0.20	5.2245	3.6642	0.05	6.8423	3.6685
50.0	0.20	4.7691	3.7834	0.20	5.3338	3.8600	0.20	7.3171	4.2282	0.05	8.1084	4.7343
70.0	0.15	5.6333	4.1107	0.15	6.5910	4.2300	0.15	8.4971	4.8691	0.05	8.6296	5.8788
100.0	0.10	7.1273	4.6144	0.10	8.4006	4.8390	0.10	9.4847	5.9911	0.04	9.0685	7.8798
150.0	0.10	9.3150	5.6700	0.10	9.9993	6.1532	0.05	10.3742	8.1572	0.03	9.4829	11.5330
200.0	0.04	10.2809	6.7884	0.05	10.8022	7.6111	0.05	10.8957	10.5353	0.03	9.7308	14.8594
250.0	0.04	10.9945	8.0813	0.05	11.3520	9.1237	0.05	11.2395	12.7653	0.03	9.9060	17.5792
300.0	0.04	11.4834	9.4251	0.05	11.7426	10.6895	0.05	11.4824	14.6809			
400.0	0.04	12.1301	11.9534	0.05	12.2523	13.3710	0.05	11.8001	17.8984			
500.0	0.04	12.5218	14.1766	0.05	12.5728	15.9449	0.05	12.0053	20.4117			

Table(6-5-10). Overall Sherwood numbers for two spheres with Zs = 3.09.

($\Delta Z = |Zs/10|$, $\Delta\eta = 6^{o}$)

	Re = 0.001			Re = 1.0			Re = 10.0			Re = 100.0		
Pe	ω_{C^*}	Sh_{AO}	Sh_{BO}	ω_{C^*}	Sh_{AO}	Sh_{BO}	ω_{C^*}	Sh_{AO}	Sh_{BO}	ω_{C^*}	Sh_{AO}	Sh_{BO}
0.001	0.80	2.0268	2.0240	0.80	2.0268	2.0240	0.80	2.0268	2.0240	0.80	2.0268	2.0240
0.01	0.80	2.0210	2.0183	0.80	2.0206	2.0178	0.80	2.0204	2.0175	0.80	2.0201	2.0173
0.1	0.70	2.0123	1.9940	0.80	2.0140	1.9917	0.70	2.0155	1.9903	0.50	2.0123	1.9989
1.0	0.70	2.3426	2.1876	0.50	2.3665	2.1734	0.50	2.4131	2.2029	0.50	2.4397	2.1545
2.4	0.30	2.5546	2.3678	0.30	2.6293	2.4029	0.30	2.7455	2.4773	0.30	2.8443	2.3723
5.0	0.30	2.9179	2.6865	0.20	2.9781	2.7015	0.25	3.2206	2.8497	0.20	3.4970	2.7055
10.0	0.20	3.3186	3.0332	0.20	3.4589	3.0889	0.20	4.0067	3.3306	0.20	4.8567	3.0380
20.0	0.20	4.0391	3.5255	0.20	4.3890	3.6415	0.20	5.9602	4.2345	0.20	6.8587	4.4758
30.0	0.20	4.8170	3.9861	0.20	5.4802	4.1958	0.20	7.3318	5.3635	0.20	7.5549	5.8772
50.0	0.20	6.7987	5.0573	0.19	7.7950	5.5884	0.20	8.5032	8.1678	0.20	8.1811	8.7339
70.0	0.15	8.3996	6.3531	0.15	8.8403	7.2702	0.15	9.0545	10.8282	0.15	8.4721	10.3713
100.0	0.10	9.4817	8.5585	0.10	9.6295	9.9166	0.10	9.5122	13.0238	0.10	8.7257	11.9759
150.0	0.05	10.2890	11.3850	0.05	10.2739	11.3242	0.05	9.8995	14.8483	0.05	8.9445	13.7849
200.0	0.05	10.6835	11.8167	0.05	10.5898	11.6404	0.05	10.1104	16.3010	0.05	9.0586	15.0810
250.0	0.05	10.9157	11.9766	0.05	10.7911	11.8213						
300.0	0.05	11.0732	12.0954	0.05	10.9314	11.9496						
400.0	0.05	11.3000	12.2568	0.04	11.1125	12.1038						
500.0	0.05	11.4208	12.3642	0.04	11.2595	12.2073						

APPENDIX F. COMPUTER PROGRAMMES.

F-1. Introduction.

Two computer programmes have been developed for solving the Navier-Stokes and diffusion equations in the present study of forced convective mass transfer from a system of two equally sized spheres with fluid flowing parallel to their line of centres. Program 1 is for the solution of the Navier-Stokes equations, while Program 2 is for the diffusion equation. The computer programmes can be used to obtain solutions for any sphere spacing by specifying a value to the sphere spacing parameter Zs, which controls the distance between the spheres.They were written in Fortran IV language and have been run on CDC6400, CDC6600, and CDC Cyber 7314 computers. The numerical techniques employed to obtain the solutions of the Navier-Stokes and diffusion equations have been presented in Chapter 4.

In the computational process, for each sphere spacing considered two magnetic tapes are needed: one for each computer programme, to store the flow information and numerical results. The Navier-Stokes equations expressed in terms of the stream function and vorticity transport equations are solved simultaneously using Program 1 for stream function and vorticity distributions in the flow region, and from which important quantities: such as the surface pressures and the drag coefficients for the spheres are calculated. The diffusion equation is solved using Program 2 for the concentration distributions over the same flow region using the stream

function distribution which has been obtained for a specific sphere spacing and Reynolds number. From the results, important quantities; such as the local and overall Sherwood numbers for the spheres are calculated.

The two computer programmes are developed solely to predict the flow conditions around two equally sized spheres parallel to their line of centres and to predict the rates of mass transfer from them, however, there is scope for these two computer programmes to be used in studies of two spheres of different sizes. Furthermore, with appropriate modification and combination, the computer programmes can be used to studies of two-sphere free convective, interacting free and forced convective mass transfer problems, as well as the time-dependent fluid dynamic and mass transfer problems.

F-2. Brief descriptions of the structures of the computer programmes.

The structures of the two computer programmes are generally similar to each other. For each programme, it consists of a main routine and some subroutines. The subroutines which perform various calculattions and operations are called at various stages of computation to perform the required operations. Some of the subroutines in the two computer programmes are identical, others differ slightly or completely.

The basic structures of the computer programmes are shown as follows, in which those subroutines related to do an operation are put together.

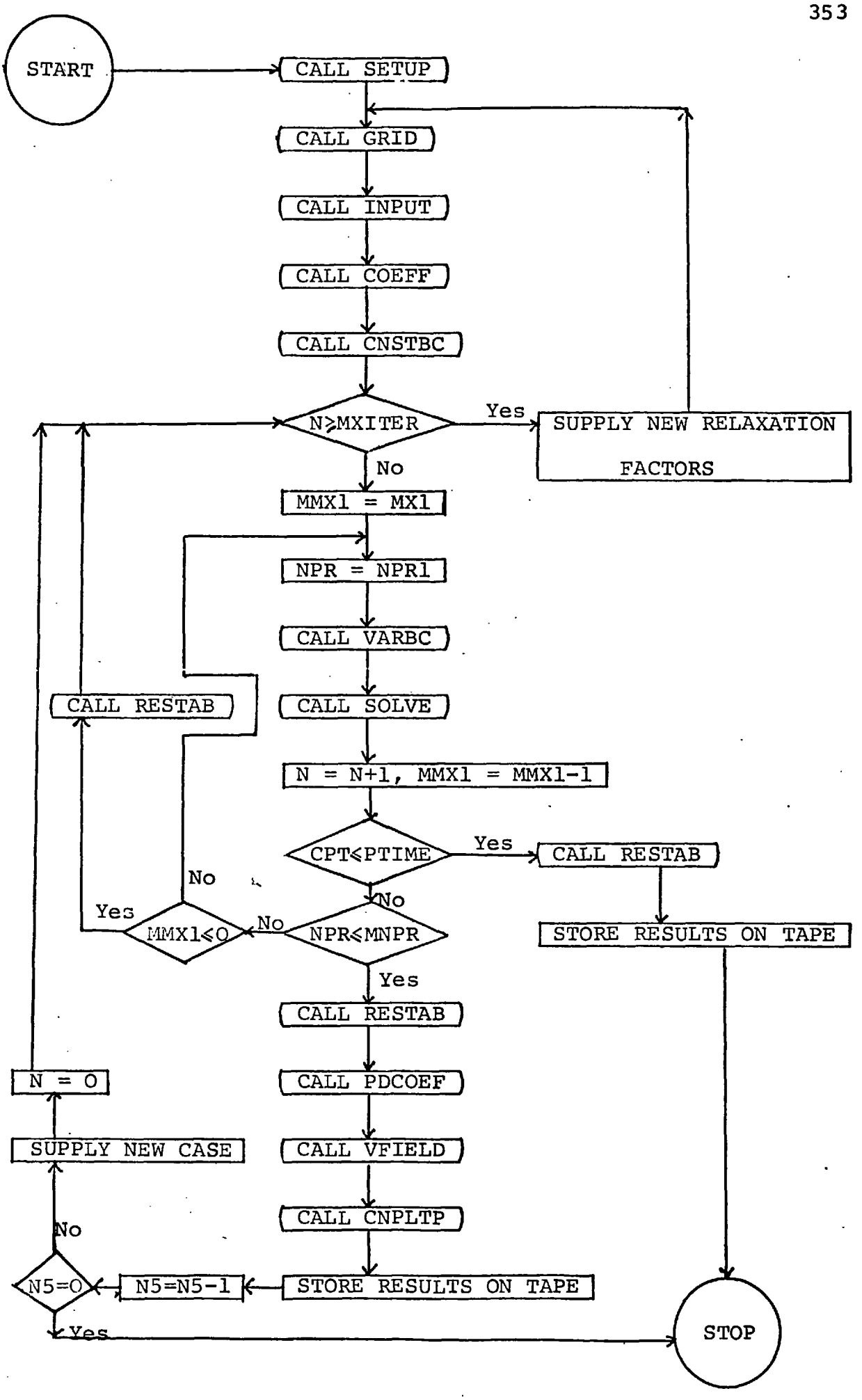

Figure(F-1). Flow chart of computer Program 1.

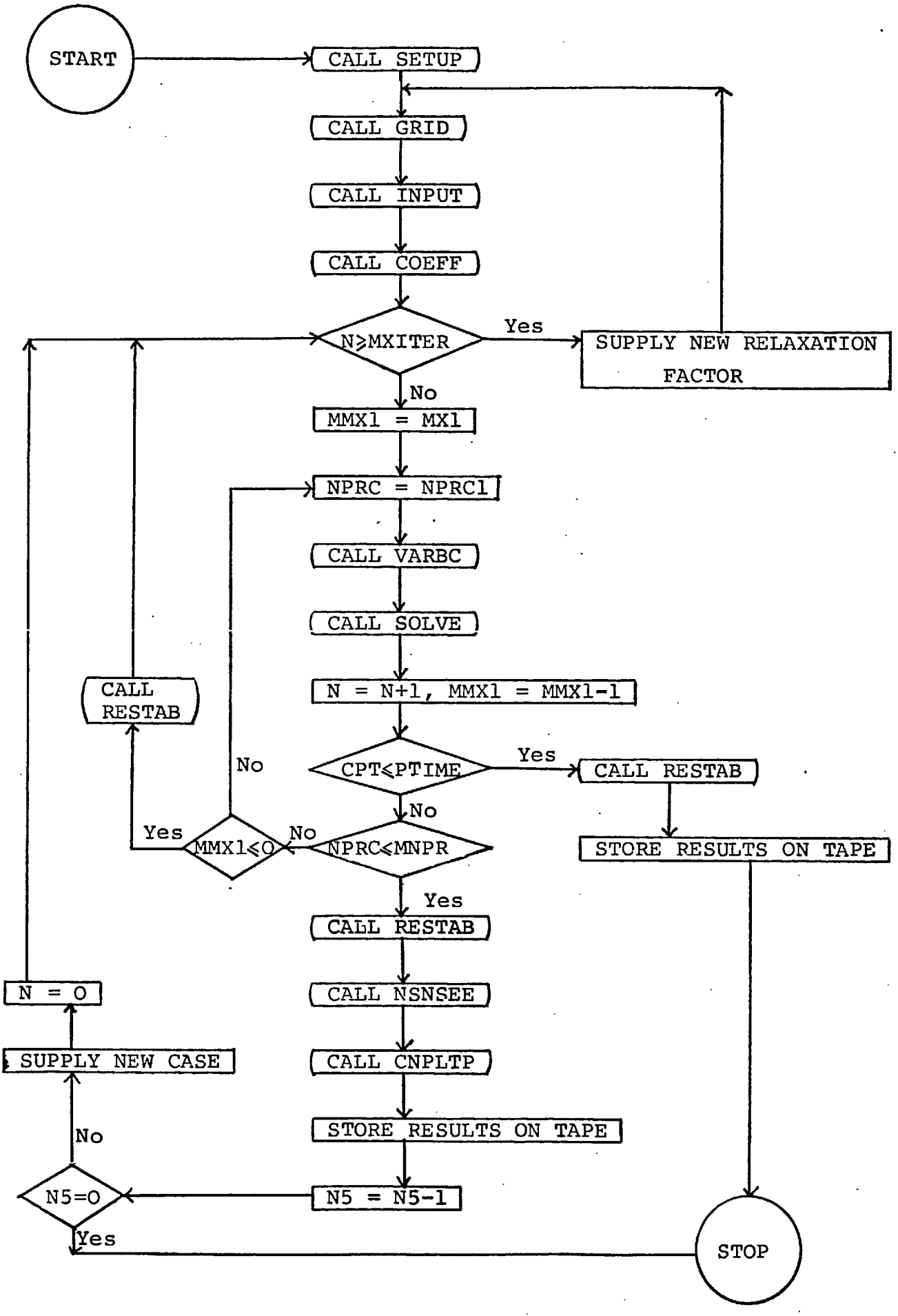

Figure(F-2). Flow chart of computer Program 2.

Program 1.	Program 2.
MAIN	MAIN
SETUP	SETUP
GRID , CNVERT	GRID
INPUT , VELDIS	INPUT
CNSTBC	
COEFF	COEFF
VARBC	VARBC
SOLVE	SOLVE
RESTAB	RESTAB
CNPLTP , CNPLOT	CNPLTP , CNPLOT
PDCOEF	NSNSEE
VFIELD	
SKPFILE	SKPFILE

The flow charts of the two computer programmes are shown in Figures(F-1) and (F-2). The function of each subroutine is described in the listings of section(F-4). Also, in section(F-3) some important Fortran symbols which are widely used in the computer programmes together with their meanings are listed. With these, the user can thus understand the computer programmes and subsequently use them without much difficulty.

F-3. List of Fortran symbols.

A list of the important Fortran symbols used in the two computer programmes is given below. All the other symbols used in the programmes are either defined in terms of these symbols or are self-explanatory in the subroutines.

Fortran symbol	Meaning
AK(J)	$K_{A\theta}$, local surface pressures for sphere A.
AKFSP	Surface pressure at the front stagnation point of sphere A.
AKRSP	Surface pressure at the rear stagnation point of sphere A.
ANU(J)	$Sh_{AL}(\theta)$, local Sherwood numbers for sphere A.
ANRAT(J)	Ratio of local Sherwood number to local Sherwood number at the front stagnation point of sphere A.
AVNU	Sh_{AO}, overall Sherwood number for sphere A.
B1(I,J)	$B_1(i,j)$ or $A_1(i,j)$.
B2(I,J)	$B_2(i,j)$ or $A_2(i,j)$.
B3(I,J)	$B_3(i,j)$ or $A_3(i,j)$.
B4(I,J)	$B_4(i,j)$ or $A_4(i,j)$.
BK(J)	$K_{B\theta}$, local surface pressures for sphere B.
BKFSP	Surface pressure at the front stagnation point of sphere B.
BKRSP	Surface pressure at the rear stagnation point of sphere B.
BNU(J)	$Sh_{BL}(\theta)$, local Sherwood numbers for sphere B.
BNRAT(J)	Ratio of local Sherwood number to local Sherwood number at the front stagnation point of sphere B.

Fortran symbol	Meaning
BVNU	Sh_{BO}, overall Sherwood number for sphere B.
C(I,J)	$C^*_{i,j}$, dimensionless concentration.
CDFA	Frictional drag coefficient for sphere A.
CDFB	Frictional drag coefficient for sphere B.
CDPA	Pressure drag coefficient for sphere A.
CDPB	Pressure drag coefficient for sphere B.
CDTA	Total drag coefficient for sphere A.
CDTB	Total drag coefficient for sphere B.
CPT	Central Processor Time(in seconds) allowed for each computer run.
COSETA(J)	$Cos\eta_j$.
CS(J)	$Cos\theta_j$.
CSH(I)	$CoshZ_i$.
D1(I)	$D_1(i)$.
D2(I)	$D_2(i)$.
D3	D_3.
DTHETA(J)	θ_j in degrees.
E1(I)	$E_1(i)$.
E2(I)	$E_2(i)$.
EPSC	Convergence criterion for concentration.
EPSG	Convergence criterion for vorticity.
EPSU	Convergence criterion for stream function.
ETHA(J)	η_j in radians.
F(I,J)	$f_{i,j}$.
FACTOR	Parameter for controlling the size of the non-linear terms of the Navier-Stokes and diffusion equations.

Fortran symbol	Meaning
FPLOT(K)	Numerical symbol used for the k^{th} contour.
G(I,J)	$g_{i,j}$, vorticity function.
H3(I,J)	$a^*/(\text{Cosh}Z_i - \text{Cos}\theta_j)$.
I	i, subscript used to indicate the increment in Z.
I1(J)	Value of i where the outer boundary begins.
I2(J)	Value of i where the outer boundary ends.
IETHA(J)	η_j in degrees.
INTAPE	When equals to 1, flow information and results for the previous case are read from magnetic tape, otherwise they are computed.
IXSTEP	Number of line-printer steps to be used for plotting half the flow region.
IYS	Scaling factor used in plotting contours on computer output.
J	j, subscript used to indicate increments in both θ and η.
JOMIT	Maximum value of j which cuts the outer boundary.
KNC	Number of concentration contours to be plotted.
KNP	General counter for contours to be plotted.
KNU	Number of stream function contours to be plotted.
KNV	Number of vorticity contours to be plotted.
KS	k, mesh spacing in the angle η.
LVC1(K),LVC2(K)	Factors control the searching of two points for each value of j for the k^{th} contour in the first and in the second halves of the flow region, respectively.

Fortran symbol	Meaning
M	Equal to m-1.
M1	m, number of the grid lines in the θ-direction.
MD	Equal to (m+1)/2.
MM	Equal to n-1.
MM1	n, number of grid lines in the Z-direction.
MMD	Equal to (n+1)/2.
MNPR	Maximum permissible number of point values unconverged, generally equal to 0.
MX1	Number of iterations after which the current solutions are to be printed out.
MMX1	Set to MX1 initially; when it becomes zero the current solutions are printed out.
MXITER	Maximum number of iterations allowed for each case of Reynolds or Peclet numbers.
N	Iteration counter.
N2	Total number of irregular points on the boundaries requiring special treatment.
N3	Equal to 0 when overall convergence of the solutions has been achieved, otherwise equal to 1.
N5	Number of cases to be solved for each computer run.
NDTAPE	When equal to 1 the flow information and results are stored on magnetic tape.
NOMIT	Number of grid points outside the outer boundary to be omitted.
NPC	Number of unconverged point values of concentration on the boundary.

Fortran symbol	Meaning
NPC1	Number of point values to be obtained for concentration on the boundaries.
NP1	Number of unconverged irregular point values.
NPR	Number of unconverged point values.
NPR1	Number of point values to be obtained for both the stream function and the vorticity.
NPRC	Number of unconverged point values for concentration.
NPRC1	Number of point values to be obtained for concentration.
NPRU	Number of unconverged point values for the stream function.
NPRU1	Number of point values to be obtained for the stream function.
NPRV	Number of unconverged point values for the vorticity.
NPRV1	Number of point values to be obtained for the vorticity.
NSKIPR	Number of files on magnetic tape to be skipped before reading data from it.
NSKIPW	Number of files on magnetic tape to be skipped before writting data on it.
NSKPR1	Number of files on magnetic tape to be skipped before reading from Tape 1 the stream function distribution in the flow region.
PE	Peclet number.
PTIME	Central Processor Time(in seconds) allowed per computer run for storing unconverged

Fortran symbol	Meaning
	results on magnetice tape.
R1(I,J)	$a^{*}Sin\theta_j/(CoshZ_i-Cos\theta_j)$.
RD	R_o or r/d.
RE	Reynolds number.
RPC	Relaxation factor for concentration.
RPG	Relaxation factor for vorticity.
RPU	Relaxation factor for stream function.
RN(J)	Equal to $\theta_j - \theta_{j-1}$, j = 2, 3, ••• , m.
RPLOT	Radius of the two spheres. Normally set to 0.
RRA	Starting point of the contours to be plotted in the flow region upstream of sphere A.
RRB	Mid-point between the spheres.
RRC	Terminating point of the contours to be plotted in the flow region downstream of sphere B.
RRCU	Terminating point of the stream function contours to be plotted in the region downstream of sphere B.
RRCV	Terminating point of the vorticity contours to be plotted in the region downstream of sphere B.
RRL	Scaling factor for the contours to be plotted on computer output.
SC	Schmidt number.
SINETA(J)	$Sin\eta_j$.
SH	h, mesh spacing in Z.
SK	K, mesh spacing in the angle η(radians).
SM(J)	Equal to $\theta_{j+1} - \theta_j$, j = 1, 2, ••• , m-1.

Fortran symbol	Meaning
SN(J)	$\mathrm{Sin}\theta_j$.
SNH(I)	$\mathrm{Sinh}Z_i$.
THETA(J)	θ_j in radians.
U(I,J)	$\psi^*_{i,j}$, dimensionless stram function.
V(I,J)	$\zeta^*_{i,j}$, dimensionless vorticity.
VCC(K)	Value of the k^{th} concentration contour.
VCU(K)	Value of the k^{th} stream function contour.
VCV(K)	Value of the k^{th} vorticity contour.
VT(I,J)	Velocity component in the θ-direction.
VZ(I,J)	Velocity component in the Z-direction.
X1(J,K),X2(J,K)	Y_1-coordinates of the first and second points on the k^{th} contour for sphere A.
X3(J,K),X4(J,K)	Y_1-coordinates of the first and second points on the k^{th} contour for sphere B.
Y1(J,K),Y2(J,K)	Y_2-coordinates of the first and second points on the k^{th} contour for sphere A.
Y3(J,K),Y4(J,K)	Y_2-coordinates of the first and second points on the k^{th} contour for sphere B
Z(I)	Z_i.
ZS	Zs, sphere spacing parameter.
ZVC1(K),ZVC2(K)	Values of Z of the first and second points on the k^{th} contour for sphere A.
ZVC3(K),ZVC4(K)	Values of Z of the first and second points on the k^{th} contour for sphere B.

F-4. Computer programmes listings.

A. Computer Program 1.

```
      PROGRAM FLOW(INPUT,OUTPUT,TAPE5=INPUT,TAPE6=OUTPUT,TAPE1)
C---- THIS PROGRAMME SIMULATES VISCOUS INCOMPRESSIBLE NEWTONIAN FLUID
C----      FLOWING AROUND A SYSTEM OF TWO EQUALLY SIZED SPHERES
C----      PARALLEL TO THEIR LINE OF CENTRES.
      COMMON/GRID1/ Z(41),SNH(41),CSH(41),SN(31),CS(31)
      COMMON/GRID2/ IETHA(31),ETHA(31),THETA(31),DTHETA(31)
      COMMON/GRID3/ H3(41,31),R1(41,31)
      COMMON/UVGFC/ U(41,31),V(41,31),G(41,31),F(41,31)
      COMMON/M1MM1C/ M,M1,MMD,MM,MM1,MD,SP,SK,KS
      COMMON/NPRC/ N,MXITER,MX1,MMX1,MNPR,N2,NOMIT,
     1             NPR,NPR1,NPRU,NPRU1,NPRV,NPRV1,NP2
      COMMON/CNTROL/ N3,L4,INTAPE,NDTAPE,NSKIPW,NSKIPR
      COMMON/CNSTC/ ZS,RE,EPSU,EPSG,RFU,RFG
      COMMON/IRREGC/ JOMIT,I1(31),I2(31)
      COMMON/RRABC/ RRA,RRB,RRC,RRCU,RRCV,RRL
      COMMON/FACTOR/ FACTOR
C---- CPT IS THE MAXIMUM TIME ALLOWED FOR EACH COMPUTER RUN.
C---- N5 IS THE COUNTER OF CASES TO BE SOLVED FOR EACH RUN.
C---- MXITER IS THE MAXIMUM NUMBER OF ITERATIONS ALLOWED FOR EACH CASE
C----      OF REYNOLDS NUMBER.
      CPT=890.0
      PTIME=5.0
      N5=1
      CALL SETUP
   60 CALL GRID
      CALL COEFF
      CALL INPUT
      CALL CNSTBC
      N=0
   50 IF(N.GE.MXITER) GO TO 4000
      WRITE(6,1000)
 1000 FORMAT(1H1,48H*****HERE STARTS A GROUP OF MX1 ITERATIONS.*****)
      WRITE(6,1001) ZS,RE,RFU,RFG,XFTOR
 1001 FORMAT(1H0,//,1X,4HZS =,F6.3,5X,4HRE =,F8.3,5X,5HRFU =,F6.2,5X,5HR
     1FG =,F6.2,5X,7HXFTOR =,F6.2)
      WRITE(6,1002) NPRU1,NPRV1,NPR1,NOMIT
 1002 FORMAT(1H0, /,10X,7HNPRU1 =,I5,11X,7HNPRV1 =,I5,10X,6HNPR1 =,I5,10
     1X,7HNOMIT =,I5,/)
      WRITE(6,1003) EPSU,EPSG
 1003 FORMAT(1H0,10X,6HEPSU =,F10.6,10X,6HEPSG =,F10.6,//)
C---- HERE BEGINS THE ITERATION SECTION FOR A GIVEN REYNOLDS NUMBER.
C---- A GROUP OF MX1 ITERATIONS IS SUPPLIED BY SETTING MMX1=MX1.
      MMX1=MX1
C---- A NEW ITERATION BEGINS WITH NPR=NPR1.
C----     NPR1 IS THE TOTAL NUMBER OF POINT VALUES TO BE OBTAINED, AND
C----      NPR IS THE TOTAL NUMBER OF UNCONVERGED POINT VALUES.
   40 NPR=NPR1
      CALL VARBC
      CALL SOLVE
      CALL SECOND(CPSEC)
      IF((N/5)*5.NE.N) GO TO 20
      WRITE(6,2000) N,CPSEC,NPRU,NPRV,NPR,NP2
 2000 FORMAT(1H0,3HN =,I5,5X,5HCPT =,F6.2,15X,6HNPRU =,I5,5X,6HNPRV =,I5
     1,5X,5HNPR =,I5,5X,5HNP2 =,I5)
```

```
   20 TLEFT=CPT-CPSEC
      IF(TLEFT.LE.PTIME) GO TO 2
C---- AN ITERATION IS COMPLETED.
      N=N+1
      MMX1=MMX1-1
C---- TEST FOR THE OVERALL CONVERGENCE. IF NPR IS LESS THAN OR EQUAL TO
C----       MNPR, THE OVERALL CONVERGENCE OF THE PRESENT SOLUTIONS HAS
C----       OBTAINED.
C---- IF MMX1=0, THE GROUP OF MX1 ITERATION HAVE BEEN PERFORMED,
C----      OTHERWISE GO TO 40 AND START A NEW ITERATION.
      IF(NPR-MNPR) 200,200,100
  100 IF(MMX1) 300,300,40
C---- SET N3 TO ZERO IF THE OVERALL CONVERGENCE HAS BEEN OBTAINED.
  200 N3=0
C---- AN EXTRA ITERATION IS ALLOWED FOR THE BOUNDARY CONDITIONS TO BE
C----       SATISFIED.
      NPR=NPR1
      CALL VARBC
      CALL SOLVE
      IF(NPR.GT.MNPR) GO TO 40
  300 CALL RESTAB
      IF(N3.EQ.1) GO TO 50
      WRITE(6,2004)
 2004 FORMAT(///,40H*****THE PRESENT CASE IS CONVERGED.*****,//)
C---- IF NDTAPE=1, STORE INFORMATION ON TAPE 1.
      IF(NDTAPE.NE.1) GO TO 3
      REWIND 1
      IF(NSKIPW.GT.0) CALL SKPFILE(NSKIPW,1)
      WRITE(1)(ETHA(J),ETHA(J),DTHETA(J),THETA(J),I1(J),I2(J),J=1,M1)
      WRITE(1) JOMIT,N2,NPRU1,NPRV1,NPR1,NOMIT
      WRITE(1) (SN(J),CS(J),J=1,M1)
      WRITE(1) ((H3(I,J),R1(I,J),I=1,MM1),J=1,M1)
      WRITE(1) ((U(I,J),I=1,MM1),J=1,M1)
      WRITE(1) ((V(I,J),I=1,MM1),J=1,M1)
      WRITE(1) ((G(I,J),I=1,MM1),J=1,M1)
      WRITE(1) ((F(I,J),I=1,MM1),J=1,M1)
      END FILE 1
      WRITE(6,3000) ZS,RE,NSKIPR,NSKIPW
 3000 FORMAT(///,10X,4HZS =,F6.3,10X,4HRE =,F8.3,10X,8HNSKIPR =,I4,10X,8
     1HNSKIPW =,I4,//)
      NSKIPR=NSKIPW
      NSKIPW=NSKIPW+1
C---- CALCULATING THE SURFACE PRESSURES AND DRAG COEFFICIENTS.
      CALL PDCOEF
C---- STREAM FUNCTION AND VORTICITY CONTOURS ARE LOCATED AND PLOTTED.
      CALL CNPLTP
C---- CALCULATE THE VELOCITY COMPONENTS.
      CALL VFIELD
    3 N5=N5+1
      N=0
      N3=1
      FACTOR=1.0
      IF(N5.EQ.2) GO TO 11
      IF(N5.EQ.3) GO TO 12
      IF(N5.EQ.4) GO TO 13
      IF(N5.EQ.5) GO TO 14
      GO TO 1
C---- SUPPLIES NEW RELAXATION FACTORS.
```

```
 4000 CONTINUE
      RFU=RFU-0.10
      RFG=RFG-0.05
      IF(RFU.LE.0.0) GO TO 1
      IF(RFG.LE.0.0) GO TO 1
      GO TO 60
   11 CONTINUE
      RE=0.01
      GO TO 50
   12 CONTINUE
      RE=0.1
      GO TO 50
   13 CONTINUE
      RE=1.0
      GO TO 50
   14 CONTINUE
      RE=2.5
      GO TO 50
C---- PRINT OUT THE CONVERGED RESULTS.
    2 CALL RESTAR
C---- IF NDTAPE=1, STORE INFORMATION ON TAPE 1.
      IF(NDTAPE.NE.1) GO TO 1
      REWIND 1
      IF(NSKIPW.GT.0) CALL SKPFILE(NSKIPW,1)
      WRITE(1)(ETHA(J),ETHA(J),DTHETA(J),THETA(J),I1(J),I2(J),J=1,M1)
      WRITE(1) JOMIT,N2,NPRU1,NPRV1,NPR1,NOMIT
      WRITE(1) (SN(J),CS(J),J=1,M1)
      WRITE(1) ((H3(I,J),R1(I,J),I=1,MM1),J=1,M1)
      WRITE(1) ((U(I,J),I=1,MM1),J=1,M1)
      WRITE(1) ((V(I,J),I=1,MM1),J=1,M1)
      WRITE(1) ((G(I,J),I=1,MM1),J=1,M1)
      WRITE(1) ((F(I,J),I=1,MM1),J=1,M1)
      END FILE 1
      WRITE(6,3001) ZS,RE,NSKIPR,NSKIPW
 3001 FORMAT(///,10X,4HZS =,F6.3,10X,4HRE =,F8.3,10X,8HNSKIPR =,I4,10X,8
     1HNSKIPW =,I4,//)
    1 STOP
      END
```

```
      SUBROUTINE SETUP
C---- THIS SUBROUTINE SUPPLIES PROGRAMME CONTROL PARAMETERS AND FLOW
C----      REGION INFORMATION.
      COMMON/GRID1/ Z(41),SNH(41),CSH(41),SN(31),CS(31)
      COMMON/GRID2/ IETHA(31),ETHA(31),THETA(31),DTHETA(31)
      COMMON/GRID3/ H3(41,31),R1(41,31)
      COMMON/NPRC/ N,MXITER,MX1,MMX1,MNPR,N2,NOMIT,
     1             NPR,NPR1,NPRU,NPRU1,NPRV,NPRV1,NP2
      COMMON/CNTROL/ N3,L4,INTAPE,NDTAPE,NSKIPW,NSKIPR
      COMMON/M1MM1C/ M,M1,MMD,MM,MM1,MD,SH,SK,KS
      COMMON/CNSTC/ ZS,RE,EPSU,EPSG,RFU,RFG
      COMMON/RPLOTC/ RPLOT,RPLOTU,RPLOTV,IYS,IXSTEP
      COMMON/PLTPCN/ VCU(10),VCV(10),KNU,KNV,KNP
      COMMON/IRREGC/ JOMIT,I1(31),I2(31)
      COMMON/RRABC/ RRA,RRB,RRC,RRCU,RRCV,RRL
      COMMON/FACTOR/ FACTOR
      COMMON/RDC/ RD
C---- SPHERE SPACING, MESH SPACING, AND BOUNDARY PARAMETERS.
      ZS=0.20
      SH=ZS/20.0
      RD=14.0
      KS=6
      SK=(3.1415926/180.0)*KS
      M=30
      MM=40
C---- CONTROL PARAMETERS FOR SOLVING THE EQUATIONS.
      FACTOR=0.00
      RE=0.001
      RFU=1.00
      RFG=0.80
      NSKIPR=0
      NSKIPW=0
      INTAPE=0
      NDTAPE=1
      MXITER=600
      MX1=300
      EPSU=0.001
      EPSG=0.001
      MNPR=0
      N3=1
      L4=0
C---- CONTROL PARAMETERS FOR PLOTTING STREAM FUNCTION AND VORTICITY
C----      CONTOURS AROUND THE SPHERES.
      RRA=5.0£RRB=COSH(ZS)
      RRL=7.0
      RRCU=6.0
      RRCV=7.0
      RPLOT=1.000
      IXSTEP=60
      IYS=1.6666*FLOAT(IXSTEP-1)+1.5
      KNU=8
      KNV=7
      VCU(1)=0.£VCU(2)=0.001£VCU(3)=0.01£VCU(4)=0.1£VCU(5)=0.5£VCU(6)=1.
      VCU(7)=2.0£VCU(8)=4.0
      VCV(1)=0.0£VCV(2)=0.05£VCV(3)=0.10£VCV(4)=0.25£VCV(5)=0.50
      VCV(6)=1.00£VCV(7)=2.00
      RETURN
      END
```

```
      SUBROUTINE GRID
C---- THIS SUBROUTINE SUPPLIES GRID INFORMATION AT EACH NODE.
      COMMON/GRID1/ Z(41),SNH(41),CSH(41),SN(31),CS(31)
      COMMON/GRID2/ IETHA(31),ETHA(31),THETA(31),DTHETA(31)
      COMMON/GRID3/ H3(41,31),R1(41,31)
      COMMON/UVGFC/ U(41,31),V(41,31),G(41,31),F(41,31)
      COMMON/M1MM1C/ M,M1,MMD,MM,MM1,MD,SH,SK,KS
      COMMON/CNSTC/ ZS,RE,EPSU,EPSG,RFU,RFG
      COMMON/NPRC/ N,MXITER,MX1,MMX1,MNPR,N2,NOMIT,
     1             NPR,NPR1,NPRU,NPRU1,NPRV,NPRV1,NP2
      COMMON/CNTROL/ N3,L4,INTAPE,NDTAPE,NSKIPW,NSKIPR
      COMMON/IRREGC/ JOMIT,I1(31),I2(31)
      COMMON/OFOSC/ OF,OF4,OF3,OF2,OS,OS4,OS3,OS2
      COMMON/PFPSC/ PF,PF4,PF3,PF2,PS,PS4,PS3,PS2
C---- CALCULATE THE FIELD DIMENSION MM1 AND M1.
      M1=M+1
      MM1=MM+1
      MD=(M1+1)/2
      MMD=(MM1+1)/2
C---- COMPUTING FIELD VARIABLES.
      Z(1)=-ZS
      SNH(1)=-SINH(ZS)
      CSH(1)=COSH(ZS)
      DO 10 I=2,MM1
      Z(I)=Z(I-1)+SH
      SNH(I)=SINH(Z(I))
      CSH(I)=COSH(Z(I))
   10 CONTINUE
C---- IF INTAPE=1, VALUES OF THE FIELD VARIABLES WILL BE READ FROM TAPE
C----     1, OTHERWISE GO TO 1 TO CALCULATE THEM.
      IF(INTAPE.NE.1) GO TO 1
      REWIND 1
      IF(NSKIPR.GT.0) CALL SKPFILE(NSKIPR,1)
      READ(1) (IETHA(J),ETHA(J),DTHETA(J),THETA(J),I1(J),I2(J),J=1,M1)
      READ(1)  JOMIT,N2,NPRU1,NPRV1,NPR1,NOMIT
      READ(1) (SN(J),CS(J),J=1,M1)
      READ(1) ((H3(I,J),R1(I,J),I=1,MM1),J=1,M1)
      READ(1) ((U(I,J),I=1,MM1),J=1,M1)
      READ(1) ((V(I,J),I=1,MM1),J=1,M1)
      READ(1) ((G(I,J),I=1,MM1),J=1,M1)
      READ(1) ((F(I,J),I=1,MM1),J=1,M1)
      GO TO 2
C---- CNVERT SUPPLIES VALUES FOR THETA(J).
    1 CALL CNVERT
      DO 20 J=1,M1
      SN(J)=SIN(THETA(J))
      CS(J)=COS(THETA(J))
   20 CONTINUE
      DO 40 J=1,M1
      DO 30 I=1,MM1
      IF(J.EQ.1.AND.I.EQ.MMD) GO TO 35
      H3(I,J)=SNH(MM1)/(CSH(I)-CS(J))
      R1(I,J)=H3(I,J)*SN(J)
      GO TO 30
   35 H3(I,J)=10.E+30
      R1(I,J)=10.E-30
   30 CONTINUE
   40 CONTINUE
    2 CONTINUE
```

```
C---- THIS SECTION SUPPLIES THE PARAMETERS FOR CALCULATION OF THE FIRST
C----    ORDER AND SECOND ORDER DERIVATIVES WITH RESPECT TO THETA.
      TM2=THETA(2)-THETA(1)
      TM3=THETA(3)-THETA(2)
      TM4=THETA(4)-THETA(3)
      OL=TM2+TM3+TM4
      OK=TM2+TM3
      OH=TM2
      OL2=OL*OL
      OK2=OK*OK
      OH2=OH*OH
      OLMK=OL-OK
      OLMH=OL-OH
      OKMH=OK-OH
      OF=OL*OK*OH*OLMK*OLMH*OKMH
      OF4=OK2*OH2*OKMH
      OF3=OL2*OH2*OLMH
      OF2=OL2*OK2*OLMK
      OS=OL*OK*OH*OLMK*OLMH*OKMH
      OS4=OK*OH*(OK2-OH2)
      OS3=OL*OH*(OL2-OH2)
      OS2=OL*OK*(OL2-OK2)
C
      TM29=THETA(29)-THETA(28)
      TM30=THETA(30)-THETA(29)
      TM31=THETA(31)-THETA(30)
      PL=TM29+TM30+TM31
      PK=TM30+TM31
      PH=TM31
      PL2=PL*PL
      PK2=PK*PK
      PH2=PH*PH
      PLMK=PL-PK
      PLMH=PL-PH
      PKMH=PK-PH
      PF=PL*PK*PH*PLMK*PLMH*PKMH
      PF4=PK2*PH2*PKMH
      PF3=PL2*PH2*PLMH
      PF2=PL2*PK2*PLMK
      PS=PL*PK*PH*PLMK*PLMH*PKMH
      PS4=PK*PH*(PK2-PH2)
      PS3=PL*PH*(PL2-PH2)
      PS2=PL*PK*(PL2-PK2)
      RETURN
      END
```

```
      SUBROUTINE COEFF
C---- THIS SUBROUTINE CALCULATES ALL THE COEFFICIENTS OF THE FINITE-
C----      DIFFERENCE EQUATIONS.
      COMMON/GRID1/ Z(41),SNH(41),CSH(41),SN(31),CS(31)
      COMMON/GRID2/ IETHA(31),ETHA(31),THETA(31),DTHETA(31)
      COMMON/GRID3/ H3(41,31),R1(41,31)
      COMMON/M1MM1C/ M,M1,MMD,MM,MM1,MD,SH,SK,KS
      COMMON/COEFF/ B1(41,31),B2(41,31),B3(41,31),B4(41,31)
      COMMON/NCOEFF/ FCOF(41),FCOFM(41),CB2(31),REG(31),A(31)
      COMMON/KMKNC/ AA(31),BB(31)
      COMMON/SMRNC/ SM(31),RN(31)
C---- B1(I,J),B2(I,J),B3(I,J),B4(I,J),ARE THE COEFFICIENTS OF THE
C----      FINITE-DIFFERENCE STREAM FUNCTION AND VORTICITY TRANSPORT
C----      EQUATIONS.
      SH2=1./(SH*SH)
      DO 1 J=1,M1
      CB2(J)=0.5*SH2/(H3(1,J)*H3(1,J))
    1 CONTINUE
      SM(1)=THETA(2)-THETA(1)
      RN(1)=0.0
      SM(M1)=0.0
      RN(M1)=THETA(M1)-THETA(M)
      DO 10 J=2,M
      SM(J)=THETA(J+1)-THETA(J)
      RN(J)=THETA(J)-THETA(J-1)
      SMTRN=SM(J)*RN(J)
      SMPRN=SM(J)+RN(J)
      SMMRN=SM(J)-RN(J)
      AA(J)=1.0-SMMRN/SM(J)
      BB(J)=1.0+SMMRN/RN(J)
      CCP=1.0+SMMRN/SMPRN
      CCM=1.0-SMMRN/SMPRN
      SKT=1.0/SMTRN
      DO 20 I=2,MM
      BA=SNH(I)/(2.0*SH*(CSH(I)-CS(J)))
      BC=(CSH(I)*CS(J)-1.0)/((CSH(I)-CS(J))*SN(J)*SMPRN)
      A(J)=2.0*SH2+2.0*SKT-(AA(J)-BB(J))*BC
      REG(J)=-1.0/(4.0*SH*SMPRN*A(J))
      B1(I,J)=(SH2+BA)/A(J)
      B2(I,J)=(SH2-BA)/A(J)
      B3(I,J)=(CCM*SKT-AA(J)*BC)/A(J)
      B4(I,J)=(CCP*SKT+BB(J)*BC)/A(J)
   20 CONTINUE
   10 CONTINUE
      DO 30 I=1,MM1
      FCOF(I)=1./(H3(I,1)*RN(2))
      FCOFM(I)=1.0/(H3(I,M1)*SM(M))
   30 CONTINUE
      WRITE(6,1000)
 1000 FORMAT(1H1,10X,5HIETHA,10X,5HTHETA,13X,2HSM,13X,2HRN,14X,1HA,12X,3
     1HREG,//)
      WRITE(6,1001) (IETHA(J),THETA(J),SM(J),RN(J),A(J),REG(J),J=2,M)
 1001 FORMAT(1H0,I15,5F15.6)
      RETURN
      END
```

```
      SUBROUTINE CNSTBC
C---- THIS SUBROUTINE SETS THE CONSTANT BOUNDARY CONDITIONS.
      COMMON/GRID1/ Z(41),SNH(41),CSH(41),SN(31),CS(31)
      COMMON/GRID2/ IETHA(31),ETHA(31),THETA(31),DTHETA(31)
      COMMON/GRID3/ H3(41,31),R1(41,31)
      COMMON/M1MM1C/ M,M1,MMD,MM,MM1,MD,SP,SK,KS
      COMMON/UVGFC/ U(41,31),V(41,31),G(41,31),F(41,31)
      COMMON/CNSTC/ ZS,RF,EPSU,EPSG,RFU,RFG
      COMMON/NPRC/ N,NXITER,MX1,MMX1,MNPR,N2,NOMIT,
     1             NPR,NPR1,NPRU,NPRU1,NPRV,NPRV1,NP2
      COMMON/IRREGC/ JOMIT,I1(31),I2(31)
C---- ALONG THE AXES OF SYMMETRY, THETA = 0 AND 180.
      DO 10 I=1,MM1
      U(I,1)=0.
      V(I,1)=0.
      G(I,1)=0.
      U(I,M1)=0.
      V(I,M1)=0.
      G(I,M1)=0.
   10 CONTINUE
C---- ON THE SPHERE SURFACES.
      DO 20 J=1,M1
      U(1,J)=0.
      U(MM1,J)=0.
   20 CONTINUE
C---- ALONG THE OUTER BOUNDARY.
      DO 30 J=1,JOMIT
      ILEFT=I1(J)
      IRIGHT=I2(J)
      DO 40 I=ILEFT,IRIGHT
      V(I,J)=0.
      G(I,J)=0.
      F(I,J)=0.
      U(I,J)=0.5*R1(I,J)*R1(I,J)
   40 CONTINUE
   30 CONTINUE
      RETURN
      END
```

```
      SUBROUTINE VARBC
C---- THIS SUBROUTINE SETS THE SPECIALLY TREATED BOUNDARY CONDITIONS.
      COMMON/GRID1/ Z(41),SNH(41),CSH(41),SN(31),CS(31)
      COMMON/GRID2/ IETHA(31),ETHA(31),THETA(31),DTHETA(31)
      COMMON/GRID3/ H3(41,31),R1(41,31)
      COMMON/MMMC/ M,M1,MMD,MM,MM1,MD,SH,SK,KS
      COMMON/UVGFC/ U(41,31),V(41,31),G(41,31),F(41,31)
      COMMON/COEFF/ B1(41,31),B2(41,31),B3(41,31),B4(41,31)
      COMMON/NCOEFF/ FCOF(41),FCOFM(41),CB2(31),REG(31),A(31)
      COMMON/KMKNC/ AA(31),BB(31)
      COMMON/IREGC/ JOMIT,I1(31),I2(31)
      COMMON/CNSTC/ ZS,RE,EPSH,EPSG,RFU,RFG
      COMMON/NPRC/ N,MXITER,MX1,MMX1,MNPR,N2,NOMIT,
     1             NPR,NPR1,NPRU,NPRU1,NPRV,NPRV1,NP2
      COMMON/CNTROL/ N3,L4,INTAPE,NDTAPE,NSKIPW,NSKIPR
      COMMON/OFOSC/ OF,OF4,OF3,OF2,OS,OS4,OS3,OS2
      COMMON/PFPSC/ PF,PF4,PF3,PF2,PS,PS4,PS3,PS2
C---- SOLUTION OF THE SPECIALLY TREATED BOUNDARY CONDITIONS.
C---- NEW ESTIMATES OF THE VORTICITY AT THE SPHERE SURFACES.
      NPRU=NPRU1
      NPRV=NPRV1
      NP2=N2
      DO 10 J=2,M
      TN=CB2(J)*(8.0*U(2,J)-U(3,J))
      IF(TN.LE.1.000) GO TO 1
      IF(ABS((G(1,J)-TN)/TN).LE.EPSG) GO TO 11
      GO TO 12
    1 IF(ABS(G(1,J)-TN).LE.EPSG) GO TO 11
      GO TO 12
   11 NP2=NP2-1
      NPRV=NPRV-1
      NPR=NPR-1
   12 G(1,J)=TN
      V(1,J)=G(1,J)/R1(1,J)
      F(1,J)=V(1,J)/R1(1,J)
   10 CONTINUE
      DO 20 J=2,M
      TN=CB2(J)*(8.*U(MM,J)-U(MM-1,J))
      IF(TN.LE.1.000) GO TO 2
      IF(ABS((G(MM1,J)-TN)/TN).LE.EPSG) GO TO 21
      GO TO 22
    2 IF(ABS(G(MM1,J)-TN).LE.EPSG) GO TO 21
      GO TO 22
   21 NP2=NP2-1
      NPRV=NPRV-1
      NPR=NPR-1
   22 G(MM1,J)=TN
      V(MM1,J)=G(MM1,J)/R1(MM1,J)
      F(MM1,J)=V(MM1,J)/R1(MM1,J)
   20 CONTINUE
C
C---- CALCULATE F(I,1) AND F(I,M1) ALONG THE AXES OF SYMMETRY.
      DO 30 I=1,MM1
      F(I,1)=(OF4*(V(I,4)-V(I,1))-OF3*(V(I,3)-V(I,1))+OF2*(V(I,2)-V(I,1)
     +))/(OF*H3(I,1))
      F(I,M1)=(PF4*(V(I,M1-3)-V(I,M1))-PF3*(V(I,M1-2)-V(I,M1))+PF2*(V(I,
     +M1-1)-V(I,M1)))/(PF*H3(I,M1))
      F(I,1)=FCOF(I)*V(I,2)
      F(I,M1)=FCOFM(I)*V(I,M)
   30 CONTINUE
      RETURN
      END
```

```
      SUBROUTINE SOLVE
C---- THIS SUBROUTINE SOLVES THE NAVIER-STOKES EQUATIONS FOR STREAM
C----      AND VORTICITY DISTRIBUTIONS IN THE FLOW REGION.
      COMMON/GRID1/ Z(41),SNH(41),CSH(41),SN(31),CS(31)
      COMMON/GRID2/ IETHA(31),ETHA(31),THETA(31),DTHETA(31)
      COMMON/GRID3/ H3(41,31),R1(41,31)
      COMMON/M1MM1C/ M,M1,MMO,MM,MM1,MO,SH,SK,KS
      COMMON/UVGFC/ U(41,31),V(41,31),G(41,31),F(41,31)
      COMMON/CNSTC/ ZS,RE,EPSU,EPSG,RFU,RFG
      COMMON/COEFF/ B1(41,31),B2(41,31),B3(41,31),B4(41,31)
      COMMON/NCOEFF/ FCOF(41),FCOFM(41),CB2(31),REG(31),A(31)
      COMMON/KMKNC/ AA(31),BB(31)
      COMMON/NPRC/ N,MXITER,MX1,MMX1,MNPR,N2,NOMIT,
     1             NPR,NPR1,NPRU,NPRU1,NPRV,NPRV1,NP2
      COMMON/IRREGC/ JOMIT,I1(31),I2(31)
      COMMON/FACTOR/ FACTOR
C---- NEW ESTIMATE OF THE VORTICITY NEAR THE OUTER BOUNDARY.
      DO 20 J=2,JOMIT
      DO 10 I=2,MM
      IF(I.GE.I1(J).AND.I.LE.I2(J)) GO TO 10
      DF1=U(I+1,J)-U(I-1,J)
      DF2=F(I,J+1)*AA(J)-F(I,J-1)*BB(J)-F(I,J)*(AA(J)-BB(J))
      DF3=U(I,J+1)*AA(J)-U(I,J-1)*BB(J)-U(I,J)*(AA(J)-BB(J))
      DF4=F(I+1,J)-F(I-1,J)
      C=DF1*DF2
      B=DF3*DF4
      D=RE*REG(J)*R1(I,J)*(C-B)
      XM=-(D/G(1,J))*FACTOR
      AGM=1.0+XM
      DP=(D+XM*G(1,J))/AGM
      BG1=B1(I,J)*G(I+1,J)
      BG2=B2(I,J)*G(I-1,J)
      BG3=B3(I,J)*G(I,J+1)
      BG4=B4(I,J)*G(I,J-1)
      TN=BG1+BG2+BG3+BG4
      TNP=TN/AGM
      TN=TNP+DP
      TN=G(I,J)+RFG*(TN-G(I,J))
      IF(TN.LE.1.000) GO TO 1
      IF(ABS((G(I,J)-TN)/TN).LE.EPSG) GO TO 11
      GO TO 12
    1 IF(ABS(G(I,J)-TN).LE.EPSG) GO TO 11
      GO TO 12
   11 NPRV=NPRV-1
      NPR=NPR-1
   12 G(I,J)=TN
      V(I,J)=G(I,J)/R1(I,J)
      F(I,J)=V(I,J)/R1(I,J)
C---- NEW ESTIMATE OF THE STREAM FUNCTION NEAR THE OUTER BOUNDARY.
      D=-(H3(I,J)*H3(I,J)/A(J))*G(I,J)
      BU1=B1(I,J)*U(I+1,J)
      BU2=B2(I,J)*U(I-1,J)
      BU3=B3(I,J)*U(I,J+1)
      BU4=B4(I,J)*U(I,J-1)
      TN=BU1+BU2+BU3+BU4
      TN=TN+D
      TN=U(I,J)+RFU*(TN-U(I,J))
      IF(TN.LE.1.000) GO TO 2
      IF(ABS((U(I,J)-TN)/TN).LE.EPSU) GO TO 13
      GO TO 14
```

```
    2 IF(ABS(U(I,J)-TN).LE.EPSU) GO TO 13
      GO TO 14
   13 NPRU=NPRU-1
      NPR=NPR-1
   14 U(I,J)=TN
   10 CONTINUE
   20 CONTINUE
C---- NEW ESTIMATE OF THE VORTICITY.
      JREG=JOMIT+1
      DO 40 J=JREG,M
      DO 30 I=2,MM
      DF1=U(I+1,J)-U(I-1,J)
      DF2=F(I,J+1)*AA(J)-F(I,J-1)*BB(J)-F(I,J)*(AA(J)-BB(J))
      DF3=U(I,J+1)*AA(J)-U(I,J-1)*BB(J)-U(I,J)*(AA(J)-BB(J))
      DF4=F(I+1,J)-F(I-1,J)
      C=DF1*DF2
      B=DF3*DF4
      D=RE*REG(J)*R1(I,J)*(C-B)
      XM=-(D/G(I,J))*FACTOR
      AGM=1.0+XM
      DP=(D+XM*G(I,J))/AGM
      BG1=B1(I,J)*G(I+1,J)
      BG2=B2(I,J)*G(I-1,J)
      BG3=B3(I,J)*G(I,J+1)
      BG4=B4(I,J)*G(I,J-1)
      TN=BG1+BG2+BG3+BG4
      TNP=TN/AGM
      TN=TNP+DP
      TN=G(I,J)+RFG*(TN-G(I,J))
      IF(TN.LE.1.000) GO TO 3
      IF(ABS((G(I,J)-TN)/TN).LE.EPSG) GO TO 31
      GO TO 32
    3 IF(ABS(G(I,J)-TN).LE.EPSG) GO TO 31
      GO TO 32
   31 NPRV=NPRV-1
      NPR=NPR-1
   32 G(I,J)=TN
      V(I,J)=G(I,J)/R1(I,J)
      F(I,J)=V(I,J)/R1(I,J)
C---- NEW ESTIMATE OF THE STREAM FUNCTION.
      D=-(H3(I,J)*H3(I,J)/A(J))*G(I,J)
      BU1=B1(I,J)*U(I+1,J)
      BU2=B2(I,J)*U(I-1,J)
      BU3=B3(I,J)*U(I,J+1)
      BU4=B4(I,J)*U(I,J-1)
      TN=BU1+BU2+BU3+BU4
      TN=TN+D
      TN=U(I,J)+RFU*(TN-U(I,J))
      IF(TN.LE.1.000) GO TO 4
      IF(ABS((U(I,J)-TN)/TN).LE.EPSU) GO TO 33
      GO TO 34
    4 IF(ABS(U(I,J)-TN).LE.EPSU) GO TO 33
      GO TO 34
   33 NPRU=NPRU-1
      NPR=NPR-1
   34 U(I,J)=TN
   30 CONTINUE
   40 CONTINUE
      RETURN
      END
```

```
      SUBROUTINE CNVERT
C---- THIS SUBROUTINE CALCULATES THE VALUES OF THETA(J) CORRESPONDING TO
C----      THE VALUES OF ETHA(J) WITH A CONSTANT INCREMENT.THE
C----      COORDINATES OF THE OUTER BOUNDARY ARE ALSO DETERMINED.
      COMMON/GRID1/ Z(41),SNH(41),CSH(41),SN(31),CS(31)
      COMMON/GRID2/ IETHA(31),ETHA(31),THETA(31),DTHETA(31)
      COMMON/GRID3/ H3(41,31),R1(41,31)
      COMMON/CNSTC/ ZS,RE,EPSU,EPSG,RFU,RFG
      COMMON/M1MM1C/ M,M1,MMD,MM,MM1,MD,SH,SK,KS
      COMMON/IRREGC/ JOMIT,I1(31),I2(31)
      COMMON/NPRC/ N,NXITER,MX1,MMX1,MNPR,N2,NOMIT,
     1             NPR,NPR1,NPRU,NPRU1,NPRV,NPRV1,NP2
      COMMON/RDC/ RD
      DIMENSION Y1A(31),Y2A(31),TN(31)
      IETHA(1)=0
      ETHA(1)=0.0
      TN(1)=0.0
      DO 20 J=2,MD
      IETHA(J)=KS*(J-1)
      ETHA(J)=SK*FLOAT(J-1)
      TN(J)=TAN(ETHA(J))
   20 CONTINUE
      MDP1=MD+1
      DO 30 J=MDP1,M1
      IETHA(J)=KS*(J-1)
      ETHA(J)=SK*FLOAT(J-1)
      TN(J)=TAN(3.1415926-ETHA(J))
      TN(J)=-TN(J)
   30 CONTINUE
C---- CONVERSION OF THE VALUES OF ETHA(J) INTO THE VALUES OF THETA(J).
      WRITE(6,1000)
 1000 FORMAT(1H1,10X,5HIETHA,10X,3HY1A,10X,3HY2A,9X,5HTHETA,9X,6HDTHETA)
      A=SINH(ZS)
      AA=COSH(ZS)
      THETA(1)=0.0
      DTHETA(1)=0.0
      Y1A(1)=(-A*A)/(AA-COS(THETA(1)))
      Y2A(1)=(A*SIN(THETA(1)))/(AA-COS(THETA(1)))
      DO 40 J=2,M1
      CHETA=THETA(J-1)
    1 CHETA=CHETA+0.017453292*0.01
      R=A*SIN(CHETA)
      RR=AA-COS(CHETA)
      A1=R/RR
      B11=(-A*A)/(AA-COS(CHETA))
      IF(J.EQ.MD) GO TO 3
      B1=TN(J)*(B11+AA)
      IF(J.GT.MD) GO TO 4
      ERROR=A1-ABS(B1)
      IF(ABS(ERROR).LE.0.000001)  GO TO 2
      IF(ERROR.GT.0.000001) GO TO 2
      GO TO 1
    3 BB=B11+AA
      IF(ABS(BB).LE.0.000001) GO TO 2
      IF(BB.GT.0.000001) GO TO 2
      GO TO 1
    4 ERROR=A1-ABS(B1)
      IF(ABS(ERROR).LE.0.000001) GO TO 2
      IF(ERROR.LT.0.000001) GO TO 2
      GO TO 1
```

```
    2 THETA(J)=CHETA
      DTHETA(J)=CHETA*(360.0/(2.0*3.1415926))
      Y1A(J)=B11
      Y2A(J)=A1
   40 CONTINUE
      WRITE(6,1001)(IETHA(J),Y1A(J),Y2A(J),THETA(J),DTHETA(J),J=1,M1)
 1001 FORMAT(11X,I4,2F13.6,F15.6,F16.6,/)
C---- DETERMINE THE BI-SPHERICAL COORDINATES OF THE OUTER BOUNDARY.
      RD2=RD*RD
      TNHZS=SINH(ZS)/COSH(ZS)
      TNHZS2=TNHZS*TNHZS
      CTP1=(RD2/TNHZS2)+1.0
      CTM1=(RD2/TNHZS2)-1.0
      C=CTP1/CTM1
      WRITE(6,2000)
 2000 FORMAT(1H0,10X,5HIETHA,10X,5HTHETA,10X,2HI1,10X,2HI2,10X,3HN2,/)
      K=0
      MM2=0
      DO 50 J=1,M1
      CS(J)=COS(THETA(J))
      CSHZ=C*CS(J)
      IF(CSHZ.LT.1.0) GO TO 5
      SNHZ=SQRT(CSHZ*CSHZ-1.0)
      EZ=CSHZ+SNHZ
      ZZ=ALOG(EZ)
      II=ZZ/SH
      I1(J)=MMD-II
      I2(J)=MMD+II
      M2=I2(J)-I1(J)+1
      MM2=MM2+M2
      K=K+1
      WRITE(6,2001)IETHA(J),DTHETA(J),I1(J),I2(J),M2,ZZ
 2001 FORMAT(1H0,I16,F15.6,3I12,F15.6)
   50 CONTINUE
    5 JOMIT=K
      WRITE(6,2002) ZS,RD,SH,MM2,JOMIT
 2002 FORMAT(///,11X,2HZS,F6.2,10X,2HRD,F6.2,10X,2HSH,F6.2,10X,3HMM2,I6,
     110X,5HJOMIT,I6,///)
C---- CALCULATION OF THE TOTAL NUMBER OF MESH POINTS OUTSIDE THE OUTER
C----       BOUNDARY WHICH IS TO BE OMITTED.
C----      N2 IS THE TOTAL NUMBER OF POINTS WHICH REQUIRE SPECIAL
C----       TREATMENT,( VORTICITY AT THE SURFACES OF THE SPHERES).
C----      NPR1 IS THE TOTAL NUMBER OF POINT VALUES TO BE OBTAINED.
C----      NOMIT IS THE NUMBER OF POINTS OUTSIDE THE OUTER BOUNDARY.
      N2=2*(M-1)
      NOMIT=0
      DO 60 J=2,JOMIT
      NOMIT=NOMIT+I2(J)-I1(J)+1
   60 CONTINUE
      NPRU1=(M-1)*(MM-1)-NOMIT
      NPRV1=(M-1)*(MM-1)+N2-NOMIT
      NPR1=NPRU1+NPRV1
      RETURN
      END
```

```
      SUBROUTINE INPUT
C---- THIS SUBROUTINE CONTROLS ALL INPUT DATA REQUIRED TO START OFF
C----      SOLUTION PROCEDURE.  IT ALSO SUPPLIES INITIAL INFORMATION
C----      FOR THE FIRST RUN.
      COMMON/GRID1/ Z(41),SNH(41),CSH(41),SN(31),CS(31)
      COMMON/GRID2/ IETHA(31),ETHA(31),THETA(31),DTHETA(31)
      COMMON/GRID3/ H3(41,31),R1(41,31)
      COMMON/UVGFC/ U(41,31),V(41,31),G(41,31),F(41,31)
      COMMON/M1MM1C/ M,M1,MM0,MM,MM1,MD,SH,SK,KS
      COMMON/CNSTC/ ZS,RE,EPSU,EPSG,RFU,RFG
      COMMON/NPRC/ N,MXITER,MX1,MMX1,MNPR,N2,NOMIT,
     1             NPR,NPR1,NPRU,NPRU1,NPRV,NPRV1,NP2
      COMMON/IRREGC/ JOMIT,I1(31),I2(31)
      COMMON/CNTROL/ N3,L4,INTAPE,NDTAPE,NSKIPW,NSKIPR
C---- INTAPE EQUAL 0, IT IS THE FIRST RUN AND STORE THE DATA ON TAPE.
      IF(INTAPE.EQ.1) GO TO 1
      DO 10 J=1,M1
      DO 10 I=1,MM1
      G(I,J)=0.0
      F(I,J)=0.0
   10 CONTINUE
C---- INTVAL SUPPLIES INITIAL VALUES FOR STREAM FUNCTION AND VORTICITY.
      CALL INTVAL
      DO 20 J=2,M
      DO 20 I=2,MM
      G(I,J)=V(I,J)*R1(I,J)
      F(I,J)=V(I,J)/R1(I,J)
   20 CONTINUE
C---- IF NDTAPE=1, STORE INFORMATION ON TAPE 1.
      IF(NDTAPE.NE.1) GO TO 1
      REWIND 1
      IF(NSKIPW.GT.0) CALL SKPFILE(NSKIPW,1)
      WRITE(1)(IETHA(J),ETHA(J),DTHETA(J),THETA(J),I1(J),I2(J),J=1,M1)
      WRITE(1) JOMIT,N2,NPRU1,NPRV1,NPR1,NOMIT
      WRITE(1) (SN(J),CS(J),J=1,M1)
      WRITE(1) ((H3(I,J),R1(I,J),I=1,MM1),J=1,M1)
      WRITE(1) ((U(I,J),I=1,MM1),J=1,M1)
      WRITE(1) ((V(I,J),I=1,MM1),J=1,M1)
      WRITE(1) ((G(I,J),I=1,MM1),J=1,M1)
      WRITE(1) ((F(I,J),I=1,MM1),J=1,M1)
      END FILE 1
      INTAPE=1
      NSKIPW=NSKIPW+1
    1 RETURN
      END
```

```
      SUBROUTINE INTVAL
C---- THIS SUBROUTINE SUPPLIES INITIAL VALUES FOR STREAM FUNCTION AND
C----      VORTICITY .
      COMMON/GRID1/ Z(41),SNH(41),CSH(41),SN(31),CS(31)
      COMMON/GRID2/ IETHA(31),ETHA(31),THETA(31),DTHETA(31)
      COMMON/GRID3/ H3(41,31),R1(41,31)
      COMMON/M1MM1C/ M,M1,MMD,MM,MM1,MD,SH,SK,KS
      COMMON/UVGFC/ U(41,31),V(41,31),G(41,31),F(41,31)
      COMMON/CNSTC/ ZS,RE,EPSU,EPSG,RFU,RFG
      COMMON/COEFF/ B1(41,31),B2(41,31),B3(41,31),B4(41,31)
      COMMON/NCOEFF/ FCOF(41),FCOFM(41),CB2(31),REG(31),A(31)
      COMMON/NPRC/ N,MXITER,MX1,MMX1,MNPR,N2,NOMIT,
     1             NPR,NPR1,NPRU,NPRU1,NPRV,NPRV1,NP2
      COMMON/IRREGC/ JOMIT,I1(31),I2(31)
      COMMON/VZVTC/ VZ(41,31), VT(41,31)
      DO 10 J=1,M1
      DO 10 I=1,MM1
      U(I,J)=0.0
      V(I,J)=0.
   10 CONTINUE
C---- INITIAL STREAM FUNCTION AT ALL INTERNAL MESH POINTS.
C---- SUPPLY STIMSON AND JEFFERY ANALYTICAL SOLUTIONS.
      CALL VELDIS
C---- INITIAL STREAM FUNCTION AT THE SURFACES OF THE SPHERES.
      DO 13 J=1,M1
      U(1,J)=0.
      U(MM1,J)=0.
   13 CONTINUE
C---- INITIAL STREAM FUNCTION ALONG THE OUTER BOUNDARY.
      DO 14 J=1,JOMIT
      ILEFT=I1(J)
      IRIGHT=I2(J)
      DO 14 I=ILEFT,IRIGHT
      U(I,J)=0.5*R1(I,J)*R1(I,J)
   14 CONTINUE
C---- INITIAL STREAM FUNCTION ALONG THE AXES OF SYMMETRY.
      DO 15 I=2,MM
      U(I,1)=0.0
      U(I,M1)=0.0
   15 CONTINUE
C---- CONVERSION OF INITIAL STREAM FUNCTION INTO VORTICITY.
      DO 100 J=2,JOMIT
      DO 100 I=2,MM
      IF(I.GE.I1(J).AND.I.LE.I2(J)) GO TO 100
      V1=(VT(I+1,J)-VT(I-1,J))/(2.0*SH*H3(I,J))
      V2=VT(I,J)*(SNH(I)/SNH(MM1))
      V3=(VZ(I,J+1)-VZ(I,J-1))/(2.0*SK*H3(I,J))
      V4=VZ(I,J)*(SN(J)/SNH(MM1))
      V(I,J)=V1-V2-V3+V4
  100 CONTINUE
      JREG=JOMIT+1
      DO 101 J=JREG,M
      DO 101 I=2,MM
      V1=(VT(I+1,J)-VT(I-1,J))/(2.0*SH*H3(I,J))
      V2=VT(I,J)*(SNH(I)/SNH(MM1))
      V3=(VZ(I,J+1)-VZ(I,J-1))/(2.0*SK*H3(I,J))
      V4=VZ(I,J)*(SN(J)/SNH(MM1))
      V(I,J)=V1-V2-V3+V4
  101 CONTINUE
```

```
      DO 110 J=2,M
      VGN1=(8.0*U(2,J)-U(3,J))*CB2(J)
      V(1,J)=VGN1/R1(1,J)
      G(1,J)=VGN1
      VGNMM1=(8.0*U(MM,J)-U(MM-1,J))*CB2(J)
      V(MM1,J)=VGNMM1/R1(MM1,J)
      G(MM1,J)=VGNMM1
  110 CONTINUE
C---- PRINT OUT INITIAL VALUES FOR STREAM FUNCTION AND VORTICITY.
      WRITE(6,2000)
 2000 FORMAT(1H1,///,30X,72H*****STREAM FUNCTION AND VORTICITY FROM STIM
     1SON-JEFFERY EXPRESSION.*****)
      WRITE(6,2002)
 2002 FORMAT(1H0,20X,29H*****U---STREAM FUNCTION*****,////)
      WRITE(6,2003) (Z(I),I=1,MMD,2)
 2003 FORMAT(1H0,7X,4HZ(I),11F11.2,//)
      WRITE(6,2004) (IETHA(J),DTHETA(J),(U(I,J),I=1,MMD,2),J=1,M1)
 2004 FORMAT(1X,I3,2X,F5.1,11F11.6)
      WRITE(6,2005) (Z(I),I=MMD,MM1,2)
 2005 FORMAT(1H1,//,7X,4HZ(I),11F11.2,//)
      WRITE(6,2006) (IETHA(J),DTHETA(J),(U(I,J),I=MMD,MM1,2),J=1,M1)
 2006 FORMAT(1X,I3,2X,F5.1,11F11.6)
      WRITE(6,2008)
 2008 FORMAT(1H1,20X,29H*****V----VORTICITY-----*****,////)
      WRITE(6,2009) (Z(I),I=1,MMD,2)
 2009 FORMAT(1H0,7X,4HZ(I),11F11.2,//)
      WRITE(6,2010) (IETHA(J),DTHETA(J),(V(I,J),I=1,MMD,2),J=1,M1)
 2010 FORMAT(1X,I3,2X,F5.1,11F11.4)
      WRITE(6,2011) (Z(I),I=MMD,MM1,2)
 2011 FORMAT(1H0,7X,4HZ(I),11F11.2,//)
      WRITE(6,2012) (IETHA(J),DTHETA(J),(V(I,J),I=MMD,MM1,2),J=1,M1)
 2012 FORMAT(1X,I3,2X,F5.1,11F11.4)
C---- STREAM FUNCTION AND VORTICITY CONTOURS ARE SEARCHED AND PLOTTED.
      CALL CNPLTP
      RETURN
      END
```

```
      SUBROUTINE VELDIS
C---- THIS SUBROUTINE SUPPLIES STIMSON-JEFFERYS ANALYTICAL SOLUTIONS.
      COMMON/GRID1/ Z(41),SNH(41),CSH(41),SN(31),CS(31)
      COMMON/GRID2/ IETHA(31),ETHA(31),THETA(31),DTHETA(31)
      COMMON/GRID3/ H3(41,31),R1(41,31)
      COMMON/M1MM1C/ M,M1,MM0,MM,MM1,MD,SH,SK,KS
      COMMON/UVGFC/ U(41,31),V(41,31),G(41,31),F(41,31)
      COMMON/CNSTC/ ZS,RF,EPSU,EPSG,RFU,RFG
      COMMON/NPRC/ N,MXITER,MX1,MMX1,MNPR,N2,NOMIT,
     1             NPR,NPR1,NPRU,NPRU1,NPRV,NPRV1,NP2
      COMMON/VZVTC/ VZ(41,31), VT(41,31)
      DIMENSION Y(31,20)
      DO 10 J=1,M1
      DO 10 I=1,MM1
      VZ(I,J)=0.0
      VT(I,J)=0.0
      U(I,J)=0.
   10 CONTINUE
C---- SUPPLY LEGENDRE POLYNOMIAL UP TO ORDER (0--19)
      NTERM=19
      DO 5 J=1,M1
      Y(J,1)=1.
      Y(J,2)=CS(J)
      DO 4 K=2,NTERM
      H=CS(J)*Y(J,K)
      Y(J,K+1)=2.0*H-Y(J,K-1)-(H-Y(J,K-1))/FLOAT(K)
    4 CONTINUE
    5 CONTINUE
      ROOT2=SQRT(2.0)
      YZ2=2.0*ZS
      E1=EXP(YZ2)
      ZSNH1=SINH(YZ2)
      DO 300 J=2,M
      X=CS(J)
      X1=SN(J)
      DO 200 I=2,MM
      X2=CSH(I)-CS(J)
      X3=SNH(I)
      X4=CSH(I)
      X2P1=SQRT(X2)
      X2M1=1.0/X2P1
      SUM1=0.
      SUM2=0.
      SUM3=0.
      SUM4=0.0
      NORDER=10
      DO 100 N=1,NORDER
      YN=N
      YN2=2.0*YN
      YN21=YN2+1.0
      AK=YN*(YN+1.0)/(ROOT2*(YN2-1.0)*YN21*(YN2+3.0))
      AKU=AK*SNH(MM1)*SNH(MM1)
C
      YZN21=YN21*ZS
      YNM=YN-0.5
      YNP=YN+1.5
      ZYNM=YNM*Z(I)
      ZYNP=YNP*Z(I)
      E2=1.0/EXP(YZN21)
      ZSNH2=SINH(YZN21)
```

```
      AB=2.0*ZSNH2+YN21*ZSNH1
      D1=2.0*(1.0-E2)
      D2=YN21*(E1-1.0)
      D3=YN21*(1.0-1.0/E1)
      AN=-(YN2+3.0)*AK*(D1+D2)/AB
      BN= (YN2-1.0)*AK*(D1+D3)/AB
      UN=AN*COSH(ZYNM)+BN*COSH(ZYNP)
      DUN=YNM*AN*SINH(ZYNM)+YNP*BN*SINH(ZYNP)
      ANU=-(YN2+3.0)*AKU*(D1+D2)/AB
      BNU=(YN2-1.0)*AKU*(D1+D3)/AB
      UNU=ANU*COSH(ZYNM)+BNU*COSH(ZYNP)
C
      PNM1=Y(J,N)
      PN=Y(J,N+1)
      PNP1=Y(J,N+2)
      PNP2=Y(J,N+3)
      VN=PNM1-PNP1
      DVN=(YN*(PN-X*PNM1)+(YN+2.0)*(X*PNP1-PNP2))/X1
      SUM1=SUM1+UN*VN
      SUM2=SUM2+UN*DVN
      SUM3=SUM3+VN*DUN
      SUM4=SUM4+UNU*VN
  100 CONTINUE
      V1=(1.0-X*X4)/X2
      V2=X2P1/X1
      V3=-X1*X3/X2
      V4=-1.5*X2M1*X3/X1
      VZ(I,J)=V1+1.5*X2M1*SUM1-V2*SUM2
      VT(I,J)=V3+V4*SUM1+V2*SUM3
      V5=0.5*R1(I,J)*R1(I,J)
      V6=X2M1*X2M1*X2M1
      U(I,J)=V5+V6*SUM4
  200 CONTINUE
  300 CONTINUE
      DO 155 I=2,MM
      VZ(I,1)=1.92*VZ(I,2)-1.44*VZ(I,3)+0.64*VZ(I,4)-0.12*VZ(I,5)
      VZ(I,M1)=1.92*VZ(I,M)-1.44*VZ(I,M-1)+0.64*VZ(I,M-2)-0.12*VZ(I,M-3)
  155 CONTINUE
      WRITE(6,1000)
 1000 FORMAT(1H1,*  VELOCITY IN THE Z-DIRECTION    *)
      WRITE(6,3010) (Z(I),I=1,MMD,2)
 3010 FORMAT(1H0,11X,11F11.2,/)
      WRITE(6,3000) (IETHA(J),DTHETA(J), (VZ(I,J),I=1,MMD,2),J=1,M1)
      WRITE(6,3020) (Z(I),I=MMD,MM1,2)
 3020 FORMAT(1H0,11X,11F11.2,/)
      WRITE(6,3000) (IETHA(J),DTHETA(J), (VZ(I,J),I=MMD,MM1,2),J=1,M1)
 3000 FORMAT(1X,I3,2X,F5.1,11F11.4)
      WRITE(6,2000)
 2000 FORMAT(1H1,*  VELOCITY IN THE THETA-DIRECTION *)
      WRITE(6,4010) (Z(I),I=1,MMD,2)
 4010 FORMAT(1H0,11X,11F11.2,/)
      WRITE(6,4000) (IETHA(J),DTHETA(J), (VT(I,J),I=1,MMD,2),J=1,M1)
      WRITE(6,4020) (Z(I),I=MMD,MM1,2)
 4020 FORMAT(1H0,11X,11F11.2,/)
      WRITE(6,4000) (IETHA(J),DTHETA(J), (VT(I,J),I=MMD,MM1,2),J=1,M1)
 4000 FORMAT(1X,I3,2X,F5.1,11F11.4)
      RETURN
      END
```

```
      SUBROUTINE RESTAB
C---- THIS SUBROUTINE PRINTS OUT THE STREAM FUNCTION AND VORTICITY
C----      DISTRIBUTIONS IN TABULATED FORM.
      COMMON/GRID1/ Z(41),SNH(41),CSH(41),SN(31),CS(31)
      COMMON/GRID2/ IETHA(31),ETHA(31),THETA(31),DTHETA(31)
      COMMON/GRID3/ H3(41,31),R1(41,31)
      COMMON/M1MM1C/ M,M1,MMD,MM,MM1,MD,SH,SK,KS
      COMMON/UVGFC/ U(41,31),V(41,31),G(41,31),F(41,31)
      COMMON/CNSTC/ ZS,RE,EPSU,EPSG,RFU,RFG
      COMMON/NPRC/ N,MXITER,MX1,MMX1,MNPR,N2,NOMIT,
     1             NPR,NPR1,NPRU,NPRU1,NPRV,NPRV1,NP2
C
      WRITE(6,100) RE,RFU,RFG
  100 FORMAT(1H1, ///,1X,4HRE =,F10.5,5X,5HRFU =,F10.5,5X,5HRFG =,F10.5)
      WRITE(6,102)  NPRU1,NPRV1,NPR1,NOMIT
  102 FORMAT(1H0,//,20X,7HNPRU1 =,I5,11X,7HNPRV1 =,I5,10X,6HNPR1 =,I5,10
     1X,7HNOMIT =,I5,//)
      WRITE(6,101) N,NPRU,NPRV,NPR,NP2
  101 FORMAT(1H0, //,1X,3HN =,I5,5X,6HNPRU =,I5,5X,6HNPRV =,I5,5X,5HNPR
     1=,I5,5X,5HNP2 =,I5,///)
      WRITE(6,200)
  200 FORMAT(1H0, 20X,29H*****U---STREAM FUNCTION*****,//)
      WRITE(6,201) (Z(I),I=1,MMD,2)
  201 FORMAT(1H0,6X,4HZ(I),11F10.2,//)
      WRITE(6,202) (IETHA(J),DTHETA(J),(U(I,J),I=1,MMD,2),J=1,M1)
  202 FORMAT(1X,I3,2X,F5.1,11F10.6)
      WRITE(6,203) (Z(I),I=MMD,MM1,2)
  203 FORMAT(///,6X,4HZ(I),11F10.2,//)
      WRITE(6,204) (IETHA(J),DTHETA(J),(U(I,J),I=MMD,MM1,2),J=1,M1)
  204 FORMAT(1X,I3,2X,F5.1,11F10.6)
      WRITE(6,300)
  300 FORMAT(1H1, ///,20X,29H*****V----VORTICITY----******,///)
      WRITE(6,301) (Z(I),I=1,MMD,2)
  301 FORMAT(1H0,6X,4HZ(I),11F10.2,//)
      WRITE(6,302) (IETHA(J),DTHETA(J),(V(I,J),I=1,MMD,2),J=1,M1)
  302 FORMAT(1X,I3,2X,F5.1,11F10.6)
      WRITE(6,303) (Z(I),I=MMD,MM1,2)
  303 FORMAT(///,6X,4HZ(I),11F10.2,//)
      WRITE(6,304) (IETHA(J),DTHETA(J),(V(I,J),I=MMD,MM1,2),J=1,M1)
  304 FORMAT(1X,I3,2X,F5.1,11F10.6)
      RETURN
      END
```

```
      SUBROUTINE PDCOEF
C---- THIS SUBROUTINE CALCULATES THE SURFACE PRESSURES AND DRAG
C----      COEFFICIENTS FOR THE TWO SPHERES.
      COMMON/GRID1/ Z(41),SNH(41),CSH(41),SN(31),CS(31)
      COMMON/GRID2/ IETHA(31),ETHA(31),THETA(31),DTHETA(31)
      COMMON/GRID3/ H3(41,31),R1(41,31)
      COMMON/UVGFC/ U(41,31),V(41,31),G(41,31),F(41,31)
      COMMON/M1MM1C/ M,M1,MMD,MM,MM1,MD,SH,SK,KS
      COMMON/CNSTC/ ZS,RE,EPSU,EPSG,RFU,RFG
      COMMON/IRREGC/ JOMIT,I1(31),I2(31)
      COMMON/OFOSC/ OF,OF4,OF3,OF2,OS,OS4,OS3,OS2
      COMMON/PFPSC/ PF,PF4,PF3,PF2,PS,PS4,PS3,PS2
      COMMON/PRESSC/ AKFSP,AKRSP,AKSTAR,BKFSP,BKRSP,BKSTAR
      COMMON/ABK/ AK(31),BK(31)
      DIMENSION SINETA(31),COSETA(31)
      DIMENSION DVDT(41)
      DIMENSION VTA(31),VTB(31),VSNA2(31),VSNB2(31),AKSN2(31),BKSN2(31)
      RE4=4.0/RE
      SS=1.0/(6.0*SH)
      DO 1 J=1,M1
      SINETA(J)=SIN(ETHA(J))
      COSETA(J)=COS(ETHA(J))
    1 CONTINUE
C---- ************************************************
C---- SURFACE PRESSURE DISTRIBUTIONS FOR SPHERE A.
C---- ************************************************
C---- CALCULATE THE PRESSURE AT THE FRONT STAGNATION POINT OF SPHERE A.
      II1=I1(1)
      DO 10 I=1,MMD
      DVDT(I)=(OF4*(V(I,4)-V(I,1))-OF3*(V(I,3)-V(I,1))+OF2*(V(I,2)-V(I,1
     1)))/OF
   10 CONTINUE
      SDVDT=0.50*DVDT(1)
      DO 11 I=2,II1
      SDVDT=SDVDT+DVDT(I)
   11 CONTINUE
      A1=SH*SDVDT
      AKFSP=1.0+8.0*A1/RE
C
C---- CALCULATE THE SURFACE PRESSURES FOR SPHERE A FROM THE FRONT TO
C----      REAR STAGNATION POINTS.
      DO 20 J=1,M1
      YY=SS*(-11.0*V(1,J)+18.0*V(2,J)-9.0*V(3,J)+2.0*V(4,J))
      AA=-SNH(1)/(CSH(1)-CS(J))
      VTA(J)=RE4*(YY+AA*V(1,J))
      VSNA2(J)=V(1,J)*SINETA(J)*H3(1,J)*R1(1,J)
   20 CONTINUE
      AK(1)=AKFSP
      AKSN2(1)=0.0
      DO 25 J=2,M1
      AK(J)=AK(J-1)+0.50*(VTA(J)+VTA(J-1))*(THETA(J)-THETA(J-1))
      AKSN2(J)=2.0*AK(J)*COSETA(J)*H3(1,J)*R1(1,J)
   25 CONTINUE
      AKRSP=AK(M1)
C---- ************************************************
C---- SURFACE PRESSURE DISTRIBUTIONS FOR SPHERE B.
C---- ************************************************
C---- CALCULATE THE PRESSURE AT THE REAR STAGNATION POINT OF SPHERE B.
      II2=I2(1)
      DO 50 I=MMD,MM1
```

```
      DVDT(I)=(OF4*(V(I,4)-V(I,1))-OF3*(V(I,3)-V(I,1))+OF2*(V(I,2)-V(I,1
     +)))/OF
   50 CONTINUE
      SDVDT=0.50*DVDT(MM1)
      DO 51 I=I12,MM
      SDVDT=SDVDT+DVDT(I)
   51 CONTINUE
      B1=SH*SDVDT
      BKRSP=1.0-8.0*B1/RE
C---- CALCULATE THE SURFACE PRESSURES FOR SPHERE B FROM THE REAR TO
C----      FRONT STAGNATION POINTS.
      DO 60 J=1,M1
      YY=SS*(-11.0*V(MM1,J)+18.0*V(MM,J)-9.0*V(MM-1,J)+2.0*V(MM-2,J))
      AA=+SNH(MM1)/(CSH(MM1)-CS(J))
      VTB(J)=RE4*(YY+AA*V(MM1,J))
      VSNB2(J)=V(MM1,J)*SINETA(J)*H3(MM1,J)*R1(MM1,J)
   60 CONTINUE
      BK(1)=BKRSP
      BKSN2(1)=0.0
      DO 65 J=2,M1
      BK(J)=BK(J-1)-0.50*(VTB(J)+VTB(J-1))*(THETA(J)-THETA(J-1))
      BKSN2(J)=-2.*BK(J)*COSETA(J)*H3(MM1,J)*R1(MM1,J)
   65 CONTINUE
      BKFSP=BK(M1)
C---- **********************************
C---- CALCULATION OF DRAG COEFFICIENTS.
C---- **********************************
      CDFA=0.0
      CDPA=0.0
      CDFB=0.0
      CDPB=0.0
      DO 100 J=2,M1
      XX=0.50*(THETA(J)-THETA(J-1))
      CDFA=CDFA+(VSNA2(J)+VSNA2(J-1))*XX*8.0/RE
      CDFB=CDFB+(VSNB2(J)+VSNB2(J-1))*XX*8.0/RE
      CDPA=CDPA+(AKSN2(J)+AKSN2(J-1))*XX
      CDPB=CDPB+(BKSN2(J)+BKSN2(J-1))*XX
  100 CONTINUE
      CDTA=CDFA+CDPA
      CDTB=CDFB+CDPB
C---- PRINTS OUT THE RESULTS.
      WRITE(6,1000) ZS,RE
 1000 FORMAT(1H1,1X,4HZS =,F6.2,5X,4HRE =,F10.3,//)
      WRITE(6,1001)
 1001 FORMAT(10X,5HIETHA,4X,6HDTHETA,7X,3HVTA,8X,2HAK,7X,3HVTB,8X,2HBK)
      WRITE(6,1002)
 1002 FORMAT(10X,5H-----,4X,6H------,7X,3H---,8X,2H--,7X,3H---,8X,2H--/)
      WRITE(6,1003) (IETHA(J),DTHETA(J),VTA(J),AK(J),VTB(J),BK(J),J=1,M1
     +)
 1003 FORMAT(5X,I10,F10.2,4F10.4)
      WRITE(6,1005)
 1005 FORMAT(///,1X,20HDVDT(I) OF SPHERE A.)
      WRITE(6,1006) (Z(I),DVDT(I),I=1,MMD)
 1006 FORMAT(5X,F6.2,5X,F10.4)
      WRITE(6,1007)
 1007 FORMAT(///,1X,20HDVDT(I) OF SPHERE B.)
      WRITE(6,1008) (Z(I),DVDT(I),I=MMD,MM1)
 1008 FORMAT(5X,F6.2,5X,F10.4)
      WRITE(6,2000) RE,CDFA,CDPA,CDTA
 2000 FORMAT(////,1X,4HRE =,F8.3,5X,6HCDFA =,F12.5,5X,6HCDPA =,F12.5,5X,
     16HCDTA =,F12.5,//)
      WRITE(6,2001) CDFB,CDPB,CDTB
 2001 FORMAT(18X,6HCDFB =, F12.5,5X,6HCDPB =,F12.5,5X,6HCDTB =,F12.5,//)
      RETURN
      END
```

```
      SUBROUTINE CNPLTP
C---- THIS SUBROUTINE EVALUATES PLOT POSITIONS OF CONTOURS AND CALLS
C----    THE LINE-PRINTER PLOTTING SUBROUTINE.
      COMMON/GRID1/ Z(41),SNH(41),CSH(41),SN(31),CS(31)
      COMMON/GRID2/ IETHA(31),ETHA(31),THETA(31),DTHETA(31)
      COMMON/GRID3/ H3(41,31),R1(41,31)
      COMMON/CNSTC/ ZS,RE,EPSU,EPSG,RFU,RFG
      COMMON/M1MM1C/ M,M1,MMD,MM,MM1,MD,SH,SK,KS
      COMMON/UVGFC/ U(41,31),V(41,31),G(41,31),F(41,31)
      COMMON/PLOT1/ X1(31,10),X2(31,10),Y1(31,10),Y2(31,10)
      COMMON/PLOT2/ X3(31,10),X4(31,10),Y3(31,10),Y4(31,10)
      COMMON/ZVC1/ ZVC1(10),ZVC2(10),LVC1(10)
      COMMON/ZVC2/ ZVC3(10),ZVC4(10),LVC2(10)
      COMMON/PLTPCN/ VCU(10),VCV(10),KNU,KNV,KNP
      COMMON/RPLOTC/ RPLOT,RPLOTU,RPLOTV,IYS,IXSTEP
      COMMON/RRABC/ RRA,RRB,RRC,RRCU,RRCV,RRL
C---- ------------------------
C---- STREAM FUNCTION CONTOURS.
C---- ------------------------
      DO 1 J=1,M1
      DO 1 K=1,KNU
      X1(J,K)=0.00£Y1(J,K)=0.00
      X2(J,K)=0.00£Y2(J,K)=0.00
      X3(J,K)=0.00£Y3(J,K)=0.00
      X4(J,K)=0.00£Y4(J,K)=0.00
    1 CONTINUE
      DO 10 K=1,KNU
      ZVC1(K)=0.00£ZVC2(K)=0.00£LVC1(K)=1
      ZVC3(K)=0.00£ZVC4(K)=0.00£LVC2(K)=1
   10 CONTINUE
C---- SEARCH AND INTERPOLATE BETWEEN TWO I-LINE.
      DO 100 J=1,M1
      DO 110 I=2,MM1
      IF(I.EQ.MMD.AND.J.EQ.1) GO TO 110
      DO 110 K=1,KNU
      IF( U(I-1,J).GE.VCU(K).AND. U(I,J).LE.VCU(K)) GO TO 200
      IF( U(I-1,J).LE.VCU(K).AND. U(I,J).GE.VCU(K)) GO TO 200
      GO TO 110
C---- SEARCH THE STREAM FUNCTION CONTOURS FOR THE FIRST SPHERE.
  200 IF(I.GT.MMD) GO TO 201
      IF(LVC1(K).EQ.0) GO TO 101
      A=(VCU(K)-U(I-1,J))
      IF(A.EQ.0.0) A=10.E-30
      B=(U(I,J)-U(I-1,J))
      IF(B.EQ.0.0) B=10.E-30
      SLOPE=A/B
      ZVC1(K)=Z(I-1)+SLOPE*(Z(I)-Z(I-1))
      ZVC2(K)=0.0
      LVC1(K)=0
      GO TO 110
  101 A=(VCU(K)-U(I-1,J))
      IF(A.EQ.0.0) A=10.E-30
      B=(U(I,J)-U(I-1,J))
      IF(B.EQ.0.0) B=10.E-30
      SLOPE=A/B
      ZVC2(K)=Z(I-1)+SLOPE*(Z(I)-Z(I-1))
      GO TO 110
C---- SEARCH THE STREAM FUNCTION CONTOURS FOR THE SECOND SPHERE.
  201 IF(LVC2(K).EQ.0) GO TO 102
      A=VCU(K)-U(I-1,J)
      IF(A.EQ.0.0) A=10.E-30
      B=(U(I,J)-U(I-1,J))
      IF(B.EQ.0.0) B=10.E-30
      SLOPE=A/B
      ZVC3(K)=Z(I-1)+SLOPE*(Z(I)-Z(I-1))
```

```
      ZVC4(K)=0.0
      LVC2(K)=0
      GO TO 110
  102 A=(VCU(K)-U(I-1,J))
      IF(A.EQ.0.0) A=10.E-30
      B=(U(I,J)-U(I-1,J))
      IF(B.EQ.0.0) B=10.E-30
      SLOPE=A/B
      ZVC4(K)=Z(I-1)+SLOPE*(Z(I)-Z(I-1))
  110 CONTINUE
C---- CONVERT TO RECTAGULAR COORDINATES
      DO 300 K=1,KNU
      IF(ZVC1(K).EQ.0.0) GO TO 301
      IF(ZVC1(K).GT.100.0) ZVC1(K)=100.0
      IF(ZVC1(K).LT.-100.) ZVC1(K)=-100.
      A1=SINH(ZVC1(K))
      B1=COSH(ZVC1(K))
      B1J=B1-CS(J)
      IF(B1J.EQ.0.0) B1J=10.E-30
      Y1(J,K)=SNH(MM1)*SN(J)/B1J
      X1(J,K)=SNH(MM1)*A1/B1J
      GO TO 300
  301 X1(J,K)=0.0£Y1(J,K)=0.0
  300 CONTINUE
      DO 310 K=1,KNU
      IF(ZVC2(K).EQ.0.0) GO TO 311
      IF(ZVC2(K).GT.100.0) ZVC2(K)=100.0
      IF(ZVC2(K).LT.-100.) ZVC2(K)=-100.
      A2=SINH(ZVC2(K))
      B2=COSH(ZVC2(K))
      B2J=B2-CS(J)
      IF(B2J.EQ.0.0) B2J=10.E-30
      Y2(J,K)=SNH(MM1)*SN(J)/B2J
      X2(J,K)=SNH(MM1)*A2/B2J
      GO TO 310
  311 X2(J,K)=0.0£Y2(J,K)=0.0
  310 CONTINUE
      DO 320 K=1,KNU
      IF(ZVC3(K).EQ.0.0) GO TO 321
      IF(ZVC3(K).GT.100.0) ZVC3(K)=100.0
      IF(ZVC3(K).LT.-100.) ZVC3(K)=-100.
      A3=SINH(ZVC3(K))
      B3=COSH(ZVC3(K))
      B3J=B3-CS(J)
      IF(B3J.EQ.0.0) B3J=10.E-30
      Y3(J,K)=SNH(MM1)*SN(J)/B3J
      X3(J,K)=SNH(MM1)*A3/B3J
      GO TO 320
  321 X3(J,K)=0.0£Y3(J,K)=0.0
  320 CONTINUE
      DO 330 K=1,KNU
      IF(ZVC4(K).EQ.0.0) GO TO 331
      IF(ZVC4(K).GT.100.0) ZVC4(K)=100.0
      IF(ZVC4(K).LT.-100.) ZVC4(K)=-100.
      A4=SINH(ZVC4(K))
      B4=COSH(ZVC4(K))
      B4J=B4-CS(J)
      IF(B4J.EQ.0.0) B4J=10.E-30
      Y4(J,K)=SNH(MM1)*SN(J)/B4J
      X4(J,K)=SNH(MM1)*A4/B4J
      GO TO 330
  331 X4(J,K)=0.0£Y4(J,K)=0.0
  330 CONTINUE
      DO 11 K=1,KNU
      ZVC1(K)=0.
      ZVC2(K)=0.
```

```
      LVC1(K)=1
      ZVC3(K)=0.
      ZVC4(K)=0.
      LVC2(K)=1
   11 CONTINUE
  100 CONTINUE
C---- PLOT STREAM FUNCTION CONTOURS AROUND THE SPHERES.
      KNP=KNU
      RRC=RRCU
      CALL CNPLOT
C---- ------------------
C---- VORTICITY CONTOURS.
C---- ------------------
      DO 2 J=1,M1
      DO 2 K=1,KNV
      X1(J,K)=0.00£Y1(J,K)=0.00
      X2(J,K)=0.00£Y2(J,K)=0.00
      X3(J,K)=0.00£Y3(J,K)=0.00
      X4(J,K)=0.00£Y4(J,K)=0.00
    2 CONTINUE
      DO 12 K=1,KNV
      ZVC1(K)=0.00£ZVC2(K)=0.00£LVC1(K)=1
      ZVC3(K)=0.00£ZVC4(K)=0.00£LVC2(K)=1
   12 CONTINUE
C---- SEARCH AND INTERPOLATE BETWEEN TWO I-LINES.
      DO 120 J=1,M1
      DO 130 I=2,MM1
      IF(I.EQ.MMD.AND.J.EQ.1) GO TO 130
      DO 130 K=1,KNV
      IF( V(I-1,J).GE.VCV(K).AND. V(I,J).LE.VCV(K)) GO TO 210
      IF( V(I-1,J).LE.VCV(K).AND. V(I,J).GE.VCV(K)) GO TO 210
      GO TO 130
C---- SEARCH THE VORTICITY CONTOURS FOR THE FIRST SPHERE.
  210 IF(1.GT.MMD) GO TO 211
      IF(LVC1(K).EQ.0) GO TO 121
      C=(VCV(K)-V(I-1,J))
      IF(C.EQ.0.0) C=10.E-30
      D=(V(I,J)-V(I-1,J))
      IF(D.EQ.0.0) D=10.E-30
      SLOPE=C/D
      ZVC1(K)=Z(I-1)+SLOPE*(Z(I)-Z(I-1))
      ZVC2(K)=0.0
      LVC1(K)=0
      GO TO 130
  121 C=(VCV(K)-V(I-1,J))
      IF(C.EQ.0.0) C=10.E-30
      D=(V(I,J)-V(I-1,J))
      IF(D.EQ.0.0) D=10.E-30
      SLOPE=C/D
      ZVC2(K)=Z(I-1)+SLOPE*(Z(I)-Z(I-1))
      GO TO 130
C---- SEARCH THE VORTICITY CONTOURS FOR THE SECOND SPHERE.
  211 IF(LVC2(K).EQ.0) GO TO 122
      C=(VCV(K)-V(I-1,J))
      IF(C.EQ.0.0) C=10.E-30
      D=(V(I,J)-V(I-1,J))
      IF(D.EQ.0.0) D=10.E-30
      SLOPE=C/D
      ZVC3(K)=Z(I-1)+SLOPE*(Z(I)-Z(I-1))
      ZVC4(K)=0.0
      LVC2(K)=0
      GO TO 130
```

```
  122 C=(VCV(K)-V(I-1,J))
      IF(C.EQ.0.0) C=10.E-30
      D=(V(I,J)-V(I-1,J))
      IF(D.EQ.0.0) D=10.E-30
      SLOPE=C/D
      ZVC4(K)=Z(I-1)+SLOPE*(Z(I)-Z(I-1))
  130 CONTINUE
C---- CONVERT TO RECTANGULAR COORDINATES
      DO 500 K=1,KNV
      IF(ZVC1(K).EQ.0.0) GO TO 501
      IF(ZVC1(K).GT.100.0) ZVC1(K)=100.0
      IF(ZVC1(K).LT.-100.) ZVC1(K)=-100.
      A1=SINH(ZVC1(K))
      B1=COSH(ZVC1(K))
      B1J=B1-CS(J)
      IF(B1J.EQ.0.0) B1J=10.E-30
      Y1(J,K)=SNH(MM1)*SN(J)/B1J
      X1(J,K)=SNH(MM1)*A1/B1J
      GO TO 500
  501 X1(J,K)=0.0£Y1(J,K)=0.0
  500 CONTINUE
      DO 510 K=1,KNV
      IF(ZVC2(K).EQ.0.0) GO TO 511
      IF(ZVC2(K).GT.100.0) ZVC2(K)=100.0
      IF(ZVC2(K).LT.-100.) ZVC2(K)=-100.
      A2=SINH(ZVC2(K))
      B2=COSH(ZVC2(K))
      B2J=B2-CS(J)
      IF(B2J.EQ.0.0) B2J=10.E-30
      Y2(J,K)=SNH(MM1)*SN(J)/B2J
      X2(J,K)=SNH(MM1)*A2/B2J
      GO TO 510
  511 X2(J,K)=0.0£Y2(J,K)=0.0
  510 CONTINUE
      DO 520 K=1,KNV
      IF(ZVC3(K).EQ.0.0) GO TO 521
      IF(ZVC3(K).GT.100.0) ZVC3(K)=100.0
      IF(ZVC3(K).LT.-100.) ZVC3(K)=-100.
      A3=SINH(ZVC3(K))
      B3=COSH(ZVC3(K))
      B3J=B3-CS(J)
      IF(B3J.EQ.0.0) B3J=10.E-30
      Y3(J,K)=SNH(MM1)*SN(J)/B3J
      X3(J,K)=SNH(MM1)*A3/B3J
      GO TO 520
  521 X3(J,K)=0.0£Y3(J,K)=0.0
  520 CONTINUE
      DO 530 K=1,KNV
      IF(ZVC4(K).EQ.0.0) GO TO 531
      IF(ZVC4(K).GT.100.0) ZVC4(K)=100.0
      IF(ZVC4(K).LT.-100.) ZVC4(K)=-100.
      A4=SINH(ZVC4(K))
      B4=COSH(ZVC4(K))
      B4J=B4-CS(J)
      IF(B4J.EQ.0.0) B4J=10.E-30
      Y4(J,K)=SNH(MM1)*SN(J)/B4J
      X4(J,K)=SNH(MM1)*A4/B4J
      GO TO 530
  531 X4(J,K)=0.0£Y4(J,K)=0.0
  530 CONTINUE
```

```
      DO 13 K=1,KNV
      ZVC1(K)=0.
      ZVC2(K)=0.
      LVC1(K)=1
      ZVC3(K)=0.
      ZVC4(K)=0.
      LVC2(K)=1
   13 CONTINUE
  120 CONTINUE
C---- PLOT VORTICITY CONTOURS AROUND THE TWO SPHERES.
      KNP=KNV
      RRC=RRCV
      CALL CNPLOT
      RETURN
      END




      SUBROUTINE CNPLOT
C---- THIS SUBROUTINE PLOTS STREAM FUNCTION AND VORTICITY CONTOURS.
      COMMON/GRID1/ Z(41),SNH(41),CSH(41),SN(31),CS(31)
      COMMON/GRID2/ IETHA(31),ETHA(31),THETA(31),DTHETA(31)
      COMMON/GRID3/ H3(41,31),R1(41,31)
      COMMON/CNSTC/ ZS,RE,EPSU,EPSG,RFU,RFG
      COMMON/M1MM1C/ M,M1,MMD,MM,MM1,MD,SH,SK,KS
      COMMON/PLOT1/ X1(31,10),X2(31,10),Y1(31,10),Y2(31,10)
      COMMON/PLOT2/ X3(31,10),X4(31,10),Y3(31,10),Y4(31,10)
      COMMON/RPLOTC/ RPLOT,RPLOTU,RPLOTV,IYS,IXSTEP
      COMMON/PLTPCN/ VCU(10),VCV(10),KNU,KNV,KNP
      COMMON/RRABC/ RRA,RRB,RRC,RRCU,RRCV,RRL
      DIMENSION CHAR(120),FPLOT(8)
      DATA BLANK,PLOT,PLUS,CROSS/1H ,1H.,1H+,1HX/
      DATA FPLOT/ 1H1,1H2,1H3,1H4,1H5,1H6,1H7,1H8/
C---- THE ZERO-CONTOUR ALONG THE AXES OF SYMMETRY, THETA = 0 AND 180.
      DO 200 K=1,KNP
      X1(1,K)=SNH(MM1)*SNH(K)/(CSH(K)-CS(1))
      Y1(1,K)=SNH(MM1)*SN(1)/(CSH(K)-CS(1))
      X3(1,K)=SNH(MM1)*SNH(MM1-K)/(CSH(MM1-K)-CS(1))
      Y3(1,K)=SNH(MM1)*SN(1)/(CSH(MM1-K)-CS(1))
C
      X1(M1,K)=SNH(MM1)*SNH(K)/(CSH(K)-CS(M1))
      Y1(M1,K)=SNH(MM1)*SN(M1)/(CSH(K)-CS(M1))
      X3(M1,K)=SNH(MM1)*SNH(MM1-K)/(CSH(MM1-K)-CS(M1))
      Y3(M1,K)=SNH(MM1)*SN(M1)/(CSH(MM1-K)-CS(M1))
  200 CONTINUE
      A=-CSH(1)
      B= CSH(1)
      RR1=A-RRA*RPLOT
      RR2=A+RRB*RPLOT
      RR3=B-RRB*RPLOT
      RR4=B+RRC*RPLOT
      XAU=-(CSH(1)+1.)
      XAUU=-(CSH(1)-1.0)
      XBU= (CSH(1)-1.)
      XBUU=(CSH(1)+1.)
      DX=RRL*RPLOT/(FLOAT(IXSTEP-1))
      DX2=DX/2.0
```

```
      DO 5 L=1,120
      CHAR(L)=PLOT
    5 CONTINUE
      WRITE(6,100) CHAR
  100 FORMAT(1H1,3H...,120A1)
      DO 10 L=1,119
      CHAR(L)=BLANK
   10 CONTINUE
C---- SPHERE A.
      XPLOT=RR1
   15 DO 25 J=1,M1
      DO 25 K=1,KNP
      DIF1=XPLOT-X1(J,K)
      ABDIF1=ABS(DIF1)
      DIF2=XPLOT-X2(J,K)
      ABDIF2=ABS(DIF2)
      IF(ABDIF1.LE.DX2) GO TO 20
   22 IF(ABDIF2.LE.DX2) GO TO 21
      GO TO 25
   20 LL=(FLOAT(IYS)/(RRL*RPLOT))*Y1(J,K)+1.0
      IF(LL.EQ.0.OR.LL.GT.119) GO TO 22
      CHAR(LL)=FPLOT(K)
      IF( J.EQ.1.OR. J.EQ.M1) CHAR(LL)=FPLOT(1)
      GO TO 22
   21 LL=(FLOAT(IYS)/(RRL*RPLOT))*Y2(J,K)+1.0
      IF(LL.EQ.0.OR.LL.GT.119) GO TO 25
      CHAR(LL)=FPLOT(K)
      IF( J.EQ.1.OR. J.EQ.M1) CHAR(LL)=FPLOT(1)
   25 CONTINUE
      IF((XPLOT.GT.XAU).AND.(XPLOT.LT.XAUU)) GO TO 1
   26 DFU=XPLOT-XAU
      DFUU=XPLOT-XAUU
      DFA=XPLOT-A
      ABDFU=ABS(DFU)
      ABDFUU=ABS(DFUU)
      ABDFA=ABS(DFA)
      IF((ABDFU.LE.DX2).OR.(ABDFUU.LE.DX2)) GO TO 40
      IF(ABDFA.LE.DX2) GO TO 41
      WRITE(6,101) CHAR
  101 FORMAT(1X,1H.,3X,120A1)
   30 DO 35 L=1,119
      CHAR(L)=BLANK
   35 CONTINUE
      XPLOT=XPLOT+DX
      IF(XPLOT.GT.RR2) GO TO 50
      GO TO 15
    1 C=XPLOT-A
      IF(C.EQ.0.0) C=10.E-30
      D=ABS(C)
      CL=1.0-D**2
      LC=(FLOAT(IYS)/(RRL*RPLOT))*SQRT(CL)+1.0
      IF(LC.EQ.1.OR.LC.GT.119) GO TO 26
      CHAR(LC)=PLUS
      GO TO 26
   40 CHAR(1)=PLUS
      WRITE(6,102) CHAR
  102 FORMAT(1X,1H.,3X,120A1)
      GO TO 30
   41 CHAR(1)=CROSS
      WRITE(6,102) CHAR
      GO TO 30
```

```
C---- SPHERE B.
   50 XPLOT=RR3
   55 DO 75 JB=1,M1
      J=M1-JB+1
      DO 75 K=1,KNP
      DIF3=XPLOT-X3(J,K)
      ABDIF3=ABS(DIF3)
      DIF4=XPLOT-X4(J,K)
      ABDIF4=ABS(DIF4)
      IF(ABDIF3.LE.DX2) GO TO 70
   72 IF(ABDIF4.LE.DX2) GO TO 71
      GO TO 75
   70 LL=(FLOAT(IYS)/(RRL*RPLOT))*Y3(J,K)+1.0
      IF(LL.EQ.0.OR.LL.GT.119) GO TO 72
      CHAR(LL)=FPLOT(K)
      IF( J.EQ.1.OR. J.EQ.M1) CHAR(LL)=FPLOT(1)
      GO TO 72
   71 LL=(FLOAT(IYS)/(RRL*RPLOT))*Y4(J,K)+1.0
      IF(LL.EQ.0.OR.LL.GT.119) GO TO 75
      CHAR(LL)=FPLOT(K)
      IF( J.EQ.1.OR. J.EQ.M1) CHAR(LL)=FPLOT(1)
   75 CONTINUE
      IF((XPLOT.LT.XBUU).AND.(XPLOT.GT.XBU)) GO TO 3
   76 DFU=XPLOT-XBU
      DFUU=XPLOT-XBUU
      DFB=XPLOT-B
      ABDFU=ABS(DFU)
      ABDFUU=ABS(DFUU)
      ABDFB=ABS(DFB)
      IF((ABDFU.LE.DX2).OR.(ABDFUU.LE.DX2)) GO TO 90
      IF(ABDFB.LE.DX2) GO TO 91
      WRITE(6,101) CHAR
      IF(XPLOT.GE.RR4) GO TO 400
   80 DO 85 L=1,119
      CHAR(L)=BLANK
   85 CONTINUE
      XPLOT=XPLOT+DX
      GO TO 55
    3 C=XPLOT-B
      IF(C.EQ.0.0) C=10.E-30
      D=ABS(C)
      CL=1.0-D**2
      LC=(FLOAT(IYS)/(RRL*RPLOT))*SQRT(CL)+1.0
      IF(LC.EQ.1.OR.LC.GT.119) GO TO 76
      CHAR(LC)=PLUS
      GO TO 76
   90 CHAR(1)=PLUS
      WRITE(6,102) CHAR
      GO TO 80
   91 CHAR(1)=CROSS
      WRITE(6,102) CHAR
      GO TO 80
  400 DO 6 L=1,120
      CHAR(L)=PLOT
    6 CONTINUE
      WRITE(6,103) CHAR
  103 FORMAT(1X,4H....,120A1)
      RETURN
      END
```

```
      SUBROUTINE VFIELD
C---- THIS SUBROUTINE CALCULATES THE VELOCITY COMPONENTS FOR THE Z- AND
C----      THETA- DIRECTIONS.
      COMMON/GRID1/ Z(41),SNH(41),CSH(41),SN(31),CS(31)
      COMMON/GRID2/ IETHA(31),ETHA(31),THETA(31),DTHETA(31)
      COMMON/GRID3/ H3(41,31),R1(41,31)
      COMMON/UVGFC/ U(41,31),V(41,31),G(41,31),F(41,31)
      COMMON/M1MM1C/ M,M1,MMD,MM,MM1,MD,SH,SK,KS
      COMMON/CNSTC/ ZS,RE,EPSU,EPSG,RFU,RFG
      COMMON/IRREGC/ JOMIT,I1(31),I2(31)
      COMMON/OFOSC/ OF,OF4,OF3,OF2,OS,OS4,OS3,OS2
      COMMON/PFPSC/ PF,PF4,PF3,PF2,PS,PS4,PS3,PS2
      COMMON/VZVTC/ VZ(41,31), VT(41,31)
      COMMON/SMRNC/ SM(31),RN(31)
      DIMENSION RS(31),SR(31)
C---- VELOCITIES IN THE FLOW REGION.
C---- VZ(I,J) IS THE VELOCITY IN THE Z-DIRECTION.
C---- VT(I,J) IS VELOCITY IN THE THETA- DIRECTION.
      DO 10 J=1,M1
      DO 10 I=1,MM1
      VZ(I,J)=0.0
      VT(I,J)=0.0
   10 CONTINUE
      DO 20 J=2,M
      RS(J)=RN(J)/SM(J)
      SR(J)=SM(J)/RN(J)
   20 CONTINUE
      DO 30 J=2,M
      DO 30 I=2,MM
      VTH=(RS(J)*U(I,J+1)-SR(J)*U(I,J-1)-(RS(J)-SR(J))*U(I,J))/(SM(J)+RN
     +(J))
      VZ(I,J)=-VTH/(H3(I,J)*H3(I,J))
      VZZ=(U(I+1,J)-U(I-1,J))/(2.0*SH)
      VT(I,J)=+VZZ/(H3(I,J)*H3(I,J))
   30 CONTINUE
      WRITE(6,200)
  200 FORMAT(1H1,1X,*++++++VELOCITY IN Z-DIRECTION,++++++*,//)
      WRITE(6,201) (Z(I),I=1,MMD,2)
C
  201 FORMAT(6X,4HZ(I),11F10.2,//)
      WRITE(6,202) (IETHA(J),DTHETA(J),(VZ(I,J),I=1,MMD,2),J=1,M1)
  202 FORMAT(1X,I3,2X,F5.1,11F10.6)
      WRITE(6,203) (Z(I),I=MMD,MM1,2)
  203 FORMAT(///,6X,4HZ(I),11F10.2,//)
      WRITE(6,204) (IETHA(J),DTHETA(J),(VZ(I,J),I=MMD,MM1,2),J=1,M1)
  204 FORMAT(1X,I3,2X,F5.1,11F10.6)
      WRITE(6,300)
  300 FORMAT(///,1X,*++++++VELOCITY IN THETA-DIRECTION,++++++*,//)
      WRITE(6,301) (Z(I),I=1,MMD,2)
  301 FORMAT(6X,4HZ(I),11F10.2,//)
      WRITE(6,302) (IETHA(J),DTHETA(J),(VT(I,J),I=1,MMD,2),J=1,M1)
  302 FORMAT(1X,I3,2X,F5.1,11F10.6)
      WRITE(6,303) (Z(I),I=MMD,MM1,2)
  303 FORMAT(///,6X,4HZ(I),11F10.2,//)
      WRITE(6,304) (IETHA(J),DTHETA(J),(VT(I,J),I=MMD,MM1,2),J=1,M1)
  304 FORMAT(1X,I3,2X,F5.1,11F10.6)
      RETURN
      END
```

```
      SUBROUTINE SKPFILE(NSKIP,NUNIT)
C---- THIS SUBROUTINE SKIPS FILES ON MAGNETIC TAPE.
      L=0
    1 READ(NUNIT) DUMMY
      IF(EOF(NUNIT)) 10,11
   10 L=L+1
      IF(L.EQ.NSKIP) RETURN
   11 GO TO 1
      END



      FUNCTION SINH(X)
      SINH=0.5*(EXP(X)-EXP(-X))
      RETURN
      END



      FUNCTION COSH(X)
      COSH=0.5*(EXP(X)+EXP(-X))
      RETURN
      END
```

B. Computer Program 2.

```
      PROGRAM MASS(INPUT,OUTPUT,TAPE5=INPUT,TAPE6=OUTPUT,TAPE1,TAPE2)
C---- THIS PROGRAMME SIMULATES FORCED CONVECTIVE MASS TRANSFER FROM A
C----      SYSTEM OF TWO EQUALLY SIZED SPHERES WITH FLUID FLOWING
C----      PARALLEL TO THEIR LINE OF CENTRES.
      COMMON/GRID1/ Z(41),SNH(41),CSH(41),SN(31),CS(31)
      COMMON/GRID2/ IETHA(31),ETHA(31),THETA(31),DTHETA(31)
      COMMON/GRID3/ H3(41,31),R1(41,31)
      COMMON/UCC/ U(41,31),C(41,31)
      COMMON/M1MM1C/ M,M1,MMD,MM,MM1,MD,SH,SK,KS
      COMMON/NPRC/ N,MXITER,MX1,MMX1,MNPR,NOMIT,NPRC,NPRC1,NPC,NPC1,N3
      COMMON/TAPEC/ INTAPE,NDTAPE,NSKIPW,NSKIPR
      COMMON/CNSTC/ ZS,RE,SC,PE,EPSC,RFC
      COMMON/IRREGC/ JOMIT,I1(31),I2(31)
      COMMON/RRABC/ RRA,RRB,RRC,RRL
      COMMON/FACTOR/ FACTOR
      CPT=890.0
      PTIME=5.0
C---- INITIAL SETTINGS
      N5=1
      CALL SETUP
   50 CALL GRID
      CALL INPUT
      N=0
      N3=1
      CALL COEFF
C---- MXITER IS THE MAXIMUM NUMBER OF ITERATIONS ALLOWED FOR EACH
C----      COMPUTER RUN.
   10 IF(N.GE.MXITER) GO TO 2
      WRITE(6,1000)
 1000 FORMAT(1H1,48H*****HERE STARTS A GROUP OF MX1 ITERATIONX.*****)
      WRITE(6,1001) ZS,RE,PE,RFC,EPSC
 1001 FORMAT(1H0,//,1X,4HZS =,F10.4,5X,4HRE =,F10.4,5X,4HPE =,F10.5,5X,
     15HRFC =,F10.4,5X,6HEPSC =,F8.6)
      WRITE(6,1002) NPRC1,NPC1,NOMIT
 1002 FORMAT(1H0,/,10X,7HNPRC1 =,I6,10X,6HNPC1 =,I4,10X,7HNOMIT =,I4,//)
C---- HERE BEGINS THE ITERATION SECTION FOR A GIVEN PECLET NUMBER.
C---- A GROUP OF MX1 ITERATIONS WILL BE STARTED WITH MMX1=MX1
      MMX1=MX1
C---- A NEW ITERATION BEGINS WITH NPRC=NPRC1
C----      NPRC1---THE TOTAL NUMBER OF POINT VALUES TO BE OBTAINED.
C----      NPRC---THE TOTAL NUMBER OF UNCONVERGED POINT VALUES.
   40 NPRC=NPRC1
      NPC=NPC1
      CALL VARBC
      CALL SOLVE
      IF(N.GE.300.AND.NPRC.EQ.NPRC1) GO TO 4000
      IF(N.GE.300.AND.NPC.EQ.NPC1) GO TO 4000
      CALL SECOND(CPSEC)
      IF((N/10)*10.NE.N) GO TO 30
      WRITE(6,2000) N,CPSEC,NPRC,NPC
 2000 FORMAT(1H0,3HN =,I5,5X,5HCPT =,F6.2,15X,6HNPRC =,I5,5X,5HNPC =,I5)
   30 TLEFT=CPT-CPSEC
      IF(TLEFT.LE.PTIME) GO TO 2
C---- AN ITERATION IS COMPLETED.
      N=N+1
      MMX1=MMX1-1
```

```
C---- TEST FOR THE OVERALL CONVERGENCE.
C----      IF NPRC IS LESS THAN OR EQUAL TO MNPR, THE CONVERGENCE OF THE
C----       PRESENT SOLUTION HAS BEEN OBTAINED.
C---- IF MMX1=0, THE GROUP OF MX1 ITERATION HAVE BEEN PERFORMED.
C----      OTHERWISE GO TO 40 AND START A NEW ITERATION.
      IF(NPRC-MNPR) 200,200,100
  100 IF(MMX1) 300,300,40
C---- SET N3 TO ZERO IF THE OVERALL CONVERGENCE HAS BEEN OBTAINED.
  200 N3=0
C---- AN EXTRA ITERATION IS ALLOWED FOR THE BOUNDARY CONDITIONS TO BE
C----       SATISFIED.
      NPRC=NPRC1
      NPC=NPC1
      CALL VARBC
      CALL SOLVE
      IF(NPRC.GT.MNPR) GO TO 40
  300 CALL RESTAB
      IF(N3.EQ.1) GO TO 10
      WRITE(6,2004)
 2004 FORMAT(///,40H*****THE PRESENT CASE IS CONVERGED.*****,//)
C---- IF NDTAPE=1, STORE INFORMATION ON TAPE 2.
      IF(NDTAPE.NE.1) GO TO 3
      REWIND 2
      IF(NSKIPW.GT.0) CALL SKPFILE(NSKIPW,2)
      WRITE(2)(ETHA(J),ETHA(J),DTHETA(J),THETA(J),I1(J),I2(J),J=1,M1)
      WRITE(2) JOMIT,NPRC1,NPC1,NOMIT
      WRITE(2) (SN(J),CS(J),J=1,M1)
      WRITE(2) ((H3(I,J),R1(I,J),I=1,MM1),J=1,M1)
      WRITE(2) ((U(I,J),I=1,MM1),J=1,M1)
      WRITE(2) ((C(I,J),I=1,MM1),J=1,M1)
      END FILE 2
      WRITE(6,3000) ZS,RE,PE,NSKIPR,NSKIPW
 3000 FORMAT(///,10X,4HZS =,F6.3,10X,4HRE =,F8.3,10X,4HPE =,F10.4,10X,8H
     1NSKIPR =,I6,10X,8HNSKIPW =,I6,//)
      NSKIPR=NSKIPW
      NSKIPW=NSKIPW+1
C---- CALCULATE THE LOCAL AND OVERALL RATES OF MASS TRANSFER.
    3 CALL NSNSEE
C---- CONCENTRATION CONTOURS AROUND THE SPHERES ARE LOCATED AND PLOTTED.
      CALL CNPLTP
C---- THIS SECTION SUPPLIES NEW VALUES FOR THE PECLET NUMBER AND
C----       RELAXATION FACTOR.
      N5=N5+1
      FACTOR=1.00
      IF(N5.EQ.2) GO TO 11
      IF(N5.EQ.3) GO TO 12
      IF(N5.EQ.4) GO TO 13
      IF(N5.EQ.5) GO TO 14
      GO TO 1
 4000 CONTINUE
      RFC=RFC-0.05
      IF(RFC.LE.0.0) GO TO 1
      GO TO 50
   11 CONTINUE
      PE=0.01
      GO TO 50
   12 CONTINUE
      PE=0.1
      GO TO 50
```

```
   13 CONTINUE
      PE=0.7
      GO TO 50
   14 CONTINUE
      PE=1.0
      GO TO 50
C
C---- PRINT OUT THE CONVERGED RESULTS.
    2 CALL RESTAB
C---- IF NDTAPE=1, STORE INFORMATION ON TAPE 2.
      IF(NDTAPE.NE.1) GO TO 1
      REWIND 2
      IF(NSKIPW.GT.0) CALL SKPFILE(NSKIPW,2)
      WRITE(2)(IETHA(J),ETHA(J),DTHETA(J),THETA(J),I1(J),I2(J),J=1,M1)
      WRITE(2) JOMIT,NPRC1,NPC1,NOMIT
      WRITE(2) (SN(J),CS(J),J=1,M1)
      WRITE(2) ((H3(I,J),R1(I,J),I=1,MM1),J=1,M1)
      WRITE(2) ((U(I,J),I=1,MM1),J=1,M1)
      WRITE(2) ((C(I,J),I=1,MM1),J=1,M1)
      END FILE 2
      WRITE(6,3001) ZS,RE,PE,NSKIPR,NSKIPW
 3001 FORMAT(///,10X,4HZS =,F6.3,10X,4HRE =,F8.3,10X,4HPE =,F10.4,10X,8H
     1NSKIPR =,I6,10X,8HNSKIPW =,I6,//)
    1 STOP
      END
```

```
      SUBROUTINE SETUP
C---- THIS SUBROUTINE SUPPLIES PROGRAMME CONTROL PARAMETERS.
      COMMON/GRID1/ Z(41),SNH(41),CSH(41),SN(31),CS(31)
      COMMON/GRID2/ IETHA(31),ETHA(31),THETA(31),DTHETA(31)
      COMMON/GRID3/ H3(41,31),R1(41,31)
      COMMON/NPRC/ N,MXITER,MX1,MMX1,MNPR,NOMIT,NPRC,NPRC1,NPC,NPC1,N3
      COMMON/TAPEC/ INTAPE,NDTAPE,NSKIPW,NSKIPR
      COMMON/M1MM1C/ M,MJ,MMD,MM,MM1,MD,SH,SK,KS
      COMMON/CNSTC/ ZS,RE,SC,PE,EPSC,RFC
      COMMON/RPLOTC/ RPLOT,IYS,IXSTEP
      COMMON/PLTPCN/ VCC(10),KNC,KNP
      COMMON/RRABC/ RRA,RRB,RRC,RRL
      COMMON/FACTOR/ FACTOR
      COMMON/NSKPRC/ NSKPR1
C---- SET SPHERE SPACING, MESH SPACING, AND BOUNDARY PARAMETERS.
      ZS=0.20
      SH=ZS/20.0
      RRL=7.0
      RRA=5.0£RRB=COSH(ZS)
      RRC=7.0
      KS=6
      SK=(3.1415926/180.0)*FLOAT(KS)
      M=30
      MM=40
C---- SET CONTROL PARAMETERS FOR SOLVING THE EQUATIONS.
      RE=0.001
      PE=0.001
      RFC=0.80
      FACTOR=0.0
      NSKIPR=0
      NSKIPW=0
      MXITER=800
      MX1=400
      MNPR=0
      INTAPE=0
      NDTAPE=1
      EPSC=0.0001
C---- PARAMETERS FOR PLOTTING CONCENTRATION CONTOURS AROUND THE SPHERES.
      RPLOT=1.000
      IXSTEP=60
      IYS=1.2500*FLOAT(IXSTEP-1)+1.5
      KNC=6
      VCC(1)=1.00£VCC(2)=0.80£VCC(3)=0.50£VCC(4)=0.25£VCC(5)=0.10
      VCC(6)=0.05
      RETURN
      END
```

```
      SUBROUTINE GRID
C---- THIS SUBROUTINE SUPPLIES GRID INFORMATION AT EACH NODE.
      COMMON/GRID1/ Z(41),SNH(41),CSH(41),SN(31),CS(31)
      COMMON/GRID2/ IETHA(31),ETHA(31),THETA(31),DTHETA(31)
      COMMON/GRID3/ H3(41,31),R1(41,31)
      COMMON/UCC/ U(41,31),C(41,31)
      COMMON/M1MM1C/ M,M1,MMD,MM,MM1,MD,SH,SK,KS
      COMMON/CNSTC/ ZS,RE,SC,PE,EPSC,REC
      COMMON/NPRC/ N,MXITER,MX1,MMX1,MNPR,NOMIT,NPRC,NPRC1,NPC,NPC1,N3
      COMMON/TAPEC/ INTAPE,NDTAPE,NSKIPW,NSKIPR
      COMMON/IREGC/ JOMIT,I1(31),I2(31)
      COMMON/NSKPRC/ NSKPR1
C---- CALCULATE THE FIELD DIMENSION MM1 AND M1.
      M1=M+1
      MM1=MM+1
      MD=(M1+1)/2
      MMD=(MM1+1)/2
C---- COMPUTE FIELD VARIABLES.
      Z(1)=-ZS
      SNH(1)=-SINH(ZS)
      CSH(1)=COSH(ZS)
      DO 10 I=2,MM1
      Z(I)=Z(I-1)+SH
      SNH(I)=SINH(Z(I))
      CSH(I)=COSH(Z(I))
   10 CONTINUE
C---- IF INTAPE=1, VALUES OF THE FIELD VARIABLES WILL BE READ FROM TAPE
C----     2, OTHERWISE GO TO 1 TO OBTAIN THEM.
      IF(INTAPE.NE.1) GO TO 1
      REWIND 2
      IF(NSKIPR.GT.0) CALL SKPFILE(NSKIPR,2)
      READ(2) (IETHA(J),ETHA(J),DTHETA(J),THETA(J),I1(J),I2(J),J=1,M1)
      READ(2) JOMIT,NPRC1,NPC1,NOMIT
      READ(2) (SN(J),CS(J),J=1,M1)
      READ(2) ((H3(I,J),R1(I,J),I=1,MM1),J=1,M1)
      READ(2) ((U(I,J),I=1,MM1),J=1,M1)
      READ(2) ((C(I,J),I=1,MM1),J=1,M1)
      GO TO 2
C
C--- READ FIELD VARIABLES AND STREAM FUNCTION DISTRIBUTIONS IN THE FLOW
C----      REGION AT THE SPECIFIED REYNOLDS NUMBER.
C---- NSKPR1 IS THE NUMBER OF FILES TO BE SKIPPED IN ORDER TO READ THE
C----      FIELD VARIABLES AND STREAM FUNCTION DISTRIBUTION FROM TAPE 1.
    1 REWIND 1
      IF(NSKPR1.GT.0) CALL SKPFILE(NSKPR1,1)
      READ(1) (IETHA(J),ETHA(J),DTHETA(J),THETA(J),I1(J),I2(J),J=1,M1)
      READ(1)  JOMIT,N2,NPRU1,NPRV1,NPR1,NOMIT
      READ(1) (SN(J),CS(J),J=1,M1)
      READ(1) ((H3(I,J),R1(I,J),I=1,MM1),J=1,M1)
      READ(1) ((U(I,J),I=1,MM1),J=1,M1)
C---- CALCULATE NPRC1 AND NPC1.
C---- NPC1 IS THE TOTAL NUMBER OF POINT VALUES WHICH REQUIRED SPECIAL
C----      TREATMENT, I.E. CONCENTRATION ALONG THE AXES OF SYMMETRY.
C---- NPPC1 IS THE TOTAL NUMBER OF POINT VALUES TO BE OBTAINED.
C---- NOMIT IS THE TOTAL NUMBER OF POINT VALUES OUTSIDE THE OUTER
C----      BOUNDARY WHICH IS TO BE OMITTED.
      NZERO=(MM-I2(1))+(I1(1)-2)
      NPI=MM-1
      NPC1=NZERO+NPI
      NPRC1=(M-1)*(MM-1)+NPC1-NOMIT
```

```
C---- IF NDTAPE=1, STORE INFORMATION ON TAPE 2.
      IF(NDTAPE.NE.1) GO TO 2
      REWIND 2
      IF(NSKIPW.GT.0) CALL SKPFILE(NSKIPW,2)
      WRITE(2)(IETHA(J),ETHA(J),DTHETA(J),THETA(J),I1(J),I2(J),J=1,M1)
      WRITE(2) JOMIT,NPRC1,NPC1,NOMIT
      WRITE(2) (SN(J),CS(J),J=1,M1)
      WRITE(2) ((H3(I,J),R1(I,J),I=1,MM1),J=1,M1)
      WRITE(2) ((U(I,J),I=1,MM1),J=1,M1)
    2 RETURN
      END



      SUBROUTINE INPUT
C---- THIS SUBROUTINE SUPPLIES INITIAL VALUES FOR CONCENTRATION.
      COMMON/GRID1/ Z(41),SNH(41),CSH(41),SN(31),CS(31)
      COMMON/GRID2/ IETHA(31),ETHA(31),THETA(31),DTHETA(31)
      COMMON/GRID3/ H3(41,31),R1(41,31)
      COMMON/UCC/ U(41,31),C(41,31)
      COMMON/M1MM1C/ M,M1,MMD,MM,MM1,MD,SH,SK,KS
      COMMON/IRREGC/ JOMIT,I1(31),I2(31)
      COMMON/NPRC/ N,MXITER,MX1,MMX1,MNPR,NOMIT,NPRC,NPRC1,NPC,NPC1,N3
      COMMON/TAPEC/ INTAPE,NDTAPE,NSKIPW,NSKIPR
C---- IF INTAPE=1, INTIAL VALUES OF CONCENTRATION ARE READ FROM TAPE.
      IF(INTAPE.EQ.1) GO TO 1
      DO 10 J=1,M1
      DO 10 I=1,MM1
      C(I,J)=0.0
   10 CONTINUE
      IF(NDTAPE.NE.1) GO TO 1
      WRITE(2) ((C(I,J),I=1,MM1),J=1,M1)
      END FILE 2
      INTAPE=1
      NSKIPW=NSKIPW+1
C---- FIXED KNOWN BOUNDARY CONDITIONS.
C---- ON THE SPHERE SURFACES.
    1 DO 30 J=1,M1
      C(1,J)=1.0
      C(MM1,J)=1.0
   30 CONTINUE
C---- ALONG THE OUTER BOUNDARY.
      DO 40 J=1,JOMIT
      ILEFT=I1(J)
      IRIGHT=I2(J)
      DO 50 I=ILEFT,IRIGHT
      C(I,J)=0.0
   50 CONTINUE
   40 CONTINUE
      RETURN
      END
```

```
      SUBROUTINE COEFF
C---- THIS SUBROUTINE CALCALATES ALL THE COEFFICIENTS NEEDED TO SOLVE
C----    THE DIFFUSION EQUATION FOR FLOW AROUND TWO-SPHERES.
      COMMON/GRID1/ Z(41),SNH(41),CSH(41),SN(31),CS(31)
      COMMON/GRID2/ IETHA(31),ETHA(31),THETA(31),DTHETA(31)
      COMMON/GRID3/ H3(41,31),R1(41,31)
      COMMON/CNSTC/ ZS,RE,SC,PE,EPSC,RFC
      COMMON/M1MM1C/ M,M1,MMD,MM,MM1,MD,SH,SK,KS
      COMMON/UCC/ U(41,31),C(41,31)
      COMMON/COEFF/ B1(41,31),B2(41,31),B3(41,31),B4(41,31)
      COMMON/VCOEFF/ D1(41),D2(41),D3,E1(41),E2(41),E3
      COMMON/DCOEFF/ BD(41,31),DB(41),EB(41)
      COMMON/KMKNC/ AA(31),BB(31)
      COMMON/SMRNC/ SM(31),RN(31)
C---- B1(I,J),B2(I,J),B3(I,J),B4(I,J)---ARE THE COEFFS OF THE FINITE-
C----    DIFFERENCE DIFFUSION EQUATIONS TO BE USED IN SUBROUTINE SOLVE.
C---- D1(I),D2(I),D3---ARE THE COEFFS. OF THE FINITE DIFFERENCE EQUATION
C----    FOR THETA=0.0 TO BE USED IN SUBROUTINE VARBC.
C---- E1(I),E2(I),E3---ARE THE COEFFS. OF THE FINITE DIFFERENCE EQUATION
C----    FOR THETA=180 TO BE USED IN SUBROUTINE VARBC.
      SH2=1.0/(SH*SH)
      SM(1)=THETA(2)-THETA(1)
      RN(1)=0.0
      SM(M1)=0.0
      RN(M1)=THETA(M1)-THETA(M)
      DO 10 J=2,M
      SM(J)=THETA(J+1)-THETA(J)
      RN(J)=THETA(J)-THETA(J-1)
      SMTRN=SM(J)*RN(J)
      SMPRN=SM(J)+RN(J)
      SMMRN=SM(J)-RN(J)
      AA(J)=1.0-SMMRN/SM(J)
      BB(J)=1.0+SMMRN/RN(J)
      CCP=1.0+SMMRN/SMPRN
      CCM=1.0-SMMRN/SMPRN
      SKT=1.0/SMTRN
      DO 20 I=2,MM
      PEHK=PE/(4.0*SH*SMPRN*R1(I,J))
      BA=SNH(I)/(2.0*SH*(CSH(I)-CS(J)))
      BC=(CSH(I)*CS(J)-1.0)/(SMPRN*SN(J)*(CSH(I)-CS(J)))
      BBB=2.0*SH2+2.0*SKT+(AA(J)-BB(J))*(BC-PEHK*(U(I+1,J)-U(I-1,J)))
      BD(I,J)=PEHK/BBB
      B1(I,J)=(SH2-BA)/BBB
      B2(I,J)=(SH2+BA)/BBB
      B3(I,J)=(CCM*SKT+AA(J)*BC)/BBB
      B4(I,J)=(CCP*SKT-BB(J)*BC)/BBB
   20 CONTINUE
   10 CONTINUE
      DO 30 I=2,MM
      IF(I.EQ.MMD) GO TO 30
      SMTRN=SM(1)*SM(1)
      SKT=1.0/SMTRN
      DDD=2.0*SH2+4.0*SKT
      DA=SNH(I)/(2.0*SH*(CSH(I)-CS(1)))
      DB(I)=PE*U(I,2)/(2.0*SH*SMTRN*H3(I,1)*DDD)
      D1(I)=(SH2-DA)/DDD
      D2(I)=(SH2+DA)/DDD
      D3=4.0*SKT/DDD
   30 CONTINUE
      DO 40 I=2,MM
      SMTRN=RN(M1)*RN(M1)
      SKT=1.0/SMTRN
```

```
      EEE=2.0*SH2+4.0*SKT
      EA=SNH(I)/(2.0*SH*(CSH(I)-CS(M1)))
      EB(I)=PE*U(I,M)/(2.0*SMTRN*H3(I,M1)*EEE)
      E1(I)=(SH2-EA)/EEE
      E2(I)=(SH2+EA)/EEE
      E3=4.0*SKT/EEE
   40 CONTINUE
      RETURN
      END

      SUBROUTINE VARBC
C---- THIS SUBROUTINE SOLVES THE SPECIALLY TREATED BOUNDARY CONDITIONS
C----      ALONG THE AXES OF SYMMETRY, THETA = 0 AND 180.
      COMMON/GRID1/ Z(41),SNH(41),CSH(41),SN(31),CS(31)
      COMMON/GRID2/ IETHA(31),ETHA(31),THETA(31),DTHETA(31)
      COMMON/GRID3/ H3(41,31),R1(41,31)
      COMMON/CNSTC/ ZS,RE,SC,PE,EPSC,RFC
      COMMON/M1MM1C/ M,M1,MMD,MM,MM1,MD,SH,SK,KS
      COMMON/UCC/ U(41,31),C(41,31)
      COMMON/IRREGC/ JOMIT,I1(31),I2(31)
      COMMON/COEFF/ B1(41,31),B2(41,31),B3(41,31),B4(41,31)
      COMMON/VCOEFF/ D1(41),D2(41),D3,E1(41),E2(41),E3
      COMMON/DCOEFF/ DD(41,31),DB(41),ER(41)
      COMMON/NPRC/ N,MXITER,MX1,MMX1,MNPR,NOMIT,NPRC,NPRC1,NPC,NPC1,N3
      COMMON/FACTOR/ FACTOR
C---- ESTIMATION OF C(I,1) ALONG THE AXIS OF SYMMETRY, THETA=0.0
      DO 10 I=2,MM
      IF(I.GE.I1(1).AND.I.LE.I2(1)) GO TO 1
      D=DB(I)*(C(I+1,1)-C(I-1,1))
      IF(C(I,1).EQ.0.00) C(I,1)=10.E-30
      IF(C(I,1).EQ.-0.00) C(I,1)=-10.E-30
      XM=-(D/C(I,1))*FACTOR
      ACM=1.0+XM
      IF(ACM.EQ.0.00) ACM=10.E-30
      IF(ACM.EQ.-0.00) ACM=-10.E-30
      DP=(D+XM*C(I,1))/ACM
      TN=D1(I)*C(I+1,1)+D2(I)*C(I-1,1)+D3*C(I,2)
      TNP=TN/ACM
      TN=TNP+DP
      TN=C(I,1)+RFC*(TN-C(I,1))
      IF(ABS(C(I,1)-TN).LE.EPSC) GO TO 20
      GO TO 30
   20 NPRC=NPRC-1
      NPC=NPC-1
   30 C(I,1)=TN
C---- ESTIMATION OF C(I,M1) ALONG THE AXIS OF SYMMETRY, THETA=180.0.
    1 D=-EB(I)*(C(I+1,M1)-C(I-1,M1))
      IF(C(I,M1).EQ.0.00) C(I,M1)=10.E-30
      IF(C(I,M1).EQ.-0.00) C(I,M1)=-10.E-30
      XM=-(D/C(I,M1))*FACTOR
      ACM=1.0+XM
      IF(ACM.EQ.0.00) ACM=10.E-30
      IF(ACM.EQ.-0.00) ACM=-10.E-30
      DP=(D+XM*C(I,M1))/ACM
      TN=E1(I)*C(I+1,M1)+E2(I)*C(I-1,M1)+E3*C(I,M)
      TNP=TN/ACM
      TN=TNP+DP
      TN=C(I,M1)+RFC*(TN-C(I,M1))
      IF(ABS(C(I,M1)-TN).LE.EPSC) GO TO 40
      GO TO 50
   40 NPRC=NPRC-1
      NPC=NPC-1
   50 C(I,M1)=TN
   10 CONTINUE
      RETURN
      END
```

```
      SUBROUTINE SOLVE
C---- THIS SUBROUTINE SOLVES THE FINITE-DIFFERENCE DIFFUSION EQUATIONS
C----      AT ALL INTERNAL MESH POINTS USING SUCESSIVE ITERATION WITH
C----      RELAXATION.
      COMMON/GRID1/ Z(41),SNH(41),CSH(41),SN(31),CS(31)
      COMMON/GRID2/ IETHA(31),ETHA(31),THETA(31),DTHETA(31)
      COMMON/GRID3/ H3(41,31),R1(41,31)
      COMMON/M1MM1C/ M,M1,MMD,MM,MM1,MD,SH,SK,KS
      COMMON/CNSTC/ ZS,RF,SC,PE,EPSC,RFC
      COMMON/UCC/ U(41,31),C(41,31)
      COMMON/COEFF/ B1(41,31),B2(41,31),B3(41,31),B4(41,31)
      COMMON/VCOEFF/ D1(41),D2(41),D3,E1(41),E2(41),E3
      COMMON/DCOEFF/ BD(41,31),DB(41),ER(41)
      COMMON/NPRC/ N,MXITER,MX1,MMX1,MNPR,NOMIT,NPRC,NPRC1,NPC,NPC1,N3
      COMMON/IRREGC/ JOMIT,I1(31),I2(31)
      COMMON/KMKNC/ AA(31),BB(31)
      COMMON/FACTOR/ FACTOR
C---- AT EACH GRID POINT, THE PROCESS OF CALCULATION IS AS FOLLOW.
C----     1. CALCULATE THE NEW VALUE OF THE CONCENTRATION, TN.
C----     2. APPLY RELAXATION (OVER- OR UNDER- RELAXATION).
C----     3. TEST FOR CONVERGENCE.
C----     4. IF THE TEST IS SATISFIED, NPRC IS REDUCED BY 1. AND THE OLD
C----        VALUE OF THE CONCENTRATUON IS REPLACED BY TN.
      JIRREG=JOMIT
      DO 10 J=2,JIRREG
      DO 20 I=2,MM
      IF(I.GE.I1(J).AND.I.LE.I2(J)) GO TO 20
      DF1=C(I+1,J)-C(I-1,J)
      DF2=(AA(J)*U(I,J+1)-BB(J)*U(I,J-1)-(AA(J)-BB(J))*U(I,J))
      DF3=AA(J)*C(I,J+1)-BB(J)*C(I,J-1)
      DF4=U(I+1,J)-U(I-1,J)
      D=BD(I,J)*(DF1*DF2-DF3*DF4)
      IF(C(I,J).EQ.0.00) C(I,J)=10.E-30
      IF(C(I,J).EQ.-0.00) C(I,J)=-10.E-30
      XM=-(D/C(I,J))*FACTOR
      ACM=1.0+XM
      IF(ACM.EQ.0.00) ACM=10.E-30
      IF(ACM.EQ.-0.00) ACM=-10.E-30
      DP=(D+XM*C(I,J))/ACM
      BC1=B1(I,J)*C(I+1,J)
      BC2=B2(I,J)*C(I-1,J)
      BC3=B3(I,J)*C(I,J+1)
      BC4=B4(I,J)*C(I,J-1)
      TN=BC1+BC2+BC3+BC4
      TNP=TN/ACM
      TN=TNP+DP
      TN=C(I,J)+RFC*(TN-C(I,J))
      IF(ABS(C(I,J)-TN).LE.EPSC) GO TO 40
      GO TO 50
   40 NPRC=NPRC-1
   50 C(I,J)=TN
   20 CONTINUE
   10 CONTINUE
C
      JREG=JOMIT+1
      DO 100 J=JREG,M
      DO 200 I=2,MM
      DF1=C(I+1,J)-C(I-1,J)
      DF2=(AA(J)*U(I,J+1)-BB(J)*U(I,J-1)-(AA(J)-BB(J))*U(I,J))
      DF3=AA(J)*C(I,J+1)-BB(J)*C(I,J-1)
      DF4=U(I+1,J)-U(I-1,J)
      D=BD(I,J)*(DF1*DF2-DF3*DF4)
```

```
      IF(C(I,J).EQ.0.00) C(I,J)=10.E-30
      IF(C(I,J).EQ.-0.00) C(I,J)=-10.E-30
      XM=-(D/C(1,J))*FACTOR
      ACM=1.0+XM
      IF(ACM.EQ.0.00) ACM=10.E-30
      IF(ACM.EQ.-0.00) ACM=-10.E-30
      DP=(D+XM*C(I,J))/ACM
      BC1=B1(I,J)*C(I+1,J)
      BC2=B2(I,J)*C(I-1,J)
      BC3=B3(I,J)*C(I,J+1)
      BC4=B4(I,J)*C(I,J-1)
      TN=BC1+BC2+BC3+BC4
      TNP=TN/ACM
      TN=TNP+DP
      TN=C(I,J)+RFC*(TN-C(I,J))
      IF(ABS(C(I,J)-TN).LE.EPSC) GO TO 400
      GO TO 500
  400 NPRC=NPRC-1
  500 C(I,J)=TN
  200 CONTINUE
  100 CONTINUE
      RETURN
      END



      SUBROUTINE RESTAB
C---- THIS SUBROUTINE PRINTS OUT THE CONCENTRATION DISTRIBUTION IN
C----      TABULATED FORM.
      COMMON/GRID1/ Z(41),SNH(41),CSH(41),SN(31),CS(31)
      COMMON/GRID2/ IETHA(31),ETHA(31),THETA(31),DTHETA(31)
      COMMON/GRID3/ H3(41,31),R1(41,31)
      COMMON/M1MM1C/ M,M1,MMD,MM,MM1,MD,SH,SK,KS
      COMMON/UCC/ U(41,31),C(41,31)
      COMMON/CNSTC/ ZS,RE,SC,PE,EPSC,RFC
      COMMON/NPRC/ N,MXITER,MX1,MMX1,MNPR,NOMIT,NPRC,NPRC1,NPC,NPC1,N3
      WRITE(6,100) ZS,RE,PE,RFC
  100 FORMAT(1H1,///,1X,4HZS =,F6.3,5X,4HRE =,F8.4,5X,4HPE =,F10.4,5X,5H
     1RFC =,F8.4)
      WRITE(6,101) NPRC1,NPC1,NOMIT
  101 FORMAT(1H0,//,20X,7HNPRC1 =,I5,11X,6HNPC1 =,I5,11X,7HNOMIT =,I5,/)
      WRITE(6,102) N,NPRC,NPC
  102 FORMAT(1H0,//,1X,3HN =,I5,5X,6HNPRC =,I5,5X,5HNPC =,I5,///)
      WRITE(6,200)
  200 FORMAT(1H0,20X,29H****C(I,J)--CONCENTRATION****,//)
      WRITE(6,201) (Z(I),I=1,MMD,2)
  201 FORMAT(1H0,6X,4HZ(I),11F10.2,//)
      WRITE(6,202) (IETHA(J),DTHETA(J),(C(I,J),I=1,MMD,2),J=1,M1)
  202 FORMAT(1X,I3,2X,F5.1,11F10.6)
      WRITE(6,300)
  300 FORMAT(1H1, ///,20X,29H****C(I,J)--CONCENTRATION****,//)
      WRITE(6,301) (Z(I),I=MMD,MM1,2)
  301 FORMAT(1H0,6X,4HZ(I),11F10.2,//)
      WRTTE(6,302) (IETHA(J),DTHETA(J),(C(I,J),I=MMD,MM1,2),J=1,M1)
  302 FORMAT(1X,I3,2X,F5.1,11F10.6)
      RETURN
      END
```

```
      SUBROUTINE NSNSEE
C---- THIS SUBROUTINE EVALUATES THE LOCAL AND OVERALL SHERWOOD NUMBERS.
      COMMON/GRID1/ Z(41),SNH(41),CSH(41),SN(31),CS(31)
      COMMON/GRID2/ IETHA(31),ETHA(31),THETA(31),DTHETA(31)
      COMMON/GRID3/ H3(41,31),R1(41,31)
      COMMON/M1MM1C/ M,M1,MMD,MM,MM1,MD,SH,SK,KS
      COMMON/UCC/ U(41,31),C(41,31)
      COMMON/CNSTC/ ZS,RE,SC,PE,EPSC,RFC
      COMMON/NPRC/ N,MXITER,MX1,MMX1,MNPR,NOMIT,NPRC,NPRC1,NPC,NPC1,N3
      COMMON/IRREGC/ JOMIT,I1(31),I2(31)
      COMMON/SMRNC/ SM(31),RN(31)
      DIMENSION ANU(31),BNU(31),ANRAT(31),BNRAT(31)
      DIMENSION SRTA(31),SRTB(31)
C---- ANU(J)---THE LOCAL SHERWOOD NUMBER FOR SPHERE A.
C---- AVNU--- THE OVERALL SHERWOOD NUMBER FOR SPHERE A.
C---- ANRAT(J)---THE RATIO OF THE LOCAL SHERWOOD NUMBER TO THE FRONT
C----              STAGNATION POINT SHERWOOD NUMBER FOR SPHERE A.
C---- BNU(J)---THE LOCAL SHERWOOD NUMBER FOR SPHERE B.
C---- BVNU--- THE OVERALL SHERWOOD NUMBER FOR SPHERE B.
C---- BNRAT(J)---THE RATIO OF THE LOCAL SHERWOOD NUMBER TO THE FRONT
C----              STAGNATION POINT SHERWOOD NUMBER FOR SPHERE B.
      SSH=-1.0/(12.0*SH)
      YA=0.0
      YB=0.0
      DO 10 J=1,M1
      CZA=SSH*(+25.0*C(1,J)-48.0*C(2,J)+36.0*C(3,J)-16.0*C(4,J)+3.0*C(5,
     1J))
      SRTA(J)=-2.0/H3(1,J)
      ANU(J)=CZA*SRTA(J)
      ANRAT(J)=ANU(J)/ANU(1)
      CZASCC=CZA*(SN(J)/(CSH(1)-CS(J)))
      YA=YA+CZASCC*SM(J)
      CZB=SSH*(+25.0*C(MM1,J)-48.0*C(MM,J)+36.0*C(MM-1,J)-16.0*C(MM-2,J)
     1+3.0*C(MM-3,J))
      SRTB(J)=-2.0/H3(MM1,J)
      BNU(J)=CZB*SRTB(J)
      BNRAT(J)=BNU(J)/ANU(1)
      CZBSCC=CZB*(SN(J)/(CSH(MM1)-CS(J)))
      YB=YB+CZBSCC*SM(J)
   10 CONTINUE
      SIS2A=(CSH(1)-CS(1))*(CSH(1)-CS(M1))/SNH(MM1)
      SIS2B=(CSH(MM1)-CS(1))*(CSH(MM1)-CS(M1))/SNH(MM1)
      AVNU=-SIS2A*YA
      BVNU=-SIS2B*YB
      WRITE(6,1000)
 1000 FORMAT(1H1,30X,19HSPHERE A (ZS = -VE),30X,19HSPHERE B (ZS = +VE))
      WRITE(6,1001) AVNU,BVNU
 1001 FORMAT(1X,25HOVER-ALL NUSSELT NUMBER =,5X,F10.5,40X,F10.5)
      WRITE(6,1010)
 1010 FORMAT(1X,//,5X,4HETHA,2X,6HDTHETA,12X,6HANU(J),4X,13HANU(J)/ANU(1
     1),28X,6HBNU(J),4X,13HBNU(J)/ANU(1))
      WRITE(6,1011)
 1011 FORMAT(5X,4H----,2X,6H------,12X,6H------,4X,13H-------------,28X,
     16H------,4X,13H-------------)
      WRITE(6,1020) (IETHA(J),DTHETA(J),ANU(J),ANRAT(J),BNU(J),BNRAT(J),
     1J=1,M1)
 1020 FORMAT(5X,I4,2X,F6.2,F18.6,F17.6,20X,F14.6,F17.6,/)
      RETURN
      END
```

```
      SUBROUTINE CNPLTP
C---- THIS SUBROUTINE EVALUATES PLOT POSITIONS OF CONTOURS AND CALLS
C----    THE LINE-PRINTER PLOTTING SUBROUTINE.
      COMMON/GRID1/ Z(41),SNH(41),CSH(41),SN(31),CS(31)
      COMMON/GRID2/ IETHA(31),ETHA(31),THETA(31),DTHETA(31)
      COMMON/GRID3/ H3(41,31),R1(41,31)
      COMMON/CNSTC/ZS,RE,EPS1,EPS2,RF1,RF2
      COMMON/M1MM1C/ M,M1,MMD,MM,MM1,MD,SH,SK,KS
      COMMON/UCC/ U(41,31),C(41,31)
      COMMON/PLOT1/ X1(31,10),X2(31,10),Y1(31,10),Y2(31,10)
      COMMON/PLOT2/ X3(31,10),X4(31,10),Y3(31,10),Y4(31,10)
      COMMON/ZVC1/ ZVC1(10),ZVC2(10),LVC1(10)
      COMMON/ZVC2/ ZVC3(10),ZVC4(10),LVC2(10)
      COMMON/PLTPCN/ VCC(10),KNC,KNP
      COMMON/RPLOTC/ RPLOT,IYS,IXSTEP
      COMMON/RRABC/ RRA,RRB,RRC,RRL
C---- ------------------------
C---- CONCENTRATION CONTOURS.
C---- ------------------------
      DO 11 K=1,KNC
      ZVC1(K)=0.
      ZVC2(K)=0.
      LVC1(K)=1
      ZVC3(K)=0.
      ZVC4(K)=0.
      LVC2(K)=1
   11 CONTINUE
C---- SEARCH AND INTERPOLATE BETWEEN TWO I-LINE---CONCENTRATION CONTOUR.
      DO 100 J=1,M1
      DO 110 I=2,MM1
      IF(I.EQ.MMD.AND.J.EQ.1) GO TO 110
      DO 110 K=1,KNC
      IF(C(I-1,J).GE.VCC(K).AND.C(I,J).LE.VCC(K)) GO TO 200
      IF(C(I-1,J).LE.VCC(K).AND.C(I,J).GE.VCC(K)) GO TO 200
      GO TO 110
C
C---- SEARCHING THE CONCENTRATION CONTOURS FOR FIRST SPHERE.
  200 IF(I.GT.MMD) GO TO 201
      IF(LVC1(K).EQ.0) GO TO 101
      A=(VCC(K)-C(I-1,J))
      IF(A.EQ.0.0) A=10.E-30
      B=(C(I,J)-C(I-1,J))
      IF(B.EQ.0.0) B=10.E-30
      SLOPE=A/B
      ZVC1(K)=Z(I-1)+SLOPE*(Z(I)-Z(I-1))
      ZVC2(K)=0.0
      LVC1(K)=0
      GO TO 110
  101 A=(VCC(K)-C(I-1,J))
      IF(A.EQ.0.0) A=10.E-30
      B=(C(I,J)-C(I-1,J))
      IF(B.EQ.0.0) B=10.E-30
      SLOPE=A/B
      ZVC2(K)=Z(I-1)+SLOPE*(Z(I)-Z(I-1))
      GO TO 110
C
C---- SEARCHING THE CONCENTRATION CONTOURS FOR SECOND SPHERE.
  201 IF(LVC2(K).EQ.0) GO TO 102
      A=VCC(K)-C(I-1,J)
      IF(A.EQ.0.0) A=10.E-30
      B=(C(I,J)-C(I-1,J))
      IF(B.EQ.0.0) B=10.E-30
```

```
      SLOPE=A/B
      ZVC3(K)=Z(I-1)+SLOPE*(Z(I)-Z(I-1))
      ZVC4(K)=0.0
      LVC2(K)=0
      GO TO 110
  102 A=VCC(K)-C(I-1,J)
      IF(A.EQ.0.0) A=10.E-30
      B=(C(I,J)-C(I-1,J))
      IF(B.EQ.0.0) B=10.E-30
      SLOPE=A/B
      ZVC4(K)=Z(I-1)+SLOPE*(Z(I)-Z(I-1))
  110 CONTINUE
C
C---- CONVERT TO RECTAGULAR COORDINATES
      DO 300 K=1,KNC
      IF(ZVC1(K).EQ.0.0) GO TO 301
      IF(ZVC1(K).GT.100.0) ZVC1(K)=100.0
      IF(ZVC1(K).LT.-100.) ZVC1(K)=-100.
      A1=SINH(ZVC1(K))
      B1=COSH(ZVC1(K))
      B1J=B1-CS(J)
      IF(B1J.EQ.0.0) B1J=10.E-30
      Y1(J,K)=SNH(MM1)*SN(J)/B1J
      X1(J,K)=SNH(MM1)*A1/B1J
      GO TO 300
  301 X1(J,K)=0.0£Y1(J,K)=0.0
  300 CONTINUE
      DO 310 K=1,KNC
      IF(ZVC2(K).EQ.0.0) GO TO 311
      IF(ZVC2(K).GT.100.0) ZVC2(K)=100.0
      IF(ZVC2(K).LT.-100.) ZVC2(K)=-100.
      A2=SINH(ZVC2(K))
      B2=COSH(ZVC2(K))
      B2J=B2-CS(J)
      IF(B2J.EQ.0.0) B2J=10.E-30
      Y2(J,K)=SNH(MM1)*SN(J)/B2J
      X2(J,K)=SNH(MM1)*A2/B2J
      GO TO 310
  311 X2(J,K)=0.0£Y2(J,K)=0.0
  310 CONTINUE
      DO 320 K=1,KNC
      IF(ZVC3(K).EQ.0.0) GO TO 321
      IF(ZVC3(K).GT.100.0) ZVC3(K)=100.0
      IF(ZVC3(K).LT.-100.) ZVC3(K)=-100.
      A3=SINH(ZVC3(K))
      B3=COSH(ZVC3(K))
      B3J=B3-CS(J)
      IF(B3J.EQ.0.0) B3J=10.E-30
      Y3(J,K)=SNH(MM1)*SN(J)/B3J
      X3(J,K)=SNH(MM1)*A3/B3J
      GO TO 320
  321 X3(J,K)=0.0£Y3(J,K)=0.0
  320 CONTINUE
      DO 330 K=1,KNC
      IF(ZVC4(K).EQ.0.0) GO TO 331
      IF(ZVC4(K).GT.100.0) ZVC4(K)=100.0
      IF(ZVC4(K).LT.-100.) ZVC4(K)=-100.
      A4=SINH(ZVC4(K))
      B4=COSH(ZVC4(K))
      B4J=B4-CS(J)
      IF(B4J.EQ.0.0) B4J=10.E-30
```

```
      Y4(J,K)=SNH(MM1)*SN(J)/B4J
      X4(J,K)=SNH(MM1)*A4/B4J
      GO TO 330
  331 X4(J,K)=0.0£Y4(J,K)=0.0
  330 CONTINUE
      DO 15 K=1,KNC
      ZVC1(K)=0.
      ZVC2(K)=0.
      LVC1(K)=1
      ZVC3(K)=0.
      ZVC4(K)=0.
      LVC2(K)=1
   15 CONTINUE
  100 CONTINUE
C---- PLOT CONCENTRATION CONTOURS AROUN THE SPHERES.
      KNP=KNC
      CALL CNPLOT
      RETURN
      END



      SUBROUTINE CNPLOT
C---- THIS SUBROUTINE PLOTS CONCENTRATION CONTOURS AROUND THE SPHERES.
      COMMON/GRID1/ Z(41),SNH(41),CSH(41),SN(31),CS(31)
      COMMON/GRID2/ IETHA(31),ETHA(31),THETA(31),DTHETA(31)
      COMMON/GRID3/ H3(41,31),R1(41,31)
      COMMON/CNSTC/ ZS,RI ,SC,PE,EPSC,RFC
      COMMON/M1MM1C/ M,M1,MMD,MM,MM1,MD,SH,SK,KS
      COMMON/PLOT1/ X1(31,10),X2(31,10),Y1(31,10),Y2(31,10)
      COMMON/PLOT2/ X3(31,10),X4(31,10),Y3(31,10),Y4(31,10)
      COMMON/RPLOTC/ RPLOT,IYS,IXSTEP
      COMMON/PLTPCN/ VCC(10),KNC,KNP
      COMMON/RRABC/ RRA,RRB,RRC,RRL
      DIMENSION CHAR(120),FPLOT(8)
      DATA BLANK,PLOT,PLUS,CROSS/1H ,1H.,1H+,1HX/
      DATA FPLOT/ 1H1,1H2,1H3,1H4,1H5,1H6,1H7,1H8/
C---- PLOTTING THE CONTOURS FOUND IN SUBROUTINE CNPLTP.
C---- ALL CONTOURS ARE MARKED BY(.).
C---- THE FRONT AND REAR STAGNATION POINTS ARE MARKED (+).
C---- THE CENTERS ARE MARKED (X).
      A=-CSH(1)
      B= CSH(1)
      RR1=A-RRA*RPLOT
      RR2=A+RRB*RPLOT
      RR3=B-RRB*RPLOT
      RR4=B+RRC*RPLOT
      XAU=-(CSH(1)+1.)
      XAUU=-(CSH(1)-1.0)
      XBU= (CSH(1)-1.)
      XBUU=(CSH(1)+1.)
      DX=RRL*RPLOT/(FLOAT(IXSTEP-1))
      DX2=DX/2.0
      DO 5 L=1,120
      CHAR(L)=PLOT
    5 CONTINUE
      WRITE(6,100) CHAR
  100 FORMAT(1H1,3H...,120A1)
      DO 10 L=1,119
      CHAR(L)=BLANK
   10 CONTINUE
```

```
C
C---- SPHERE A.
      XPLOT=RR1
   15 DO 25 J=1,M1
      DO 25 K=1,KNP
      DIF1=XPLOT-X1(J,K)
      ABDIF1=ABS(DIF1)
      DIF2=XPLOT-X2(J,K)
      ABDIF2=ABS(DIF2)
      IF(ABDIF1.LE.DX2) GO TO 20
   22 IF(ABDIF2.LE.DX2) GO TO 21
      GO TO 25
   20 LL=(FLOAT(IYS)/(RRL*RPLOT))*Y1(J,K)+1.0
      IF(LL.EQ.0.OR.LL.GT.119) GO TO 22
      CHAR(LL)=PLOT(K)
      GO TO 22
   21 LL=(FLOAT(IYS)/(RRL*RPLOT))*Y2(J,K)+1.0
      IF(LL.EQ.0.OR.LL.GT.119) GO TO 25
      CHAR(LL)=PLOT(K)
   25 CONTINUE
      IF((XPLOT.GT.XAU).AND.(XPLOT.LT.XAUU)) GO TO 1
   26 DFU=XPLOT-XAU
      DFUU=XPLOT-XAUU
      DFA=XPLOT-A
      ABDFU=ABS(DFU)
      ABDFUU=ABS(DFUU)
      ABDFA=ABS(DFA)
      IF((ABDFU.LE.DX2).OR.(ABDFUU.LE.DX2)) GO TO 40
      IF(ABDFA.LE.DX2) GO TO 41
      WRITE(6,101) CHAR
  101 FORMAT(1X,1H.,3X,120A1)
   30 CONTINUE
      DO 35 L=1,119
      CHAR(L)=BLANK
   35 CONTINUE
      XPLOT=XPLOT+DX
      IF(XPLOT.GT.RR2) GO TO 50
      GO TO 15
    1 C=XPLOT-A
      IF(C.EQ.0.0) C=10.E-30
      D=ABS(C)
      CL=1.0-D**2
      LC=(FLOAT(IYS)/(RRL*RPLOT))*SQRT(CL)+1.0
      IF(LC.EQ.1.OR.LC.GT.119) GO TO 26
      CHAR(LC)=PLUS
      GO TO 26
   40 CHAR(1)=PLUS
      WRITE(6,102) CHAR
  102 FORMAT(1X,1H.,3X,120A1)
      GO TO 30
   41 CHAR(1)=CROSS
      WRITE(6,102) CHAR
      GO TO 30
C
C---- SPHERE B.
   50 XPLOT=RR3
   55 DO 75 JB=1,M1
      J=M1-JB+1
      DO 75 K=1,KNP
      DIF3=XPLOT-X3(J,K)
      ABDIF3=ABS(DIF3)
      DIF4=XPLOT-X4(J,K)
      ABDIF4=ABS(DIF4)
```

```
      IF(ABDIF3.LE.DX2) GO TO 70
   72 IF(ABDIF4.LE.DX2) GO TO 71
      GO TO 75
   70 LL=(FLOAT(IYS)/(RRL*RPLOT))*Y3(J,K)+1.0
      IF(LL.EQ.0.OR.LL.GT.119) GO TO 72
      CHAR(LL)=FPLOT(K)
      GO TO 72
   71 LL=(FLOAT(IYS)/(RRL*RPLOT))*Y4(J,K)+1.0
      IF(LL.EQ.0.OR.LL.GT.119) GO TO 75
      CHAR(LL)=FPLOT(K)
   75 CONTINUE
      IF((XPLOT.LT.XBUU).AND.(XPLOT.GT.XBU)) GO TO 3
   76 DFU=XPLOT-XBU
      DFUU=XPLOT-XBUU
      DFB=XPLOT-B
      ABDFU=ABS(DFU)
      ABDFUU=ABS(DFUU)
      ABDFB=ABS(DFB)
      IF((ABDFU.LE.DX2).OR.(ABDFUU.LE.DX2)) GO TO 90
      IF(ABDFB.LE.DX2) GO TO 91
      WRITE(6,101) CHAR
      IF(XPLOT.GE.RR4) GO TO 400
   80 DO 85 L=1,119
      CHAR(L)=BLANK
   85 CONTINUE
      XPLOT=XPLOT+DX
      GO TO 55
    3 C=XPLOT-B
      IF(C.EQ.0.0) C=10.E-30
      D=ABS(C)
      CL=1.0-D**2
      LC=(FLOAT(IYS)/(RRL*RPLOT))*SQRT(CL)+1.0
      IF(LC.EQ.1.OR.LC.GT.119) GO TO 76
      CHAR(LC)=PLUS
      GO TO 76
   90 CHAR(1)=PLUS
      WRITE(6,102) CHAR
      GO TO 80
   91 CHAR(1)=CROSS
      WRITE(6,102) CHAR
      GO TO 80
  400 DO 6 L=1,120
      CHAR(L)=PLOT
    6 CONTINUE
      WRITE(6,103) CHAR
  103 FORMAT(1X,4H....,120A1)
      RETURN
      END
      SUBROUTINE SKPFILE(NSKIP,NUNIT)
C---- THIS SUBROUTINE SKIPS FILES ON MAGNETIC TAPE.
      L=0
    1 READ(NUNIT) DUMMY
      IF(EOF(NUNIT)) 10,11
   10 L=L+1
      IF(L.EQ.NSKIP) RETURN
   11 GO TO 1
      END
      FUNCTION SINH(X)
      SINH=0.5*(EXP(X)-EXP(-X))
      RETURN
      END
      FUNCTION COSH(X)
      COSH=0.5*(EXP(X)+EXP(-X))
      RETURN
      END
```

Bibliography.

Acrivos,A. and Taylor,T.D.

Phys. of fluid, 5, 387(1962).

Aksel'rud,S.A.

Zh. Fiz. Khim. 27, 1445(1953).

Al-Taha,T.R.

Ph.D. Thesis, Imperial College, Univ. of London(1969).

Aminzadeh,K.

M.Sc. Thesis, Imperial College, Univ. of London(197)).

Aminzadeh,K., Al-Taha,T.R., Cornish,A.R.H, Kolansky,M.S., and Pfeffer,R.

Int. J. Heat Mass transfer, V17, 1425(1974).

Baird,A.H.I. and Hamilec,A.E.

Can. J. Chem. Eng., 40, 119(1962).

Bart,E.

M.Ch.E. Thesis, New York university(1959).

Brenner,H.

Chem. Eng. Sci., 16, 242(1961).

Cornish,A.R.H.

Ph.D. Thesis, Illinos Institute of Technology(1961).

Cornish,A.R.H.

Trans. Instn. Chem. Engrs., V43, 332(1965).

Dean,W.R. and O'Neill,M.E.

Mathematika, 10, 13(.963).

Evenson,G.F., Hall,E.W., and Wart,S.G.

Brit. J. Appl. Phys., 10, 43(1959).

Faxen,H. and Dahl,H.

Arkiv. Mat. Astron. Fys. 19A, no.13(1925).

Frossling,N.

Lung Univ. Arsskr. N. F. avd. 36, no. 4(1940).

Goldman,A.J., Cox,R.G., and Brenner,H.

Chem. Eng. Sci., 21, 1151(1966).

Grafton,R.W.

Chem. Eng. Sci., 18, 457(1963).

Green,M.B.

Ph.D. Thesis, Imperial College, Univ. of London(1968).

Hamielec,A.E., Hoffman,T.W., and Ross,L.L.

A.I.C.E.J. 13, no.2, 212(1967).

Happel,J. and Pfeffer,R.

A.I.C.E.J., 6, 129(1960).

Happel,J. and Brenner,H.

"Low Reynolds Number Hydrodynamics", Prentice-Hall(1965).

Hocking,L.M.

Ph.D. Thesis, Univ. of London(1958).

Hocking,L.M.

Quart. J. Roc. Meteorol. Soc., 85, 44(1959).

Issakyan,S.M. and Gasparyan,A.M.

Int. Chem. Eng., 6, 74(1966).

Jeffery,G.B.

Proc. Lond. Math. Soc., 14, 327(1915).

Jenson,V.G.

Proc. Roy. Soc.(London), A249, 346(1959).

Kawaguti,M.

Rept. Inst. Sci. Tech.(Tokyo), 4, 154(1950).

Kronig,R. and Bruijsten,J.

Appl. Sci. Res. A2, 439(1951).

Kynch,G.J.

J. Fluid. Mech., 5, 193(1959).

Langmuir,I.

Phys. Review, 12, 368(1918).

Levich,V.G.

"Physicochemical Hydrodynamics", Prentice-Hall(1962).

Navier.

Mem. de l'Acad. des. Sciences, Vl, 389(1822).

O'Neill,M.E.

Mathematika, lO, 13(1963).

O'Neill, M.E.

Ph.D. Thesis, Univ. of London(1964).

O'Neill,M.E.

Appl. Sci. Res., 21, 452(1970).

Oseen,C.W.

"Hydrodynamics", Leipzig, Akademische Verlag(1927).

Pfeffer,R. and Happel,J.

A.I.C.E.J., lO, 605(1964).

Pfeffer,R. and Happel,J.

Ind. Eng. Chem. Fundamentals, 3, 380(1964).

Prandtl,L.

"Verber Fhussigkeitbewegen mit Kheniner Reibung",(1904).

Rojey,A.

M.Sc. Thesis, Univ. of London(1967).

Smoluchowski,M.

Bull. Inter. Acad. Palonaise. Sci. lett., lA, 28(1911).

Steinberger,E.H., Pruppacher,H.R., and Neiburger,M.

J. Fluid Mech., 34, 809(1968).

Atimson,M. and Jeffery,G.B.

Proc. Roy. Soc., Alll, llO(1926).

Stokes,G.G.

Trans. Camb. Phil. Soc., 9, Part 2, 8(1851).

Thom,A.

Aero. Res. Council, Rep. and Memo., no.1194(1928).

Tomotika,S. and Aoi,T.

Quart. J. Mech. Appl. Math., 3, 140(1950).

Wakiya,S.

Niigata Univ.(Nagaoka, Japan), Coll. Eng. Res. Report, no.6, Mar.30(1957).

Wakiya,S.

J. Phys. Soc., Japan, 22,4(1967).

Yuge,T.

Rept. Inst. High Speed Mech., (Tohoku University), 6, 146(1956).